

Max Wolfsberg
W. Alexander Van Hook
Piotr Paneth

With contributions from:
Luís Paulo N. Rebelo

18O Isotope Effects

in the Chemical, Geological,
and Bio Sciences

k_H
/
 k_D

 Springer

Isotope Effects

Max Wolfsberg • W. Alexander Van Hook
Piotr Paneth
with contributions from Luís Paulo N. Rebelo

Isotope Effects

in the Chemical, Geological, and Bio Sciences

 Springer

Max Wolfsberg
University of California Irvine
School of Physical Sciences
Dept. Chemistry
Irvine CA 92697-2025
1102, Natural Sciences II
USA
mwolfsbe@uci.edu

W. Alexander Van Hook
University of Tennessee
Dept. Chemistry
552 Buehler Hall
Knoxville TN 37996-1600
USA
avanhook@utk.edu

Piotr Paneth
Technical University of Lodz
Inst. Applied Radiation Chemistry
Dept. Chemistry
Zeromskiego 116
90-924 Lodz
Poland
paneth@p.lodz.pl

Luís Paulo N. Rebelo
Universidade Nova de Lisboa
Inst. Tecnologia Química e Biológica
Av. da Republica
2781-901 Oeiras
Portugal
luis.rebelo@itqb.unl.pt

ISBN 978-90-481-2264-6 e-ISBN 978-90-481-2265-3

DOI 10.1007/978-90-481-2265-3

Springer Dordrecht Heidelberg London New York

Library of Congress Control Number: 2009942349

©Springer Science+Business Media B.V. 2010

No part of this work may be reproduced, stored in a retrieval system, or transmitted in any form or by any means, electronic, mechanical, photocopying, microfilming, recording or otherwise, without written permission from the Publisher, with the exception of any material supplied specifically for the purpose of being entered and executed on a computer system, for exclusive use by the purchaser of the work.

Cover design: Design by Luís Morgado, implementation by WMX Design.

Printed on acid-free paper

Springer is part of Springer Science+Business Media (www.springer.com)

Preface

This book is an educational monograph addressed to graduate students and others undertaking isotope effect research. The fundamental principles needed to understand isotope effects are presented in appropriate detail. While it is true that these principles in the beginning will be more familiar to students of physical chemistry, and some background in physical chemistry is strongly recommended, the text provides enough detail to make the book an asset to students in organic and biochemistry, and geochemistry. Isotope effects are widely employed in many fields of science because of their utility. The underlying scientific principles needed to apply isotope effects to problems in physical chemistry, in organic and biochemistry, and in geochemistry are all the same or similar. This accounts for widespread communication between scientists in very different disciplines who share a fundamental interest in isotope effects. Nowhere has this been better exemplified than at the Gordon Conference on Isotope Effects which has met regularly for more than 50 years and has just as regularly stimulated cooperative efforts.

The title indicates the scope of the text. The term “isotope effects” is used rather than “applications of isotopes” to indicate clearly that it deals with differences in the properties of isotopically substituted molecules, for example differences in the chemical and physical properties of water and the heavy waters (H_2O , HDO, D_2O , HTO, etc.). Thus H_2O , HDO and D_2O have different thermodynamic properties. Also reactions in solvent mixtures of light and heavy water proceed at different rates than they do in pure H_2O . On the other hand, the differences are not large and consequently, to the extent the difference in properties can be ignored, HDO or HTO can be used as tracers for H_2O . An important point, however, is that this book does not deal with isotopes as tracers in spite of the widespread importance of tracer studies, particularly in the bio and medical sciences. Also the title specifically does not mention physics which would necessarily have been included if the term “Physical Sciences” had been used. Thus the text does not deal with differences in the nuclear properties of isotopic atoms. Such differences are in the realm of nuclear physics and will not be discussed.

A synopsis of the topics treated in this monograph follows. Chapter 1 is a brief survey of historical developments in the field of isotope effects through the early 1930s. Chapters 2 and 3 give developments of the fundamental quantum mechanical, thermodynamic, and molecular vibration theory required to under-

stand isotopic differences on molecular properties. Chapter 4 considers the theory of isotope effects on thermodynamic and equilibrium properties, and follows that development with a short discussion of rate isotope effects. Chapter 5 treats condensed phase isotope effects in considerable detail, and Chapter 6 returns attention to kinetic isotope effects by contrasting ordinary activated complex theory with variational transition state theory. Chapter 7 deals with the instrumentation and experimental techniques of isotope science. The final seven chapters discuss applications of fundamental isotope effect theory to isotope separation (Chapter 8), environmental and geo-science (Chapter 9), physical organic chemistry (Chapter 10), enzymes and biochemistry (Chapter 11), molecular properties dependent on vibrational amplitudes (Chapter 12), corresponding states theory of fluids (Chapter 13), and isotope effects on rates of unimolecular reactions and mass independent isotope effects (Chapter 14). We hope this work will prove to be a helpful introduction to those planning studies using isotope effects, and a useful reference for those already in the field.

It is a pleasure for two of the authors (AVH and MW) to express their appreciation to Jacob Bigeleisen, who during our postdoctoral years ignited our lifelong interest in isotope effects.

Irvine,
Knoxville,
Lodz,
Lisbon,

Max Wolfsberg
Alexander Van Hook
Piotr Paneth
Luís Paulo N. Rebelo

Contents

1	A Short History of Early Work on Isotopes	1
1.1	Introduction	1
1.2	From Dalton to the Discovery of Isotopes	2
1.2.1	The Periodic Table	3
1.3	From the Discovery of Isotopes through the Invention of the Mass Spectrograph by Aston	6
1.3.1	The Historic Papers of Soddy and Fajans in 1913 and the Work Leading up to These Papers	6
1.3.2	Further Elucidation of the Concepts of Elements and Isotopes Including Works of van den Broek, Moseley, Rutherford, Thomson, Aston and Lindemann	14
1.3.3	The Work of Harkins on the Whole Number Rule	21
1.3.4	Understanding the “Modern” Periodic Table	23
1.4	The 1920s and 1930s Through the Discovery of Deuterium	25
1.4.1	Early Work on Isotope Effects on Spectra	25
1.4.2	The Discovery of Isotopes of Carbon, Nitrogen, and Oxygen, and Hydrogen	30
1.4.3	Deuterium	31
1.5	A Brief Look at the Position of Theoretical and Experimental Developments at the Time of the Discovery of Deuterium	33
1.5.1	Quantum Theory	33
1.5.2	Thermodynamics and Statistical Mechanics	33
1.5.3	Instrumentation – The Mass Spectrometer	34
	References	34
2	The Born–Oppenheimer Approximation: Potential Energy Surfaces ..	37
2.1	Introduction	37
2.2	The Quantum Mechanical Schrödinger Equation of the Molecule ..	37
2.3	The Separation of the Nuclear and Electronic Parts of the Schrödinger Equation	39
2.3.1	Solutions of the Electronic Schrödinger Equation for Molecules	40

2.3.2	Nuclear Motion	42
2.3.3	Corrections.....	42
2.3.4	Substituent Effects, Isotope Effects, and the First Law of Isotopics	42
2.3.5	Separation of Internal and External Degrees of Freedom.....	43
2.4	The Adiabatic Correction	44
2.4.1	An Example.....	45
2.4.2	Adiabatic BO Corrections for Hydrogenic Atoms.....	47
2.4.3	Muonium (Mu)	50
2.5	Numerical Calculations of $E_{\text{elec}}(S)$	51
2.5.1	Historical Development	51
2.5.2	Present Day Approaches	52
	References/Suggestions for Further Reading	53
3	Molecular Vibrations.....	55
3.1	Introduction	55
3.1.1	Vibrations in Diatomic Molecules	55
3.1.2	Extension to Polyatomics	58
3.1.3	Remarks.....	60
3.2	Discussion of Two Types of Coordinate Systems	60
3.3	Calculations in Cartesian Coordinates	62
3.3.1	Separation of Translation and Rotation from Vibration ...	67
3.4	Calculations Employing Valence (Internal) Coordinates	68
3.5	Two Important Rules for Harmonic Vibrational Frequencies	70
3.5.1	The Teller–Redlich Product Rule	70
3.5.2	The Sum Rule	71
3.A1	Appendix: Matrix Operations	71
3.A1.1	Some Definitions	71
3.A1.2	Matrix Diagonalization.....	72
3.A2	An Equality for Use in the Derivation of the Teller– Redlich Product Rule	75
	Reading List.....	76
4	Isotope Effects on Equilibrium Constants of Chemical Reactions; Transition State Theory of Isotope Effects	77
4.1	Introduction	77
4.2	Brief Review of the Laws of Thermodynamics	77
4.2.1	The First Law	77
4.2.2	The Second Law	78
4.2.3	The Third Law.....	79
4.3	The Free Energies and the Concept of Equilibrium	80
4.3.1	The Helmholtz Free Energy	80
4.3.2	The Gibbs Free Energy.....	81
4.3.3	Relations Involving A , ΔA , G and ΔG	81

4.4	Application to Ideal Gases at Equilibrium.....	84
4.4.1	Remarks, Nonideality, Condensed Phases	85
4.5	Statistical Mechanics of Ideal Gases and Isotope Effects.....	86
4.5.1	General Remarks	86
4.5.2	Equilibrium Constants and Partition Functions	88
4.6	Evaluation of Partition Functions, q , and Isotope Effects on Partition Functions, $q_{\text{heavy}}/q_{\text{light}}$ for Ideal Gases	89
4.6.1	The Rigid Rotor Harmonic Oscillator Approximation	89
4.6.2	Considerations of Level Spacing	91
4.6.3	The Energy Zero.....	92
4.6.4	Bigeleisen and Mayer; The Reduced Isotopic Partition Function Ratio	93
4.6.5	Limiting Values for the Isotope Effects	96
4.7	The High Temperature Limit: Generalization, (No Classical) Isotope Effects on Chemical Equilibrium.....	97
4.7.1	Further Remarks, RRHO Ideal Gas	101
4.8	The First Quantum Correction	102
4.8.1	Application to an Equilibrium	104
4.8.2	Polynomial Expansions of $(s_2/s_1)_f$: Orthogonal Polynomial Methods	105
4.9	Symmetry Numbers	106
4.9.1	Symmetry Numbers; Diatomic Molecules	106
4.9.2	Symmetry Numbers Continued, Comments, Polyatomics	110
4.9.3	The Determination of Relative Symmetry Numbers for Isotopomers	112
4.9.4	More Comments, Symmetry Numbers Do Not Lead to Isotope Enrichment.....	113
4.10	Further Remarks on Temperature Dependence of $(s/s')_f$: Limiting Forms: An Example	115
4.11	Transition State Theory of Isotope Effects	117
4.11.1	Fundamentals of Transition State Theory	117
4.11.2	Introduction of the Partition Functions	121
4.11.3	Comments	126
4.12	The Development of Modern Methods to Calculate Reduced Isotopic Partition Function Ratios	127
4.12.1	The Calculation of $(s/s')_f$ for Normal Molecular Species	128
4.13	Corrections to the Bigeleisen–Mayer Equation: The Nuclear Field Shift Effect	130
4.A1	Appendix: The Connection Between the Equilibrium Constant, Its Isotope Effects, and Pressure or Concentration Ratios: Corrections for Nonideality	132
4.A2	Corrections to the Rigid Rotor Harmonic Oscillator Approximation in the Calculation of Equilibrium Constants.....	134
4.A2.1	Corrections to RRHO: Diatomic Molecules	134
	Reading List.....	136

5	Condensed Phase Isotope Effects: Isotope Effects	
	in Non-ideal Gases	139
5.1	Introduction	139
5.2	Thermodynamic Formalism	139
	5.2.1 The Vapor Phase Reference	140
	5.2.2 The Condensed Phase	141
	5.2.3 The Vapor Pressure Isotope Effect, Separated Isotopes ...	141
	5.2.4 Fractionation Factors	142
5.3	Reprise: Remarks Concerning the Partition Functions: The Relation of VPIE to Condensed Phase Molecular Properties and Vibrational Dynamics	144
	5.3.1 Application to Polyatomics	144
	5.3.2 What Happens When Molecules Interact or Condense? A Simplified Physical Picture	145
5.4	VPIE's in Monatomic and Polyatomic Systems: Approximate Vibrational Analysis	147
	5.4.1 Dispersion Forces, Frequency Shifts on Condensation, and the VPIE	149
	5.4.2 Polyatomic Systems in Approximation: The Cell Model	150
	5.4.3 A Further Approximation: The AB Equation	151
5.5	Non-ideal Gases: Virial Coefficient Isotope Effects (VCIE)	152
5.6	Further Discussion of VPIE's	154
	5.6.1 Representative Effects, Especially H/D Effects and Solvent Dependence	154
	5.6.2 Interpretation of VPIE Using Model Calculations: Preliminary Remarks	157
	5.6.3 Anharmonic Corrections	157
	5.6.4 Corrections for the Dielectric Effect	160
5.7	Some Examples	162
	5.7.1 Example #1: Monatomic Systems Reconsidered: Accurate Calculations	162
	5.7.2 Example #2: VPIE's of Ethylene Isotopomers	163
	5.7.3 Example #3: VPIE's of Benzene Isotopomers; Excess Pressures of Isotopomer Solutions ..	165
	5.7.4 Example #4: Water	166
5.8	Excess Free Energies in Solutions of Isotopes: Connections Between VPIE, the Liquid Vapor Fractionation Factor, α , and RPF	170
	5.8.1 Excess Free Energies and Demixing in Isotopomer Solutions, Further Discussion	172
5.9	The Isotope Effect on T_{CR} for the Superconducting/ Resistive Transition in Metals	173
5.10	Isotope Effects on Solubility	174
	5.10.1 Liquid-Liquid Equilibria: Two Component Systems	174

5.10.2	Small Molecule Solutions Including Aqueous Systems ...	175
5.10.3	IE's on Solubility of Gases in Liquids, Chromatographic IE's	177
5.10.4	Solubility of Ionic Solids in H ₂ O/D ₂ O	179
	Further Reading	180
6	Kinetic Isotope Effects Continued: Variational Transition State Theory and Tunneling	181
6.1	Introduction: Transition State Theory, Variational Transition State Theory, and Tunneling	181
6.1.1	Transition State Theory	181
6.2	The Basics of Variational Transition State Theory and How It Differs from Conventional Transition State Theory	182
6.2.1	The Dividing Surface for the Reaction	182
6.2.2	The Minimum Energy Path	185
6.2.3	Classical Trajectory Calculations	185
6.2.4	The Differences Between TST and VTST	186
6.2.5	Locating Dividing Surfaces	187
6.2.6	Quantum Mechanical VTST	187
6.2.7	Isotope Effects, Comments	188
6.3	Tunneling	189
6.3.1	Tunneling in TST	189
6.3.2	Tunneling in VTST	192
6.3.3	Tunneling in Three Center Collinear Reactions	196
6.4	Tests of Variational Transition State Theory (Including Tunneling)	199
6.4.1	Collinear Three Center Reactions	199
	Further Reading	201
7	Instrumentation and Experimental Techniques	203
7.1	Experimental Determination of Kinetic Isotope Effects	203
7.1.1	The Non-competitive or "Direct" Method	203
7.1.2	Simultaneous Non-competitive Measurements	206
7.1.3	KIE's of Enzyme Catalyzed Reactions by Isotope Perturbation	207
7.1.4	Competitive Measurements of KIE's	208
7.1.5	Error Analysis	212
7.2	Mass Spectrometry and Isotope Ratio Mass Spectrometry	215
7.2.1	Whole Molecule Mass Spectrometry	215
7.2.2	Isotope-Ratio Mass Spectrometry	219
7.3	NMR Measurements of Isotope Effects: Isotope Effects on NMR Spectra	225
7.3.1	Isotope Labeling in NMR Investigations of Molecular Structure	225
7.3.2	Rovibrational NMR Isotope Effects	226

7.3.3	NMR as an Analytical Tool: NMR Measurements of Carbon IE's	231
7.4	Radioisotopes	233
7.4.1	Errors.....	233
7.5	Equilibrium Isotope Effects	234
7.5.1	Fractionation Measurements	234
7.5.2	Studies Using Separated Isotopes	235
7.5.3	Liquid–Vapor Isotope Fractionation Measurements	238
7.5.4	Isotope Effects on Liquid–Liquid Equilibria	238
7.6	H/D Isotope Effects and Small Angle Neutron Scattering	242
	Further Reading	244
8	Isotope Separation	245
8.1	Introduction	245
8.2	Theory of Cascades: Terminology	247
8.2.1	Gaseous Diffusion of UF ₆	248
8.2.2	Types of Separations: Cascades	249
8.2.3	Further Discussion of Gaseous Diffusion: Separative Work	254
8.3	Practical Isotope Separation: Some Examples	255
8.3.1	Electromagnetic Separation	256
8.3.2	Thermal Diffusion of Gases.....	259
8.3.3	Large Scale Separations and Energy Demands	261
8.3.4	Centrifuge Based Separations.....	264
8.3.5	Aerodynamic Isotope Separation	267
8.4	Distillation and Exchange Distillation: The Large Scale Production of Deuterium	267
8.4.1	An Aside: Monothermal Isotope Exchange with Chemical Reflux; ¹⁵ N Enrichment	269
8.4.2	Dual Temperature Exchange: The GS Process for Deuterium Enrichment	270
8.4.3	Other Exchange Reactions for Deuterium Enrichment	272
8.4.4	Distillation	272
8.4.5	Specific Examples, Isotope Separation by Distillation	274
8.4.6	Exchange Distillation: ¹⁰ B Enrichment	276
8.4.7	Liquid–Liquid Exchange: Lithium Enrichment.....	277
8.5	Chromatography	277
8.5.1	Gas Chromatography	278
8.5.2	Redox Ion Exchange Chromatography	280
8.6	Photochemical and Laser Isotope Separation	282
8.6.1	Outline of a Laser Isotope Separation Scheme.....	282
8.6.2	LIS of Deuterium	285
8.6.3	LIS for Uranium	285
8.7	Other Isotope Separation Processes.....	286
	Further Reading	287

9	Isotope Effects in Nature: Geochemical and Environmental Studies	289
9.1	Introduction	289
9.2	Notation and Standards	290
9.2.1	The Delta, δ , Notation	290
9.2.2	Standards	290
9.2.3	Conversion from One Standard to Another	292
9.2.4	Remarks, Experimental Technique	292
9.3	Geochemical Temperature Scales	293
9.4	Isotope Hydrology; Rayleigh Fractionation	296
9.4.1	Fractionation in Hydrology; the Meteoric Water Line	298
9.4.2	Ice Cores	298
9.4.3	Clay Cores: ^{13}C Enrichment in Paleo-Organics	301
9.5	Three Isotope Plots of Terrestrial and Extraterrestrial Samples	302
9.6	Isotope Fractionation by Living or Once Living Organisms	302
9.6.1	“We Are What We Eat, \pm a Few per Mil”	303
9.6.2	Isotope Fractionation and Dendrochronology of Bristlecone Pines	305
9.6.3	$\delta^{18}\text{O}$ as a Probe for Storm Patterns	306
9.7	Coal, Petroleum and Natural Gas	307
9.8	Further Examples, Food Authentication	308
9.8.1	Food Authentication	308
9.8.2	Athletic ‘Doping’	310
9.9	Stable Isotopes as Tracers in Biological, Agricultural, Nutritional and Medical Research	310
	Suggestions for Further Reading	310
10	Kinetic Isotope Effects on Chemical Reactions	313
10.1	Introduction	313
10.2	KIE’s on the “Simplest” Chemical Reaction (Hydrogen Atom + Diatomic Hydrogen)	313
10.3	The Reaction Between Methane and Hydroxyl Radical	318
10.4	Further Discussion, Heavy Atom Isotope Effects, Secondary Isotope Effects	319
10.4.1	α - 2° Isotope Effects	320
10.4.2	β - 2° Isotope Effects	322
10.4.3	Steric Arguments and β , γ ... 2° Isotope Effects	323
10.4.4	Comment	324
10.5	Relative Values for Deuterium and Tritium Isotope Effects: The Swain–Schaad Relation	325
10.6	Alternative Reaction Paths, $\text{S}_{\text{N}}2$ and $\text{E}2$: Condensed and Vapor Phase Studies	327
10.7	KIE’s as Probes of Transition State Structure	329
10.7.1	$\text{S}_{\text{N}}2$ Reactions for CN^- Attack on Substituted Benzyl Chlorides	330

10.7.2	Reaction of Substituted Anilines with Methyl Iodide	331
10.7.3	More on KIE's in Menshutkin Reactions	332
10.7.4	Decarboxylation Reactions	334
10.7.5	Bond Order Dependence of the KIE	335
10.7.6	Mechanism of the Diels–Alder Reaction	336
10.8	Remarks	339
10.8.1	Protocol of Harmonic TST Calculations of Kinetic Isotope Effects	339
10.8.2	The TST/VTST Interface	340
	Reading List	341
11	Enzymes; Aqueous Solvent IE'S	343
11.1	Introduction	343
11.2	Some Simple Enzyme Kinetics	344
11.2.1	Introduction: The Michaelis–Menten Mechanism	344
11.2.2	The Incorporation of Product Binding	347
11.2.3	A Simpler Notation	349
11.2.4	The Intrinsic IE, Commitments, and Partitioning Factor	350
11.3	More Complicated Enzyme Reactions	351
11.3.1	Reversible Reaction at the Active Site	351
11.3.2	Ordered Sequential Reactions	352
11.3.3	Random Binding	354
11.3.4	Comments	354
11.3.5	Multiple Isotope Effects	355
11.3.6	Multiple Isotope Effects, Different Steps	356
11.3.7	Reversible Competitive Inhibitors	357
11.4	Aqueous Solvent Equilibrium and Kinetic Isotope Effects	358
11.4.1	H ₂ O/D ₂ O Solvent Effects on pH (pD) and pK _a	358
11.4.2	Monoprotic Acid/Base Equilibria in Mixed Solvents	360
11.4.3	Kinetic Isotope Effects in Mixed Solvents	362
11.5	Examples, Enzyme Catalysis	365
11.5.1	Decarboxylation KIE's	365
11.5.2	Glucose-6-Phosphate Dehydrogenase	366
11.5.3	Concentration Dependence of KIE; Phosphoenolpyruvate Carboxylase	368
11.5.4	Other Factors Influencing Commitment	371
11.6	Solvent Kinetic Isotope Effects in Enzyme Reactions (See Also Section 11.4)	372
11.6.1	Examples	373
11.6.2	Coupled Motion	375
11.7	Tunneling (See Also Section 11.8)	376
11.7.1	Tunneling in Alcohol Dehydrogenases	376
11.7.2	Hydrogen Atom Transfer in Methylmalonyl- CoA Mutase	377

11.8	Modeling Isotope Effects on Enzyme-Catalyzed Reactions	379
11.8.1	Examples of VTST QM/MM Calculations for Enzyme Reactions	380
11.8.2	QM/MM for Haloalkane Dehalogenase: TST Calculations.....	385
11.8.3	Comment	388
	Reading List.....	388
12	Isotope Effects on Dipole Moments, Polarizability, NMR Shielding, and Molar Volume	389
12.1	Introduction	389
12.1.1	Dipole Moments, Polarizabilities and Hyperpolarizabilities	389
12.2	Dipole Moments and Their Isotope Effects	393
12.2.1	Experimental Methods	393
12.2.2	The IE on μ_0 , Discussion	394
12.2.3	Dipole Moments for Diatomic Isotopomers	396
12.2.4	Theoretical Approaches	398
12.3	Induced Moments, Polarizability Isotope Effects	398
12.3.1	The Polarizability.....	398
12.3.2	Frequency Dependence	398
12.3.3	Experimental Methods, Results, Discussion	400
12.4	Isotope Effects on NMR Shielding	403
12.4.1	Introduction.....	403
12.4.2	Application of the Rovibrational Theory	403
12.5	Molar Volume Isotope Effects	406
12.5.1	The Bartell Mechanical Model for MVIE.....	408
12.5.2	Hydrogen Bonded Liquids	409
12.5.3	Limitations of the Mechanical Model, the Temperature Dependence	411
	Reading List.....	412
13	Reduced Equations of State: Critical Property Isotope Effects	413
13.1	Introduction, Corresponding States	413
13.1.1	Equations of State, Corresponding States	413
13.2	Reference Systems; Critical Property Data for Some Isotopomer Pairs	414
13.2.1	The PVT Surface for Isotopomer Pairs.....	414
13.2.2	IE's of Reference Pairs	417
13.2.3	PVT Isotope Effects and the Modified Van der Waals Equation	418
13.2.4	Reference Systems, Isotope Effects	418
13.3	Critical Property Isotope Effects	419
13.3.1	Experimental Data.....	419

13.3.2	Correlations Between Critical Property and Vapor Pressure IE's: $\ln(T_c'/T_c)$ and $\ln(P'/P)$	420
13.3.3	Uncertainties in Critical Property IE's	421
13.4	CS Calculations for Some Isotopomer Pairs	422
13.4.1	The Lighter Pairs	422
13.4.2	VdW1 Parameters for Heavier Pairs.....	424
13.5	Remarks	424
	Further Reading	426
14	Isotope Effects in Unimolecular Processes: “Mass Independent” Isotope Fractionation and the Ozone Problem	427
14.1	Introduction: Isotope Effects in Unimolecular Reactions.....	427
14.2	The RRKM Mechanism for Unimolecular Gas Phase Reactions ...	428
14.2.1	The Expression for $\delta k_1(E, dE)/k_2$	431
14.2.2	Discussion of $k_a(E)$	431
14.2.3	The Expression for $k_a(E)$	433
14.2.4	The Pressure Dependence of the Rate Constant k_{uni}	435
14.2.5	Experimental Measurements of Isotope Effects in Unimolecular Reactions and the RRKM theory	436
14.2.6	Thermal Activation: Inverse 2°-D-KIE's at Low Pressure	437
14.2.7	Primary Isotope Effects	441
14.3	¹⁷ O and ¹⁸ O Enrichment in Terrestrial and Extraterrestrial Samples: “Mass Independent” Isotope Fractionation and the Ozone Problem	442
14.3.1	Introduction	442
14.3.2	Oxygen Isotope Fractionation in Earth, Moon, and Meteorite Samples	443
14.3.3	Mass Independent Isotope Fractionation in the Laboratory, the Stratosphere, and the Troposphere.....	444
14.3.4	MIF's for Ozone from Natural Abundance and Enriched Starting Materials	446
14.4	Theory of Mass Independent Isotope Fractionation of Ozone.....	448
14.4.1	Comment	450
	Further Reading	450
	Author Index	453
	Subject Index	459

Chapter 1

A Short History of Early Work on Isotopes

Abstract A brief introduction deals with the time period from Dalton to the discovery of isotopes by Soddy and Fajans in the early twentieth century which was soon followed by the invention of the mass spectrograph (1922). The next section covers the period from 1922 to the discovery of deuterium by Urey and his colleagues. It includes a discussion of isotope effects in spectroscopy, particularly band spectra of diatomic molecules, and also discusses the discovery of the important stable isotopes in the second row of the periodic table. It ends with the discovery of deuterium, probably the most “popular” isotope for isotope effect studies. The chapter ends with a short description of the “apparatus” of theory and experimentation available for isotope effect work at the time of the discovery of deuterium.

1.1 Introduction

The concept of the atom as the smallest “particle” of matter (from the Greek word for indivisible) was promulgated by John Dalton about 1803. Within about a century and a quarter of scientific investigation which will be briefly described in this chapter, this concept yielded the idea of the periodic table and the understanding of the periodic table including the nuclear atom, the concept of isotopes, and the discovery of the majority of the isotopes which are used in the studies of the isotope effects. It is appropriate to point out that this book deals with the study of the effect of isotopic substitution on the physical and chemical properties of molecular (or atomic) systems. The book does not deal with the use of isotopes as tracers, a use which usually depends on the assumption that isotope effects are small and can be ignored in tracer studies.

Section 1.2 deals with the time period from Dalton to the discovery of isotopes by Soddy and Fajans. Much of the discussion elaborates on the type of material found in introductory chemistry texts. It ends with the discovery of radioactivity by Becquerel and the developments which quickly followed. Section 1.3 starts with the discovery of the concept of isotopes in the early years of the twentieth century and ends with the invention of the mass spectrograph in 1922 by Aston. The literature relating to the work leading up to the 1913 papers by Soddy and Fajans is well and

even-handedly reviewed in the Nobel Lecture of F. Soddy (NLC1921*) who himself was a main contributor to this development. This Lecture (Soddy 1922) is used as almost the sole literature reference to this material. Subsequent material in this chapter will contain appropriate references. The references should be regarded as a survey of some of the relevant literature. It would be a mistake to conclude that they are in any way complete or that they even contain all the “important” publications. The chief personalities related to isotope chemistry that appear in this section include Soddy, Fajans, Paneth, de Hevesy, Rutherford, van den Broek, Moseley, Lindemann, Aston, and Harkins.

Section 1.4 starts after the invention of the mass spectrograph; it covers the period from 1922 to the discovery of deuterium by Urey and his colleagues. This section includes discussion of isotope effects in spectroscopy, particularly band spectra of diatomic molecules. It also discusses the discovery of the important stable isotopes in the second row of the periodic table. It ends with the discovery of deuterium, probably the most “popular” isotope for isotope effect studies.

The chapter ends with Section 1.5, a very short discussion of the “apparatus” of theory and of experimentation available for isotope effect work at the time of the discovery of deuterium.

1.2 From Dalton to the Discovery of Isotopes

As already noted, in 1803, Dalton referred to the smallest particle of matter as an atom. Atoms of elements combine to form compounds/molecules. Dalton measured the weight of an elemental material which combines with a given weight of another elemental material. He observed that, on a relative basis, hydrogen gas is the lightest material and, on the assumption that hydrogen has a weight of 1.00 and that molecules made up from elements consist of one atom each from two elements which reacted, he determined the relative weights of various elements. Thus, he assigned masses to the atoms of various elements as shown in Table 1.1. The above naive discussion, of course, over-simplifies the situation. How do you decide that a material is an elemental material? Obviously, elemental materials cannot be decomposed into other elemental materials whereas compounds can. How do you know that water is not an elemental material? You can electrolyze water and obtain hydrogen and oxygen which you have already established to be elements. Such questions must have come up and indeed it is almost certain that people misidentified compounds as elements and vice versa. As we see from the table, Dalton came up with combining weights for materials which we do recognize as elements.

Nobel Prizes in Chemistry and Physics were awarded starting in 1901. In this chapter (the first mention of the name of a Nobel Laureate in the running text will be followed by the notation (NLP xxxx) or (NLCxxxx*) where NLP and NLC stand for Nobel Laureate Physics and Nobel Laureate Chemistry respectively while xxxx notes the year of the award.

Table 1.1 Dalton's system of relative atomic weights, 1810

	Relative to H = 1.000 1810	1810 values recalculated relative to O = 16.000 assuming modern formulae	Modern values
Hydrogen	1	1.14	1.008
Oxygen	7	16	16
Azote (nitrogen)	5	11.4 ^a 15	14
Carbon	5.4	12.3	12
Sulfur	13	29.7	32
Phosphorus	9	25.7 ^a 27	31

^aFor nitrogen and phosphorus two numbers are given, the upper calculated from Dalton's formula for the hydride, the lower from that for the oxide.

The finding that two elements can give rise to more than one product molecule so that there could be more than one combining ratio for two given elements leads to the concept that molecules need not be diatomic. Avogadro's hypothesis that equal volumes of gas at a given pressure and temperature contain the same number of molecules permitted further refinements leading to the concept of atomic weights. By 1826, the Swedish chemist J. Berzelius, who was the discoverer of a number of new elemental substances, published a table of atomic weights relative to oxygen which was taken to have an atomic weight of 100 (Table 1.2). While some of his relative atomic weights differ by factors of approximately 3/2 or 2 from present day values, many are in quite close agreement. Berzelius introduced the modern usage of one or two letter abbreviations for the names of the elements and wrote formulae for chemical compounds indicating by superscripts (rather than by modern subscripts) the relative number of atoms of each kind in a molecule. Berzelius also showed that atomic weights are not just integer multiples of the atomic weight of hydrogen (Prout's hypothesis).

1.2.1 The Periodic Table

Although a number of chemists noted similarities in groups of elements, it is the Russian chemist D. I. Mendeleev who is credited as the Father of the Periodic Table. He observed periodicity of chemical properties when he grouped elements in order of increasing atomic weight in rows and columns in the way familiar to chemists (see Figs. 1.3 and 1.4). The periodicity in properties is associated with the columns of the table. It is noted that the theoretical foundation underlying the construction of the table did not become clear until after the introduction of quantum theory in the early twentieth century. The importance of Mendeleev's table to chemistry in 1872 was that the table enabled him to predict (correctly) missing elements and their properties, as well as properties of the compounds which could be formed from them.

Table 1.2 Berzelius's atomic weights^a of 1826 (Cited from Partington, J. R. *A history of chemistry*, Macmillan & Co., London 4, 166 (1964))

	Relative to O = 16	Relative to H = 1	Modern value
O	16	16.026	16
S	32.19	32.24	32.07
P	31.38 × 2	31.436	30.97
Cl	35.41	35.47	35.45
C	12.23	12.25	12.01
N	14.16	14.186	14.007
H	0.998	1.000	1.008
As	75.21	75.329	74.92
Cr	56.29	56.38	52.00
Sb	129.03	129.24	121.75
Si	29.58 × 3/2	29.61 × 3/2	28.09
Hg	202.5	202.863	200.59
Ag	108.12 × 2	108.31 × 2	107.87
Cu	66.31	63.415	63.55
Bi	212.80	213.208	208.98
Pb	207.12	207.458	207.21
Sn	117.6 × 2	117.84	118.71
Fe	54.27	54.363	55.85
Zn	64.51	64.621	65.39
Mn	56.92	57.019	54.94
Al	27.38	27.431	26.98
Mg	25.33	25.378	24.31
Ca	40.96	41.03	40.08
Ba	137.1	137.325	137.33
Na	23.27 × 2	23.31 × 2	22.99
K	39.19 × 2	39.26 × 2	39.10

^aBerzelius's figures relative to O = 100 have been recalculated in the table above to facilitate comparisons with modern values.

While the emphasis here is on the beginnings of modern chemistry in terms of atomic weights and atomic theory, one should not forget that the nineteenth century saw large strides in many other aspects of chemistry. We name here just a few of the scientists involved. In physical chemistry, there were, for instance, S. Carnot (1796–1832) and R. Clusius (1822–1888). In organic chemistry, there were F. Woehler (1800–1882) and J. F. Von Liebig (1803–1878). By 1864, J. C. Maxwell had published his famous equations of the electromagnetic field. Around 1886, H. Hertz demonstrated the existence of radio waves. On January 1, 1896, W. C. Roentgen (NPP 1901*) announced the discovery of x-rays. Subsequently, H. Becquerel [NLP 1903*] studied the fluorescence and phosphorescence of certain salts; fluorescence refers to the phenomenon where a material emits light of a different frequency while, or immediately after, being irradiated by light of another frequency (often sunlight), while phosphorescence refers to the delayed emission of light by the material. Soon after Roentgen's discovery of x-rays, in March 1896, Becquerel found that uranyl

salts emitted a new type of radiation which, like x-rays, could pass through pieces of paper as well as sheets of metal; however, this new radiation required no initiating energy source unlike phosphorescence and fluorescence. Becquerel also found that the uranium emanations turned air into a conductor of electricity.

Marie (NLP 1903*, NLC 1911*) and Pierre (NLP 1903*) Curie took up further study of Becquerel's discovery. In their studies, they made use of instrumental apparatus, designed by Pierre Curie and his brother, to measure the uranium emanations based on the fact that these emanations turn air into a conductor of electricity. In 1898, they tested an ore named pitchblende from which the element uranium was extracted and found that the electric current produced by the pitchblende in their measuring instrument was much stronger than that produced by pure uranium. They then undertook the herculean task of isolating demonstrable amounts of two new radioactive elements, polonium and radium, from the pitchblende. In their publications, they first introduced the term "radio-activity" to describe the phenomenon originally discovered by Becquerel. After P. Curie's early death, M. Curie did recognize that radioactive decay (radioactivity) is an atomic property. Further understanding of radioactivity awaited the contributions of E. Rutherford.

Meanwhile, in 1897, J. J. Thomson (NLP 1906*) observed that the cathode rays produced in a so-called cathode ray tube were a stream of negatively charged particles. He studied the motion of these particles in a magnetic field and was able to deduce the charge to mass ratio (e/m). He also found a number of ways to estimate the charge of these particles, which he referred to as corpuscles and we now term electrons. One method towards this end devised by A. H. Wilson is remarkably similar to the famous oil drop apparatus by which R. E. Millikan (NLP 1923*) made his accurate determination of the charge (e) of an electron in 1909. From the value obtained, Thomson found that the charge on the electron, while opposite in sign to that of a hydrogen ion, is the same magnitude. On the other hand, he found that the mass (m) is approximately $1/1,800$ that of a hydrogen ion. He concluded that the corpuscles had been produced from atomic material. Thus, he reluctantly concluded at a meeting of the Royal Society (London) that Dalton's hypothesis of the indivisibility of the atom is erroneous.

The early years of the twentieth century saw giant advances in man's understanding of nature which must be mentioned in any synopsis of the scientific history of this era. Thus, in 1901, M. Planck (NLP 1918*) published his first paper on the black-body radiation law which ushered in the era of quantum mechanics. In 1905, A. Einstein (NLP 1918*) published his *Anna Mirabilis Papers* on the photo effect, on Brownian motion, and on the theory of special relativity and the equivalence of matter and energy.

In the meantime, E. Rutherford (NLC 1908*) studied the radioactivity discovered by Becquerel and the Curies. He determined that the emanations of radioactive materials include alpha particles (or rays) which are positively charged helium atoms, beta particles (or rays) which are negatively charged electrons, and gamma rays which are similar to x-rays. He also studied the radioactive decay process and deduced the first order rate law for the disappearance of a radioactive atom, characterized by the half-life, the time in which 50% of a given radioactive species disappears, and which is independent of the concentration of that species.

1.3 From the Discovery of Isotopes through the Invention of the Mass Spectrograph by Aston

1.3.1 *The Historic Papers of Soddy and Fajans in 1913 and the Work Leading up to These Papers*

As already noted, while it is the intention for the rest of this chapter to give references to original literature, this will not be done for the (extensive) literature on studies of radioactive decay series which preceded the publication of the historic papers of Soddy and Fajans in 1913. This material was well reviewed by F. Soddy (NLC 1921*) in his Nobel Lecture which is used as the sole reference here (Soddy 1922).

Three radioactive series (or radioactive chains) were discovered, each starting with a known naturally occurring element with a long half-life which decays by emitting either an alpha(α) or a beta(β) particle to yield a daughter material which in turn decays with a different half-life to another daughter material. This process continues until a stable (non-radioactive) daughter material is obtained. It was determined that the gamma (γ) rays of Rutherford are electromagnetic radiation of very high frequency, like x-rays, and these are always accompanied by either α or β emission. Consequently, each decay process can be described as an α or β decay. It will be seen subsequently that the “rules” deduced by Soddy and Fajans for the decay process state that the gamma rays have no effect on the determination of the atomic weight of the daughter element. One knows now that gamma rays are emitted if the daughter is initially produced in an excited nuclear state. Figure 1.1 shows the displacement law as it was understood in 1913, and Fig. 1.2 shows the sequence of parent to daughter transformations for the three natural radioactive series taken from the work of Soddy (1917, 1922) and of Fajans (1913a, 1914).

A number of chemists worked on the radioactive decay series and on the characterization of the various products (daughters) observed in the decays. The characterizations involved determining whether the products were new elements and, if so, where they would fit into the periodic table. The procedures used involved electrochemistry and precipitation reactions in which the new materials were compared with known elements, and with each other. The new “elements” were often available in such small quantities that the radioactivity was used as a tracer to follow precipitation or other reactions. In a number of cases it was soon determined that the new elements are inseparable from and identical to elements that were already known (often as elements in a radioactive series). Soddy (1922) records that the first such report was that of H. N. McCoy and W. H. Ross of the University of Chicago in a paper published in 1907 (McCoy and Ross 1907) on the radioactivity of thorium. The parent of the thorium radioactive series designated in Fig. 1.1 as Th was found to be identical to RadTh (Radiothorium). It is not the intention here to discuss in detail the findings of McCoy and Ross but merely to note that they pointed out that the separation of radiothorium from the parent thorium of the series is “remarkably difficult if not impossible.” Over the next several years, there were many reports of members of radioactive decay series being chemically equivalent to other members of the same series or to a member of another decay series.

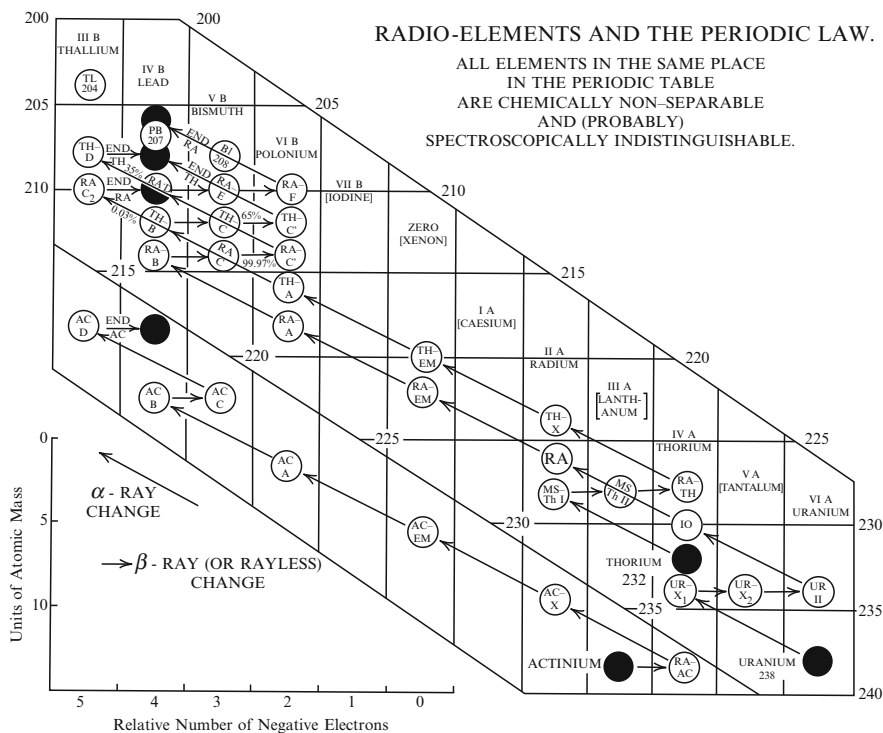


Fig. 1.1 The displacement law as it was understood in 1913 by F. Soddy

In this connection, A. B. Garrett (1963) reports the following as a direct quote from G. de Hevesy (NLC 1943*) who worked with E. Rutherford in Manchester between 1910 and 1913.

A few hundred kilograms of lead chloride containing appreciable amounts of radium D obtained from pitchblende were presented to Rutherford by the Austrian government. The lead chloride was stored in the cellar of the institute. One day when I met Rutherford in the cellar, he suggested that if I were worth my salt, I would separate radium D from all that nuisance of lead. Being a young man, I was an optimist and fully convinced that I would succeed; but even though I worked very hard for a year, trying a large number of separations, I failed entirely. To make the best of a depressing situation, I decided to make use of the inseparability of radium D from lead.

The last part of de Hevesy's statement does, of course, allude to his pioneering work on the use of radioactive tracers.

Soddy was very interested in nuclear emissions which give rise to products which are chemically equivalent to other elements which had previously been studied. While they were chemically equivalent (*vide infra*), these new elements often differed in their radioactive properties. Both Soddy and K. Fajans (*vide infra*) state that Soddy had generalized the available experimental results on what happens in

THE NATURAL DISINTEGRATION SERIES.

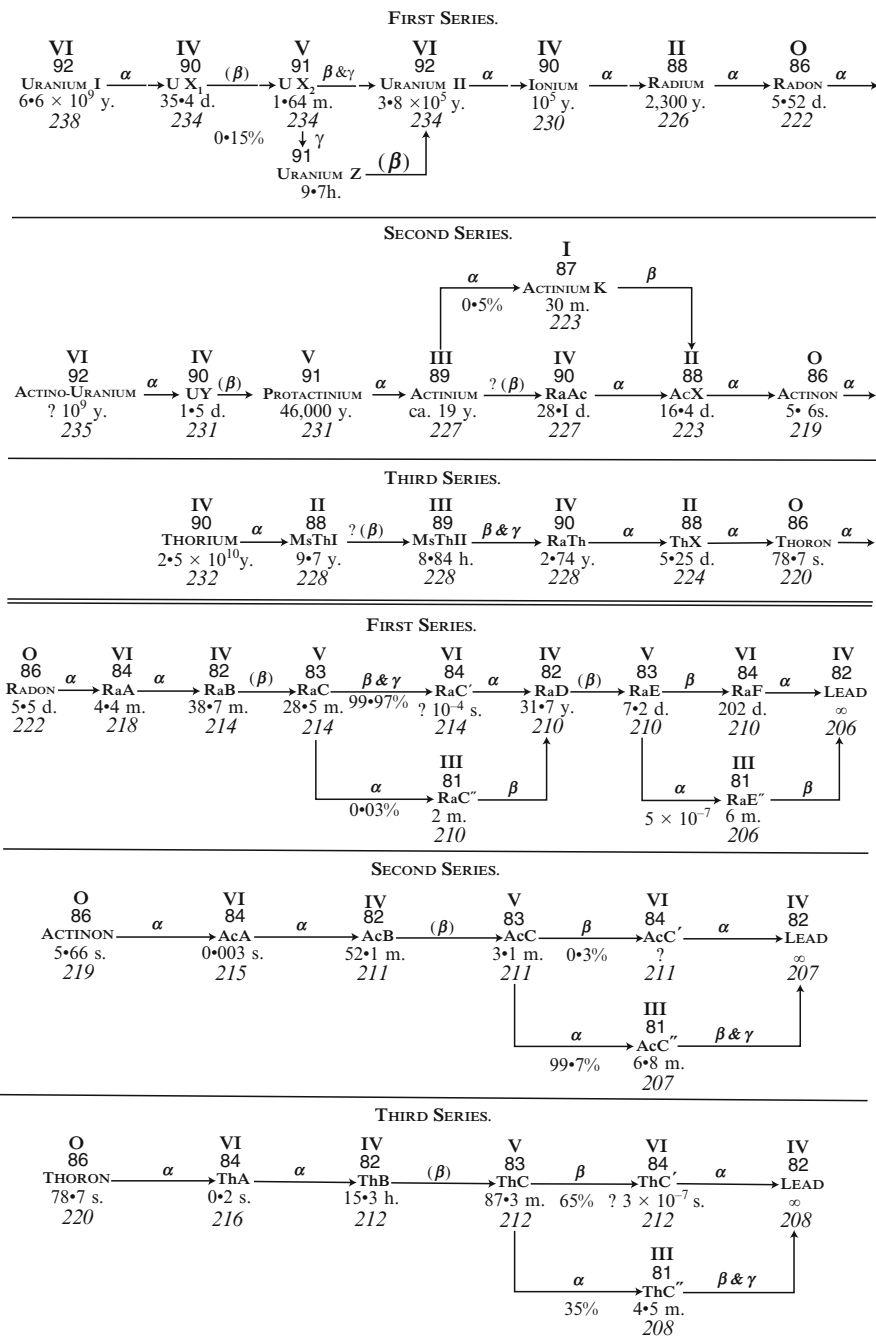


Fig. 1.2 The three natural radioactive decay series as understood by F. Soddy and K. Fajans in the period 1913–1920

α decay already in 1911 or 1912 in his book “Chemistry of the Radio-Elements”. Fajans refers to this as Soddy’s Rule. This rule, which states the relationship in the periodic table of a parent element in α decay to the daughter element, is the first of the generalizations of the experimental observations on radioactive decay promulgated by Fajans and Soddy in their 1913 papers (*vide infra*). Both G. de Hevesy and A. S. Russell proposed rules on what happens in β decay but neither of these “worked out”. In the meantime, Soddy had requested his assistant A. Fleck (1971) to investigate the products of β decay in the radioactive decay series, particularly to investigate the chemical identities of these decay products. Two of Fleck’s important papers were published in 1913. Soddy has stated that he knew all of Fleck’s results when he wrote his historic paper published early in 1913 (Historical Vignette 1.1).

The stage was now set for the 1913 papers published independently by Fajans (1913b) and by Soddy (1913a). The paper by Fajans was published a couple of weeks prior to that by Soddy. Soddy has stated that he had not seen the Fajans paper at the time when he wrote his paper. Both papers try to generalize experimental observations on the chemical identities of decay products in the three natural radioactive decay series.



[Historical Vignette 1.1] Frederick Soddy (1882–1956) graduated from Merton College, Oxford. After 2 years of research at Oxford he joined Sir Ernest Rutherford in Canada to work on problems of radioactivity. Returning to Britain in 1902 he worked with Sir William Ramsey at University College, London, demonstrating that helium is evolved during the radioactive decay of radium. Soddy served as lecturer on physical chemistry and radioactivity at the University of Glasgow from 1904 to 1914. It was here that he published the so-called “Displacement Law” of radioactive decay, and formulated the concept of isotopes which stated that certain elements exist in two or more forms which have different atomic weights but are indistinguishable chemically. Soddy served as Professor of Chemistry at the University of Aberdeen from 1914 to 1919, when he moved to Oxford as Dr. Lees Professor of Chemistry, retiring in 1937. He was awarded the Nobel Prize in Chemistry in 1921. (Photo credit www.wikipedia.com, public domain)

The Soddy/Fajans papers both identify the chemical nature of a given species by reference to the column of the periodic table in which it is found. A copy of a periodic table published in 1912 by Soddy (1914) is given in Fig. 1.3. Here the columns are designated by Roman numerals. One recognizes, of course, that this 1912 periodic table, the organization of which is based on Mendeleev's periodic table, differs from the modern periodic table which is based on a knowledge of atomic structure gained from quantum mechanics (Fig. 1.4). Thus, polonium (Po) is in group VI along with oxygen, sulfur, selenium, and Soddy points out that the properties of Po mirror those of Te as predicted by the "periodic law". This result also follows from the modern periodic table where these five elements are in one column, sometimes called VI-A. On the other hand, uranium (U) is also in column VI of the old periodic table. In the modern periodic table, U is, of course in the actinide series. The properties of the actinides are not expected to reflect the properties of the column VI-A elements of the modern periodic table. In the same vein, Soddy refers to the element in the last row of the 1912 table, one column to the left of uranium, column V, as ekatantalum and likens its chemistry to tantalum (Ta) which is also in group V. From the modern point of view this is a questionable procedure. The procedure of identifying elements in the radioactive series belonging to particular groups in the periodic table, depended strongly on demonstrating that elements given the same Latin numeral have identical properties and are inseparable. Whether the element belonged to the last row of the periodic table or to the row above is always readily established from the Fajans/Soddy "rules". Note finally that each of the radioactive series yielded one gaseous element which was labeled by the suffix Em (for emanation). The Em's all acted like noble gases and had the same properties (non-reactive and with the same condensation temperature at a given pressure). They were assigned to column 0 in the periodic table which is the column of noble gases.

The conclusions of the two papers are identical. The generalizations are the following:

1. Alpha decay leads to a product which is two columns to the left of the decaying atom. This, as already noted, is Soddy's rule. Since an alpha particle is an ionized helium atom and the atomic weight of a helium atom was known to be four units, it is assumed that the daughter element has an atomic weight four units less than that of the parent. Since electrons have a weight of approximately $1/1,800$ that of a hydrogen atom, any consideration of electrons in determining atomic weight is ignored.
2. The rule on beta decay is new. It is that, when an atom emits a beta particle, which was known to be an electron, the resulting element is chemically equivalent to an element one column to the right from the parent in the periodic table. Consistent with rule 1, it is assumed that there is no change in atomic weight from this decay.
3. Gamma rays, which are like x-rays, are assumed not to change the chemical identity of the emitting atom. It was recognized that the change in mass from the Einstein's relativistic expression ($E = mc^2$) is so small that it could be ignored

a

0	I	II	III	IV	V	VI	VII	<u>VIII</u>		
He 3.99	Li 6.94	Be 9.1	B 11.0	C 12.00	N 14.01	O 16.00	F 19.0			
Ne 20.2	Na 23.00	Mg 24.33	Al 27.1	Si 28.3	P 31.04	S 32.07	Cl 35.46			
A 39.88	K 39.10	Ca 40.07	Sc 44.1	Ti 48.1	V 51.0	Cr 52.0	Mn 54.98	Fe 55.84	Co 58.97	Ni 58.08
	Cu 63.57	Zn 65.37	Ga 69.9	Ge 72.5	As 74.96	Se 79.2	Br 79.92			
Kr 82.92	Rb 88.45	Sr 87.63	Yt 89.0	Zr 90.6	Nb 93.5	Mo 96.0		Ru 101.7	Rh 102.9	Pd 106.7
	Ag 107.88	Cd 112.4	In 114.8	Sn 119.0	Sb 120.2	Te 127.6	I 126.92			
Xe 130.2	Cs 132.81	Ba 137.37	[<i>La</i> 139.0		<i>Ce</i> 140.25	<i>Pr</i> 140.6		<i>Nd</i> 144.3	<i>Sm</i> 150.4	
	<i>Eu</i> 152.0		<i>Gd</i> 157.3		<i>Tb</i> 159.2	<i>Dy</i> 162.5		<i>Er</i> 167.7		
	<i>Tm</i> 168.8	<i>Yb</i> 172.0		<i>Lu</i>] 174.0	Ta 181.5					
	Au 197.2	Hg 200.6	Tl 204.0	Pb 207.10	Bi 208.0	W 184.0		Os 190.9	Ir 193.1	Pt 196.3
Ra' 222		Ra 226.4		Th 232.4		(Po)				
							U 238.5			

Note Dy and Er have been aligned with Eu, Gd, Tb. In the original table they were aligned with Lu, Ta etc. This was probably a misprint.

b

Element	Soddy's weight	Modern Weight
Rb	88.45	85.47
Sb	120.2	121.75
Xe	130.3	131.3
Yb	172.0	173.04
Lu	174.0	174.97
Bi	208.0	208.98
Pt	196.3	195.1

Fig. 1.3 (a) Periodic Table of the Elements (Soddy 1912). (b) Elements for which Soddy's atomic weights (1912) differ by 1.0 unit or more from currently accepted values

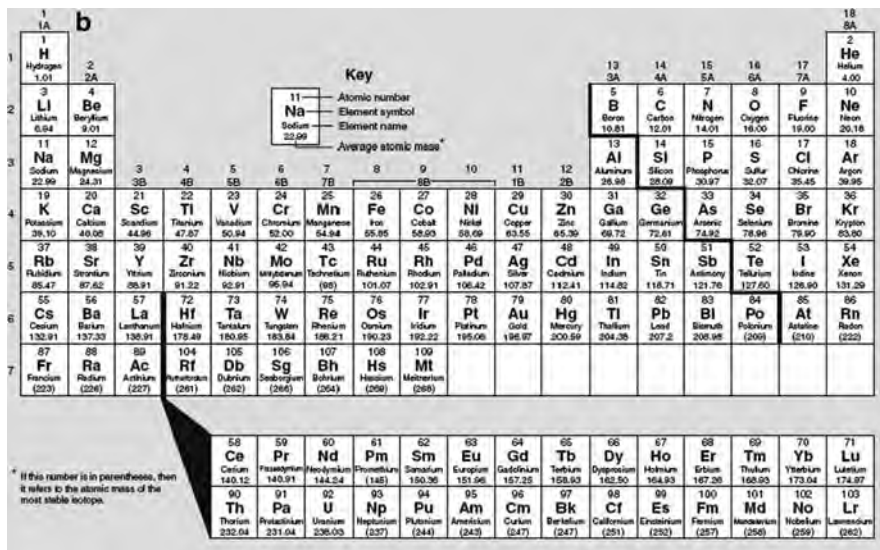
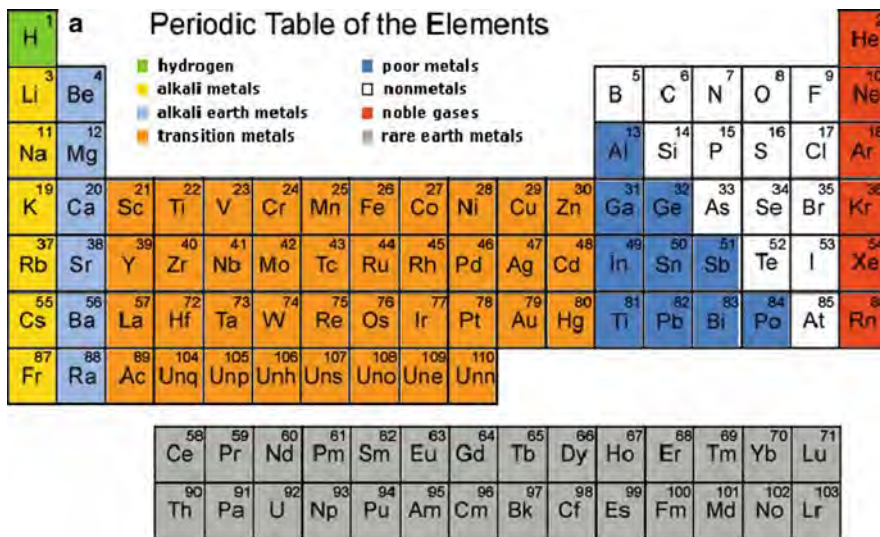


Fig. 1.4 (a, b) Modern versions of the periodic table, 2008

in considering atomic mass. (Similarly, the kinetic energies of the alpha particles and beta particles in radioactive decay are ignored.) Thus, gamma emission is also ignored.

These rules can now be applied to the three radioactive series in Figs. 1.1 and 1.2. The names of the various elemental materials are given in the figures. The atomic weights of each can be determined from the rules above, given the respective atomic weights of the parent of each series, taken here as $U_{r1} = 238.5$, $Th = 232.4$, and

Act = 226.5; the naming of the parents follows the nomenclature employed by Fajans in which the element uranium is referred to as UrI . A place in the periodic table is then defined by a specific row and a specific column. From the data, one then readily obtains the row and column of each of the elemental daughters. Since the characterization of decay products emphasized the fact that many of these products are chemically indistinguishable from one another, it is of course expected that many of the places in the last two rows of the periodic table are occupied by more than one elementary material. What is surprising is that these chemically equivalent materials have different atomic weights, some differing by as much as eight units.

In subsequent papers, Fajans (1914) refers to a group of elements which have the same chemical properties but different atomic masses as a “plejade” (in the German article), a word derived from a stellar constellation of seven stars to which the ancient Greeks gave the name “pleiade”. On the other hand, Soddy (1917) called the individual elements which made up the plejade of Fajans, “isotopes”. The word isotope was suggested to Soddy by one of his relatives and is derived from the Greek (iso = same, top = place), referring to the place in the periodic table. Soddy’s nomenclature gained general acceptance; the word “plejade” is not commonly used in the chemical literature.

It is, of course, quite clear now that the element radiothorium which the U.S. workers McCoy and Ross could not separate from the parent (^{232}Th) of the thorium decay series is indeed an isotope of thorium (^{228}Th); it arises from thorium (^{232}Th) after the emissions of an α and two β particles. (A common practice has been followed by noting the mass number (the atomic weight of an isotope rounded off to the closest integer) as pre-superscript.) Likewise, the radium D which Rutherford asked de Hevesy to separate from lead chloride obtained from pitchblende was a radioactive isotope of lead. Several of the workers who were involved in finding the chemical identities observed in radioactive decay noted that their inability to separate such materials from each other implies that any possible separation of these materials would be more difficult to carry out than the separation of the rare earth elements. In some cases this demonstration of chemical equality of different materials even involved quantitative tests. Thus, chemical equilibrium constants were well understood in the early twentieth century as involving concentrations of reactants and products. Tests were carried out in many cases showing that, if different isotopes are mixed, the proper concentrations to be used in equilibrium expressions (e.g., for solubility products and/or for expressions giving the emf of electrochemical cells in terms of concentrations) is the sum of the concentration of the isotopes of a given material. Especially noted in this regard should be the work of de Hevesy and F. Paneth (1915).

From Figs. 1.1 and 1.2 it follows that the main end products of the uranium and thorium series are isotopes of lead (at the time referred to as $\text{Pb}206.5$ and $\text{ThO}_2208.4$). The end products are thus isotopes of lead differing by two mass units. This observation became the motivation for the measurement of atomic weights of lead samples separated from thorium and uranium minerals. In his Nobel Lecture, Soddy describes this work as follows:

... determinations were undertaken of the atomic weight of lead separated from thorium minerals as free as possible from uranium, and of that from uranium minerals as free as possible from thorium. These resulted in the complete verification of the prediction. The highest value yet found for "thorium-lead" is 207.9 (Fajans and Honigschmid) and the lowest value for "uranium-lead" 206.05, the accepted value for common lead being 207.20.

Extensive references to this work are given by Soddy. It is noted that a major contributor to these studies was the Harvard University chemist T.W. Richards (NLC1914), an expert on atomic weight determinations.

So, now (1913) one has a set of rules which characterize the daughter atom in terms of a knowledge of the parent element and the type of radioactive decay. The rules "work"; they give rise to the concept of isotopes: elements which correspond to different atomic weights but which are chemically identical. However, the rules are purely empirical; no explanation exists for the rules as the matter now stands. Something is still missing in this story.

1.3.2 Further Elucidation of the Concepts of Elements and Isotopes Including Works of van den Broek, Moseley, Rutherford, Thomson, Aston and Lindemann

What is needed now (1913) is an answer to the question "what is an element?" Up to this time elements had been characterized by their respective masses. But now different masses (isotopes) all correspond to the same element. As already noted, Mendeleev had assembled the elements into a table by writing down the elements in order of increasing mass and had found, by making the table two dimensional through the introduction of rows and columns, that he was able to construct the table so that elements in given columns had similar properties. The similarities included physical properties as well as chemical properties. The table was therefore called a periodic table (there was periodicity). However, Mendeleev noted immediately that, in order to make his table "work", he needed to introduce blank spaces for missing elements. This was fine because it led to the prediction of "new" elements which were later actually found. However, there were also places in the table where he had to reverse the ordering demanded by the masses in order to obtain periodicity (e.g. Co and Ni).

1.3.2.1 Van den Broek

The next step was taken by A. van den Broek, a Dutch physicist (and a lawyer by training), in a very short letter to the editor published in *Nature* (van den Broek 1913a). His thoughts were based on the Rutherford model of the atom as a positively charged nucleus concentrated in a small volume at its center surrounded by electrons occupying a much larger volume. He used the term intra-atomic charge to designate the positive charge on the nucleus which is equal in magnitude but opposite in sign to the total charge of the surrounding electrons. In this context charge

is measured in units of the charge on one electron. Van den Broek hypothesized that the charge on the nucleus, the positive intra-atomic charge of an element, is given by the number of that element in a series in which all the elements are arranged in order of increasing atomic weight, as is done in the periodic table. He thus was the first to use the concept of what we now call the atomic number to characterize an element.

Van den Broek's hypothesis was based on Rutherford's idea that the experimental observation of large angle scattering of particles by atoms leads to the conclusion that the atom consists "of a strong positive or negative central charge concentrated in a sphere of radius about 3×10^{-12} cm surrounded by electricity of the opposite sign distributed throughout the remainder of the atom of about 10^{-8} cm radius" (Rutherford, 1911,1913; Geiger and Marsden 1913). The quote is from Geiger and Marsden (1913). Moreover, Rutherford showed the magnitude of the scattering is proportional to the square of the charge on the central core, which was taken to be positive. According to Geiger and Marsden (1913), Rutherford encouraged them to undertake studies to test his scattering formula, in particular the dependence on the magnitude of the central charge. Moreover, it was Rutherford who submitted the paper of Geiger and Marsden (GM 1913) to the journal. It is clear that Rutherford and GM believed that the central charge of the atom is proportional to its atomic weight A . GM examined six elements (Au, Pt, Sn, Ag, Cu, Al) for which they report scattering per atom divided by A^2 . Except for Cu, for which they give a value of 3.83, their mean results are 3.37 ± 0.23 . They concluded their experimental results show the ratio to be constant "within the experimental error". Van den Broek, in order to test his hypothesis that the charge on the dense atomic nucleus is equal to the number attached to the element in the sequence of the elements arranged in increasing atomic weight (the present day atomic number which he refers to as M), multiplied the GM scattering value per atom divided by A^2 by A^2/M^2 (to find scattering value divided by M^2) and obtained 18.7 ± 0.3 for the elements listed above except Al, for which he would have found 15.1. In his paper, van den Broek omits the data on Al. He does not refer to the fact that results for Al exist in the GM paper. If the Al data are omitted, van den Broek's conclusion that the GM experimental data indicates that the scattering per atom is proportional to $1/M^2$ rather than $1/A^2$ as Rutherford and GM had supposed. However, as it is, it does not seem to us that the GM data can be used to distinguish whether the scattering per atom is proportional to $1/M^2$ or $1/A^2$. Van den Broek's conclusion must be described as a "stretch". This criticism should not be construed as a lack of admiration for van den Broek's physical insight in recognizing that it is the charge on the nucleus of the atom, which characterizes the particular element. There is no question that he first proposed what we now call the atomic number. Rutherford, Soddy and GM all acknowledge that the value of the charge of the nucleus of an atom of an element was first correctly given by Van den Broek. The paper by van den Broek (1913a) was published in *Nature* in the issue of November 27, 1913. Soddy (1913) commented on Van den Broek's paper just a week later in the issue of December 4, 1913. Assuming that radioactive changes only involve the intra-atomic charge on the nucleus, he points out that the van den Broek hypothesis leads to the generalizations on radioactive decay that he

and Fajans had proposed earlier in the year. Thus α decay involves the emission of a particle (alpha particle) of mass 4 and charge +2 and results in a daughter element the intra-atomic charge on the nucleus of which has been reduced by two units and the atomic weight reduced by 4; thus the result is a daughter element which corresponds to the element two columns to the left of the parent and with the appropriate mass. Likewise β decay leads to the loss of a unit of negative intra-atomic charge in the nucleus of the daughter which means that the intra-atomic nuclear charge increases by one unit and corresponds to the element one column to the right of the parent in the periodic table with the mass of the parent. There is an assumption here that the negative intra-atomic charge of the electrons outside of the nucleus takes care of itself by interacting with its environment as necessary. At this point, there must have been some private communication between Soddy and van den Broek since Soddy states that van den Broek's atomic nucleus has a net positive inter-atomic charge but contains both positive charges and negatively charged electrons while Rutherford's nucleus contains only positive charges. Van den Broek does not introduce the alpha particle/electron model of the nucleus until 3 weeks later in another letter in *Nature* (van den Broek 1913b). In this letter, van den Broek assumes that the nucleus is made up of alpha particles and electrons in such a way that the nuclear mass is all due to alpha particles each of mass 4 and each contributing two units to the nuclear intra-atomic charge while the number of electrons is chosen so that the intra-atomic charge of the nucleus is the correct one. This second *Nature* paper of van den Broek will not be further discussed here.

Soddy (1913) further discusses a statement made by Fajans in his first paper on the generalization of the decay rules (Fajans 1913b). There, Fajans did point out that the processes involved in radioactive decay are very similar to electrochemical processes. So both radioactive decay and electrochemical processes involve the gain or loss of charge by atoms. Thus, Fajans reasoned that both processes involve the same electrons. Soddy correctly states that this is a mistake on the part of Fajans. The chemistry of the radioactive compounds amply demonstrates that chemical reactions involve the extra-nuclear electrons which make up the intra-atomic negative charge while nuclear decay involves the electrons and nuclear charges of the particles which make up the positively charged nucleus; there is no exchange between the two types of electrons.

1.3.2.2 Moseley

It was H. G. J. Moseley (Heilbronn 1974) who brought the atomic number story to its conclusion. Moseley was a young British chemist who went to Manchester in 1910 to work with Rutherford. He became aware of van den Broek's postulate on the intra-atomic charges in 1913. While in Manchester he started the measurement of the wavelengths of x-rays emitted by targets after bombardment by energetic electrons and reported this work in his first paper (Moseley 1913) by November 1913. He continued his work in Oxford and reported further in a second classic paper in 1914 (Moseley 1914). Moseley measured the x-ray wavelengths by scattering

them from a potassium ferrocyanide crystal and using the Bragg diffraction formula. He made measurements on more than 30 target elements. They spanned atomic numbers (a term first used by Moseley and referred to as N) from 13 (Al) to 79 (Au). He measured two series of lines, the so-called K series for atomic numbers, $N \leq 47$ and the L series for atomic numbers, $40 \leq N \leq 79$. The K series lines correspond to shorter wavelengths than the L series lines. Each of these series has an intense line referred to as alpha and less intense longer wavelengths referred to as beta, phi and gamma. From his nomenclature, he obviously recognized the K-series as analogous to the Lyman series in the hydrogen atom spectrum, while the L series is the analogue of the Balmer series in hydrogen. He plotted the square roots of the frequencies of the various x-ray lines versus N , the atomic number, and found straight lines if he chose the atomic numbers N with the proviso that N increases with increasing atomic weights “except in the cases of Ag, Co, and Te where this clashes with the order of the chemical properties” in the periodic table. He also had to reserve N values for an unknown element each between Mo and Ru, between Nd and Sm, and between W and Os. Moseley also calculated the parameters Q_K and Q_L for the alpha lines of the K and L series respectively

$$Q_K = (\nu/(3/4)\nu_0)^{1/2} \text{ and } Q_L = (\nu/(5/36)\nu_0)^{1/2} \quad (1.1)$$

where ν refers to the frequency of the observed x-ray and ν_0 to the frequency corresponding to the Rydberg constant for the hydrogen atom, respectively. Notice that the denominators in Equation 1.1 correspond to the frequencies of the first (longest wave lengths) members of the hydrogen atom spectrum. Thus, Q_K and Q_L for a hydrogenic atom would equal the nuclear charges of the atom. For the 15 Q_K values that he evaluated, Moseley found Q_K almost exactly equaled $N - 1$ (except for the very lowest wavelengths) and increased by almost exactly one unit from one element to its neighbor, while Q_L similarly equaled $(N - 7.4)$. Moseley concluded his second paper as follows:

Now if either the elements were not characterized by these integers, or any mistake had been made in the order chosen or in the number of places left for unknown elements, these regularities would at once disappear. We can therefore conclude from the evidence of the X-ray spectra alone, without using any theory of atomic structure, that these integers are really characteristic of the elements. Further, as it is improbable that two different stable elements should have the same integer, three, and only three, more elements are likely to exist between Al and Au. As the X-ray spectra of these elements can be confidently predicted, they should not be difficult to find. The examination of keltium would be of exceptional interest, as no place has been assigned to this element. (For keltium see footnote¹)

Now Rutherford has proved that the most important constituent of an atom is its central positively charge nucleus, and van den Broek has put forward the view that the charge carried by this nucleus is in all cases an integral multiple of the charge on the hydrogen nucleus. There is every reason to suppose that the integer which controls the X-ray spectrum is the same as the number of electrical units in the nucleus, and these experiments therefore give

¹ The reference to keltium is to a rare element which the French chemist G. Urbain claimed to have discovered. Moseley was able convince Urbain that keltium did not exist (Heilbronn 1974).

the strongest possible support to the hypothesis of van den Broek. Soddy has pointed out that the chemical properties of the radio-elements are strong evidence that this hypothesis is true for the elements from thallium to uranium, so that its general validity would now seem to be established.

It is noted without further comment that Moseley was able to characterize his observed x-ray spectra in such a way that the individual elements are identified purely by their respective atomic numbers without any use of an atomic model. Note again, however, that the denominators in the Q_K and Q_L expressions are exactly the frequencies of the hydrogenic Lyman and Balmer alpha lines (Moseley's nomenclature) and that therefore Q_K and Q_L exactly equal the nuclear charge of a "one-electron" hydrogenic atom which would be deduced from the frequency ν of its observed Lyman and Balmer alpha lines².

In the summer of 1914, Moseley traveled to Australia to report his new results. War broke out and he hurried back to England. He enlisted as a second lieutenant in the Royal Engineers and was killed in action in Gallipoli in 1915, a victim of World War I.

1.3.2.3 Thomson

The year 1913 produced yet another important discovery in isotope chemistry. J. J. Thomson (1913), previously cited here for his discovery of electrons, reported work on the positive ions produced by electrical discharge in a vacuum tube and which Goldstein had earlier seen in 1886 and referred to as Kanalstrahlen. (They had not been recognized as positively charged until Wein was able to determine their polarity by the use of a strong magnetic field.) Using appropriate electric and magnetic fields Thomson measured the charge to mass ratio e/m for these positive ions and determined the number of charges per ion. As an example of the use of his instrument, Thomson analyzed residues of liquid air samples enriched in the rare gases present in the atmosphere, which he obtained from James Dewar. He did find xenon, krypton, argon and neon in these samples with atomic masses corresponding to the ones in the periodic table. However, whenever he found neon (mass 20), he found it was always accompanied by a heavier gas of mass approximately 22 present in an amount that he stated formed "only a small percentage of the mixture of 20 and 22". He thus concluded that there are two isotopes of neon. All the previously known isotopes had been formed in processes involving natural radioactivity. Neon represents the first known example of isotopes in that part of the periodic table far removed from natural radioactivity.

² While we have not carefully studied all of the tabular material in Moseley's papers, we note that Moseley's atomic numbers agree with the values accepted today, with one exception. Thus, Moseley assigns $N = 66$ to Ho and $N = 67$ to Dy; the presently accepted assignment reverses these two elements in the periodic table.

1.3.2.4 Lindemann

The war inhibited the rate of scientific progress. The date of the next scientific publication (Lindemann and Aston 1919), cited here is 1919. There F. W. Aston (NLC 1922*), a student of Thomson, and F. A. Lindemann, a student of the German chemist W.H. Nernst (NLC 1920*), discuss the possibility of separating a mixture of isotopes or enriching such a mixture in one isotope or another by fractional distillation, by diffusion, by gravitational effects, by centrifuge, or by producing positive rays and subjecting them to electric and magnetic fields as in Thomson's experiment leading to evidence for the existence of two isotopes of neon. They conclude that all of these methods should lead to isotope separation in principal "though possibly not in practice". They briefly discuss unsuccessful experimental attempts in 1914 by Aston to separate the neon isotopes by fractional distillation and by diffusion.

Shortly after the publication of this paper, Lindemann (1919) published another paper in which he analyzed vapor pressure isotope effects of monatomic solids. He used an integrated Clausius–Clapeyron equation, assumed the gas to be ideal and used the Debye model to calculate the necessary heat capacity of the solid. In the Debye model, there is a continuous distribution of frequencies ν of the solid from zero to a maximum frequency; further details are beyond the scope of this discussion. Lindemann made application to the isotopes of lead and used the experimental result that the melting point of the lead isotopes show no observable isotope effects. While in 1919 he, of course, did not know anything about the Born–Oppenheimer approximation (see Chapter 2) of quantum mechanics, he made several assumptions that follow from this approximation, among them that the Debye frequency ν is given by $(1/(2\pi))(f/m)^{1/2}$ where m is the mass of the atom and f is an isotope independent force constant. Lindemann also did not know the solutions to the quantum mechanical problem of the harmonic oscillator. He was, however, aware of Planck's solutions of the black-body radiation problem (Einstein and Stern (1913), Millonni and Shih (1991); Dahl (1998)), the first of which involved a "resonator" of frequency ν with energy levels $n h \nu$ (n a positive integer or zero) and a second and more successful expression with energy levels $(n + 1/2) h \nu$. The second formula contains a zero-point energy (i.e. $(1/2) h \nu$). Lindemann, like others, regarded these relations as formulae for quantum energy levels of an oscillator. In fact, he decided to use the isotope effect on the vapor pressure of a monatomic solid as a device for finding out which of the two is correct. He assumed that $h \nu / k T$ is sufficiently small so that $\exp(-h \nu / k T)$ is well represented by an expansion containing terms in powers of $1/T$ up to $1/T^2$. The result of his theoretical calculation was that, in the absence of a zero-point energy term in the harmonic oscillator energy, the isotope effect on the vapor pressure would have the form $(1 + A/T)$ with the heavy isotope having the higher vapor pressure while, in the presence of the zero-point energy, the isotope effect would be of the form $(1 + B/T^2)$ with the lighter isotope having the higher vapor pressure. This result was tested in 1931/1935 when the isotope effect on the vapor pressures of isotopic neon crystals was experimentally measured by Keesom and van Dijk 1935. The experimental result confirmed that the quantum formula for the energy levels of a harmonic oscillator does contain a zero-point energy term. In

Chapter 5, vapor pressure isotope effects are discussed. There, a very simple model for the condensed phase frequencies is used, the Einstein model, in which all the frequencies of a condensed phase are assumed to be the same. From this model, one can derive the same result for the relationship between vapor pressure isotope effect and zero-point energy of the oscillator as that derived by Lindemann.

1.3.2.5 Another Component of the Nucleus

In 1919 continuing his studies of the nucleus, Rutherford (1919) experimented on collisions of α particles with light atoms, in particular with nitrogen. Here he found a new phenomenon, namely in the collision he disintegrated the stable atom, nitrogen, producing hydrogen atoms. Thus, he concluded that the nucleus contains protons. From radioactive decay, it had previously been agreed that atomic nuclei contain only alpha particles and electrons. Now, there was still another component.

1.3.2.6 Aston, the Mass Spectrograph, the Whole Number Rule

Another piece of information was necessary before one arrives at a periodic table which is close to the modern view. This is the whole number rule which states that the masses of atoms on the ^{16}O scale (i.e. mass of the major isotope of oxygen is 16.00) tend to have close to integer values. This information was provided by W. D. Harkins (*vide infra*) and F. W. Aston (Historical Vignette 1.2).

F. W. Aston has already been mentioned in connection with the unsuccessful attempt to separate neon isotopes. His motivation (Aston (1920a)) had been to clear up an uncertainty in Thomson's discovery of the two isotopes of neon; namely Thomson's positive ray instrument did not yield a sufficiently precise measure of the mass of the ion of mass 20 to distinguish mass 20.0 from mass 20.2. Note that the (average) atomic weight of neon is 20.2. At the time, it was conceivable that the large peak observed by Thomson around mass 20 was really mass 20.2 and corresponded to mono-isotopic neon, while the observed smaller peak at mass 22 was just another element. Having failed to separate two neon isotopes, Aston then set out to build a positive ray instrument capable of distinguishing between mass 20.0 and mass 20.2. In this instrument, which he later called a mass spectrograph, he used collimators and electric and magnetic fields in such manner and such geometry that he lost less of the ion beam and was able to obtain more precise mass values than did Thomson in the earlier experiment. Masses in the Aston instrument were not measured absolutely but relative to other "known" masses. Reference here is made to a few of Aston's earlier papers (Aston 1920b, c) and also to his later Nobel Lecture (Aston 1922). In the first of these papers, he did show that a sample of neon gas gives rise to two peaks at masses 20.0 and 22.0 respectively, and to no peak at mass 20.2, the (average) atomic weight of neon. In the next paper, which followed shortly, he discovered the isotopes of chlorine, at mass 35 and mass 37, ^{35}Cl and ^{37}Cl . He also found molecular ions. Thus, he observed peaks at mass 36 and mass



[Historical Vignette 1.2] Francis W. Aston (1877–1945) studied chemistry and physics at Birmingham University and its predecessor, Mason College. At Birmingham he worked on discharge tubes and discovered the phenomenon now known as the Aston Dark Space. In 1909 he joined Sir J. J. Thomson at Cambridge to work on studies of positive rays. During this period he obtained definite evidence for the existence of two isotopes of neon. During World War I Aston was at the Royal Aircraft establishment. Returning to Cambridge Aston attacked the problem of separating the neon isotopes. He achieved success in this by his invention of the mass spectrograph. Extending the technique to other elements he discovered no less than 212 of the naturally occurring isotopes. From these results he was able to formulate the Whole Number Rule. Aston was awarded the Nobel Prize in Chemistry in 1922. He was a fine amateur musician and an enthusiastic sportsman, excelling at skiing, rock climbing, and tennis. (Photo credit www.wikipedia.com, public domain)

38 which he attributed to HCl. Phosgene gave rise to peaks at mass 63 and mass 65 which he attributed to CO^{35}Cl and CO^{37}Cl . By the time he published this paper (Aston 1920b), he had measured a large number of masses of various ions and concluded: “A fact of greatest theoretical interest appears to underlie these results, namely that of more than forty different values of atomic and molecular mass so far measured, all, without a single exception, fall on whole numbers, carbon and oxygen being taken as 12 and 16 exactly. . .”.

1.3.3 The Work of Harkins on the Whole Number Rule

There is anecdotal material that W. D. Harkins, whose career at the University of Chicago started around the time of World War I, felt that his scientific contributions were not adequately recognized by the community. It is indeed correct that he is not well known for his contributions to the “Whole Number Rule”.

In 1915, Harkins and his student E. D. Wilson (HW) published a series of three papers (Harkins and Wilson 1915a, b, c) in the *Journal of the American Chemical*

Society. In the first paper, they start with Prout's Rule which dates to 1814/1815 and states that the then known atomic weights of the elements are integral multiples of the atomic weight of hydrogen and that hydrogen is the primary element (this is not the language used by Prout). HW then tabulate the atomic weights of the lighter elements (27 elements, H through Co) on a scale with H = 1.00 (the " ^1H scale"). They studied the deviations of the atomic weights from integer values and found, omitting Be because its atomic weight was not well known, and Ne because Thomson believed there are two isotopes of that element, that the average deviation is 0.21. If the atomic weights were randomly distributed, one would expect an average deviation from integer values to be 0.25. Moreover, for five of the elements, the percent deviation of the atomic weight from an integer value is -0.77% while for a seventh element this deviation is -0.70% . With the exception of Mg, Si, and Cl, all the deviations are negative. On the assumption that atoms are built from hydrogen, HW recognized that the negative values of these deviations mean that, when the hydrogen atoms are "packed" to produce these elements, the energy must be lowered and, in accordance with the Einstein mass/energy relationship, the element being formed is more stable than the hydrogen atoms from which it is formed. They then carried out a similar investigation of the atomic weights of these 27 elements based on a scale with O = 16.00 (the " ^{16}O scale"). With the ^{16}O scale, not only are the atomic weights of seven of the 27 light elements exactly integer values but also the average deviation of all these "light" elements from integer values is 0.05 if Mg, Si, and Cl are omitted. There is no way of omitting a few elements on the ^1H scale which leads to a similarly small deviation of atomic weights from integer values. Historically, atomic weight scales were usually based on either the ^1H scale or the ^{16}O scale and it was noted already by previous workers (prior to HW) that the ^{16}O scale tends to predict atomic weights closer to integer values than does the ^1H scale. However, it is doubtful that anyone had previously gone through the analysis of this effect as carefully as HW. Thus, on looking at the packing effect of hydrogen atoms used as building blocks for the heavier elements, they found that this factor was close to 0.77% of the total atomic weight for the first 27 of the heavier elements. Consequently when they multiplied the atomic weights on the ^1H scale by 1.0078 they obtained the weight of H as 1.0078 and found integer values for all the other elements (excluding Mg, Si, Cl) with a deviation 0.2 or less.

HW noted that past atomic number 27 the whole number rule did not "work" for the atomic weights. They attributed this fact either to the presence of isotopes for all of these elements or to some phenomenon which they did not understand. The first explanation (isotopes) is correct. The mass spectrograph, already mentioned as an invention of Aston, shows that all isotopic masses on the ^{16}O scale (or the very similar ^{12}C scale used today) tend to differ from integer values by less than 0.1% .

Of more relevance, in the present context, HW reasoned that large deviations from the whole number rule among the light elements indicates the existence of isotopes. They, thus, predicted that Mg, Si, and Cl had isotopes (were not monoisotopic). Harkins decided to show that the element chlorine which had the atomic weight deviating the most from integer value among the 27 low atomic number

elements contains more than one isotope. He assumed that there are two isotopes ^{35}Cl and ^{37}Cl . To show that there is more than one isotope he followed the same path originally used by Aston in the case of neon; he decided to try to separate the isotopes or to initiate a separation process and show that he could change the atomic weight of the material (i.e. isotopically enrich some fraction of the sample).

As detailed earlier, Aston had been faced with this problem for the case of neon where he was not convinced by Thomsons's conclusion that there are two neon isotopes of masses 20 and 22. He attempted to show that indeed neon consists of two isotopes by trying to separate the two isotopes using thermal diffusion. The result proved unsatisfactory and he then proceeded to invent the mass spectrograph.

Harkins started work to separate the chlorine isotopes in 1915 by gaseous diffusion through "porous pipe stems". Originally, he used chlorine gas. He later switched to hydrogen chloride. The work was resumed during 1919 (Harkins 1920) and, in 1921 he reported (Harkins and Hayes 1921) the first partial separation of an element into isotopes, having found that the atomic weight of the chlorine had increased by 0.05 units from 35.46 to 35.51 in the heavy (i.e. residual) fraction. The result was published in short notes, not only in *Nature* to which reference is made above, but also in *Physical Review* and *Science*. The result has not been disputed, and moreover was confirmed by later work of Harkins and his students. The next separation of isotopes was reported by Bronsted and de Hevesy (1920) in September, 1920; they measured a change of 1 part in 20,000 in the atomic weight of mercury. Mulliken and Harkins (1922), in a paper in 1921, dealing in part with the theory of isotope separation, confirmed the results of Bronsted and de Hevesy.

It is clear from the tone of Harkins' publications and by his sometime repetitive publications that he feared that he would not receive credit for his accomplishments. Aston was awarded the Nobel Prize in Physics in 1922; the citation for the Prize refers to the whole number rule and to the mass spectrograph. It is of course true that the invention of the mass spectrograph ranks among the most important scientific inventions of the twentieth century, and not only for isotope science. It is also true that the investigation of the whole number rule using the mass spectrograph is by far the most elegant approach to such a study. What is surprising is that Aston made no reference to Harkins in the Nobel Lecture. By comparison, Soddy in his Nobel Lecture made copious reference to his contemporaries and especially to Fajans.

1.3.4 Understanding the "Modern" Periodic Table

In the second of their 1915 papers (Harkins and Wilson 1915b), Harkins and Wilson note from their study of the light elements (up to atomic number 27) that the main isotopic species had atomic masses which are integral multiples of 4. They concluded from this that, for those light nuclei, an important constituent must be the alpha particle just as it must be in the heavier radioactive nuclei which undergo alpha decay. In order to rationalize all the nuclei, including their nuclear charges, they

then postulated that nuclei contain alpha particles, protons, and nuclear electrons. Such a postulate taken together with the postulate of the constancy of the packing fraction leads to the whole number rule for nuclear masses.

Similarly in his Bakerian Lecture (Royal Society of London) for 1920, Rutherford (1920) states “In considering the possible constitution of the elements, it is natural to suppose that they are built up ultimately of hydrogen nuclei and electrons.” On this view the helium nucleus is composed of four hydrogen nuclei and two negative electrons with a resultant charge of 2. In the Lecture, he emphasizes the difference between the extra-nuclear electrons and the electrons which are closely bound to the charged particles which he supposes make up the nucleus. He does talk about a neutral particle in the nucleus of mass approximately equal to unity consisting of a proton and a closely bound electron. In discussing the possible nuclear structure of the nucleus of nitrogen of mass 14, he considers that the nucleus may be made up of four double charged helium 3 nuclei plus two protons with closely bound electrons. Aside from the quote at the beginning of this paragraph, Rutherford did not give an example of a nucleus made up only of protons and of protons with closely bound electrons. However, as time went on, this (nucleus made up of protons and neutral particles of unit mass) did become the accepted view. In this history, this latter view of the atomic nuclei will be accepted. Over the next few years, both Rutherford and Harkins tried to find evidence for a neutral particle with mass close to that of a proton. They did not succeed. That discovery was not made until 1932 by a former student of Rutherford, J. Chadwick (NLP 1932*) (1932). The particle was called a neutron. From the point of view of isotope effects discussed in this book, all we need to know about the nucleus is that it is made up of protons and neutrons, that the number of protons is equal to the charge on the nucleus which is called the atomic number, and that the sum of the number of protons plus the number of neutrons is called the mass number which yields the atomic weight corresponding to that nucleus. The mass number is, of course, an integer. The actual atomic weights show small deviations from these integers and these are related to nuclear stabilities.

It should be noted that both Harkins and Rutherford were interested in the details of nuclear structure from the point of view of understanding stability of nuclei and understanding which mass numbers are stable. This is an important study but it is really nuclear physics and is beyond the scope of this book.

This section started with the discovery of Soddy and Fajans on radioactive decay around 1910 and the relationship of radioactive decay to the periodic table. At this point in the history, we understand the periodic table and we understand the role of isotopes in the periodic table. We have not yet understood the structure of the modern Table, i.e. first row two elements, second row eight elements, etc. That understanding can be based on Bohr theory of the hydrogen atom originally developed in 1911 and is summarized in Bohr’s famous article in *Zeitschrift für Physik* (Bohr 1922).

1.4 The 1920s and 1930s Through the Discovery of Deuterium

This part of the history will be much less detailed than the previous ones which dealt with the development of the concept of isotopes. While, in the previous section, much of the focus was on the fact that the isotopes of an element all have the “same” properties, much of the focus now changes to the (small) “differences” in the properties.

This period also focuses on the discovery of isotopes of light weight elements some of which have such low natural abundance that they could not be detected by the mass spectrographs available in the early part of the twentieth century, but which may be very desirable for study because isotope effects involving lightweight elements tend to be much larger than those for heavier elements. A prime example is the discovery of deuterium in 1932, one of the major events in isotope chemistry during this time period.

1.4.1 Early Work on Isotope Effects on Spectra

In 1920, [Kratzer \(1920\)](#) and [Loomis \(1920\)](#) independently noted that vibrational frequencies of isotopic diatomic molecules should depend inversely on the square root of the reduced masses of the molecules (see Chapter 3, Equation 3.4) on the assumption that isotopic substitution does not affect the force constant f . One knows from the Born–Oppenheimer approximation (*vide infra* and Chapter 2) that this is a correct assumption. While 1920 precedes the publication of the Born–Oppenheimer approximation (1927), it was commonly assumed at that time that isotopic substitution does not have significant effect on chemical bonding or on the force constants associated with chemical bonds. Kratzer and Loomis were aware of the existence of two isotopes of chlorine and were able to calculate the ratio of the stretching vibrations of H^{35}Cl and H^{37}Cl . The far infrared spectrum had been measured by [Imes \(1919\)](#). Identifying the lowest observed transition in HCl as corresponding to the fundamental vibration of the more abundant H^{35}Cl molecule, they were able to calculate $\Delta\nu$, the expected difference between the frequencies of the two isotopic HCl molecules, H^{35}Cl and H^{37}Cl . While Kratzer and Loomis found no evidence of an isotopic molecule in the fundamental vibrational band since their instrumental resolution was not sufficient, the splitting was apparent in the overtone band at frequency 2ν with isotopic splitting $2\Delta\nu$. The calculated and observed values of the isotopic splitting were in excellent agreement. Arguably, this represents the first quantitative study of an isotope effect.

Kratzer and Loomis as well as [Haas \(1921\)](#) also discussed the isotope effect on the rotational energy levels of a diatomic molecule resulting from the isotope effect on the moment of inertia, which for a diatomic molecule, again depends on the reduced mass. They noted that isotope effects should be seen in pure rotational spectra, as well as in vibrational spectra with rotational fine structure, and in electronic spectra with fine structure. They pointed out the lack of experimental data then available for making comparison.

R. S. Mulliken (1925a), whose name has previously appeared in these pages as a student of Harkins carried out the first detailed study of isotope effects on the electronic spectrum of a diatomic molecules. His first paper on isotope effects in band spectra of diatomic molecules dealt with theory of the energy levels of diatomic molecules and with the spectrum that results from a transition between two electronic states. Corresponding to a given electronic state there is a vibrational force constant f and a corresponding vibrational frequency ν which depends, as already noted, on the force constant and on the diatomic molecule reduced mass. The vibrational energy levels corresponded in the old (Sommerfeld) quantum theory to $n h \nu$ with n integer or zero and ν the vibrational frequency. The corresponding rotational energy levels of the diatomic molecule as a rigid rotor were given in the old theory by $j^2 h^2 / 8 \pi^2 I$. Here j , the rotational quantum number, is an integer, I is the moment of inertia of the diatomic molecule which is isotope dependent and h is Planck's constant. Mulliken assumed that the electronic states of the diatomic molecule are isotope independent as is the vibrational force constant f . Thus, he implicitly assumed the relation which later became the Born–Oppenheimer approximation in the new quantum mechanics (see Chapter 2). Mulliken's formulation did include rotational–vibrational interaction.

In a second paper, Mulliken (1925b) employed the result just discussed to interpret the emission spectrum of BO which had previously been measured by Jevons (1915) by introducing BCl_3 vapor into the afterglow of “active nitrogen”. “Active nitrogen” is produced by an electric discharge through nitrogen (containing some air). Jevons “reasonably” assigned the observed band spectrum to BN. Two bands were observed, one starting at about $24,000 \text{ cm}^{-1}$ and a shorter wavelength one starting around $44,000 \text{ cm}^{-1}$. (Note that wave number, cm^{-1} , is a unit of frequency which can be converted to frequency in per sec by multiplying by the velocity of light c . High frequency corresponds to short wave length.) Each band system is made up of two similar superimposed band systems, the weaker of which is assigned to the compound of the less abundant ^{10}B isotope of boron and the stronger assigned to the ^{11}B isotope. Mulliken re-measured the electronic transition frequencies which were assigned to a vibrational integer quantum number n' of the initial state and a vibrational integer quantum number n'' of the final state. He was able to fit the energies (in units of reciprocal centimeters, cm^{-1}) of the observed band heads for each of the four spectra with a power series of n' and n'' containing terms up to quadratic.

$$\nu(\text{cm}^{-1}) = \text{constant} + (a_1 n' + a_2 n'^2 + \dots) - (b_1 n'' + b_2 n''^2 + \dots) \quad (1.2)$$

From his first paper (Mulliken 1925a), Mulliken understood that the band heads did not represent a transition from a non-rotating initial state to non-rotating final state. Yet, he used the band heads to study the vibrational isotope effect since he could measure the band heads more easily and since the rotational energy differences are very small compared to the vibrational energy difference. From the theory, the terms linear in n' and n'' ($a_1 n'$ and $b_1 n''$) arise from the harmonic approximation with the coefficients a_1 and b_1 corresponding to the harmonic vibrational frequencies in the



[Historical Vignette 1.3] Robert S. Mulliken (1896–1986) took his undergraduate degree at Massachusetts Institute of Technology and later, after serving in the US Army’s Chemical Corps during World War I, received his Ph.D. in 1922 from the University of Chicago working with W. D. Harkins on the separation of mercury isotopes. During the 1920s he held several prestigious fellowships which he spent abroad focusing his interests on molecular spectroscopy and quantum theory. On his return to the US he joined the faculty at the University of Chicago. Mulliken is best known for his development of molecular orbital theory for which he was awarded the Nobel Prize in Chemistry in 1966. He continued active theoretical (large scale molecular orbital calculations) and experimental (high resolution electronic molecular spectroscopy) programs until his retirement in 1985. (Harris and Ewing photograph from National Academy of Sciences Archives)

initial and final electronic states respectively. Thus, Mulliken determined that the final state in both the long wavelength band system and the short wavelength band system corresponds to the same state, presumably the electronic ground state of the system (Historical Vignette 1.3).

A major interest here is, of course, the isotope effect on the a_1 and b_1 coefficients for the ^{11}B system and the ^{10}B system. As already noted, this isotope effect should reflect the isotope effect on the harmonic vibrational frequencies in the various electronic states. Within the implicit Born–Oppenheimer approximation the ratio of these coefficients should be equal to the inverse ratio of the square roots of the reduced masses of the isotopic diatomic molecules. For the ratio $^{10}\text{BN}/^{11}\text{BN}$, one calculates with the use of atomic masses measured by Aston with the mass spectrometer a value of 1.0276. The values obtained from Mulliken’s measurements for the ratios of the a and b terms were 1.0302 and 1.0286 for the long wavelength bands and 1.0282 and 1.0294 for the short wavelength bands. The weighted average (Mulliken assigned weights to the measured values) of these values is 1.0291 ± 0.0003 . Mulliken concluded that the deviation from the theoretical value is so large that the isotope effect shows that the spectrum does not correspond to BN but rather to BO. For BO one calculates the appropriate theoretical ratio to be 1.0292. Mulliken’s reasoning on the identification of the molecule as BO is quite

convincing, all the more so since he also presents chemical evidence supporting this assignment. Later studies of the BO spectrum (*vide infra*) have supported Mulliken's assignment.

It should be noted in passing that Mulliken also examined the isotope effect on the quadratic terms in the equations for the band heads. These ratios should theoretically show an isotope effect proportional to the reduced masses of the diatomic molecules (rather than the square root of the reduced masses). While Mulliken concludes that these ratios also confirm that the molecule is BO rather than BN, the four experimental ratios show a fairly large scatter so that the case for identifying the molecule is not as strong as that from the experimental a and b ratios. He also measured some of the rotational lines in the spectra of BO and considered the measured and theoretical isotope effects. Here one experimental isotope ratio checks the theoretically calculated ratio quite well, but for the other two the result was unsatisfactory. However, Mulliken judged the error to be within the experimental uncertainty.

Mulliken's analysis of the isotope effect on the band spectrum of BO is regarded as arguably the first analysis of isotope effects on the band spectra of diatomic molecules. It is, however, also recognized as the first experimental measurement of a zero-point energy. It has been noted that Mulliken expressed the observed transition energies as a power series in n' and n'' (the integer vibrational quantum numbers of the initial and final states respectively). There is obviously also a constant term in this series which corresponds to the transition energy between ground states ($n' = 0$, $n'' = 0$) with no vibrational energy. This constant term is the difference in electronic energy between the initial and the final states. The dilemma that Mulliken faced is that the isotope effect observed for this constant term is too large; the difference between the ^{10}B molecule and the ^{11}B molecule is -9.4 and -6.3 cm^{-1} for the long wavelength band systems and the short wavelength band systems respectively. Such a difference would be called an electronic isotope effect. Within the Born–Oppenheimer approximation or even the implied Born–Oppenheimer approximation, this electronic isotope effect should be small, much smaller than 5 or 10 cm^{-1} . In Chapter 2, corrections to the Born–Oppenheimer approximation are discussed. Only one such correction is discussed in detail and that is the so-called Rydberg correction for the hydrogenic atom (the one electron atom). The Rydberg correction depends on the nuclear mass of the atom. Mulliken reasons that a knowledge of the difference in the Rydberg correction between ^{10}B and ^{11}B nuclei will give an estimate of the order of the electronic isotope effect to be expected for ^{10}BO and ^{11}BO . This is a bold assumption, but it is probably reasonable. On this basis, he expects an isotope effect on the electronic energy of a few tenths of a wave number. Thus, he reasons that the electronic isotope effect that he calculated above is unreasonably large. While he makes no reference to the Einstein–Stern paper (1913) or to the Lindemann paper (1919), he was probably aware that these authors had considered that the energy levels of a harmonic oscillator are given by a formula $(n + 1/2)h\nu$ rather than $n h\nu$ with the vibrational quantum number n being a positive integer or zero (as was assumed in the early quantum mechanics). Mulliken does refer to some work which indicates half integer quantum numbers.

Be that as it may, Mulliken decided to assume that the energy levels of the oscillators are given by $(1/2)h\nu$, $(3/2)h\nu$, etc. He then introduced new quantum numbers η' and η''

$$\eta' = \left(n' + \frac{1}{2} \right) \quad (1.3)$$

$$\eta'' = \left(n'' + \frac{1}{2} \right) \quad (1.4)$$

and, in a straightforward manner, he rewrote the equations for the transition energies of the two band systems in terms of η' and η'' and in this way, included the zero-point energy in the constant terms. Carrying this procedure through, he found for the electronic isotope effect, values of -2.3 and $+2.4 \text{ cm}^{-1}$ where he had found above -9.4 and -6.3 cm^{-1} . Mulliken admits that -2.3 and $+2.4$ are still too large for the electronic isotope effects but concludes that such values could result from experimental error. He also tried a zero-point energy of $1h\nu$ (rather than $1/2h\nu$) for the harmonic oscillator but that did not “work” at all. He concludes since half integer quantum numbers with a minimum value of $+1/2$ “are by far more probable than large electronic isotope effects or other serious failure of the theory – unless one wishes to entertain the possibility of fractional values of quantum numbers other than $1/2$ ”. This was written in September, 1924. The Schrödinger equation which leads directly to the concept of the $1/2h\nu$ zero-point energy was not published until 1926. It will be seen that the vibrational zero-point energy is one of the principal concepts underlying all concepts of isotope effects on chemical and physical properties.

Mulliken also studied other band spectra of diatomic molecules. Only one such study will be mentioned here and that is his study of copper iodide (Mulliken 1925c), where he examined the copper isotope effect. Mulliken’s pioneering work was followed by more papers on isotope effects on electronic spectra (visible and UV) which will not be detailed here. Many of these papers deal with diatomics since the theory of such spectra is much better understood than that for general polyatomic systems. Further discussion of isotope effects on spectra will be mainly restricted to their use in the discovery of less abundant isotopes.

It should, however, be mentioned that Mulliken’s study of the BO system has been followed over the years by many others. An extensive study by Jenkins and McKellar (1932) should be mentioned explicitly. This study involved the long wavelength band of BO. The same method as that used by both Jevons and Mulliken to produce the BO was used in this work. The new (present day) quantum mechanics was used in the theoretical interpretation. Both the vibrational and the rotational isotope effects were observed and agree with theory. One motivation for this work was to determine how well the isotopic ratio of the square roots of the two relevant isotopic masses (^{10}B and ^{11}B) agrees with the ratio obtained from Aston’s mass spectrometric measurements and hence how well isotopic mass ratios determined from band spectra compare with those obtained using Aston’s mass spectrograph.

The reduced mass ratios agree exactly with Aston's to the five significant figures reported by Aston. An interesting result obtained in this study, where there was no longer any question about zero-point energy, is the electronic isotope effect reported as $0.33 \pm 0.08 \text{ cm}^{-1}$, a result which appears much more satisfactory than that obtained earlier by Mulliken.

As already noted, the study of BO above was carried out about 7 years after Mulliken's study. It is included here to indicate that Mulliken's earlier study did reach the correct conclusions even though it had available only much poorer theoretical and experimental "apparatus." The next section returns to an earlier time period, closer to the time of Mulliken's BO study.

1.4.2 The Discovery of Isotopes of Carbon, Nitrogen, and Oxygen, and Hydrogen

Aston and his colleagues discovered a fairly large number of isotopic atoms during the 1920s using the mass spectrograph. However, there was no evidence that hydrogen, carbon, nitrogen, and oxygen, the elements that account for about 96% of the mass of the human body, had isotopes. This might mean that these elements did indeed have no isotopes or, alternatively, that the existing mass spectrographs were unable to detect these isotopes because of their low abundance in natural materials. This section deals with the discovery of the isotopes of carbon, nitrogen, oxygen, and hydrogen.

In connection with their interest in calculating Third Law entropies, W.F. Giauque (NPC1949*) and H. L. Johnston (1929a) studied the atmospheric absorption spectral bands which had been observed by Dieke and Babcock (1927). Around $13,000 \text{ cm}^{-1}$, bands are observed which are designated as the A bands and are ascribed to O_2 . There is also a much weaker A' band in the observed spectrum. Mulliken had apparently also noted this weak band but then expressed the opinion that a "revised interpretation will probably be necessary to include such a weak band." The quote is from Giauque and Johnston (1929a). The band structures of the A and A' bands are quite similar, except the spacings are different. Giauque and Johnston were able to rationalize the observed spacings by assigning the A bands to 16–16 oxygen molecules and the A' bands to 16–18 molecules, thereby discovering the ^{18}O isotope of oxygen. Historically, it would be interesting to determine how Mulliken, the expert on isotope effects on band spectra of diatomic molecules, missed this solution. Maybe, he did not have all the experimental data available.

Shortly after their discovery of ^{18}O Giauque and Johnston (1929b) (see also Babcock (1929)) studied newer and more extensive data on the atmospheric absorption of sunlight. Here they found a band referred to as A'' with band structure similar to the A and A' bands but much weaker even than the A' band. The spectral results agreed with the assignment of this band to the 17–16 O_2 molecule, and thereby they discovered the third and least abundant isotope of oxygen.

Following the discovery of the oxygen isotopes, the carbon 13 isotope was discovered by [King and Birge \(1930\)](#). This discovery was made by observing a band spectrum in the diatomic molecule C_2 . While in the case of O_2 , an absorption band was studied, the observed C_2 band here (the so-called Swan band) is in the emission spectrum from an electric furnace (presumably from the material of the graphite tube in the furnace). While the observation of the rare oxygen isotopes in the sunlight was made possible by the long path length through the atmosphere (particularly at low sun), the rare carbon isotope was detected by long exposure.

The last discovery of an isotope of an element in the second row of the periodic table was that of ^{15}N . This is credited to [R. Naudé \(1929\)](#). In the band spectrum of NO , he observed band heads for not only $^{15}N^{16}O$ but also $^{14}N^{18}O$ and $^{14}N^{17}O$ on the basis of the expected isotope effect on the reduced mass of the molecule.

1.4.3 Deuterium

We now arrive at the experiment which, for the purpose of this chapter, is regarded as the last act of the early history of isotope effects and also the first act of the modern history. The modern history of isotope effects is not a part of this chapter; it is still being written.

[Aston \(1927\)](#) had accurately measured the atomic weight of the mass 1 positive ion relative to the mass of the oxygen at mass 16, taken to have a mass exactly equal to 16.0000. The atomic mass that he obtained in this way was in close agreement with the atomic weight for hydrogen obtained by chemical means. This result indicates that, if natural oxygen is mono-isotopic, then so is hydrogen. This situation changed when [Giauque and Johnston](#) showed that natural oxygen is not mono-isotopic. To determine the meaning of Aston's atomic weight measurement of hydrogen corresponding to mass = unity, one then needs to know the relative abundance of ^{16}O and ^{18}O in oxygen. [Birge and Menzel \(1931\)](#) reviewed the available data (and this was not a straightforward matter) and estimated that the abundance of hydrogen of mass 2 relative to hydrogen of mass 1 is 1:4,500. It should be pointed out that this result would mean that the hydrogen isotope of mass 2 is much less abundant than any isotope then yet discovered and that finding it either mass spectroscopically or by study of band spectra would not be experimentally possible (at that time).

One of the authors of this book heard a story while he was a graduate student, that [Harold Urey](#), [W. C. Harkins](#), and [G. N. Lewis](#) met at an American Chemical Society Meeting and privately discussed the possibility of finding hydrogen of mass 2. When the meeting broke up, the other two turned to Urey and said "OK, Harold, you discover it." He has been unable to verify this story or find any evidence that such a conversation took place between these three eminent chemists, but it is a fact that "Harold and his colleagues did discover it."

[Urey](#), [Brickwedde](#), and [Murphy \(UBM\)](#) set out to discover isotopes of hydrogen. They knew the energy levels of the hydrogen atom and they knew the effect of the mass of the nucleus on these energy levels. The Rydberg constant depends on the

mass of the nucleus and this dependence is given by the Bohr theory. They also knew that the new quantum mechanics yields exactly the same result, which for the hydrogen atom of mass 1 agrees with experiment. They also realized that if they wanted to find new isotopes of hydrogen by their spectral “signature” after passing an electrical discharge through a sample of hydrogen gas, they would need first to enrich the gas with respect to the rarer isotopes to which they gave the names deuterium (mass 2) and tritium (mass 3). They made calculations on the isotope effect on the vapor pressure of solid hydrogen using the same type of theory that Lindemann had used to calculate the isotope effect on the vapor pressure of the lead isotopes, discussed earlier in this chapter (Lindemann 1919). Assuming that the vibrational frequencies of hydrogen as well as the molecular inter-atomic distances are the same in the crystal and the gas phases and further assuming the Born–Oppenheimer approximation, UBM estimated a considerable isotope effect with the lighter isotope leading to the higher vapor pressure. Instead of using solid hydrogen, they decided to use fractional distillation of liquid hydrogen. They obtained the atomic spectra of hydrogen both from tank hydrogen and from the residue from evaporating 4L of liquid hydrogen. They observed deuterium spectral lines in both samples but the residue from the distillation was much enriched. No evidence of tritium was found in either sample. The discovery of deuterium was first announced by the American Physical Society meeting in December 1931 and then published in *Physical Review* (Urey et al. 1932).

The results for deuterium were confirmed by Bleakney (1932) using mass spectroscopy. Bleakney built a special instrument for the purpose of the experiment. The mass spectrum of H_2 was known to yield an ion at mass 3 corresponding to H_3^+ which results from an ion molecule reaction in the source, probably $H_2^+ + H_2 \rightarrow H_3^+ + H$ or possibly $H^+ + H_2 \rightarrow H_3^+$. The intensity of the mass 3 H_3^+ peak should depend on the square of the pressure of hydrogen in the ion source. On the other hand, the intensity of the mass 3 peak resulting from deuterium, HD^+ , should depend linearly on the pressure of the hydrogen in the ion source. Bleakney investigated the two samples which had been studied in Urey et al. (1932). He found a large increase of the mass 3 peak in the concentrated H_2 sample when compared to the tank hydrogen and found that this increase varies linearly with the pressure of the hydrogen gas, thus confirming the UBM discovery.

While our description of this experiment ends this chapter on the discussion of isotope history, a few more notes are appropriate. The discovery of deuterium led to a rush of new work on deuterium, so much so that Urey published a review article on deuterium in 1935, including both work by himself and by his collaborators but also work by other groups (Urey and Teal 1935). Reading or perusing of this article is highly recommended.

It is of interest to point out that Washburn and Urey proposed a method for enriching deuterium based on the experience that, during electrolysis, the cathodic reaction with the lower cathodic potential will occur almost to the exclusion of other cathodic reactions. Reasoning that the reduction potentials of H^+ and D^+ may differ, they proposed electrolysis could be used to enrich deuterium. Pursuing that idea they found the residual water in a commercial water electrolysis apparatus used for

the production of oxygen was significantly enriched in deuterium. Washburn and Urey (1932) describe several schemes for making practical use of electrolysis to obtain enriched deuterium. This reference also makes it clear that Urey no longer believed that the isotope effect in electrolysis reflects an isotope effect on a reduction potential.

1.5 A Brief Look at the Position of Theoretical and Experimental Developments at the Time of the Discovery of Deuterium

1.5.1 Quantum Theory

It has already been noted that the new quantum theory and the Schrödinger equation were introduced in 1926. This theory led to a solution for the hydrogen atom energy levels which agrees with Bohr theory. It also led to harmonic oscillator energy levels which differ from those of the older quantum mechanics by including a zero-point energy term. The developments of M. Born and J. R. Oppenheimer followed soon thereafter; referred to as the Born–Oppenheimer approximation, these developments are the cornerstone of most modern considerations of isotope effects.

1.5.2 Thermodynamics and Statistical Mechanics

Equilibrium thermodynamics as we know it became complete with the Third Law of Thermodynamics developed by W. Nernst and by G. N. Lewis. The ideas of activities and activity coefficients for real systems were well developed by 1932.

Giauque, whose name has already been mentioned in connection with the discovery of the oxygen isotopes, calculated Third Law entropies with the use of the low temperature heat capacities that he measured; he also applied statistical mechanics to calculate entropies for comparison with Third Law entropies. Very soon after the discovery of deuterium Urey made statistical mechanical calculations of isotope effects on equilibrium constants, in principle quite similar to the calculations described in Chapter IV. J. Kirkwood's development showing that quantum mechanical statistical mechanics goes over into classical statistical mechanics in the limit of high temperature dates to the 1930s. Kirkwood also developed the quantum corrections to the classical mechanical approximation.

Transition state theory, a quasi-thermodynamic/statistical mechanical approach to the theory of reaction rates was developed in the early 1930s by a number of workers including H. Eyring, E. P. Wigner, and J. C. Polanyi and was very quickly applied to the consideration of isotope effects on rates of simple molecular reactions.

1.5.3 Instrumentation – The Mass Spectrometer

The mass spectrometer (called mass spectrograph by its “discoverer” Aston) is an important tool of the isotope chemist. Improvements in the 1920s and the 1930s leading to higher sensitivity and higher resolution were introduced by Aston himself and a number of others including A. J. Dempster, K. T. Bainbridge and A. O. Nier. Commercial isotope ratio machines did not become generally available until after World War II.

References

- Aston, F. W. Neon. *Nature* **104**, 334 (1920a).
- Aston, F. W. The constitution of the elements. *Nature* **104**, 393 (1920b).
- Aston, F. W. Isotopes and atomic weights. *Nature* **105**, 617–619 (1920c).
- Aston, F. W. *Mass Spectra and Isotopy*, Nobel Lecture, December 12, 1922 available at http://nobelprize.org/nobel_prizes/chemistry/laureates/1922/aston-lectures.pdf
- Aston, F. W. A new spectrograph and the whole number rule. *Proc. Roy. Soc. Lond.* **A115**, 487–514 (1927).
- Babcock, H. D. Some new features of the atmospheric oxygen bands, and the relative abundance of the isotopes 0–16, 0–18. *Proc. Nat. Acad. Sci. USA* **15**, 471–477 (1929).
- Birge, R. T. and Menzel, D. H. The relative abundance of the oxygen isotopes, and the basis of the atomic weight system. *Phys. Rev.* **37**, 1669–1671 (1931).
- Bleakney, W. Additional evidence for an isotope of hydrogen of mass 2. *Phys. Rev.* **39**, 536 (1932).
- Bronsted, J. N. and de Hevesy, G. The separation of the isotopes of mercury. *Nature* **106**, 144 (1920).
- Bohr, N. Der Bau der Atome und die Physikalischen und Chemischen Eigenschaften der Elemente. *Z. f. Physik* **19**, 1–67 (1922).
- Chadwick, J. The existence of a neutron. *Proc. Roy. Soc. Lond.* **A136**, 692–708 (1932).
- Dahl, J. P. On the Einstein-Stern model of rotational heat capacities. *J. Chem. Phys.* **109**, 10688–10691 (1998).
- de Hevesy, G. and Paneth, F. Zur Frage der Isotopen Elemente. *Monatshefte für Chemie* **36**, 75–93 (1915).
- Dieke, G. H. and Babcock, H. D. The structure of the atmospheric absorption bands of oxygen. *Proc. Nat. Acad. Sci.* **13** 670–678 (1927).
- Einstein, A. and Stern, O. Einige Argumente für die Annahme einer Molekularen Agitation beim Absoluten Nullpunkt. *Ann. Physik* **40**, 551–560 (1913).
- Fajans, K. Über eine Beziehung Zwischen der Art einer radioaktiven Umwandlung und dem elektro chemischer Verhalten der betreffenden Radioelemente. *Phys. Z.* **14**, 131–136 (1913a); Fajans, K. Die Stellung der Radioelemente in Periodischen System. *Phys. Z.* **14**, 136 (1913a).
- Fajans, K. Radioactive transformations and the periodic system of the elements. *Berichte der Deutschen Chemischen Gesellschaft* **46**, 422–439 (1913b).
- Fajans, K. The radioelements and the periodic system. *Naturwissenschaften* **2**, 429, 463, 543 (1914).
- Fleck, A. See Biographical Memoirs of Fellows of the Royal Society, *Alexander Fleck, Baron Fleck of Saltcoats*, **17**, 242–454 (1971). He received his chemistry degree in 1911 at Glasgow and remained with Soddy as an assistant until 1913. He stayed in close contact with Soddy for another 2 years. He then moved on to industry and had a very successful career, serving as chairman of ICI from 1953–1960. His papers on radioactivity were all single author publications.
- Garrett, A. B. Radioactive Tracers: G. de Hevesy. *J. Chem. Ed.* **40**, 36–37 (1963).

- Geiger, H. and Marsden, F. The laws of deflexion of α particles through large angles. *Phil. Mag.* **25**, 604–623 (1913).
- Giauque, W. F. and Johnston, H. L. An isotope of oxygen, mass 18. Interpretation of the atmospheric absorption bands. *J. Am. Chem. Soc.* **51**, 1436–1441 (1929a).
- Giauque, W. F. and Johnston, H. L. An isotope of oxygen, mass 17, in the earth's atmosphere. *J. Am. Chem. Soc.* **51**, 3528–3534 (1929b).
- Haas, A. Rotation spectrum and isotopy. *Z. f. Physik* **40**, 68–72 (1921).
- Harkins, W. D. and Wilson, E. D. The changes of mass and weight involved in the formation of complex atoms. *J. Am. Chem. Soc.* **37**, 1367–1383 (1915a).
- Harkins, W. D. and Wilson, E. D. The structure of complex atoms, the hydrogen–helium system. *J. Am. Chem. Soc.* **37**, 1383–1396 (1915b).
- Harkins, W. D. and Wilson, E. D. Recent work on the structure of the atom. *J. Am. Chem. Soc.* **37**, 1396–1420 (1915c).
- Harkins, W. D. The separation of the element chlorine and meta chlorine and the positive electron. *Nature* **105**, 230–231 (1920).
- Harkins, W. D. and Hayes, A. The separation of the element chlorine into isotopes (isotopic elements). *J. Am. Chem. Soc.* **43**, 1803–1825 (1921).
- Heilbronn, J. L. *H. G. J. Moseley: The Life and Letters of an English Physicist, 1887–1915*, University of California Press, Berkeley, CA (1974).
- Imes, E. S. Measurements on the near infrared absorption of some diatomic gases. *Astrophys. J.* **50**, 251–276 (1919).
- Jenkins, F. A. and McKellar, A. Mass ratio of the boron isotopes from the spectrum of BO. *Phys. Rev.* **42**, 464–487 (1932).
- Jevons, W. Spectroscopic investigations in connection with the active modification of nitrogen IV – a band spectrum of boron nitride. *Proc. Roy. Soc. Lond.* **91A**, 120–134 (1915).
- Keesom, W. H. and van Dijk, H. On the possibility of separating neon and its isotopic components by rectification. *Koninklijke Akademie van Wetenschappen te Amsterdam*, Proc. of the Sect. of Sciences XXXIV, 42–50 (1931); Keesom, W. H. and Hantjes, Vapor pressures of neon of different isotopic compositions. *J. Physica* **2**, 986–999 (1935).
- King, A. S. and Birge, R. T. Evidence from band spectra of the existence of a carbon isotope of mass 13. *Astrophys. J.* **72**, 19–40 (1930).
- Kratzer, A. A spectroscopic confirmation of the isotopes of chlorine. *Z. f. Physik* **30**, 460–465 (1920).
- Lindemann F. A. and Aston, F. W. The possibility of separating isotopes. *Phil. Mag.* **37**, 523–534 (1919).
- Lindemann, F. A. Note on the vapour pressure and affinity of isotopes. *Phil. Mag.* **38**, 173–181 (1919).
- Loomis, F. W. Infra-red spectra of isotopes. *Astrophys. J.* **52**, 248–256 (1920).
- McCoy, H. N. and Ross, W. H. The specific radioactivity of thorium and the variation of the activity with chemical treatment and with time. *J. Am. Chem. Soc.* **29**, 1709–1718 (1907).
- Millonni, P. W. and Shih, M. L. Zero-point energy in early quantum theory. *Am. J. Phys.* **59**, 684–698 (1991).
- Moseley, H. G. J. The high frequency spectra of the elements. *Phil. Mag.* **26**, 1024–1034 (1913).
- Moseley, H. G. J. The high frequency spectra of the elements, Part II. *Phil. Mag.* **27**, 703–713 (1914).
- Mulliken, R. S. and Harkins, W. D. The separation of isotopes. Theory of resolution of isotopic mixtures by diffusion and similar processes. Experimental separation of mercury by evaporation in a vacuum. *J. Am. Chem. Soc.* **44**, 37–65 (1922).
- Mulliken, R. S. The isotope effect in band spectra, Part I. *Phys. Rev.* **25**, 119–138 (1925a).
- Mulliken, R. S. The isotope effect in band spectra, II: the spectrum of boron monoxide. *Phys. Rev.* **25**, 259–296 (1925b).
- Mulliken, R. S. The isotope effect in band spectra III. The spectrum of copper iodide as excited by active nitrogen. *Phys. Rev.* **26**, 1–34 (1925c).

- Naudé, R. An isotope of nitrogen, mass 15. *Phys. Rev.* **34**, 1498–1499 (1929). Note that Naudé refers in this paper to two earlier communications by King and Birge (1930) on the discovery of ^{13}C .
- Rutherford, E. The scattering of the α and β rays and the structure of the atom. *Phil. Mag.* **21**, 669–688 (1911).
- Rutherford, E. The structure of the atom. *Nature* **92**, 423 (1913).
- Rutherford, E. Collisions of alpha particles with light atoms. IV An anomalous effect in nitrogen. *Phil. Mag.* **37**, 581–587 (1919).
- Rutherford, E. Nuclear constitution of atoms. *Proc. Roy. Soc. Lond.* **A97**, 374–400 (1920).
- Soddy, F. The radio-elements and the periodic law. *Chem. News* **107**, 97–99 (1913a).
- Soddy, F. Intra-atomic charge. *Nature* **92**, 399–400 (1913b).
- Soddy, F. The periodic table of the elements. *Le Radium* **11**, 6 (1914).
- Soddy, F. The complexity of the chemical elements. *Scientific Monthly* **5**, 451 (1917). *The Interpretation of Radium*. 4th Ed. G. P. Putnam's Sons, New York 1922. *The Story of Atomic Energy*, Nova Atlantis, London 1949.
- Soddy, F. *The Origins of the Conceptions of Isotopes*, Nobel Lecture 1922, available at http://nobelprize.org/nobel_prizes/chemistry/laureates/1921/soddy-lectures.pdf.
- Thomson, J. J. Rays of positive electricity. *Proc. Roy. Soc. Lond.* **A89**, 1–20 (1913).
- Urey, H. C. Brickwedde, H. G. and Murphy, G. M. A hydrogen isotope of mass 2. *Phys. Rev.* **39**, 164–165 (1932).
- Urey, H. C. and Teal, G. K. The hydrogen isotope of atomic weight two. *Rev. Mod. Phys.* **7**, 34–94 (1935).
- van den Broek, A. Intra-atomic charge. *Nature* **92**, 372–373 (1913a).
- van den Broek, A. Intra-atomic charge and structure of the atom. *Nature* **92**, 470–478 (1913b).
- Washburn, E. W. and Urey, H. C. Concentration of the ^2H isotope of hydrogen by the fractional electrolysis of water. *Proc. Nat. Acad. Sci. USA* **18**, 496–498 (1932).

Chapter 2

The Born–Oppenheimer Approximation: Potential Energy Surfaces

Abstract The Born–Oppenheimer approximation is introduced and discussed. This approximation, which states the potential energy surface on which the molecule vibrates/rotates is independent of isotopic substitution, is of central importance in the theory of isotope effects.

2.1 Introduction

An understanding of isotope effects on the molecular level requires some acquaintance with mechanics, both classical and quantum, on the level of an undergraduate physical chemistry course; such acquaintance will be assumed here. The central unifying concept used for the theoretical rationalization of isotope effects is the molecular potential energy function. The potential energy function expresses the electronic energy of the ground state of the molecular system of interest as a function of the geometrical configuration of the atomic nuclei. On the one hand, as will be shown later, the theoretical calculation of an isotope effect usually requires knowledge of this function; conversely, on the other, the observation of an isotope effect usually leads to some knowledge of this function. The potential energy function is independent of isotopic substitution within the Born–Oppenheimer approximation, it depends on the charges of the nuclei but not their masses. The potential energy function is defined in terms of quantities referred to as force constants which are independent of isotopic substitution. Clarification of these ideas requires an understanding of molecular quantum mechanics; in the sections below we will attempt to present some of the basic concepts of molecular quantum mechanics without getting bogged down in mathematical detail.

2.2 The Quantum Mechanical Schrödinger Equation of the Molecule

In classical mechanics, the Hamiltonian function is the expression of the energy of a molecular system in terms of the momenta of the particles in the system and

the coordinates corresponding to these particles. The total energy is the sum of the kinetic energies of all the particles in the system (the atomic nuclei and the electrons which make up the molecule) and the potential energy. The nuclei are positively charged while the electrons are negatively charged; the electronic potential energy is evaluated by summing terms which correspond to Coulomb attraction between particles of opposite charge and Coulomb repulsion between particles of like charge. The Coulomb potential energy between two particles i and j with charges c_i and c_j at inter-particle distance R_{ij} is given by

$$V_{ij} = \frac{c_i c_j}{R_{ij}} \quad (2.1)$$

where c is positive or negative depending on whether the particles are positively or negatively charged. Thus, the Coulomb potential terms between electrons and nuclei will be negative (lowering the energy, corresponding to attraction) while the electron–electron terms and the nucleus–nucleus Coulomb terms will raise the energy and lead to repulsion. The kinetic energy of each particle j is expressed in terms of the squares of its Cartesian momenta (p_{xj} , p_{yj} , p_{zj}) divided by $2m_j$, where m_j is the particle mass.

$$T_j = \frac{1}{2m_j} (p_{xj}^2 + p_{yj}^2 + p_{zj}^2) \quad (2.2)$$

The Cartesian momenta can be expressed in terms of Cartesian velocities v_{xj} , v_{yj} , v_{zj} by the familiar relationship

$$p_{xj} = m_j v_{xj} = m_j \dot{x}_j \quad (2.3)$$

where we have indicated that the velocity in the x direction v_x is given by the time derivative of x (\dot{x}). The total Hamiltonian function for the molecular system in classical mechanics is then given by

$$H = T_E + T_N + V \quad (2.4)$$

T_E and T_N refer respectively to the kinetic energy terms from all the electrons and all of the nuclei, and V contains all the Coulomb terms.

The interest here is in the energy levels of molecular systems. It is well known that an understanding of these energy levels requires quantum mechanics. The use of quantum mechanics requires knowledge of the Hamiltonian operator H_{op} which, in Cartesian coordinates, is easily derived from the classical Hamiltonian. Throughout this chapter quantum mechanical operators will be denoted by subscript “op”. If the classical Hamiltonian function H is written in terms of Cartesian momenta and of interparticle distances appropriate for the system, then the rule for transforming H to H_{op} is quite straightforward. Just replace each Cartesian momentum component of particle j , p_j , by $(-\hbar/i) \frac{\partial}{\partial q_j}$ where $\frac{\partial}{\partial q_j}$ is a derivative with respect to Cartesian coordinate q_j , i equals $\sqrt{-1}$, and \hbar is Planck’s constant divided by 2π . Thus the kinetic energy of particle j is replaced by the operator $T_{op,j}$

$$T_{op,j} = -\frac{\hbar^2}{2m_j} \left(\frac{\partial^2}{\partial x_j^2} + \frac{\partial^2}{\partial y_j^2} + \frac{\partial^2}{\partial z_j^2} \right) = -\frac{\hbar^2}{2m_j} \nabla_j^2 \quad (2.5)$$

Here $\frac{\partial^2}{\partial x_j^2}$ is the second derivative with respect to the coordinate x_j . The discussion here is abbreviated and is intended to just give a preliminary insight into the quantum mechanics of molecules. Thus, Cartesian coordinates are introduced but there is no discussion of molecule fixed coordinates and space fixed coordinates: particle spin is not mentioned; there is no mention of interaction between rotation and vibration; etc.

The classical potential energy term is just a sum of the Coulomb interaction terms (Equation 2.1) that depend on the various inter-particle distances. The potential energy term in the quantum mechanical operator is exactly the same as in classical mechanics. The operator H_{op} has now been obtained in terms of second derivatives with respect to Cartesian coordinates and inter-particle distances. If one desires to use other coordinates (e.g., spherical polar coordinates, elliptical coordinates, etc.), a transformation presents no difficulties in principle. The solution of a differential equation, known as the Schrödinger equation, gives the energy levels E_{mol} of the molecular system

$$H_{op,mol} \Psi_{mol} = E_{mol} \Psi_{mol} \quad (2.6)$$

and also the corresponding wave functions Ψ_{mol} . The eigenfunctions (wave functions) can be employed to calculate electronic probability densities but further discussion of this point lies outside our present interest. The rules of quantum mechanics instruct that one must solve Equation 2.6 subject to conditions that “ Ψ_{mol} is well behaved” – the detailed collection of these conditions is referred to as the set of boundary conditions. It is these boundary conditions that lead to the fact that many of the energy levels of the molecular system are quantized, although there also exist continua.

While details of the solution of the quantum mechanical eigenvalue problem for specific molecules will not be explicitly considered in this book, we will introduce various conventions that are used in making quantum calculations of molecular energy levels. It is important to note that knowledge of energy levels will make it possible to calculate thermal properties of molecules using the methods of statistical mechanics (for examples, see Chapter 4). Within approximation procedures to be discussed in later chapters, a similar statement applies to the rates of chemical reactions.

2.3 The Separation of the Nuclear and Electronic Parts of the Schrödinger Equation

Molecules which differ from each other only because one or more nuclei in one molecule have been replaced by a different isotope of that nucleus are referred to as isotopic isomers or isotopomers. [Born and Oppenheimer \(1927\)](#) were the first to

formally demonstrate that to good approximation the quantum mechanical problem of a stable molecule can be separated into two independent problems, one dealing with the electronic motion within the molecule corresponding to fixed positions of the nuclei, and the other dealing with the motion of the nuclei. The approximations result from the need to introduce appropriate transformations to new coordinate systems and the omission of certain small terms which result from the transformations. In the end that omission is justified because the electrons are much lighter in mass than the nuclei. The electronic Schrödinger equation contains the kinetic energy operators for the electrons as well as the various electrostatic potential energy terms previously mentioned. These include the nuclear Coulomb repulsion terms which are now constant at the fixed configuration of the nuclei. The electronic Schrödinger equation can be written as

$$H_{\text{op,elec}}(\mathbf{S}, \mathbf{r}_i) = (T_{\text{op,elec}} + V(\mathbf{S}, \mathbf{r}_i)) \psi_{\text{elec}}(\mathbf{S}, \mathbf{r}_i) = E_{\text{elec}}(\mathbf{S}) \psi_{\text{elec}}(\mathbf{S}, \mathbf{r}_i) \quad (2.7)$$

In Equation 2.7 the collective coordinates defining nuclear geometry are designated by \mathbf{S} ; \mathbf{r}_i stands for the coordinates of the electrons. Again, it must be confessed that matters are being simplified here but this need not concern us; thus, the terms in $T_{\text{op,elec}}$ above have the form of the terms for individual electrons in the molecular Hamiltonian as given by Equation 2.5. In Equation 2.5, however, the electronic coordinates are space fixed while in Equation 2.6 the electronic coordinates are molecule fixed. Equation 2.7 is solved for fixed internuclear configuration \mathbf{S} to obtain $E_{\text{elec}}(\mathbf{S})$. One finds $E_{\text{elec}}(\mathbf{S})$ for a number of different configurations \mathbf{S} , and it is this process which is used to define the total electronic energy surface and thence the potential energy surface. Note that Equation 2.7 contains the nuclear charges through the Coulomb potentials, but it does not include any reference to nuclear mass. Thus, E_{elec} , the eigenvalue (energy) of the electronic Schrödinger equation is the same for all isotopomers of a molecular system. This is an important result (Historical Vignettes 2.1 and 2.2).

2.3.1 *Solutions of the Electronic Schrödinger Equation for Molecules*

The electronic Schrödinger equation has solutions corresponding to the ground electronic state and numerous electronic excited states. The interest here will be only in the ground electronic state. If one were discussing isotope effects in photochemical reactions, then there might be an interest in excited electronic states. However, in this book, unless a statement is made to the contrary, it is assumed that E_{elec} refers to the electronic ground state. One seeks to find the minimum value of $E_{\text{elec}}(\mathbf{S})$ for the electronic ground state as well as the second derivatives of $E_{\text{elec}}(\mathbf{S})$ with respect to nuclear distortion from this minimum. The nuclear configuration corresponding to this minimum energy will be referred to as the equilibrium internuclear configuration of the stable molecule, \mathbf{S}_0 . The second derivatives at \mathbf{S}_0 will be referred to as force constants. The following section contains a brief discussion of methods used to solve the electronic Schrödinger equation.



[Historical Vignette 2.1] Max Born (1882–1970) served as a professor of theoretical physics in several German universities prior to the 1930s where he became well known for his contribution to the theory of the properties of crystals, quantum theory, and the statistical interpretation of quantum mechanics. He was awarded the Nobel Prize in Physics for 1954. As were so many other Jewish–German scientists, Born was forced to emigrate in 1933 and was invited to Cambridge, where he taught for 3 years. In 1936 he was appointed Tait Professor of Natural Philosophy in Edinburgh, where he worked until his retirement in 1953. (Photo credit www.wikipedia.org, public domain)



[Historical Vignette 2.2] J. Robert Oppenheimer (1904–1967) was an American theoretical physicist best known for his role as director of the Manhattan project at Los Alamos, the World War II effort to develop the first nuclear weapons. After study abroad in England and Germany (with Born) he was appointed to the University of California, Berkeley where he is noted as being the chief founder of the American school of theoretical physics. Following WW II he was director of The Institute for Advanced Study, Princeton, and served as an advisor to the United States Atomic Energy Commission. He used that position to lobby for control of atomic energy and against the development of the H-bomb (“super”). This aroused the ire of many politicians and scientists and his security clearance was revoked in 1954 at the end of a highly publicized and politicized hearing. Oppenheimer’s controversial career has resulted in several thoughtful biographies. His role in the Manhattan project was musically dramatized in the opera “Dr. Atomic” which premiered in 2005. (Photo credit www.wikipedia.org, public domain)

2.3.2 Nuclear Motion

The Schrödinger equation for nuclear motion contains a Hamiltonian operator $H_{\text{op,nuc}}$ consisting of the nuclear kinetic energy and a potential energy term which is $E_{\text{elec}}(\mathbf{S})$ of Equation 2.7. Thus

$$H_{\text{op,nuc}} \psi_{\text{nuc}} = (T_{\text{op,nuc}} + E_{\text{elec}}(\mathbf{S}))\psi_{\text{nuc}} = E_{\text{mol}}\psi_{\text{nuc}} \quad (2.8)$$

Here, in the Born–Oppenheimer approximation, E_{mol} is the molecular energy. Note that Equation 2.8 is the nuclear Schrödinger equation with the energy eigenvalue E_{mol} being the molecular energy of Equation 2.6. Thus the energy $E_{\text{elec}}(\mathbf{S})$ is the potential function for nuclear motion. As has already been emphasized, $E_{\text{elec}}(\mathbf{S})$ is independent of isotopic substitution. This is the essence of the Born–Oppenheimer approximation. The details of the mathematics of proceeding from Equation 2.1 through 2.8 require ignoring various terms which are small because the electronic mass is much less than the nuclear masses in Equation 2.6, but also involves other consequences of this mass difference; for instance the electronic wave function of Equation 2.7 varies very slowly with respect to change in nuclear coordinates.

2.3.3 Corrections

Corrections to the Born–Oppenheimer approximation, which will not be explored here in any detail, can be studied by perturbation theory. In first order perturbation theory the neglected terms in the Hamiltonian are averaged over the particular molecular state being considered and the concept of a given electronic state of the molecule remains a valid concept. One is said to be “working” in the adiabatic approximation. If one proceeds to higher orders in the perturbation, the concept of a given electronic state no longer remains valid (states are mixed); one is said to be working in a non-adiabatic regime. For most isotope effect considerations, corrections to the Born–Oppenheimer approximation are ignored and such procedure is adequate. Where corrections to the Born–Oppenheimer approximation have been considered, the process is usually carried out by first order perturbation theory in the adiabatic approximation.

2.3.4 Substituent Effects, Isotope Effects, and the First Law of Isotopics

Substituent effects occur when one substituent in a molecule is substituted by another (e.g. replacing a Cl atom in CH_3Cl by a Br atom). Studies of the changes in the physical properties (both equilibrium and dynamical) of that molecule resulting

from this substituent effect have been very useful tools for chemists for many years. Such work was pioneered by L.P. Hammett and subsequently expanded by R. W. Taft and others (see reading list). While Hammett and his successors did not actually study isotope effects (e.g. replacing H by D in a molecule), an isotope effect is a special type of substituent effect. The fact that the two isotopomers have the same potential energy curve for nuclear motion to good approximation means, on the one hand, that isotope effects are theoretically accessible if one knows the potential energy curve, while, on the other hand, if one does not know the potential curve, the isotope effect can be used to “probe” the potential curve. The Born–Oppenheimer isotope independent potential energy curve is central to most discussions of isotope effects and has sometimes been referred to as the First Law of Isotopics.

2.3.5 Separation of Internal and External Degrees of Freedom

Equation 2.8 can be further simplified. The motion of the molecular center of mass could have been rigorously separated from Equation 2.6, to get a Schrödinger equation for the center of mass and a separate equation for the other degrees of freedom of the molecule. In the approach here, the center of the mass is separated from Equation 2.8 rigorously. Subsequently one typically uses the rigid rotor approximation to separate the rotational motion of a rigid rotor (a non-vibrating rotor) from the motion of the vibrating molecule. The latter separation requires omitting terms corresponding to rotation–vibration interaction. By this process Equation 2.8 is replaced by three equations:

$$H_{\text{op,trans}} \psi_{\text{trans}} = T_{\text{op,trans}} \psi_{\text{trans}} = E_{\text{trans}} \psi_{\text{trans}} \quad (2.9)$$

$$H_{\text{op,rot}} \psi_{\text{rot}} = T_{\text{op,rot}} \psi_{\text{rot}} = E_{\text{rot}} \psi_{\text{rot}} \quad (2.10)$$

$$H_{\text{op,vib}} \psi_{\text{vib}} = (T_{\text{op,vib}} + E_{\text{elec}}(\mathbf{S})) \psi_{\text{vib}} = E_{\text{vib}} \psi_{\text{vib}} \quad (2.11)$$

Equation 2.11 explicitly indicates that the zero of (vibrational) energy corresponds to the electronic energy of the equilibrium configuration of the relevant electronic state. In the above, it has been assumed that there is no potential function acting on the translational motion; in practice one often assumes that the molecule is in a box. Then, the energy levels and wave functions of Equation 2.9 correspond to the particle in the box problem treated in most courses on elementary quantum mechanics. In the absence of rotational vibrational interaction, the rotational motion Hamiltonian operator and consequently the rotational energy correspond to the kinetic energy of rotation. The potential function for vibration is the isotope independent electronic energy of Equation 2.8, $E_{\text{elec}}(\mathbf{S})$. The solution of Equation 2.11 provides theoretical values of vibrational energy levels which may be studied in the laboratory using infrared and Raman spectroscopies. The solution of this equation and the isotope effects on the vibrational energy levels, which can be observed experimentally, will be the subject of Chapter 3.

The molecular wave function Ψ_{mol} can then be written as a product of the four wave functions of Equations 2.8 through 2.11 while the total energy E_{mol} can be expressed as a sum of four energy terms.

$$\psi_{\text{mol}} = \psi_{\text{elec}} \psi_{\text{trans}} \psi_{\text{rot}} \psi_{\text{vib}} \quad (2.12a)$$

$$E_{\text{mol}} = E_{\text{trans}} + E_{\text{rot}} + E_{\text{vib}} + E(S_0) \quad (2.12b)$$

Here it has been recognized that the vibrational Schrödinger equation includes a potential with its minimum corresponding to the minimum in the electronic energy of the state being considered. E_{vib} corresponds to the vibrational energy referenced to this minimum.

2.4 The Adiabatic Correction

A detailed discussion of the theoretical evaluation of the adiabatic correction for a molecular system is beyond the scope of this book. The full development involves, among other matters, the investigation of the action of the kinetic energy operators for the nuclei (which involve inverse nuclear masses) on the electronic wave function. Such terms are completely ignored in the Born–Oppenheimer approximation. In order to go beyond the Born–Oppenheimer approximation as a first step one can expand the molecular wave function in terms of a set of Born–Oppenheimer states (designated as $\psi_{\text{elec}}^{\Gamma}(S, r_i)$)

$$\Psi_{\text{mol}} = \sum_{\Gamma} F^{\Gamma}(S) \psi_{\text{elec}}^{\Gamma}(S, r_i) \quad (2.13)$$

Thus, when one considers the corrected Born–Oppenheimer (BO) approximation, one can no longer speak about being in a single BO electronic state. This kind of BO state mixing clearly occurs when the system jumps from one electronic state to another (usually as a result of “curve crossing”). Also such state mixing often occurs when an excited electronic state of a molecule decays by a non-radiative process. Ordinarily, one need not consider such mixing of electronic states unless the states are close lying in energy. In such a situation, one can make a first order correction to the Born–Oppenheimer approximation by averaging the terms in the BO electronic Hamiltonian operator over the electronic wave function and replacing Equation 2.8 by

$$(T_{\text{op,vib}} + E_{\text{elec}}(S) + C(S)) \psi_{\text{vib}} = E_{\text{vib}} \psi_{\text{vib}}(S) \quad (2.14)$$

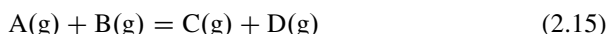
where $C(S)$ is the averaged perturbation. $C(S)$ may depend on nuclear mass and is often referred to as the adiabatic correction. Generally $C(S)$ does depend on nuclear configuration and will therefore affect the vibrational energy levels. In practice (see further reading at the end of the chapter) this effect is neglected here and C is

evaluated only at the equilibrium nuclear configuration of the stable molecule. In that case it reduces to an isotopic mass dependent constant to be added to the zero of vibrational energy.

The important fact that must be remembered is that in the Born–Oppenheimer approximation, Equation 2.8, the potential energy for vibrational motion is $E_{\text{elec}}(S)$ which is independent of isotopic mass of the atoms. In the adiabatic approximation, the potential energy function is $E_{\text{elec}}(S) + C$ and this potential will depend on nuclear mass if C depends on nuclear mass.

2.4.1 An Example

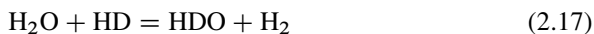
In the context of Section 2.4, consider a chemical equilibrium in the gas phase



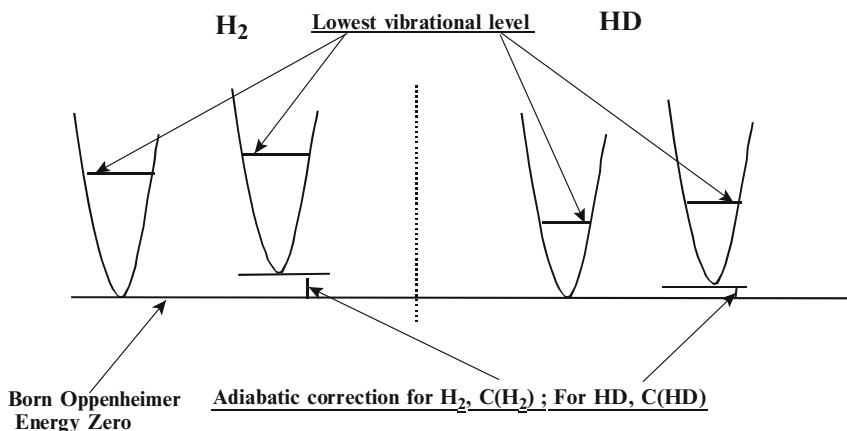
With the temperature sufficiently low so that all the molecules can be considered to be in their respective ground electronic states, the usual situation, the methods of statistical mechanics which will be explored in Chapter 4 then enable one to calculate the numerical value of the equilibrium constant K for this reaction from a knowledge of the molecular energy levels which are thermally accessible. With the assumption that all the molecules are in their respective ground electronic states, the relevant energy levels are then the respective rotational–vibrational energy levels. Within the BO approximation, it is customary to measure these energy levels with respect to the electronic energy E_{elec} in the equilibrium internuclear configuration. For the usual chemical equilibrium, the main contribution to the chemical equilibrium arises from ΔE_{elec} , the electronic energy difference between the sums of the electronic energies of the products and the reactants, and is given by

$$K_{\text{elec}} = \exp(-\Delta E_{\text{elec}}/kT) \quad (2.16)$$

where k is Boltzmann’s constant and T is the absolute temperature. Given that rotational and vibrational energy spacings tend to be quite small compared to the electronic energy differences between different molecules, it is quite usual that K_{elec} by itself determines whether an equilibrium constant is large or small. The exception to this rule is an isotopic exchange equilibrium. For example,



since ΔE_{elec} is identically equal to zero; E_{elec} in the BO approximation is the same for each isotopomer in each pair (H_2O , HDO) and (H_2 , HD) If one now includes the contribution of the adiabatic correction to the BO approximation, then



The adiabatic correction to the Born Oppenheimer approximation for H₂ and HD: Schematic, Not to Scale: $\Delta C = C(\text{H}_2) - C(\text{HD})$

In each case the uncorrected potential lies to the left, the corrected to the right

Fig. 2.1 The adiabatic correction to the Born–Oppenheimer approximation for H₂ and HD: schematic, not to scale: $\Delta C = C(\text{H}_2) - C(\text{HD})$. In each case the uncorrected potential lies to the *left*, the corrected to the *right*

$$K_{\text{elec}} = \exp(-(C(\text{HDO}) + C(\text{H}_2) - C(\text{H}_2\text{O}) - C(\text{HD}))/kT) \quad (2.18)$$

$$= \exp(+\Delta C(\text{HDO}) - \Delta C(\text{HD}))/kT \quad (2.19)$$

$$= \exp(-\Delta\Delta C/kT) \quad (2.20)$$

The K_{elec} value for an isotopic exchange reaction resulting from a failure of the Born–Oppenheimer approximation is sometimes referred to as K_{BOELE} . With the notation employed above $\Delta\Delta C$ is the value of ΔE_{elec} for the reaction (see Fig. 2.1).

In Chapter 4 we will learn to calculate the equilibrium constant for an exchange reaction like Equation 2.15 using the Born–Oppenheimer approximation. If, in addition, the adiabatic correction is included, the equilibrium constant calculated in the Born–Oppenheimer approximation must be multiplied by a correction factor containing the energy difference $\Delta\Delta C$.

The nuclear mass dependence of C values has the form

$$C = \sum_i \frac{b_i}{m_i} \quad (2.21)$$

where the sum is over the atoms in the relevant molecule, m_i is the nuclear mass of the isotope i , and b_i is a mass independent constant for each particular nucleus (element) in the molecule or separated atom of interest. Thus $b_{\text{H}}(\text{H}_2)$, $b_{\text{H}}(\text{LiH})$ and $b_{\text{H}}(\text{H}^-)$ are all different (see Table 2.1), but $b_{\text{H}}(\text{H}_2) = b_{\text{H}}(\text{HD}) = b_{\text{H}}(\text{D}_2)$, $b_{\text{H}}(\text{LiH}) = b_{\text{H}}(\text{LiD})$, etc. Table 2.1 lists C values and corresponding b values taken

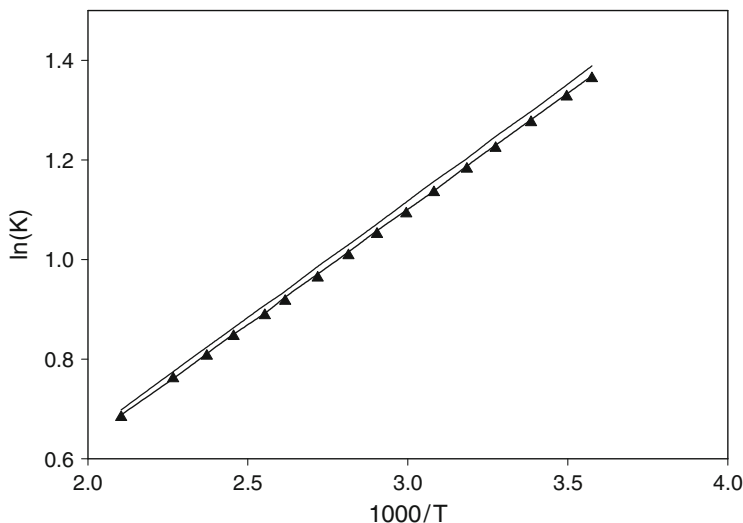


Fig. 2.2 $\ln(K_{\text{EQ}})$ for the isotope exchange reaction, equation 2.15 plotted vs. $1,000/T$: (*lighter solid line*, uppermost line) K_{EQ} calculated within the BO approximation; (*—, heavier solid middle line*) K_{EQ} calculated including adiabatic correction using equation 2.17; points are taken from a least squares fit to experimental values for the temperature range ($280 < T/K < 475$) (Modified with permission from Bardo, R. D. and Wolfsberg, M., *J. Phys. Chem.* **80**, 1068, (1976)).

from the literature. A few diatomic and atomic values are given as well as a single polyatomic value (H_2O) which may be the only such value available. Using the data in Table 2.1 one obtains $\Delta\Delta C = 3.8 \text{ cm}^{-1}$ for reaction 2.17. This corresponds to $K_{\text{BOELE}} = \exp(-3.8hc/(kT)) = \exp(-5.5/T)$ and amounts to a 2% correction to the Born–Oppenheimer isotopic equilibrium constant at room temperature. This is not a large effect but it so happens that there are very accurate experimental measurements of this particular isotopic gas phase equilibrium constant while at the same time the energy levels of all the molecules involved in this exchange reaction are quite well known. The comparison of the experimental measurement of this isotopic exchange equilibrium constant and the theoretically calculated value with and without the K_{BOELE} correction is shown in Fig. 2.2; the result is gratifying.

2.4.2 Adiabatic BO Corrections for Hydrogenic Atoms

To give the reader some further appreciation of the adiabatic correction, we next discuss the so-called Rydberg correction of the hydrogenic atom. The kinetic energy of the electron in the hydrogen atom is expressed by Equation 2.5, where m_j is set equal to the electron mass, m_e . It is well known that the Schrödinger equation for the hydrogen atom separates into two equations, one of which deals with the motion of the center of mass of the system and the other with the motion of the electron

with respect to the proton. The latter is the well-known equation:

$$\left(-\frac{\hbar^2}{2\mu}\nabla^2 - \frac{e^2}{r}\right)\psi = E\psi \quad (2.22)$$

where r is the distance from the proton to the electron. Here μ is the electron/proton reduced mass

$$\mu = \frac{m_e M}{m_e + M} \quad (2.23)$$

with M the mass of the proton and m_e the electronic mass. The eigenfunctions of Equation 2.22 are well known. The energy level formulae contain the Rydberg constant which leads to the appearance of a factor μ in the numerator. There are two Rydberg constants R_∞ and R_M , the first of which corresponds to replacing μ by m_e (equivalent to setting m_e/M equal to $1/\infty$ or 0) and the second to using the actual value of M . Substituting Equation 2.23 into Equation 2.22, one obtains

$$\left(-\frac{\hbar^2}{2m_e}\nabla_i^2 - \frac{e^2}{r} - \frac{\hbar^2}{2M}\nabla_i^2\right)\psi = E\psi \quad (2.24)$$

Both Equations 2.22 and 2.24 are exact Schrödinger equations for the coordinate r in the hydrogen atom. The attraction of Equation 2.24 is that it contains a kinetic energy term that involves only the mass of the electron and not the mass of the nucleus. In molecular calculations on electronic motion, one conventionally (usually) expresses the kinetic energy of electrons in the form given by the first term on the left hand side in Equation 2.24. Terms involving nuclear mass (i.e. the third term) are treated by perturbation theory. The first term on the left hand side of Equation 2.24 is just the kinetic energy of an electron of mass m_e . The third term on the left is a kinetic energy term which contains the nuclear mass M , and which would vanish for infinite nuclear mass. With M set infinite, Equation 2.24 is the hydrogen atom equation equivalent to Equation 2.14 for the molecular electronic Schrödinger equation. In Equation 2.14 the standard assumption of infinite nuclear mass (compared to electronic mass) was introduced at the outset,

$$\left(-\frac{\hbar^2}{2m_e}\nabla_i^2 - \frac{e^2}{r}\right)\psi = E\psi \quad (2.25)$$

The electronic energy of the ground (1s) state of the hydrogen atom corresponding to infinite nuclear mass is given by

$$E_{1s} = -R_\infty \quad (2.26)$$

Equation 2.24 can be thought of as having been derived from Equation 2.25 by adding the third term on the left hand side of Equation 2.24 as a perturbation. In first order quantum mechanical perturbation theory (see any introductory quantum text), the perturbation on the ground state of Equation 2.25 is obtained by averaging the perturbation over the ground state wave function of Equation 2.25. The effect of this

perturbation on the energy levels of Equation 2.25 is found by evaluating the value of the perturbation term averaged over the wave functions of the unperturbed problem. It is well known that the average kinetic energy of the electron in the ground state of the hydrogen atom (see any introductory quantum text) corresponding to Equation 2.25 is given by

$$\left\langle \left(-\frac{\hbar^2}{2m_e} \nabla_i^2 \right) \psi \right\rangle = R_\infty \quad (2.27)$$

so that

$$\langle \nabla_i^2 \psi \rangle = -\frac{2m_e}{\hbar^2} R_\infty \quad (2.28)$$

Note the usual quantum mechanical notation of using brackets ($\langle X \rangle$) to indicate an average of X . Therefore, the average value (averaged over the ground state of the hydrogen atom, Equation 2.25) of the third term on the left of Equation 2.24, which is the “adiabatic correction” C for the hydrogen atom is given by

$$C(\text{H}) = \left\langle \left(-\frac{\hbar^2}{2M} \nabla_i^2 \right) \psi \right\rangle = \frac{m_e}{M} R_\infty \quad (2.29)$$

The meaning of adiabatic correction is that the addition of C to the ground state energy calculated with R_∞ should yield a value equal to (close to) the exact ground state energy of the hydrogen atom

$$E_{1s} = -R_\infty + C = -R_\infty + (m_e/M) R_\infty \quad (2.30)$$

It is well known that the exact value of the energy of the ground state of the H atom is

$$E_{1s} = -R_M \quad (2.31)$$

where M refers to the mass of the proton. From the definition of R_M and R_∞

$$R_M/\mu = R_\infty/m_e$$

And therefore

$$R_M = (m/m_e) R_\infty = [M/(M + m_e)] R_\infty = [1 - (m_e/M) + K] R_\infty \quad (2.32)$$

where the higher order terms in m_e/M are collected in the correction term K . Comparison of Equations 2.30 and 2.32 shows that the adiabatic correction “works” through terms first order in m_e/M .

With M the mass of the hydrogenic nucleus (proton), the atomic C value in Table 2.1 does have exactly the mass dependence given by Equation 2.18. There is no approximation in the quantum mechanical solution for the hydrogenic atom. The C and ΔC values (Table 2.1) for H and D are accurate (except for higher or-

Table 2.1 Adiabatic corrections (cm^{-1}) for H–D and Mu–H isotope effects (Bardo, R. D., Kleinman, L. I., Raczkowski, A. W. and Wolfsberg, M., *J. Chem. Phys.* **69**, 1106, 1978)

Molecule	C(HX)	C(DX)	$\Delta C(\text{H–D})^1$	$b_{\text{H}}(\text{cm}^{-1} \text{amu})$	$\Delta C(\text{Mu–H})^2$
H ₂	114.6	86.0	28.6	57.7	452
LiH	198.3	163.8	34.5	69.6	544
H [−]	67.0	33.5	33.5	67.5	528
H	59.8	29.9	29.9	60.2	471
H ⁺	0	0	0	0	0
H ₂ O	–	–	24.8 ³	50.0	–

¹ $\Delta C(\text{H–D}) = C(\text{HX}) - C(\text{DX})$; $m_{\text{H}} = 1.00728 \text{ amu}$, $m_{\text{D}} = 2.01345 \text{ amu}$.

² $\Delta C(\text{Mu–H}) = C(\text{MuX}) - C(\text{HX})$; $m_{\text{Mu}} = 0.11343 \text{ amu}$. Mu represents muonium (Section 2.4.3).

³Bardo, R. D. and Wolfsberg, M., *J. Phys. Chem.* **80**, 1068 (1976). The value is that for $C(\text{H}_2\text{O}) - C(\text{HDO})$.

der perturbations). Accurate C and b values from the work of Bardo et al. for H₂, LiH, H, H[−], H⁺ and H₂O are given in Table 2.1. From this table, one can calculate $\Delta\Delta C$ values for corresponding H/D isotopic exchange reactions and K_{BOELE} values, correction factors for the equilibrium calculated from statistical mechanics in the Born–Oppenheimer approximation. Omitting the H⁺ system from consideration, the largest magnitude $\Delta\Delta C$ value from Table 2.1 is 5.9 cm^{-1} , which gives rise to a K_{BOELE} value in the room temperature region that differs from unity by less than 3%. For heavy atom isotope effects (atoms heavier than hydrogen) K_{BOELE} differs negligibly from unity at room temperature. Thus, for equilibria involving ¹⁴N/¹⁵N and ⁶Li/⁷Li, the difference is less than 0.001 (0.1%). In the one case (Equation 2.15) for hydrogen isotope exchange where accurate experimental data are available at room temperature, and where very accurate statistical mechanical values of the equilibrium constant have been calculated, the deviation of K_{BOELE} from unity at 300 K is less than 2%. Even so its application visibly improved the agreement between theory and experiment. See Chapter 4.

2.4.3 Muonium (Mu)

Mu is a very light and unstable ($t_{1/2}$ (half live) = $2 \mu\text{s}$) isotope of hydrogen consisting of a nucleus which is a positive muon (μ^+) and an electron. The nuclear mass of Mu is 0.113 amu. For this isotope one would expect much larger K_{BOELE} values than those discussed above.

$$\Delta C(\text{Mu, H}) / \Delta C(\text{H, D}) = (m_{\text{Mu}}^{-1} - m_{\text{H}}^{-1}) / (m_{\text{H}}^{-1} - m_{\text{D}}^{-1}) = 15.77 \quad (2.33)$$

The ΔC values for muonium hydrogen isotope effects are listed in Table 2.1. The $\Delta\Delta C$ value obtained for LiH, H₂ isotopic exchange involving Mu–H is 92 cm^{-1} ,

leading to K_{BOELE} differing from unity by 0.4 at room temperature. Clearly one cannot ignore K_{BOELE} effects in considering the thermodynamics of reactions involving Mu.

2.5 Numerical Calculations of $E_{\text{elec}}(S)$

2.5.1 *Historical Development*

The ground state electronic energy of the system on the right hand side of Equation 2.7 is the isotope independent potential energy for nuclear motion (in particular the molecular vibrations) in Equation 2.11. Within the Born–Oppenheimer approximation all isotope effects result from the motion of different isotopic masses on this potential energy surface. In the following we show how one can calculate isotope effects on thermodynamic properties of a molecular system from a knowledge of this surface, in particular from a knowledge of the position of the minimum of the ground state electronic energy surface, together with the second derivatives which describe the distortions of the atoms (really the nuclei) from their respective positions at the so-called equilibrium geometry.

The first electronic Schrödinger equation to be solved was that for the hydrogen atom, a proton and a single electron. This problem was solved exactly and led to the well known ground state wave function which is now described as a 1s atomic orbital, and excited states 2p, 3s, 3p, etc. Already, at the next level of difficulty, the two electron problem could not be solved exactly but highly accurate approximate solutions usually based on the variational principal of quantum mechanics soon became available. Most of these were “take-offs” on the solutions for the ground state and excited state quantum mechanical solutions to the hydrogen atom problem. Thus the helium atom was described as $(1s)^2$, lithium as $(1s)^2(2s)^1$, etc. A number of refinements were introduced including electron spin and the exclusion principle. The idea that each electron moves in the electric field of the nucleus and in the field created by all the other electrons led to Hartree–Fock calculations which yield the atomic orbitals of the polyelectron atom and the energy of the atomic system.

The first calculations on a two-electron bond was undertaken by Heitler and London for the H_2 molecule and led to what is known as the valence bond approach. While the valence bond approach gained general acceptance in the chemical community, Robert S. Mulliken and others developed the molecular orbital approach for solving the electronic structure problem for molecules. The molecular orbital approach for molecules is the analogue of the atomic orbital approach for atoms. Each electron is subject to the electric field created by the nuclei plus that of the other electrons. Thus, one was led to a Hartree–Fock approach for molecules just as one had been for atoms. The molecular orbitals were written as linear combinations of atomic orbitals (i.e. hydrogen atom type atomic orbitals). The integrals that needed to be calculated presented great difficulty and the computations needed were

very labor intensive. In the early 1950s, S.F. Boys in Cambridge, UK proposed the replacement of hydrogenic atomic orbitals (which behave like $\exp(-Zr)$) by Gaussian type orbitals (which behave like $\exp(-\alpha r^2)$, where r is the distance of the electron from a nucleus and Z and α are constants. This suggestion removed the difficulties in evaluating the integrals but at the same time it made the computation even more laborious. Then came large digital computers that were able to perform the computational labor! By the mid 1960s, John Pople and his colleagues were creating the Gaussian computer programs that enabled electronic structure calculations on chemically interesting molecules. Various versions of this program have become commercially available (Frisch et al. (2004)). The present version is labeled g09.

The original computer programs were used for carrying out Hartree–Fock calculations. Hartree–Fock calculations are still standard today. However, just as for atoms, Hartree–Fock calculations were not sufficient for very accurate calculations. Thus for the helium atom, $(1s)^2$ is a fair representation for the ground state; for better descriptions of ground states one has to mix in other configurations, $(1s)^2(2s)^1$, $(2s)^2$, $(2p)^2$, etc. This is known as configuration interaction. Configuration interaction is a method for taking proper account of the “correlation” between the electrons. Among the methods that take correlation into account are ones with acronyms like MP and CI.

2.5.2 *Present Day Approaches*

The methods described above are still in use today. However, in the 1970s Walter Kohn proposed an entirely different approach for solving both the atomic and the molecular problems. This new approach is known as density functional theory (DFT). The electronic wavefunction Ψ_{elec} that appears in the electronic Schrödinger equation is a function of the positions of all of the electrons. The electronic density is a function that indicates where the electronic charge in the molecule is located with respect to the various atomic nuclei. The Born–Oppenheimer approximation applies to the electronic density function just as it does to wavefunctions based quantum mechanics. Again, note that the electronic Schrödinger equation yields $E_{\text{elec}}(\mathbf{S})$, the electronic energy at given geometrical configurations \mathbf{S} of the nuclei, which is the isotope independent potential function for vibrational motion. The Kohn Hohenberg Theorem states that the solution of this problem depends only on the electron density. However, the theorem does not tell one how to calculate the energy from the electron density. Thus, the “fly in the ointment”, as far as DFT is concerned, is that we don’t know the functional, that is at least we don’t know the exact functional. However, approximate functionals have been developed which work quite well. The fact that the exact functional is not known means that DFT is not fully an “a priori theory”. A discussion of functionals is beyond the scope of this book. In our experience and that of a large chemistry community, the functional known as B3LYP “works quite well” and is adequate for our purpose; we use it. Thus, while we refer to ordinary electronic structure calculations as HF (Hartree–Fock) or as MP2 and

CI (types of calculations with correlation), we refer to DFT calculations as B3LYP. For a more complete discussion of functions, functionals, and DFT see any recent text on quantum chemistry (e.g., Levine, reading list).

The molecular orbitals in ordinary Gaussian calculations are expanded in terms of Gaussian types of atomic orbitals, which are referred to as basis functions. These Gaussian orbitals are available for most atoms in the periodic table and are described in the manuals that are available for the various types of electronic structure programs now in wide use, among them g03. Larger sets of basis functions tend to yield better results for $E_{\text{elec}}(S)$. DFT calculations do not employ molecular orbitals; they do use Kohn–Sham orbitals, which in many ways are similar to molecular orbitals. The mathematics of determining the Kohn–Sham orbitals turns out to be similar to the mathematics of constructing molecular orbitals from Hartree–Fock calculations. In fact, once a computer program has been constructed to carry out Hartree–Fock calculations, that program can also be used to find the Kohn–Sham orbitals and the electron density which can be evaluated from these orbitals. Thus, both ordinary molecular orbital calculations and DFT calculations require the completion of a Hartree–Fock calculation. If one wants to go beyond Hartree–Fock to include correlation (say MP2 or CI), then one has to do a great deal of additional computation. If one is doing DFT, the calculation is almost complete at the Hartree–Fock level. Thus, the advantage of DFT is that it includes electron-correlation in a calculation which costs (in computer time) only about as much as a Hartree–Fock calculation. MP2 and CI (and other types of calculation including electron correlation) are much more expensive. As noted, the basis sets are discussed in the relevant computer program manuals. The basis sets are the same in both types of calculations. Larger basis sets tend to have longer names and should give better results. The basis sets used in this book include ST0-3G (very minimal), 6–31G, 6–311G, 6–311**G. These are the so called Pople type basis sets. Other computer programs often refer to available basis sets in terms of g03 calculations.

References/Suggestions for Further Reading

- Born, M. and Oppenheimer, J. R. Zur Quantentheorie der Molekeln. *Ann. D. Phys.* **84**, 457 (1927).
- Frisch, M. J., Trucks, G. W., Schlegel, H. B., Scuseria, G. E., Robb, M. A., Cheeseman, J. R., Montgomery, Jr., J. A., Vreven, T., Kudin, K. N., Burant, J. C., Millam, J. M., Iyengar, S. S., Tomasi, J., Barone, V., Mennucci, B., Cossi, M., Scalmani, G., Rega, N., Petersson, G. A., Nakatsuji, H., Hada, M., Ehara, M., Toyota, K., Fukuda, R., Hasegawa, J., Ishida, M., Nakajima, T., Honda, Y., Kitao, O., Nakai, H., Klene, M., Li, X., Knox, J. E., Hratchian, H. P., Cross, J. B., Bakken, V., Adamo, C., Jaramillo, J., Gomperts, R., Stratmann, R. E., Yazyev, O., Austin, A. J., Cammi, R., Pomelli, C., Ochterski, J. W., Ayala, P. Y., Morokuma, K., Voth, G. A., Salvador, P., Dannenberg, J. J., Zakrzewski, V. G., Dapprich, S., Daniels, A. D., Strain, M. C., Farkas, O., Malick, D. K., Rabuck, A. D., Raghavachari, K., Foresman, J. B., Ortiz, J. V., Cui, Q., Baboul, A. G., Clifford, S., Cioslowski, J., Stefanov, B. B., Liu, G., Liashenko, A., Piskorz, P., Komaromi, I., Martin, R. L., Fox, D. J., Keith, T., Al-Laham, M. A., Peng, C. Y., Nanayakkara, A., Challacombe, M., Gill, P. M. W., Johnson, B., Chen, W., Wong, M. W., Gonzalez, C., and Pople, J. A.: Gaussian 03, Revision C.02, Gaussian, Inc., Wallingford CT, 2004.

- Hammett, L. P. *Physical Organic Chemistry*, McGraw-Hill, New York (1940); *Chem. Rev.* **17**, 125 (1935).
- Levine, I. M. *Quantum Chemistry*, 6th Ed. Prentice-Hall, Saddle River, NJ (2009).
- Taft, R. W. and Lewis, I. C. The general applicability of a fixed scale of inductive effects. II. Inductive effects of dipolar substituents in the reactivities of m- and p-substituted derivatives of benzene. *J. Am. Chem. Soc.* **80**, 2436 (1958).
- Wolfsberg, M. In Kohen, A. and Limbach, Eds. *Isotope Effects in Chemistry and Biology*, CRC Taylor & Francis, Boca Raton, FL (2006), Chapter 3, p. 89.

Chapter 3

Molecular Vibrations

Abstract The theory of molecular vibrations of molecular systems, particularly in the harmonic approximation, is outlined. Application to the calculation of isotope effects on equilibrium and kinetics is discussed.

3.1 Introduction

The most isotope sensitive motions in molecules are the vibrations, and many thermodynamic and kinetic isotope effects are determined by isotope effects on vibrational frequencies. For that reason it is essential that we have a thorough understanding of the vibrational properties of molecules and their isotope dependence. To that purpose Sections 3.1.1, 3.1.2 and 3.2 present the essentials required for calculations of vibrational frequencies, isotope effects on vibrational frequencies (and by implication calculation of isotope effects on thermodynamic and kinetic properties). Sections 3.3 and 3.4, and Appendices 3.A1 and 3.A2 treat the polyatomic vibrational problem in more detail. Students interested primarily in the results of vibrational calculations, and not in the details by which those results have been obtained, are advised to give these sections “the once-over lightly”.

3.1.1 *Vibrations in Diatomic Molecules*

Consider a stable diatomic molecule with nuclei denoted as A and B. The Born–Oppenheimer potential V for such a molecule will depend on the internuclear distance r_{AB} and will typically have the form shown in Fig. 3.1. The potential energy has a minimum at r_0 , which is often referred to as the equilibrium internuclear distance. As the distance r_{AB} increases, the potential V increases and finally reaches a limiting value where the molecule is now better described as two separated atoms (or depending on the electronic state of the system, two separated atomic species one or both of which may be ions). The difference in energy between the two separated atoms and the minimum of the potential is the dissociation energy D_e of the molecule. As the internuclear distance of the diatomic molecule is decreased

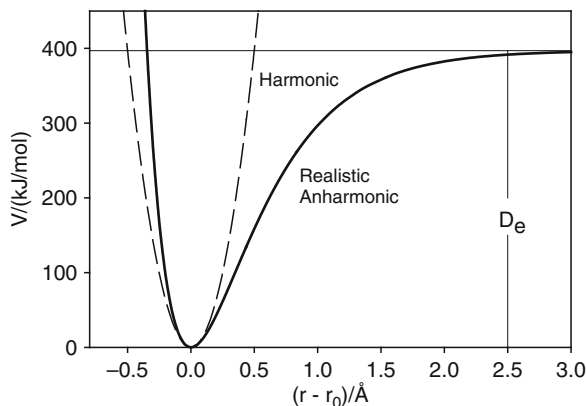


Fig. 3.1 Born–Oppenheimer vibrational potentials for a diatomic molecule corresponding to the CH fragment. The experimentally realistic anharmonic potential (*solid line*) is accurately described by the Morse function $V_{\text{MORSE}} = D_e[1 - \exp(a(r - r_0))]^2$ with $D_e = 397 \text{ kJ/mol}$, $a = 2 \text{ \AA}^{-1}$ and $r_0 = 1.086 \text{ \AA}$ ($\text{\AA} = \text{Angstrom} = 10^{-10} \text{ m}$). Near the origin the BO potential is adequately approximated by the harmonic oscillator (Hooke’s Law) function (*dashed line*), $V_{\text{HARM OSC}} = f(r - r_0)^2/2$. The harmonic oscillator force constant $f = 2a^2D_e$.

from the equilibrium internuclear distance, the potential rises at an ever increasing rate and tends to infinity as the internuclear distance tends toward zero.

At r_0 , the first derivative of the potential energy with respect to r_{AB} vanishes (the potential is at a minimum) The second derivative of the potential with respect to distance is the first non-vanishing derivative and is referred to as a force constant, designated here as f . If one replaces the potential of Fig. 3.1 by a curve with a minimum at r_0 , a second derivative equal to f , and no higher derivatives, i.e. if one replaces the Born–Oppenheimer potential by the parabola

$$V = \frac{1}{2}f(r - r_0)^2 \quad (3.1)$$

one is then working in the harmonic approximation. Equation 3.1 is also known as Hooke’s Law. For stable molecules at room temperature and below the harmonic approximation is usually appropriate. The harmonic potential, Equation 3.1, is depicted in Fig. 3.1 as a dashed curve, labeled V_{harmonic} . Much of the discussion in this chapter will be carried out in the harmonic approximation. It was noted in the previous chapter that the Born–Oppenheimer potential is independent of isotopic substitution. Consequently in the harmonic approximation the force constant of various isotopic isomers of a given molecule are all the same, for example in the case of HCl, $f(\text{H}^{35}\text{Cl}) = f(\text{H}^{37}\text{Cl}) = f(\text{D}^{35}\text{Cl}) = f(\text{D}^{37}\text{Cl})$.

As pointed out in Chapter 2, nuclear motion takes place on the Born–Oppenheimer potential surface. The motion of the center of mass (corresponding to translation) rigorously separates from the other motions of the atoms. Translational motion may be subject to a potential corresponding to the fact that the molecule

may move within an enclosure (a “bottle”). To good approximation, one can usually consider rotation to be independent of vibration although evidence of some rotational–vibrational interaction is found in rotational spectroscopy.

Consider now the vibration of the AB diatomic molecule. The potential energy of vibration depends on the displacement of the diatomic molecule internuclear distance from its equilibrium value, $S = r - r_e$. The kinetic energy involves the velocity (time derivative), $\dot{S} = d(r - r_e)/dt$, and is given by

$$T = \frac{1}{2} \mu \dot{S}^2 \quad (3.2)$$

where μ is the reduced mass of the diatomic molecule

$$\mu = \frac{m_A m_B}{m_A + m_B} \quad (3.3)$$

It is mentioned in passing that the proper masses m_A and m_B to be used in Equation 3.3 are the atomic masses (nucleus + electrons) rather than the respective nuclear masses as might be expected from a strict Born–Oppenheimer approximation. For further discussion of this point, reference should be made to the reading lists at the end of this chapter and of Chapter 2. The combination of Equations 3.1 and 3.2 corresponds to a classical harmonic oscillator with force constant f and mass μ . The harmonic oscillator frequency ν is given by the well-known formula

$$\nu = \frac{1}{2\pi} \sqrt{\frac{f}{\mu}} \quad (3.4)$$

The motion in the classical domain corresponds to a harmonic oscillator of frequency ν , with the displacement from equilibrium varying sinusoidally with time. The transcription of this problem into quantum mechanics is simple and straightforward; it is a standard problem in introductory quantum mechanics texts. The energy levels of the quantum system are given by

$$E_n = \left(n + \frac{1}{2} \right) h\nu \quad n = 0, 1, 2, \dots \quad (3.5)$$

where ν is the classical frequency, and n is a quantum number with the ground or bottom-most state corresponding to $n = 0$. The ground state energy, $\frac{1}{2}h\nu$, referred to as the zero-point energy, corresponds to an energy greater than that of the non-oscillating classical system ($E_{((r-re)=0)} = 0$). The solution of the classical mechanical problem yields harmonic motion with frequency ν and transcription to quantum mechanics gives rise to quantized energy levels which depend on the classical vibrational frequency. Thus, the solution of the classical problem includes the vibrational frequency, which is needed in the formula for the quantum energy levels. This conclusion carries over to the vibrational problem of polyatomic molecules in the harmonic approximation. As will be seen shortly, the solution of the general

non-linear N -atomic harmonic molecule gives rise to $3N - 6$ normal mode harmonic frequencies. For this general molecule, the determination of these classical frequencies requires more mathematical manipulation than it does for the diatomic harmonic oscillator. However, once the classical system is solved, the transcription to quantum mechanics requires only the understanding that there are quantum energy levels for each of the normal modes of vibration with corresponding normal mode frequencies ν_i and quantum numbers n_i corresponding to each of the normal modes. Thus, the problem that requires some mathematical sophistication (namely finding the normal mode frequencies ν_i) is a purely classical problem. The quantization of the energy levels requires little or no further effort.

Obviously, there is an isotope effect on the vibrational frequency ν_i . For heteroatomic molecules (e.g. HCl and DCl), infrared spectroscopy permits the experimental observation of the molecular frequencies for two isotopomers. What does one learn from the experimental observation of the diatomic molecule frequencies of HCl and DCl? To the extent that the theoretical consequences of the Born–Oppenheimer Approximation have been correctly developed here, one can deduce the diatomic molecule force constant f from either observation and the force constant will be independent of whether HCl or DCl was employed and, for that matter, which isotope of chlorine corresponded to the measurement as long as the masses of the relevant isotopes are known. Thus, from the point of view of isotope effects, the study of vibrational frequencies of isotopic isomers of diatomic molecules is a study involving the confirmation of the Born–Oppenheimer Approximation.

3.1.2 *Extension to Polyatomics*

3.1.2.1 **Degrees of Freedom**

The situation described above for diatomics is different for polyatomic molecules. Proper description of the motion of each atom in a molecule requires the use of three degrees of freedom (for example the x , y , and z Cartesian coordinates), so for the N -atomic molecule a total of $3N$ degrees of freedom corresponding to nuclear (atomic) motion are required. Three of these degrees of freedom correspond to the x , y , and z translations of the center of mass. For a non-linear molecule, there are three degrees of freedom that correspond to the rotation of the molecule; for a linear molecule there are only two. The remaining degrees of freedom, $3N - 6$ ($\{3N - 5\}$ for a linear molecule), correspond to molecular vibrations. Thus, the triatomic water molecule has three translational, three rotational, and three vibrational degrees of freedom.

3.1.2.2 **Coordinate Systems**

While it is possible to solve the vibrational problem using any one of a number of coordinate systems (Cartesian coordinates, spherical polar coordinates, valence coordinates, etc.), it is often most convenient to employ some type of valence

coordinate system. In this approach one chooses a set of $3N - 6$ ($3N - 5$ for linear molecules) independent (orthogonal) displacement coordinates to describe the motions of the various atoms in the molecule. These, for example, might be bond extensions, angle distortions, torsional motions, etc. In any case the physical problem must be independent of the (always arbitrary) choice of coordinates used to describe that problem. It is possible, although not always convenient to transform the problem from one coordinate system to another, the mathematical details are described in introductory texts on molecular spectroscopy (see the reading list at the end of this chapter).

For a simple molecule like water the choice of valence coordinates is straightforward. For water three valence displacement coordinates are required: Δr_1 the displacement of one of the O–H bond distances from its equilibrium value, Δr_2 the corresponding displacement of the other bond length, and $\Delta \alpha$ the displacement of the bond angle bend from its equilibrium value. These three coordinates are independent and one can discuss the three vibrational degrees of freedom of the water molecule in terms of these three coordinates (*vide infra*). The harmonic potential function is a quadratic expression in terms of these displacements (as in the case of the diatomic molecule) but, unlike the case of a diatomic molecule, there are interaction force constants, $f_{rr'}$ and $f_{r\alpha}$, which couple the two stretching motions and the stretches and the bends, in addition to the pure stretching and bending force constants, f_{rr} and $f_{\alpha\alpha}$. Thus, the Born–Oppenheimer potential function for the water molecule in the harmonic approximation has the form

$$V = \frac{1}{2}f_{rr}((\Delta r_1)^2 + (\Delta r_2)^2) + \frac{1}{2}f_{\alpha\alpha}(\Delta \alpha)^2 + f_{rr'}(\Delta r_1 \Delta r_2) + f_{r\alpha}(\Delta r_1 \Delta \alpha + \Delta r_2 \Delta \alpha) \quad (3.6)$$

It will be noted that the force constants reflect the symmetry of the water molecule in its equilibrium configuration with two equal equilibrium O–H distances.

3.1.2.3 Vibrations of Water Isotopomers

How one obtains the three normal mode vibrational frequencies of the water molecule corresponding to the three vibrational degrees of freedom of the water molecule will be the subject of the following section. The H_2O molecule has three normal vibrational frequencies which can be determined by vibrational spectroscopy. There are four force constants in the harmonic force field that are not known (see Equation 3.6). The values of four force constants cannot be determined from three observed frequencies. One needs additional information about the potential function in order to determine all four force constants. Here comes one of the first applications of isotope effects. If one has frequencies for both H_2O and D_2O , one knows that these frequencies result from different atomic masses vibrating on the same potential function within the Born–Oppenheimer approximation. Thus, we

now have six frequencies and still only four force constants. Here the isotope effect is a tool for obtaining information about the isotope independent force fields on which isotopomers vibrate.

3.1.3 *Remarks*

The vibrational frequencies of isotopic isotopomers obey certain combining rules (such as the Teller–Redlich product rule which states that the ratio of the products of the frequencies of two isotopic isotopomers depends only on molecular geometry and atomic masses). As a consequence not all of the $2(3N - 6)$ normal mode frequencies in a given isotopomer pair provide independent information. Even for a simple case like water with only three frequencies and four force constants, it is better to know the frequencies for three or more isotopic isotopomers in order to deduce values of the harmonic force constants. One of the difficulties is that the exact normal mode (harmonic) frequencies need to be determined from spectroscopic information and this process involves some uncertainty. Thus, in the end, there is no isotope independent force field that leads to perfect agreement with experimental results. One looks for a best fit of all the data. At the end of this chapter reference will be made to the extensive literature on the use of vibrational isotope effects to deduce isotope independent harmonic force constants from spectroscopic measurements.

It is important to point out here, in an early chapter, that the Born–Oppenheimer approximation leads to several of the major applications of isotope effect theory. For example the measurement of isotope effects on vapor pressures of isotopomers leads to an understanding of the differences in the isotope independent force fields of liquids (or solids) and the corresponding vapor molecules with which they are in equilibrium through use of statistical mechanical theories which involve vibrational motions on isotope independent potential functions. Similarly, when one goes on to the consideration of isotope effects on rate constants, one can obtain information about the isotope independent force constants which characterize the transition state, and how they compare with those of the reactants.

As will be shown further on, the most interesting isotope effects are quantum effects. Since the most important quantized motions in molecules are vibrations it makes sense that isotope effects yield information about the isotope independent surface (the vibrational force field) on which these quantized motions take place.

3.2 Discussion of Two Types of Coordinate Systems

The discussion of the previous section amounts to a qualitative treatment of harmonic vibrational motion. The harmonic potential function on which the molecule vibrates has been described in terms of displacement of bond stretches from the equilibrium configuration for the diatomic molecule; for water, displacement of

the bond angle from its equilibrium value has also been drawn into consideration. These types of coordinates, first proposed by N. Bjerrum, are known as valence coordinates. They are attractive to chemists because chemists have developed qualitative feelings about various types of bonds which are conveniently expressed in terms of valence coordinates. For instance, chemists know that CH bonds in alkanes are very similar and they expect that the corresponding stretching force constants in alkanes are similar. They also expect the stretching force constant for the C=C double bond in ethylene to be larger than the corresponding C-C stretching force constant in singly-bonded ethane. Also, when valence force coordinates were first introduced, it was expected that interaction force constants (e.g. $f_{rr'}$, $f_{r\alpha}$ in the water force field) would be much smaller than the diagonal force constants (e.g. f_r and f_α in the water force field). This expectation was pretty much fulfilled when calculations were carried out in order to deduce numerical force constants from spectroscopic data. Additionally, chemists intuitively expect that it is much more difficult to distort bond lengths than bond angles. This expectation is reflected in the relative magnitudes of bond stretching force constants and of bond angle bending force constants.

To solve the classical vibration problem for a molecule, one needs an expression for the vibrational kinetic energy in terms of time derivatives of the same coordinates that are used to express the potential energy. In Equation 3.1, the kinetic energy for the diatomic molecule is given in terms of the time derivative of the stretching coordinate. Although simple for the diatomic case, the analogous equations for polyatomic molecules using valence coordinates are much more complicated and may be tedious to solve. While a method for determining the appropriate kinetic energy expression in valence coordinates will be outlined in a following section, we want to emphasize here that the kinetic energy expression in Cartesian coordinates is very simple, and relatively easy to solve. The drawback with use of Cartesian coordinates is that the force constants which describe atom-atom distortions in this coordinate system have little appeal to chemists because they do not correspond to simple bond length extensions or angle distortions, and hence are difficult to translate into arguments based on chemical intuition. It is, of course, true that one can transform from one coordinate system to another. Yet, it is also true that vibrational calculations on molecular systems were almost exclusively done in valence coordinates until digital computers became widely available. Computers made it possible to calculate Born-Oppenheimer potentials for quite large molecules by carrying out electronic structure calculations. Two examples of widely available computer programs for carrying out such calculations are Gaussian and Turbomole. These programs have already been briefly discussed in Chapter 2. For the present discussion of electronic ground states, it suffices to point out that in these programs one can “optimize” the configuration of a molecule to find the equilibrium geometry. This optimization may be carried out either by varying valence coordinates or by varying the Cartesian coordinates of the nuclei to obtain the minimum of the energy of the system. This equilibrium geometry is, of course, the minimum of the isotope independent potential energy surface, which is the potential energy surface for vibrational motion. Quantum mechanical methods are used to calculate the second derivative of this potential at the minimum with respect to displacements in

Cartesian coordinates of the individual nuclei in the molecule from their respective positions at the minimum. These are the so-called Cartesian displacement coordinates. These second derivatives are the force constants of the Born–Oppenheimer approximation in this coordinate system and are the theoretical basis for harmonic calculations of the $3N - 6(3N - 5)$ harmonic vibrational frequencies of the isotopomers being considered. While the computer programs can (and do) translate the Cartesian force constants into valence displacement coordinates, it turns out that it is most convenient to carry out the calculation of the vibrational frequencies in Cartesian coordinates because of the simplicity of the kinetic energy expression for vibrational energy in these coordinates. The output of the Gaussian program (g03) produces a file with the Cartesian force constants. This output can be used directly to compute harmonic vibrational frequencies for isotopomers with desired isotopic substitution. One such program, THERMISTP, has been described by Wolfsberg (reading list). This program calculates isotope effects from molecular force constants calculated from Born–Oppenheimer surfaces using Gaussian03 or similar quantum mechanical packages (see Chapter 2). The calculation of the harmonic vibrational frequencies of a molecule from the isotope independent Cartesian force constants is briefly outlined in Section 3.3. In Section 3.4, the use of valence coordinate force constants is discussed. While it may seem that the discussion here indicates that Cartesian force constants should be preferred, one should bear in mind that, for certain types of calculations, valence coordinate force constants may be more convenient. For example, if one is trying to deduce numerical values of force constants through procedures to find best fits for observed infrared and Raman frequencies of isotopomers, convergence is much more rapid if one has ways of estimating “good” starting values for the force constants. Thus, the idea of transferability of force constants between similar molecules might lead to a preference for valence coordinates in this situation. In the end, however, keep in mind that it is always possible to transform from a potential expressed in one set of coordinates into an equivalent potential expressed in any other.

3.3 Calculations in Cartesian Coordinates

Take an N -atomic molecule with the nuclei each at their equilibrium internuclear position. Establish a Cartesian x , y , z coordinate system for each of the nuclei such that, for x_i with $i = 1, \dots, 3N$, x_1 is the Cartesian x displacement of nucleus 1, x_2 is the Cartesian y displacement coordinate for nucleus 1, x_3 is the Cartesian z displacement coordinate for nucleus 1, \dots , x_{3N} is the Cartesian z displacement for nucleus N . Use of one or another quantum chemistry program yields a set of force constants f_{ij} in Cartesian displacement coordinates

$$E_{\text{elec}} = \frac{1}{2} \sum_{ij}^{3N} f_{ij} x_i x_j \quad (3.7)$$

where

$$f_{ij} = \left(\frac{\partial^2 E_{\text{elec}}}{\partial x_i \partial x_j} \right)_{x_k, k \neq i, j} \quad (3.8)$$

One remembers that E_{elec} is the isotope independent potential energy surface for vibration in the Born–Oppenheimer approximation, $E_{\text{elec}} = V$. Note

$$\left(\frac{\partial^2 V}{\partial x_a \partial x_b} \right) = \left(\frac{\partial^2 V}{\partial x_b \partial x_a} \right) \quad (3.9)$$

so that the force constant matrix \mathbf{F} is symmetric (see Appendix 3.A1 for definitions of some matrix properties),

$$f_{ab} = f_{ba} \quad (3.10)$$

The classical kinetic energy T is given by the usual formula involving the time derivatives (velocities) of the Cartesian coordinates \dot{x}_i ,

$$T = \frac{1}{2} \sum_i^{3N} m_i \dot{x}_i^2 \quad (3.11)$$

In the numbering scheme used here $m_1 = m_2 = m_3 =$ mass of atom 1, etc., $m_{3N-2} = m_{3N-1}$, $m_{3N} =$ mass of atom N .

For convenience we introduce mass weighted coordinates (designated by a prime)

$$x'_i = \sqrt{m_i} x_i \text{ and } x_i = \frac{x'_i}{\sqrt{m_i}} \quad (3.12)$$

Then

$$E_{\text{elec}} = \frac{1}{2} \sum_{i,j}^{3N} \frac{f_{ij}}{\sqrt{m_i m_j}} x'_i x'_j \quad (3.13)$$

$$T = \frac{1}{2} \sum_i^{3N} \dot{x}'_i{}^2 \quad (3.14)$$

Again, for convenience, introduce a set of mass weighted force constants

$$f_{ij}^m = \frac{f_{ij}}{\sqrt{m_i m_j}} \quad (3.15)$$

Also note that E_{elec} is the potential energy for nuclear motion in the Born–Oppenheimer approximation. Thus the classical Hamiltonian H for nuclear (vibrational) motion is given by

$$H = T + V = \frac{1}{2} \sum_i^{3N} \dot{x}_i'^2 + \frac{1}{2} \sum_{i,j} f_{ij}^m x_i' x_j' \quad (3.16)$$

The second term on the right hand side of Equation 3.16 introduces complications because it couples x_i' and x_j' . The first term, on the other hand is easily solved because it involves no coupling. The resolution of the difficulty introduced by the second term is to take advantage of the symmetry of the f_{ij} matrix. Note that each f_{ij}^m is an element of a symmetric matrix and the second derivatives f_{ij} are independent of the order of differentiation. There is a well known mathematical theorem on the diagonalization of symmetric matrices which states (as applied to Equation 3.16) that when we introduce a new coordinate Q_i

$$Q_i = \sum_k^{3N} b_{ik} x_k \quad (3.17)$$

it is possible to find coefficients b_{ik} such that

$$\sum_{i,j} f_{ij}^m x_i' x_j' \text{ becomes } \sum_i^{3N} \lambda_i Q_i^2 \quad (3.18a)$$

while

$$\sum_i \dot{x}_i'^2 \text{ becomes } \sum_i \dot{Q}_i^2 \quad (3.18b)$$

This is explicitly demonstrated in Appendix 3.A2. The mathematical process involved is appropriately called a diagonalization because both the kinetic and the potential energy terms in Q_i only involve diagonal (squared) terms. Thus, in terms of the new coordinates which are usually called the normal coordinates

$$H = T + V = \frac{1}{2} \sum_i^{3N} \dot{Q}_i^2 + \frac{1}{2} \sum_i^{3N} \lambda_i Q_i^2 \quad (3.19a)$$

$$= \sum_{i=1}^{3N} \left(\frac{1}{2} \dot{Q}_i^2 + \frac{1}{2} \lambda_i Q_i^2 \right) \quad (3.19b)$$

So Equation 3.19 shows the Hamiltonian, the total energy function of classical mechanics, is the sum of $3N$ terms each of the form

$$\left(\frac{1}{2} \dot{Q}_i^2 + \frac{1}{2} \lambda_i Q_i^2 \right) \quad (3.20)$$

Note that λ_i is a numerical factor that arises from the diagonalization of the \mathbf{F}^m matrix. The λ_i 's are known as the eigenvalues of the \mathbf{F}^m matrix. The first term in Equation 3.20 is the kinetic energy and the second term is the potential energy for

the coordinate Q_i . We can immediately write down the classical equation of motion for Q_i from Newton's Second Law,

$$F = ma \quad (3.21)$$

with F , the force, and a the acceleration equal to

$$\frac{d}{dt}\dot{Q}_i = \ddot{Q}_i \quad (3.22)$$

The force can be derived from the potential energy by the classical equation

$$F = -\frac{\partial V}{\partial Q_i} = -\frac{\partial}{\partial Q_i} \left(\frac{1}{2} \lambda_i Q_i^2 \right) = -\lambda_i Q_i \quad (3.23)$$

Then Equation 3.21 becomes

$$-\lambda_i Q_i = \ddot{Q}_i \quad (3.24)$$

Here we have recognized that the effective mass corresponding to coordinate Q_i is unity since the kinetic energy is given by $\frac{1}{2}\dot{Q}_i^2 = \frac{1}{2}mv^2$. The solution of Equation 3.24, the equation of motion for a harmonic oscillator with a frequency ν_i , is

$$Q_i = K_i \cos \left(\lambda_i^{\frac{1}{2}} t + \delta_i \right) \quad (3.25)$$

with

$$\lambda_i^{\frac{1}{2}} = 2\pi \nu_i \quad (3.26)$$

In Equation 3.25, δ_i is a phase which can be determined from the boundary conditions at time $t = 0$, and K_i is the amplitude which can be determined from the energy of coordinate i . From Equation 3.25

$$\begin{aligned} H(\text{coordinate } i) &= \text{Energy}(\text{coordinate } i) \\ &= \frac{1}{2} \left(\lambda_i \sin^2 \left(\lambda_i^{1/2} t + \delta_i \right) + \lambda_i \cos^2 \left(\lambda_i^{1/2} t + \delta_i \right) \right) K_i^2 \\ &= \frac{1}{2} \lambda_i K_i^2 = 2\pi^2 \nu_i^2 K_i^2 \end{aligned} \quad (3.27)$$

Thus, the solution to the classical problem with the Hamiltonian (energy) function given by Equation 3.19 is a set of $3N$ harmonic oscillators with $3N$ frequencies $\lambda_i = 4\pi^2 \nu_i^2$. The λ_i 's result from the diagonalization of the \mathbf{F}' matrix of Equation 3.15.

The quantum mechanical approach to the problem is based on the Hamiltonian of Equation 3.19b with velocities \dot{Q}_i replaced by momenta P_i conjugate to the coordinate Q_i . P_i is classically defined

$$P_i = \frac{\partial T}{\partial \dot{Q}_i} = \dot{Q}_i \quad (3.28)$$

(Remember that the effective mass of coordinate Q_i is unity). In terms of momenta, the classical Hamiltonian is, from Equation 3.19,

$$H = \sum_{i=1}^{3N} \frac{1}{2} (P_i^2 + \lambda_i Q_i^2) \quad (3.29)$$

The Hamiltonian operator of quantum mechanics is then

$$H_{\text{op}} = \sum_{i=1}^{3N} \frac{1}{2} \left(-\hbar^2 \frac{\partial^2}{\partial Q_i^2} + \lambda_i Q_i^2 \right) \quad (3.30)$$

where we have replaced the operator $P_{\text{op},i}$ appropriately by

$$-i\hbar \left(\frac{\partial}{\partial Q_i} \right) \quad (3.31)$$

$$\hbar = \frac{h}{2\pi} \quad (3.32)$$

where h is Planck's constant.

The quantum mechanical problem is expressed by the Schrödinger equation

$$H_{\text{op},j} \psi_j = E_j \psi_j \quad (3.33)$$

where E_j are the quantized energy levels of the molecular system. Equation 3.30 corresponds to a sum of Hamiltonian operators for coordinates Q_i . The Schrödinger equation for any one coordinate Q_i is

$$\frac{1}{2} \left(-\hbar^2 \frac{\partial^2}{\partial Q_i^2} + \lambda_i Q_i^2 \right) \psi_i = E_i \psi_i \quad (3.34)$$

This is the Schrödinger for a harmonic oscillator with frequency ν_i corresponding to $\lambda_i = 4\pi^2\nu_i^2$. The energy levels for this system are given by

$$E_i = \left(n_i + \frac{1}{2} \right) h\nu_i \quad (3.35)$$

with the quantum number n_i having the possible values of 0, 1, 2, 3, ... The ground state has the zero-point energy ($n_i = 0$), E_0 ,

$$E_{0i} = \frac{1}{2} h\nu_i \quad (3.36)$$

It is easy to show, analogously to the classical system, the quantum problem also has solutions corresponding to $3N$ uncoupled harmonic oscillators. The total wave

function is just a product of individual harmonic oscillator wave functions and the total energy is expressed in terms of $3N$ quantum numbers n_i each of which can take values $0, 1, 2, 3, \dots$. Thus the energy levels of the molecular system are

$$E_{n,i} = \sum_{i=1}^{3N} \left(n_i + \frac{1}{2} \right) h\nu_i \quad n_i = 0, 1, 2, 3, \dots \quad (3.37)$$

Remember again the ν_i 's are obtained from the λ_i 's, which arise from the diagonalization of the \mathbf{F}' matrix, which is a classical problem.

3.3.1 Separation of Translation and Rotation from Vibration

We can now explore further the properties of the frequencies. The force constants f_{ij} are second derivatives of the electronic energy with respect to displacements of the Cartesian coordinates of the nuclei from their minimum energy positions (the so-called equilibrium configuration). Suppose that we displace all the nuclei by the same amount along the x-axis of an appropriate coordinate system. This motion would correspond to a translation of the molecule in the X direction. In this displacement, the nuclei do not move with respect to each other and there would be no energy change. The same will happen if we move the molecule in the Y direction or in the Z direction. There are three independent translations which are possible.

Also, each non-linear molecule has three principal axes around which it can rotate and any rotation of the molecule can be analyzed in terms of these rotations just as any translation of the molecule can be analyzed in terms of the three translations along X, Y and Z axes. For a linear molecule, there are only two independent rotations. Again, just as for a translation, a displacement of nuclei which corresponds to rotation does not lead to a change of E_{elec} of that molecule. As a consequence of this analysis there are SIX zeroes among the λ_i 's in Equation 3.19 for a non-linear molecule. For a linear molecule, there are only FIVE zero λ_i 's because there are only two rotations. Thus, again for emphasis, a non-linear N-atomic molecule has six zero frequencies and $3N - 6$ non-zero frequencies, while for a linear molecule the corresponding numbers are five and $3N - 5$. The mass associated with translational motion is the molecular mass. For rotation the appropriate masses are the principal moments of inertia corresponding to the principal axes of rotation. These are referred to as I_A, I_B, I_C . For a linear molecule, there are only two rotations and, moreover, the two principal axes are both perpendicular to the molecular axis and the corresponding moments of inertia are equal to each other. For a diatomic molecule A-B the moment of inertia is

$$I = \mu r_e^2 = \frac{m_A m_B}{m_A + m_B} r_e^2 \quad (3.38)$$

where r_e is the equilibrium bond distance.

3.4 Calculations Employing Valence (Internal) Coordinates

The well-known GF matrix technique of E. B. Wilson and his colleagues for calculating the harmonic frequencies of polyatomic molecules is based on the use of valence coordinates, also referred to as internal coordinates. What is presented here is merely a sketch of the method; a fuller discussion would require extensive use of matrix algebra, which is beyond the scope of this book. The appendix on matrices in this chapter serves only as a very short introduction to such methods. For details reference should be made to the classical work of E. B. Wilson, J. C. Decius and P. C. Cross (WDC) in the reading list.

From the prior discussion, it follows that valence coordinates S_t are displacement coordinates and include bond stretches and valence angle bends. Additionally, there are torsional coordinates defined by displacement from the equilibrium configuration of the angle between two planes containing three atoms each, one of which contains atoms 1, 2, and 3 and the other atoms 4, 5 and 6. For example in ethylene, which is planar, the two methylene groups (atoms 1, 2 and 3, and 4, 5 and 6) at equilibrium lie in the same plane but twist about the carbon-carbon bond joining atoms 2 and 5 thus periodically displacing the torsional angle from its equilibrium value of 0° with a frequency of 1027 cm^{-1} . There may also be other kinds of coordinate such as the vertical distance of a given atom from the plane defined by three other atoms. The coordinates for a given molecule may also be chosen as redundant (for convenience) or non-redundant. If the choice is non-redundant, there will be as many coordinates for the molecule as there are vibrational frequencies ($3N - 6$ or $3N - 5$ for an N-atomic molecule as appropriate). If the number of internal coordinates is larger than this, there will be a redundancy. This means that the coordinates are not independent. The use of redundant coordinates is often convenient for symmetry purposes. A thorough discussion of redundant coordinates is found in WDC (reading list). The coordinates are considered to be linearized, i.e. they are taken to be linearly related to Cartesian displacement coordinates. Thus,

$$S_t = \sum_{i=1}^{3N} B_{ti} x_i \quad (3.39)$$

where the x_i are Cartesian displacement coordinates. Here the matrix \mathbf{B} (see Appendix 3.A1 for discussion of matrices) has a number of rows equal to the number of internal coordinates and a number of columns equal to $3N$, with 1,2,3 referring to x, y, z coordinates of atom 1; 4, 5, 6 referring to atom 2; etc. Since the kinetic energy can be expressed exactly by a quadratic form of the time derivatives of x_i (i.e. the velocity), it follows that it can also be expressed in terms of valence coordinate velocities by a quadratic form. WDC introduced the \mathbf{G} matrix with elements given by

$$G_{ss'} = \sum_j^{3N} m_j^{-1} B_{sj} B_{s'j} \quad (3.40)$$

where m_j refers to the atomic mass associated with the Cartesian displacement coordinate, x_j . The kinetic energy expression in terms of valence coordinates is not as simple as the corresponding expression using Cartesian coordinates. In terms of momenta P_i conjugate to the internal coordinates S_i (Equation 3.28).

$$T = \frac{1}{2} \sum_{i,j} G_{i,j} P_i P_j \quad (3.41)$$

The contribution of the potential energy to the Hamiltonian is given in the harmonic approximation by

$$V = \frac{1}{2} \sum f_{ij} S_i S_j \quad (3.42)$$

where the f_{ij} are the harmonic force constants in valence coordinates. As when Cartesian force constants and Cartesian displacement coordinates were employed, one again finds $3N - 6$ ($3N - 5$ for a linear molecule) non-zero normal modes of vibration. Again the frequencies are related to the eigenvalues resulting from the diagonalization of a matrix, namely the eigenvalues of the matrix product (see Appendix 3.A1)

$$\mathbf{GF} = \lambda \mathbf{E} \quad (3.43)$$

In Equation 3.43 \mathbf{F} now is the matrix of the force constants in valence coordinates. Again one finds normal mode coordinates, Q_i , corresponding to the normal mode frequencies ν_i .

In fact, the result of Equation 3.43 not only applies to internal displacement coordinates but also to Cartesian displacements. The kinetic energy in terms of Cartesian coordinates (Equation 3.11) can easily be transformed into an expression in terms of Cartesian momenta (Equation 3.28)

$$P_{x_i} = m_i x_i \quad i = 1, \dots, 3N \quad (3.44)$$

Then, in terms of Cartesian momenta

$$2T = \sum \frac{P_i^2}{m_i} \quad (3.45)$$

so that the \mathbf{G} matrix in Cartesian momenta is a diagonal matrix with

$$g_{ij} = \frac{1}{m_i} \delta_{ij} \quad (3.46)$$

where

$$\delta_{ij} = 1 \quad \text{for } i = j \quad (3.47a)$$

$$= 0 \quad \text{for } i \neq j \quad (3.47b)$$

The matrix to be diagonalized for finding the vibrational frequencies is the matrix product of the above \mathbf{G} matrix for Cartesian coordinates and the corresponding \mathbf{F} matrix for Cartesian displacement coordinates. It is noted in passing that the \mathbf{GF} matrix is generally not symmetric, i.e.

$$(\mathbf{GF})_{ij} \neq (\mathbf{GF})_{ji} \quad (3.48)$$

The theorem on matrix diagonalization (Appendix 3.A2) applies only to symmetric matrices. This difficulty can be avoided by use of a method suggested by T. Mayezawa, attention to which has been drawn by Schachtschneider and Snyder (see References).

3.5 Two Important Rules for Harmonic Vibrational Frequencies

3.5.1 The Teller–Redlich Product Rule

There are two important rules involving harmonic vibrational frequencies that are well known to spectroscopists. They are important in the present context because they permit the simplification of some of the statistical mechanics results for isotopomers in Chapter 4. The first rule, the Teller–Redlich (TR) product rule, follows straightforwardly from Equation 3.A1.13 (Appendix 3.A1) if one remembers that $\Lambda_i = 4\pi^2\nu_i^2$ and that there are six frequencies for the non-linear molecule which are zero, three corresponding to translations in the X, Y, and Z directions, each with a mass dependence $(M)^{-\frac{1}{2}}$, and three rotations with mass dependence $I_A^{-\frac{1}{2}}$, $I_B^{-\frac{1}{2}}$, $I_C^{-\frac{1}{2}}$ (I = principal moment of inertia) respectively. It then follows for the ratio of the products of the Λ_i 's of two isotopomers

$$\prod_i^{3N} \Lambda_{1i} / \Lambda_{2i} = \prod_i^{3N-6} \left(\frac{\nu_{1i}}{\nu_{2i}} \right)^2 \left(\frac{M_2}{M_1} \right)^3 \left(\frac{I_{2A}I_{2B}I_{2C}}{I_{1A}I_{1B}I_{1C}} \right) = \prod_j^N \left(\frac{m_{2j}}{m_{1j}} \right)^3 \quad (3.49)$$

The subscripts 1 and 2 refer to the two isotopomers being compared. On the right hand side of the equation the product is over the N atoms of the molecule rather than the $3N$ Cartesian coordinates. From Equation 3.49, one obtains the Teller–Redlich product rule after some rearrangement

$$\prod_i^{3N-6} \left(\frac{\nu_{1i}}{\nu_{2i}} \right) = \left(\frac{M_1}{M_2} \right)^{3/2} \left(\frac{I_{1A}I_{1B}I_{1C}}{I_{2A}I_{2B}I_{2C}} \right)^{1/2} \prod_{j=1}^N \left(\frac{m_{2j}}{m_{1j}} \right)^{3/2} \quad (3.50)$$

For a non-linear molecule, there are only $3N - 5$ frequencies and two moments of inertia which are equal.

3.5.2 The Sum Rule

The second rule for isotopomer harmonic frequencies is the so-called Sum Rule which follows from Equation 3.A1.8. Equation 3.A1.8 relates the sum of the squares of all the frequencies to the sum of the diagonal matrix elements of the (**FG**) matrix diagonalized to obtain the frequencies. When mass weighted Cartesian displacement coordinates are used to calculate the vibration frequencies, this means that the sum of the Λ_i 's ($\Lambda_i = 4\pi^2\nu_i^2$) can be found as follows (Equation 3.51)

$$4\pi^2 \sum_i^{3N} \nu_i^2 = \sum_i^{3N} f'_{ii} = \sum_i^{3N} \frac{f_{ii}}{m_i} = \sum_i^N \frac{f_{xx_i} + f_{yy_i} + f_{zz_i}}{m_i} \quad (3.51)$$

where the f' force constants refer to mass weighted Cartesian coordinates and the f force constants to mass independent (ordinary) Cartesian displacement coordinates. Note that the diagonal force constants in mass weighted Cartesian coordinates refer only to the atomic mass of one atom (m_i) while off-diagonal constants involve two masses ($m_i m_j$)^{1/2}. The last equality in Equation 3.51 emphasizes that for each element referring to a given atomic mass, there are three diagonal force constants f_{xx} , f_{yy} and f_{zz} . We apply the formula to the case where the two isotopomers differ by the replacement of one particular atom with mass m_1^* by another isotope in Cartesian coordinates with mass m_2^* . We designate the sum of the three diagonal Cartesian force constants at the position of isotopic substitution

$$f^* = f_{xx}^* + f_{yy}^* + f_{zz}^* \quad (3.52)$$

and obtain for the difference between the sums of the squares of the frequencies

$$\sum (v_{1i}^2 - v_{2i}^2) = \frac{1}{4\pi^2} (f^*) \left(\frac{1}{m_1^*} - \frac{1}{m_2^*} \right) \quad (3.53)$$

The frequency sum here needs, of course, only to be taken over the $3N-6$ (or $3N-5$ for a linear molecule) non-zero frequencies of the molecule.

3.A1 Appendix: Matrix Operations

3.A1.1 Some Definitions

A matrix **B** contains matrix elements b_{ij} where i refers to the column of the matrix and j the row of the matrix. Thus, the three-dimensional square matrix is defined as follows,

$$\mathbf{B} = \begin{pmatrix} b_{11} & b_{12} & b_{13} \\ b_{21} & b_{22} & b_{23} \\ b_{31} & b_{32} & b_{33} \end{pmatrix} \quad (3.A1.1)$$

While matrices in this chapter are all square, there are also matrices with the number of columns not equal to the number of rows. Thus, there are column matrices (and row matrices). A column matrix has one column and a given number of rows. Thus, \mathbf{Y} below is a column matrix

$$\mathbf{Y} = \begin{pmatrix} y_{11} \\ y_{21} \\ y_{31} \end{pmatrix} \quad (3.A1.2)$$

Matrix multiplication is a defined operation. Given two matrices \mathbf{A} and \mathbf{B} , the product is \mathbf{C} means

$$\mathbf{A}\mathbf{B} = \mathbf{C} \quad (3.A1.3)$$

$$c_{ij} = \sum_k a_{ik} b_{kj} \quad (3.A1.4)$$

To find the ij element of the product, one multiplies the i th row of \mathbf{A} , term by term, with the j th column of \mathbf{B} . To form the product of the two matrices, the number of columns of the first matrix must equal the number of rows of the second matrix.

The inverse of \mathbf{B} is called \mathbf{B}^{-1} . \mathbf{B}^{-1} has the property that

$$\mathbf{B}\mathbf{B}^{-1} = \mathbf{B}^{-1}\mathbf{B} = \mathbf{1} \quad (3.A1.5)$$

$\mathbf{1}$ here is the unit matrix. It has unity in the diagonal elements ($i = j$) and zero everywhere else. The transpose of a matrix \mathbf{A} is called \mathbf{A}' and is obtained from \mathbf{A} by exchanging rows and columns. Thus

$$\mathbf{B} = \mathbf{A}' \quad (3.A1.6a)$$

$$b_{ij} = a_{ji} \quad (3.A1.6b)$$

3.A1.2 Matrix Diagonalization

Matrix diagonalization of \mathbf{F}^m requires finding a matrix \mathbf{B} such that

$$\mathbf{B}^{-1} \mathbf{F}^m \mathbf{B} = \begin{pmatrix} \lambda_1 & 0 & 0 & 0 & 0 \\ 0 & \lambda_2 & 0 & 0 & 0 \\ 0 & 0 & \lambda_3 & 0 & 0 \\ 0 & 0 & 0 & \dots & 0 \\ 0 & 0 & 0 & 0 & \lambda_N \end{pmatrix} \quad (3.A1.7)$$

where \mathbf{B} , \mathbf{B}^{-1} , \mathbf{F}^m are all N -dimensional square matrices. The triple product has $\lambda_1, 2, \dots, \lambda_N$ along the diagonals and zeros everywhere else. The λ_i 's are known as the eigenvalues of the matrix \mathbf{F}^m . It can be shown that the sum of the eigenvalues of \mathbf{F}^m is the sum of the diagonal elements of \mathbf{F}^m . This means

$$\sum_i \lambda_i = \sum_j f_{jj}^m \quad (3.A1.8)$$

It can also be shown that the product of the eigenvalues is given by the determinant of \mathbf{F}^m ,

$$\prod_i \lambda_i = \det \mathbf{F}^m \quad (3.A1.9)$$

The theorem on matrix diagonalization states that symmetric matrices can be diagonalized and, moreover, \mathbf{B} can be taken such that

$$\mathbf{B}^{-1} = \mathbf{B}' \quad (3.A1.10)$$

A matrix \mathbf{B} that has this property is called an orthogonal matrix.

In the following it will be shown how matrix diagonalization enters the problem of harmonic vibrational motion of molecules, specifically when mass weighted Cartesian coordinates are employed (see Section 3.3). This analysis employs more matrix algebra than is generally used in this chapter. Some readers may prefer to skip this material on a first reading; those who do read it will be rewarded with a better understanding of the use of matrix diagonalization in the study of molecular vibrations.

Equation (3.16) presents expressions for the kinetic T and potential V energies in Cartesian mass weighted displacement coordinates x'_i and corresponding velocities \dot{x}'_i

$$2T = \sum_i \dot{x}'_i{}^2 \quad (3.A1.11)$$

$$2V = \sum_{i,j} f_{ij}^m x'_i x'_j \quad (3.A1.12)$$

Given that a matrix diagonalization (Equation 3.A1.7) of the matrix \mathbf{F}^m has been carried out with the matrix \mathbf{B} to yield eigenvalues λ_i , investigate now what happens to the expressions for T and V when new coordinates and corresponding velocities, Q_i and \dot{Q}_i , are introduced

$$x'_i = \sum_k b_{ik} Q_k \quad \dot{x}'_i = \sum_k b_{ik} \dot{Q}_k \quad (3.A1.13)$$

where the b_{ik} 's are the elements of the \mathbf{B} matrix. First look at Equation 3.A1.12

$$2V = \sum_i f_i^m \sum_k b_{ik} Q_k \sum_s b_{js} Q_s \quad (3.A1.14a)$$

$$= \sum_{i,j,k,s} f_{ij}^m b_{ik} b_{js} Q_k Q_s \quad (3.A1.14b)$$

$$= \sum_{i,j,k,s} b'_{ki} f_{ij}^m b_{js} Q_k Q_s \quad (3.A1.14c)$$

$$= \sum_{k,s} (\mathbf{B}' \mathbf{F}^m \mathbf{B})_{ks} Q_k Q_s \quad (3.A1.14d)$$

$$= \sum_k \lambda_k Q_k \quad (3.A1.14e)$$

In Equation 3.A1.14b it has been indicated that the sum is independent of the order of summation. In Equation 3.A1.14c, the order of the terms has been interchanged for convenience and the transpose of the \mathbf{B} matrix has been introduced, $b_{ik} = b'_{ki}$. In Equation 3.A1.14d, it has been recognized that the sum over i and j carried out in Equation 3.A1.14c produces the ks 'th element of the triple matrix product $\mathbf{B}' \mathbf{F}^m \mathbf{B}$. In Equation 3.A1.14e, we see that \mathbf{B}' in Equation 3.A1.14d is identical to \mathbf{B}^{-1} and therefore the triple matrix product is just the diagonal matrix from the right hand side of Equation 3.A1.7. Thus, the matrix diagonalization has led to a coordinate transformation, which makes the potential a sum of square terms.

Next look at what happens to Equation 3.11 when the transformation 3.A1.13 is introduced

$$2T = \sum_i \sum_k b_{ik} \dot{Q}_k \sum_s b_{is} \dot{Q}_s \quad (3.A1.15a)$$

$$= \sum_{i,k,s} b_{ik} b_{is} \dot{Q}_k \dot{Q}_s \quad (3.A1.15b)$$

$$= \sum_{i,k,s} (b'_{ki} b_{is}) \dot{Q}_k \dot{Q}_s \quad (3.A1.15c)$$

$$= \sum_{k,s} (\mathbf{B}' \mathbf{B})_{ks} \dot{Q}_k \dot{Q}_s \quad (3.A1.15d)$$

$$= \sum_k \dot{Q}_k^2 \quad (3.A1.15e)$$

Again, in Equation 3.A1.15b, it is indicated that the sum is independent of the order of the summation. In Equation 3.A1.15c the order of the terms has been changed to produce a convenient expression and the transpose of the \mathbf{B} matrix has been introduced, $b'_{ki} = b_{ik}$. In Equation 3.A1.15d, we see that the sum over i produces the ks 'th element of the matrix product $\mathbf{B}' \mathbf{B}$. Lastly, in Equation 3.A1.15e, it is recognized that \mathbf{B}' is the inverse of \mathbf{B} and that the matrix product has only diagonal elements, all of which are equal to unity. Thus, the kinetic energy is a sum of

squares in both coordinate systems. The consequences of this transformation from mass weighted Cartesian coordinates x' to normal coordinates Q in the analysis of molecular vibrations and the treatment of redundant coordinates are discussed in WDC (reading list).

3.A2 An Equality for Use in the Derivation of the Teller–Redlich Product Rule

The relationship between the force constant matrix in Cartesian displacement coordinates \mathbf{F}_{ij} , and the force constant matrix for mass weighted Cartesian coordinates \mathbf{F}^m can be written as follows (only the first three rows and columns of the matrices are explicitly shown):

$$\begin{pmatrix} f_{11}^m & f_{12}^m & f_{13}^m \\ f_{21}^m & f_{22}^m & f_{23}^m \\ f_{31}^m & f_{32}^m & f_{33}^m \end{pmatrix} = \begin{pmatrix} \frac{f_{11}}{\sqrt{m_1 m_1}} & \frac{f_{12}}{\sqrt{m_1 m_2}} & \frac{f_{13}}{\sqrt{m_1 m_3}} \\ \frac{f_{21}}{\sqrt{m_2 m_1}} & \frac{f_{22}}{\sqrt{m_2 m_2}} & \frac{f_{23}}{\sqrt{m_2 m_3}} \\ \frac{f_{31}}{\sqrt{m_3 m_1}} & \frac{f_{32}}{\sqrt{m_3 m_2}} & \frac{f_{33}}{\sqrt{m_3 m_3}} \end{pmatrix} \quad (3.A2.1)$$

$$= \begin{pmatrix} \frac{1}{\sqrt{m_1}} & 0 & 0 \\ 0 & \frac{1}{\sqrt{m_2}} & 0 \\ 0 & 0 & \frac{1}{\sqrt{m_3}} \end{pmatrix} \begin{pmatrix} f_{11} & f_{12} & f_{13} \\ f_{21} & f_{22} & f_{23} \\ f_{31} & f_{32} & f_{33} \end{pmatrix} \begin{pmatrix} \frac{1}{\sqrt{m_1}} & 0 & 0 \\ 0 & \frac{1}{\sqrt{m_2}} & 0 \\ 0 & 0 & \frac{1}{\sqrt{m_3}} \end{pmatrix}$$

Assume now that weak forces have been applied to the molecular rotations and translations so that the eigenvalues λ_i of the \mathbf{F}^m matrix correspond to the $3N - 6$ ($3N - 5$ for a linear molecule) real frequencies $\lambda_i = 4\pi^2\nu_i^2$ of the molecule plus six (or five) very low frequencies (ordinarily calculated as zero frequencies) that correspond to translations and rotations, uncoupled from the larger molecular vibrations. Then, if one recognizes that: (1) the determinant of a diagonal matrix is just the product of its diagonal elements, and (2) if a matrix \mathbf{A} can be written as a matrix product of \mathbf{B} and \mathbf{C} , then

$$\det \mathbf{A} = (\det \mathbf{B})(\det \mathbf{C}) \quad (3.A2.2)$$

It follows that the determinant of a matrix is equal to the product of its eigenvalues and, furthermore,

$$\prod_i^{3N} \lambda_i = \prod_i^{3N} (m_i)^{-1} \det |\mathbf{F}| \quad (3.A2.3)$$

In the use of Equation 3.A2.3, it should be remembered that the f_{ij} force constants, which are the elements of \mathbf{F} , are isotope independent, as is the determinant.

Reading List

- Bernath, P. F. *Spectra of Atoms and Molecules. 2nd Ed.* Oxford University Press, Oxford (2005).
- Miyazawa, T. Symmetrization of secular determinant for normal vibration calculation. *J. Chem. Phys.* **29**, 246 (1958).
- Schachtsneider, J. H. and Snyder, R. G. Vibrational analysis of the n-paraffins – II: Normal coordinate calculations. *Spectrochim. Acta* **19**, 117 (1963).
- Wilson, E. B. Jr., Decius, J. C. and Cross, P. C. *Molecular Vibrations*, McGraw-Hill, New York (1955).
- Wolfsberg, M. *Comments on selected topics in isotope theoretical chemistry*. In: Kohen, A. and Limbach, H. H., Eds. *Isotope Effects in Chemistry and Biology*, CRC Press/Taylor & Francis, Boca Raton, FL (2006), Chapter 3, p. 89.

Chapter 4

Isotope Effects on Equilibrium Constants of Chemical Reactions; Transition State Theory of Isotope Effects

Abstract The statistical thermodynamic theory of isotope effects on chemical equilibrium constants is developed in detail. The extension of the method to treat kinetic isotope effects using the transition state model is briefly described.

4.1 Introduction

The understanding of isotope effects on chemical equilibria, condensed phase equilibria, isotope separation, rates of reaction, and geochemical and meteorological phenomena, share a common foundation, which is the statistical thermodynamic treatment of isotopic differences on the properties of equilibrating species. For that reason the theory of isotope effects on equilibrium constants will be explored in considerable detail in this chapter. The results will carry over to later chapters which treat kinetic isotope effects, condensed phase phenomena, isotope separation, geochemical and biological fractionation, etc.

The chapter starts with a brief review of thermodynamic principles as they apply to the concept of the chemical equilibrium. That section is followed by a short review of the use of statistical thermodynamics for the numerical calculation of thermodynamic equilibrium constants in terms of the chemical potential (often designated as μ). Lastly, this statistical mechanical development is applied to the calculation of isotope effects on equilibrium constants, and then extended to treat kinetic isotope effects using the transition state model. These applications will concentrate on equilibrium constants in the ideal gas phase with the molecules considered in the rigid rotor, harmonic oscillator approximation.

4.2 Brief Review of the Laws of Thermodynamics

4.2.1 *The First Law*

The first law of thermodynamics is the law of conservation of energy for a thermodynamic system. The “system” is that which is of interest. It is usually defined by the mole numbers n_i of the various molecular species in the system, the volume V ,

the pressure P , and the temperature T (in Kelvin). Everything outside of the system is considered as “surroundings”. The system plus the surroundings makes up the universe. The state of the system is defined by the molecules it contains, their respective mole numbers, as well as T , P and V . Two forms of energy change ΔU are considered: q , the heat added to the system, and w , the work done on the system. The work is usually restricted to PdV work, the work done by compressing the volume by an amount dV against a pressure P . Should it become necessary to consider other kinds of work additional terms may be required. The first law of thermodynamics states that

$$\Delta U = q + w \quad (4.1)$$

and furthermore, that ΔU going from a given initial state of the system to a given final state depends only on the initial and final state and is independent of the “path” taken to go from the initial to the final state; q and w individually do depend on the pathway. The energy U is consequently called a function of state. For a change of state in which there is no volume change, there will be no work ($w = 0$) and consequently ΔU is the heat added to the system for a process carried out at constant volume. (Following the custom employed in most modern thermodynamics texts, in this chapter we use the symbol U to denote the energy of (macroscopic) systems, reserving the symbols E and ϵ to denote microscopic energies throughout the balance of the text.)

It is appropriate at this point to define another function of state, the enthalpy H ,

$$H = U + PV \quad (4.2)$$

For a process carried out at constant pressure,

$$\Delta H = \Delta U + P\Delta V \quad (4.3)$$

For this process, the work done on the system is

$$w = -P\Delta V \quad (4.4)$$

Note the minus sign to indicate that work is done on the system when ΔV is negative. Combining Equations 4.1, 4.3, and 4.4, one obtains for a process at constant pressure

$$\Delta H = q \quad (4.5)$$

so ΔH is the heat added to the system at constant pressure.

4.2.2 *The Second Law*

The second law of thermodynamics introduces a new function of state, the entropy, S , in order to quantify the spontaneity and direction of change for natural systems

(plus their surroundings), and the conditions of the equilibrium state toward which change occurs. It is useful to contrast natural changes, always spontaneous and irreversible to some extent, with idealized reversible processes (ones capable of restoring system plus surroundings to their original condition). Thus, a gas at pressure P expanding against an external pressure, which is kept throughout the expansion at a pressure infinitesimally smaller than the pressure of the gas, is a typical example of a reversible process. A truly reversible process would be carried out infinitely slowly. During a reversible expansion (or compression) for example, the thermodynamic parameters (T , P , V , concentrations) of the system are completely defined at each step. A spontaneous process is one that happens naturally and unidirectionally. Thus, the expansion of gas into a vacuum is a spontaneous process; so is the temperature equilibration between a hot material and a cold material when they are brought together. The second law of thermodynamics may be stated as follows:

There exists a thermodynamic function S , called the entropy, such that the change in entropy ΔS in going from an initial state i to a final state f has the following property

$$\Delta S \geq \int_i^f \frac{\delta q}{T} \quad (4.6)$$

where T is the temperature and δq is the incremental addition of the heat added to the system at T .

The equal sign in Equation 4.6 only applies if the process is carried out reversibly. Note that Equation 4.6 contains the recipe for obtaining ΔS exactly by carrying out the change of state reversibly.

It follows from Equation 4.6 for a thermally isolated system (hence $q = 0$) that

$$\Delta S \geq 0 \quad (4.7)$$

The universe is a thermally isolated system. Hence one can write

$$\Delta S_{\text{universe}} \geq 0 \quad (4.8)$$

It can be shown that Equation 4.6 can also be derived from Equation 4.8, so Equation 4.8 is an alternate statement of the second law.

4.2.3 *The Third Law*

There is a third law of thermodynamics. It can be stated in the following way: “The entropy of a perfect crystal at 0 K is zero.” A perfect crystal is one with no lattice defects. The third law gives rise to the concept of absolute entropy. There will be no further mention of the third law in this book.

4.3 The Free Energies and the Concept of Equilibrium

When a system cannot undergo a change of state in which the entropy of the universe (S_{universe}) increases, then that system is said to be at equilibrium. Implementation of this criterion of equilibrium requires one to quantitatively examine both the system and its surroundings, and this is often inconvenient or impossible. The introduction of the free energy functions, however, permits one to make statements about $\Delta S_{\text{universe}}$ for certain special systems without explicitly considering the surroundings, and this is a great convenience. The specialized systems considered here are those at constant volume and constant temperature, or constant pressure and constant temperature.

4.3.1 The Helmholtz Free Energy

For a system at constant volume, there can be no $P\Delta V$ work and, since the only work we are presently considering is $P\Delta V$ work, $w = 0$. Therefore, from the first law of thermodynamics

$$\Delta U = q \quad (4.9)$$

It follows from Equation 4.6, for a system at constant temperature, that

$$\Delta S \geq \frac{q}{T} \quad (4.10)$$

or

$$q \leq T\Delta S \quad (4.11)$$

Hence, from Equation 4.9

$$\Delta U - T\Delta S = q - T\Delta S \leq 0 \quad (4.12)$$

Define, now, a new thermodynamic function, the Helmholtz free energy A ,

$$A = U - TS \quad (4.13)$$

For a system at constant temperature with no PdV work, the second law states

$$\Delta A = \Delta U - T\Delta S \leq 0 \quad (4.14)$$

where the equal sign applies to a reversible process, and the inequality applies to all other (irreversible) processes. Thus, for a system at constant volume and constant temperature, the Helmholtz free energy will decrease until it reaches a minimum, at which point the system is said to be at equilibrium.

4.3.2 *The Gibbs Free Energy*

Similarly we consider a system held at constant temperature and constant pressure, where the process of interest involves adding an amount of heat q to the system and also an amount of work

$$w = -P\Delta V = -\Delta(PV) \quad (4.15)$$

Then, from the first law and Equation 4.11

$$\Delta U = q + w \leq T\Delta S - \Delta(PV) \quad (4.16)$$

so that

$$\Delta U + \Delta(PV) - T\Delta S \leq 0 \quad (4.17)$$

Finally, remembering the definition of enthalpy H (Equation 4.2)

$$H = U + PV \quad (4.18)$$

one obtains

$$\Delta H - T\Delta S \leq 0 \quad (4.19)$$

Note that ΔH is the heat absorbed by the system in a process carried out at constant T and P .

Now introduce the Gibbs free energy G

$$G = H - TS \quad (4.20)$$

So that, for a system at constant T and P , the second law states

$$\Delta G \leq 0 \quad (4.21)$$

where the equal sign applies to a system in equilibrium, and the inequality applies to irreversible processes.

4.3.3 *Relations Involving A , ΔA , G and ΔG*

Let us investigate free energies a bit further by writing relevant expressions for the differentials ΔA and ΔG employing the definitions 4.13 and 4.20. With use of the rules of differential calculus

$$dA = dU - TdS - SdT \quad (4.22)$$

From Equation 4.1

$$dU = \delta q + \delta w \quad (4.23)$$

where a small change in U , a function of state, is indicated by dU while a small quantity of heat energy q and work energy w (both of which depend on the pathway taken from the energy state U to that with energy $U + dU$) are expressed by δq and δw , respectively. (The symbol “ δ ” specifies the derivatives as inexact.) If a reversible pathway is taken between the two states, then from the definition of entropy S , Equation 4.11, $dq_{\text{rev}} = TdS$ while the corresponding work is given by $-PdV$. Thus Equation 4.13 becomes

$$dU = TdS - PdV \quad (4.24)$$

Correspondingly Equation 4.22 becomes

$$dA = TdS - PdV - TdS - SdT \quad (4.25)$$

$$dA = -PdV - SdT \quad (4.26)$$

Thus the differential of A has been obtained in terms of the changes in volume and temperature. The partial derivatives of A are given by

$$\left(\frac{\partial A}{\partial V}\right)_T = -P \quad (4.27)$$

and

$$\left(\frac{\partial A}{\partial T}\right)_V = -S \quad (4.28)$$

For a system containing n_i moles of molecular species i , one can then write for the differential dA of A

$$dA = -PdV - SdT + \sum_i dn_i \left(\frac{\partial A}{\partial n_i}\right)_{T,V,n_j \neq i} \quad (4.29)$$

One can similarly derive for the differential of the Gibbs free energy

$$dG = VdP - SdT + \sum_i dn_i \left(\frac{\partial G}{\partial n_i}\right)_{T,P,n_j \neq i} \quad (4.30)$$

In both Equations 4.29 and 4.30, the subscript $n_j \neq n_i$ in the partial derivatives signifies that all mole numbers are kept constant except that of molecule i .

From Equations 4.13, 4.18, and 4.20, it follows that

$$G = A + PV \quad (4.31)$$

and

$$dG = dA + PdV + VdP \quad (4.32)$$

$$= VdP - SdT + \sum_i dn_i \left(\frac{\partial A}{\partial n_i}\right)_{T,V,n_j \neq i} \quad (4.33)$$

Comparing Equations 4.30 and 4.33, one finds

$$\left(\frac{\partial A}{\partial n_i}\right)_{T,V,n_j \neq n_i} = \left(\frac{\partial G}{\partial n_i}\right)_{T,P,n_j \neq n_i} \quad (4.34)$$

The two partial derivatives in Equation 4.34, which are equal to each other, are very important in the thermodynamics of chemical equilibrium, and are referred to as the chemical potential, μ_i .

The combined first and second laws state that, at constant T and V, a system seeks to minimize A until dA for any subsequent change is zero (Equation 4.14), and likewise, at constant T and P, the Gibbs free energy decreases until dG for any subsequent change equals zero (Equation 4.20). One then recognizes that the condition for equilibrium is exactly the same at constant T and V as it is at constant T, P.

$$\sum_i \mu_i dn_i = 0 \quad (4.35)$$

Notice most often that studies on chemical equilibrium in the gas phase are carried out at constant T and V, while those involving only condensed phases will usually be studied at constant T and P. Condition 4.35 applies to either situation.

Consider now a system in which a chemical reaction is taking place



where the A, B, C, ... refer to the various molecular species in the system, and v_A , v_B , ... etc, refer to the relevant mole numbers in the reaction taking place. If one considers a differential extent of reaction $d\xi$ in Equation 4.36, proceeding from left to right, one obtains

$$\begin{aligned} dn_A &= -v_A d\xi \\ dn_B &= -v_B d\xi \\ dn_C &= +v_C d\xi \\ dn_D &= +v_D d\xi \end{aligned} \quad (4.37)$$

and further obtains at constant T and V, at equilibrium

$$\sum_i v_i \mu_i d\xi = 0 \quad (4.38)$$

since at equilibrium $dn_A = dn_B = dn_C = dn_D = 0$. The same equation is deduced at constant T and P, where the v_i refer to the mole numbers in Equation 4.36, the v_i 's being positive for products and negative for reactants. Since Equation 4.38 must hold for any value $d\xi$, it follows that the condition for equilibrium requires

$$\sum_i v_i \mu_i = 0 \quad (4.39)$$

4.4 Application to Ideal Gases at Equilibrium

All the applications in this chapter will be to the gas phase, in particular to ideal gases. In later chapters the discussion will treat isotope effects on equilibria for condensed phase systems.

At very low pressure all gases obey the ideal gas law, $PV = nRT$, where P is the pressure, V is the volume and, T is the temperature. The gas constant, R , is a universal constant, and T is the absolute temperature in kelvin. A mixture of gases at sufficiently low pressure also behaves ideally

$$PV = nRT \quad (4.40)$$

where n is the total number of moles,

$$n = \sum_i n_i \quad (4.41)$$

and V and P are the total volume and the total pressure respectively. For the individual gases, the perfect gas law V is also valid with

$$P_i V = n_i RT \quad (4.42)$$

with P_i referred to as the partial pressure of gas component i . The total pressure in Equation 4.40 is then the sum of partial pressures.

$$P = \sum_i P_i \quad (4.43)$$

Equations 4.42 and 4.43 are a statement of Dalton's law.

From Equation 4.30, one can write for a gas consisting of one molecular species

$$dG = VdP - SdT \quad (4.44)$$

For an ideal gas at constant temperature $-SdT = 0$, and

$$dG = VdP = n \frac{RT}{P} dP = nRT d \ln P \quad (4.45)$$

and consequently one obtains at given temperature T

$$\begin{aligned} G(T, P) &= G^0(T) + nRT \int_{P^0}^P d \ln P \\ &= G^0(T) + nRT \ln \frac{P}{P^0} \end{aligned} \quad (4.46)$$

Here $G^0(T)$ refers to an n mole ideal gas system at a standard pressure designated as P^0 (usually 1 bar). The chemical potential of a one component i ideal gas system is then

$$\begin{aligned}\mu_i &= \left(\frac{\partial G_i}{\partial n_i} \right)_{T,P} = \left(\frac{\partial G_i^0}{\partial n_i} \right)_{T,P} + RT \ln \frac{P_i}{P^0} \\ &= \mu_i^0(T) + RT \ln \frac{P_i}{P^0}\end{aligned}\quad (4.47)$$

Here $\mu_i^0(T)$ is the Gibbs free energy per mole of an ideal gas at temperature T and standard pressure P^0 . Thus the condition of equilibrium for a gas phase system subject to a chemical reaction (Equation 4.36), whether at constant T and P or constant T and V , is given by

$$\begin{aligned}\sum v_i \mu_i &= \sum_i v_i \mu_i^0 + v_i RT \ln \frac{P_i}{P^0} \\ &= \Delta G_r^0 + \sum_i RT \ln \left(\frac{P_i}{P^0} \right)^{v_i} = \Delta G_r^0 + RT \ln K_P = 0\end{aligned}\quad (4.48)$$

Here ΔG_r^0 is the Gibbs free energy change in the ideal gas phase reaction system when all the gases are in their respective standard states. The equilibrium constant K_P is given in terms of the partial pressures at equilibrium by

$$K_P = \prod_i \left(\frac{P_i}{P^0} \right)^{v_i}\quad (4.49)$$

Condition 4.48 can be written

$$\Delta G_r^0 = -RT \ln K_P\quad (4.50)$$

The equilibrium constant, K_P , takes the well known form of a ratio of products of pressures raised to various stoichiometric powers, remembering that the v_i 's for products in Equation 4.36 are positive while those for reactants are negative.

4.4.1 Remarks, Nonideality, Condensed Phases

The thermodynamic development above has been strictly limited to the case of ideal gases and mixtures of ideal gases. As pressure increases, corrections for vapor nonideality become increasingly important. They cannot be neglected at elevated pressures (particularly in the critical region). Similar corrections are necessary in the condensed phase for solutions which show marked departures from Raoult's or Henry's laws which are the common ideal reference solutions of choice. For non-ideal solutions, in both gas and condensed phases, there is no longer any direct

proportionality between measured isotope effects on logarithmic concentration or pressure ratios and isotopic differences in the corresponding standard state free energy differences. Appreciable corrections may be required. Further details are found in Appendix 4.A1 and in Chapter 5.

4.5 Statistical Mechanics of Ideal Gases and Isotope Effects

4.5.1 General Remarks

Statistical mechanics enables one to express the chemical potential μ_i for an ideal gas phase system in terms of the spectroscopic properties of individual gas phase molecules. The reader is referred to standard statistical mechanics texts (e.g. D. A. McQuarrie “Statistical Mechanics”, reading list) for the development of the relationship between the system Helmholtz free energy, A_i , and the corresponding canonical partition function Q_i

$$A_i = -kT \ln Q_i \quad (4.51)$$

$$Q_i = \sum_s e^{-E_{is}/kT} \quad (4.52)$$

In Equations 4.51 and 4.52 k is Boltzmann’s constant, T is the absolute temperature and the E_{is} ’s are the energy states of the molecules i . The statistical mechanical considerations in this book will refer to an ideal gas unless explicit mention is made to the contrary. For an ideal gas, a gas of non-interacting molecules, one can express the partition function Q_i of a collection of \tilde{N}_i molecules of species i in terms of the single molecule partition functions q_i as follows¹

$$Q_i = \frac{q_i^{\tilde{N}_i}}{\tilde{N}_i!} \quad (4.53)$$

$$q_i = \sum_s e^{-\epsilon_{is}/kT} \quad (4.54)$$

Here the ϵ_{is} ’s are the energy levels of the individual molecules. Equation 4.53 follows from the use of Boltzmann statistics for \tilde{N}_i distinguishable non-interacting molecules when the number of energy states of the \tilde{N}_i molecule system is very large compared to the number of molecules. The latter condition is satisfied for most systems of practical interest. For detailed consideration of this point, the reader should consult the McQuarrie reference.

¹ The authors recognize that the symbol q has previously been used for thermodynamic heat. In using the letter q to symbolize the molecular partition function, usual practice is being followed. This usage should not give rise to confusion.

One now recognizes that in situations of chemical interest \tilde{N}_i is very large so that $\tilde{N}_i!$ in Equation 4.53 can be well approximated by Stirling's formula

$$\ln \tilde{N}_i! = \tilde{N}_i \ln \tilde{N}_i - \tilde{N}_i \quad (4.55)$$

Then

$$\ln Q_i = \tilde{N}_i \ln q_i - \tilde{N}_i \ln \tilde{N}_i + \tilde{N}_i \quad (4.56)$$

Moreover, with the number of molecules \tilde{N}_i related to the number of moles of species i by Avogadro's number N_A

$$n_i = \frac{\tilde{N}_i}{N_A} \quad (4.57)$$

and with the gas constant R (of the ideal gas law) related to Boltzmann's constant k

$$R = N_A k \quad (4.58)$$

one obtains for the chemical potential μ_i

$$\mu_i = -kT \left(\frac{\partial \ln Q_i}{\partial n_i} \right)_{T,V} = -RT \left(\frac{\partial \ln Q_i}{\partial \tilde{N}_i} \right)_{T,V} \quad (4.59a)$$

$$= -RT (\ln q_i - \ln \tilde{N}_i - 1) \quad (4.59b)$$

$$= -RT \ln \frac{q_i}{\tilde{N}_i} \quad (4.59c)$$

$$= -RT \ln \left(\frac{q_i V}{V \tilde{N}_i} \right) \quad (4.59d)$$

$$= -RT \ln \left(\frac{q_i kT}{V P_i} \right) \quad (4.59e)$$

with V the volume of the gas. Use has been made of the ideal gas law (Equation 4.40) where P_i is the pressure (or partial pressure) of the ideal gas i .

We now introduce the standard pressure P^0 (usually 1 bar) and obtain

$$\mu_i = -RT \ln \frac{q_i kT}{V P^0} + RT \ln \frac{P_i}{P^0} \quad (4.60)$$

$$\mu_i = \mu_i^0 + RT \ln \frac{P_i}{P^0} \quad (4.61)$$

Here μ_i^0 is the chemical potential of the ideal gas at the standard pressure. It will be seen subsequently that q_i for an ideal gas depends linearly on the volume V , so μ_i^0 is a function only of the temperature. It does of course depend on the distribution of energy levels of the ideal gas molecules. The form of Equation 4.59 for the chemical potential of an ideal gas component is the same as that previously derived from thermodynamics (Equation 4.47). The present approach shows how to calculate μ_i^0 through the evaluation of the molecular partition function. Furthermore, the

evaluation of molecular partition functions for the relevant ideal gases permits the calculation of the standard state free energy change

$$\Delta G_i^0 = \sum \nu_i \mu_i^0 \quad (4.62)$$

for any gas phase reaction, Equation 4.36, and consequently permits the calculation of the equilibrium constant for the reaction. It should be noted in passing that Equation 4.62 refers to ΔG for the reaction when all the molecules are in their respective standard states. It has been pointed out that the standard state for a gas is 1 bar at the given temperature T . That is an incomplete definition. In thermodynamics the definition also contains the provision that the gas in its standard state behaves as an ideal gas (which is always a correct description of any gas at very low pressure). Non-ideal gas behavior is handled by introducing activity coefficients (see Appendix 4.A1 or any thermodynamics text).

4.5.2 Equilibrium Constants and Partition Functions

From Equations 4.60 and 4.61,

$$\sum_i \nu_i \mu_i^0 = -RT \ln \prod_i \left(\frac{q_i}{V} \frac{kT}{P^0} \right)^{\nu_i} \quad (4.63)$$

and using Equations 4.49 and 4.50, one obtains

$$K_p = \prod_i \left(\frac{P_i}{P^0} \right)^{\nu_i} = \prod_i \left(\frac{q_i}{V} \frac{kT}{P^0} \right)^{\nu_i} \quad (4.64)$$

In the context of this book our interest is in the isotope effect on the equilibrium constant K_p . This is illustrated below for an isotope effect involving the replacement of a hydrogen atom by a deuterium atom



A, B, C, and E are identical in the two reactions. The two equilibrium constants are K_1 and K_2 . Thus in Equation 4.64, in the evaluation of K_1/K_2 all factors drop out except the partition functions of the isotopically substituted molecules and one obtains

$$\frac{K_1}{K_2} = \left(\frac{q_{AD}}{q_{AH}} \frac{q_{CD}}{q_{CH}} \right) \quad (4.67)$$

We see here that one calculates an isotope effect on an equilibrium constant as a ratio of isotopic partition ratios. Moreover, we also see that the subtraction of

equilibrium (4.66) from equilibrium (4.65) in the usual chemical fashion yields a third equilibrium



This latter equilibrium is called an isotopic exchange equilibrium. Its equilibrium constant in terms of partition functions is from Equation 4.64

$$K_3 = \frac{q_{\text{AD}} q_{\text{CH}}}{q_{\text{AH}} q_{\text{CD}}} = \left(\frac{q_{\text{AD}}}{q_{\text{AH}}} \right) / \left(\frac{q_{\text{CD}}}{q_{\text{CH}}} \right) \quad (4.69)$$

It is clear that the exchange equilibrium constant K_3 is equal to the isotopic ratio of equilibrium constants, K_1/K_2 .

4.6 Evaluation of Partition Functions, q , and Isotope Effects on Partition Functions, $q_{\text{heavy}}/q_{\text{light}}$ for Ideal Gases

The evaluation of partition functions for ideal gases forms a major portion of introductory statistical mechanics textbooks and the reader is referred to these for the details (e.g. McQuarrie, reading list, below the statistical mechanical conventions of McQuarrie are followed). This discussion is carried out within the framework of the Born–Oppenheimer approximation (see Chapter 2). The molecule (or atom) is taken to be in its ground electronic state. The eigenvalues of the Schrödinger equation corresponding to the molecular energy states ε_i needed for the evaluation of q (Equation 4.54) are found by solving the equation corresponding to the N -nuclei of the N -atomic system moving on the Born–Oppenheimer potential energy surface of that molecule or atom. Recall that the BO surface expresses the electronic energy of the molecular system as a function of the configuration of the nuclei. An exact solution of this problem can be quite complex; however, for many applications, it is sufficient to introduce simplifying approximations. Before proceeding, it should be said that the majority of calculations in isotope chemistry (including all calculations in this book) are carried out with use of these simplifying assumptions. At the end of this chapter (Appendix 4.A2), references are given to more sophisticated and detailed calculations that test certain of these approximations (e.g. Wolfsberg and coworkers, reading list). On the one hand, such higher level studies show that the standard simplifying assumptions lead to theoretically calculated results with errors usually smaller or comparable to normal experimental error and establish the validity of the simplified approach; on the other, such calculations enable the comparison between theory and accurate high precision experiments.

4.6.1 *The Rigid Rotor Harmonic Oscillator Approximation*

This simplification was already introduced in Chapter 2. In the rigid rotor approximation there is no rotational–vibrational interaction. The molecular Schrödinger

equation factors into equations for describing motion of the center of mass, for rotation about the center of mass, and for describing the molecular vibrations. As in Chapter 2, we introduce the additional approximation that the vibrational frequencies be harmonic. Using this approximation, the vibrational problem of the N -atomic molecule factors into $3N - 6$ [$(3N - 5)$ for a linear molecule] independent harmonic vibrational problems, one corresponding to each of the normal modes of the molecule. Combining the rigid rotor and harmonic oscillator approximations, we see that the individual energy levels of the molecular partition function q can be written as a sum

$$E_i = E_{\text{Trans}} + E_{\text{rot}} + \sum_i E_{\text{vib}}(i) \quad (4.70)$$

The last term refers to the $3N - 6$ (or $3N - 5$) vibrations. Corresponding to each of the terms in Equation 4.70 are sets of quantum numbers (e.g. translational quantum numbers, rotational quantum numbers, etc.) which are independent of each other. From this point it is quite straightforward to show that the partition function can be factored into a product of partition functions corresponding to translation, rotation, etc.

$$q = q_{\text{Trans}} q_{\text{rot}} \prod_i q_{\text{vib}}(\nu_i) \quad (4.71)$$

In Equation 4.71 the individual q_{vib} 's have been specified $q_{\text{vib}}(\nu_i)$ to indicate that these partition functions depend on the normal mode frequencies. It is interesting to note that the partition function for translation, which is usually considered in terms of the problem of the particle in a three dimensional rectangular box, is, itself a product of three partition functions; one for motion in the x dimension, one for y , etc.

4.6.1.1 Degrees of Freedom

A brief discussion of degrees of freedom is included here. The quantum mechanical equation for nuclear motion contains a kinetic energy term for the nuclei which is usually written in terms of three Cartesian coordinates fixed to each of the nuclei of the N -atomic molecule. The potential energy term in this equation can also be written in terms of these $3N$ coordinates. By transforming to a set of new coordinates, which are linear combinations of these Cartesian coordinates, one can factor this so-called Born–Oppenheimer equation into a set of separate and independent equations. The important fact to remember is that the number of degrees of freedom that lead to these coordinates must be exactly equal to $3N$. This fact enables the determination of the number of vibrational degrees of freedom. The motion of the center of mass involves the three Cartesian coordinates of the center of mass. The rotations of the general rigid body involve three angles (three degrees of freedom). However, the rotations of a linear molecule (a molecule is linear if its minimum electronic energy corresponds to a nuclear geometry in which the nuclei lie along a straight line) involve only two angles. Thus, for a linear molecule, there must be $3N - 5$ vibrational

Table 4.1 Partition functions evaluated in the rigid rotor harmonic oscillator approximation

$$q = q_{\text{Trans}} q_{\text{rot}} q_{\text{vib}}$$

$$q_{\text{Trans}} = \left(\frac{2\pi M k T}{h^2} \right)^{3/2} V^a$$

$$q_{\text{rot}} = \frac{8\pi^2 I k T}{s h^2} \text{--- linear molecule}^b$$

$$q_{\text{rot}} = \frac{\pi^{1/2}}{s} \left(\frac{8\pi^2 I_A k T}{h^2} \right)^{1/2} \left(\frac{8\pi^2 I_B k T}{h^2} \right)^{1/2} \left(\frac{8\pi^2 I_C k T}{h^2} \right)^{1/2} \text{--- non-linear molecule}^b$$

$$q_{\text{vib}} = \prod_i \frac{e^{-u_i/2}}{1 - e^{-u_i}}$$

^a M is the molecular mass.

^b I is the moment of inertia of a linear molecule (see Chapter 3). I_A , I_B , I_C , are the three principal moments of the nonlinear molecules. s is the symmetry number. It is equal to the number of rotations that take the molecule into itself. If one knows the point group of the equilibrium configuration of the molecule, s is the number of rotation operations in the point group including the identity operator E . Thus s has a minimum value of unity. Actually, s is a concept of classical statistical mechanics (remember that the rotational partition function is calculated here in the classical limit) and division by s prevents over-counting the number of states. For further discussion see Section 4.9 and/or a statistical mechanics text.

^cThe product, for the N -atomic molecule, is over the $3N-6$ normal vibrational modes ν_i ($3N-5$ for a linear molecule). For ν in units of sec^{-1} , $u = h\nu/kT$; for ν in cm^{-1} , $u = hc\nu/kT$. See footnote 2, page 92

degrees of freedom while, for a non-linear molecule, there are $3N-6$ vibrational degrees of freedom. The actual calculation of the molecular partition function in the rigid-rotor-harmonic-oscillator approximation requires more detail. The results are presented in Table 4.1. For the full details, a standard textbook in statistical mechanics (e.g. McQuarrie) again needs to be consulted. As already noted, q is calculated as a product, Equation 4.71. Thus, if possible, one wants to evaluate q_{Trans} , q_{rot} , and q_{vib} by means of simple formulae rather than explicitly calculating the sum over the quantized energy levels implied by Equation 4.54.

4.6.2 Considerations of Level Spacing

If the spacing between quantized energy levels is sufficiently small compared to kT (Equation 4.54) and if one knows the explicit formula for the quantized energy levels, then one can integrate over the quantum numbers rather than carrying out the direct summation. The result so obtained is identical to the partition function in the classical mechanical-limit (*vide infra*). For practical purposes, one can always replace the quantum expression for q_{Trans} by the corresponding classical expression. The same is almost always true for q_{rot} . The rotational energy spacing tends to be somewhat larger than the spacing for translational energy levels. Very occasionally, one may need to correct the classical expression for q_{rot} for quantum spacing and

methods for making quantum corrections to q_{rot} are available in standard sources (e.g. McQuarrie, reading list). The formulae for both q_{Trans} and q_{rot} in Table 4.1 are the classical formulae for these quantities.

The spacing between vibrational energy levels cannot be ignored for calculations of q_{vib} at room temperature. For a single harmonic vibration, the energy levels are given by

$$\varepsilon_n = \left(n + \frac{1}{2} \right) h\nu \quad n = 0, 1, 2, \dots \quad (4.72)$$

where n is the vibrational quantum number, ν is the vibrational frequency², and h is Planck's constant. One obtains

$$\begin{aligned} q_{\text{vib}} &= e^{-\frac{1}{2}h\nu/kT} + e^{-\frac{3}{2}h\nu/kT} + e^{-\frac{5}{2}h\nu/kT} \dots \\ &= \frac{e^{-\frac{1}{2}h\nu/kT}}{1 - e^{-h\nu/kT}} \end{aligned} \quad (4.73)$$

Again, for detail, see a statistical mechanics text. For a general N -atomic molecule, there are $(3N - 6)$ normal vibrations ν_i ($3N - 5$ for a linear molecule) and the corresponding vibrational partition function is

$$q_{\text{vib}} = \prod_i^{3N-6(5)} \frac{e^{-\frac{1}{2}h\nu_i/kT}}{1 - e^{-h\nu_i/kT}} \quad (4.74)$$

The formulae for the partition function of a molecule in the rigid-rotor-harmonic-oscillator approximation are summarized in Table 4.1.

4.6.3 The Energy Zero

The formulae given in Table 4.1 for the molecular partition functions enable us to write the partition function ratio $q_{\text{heavy}}/q_{\text{light}}$ or q_2/q_1 where, by the usual convention, the subscript 2 refers to the heavy isotopomer and 1 refers to the light isotopomer if "heavy" and "light" are appropriate designations. Then, a ratio of such partition function ratios enables one to evaluate the isotope effect on a gas phase equilibrium constant, as pointed out above. Before continuing, it is appropriate to

² In the equations in this part of the text the frequency ν (cycles per second) has units of sec^{-1} . The units of Planck's constant h and the Boltzmann constant k are J s and J K^{-1} , respectively. Consequently the exponents, $-h\nu/kT$, as mathematically required are unitless, $(\text{J s s}^{-1})/(\text{J K}^{-1} \text{K})$. Chemists, however, are fond of expressing frequency in units of reciprocal wave length or wave numbers, cm^{-1} . Recall $\nu(\text{s}^{-1}) = c/\lambda(\text{cm}) = c\nu(\text{cm}^{-1})$ where c is the velocity of light, $3 \times 10^{10} \text{ cm s}^{-1}$ and λ is the wave length. Therefore should one choose to express frequency in units of cm^{-1} the exponents in equations of type 4.73 become $-hc\nu/kT$. It is unfortunate that both conventions, as here, often employ the same symbol, ν .

discuss the “zero of energies”. For translation and rotation, the zero of energy is the non-translating, non-rotating molecule so the zeros of molecule 1 and 2 are identical. For vibrations, the lowest vibration energy for each of the normal mode frequencies ν_i is the well-known zero point energy $\frac{1}{2}h\nu_i$, this energy being taken with respect to the Born–Oppenheimer minimum which is the same for all the isotopomers of a given molecule. Thus the zero of energies has been chosen the same for all the isotopomers and automatically cancels out when one evaluates q_2/q_1 . Then from Table 4.1 for a non-linear molecule

$$\frac{q_2}{q_1} = \frac{s_1}{s_2} \frac{M_2^{\frac{3}{2}}}{M_1^{\frac{3}{2}}} \frac{(I_{A_2} I_{B_2} I_{C_2})^{\frac{1}{2}}}{(I_{A_1} I_{B_1} I_{C_1})^{\frac{1}{2}}} \prod_i^{3N-6} \left(\frac{1 - e^{-h\nu_{1i}/kT}}{1 - e^{-h\nu_{2i}/kT}} \right) e^{\frac{1}{2}h \sum_i^{3N-6} (\nu_{1i} - \nu_{2i})/kT} \quad (4.75)$$

For a linear molecule

$$\frac{q_2}{q_1} = \frac{s_1}{s_2} \frac{M_2^{\frac{3}{2}}}{M_1^{\frac{3}{2}}} \frac{I_2}{I_1} \prod_i^{3N-5} \left(\frac{1 - e^{-h\nu_{1i}/kT}}{1 - e^{-h\nu_{2i}/kT}} \right) e^{\frac{1}{2}h \sum_i^{3N-5} (\nu_{1i} - \nu_{2i})/kT} \quad (4.76)$$

Equation 4.76 is written for a non-linear molecule with $3N - 6$ vibrations. For linear molecules (including diatomics), there are $3N - 5$ vibrations, two of the moments of inertia, say I_A and I_B , are equal, and there is no third moment of inertia. Using $u = h\nu/kT$, we obtain a more compact formula.

$$(s_2/s_1) q_2/q_1 = \frac{M_2^{\frac{3}{2}}}{M_1^{\frac{3}{2}}} \frac{(I_{A_2} I_{B_2} I_{C_2})^{\frac{1}{2}}}{(I_{A_1} I_{B_1} I_{C_1})^{\frac{1}{2}}} \prod_i \left(\frac{1 - e^{-u_{1i}}}{1 - e^{-u_{2i}}} \right) e^{\frac{1}{2}(u_{1i} - u_{2i})} \quad (4.77)$$

In Chapter 3, a formula was presented which connects the normal vibrational frequencies of two rigid-rotor-harmonic-oscillator isotopomers with their respective atomic masses m_i , molecular masses M_i and moments of inertia (the Teller–Redlich product rule). If this identity is substituted into Equation 4.77, one obtains

$$\frac{s_2}{s_1} \frac{q_2}{q_1} = \prod_i^N \left(\frac{m_{2i}}{m_{1i}} \right)^{\frac{3}{2}} \prod_i \frac{u_{2i}}{u_{1i}} \left(\frac{1 - e^{-u_{1i}}}{1 - e^{-u_{2i}}} \right) e^{\frac{1}{2}(u_{1i} - u_{2i})} \quad (4.78)$$

where the first product is taken over all the atoms in the two isotopomers and the second product is taken over the $3N - 6(3N - 5)$ normal mode vibrational frequencies.

4.6.4 Bigeleisen and Mayer; The Reduced Isotopic Partition Function Ratio

Bigeleisen and Mayer (Historical Vignettes 4.1 and 4.2), recognizing that the term in Equation 4.78 involving isotopic masses would always cancel in the calculation of



[Historical Vignette 4.1] **Jacob Bigeleisen** (1919–present) was educated at New York University (AB 1939), Washington State University (MS 1941), and the University of California at Berkeley (Ph.D. 1943). After receiving his degree he joined the Manhattan Project where, together with Maria Mayer he worked out the Bigeleisen–Mayer formalism for the theory of isotope effects. Later Bigeleisen held appointments at the University of Chicago, Brookhaven National Laboratory, Rochester University, and the State University of New York at Stony Brook. In addition to his work on the Bigeleisen–Mayer theory he has made many important theoretical and experimental contributions to kinetic isotope effects, condensed phase isotope effects, isotope separation, etc. He has been instrumental in promoting the development of isotope science by his numerous writings and by organizing the first Gordon Conference on the Chemistry and Physics of Isotopes in 1954 and encouraging its continuation for now more than a half-century. (Photo courtesy of J. Bigeleisen)

an isotope effect on an equilibrium constant (since the heavy/light isotopic substitution in both pairs of isotopomers must be identical), introduced the reduced isotopic partition function ratio (s_2/s_1) f ,

$$\frac{s_2}{s_1} f = \left(\frac{s_2}{s_1} \frac{q_2}{q_1} \right) \prod_i^N \left(\frac{m_{2i}}{m_{1i}} \right)^{-3/2} = \prod_i \frac{u_{2i}}{u_{1i}} \left(\frac{1 - e^{-u_{1i}}}{1 - e^{-u_{2i}}} \right) e^{\frac{1}{2}(u_{1i} - u_{2i})} \quad (4.79)$$

$$= (\text{PF})(\text{EXC})(\text{ZPE}) \quad (4.79a)$$

Equation 4.79a points out the Reduced Isotopic Partition Function Ratio (RPFRR) may be considered as the product of three factors: the product factor (PF), the excitation factor (EXC), and the zero-point energy factor (ZPE). Note that in terms of RPFRR's, the isotope effects corresponding to Equations 4.65, 4.66, and 4.68 can be written

$$\frac{K_1}{K_2} = K_3 = (\text{symmetry number factor}) \times \frac{\left(\frac{s_2}{s_1} f \right) [\text{AD/AH}]}{\left(\frac{s_2}{s_1} f \right) [\text{CD/CH}]} \quad (4.80)$$



[Historical Vignette 4.2] **Maria Goeppert Mayer** (1906–1972, Nobel Prize in Physics 1963) studied physics at the University of Göttingen (Ph.D., 1930). In 1930 she married the American chemical physicist Joseph E. Mayer and accompanied him to the United States. During the 1930s she was at Johns Hopkins University as a volunteer associate. In 1939 she received an appointment in chemistry at Columbia University, and worked on the separation of uranium isotopes for the Manhattan project (1939–1945). It was during this period that she collaborated with J. Bigeleisen in developing the molecular theory of isotope effects. After the war Mayer's interests centered increasingly on nuclear physics. In 1945 she became a volunteer professor of physics in the Enrico Fermi Institute for Nuclear Studies at the University of Chicago receiving a regular appointment as full professor in 1959. She moved to the University of California at San Diego in 1960 where she spent the balance of her career. She was instrumental in developing the shell model of the nucleus, and it is for that work she shared the 1963 Nobel Prize in Physics. It is worth mentioning that even as late as 1945 Maria G. Mayer remained a volunteer research associate by which time she was a quite distinguished scientist. This historical detail calls attention to the shameful policies in US academia which then severely limited opportunities for women. (Photo credit: www.wikipedia.org, public domain)

where the symmetry number factor is given by

$$\frac{\left(\frac{S_{AH}}{S_{AD}}\right)}{\left(\frac{S_{CH}}{S_{CD}}\right)} \quad (4.80a)$$

From Equation 4.79, it is then recognized that the isotope effect is given by a symmetry number factor and terms which depend only on the normal mode vibrational frequencies. There are no terms in the equality that depend explicitly on atomic and molecular masses or on moments of inertia.

The introduction of the concept of the reduced isotopic partition function ratio had a profound effect on the development of the study of isotope effects. Equation 4.79 in which no reference is made to moments of inertia appears much less formidable than Equation 4.77 and focuses the reader's attention on the isotope

effect on the frequencies and on the molecular force constants which underlie these frequencies. As has been pointed out repeatedly, isotope effects reflect force constant differences at or near the position of isotopic substitution. It is well to keep in mind that the reduced isotopic partition function ratio for an unbound atom is exactly unity. Thus, for example, neglecting symmetry number effects, the reduced isotopic partition function ratio for $\text{CH}_3\text{D}/\text{CH}_4$ is the equilibrium constant for the reaction $\text{CH}_4 + \text{D} = \text{CH}_3\text{D} + \text{H}$. Nevertheless, when comparing calculations based on reduced partition function ratios (s/s)f with experimental observation it is important to keep in mind that one must multiply the theoretical value by the symmetry number factor (Equation 4.80a).

4.6.5 Limiting Values for the Isotope Effects

4.6.5.1 The High Temperature Limit

As pointed out in Chapter 3, the vibrational frequencies ν_i of an isotopomer pair obey the rule $\nu_{1i} \geq \nu_{2i}$. Since $e^{-x} = 1 - x$ for x sufficiently small, it is clear that at high temperature PF and EXC cancel exactly. At sufficiently high temperature the exponent in ZPE will become small. ZPE will also approach unity. Consequently (PF)(EXC) also approaches unity.

$$\lim_{u_i \rightarrow 0} \prod_i \frac{u_{2i}}{u_{1i}} \left(\frac{1 - e^{-u_{1i}}}{1 - e^{-u_{2i}}} \right) = \prod_i \frac{u_{2i}}{u_{1i}} \frac{u_{1i}}{u_{2i}} = 1 \quad (4.80b)$$

and, overall, $(s_2/s_1)f$ also approaches unity at high temperature. The isotope effect (K_1/K_2 , Equation 4.80) can be represented by a ratio of q_2/q_1 values and at limiting high temperature will be given by a ratio of symmetry numbers. The symmetry number ratio is a purely statistical factor which insures correct counting of probabilities. It will not lead to any enrichment of isotopes and therefore is recognized as a “non-effect”. Thus, there are no isotope effects at sufficiently high temperature. As we already know, quantum mechanics goes over into classical mechanics in the high temperature limit (when the spacing between quantum energy states becomes small compared to kT). Thus, in the formulation above isotope effects are quantum effects. In the following section, it will be pointed out that this result is not a consequence of the rigid-rotor, harmonic oscillator, ideal gas approximation but is a general truth.

4.6.5.2 The Low Temperature Limit: The ZPE Approximation

As temperature falls $u = hc\nu/kT$ increases,³ $(1 - e^{-u}) \rightarrow 1$. The harmonic oscillator partition function for each frequency simplifies, $q_{\text{HO}} = e^{-u/2}/(1 - e^{-u}) \rightarrow e^{-u/2}$

³ See footnote 2.

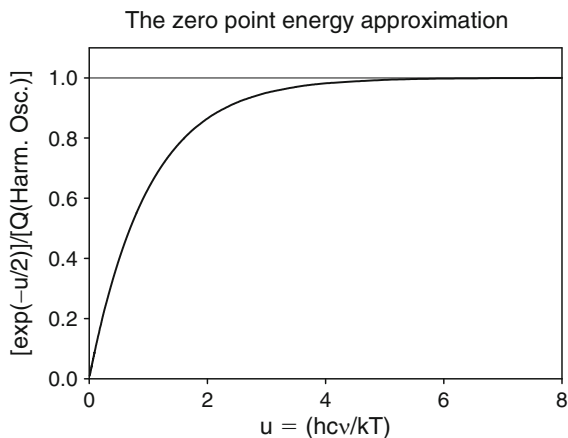


Fig. 4.1 The zero point energy or low temperature approximation: As temperature drops and u increases above $u \sim 4$ the harmonic oscillator partition function Q (Harm. Osc.) is better and better approximated by the zero point energy term, $\exp(-u/2)$. For a typical CH stretching frequency, $\nu = 3000 \text{ cm}^{-1}$, $u \sim 4$ at 1050 K and it is reasonable to use the ZPE approximation for that frequency at temperatures below $\sim 1000 \text{ K}$

with concomitant simplification in the reduced partition function ratio, $(s_2/s_1)f = (\text{PF})(\text{EXC})(\text{ZPE}) \rightarrow \Pi(u_{2i}/u_{1i})(\exp[-(u_{2i} - u_{1i})/2])$. No upper vibrational levels are populated and we refer to this condition as the “zero point energy approximation”. The approach to conditions where the ZPE approximation is valid is shown in Fig. 4.1. Note that at very low temperatures ZPE isotope effects can get very large. In fact as $T \rightarrow 0$ they increase without limit.

4.7 The High Temperature Limit: Generalization, (No Classical) Isotope Effects on Chemical Equilibrium

In 1933, J.G. Kirkwood explicitly showed that the canonical partition function Q for a system of \tilde{N} monatomic particles reduces to an integral over phase space in the limit of high temperature (Equation 4.81). The result corresponds to classical mechanics (i.e. the spacing between energy levels is small compared to kT)

$$Q_C = \frac{1}{\tilde{N}! h^{3\tilde{N}}} \int \dots \int e^{-H/kT} dp_1 \dots dp_{\tilde{N}} dq_1 \dots dq_{\tilde{N}} \quad (4.81)$$

Note the subscript C to indicate classical (or high temperature). In Equation 4.81 the p 's are momenta and the q 's the associated coordinates (not to be confused with q 's previously used to symbolize molecular partition functions). In Cartesian coordinates $dp_1 dq_1 = dp_{x_1} dp_{y_1} dp_{z_1} dx_1 dy_1 dz_1$ with x_1, y_1, z_1 , the coordinates of atom

1 and p_{x_1} , p_{y_1} , p_{z_1} , the corresponding momenta used to express the kinetic energy KE of atom 1. H is the classical Hamiltonian function for the \tilde{N} atom system with kinetic energy K.E. (expressed in terms of Cartesian momenta) and V the interatomic potential (expressed in Cartesian coordinates). While Kirkwood originally wrote this equation for the case of a noble gas, this system will be considered here to be a system of \tilde{N} N-atomic molecules so that then the integration will be over $3\tilde{N}N$ coordinates and momenta, and the divisor h appropriately needs an exponent $3\tilde{N}N$. The Hamiltonian function is expressed as

$$H = \text{K.E.} + V = \sum_i^{3\tilde{N}N} \frac{p_{x_i}^2 + p_{y_i}^2 + p_{z_i}^2}{2m_i} + V = T + V \quad (4.82)$$

The space of the integration is referred to as phase space. The justification of the integration over phase space in order to calculate “high temperature” partition functions is beyond the scope of this book but discussion addressed to readers of various backgrounds may be found in many works ranging from beginning physical chemistry texts to advanced monographs on statistical mechanics. Briefly, it is expected that the integration over the p’s and q’s considering H to be a continuous function of these variables (in a classical sense), and expressing the fundamental volume of phase space in terms of Planck’s constant raised to an appropriate power, will yield the correct value of the partition function at temperatures large enough that the spacing between energy levels is small compared to kT ; k is the Boltzmann constant and T the absolute temperature.

The factor $1/\tilde{N}!$ included in Equation 4.81 corrects the classical integrals for over-counting. It is necessary because the purely classical derivation ignores the quantum mechanical principle of indistinguishability. The classical integration is over the space of every particle without any restriction. However, indistinguishability means when integrating over phase space, which is the equivalent of summing over quantum states, one is over-counting by a factor of $\tilde{N}!$ which is the number of ways of arranging \tilde{N} distinguishable objects. (e.g., for $\tilde{N} = 2$ identical objects the classical integration separately “counts” the arrangements “ab” and “ba”, which is incorrect according to quantum mechanical indistinguishability). The factor $1/\tilde{N}!$ also appears in the canonical partition function (Equation 4.53) derived similarly.

As noted in the discussion leading to Table 4.1, when calculating molecular partition functions, one needs the translational, rotational, and vibrational parts. For translation the spacing between energy levels is very small compared to kT and one can obtain the classical partition function by integrating over quantum numbers and subsequently dividing by \tilde{N} as noted above to obtain the canonical partition function. Also, the spacing between rotational states is small compared to kT around room temperature and above (except for hydrogen gas and its isotopomers), but symmetric molecules may have two or more equivalent orientations and it is necessary to correct the classical partition function for rotation for over-counting by inserting a factor $1/s$, where s is the symmetry number of the molecule. Symmetry numbers and symmetry number isotope effects are considered in detail in

Section 4.9. To sum up, Equation 4.81 can be generalized to molecules by dividing by a symmetry number factor (see Section 4.9). Equation 4.81 is the classical analogue of the quantum canonical partition function. An important finding is that the elemental volume in phase space is h^3 per particle. The division by $h^{3\tilde{N}}$ makes the integral dimensionless. The exponent in Equation 4.80, for an ideal gas of \tilde{N} molecules (or \tilde{N} monatomic particles) is a sum of \tilde{N} classical Hamiltonian functions ($KE + V$), one for each molecule with no interaction terms between different molecules (ideal gas). The assumption of gas ideality immediately leads to the separation of the integral of Equation 4.81 into a product of \tilde{N} integrals, one for each molecule. Comparison with Equation 4.53 leads to the identification of the classical molecular partition function $q_{i,\text{classical}}$ corresponding to the classical canonical partition function of Equation 4.83,

$$q_{i,\text{classical}} = (1/s_i)(1/h^{3N}) \int e^{-H_i/kT} dx_{i,1} dy_{i,1} \dots dy_{i,N} dz_{i,N} dp_{x,i,1} dp_{y,i,1} dp_{z,i,1} \dots dp_{y,i,N} dp_{z,i,N} \quad (4.83)$$

Here H_i is the Hamiltonian function for one N atomic molecule (i) and s_i is its symmetry number. One might have expected this result immediately from the Kirkwood formulation for the classical canonical partition function. H_i is a function of the $3N$ Cartesian momenta and the $3N$ Cartesian coordinates of molecule i .

Equation 4.83 can be straightforwardly applied to the calculation of the isotopic partition function ratio q_2/q_1 , needed for the calculation of classical isotope effects on equilibrium constants. The use of the Born–Oppenheimer approximation that the potential V is independent of nuclear mass yields a very simple result. One recognizes that the mass independent potential function V does not depend on momenta, and the kinetic energy does not depend on coordinates. Consequently each of the phase space integrals factors into a kinetic energy integral over momenta and a potential energy integral over coordinates, and moreover, the potential energy integral is the same in both the numerator and denominator so this integral cancels in the ratio. Thus, after introducing the relevant symmetry numbers into Equation 4.83, the ratio of the partition functions for molecular systems with N atoms per molecule becomes

$$\frac{q_{2,C}}{q_{1,C}} = \frac{s_1 \int \dots \int e^{-KE(1)/kT} dp_1 \dots dp_{3N}}{s_2 \int \dots \int e^{-KE(2)/kT} dp_1 \dots dp_{3N}} \quad (4.84)$$

Here $KE(1)$ and $KE(2)$ are classical kinetic energy expressions for isotopomer 1 and isotopomer 2 respectively, each containing terms for the kinetic energy of each atom in each of the three coordinates. For N -atomic molecules there are three Cartesian momenta for each atom, $3N$ Cartesian momenta for each molecule, and consequently $3N\tilde{N}$ Cartesian momenta for the \tilde{N} molecule system. The integrals in the numerator and denominator can thus be written as a product of 3 integrals of the type

$$\int_{-\infty}^{\infty} e^{-p^2/2mkT} dp = \left(\int_{-\infty}^{\infty} e^{-p'^2/2kT} dp' \right) m^{1/2} \quad (4.85)$$

by setting $p^2/m = p'^2$. All the integrals $\left(\int_{-\infty}^{\infty} e^{-p'^2/2kT} dp'\right)$ will cancel between numerator and denominator and one finally obtains

$$q_{2,C} / q_{1,C} = (s_2 / s_1) \prod_{i=1}^N (m_{2,i}/m_{1,i})^{3/2} \quad (4.86)$$

where m_{1i} and m_{2i} refer to the atomic masses in isotopomers (1) and (2) respectively. This result is completely independent of the form of the isotope independent Born–Oppenheimer potential for nuclear motion. It does not require the assumption of harmonic forces. For a simple illustration apply Equation 4.86 to two isotopomers which differ only by substitution of one H by D so that (deferring consideration of symmetry number effects to a later section where it will be shown that symmetry effects do not lead to isotopic enrichment or depletion) $q_2/q_1 = (m_D/m_H)^{3/2}$ for the \tilde{N} atom molecule. It follows from Equation 4.86 that the isotope effect on the Helmholtz free energy of \tilde{N} molecules or monatomic particles is

$$(A_1 - A_2)_C = -\tilde{N}kT \ln(q_{1,C}/q_{2,C}) = \tilde{N}kT \ln\left(\frac{q_{2,C}}{q_{1,C}}\right) \quad (4.87)$$

so

$$(A_1 - A_2)_C = \tilde{N}kT \ln\left(\frac{m_D}{m_H}\right)^{3/2} = \frac{3}{2}nN_A kT \ln\frac{m_D}{m_H} \quad (4.88)$$

where N_A is Avogadro's number and n is the number of moles in \tilde{N} molecules. Since the chemical potential, μ , equals $\frac{\partial A}{\partial n}$, it follows the difference between the chemical potential of two isotopomers which differ by replacing one hydrogen by a deuterium is independent of the molecular structures of the molecules involved. This result means that ΔA will be zero (and $K_{eq} = 1$) in the limit of classical mechanics for any such chemical equilibrium, for example



The statement applies not only to chemical equilibrium but also to phase equilibrium. It is obviously true that it also applies to multiple substitutions. Classically isotopes cannot be separated (enriched or depleted) in one molecular species (or phase) from another species (or phase) by chemical equilibrium processes. Statements of this truth appeared clearly in the early chemical literature. The previously derived Equation 4.80 leads to exactly the same conclusion but that equation is limited to the case of an ideal gas in the rigid rotor harmonic oscillator approximation. The present conclusion about isotope effects in classical mechanics is stronger. It only requires the Born–Oppenheimer approximation.

4.7.1 Further Remarks, RRHO Ideal Gas

It is useful to rewrite Equation 4.78 as

$$\begin{aligned} \frac{s_2}{s_1} \frac{q_2}{q_1} &= \prod_{i=1}^3 \left(\frac{m_{2i}}{m_{1i}} \right)^{3/2} \prod_i \frac{u_{2i}}{u_{1i}} \left(\frac{1 - e^{-u_{1i}}}{1 - e^{-u_{2i}}} \right) e^{\frac{1}{2}(u_{1i} - u_{2i})} \\ &= \frac{s_2}{s_1} \left(\frac{q_{2,C}}{q_{1,C}} \right) \prod_i \frac{u_{2i}}{u_{1i}} \left(\frac{1 - e^{-u_{1i}}}{1 - e^{-u_{2i}}} \right) e^{\frac{1}{2}(u_{1i} - u_{2i})} \end{aligned} \quad (4.90)$$

The second product is over the $3N - 6(3N - 5)$ normal mode frequencies of the ideal gas harmonic molecule to which Equation 4.78 applies. Thus the product over vibrations Equation 4.90 is indeed the quantum mechanical contribution to the molecular partition function for the ideal gas.

The result (Equation 4.90) could have been derived more simply. It has been emphasized that the quantum mechanical contribution to the partition function ratio arises from the quantization of vibrational energy levels. For the molecular translations and rotations quantization has been ignored because the spacing of translational and rotational energy levels is so close as to be essentially continuous ($\Delta\varepsilon/kT \ll 1$).

Now look at the partition function for each normal mode of vibration (Table 4.1)

$$q_{\text{harmonic}} = \frac{1}{1 - e^{-u}} e^{-u/2} \quad (4.91)$$

The classical vibrational partition function can be found by letting the temperature go to infinity. This means that we take the limit of Equation 4.91 as $u \rightarrow 0$ ($u = h\nu/kT$).

$$\lim_{u \rightarrow 0} \left(\frac{e^{-u/2}}{1 - e^{-u}} \right) = \frac{1}{1 - (1 - u)} = \frac{1}{u} \quad (4.92)$$

where the Taylor expansion of e^{-x} has been used for x vanishingly small. The quantum effect on the molecular vibrational partition function is found by taking the ratio q_2/q_1

$$\left(\frac{q_2}{q_1} \right)_{\text{quantum effect}} = \prod_i^{3N-6} \left(\frac{u_{2i}}{u_{1i}} \right) \frac{1 - e^{-u_{1i}}}{1 - e^{-u_{2i}}} e^{(u_{1i} - u_{2i})/2} \quad (4.93)$$

This result indicates that $(s_2/s_1)f$ (compare Equations 4.78 and 4.93) is just the quantum effect on the molecular partition functions of the normal mode vibrations. This result has now been derived without the explicit use of the Teller–Redlich product rule.

Considerations like the above led the German statistical mechanician L. Waldman independently to an equation similar to the $(s_1/s_2)f$ equation of Bigeleisen and Mayer. The foregoing can be regarded as an independent proof of the Teller–Redlich product rule but this statement depends on the assumption of no rotational–vibrational interaction.

4.8 The First Quantum Correction

In the previous section, it was shown that $(s_1/s_2)f$ goes to unity at high temperature when u tends to zero as the temperature increases. Thus, at high temperature we replace e^{-u} by 1 and $(1 - e^{-u})$ by u . If an additional term is carried in the expansion for e^{-u} when u is very small, one obtains a deviation of $(s_1/s_2)f$ from unity which scales as h^2 and this term gives the first order correction to the classical mechanical value of $(s_1/s_2)f$, which is unity.

The first quantum correction is deduced by recognizing that for small u

$$e^{-u} = 1 - u + \frac{u^2}{2} - \frac{u^3}{6} + \dots \quad (4.93a)$$

and

$$1 - e^{-u} = u - \frac{u^2}{2} + \frac{u^3}{6} - \dots \quad (4.93b)$$

so that

$$\begin{aligned} \phi(u) &= \frac{1 - e^{-u}}{u} e^{\frac{u}{2}} = \frac{u - \frac{u^2}{2} + \frac{u^3}{6} - \dots}{u} \left(1 + \frac{u}{2} + \frac{u^2}{8} + \frac{u^3}{48} + \dots \right) \\ &= \left(1 - \frac{u}{2} + \frac{u^2}{6} - K \right) \left(1 + \frac{u}{2} + \frac{u^2}{8} + \frac{u^3}{48} + \dots \right) \\ &= 1 - \frac{u}{2} + \frac{u}{2} + \frac{u^2}{8} - \frac{u^2}{4} + \frac{u^2}{6} + u^3(\dots) \\ &= 1 + \frac{u^2}{24} + \text{higher order terms in } u \end{aligned} \quad (4.94)$$

Thus to order u^2 , for small u (high temperature) one obtains

$$\begin{aligned} \frac{s_2}{s_1} f &= \prod_i^{3N-6} \frac{\phi(u_{1i})}{\phi(u_{2i})} = \prod_i^{3N-6} \frac{\left(1 + \frac{u_{1i}^2}{24} \right)}{\left(1 + \frac{u_{2i}^2}{24} \right)} \\ &= 1 + \sum_i \frac{1}{24} (u_{1i}^2 - u_{2i}^2) \\ &= 1 + \frac{1}{24} \left(\frac{h}{kT} \right)^2 \sum_i (v_{1i}^2 - v_{2i}^2) \end{aligned} \quad (4.95)$$

Thus the first correction to the classical statistical mechanics at high temperature goes as h^2 . There are higher order corrections. The result obtained here is identical to that found by J. Kirkwood for a harmonic oscillator. The approach to the

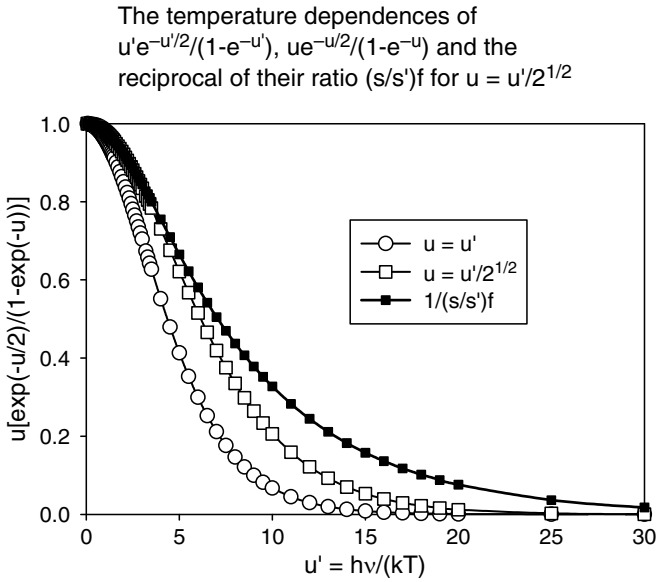


Fig. 4.2 The temperature dependences of $u'e^{-u'/2}/(1-e^{-u'})$, $ue^{-u/2}/(1-e^{-u})$ and the reciprocal of their ratio $(s/s')f$ for $u = u'/2^{1/2}$

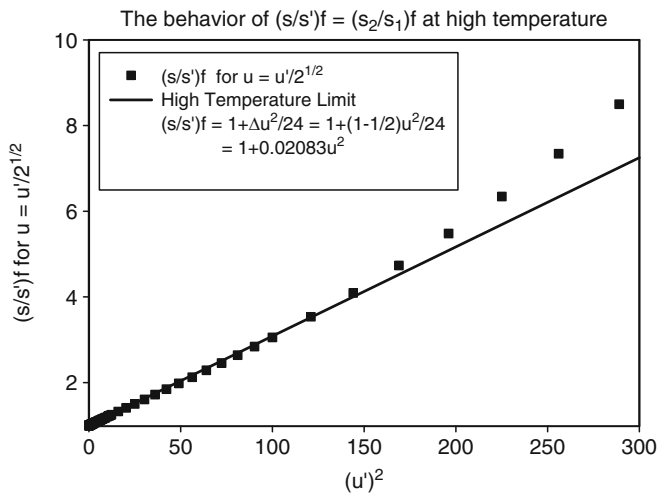


Fig. 4.3 The behavior of $(s/s')f = (s_2/s_1)f$ at high temperature

$u^2/24$ high temperature approximation is illustrated in Figs. 4.2 and 4.3 for the case $v_1^2/v_2^2 = v'^2/v^2 = 2$. Here, for future convenience, we have introduced (primed/unprimed) = (light/heavy) to supplement the (subscript₁/subscript₂) = (light/heavy) notation we have been using to this point.

One can simplify Equation 4.95 and obtain a very interesting result. We previously obtained the normal mode vibrational frequencies ν_i by diagonalization of the matrix of the harmonic force constants in mass weighted Cartesian coordinates (Chapter 3). These force constants F_{ij} were obtained from the force constants in Cartesian coordinates f_{ij} by using

$$F_{ij} = \frac{f_{ij}}{\sqrt{m_i m_j}} \quad (4.96)$$

The f_{ij} 's, the force constants in ordinary Cartesian coordinates, are the ones obtained from the Born-Oppenheimer potential, and are independent of isotopic substitution. Remember that the m_i 's in Equation 4.96 are the masses of the atoms in the molecule.

The $(3N - 6)$ non-zero eigenvalues Λ_i of the matrix F are related to the normal mode vibrational frequencies by

$$\Lambda_i = (2\pi\nu_i)^2 \quad (4.97)$$

There is an important theorem in matrix algebra which states that the sum of the eigenvalues of a matrix is equal to the sum of the diagonal matrix elements. Thus

$$\sum_i^{3N-6} \Lambda_i = \sum_i^{3N-6} 4\pi^2 \nu_i^2 = \sum_i^{3N} \frac{f_{ii}}{m_i} \quad (4.98)$$

Remember now that the numbering of the subscripts in F_{ij} corresponds to Cartesian coordinates with 1, 2, 3 corresponding to x, y, z of atom 1; 4, 5, 6 corresponding to x, y, z of atom 2; etc.; with $3N - 2$, $3N - 1$, $3N$ corresponding to x, y, z of the N th atom. We then obtain the important sum rule for frequencies (previously derived similarly (Equation 3.51))

$$4\pi^2 \sum_i^{3N-6} \nu_i^2 = \sum_i^{3N-6} \frac{(f_{xx} + f_{yy} + f_{zz})_i}{m_i} \quad (4.99)$$

where f_{xx} , f_{yy} , and f_{zz} are the diagonal Cartesian force constants for the displacement x^2 , y^2 , and z^2 of the i th atom from the equilibrium nuclear configuration.

4.8.1 Application to an Equilibrium

We have seen that Equation 4.95 for $(s_2/s_1)f$ involves the difference between the sums of the squares of the frequencies for two isotopomers. Consider now two isotopic atoms X^α and X^β with masses m_α and m_β and two isotopomers AX^α and AX^β with $m_\beta > m_\alpha$. Then, from Equations 4.95 and 4.99, according to the first quantum correction

$$\frac{s_2}{s_1} f(\text{AX}^\beta / \text{AX}^\alpha) = 1 + \frac{1}{24} \left(\frac{h}{kT} \right)^2 \sum_i^{3N-6} (v_i^2(\text{AX}^\alpha) - v_i^2(\text{AX}^\beta)) \quad (4.100a)$$

$$= 1 + \frac{1}{24} \left(\frac{h}{kT} \right)^2 \frac{1}{4\pi^2} (f_{xx} + f_{yy} + f_{zz})^* \left(\frac{1}{m_\alpha} - \frac{1}{m_\beta} \right) \quad (4.100b)$$

In Equation 4.100, $(f_{xx} + f_{yy} + f_{zz})^*$ is the sum of the three diagonal Cartesian force constants at the position of isotopic substitution, this sum being isotope independent.

In addition now consider a second set of isotopomers BX^α and BX^β . Then we obtain a second equation similar to Equation 4.100 for $(s_2/s_1)f$ for this pair of isotopomers and can write the equilibrium constant for the isotopic exchange reaction



as

$$K = (s_2/s_1) f(\text{AX}^\beta / \text{AX}^\alpha) / (s_2/s_1) f(\text{BX}^\beta / \text{BX}^\alpha) \quad (4.102)$$

In the first quantum correction, we find, since

$$\frac{1+x}{1+y} \approx 1 + x - y \quad (4.103)$$

for small x and y , that K can be written as

$$K = 1 + \frac{1}{24} \left(\frac{h}{kT} \right)^2 \frac{1}{4\pi^2} [(f_{xx} + f_{yy} + f_{zz})_{\text{AX}}^* - (f_{xx} + f_{yy} + f_{zz})_{\text{BX}}^*] \left(\frac{1}{m_\alpha} - \frac{1}{m_\beta} \right) \quad (4.104)$$

Thus, in the first quantum correction approximation, the isotope effect reflects the change in the force constants at the position of isotopic substitution between the two molecules involved in the isotopic fractionation. Moreover, the fractionation is such that the light atom enriches in the molecular species that has the smaller force constant. While this statement has been derived here only at high temperature, it can be generalized to state that **“isotope effects are probes for force constant changes at the position of isotopic substitution.”** That is what isotope effects are all about.

4.8.2 Polynomial Expansions of $(s_2/s_1)f$: Orthogonal Polynomial Methods

Bigeleisen and Ishida (BI) (see reading list) have explored the use of expansion methods to evaluate RPF. The Bernoulli expansion is an infinite series in even powers of frequencies and is expressed

$$\begin{aligned} \ln \frac{s_2}{s_1} f &= \sum_i \sum_{j=1}^{\infty} \frac{(-1)^{j+1} B_{2j-1} \delta u_i^{2j}}{2j (2j)!} \\ &= \sum_i \left(\frac{\delta u_i^2}{24} - \frac{\delta u_i^2}{2880} + \frac{\delta u_i^2}{181440} - \dots \right) \quad (u_i < 2\pi) \quad (4.105) \end{aligned}$$

where $\delta u_i^{2j} = (u_{1i}^{2j} - u_{2i}^{2j})$ and the B's are Bernoulli numbers ($B_1 = 1/6$, $B_2 = 1/30$, $B_3 = 1/42$, etc.) and the sum over i refers to frequencies. The first term is just that found in Equations 4.94 and 4.95. Equation 4.105 is of special interest because it provides means for calculating contributions to the thermodynamic functions and their isotope effects from shifts in individual force constants without solving the secular equations (by methods outlined in Chapter 3). The physical origin of the isotope effects is thus directly expressed. The sum of u_i^{2j} over all normal mode frequencies is equal to the trace of a matrix \mathbf{H}^j obtained by multiplying the Hamiltonian \mathbf{H} by itself ($j - 1$) times. Equation 4.105 is an example of a Taylor expansion but, unfortunately, is limited to $u_i < 2\pi$. BI point out that extension of this approach to $u_i > 2\pi$ is made possible by using orthogonal Jacobi and Chebyshev polynomial expansions as weighting functions. Although this approach to evaluating $(s_2/s_1)f$ was thoroughly explored in the late sixties and early seventies it is rarely employed at present because of the convenience and high accuracy of modern computer methods for solving the secular equations and evaluating complete expressions for isotopic partition function ratios.

4.9 Symmetry Numbers

4.9.1 Symmetry Numbers; Diatomic Molecules

We now explore the origins of the symmetry number, s , employed in the partition functions developed in Section 4.6 and listed in Table 4.1. Quantum mechanics requires the wave function for any system containing identical particles to either remain unchanged or to change sign if one interchanges any two of the identical particles. There are two physically distinct cases. If the wave function is unchanged then $\psi(1, 2) = \psi(2, 1)$ and we say that $\psi(1, 2)$ is symmetric with respect to the two particles which were exchanged. Particles with symmetric wave functions (Bosons) include photons and all other particles with integral spin. If the wave function changes sign then $\psi(1, 2) = -\psi(2, 1)$ and we say that $\psi(1, 2)$ is antisymmetric. Particles with antisymmetric wave functions (Fermions) include electrons, protons, neutrons and all other particles with half-integer spin.

We begin by considering the diatomic molecule as an example. The overall symmetry of the molecular wave function must include the properties of the nuclear wave function when the nuclei are permuted within the molecule. For an heteronuclear diatomic molecule with nuclei a and b the only permutation of nuclei allowed

is the identity operation. There are a number closely spaced nuclear spin wave functions $g_a = 2I_a + 1$ and $g_b = 2I_b + 1$ where I_a and I_b are the nuclear spins of the two atoms. For the molecule, the combined wave nuclear spin wave function is symmetric (since the identity operation does not give a change in sign), and yields a corresponding degeneracy in the nuclear spin partition function, $g_a g_b$. For an homonuclear diatomic each individual nucleus has the same wave function and degeneracy as before, but for the combined nuclear spin wave function both antisymmetric and symmetric combinations are possible. The antisymmetric combinations are catalogued as $[\psi_a(a)\psi_s(b) - \psi_s(a)\psi_a(b)]$, there are $[(g - 1)g/2]$ of these antisymmetric combinations, while the possible symmetric combinations are $[(\psi_a(a)\psi_s(b) + \psi_s(a)\psi_a(b))]$, there are $[(g - 1)g/2]$ of these, and $(\psi_{as}(a)\psi_s(b))$ $[(g)$ of these], for a total of $[(g + 1)g/2]$ symmetric combinations. The total number of possible wave functions of both types (the degeneracy) is then $g(g - 1)/2 + g(g + 1)/2 = g^2 (=g_a g_b)$, which is the same as for the heteronuclear case.

We must now combine the nuclear wave functions with the rest of the molecular wave function to generate a total wave function which is antisymmetric with respect to exchange of Fermions. For Bosons the total wave function must be symmetric. To do so we write $\psi = \psi_{\text{TRANS}} \psi_{\text{VIB}} \psi_{\text{ROT}} \psi_{\text{NUC-SPIN}}$ and recognize that both the vibrational and translational wave functions are symmetric. Rotational wave functions with even quantum numbers $J = 0, 2, 4, 6 \dots$ are symmetric and those with odd $J = 1, 3, 5 \dots$ are antisymmetric with respect to the nuclear coordinates. It follows that homonuclear diatomic molecules with anti-symmetric nuclear spin wave functions (nuclei with half-integer $I = 1/2, 3/2 \dots$) can combine only with symmetric rotational functions (even $J = 0, 2, 4 \dots$), while those with symmetric nuclear spin wave functions (even I) can combine only with antisymmetric rotational functions (odd $J = 1, 3, 5 \dots$). The partition function for rigid body rotation of a diatomic molecule, including effects of nuclear spin for a homonuclear diatomic molecule with nuclei of half integer spin is,

$$q_{\text{NS,ROT}} = \left[\frac{1}{2} g(g - 1) \right] \sum_{J=0,2,4..}^{\infty} (2J + 1) \exp[-J(J + 1)\Theta_{\text{ROT}}/T] \\ + \left[\frac{1}{2} g(g + 1) \right] \sum_{J=1,3,5..}^{\infty} (2J + 1) \exp[-J(J + 1)\Theta_{\text{ROT}}/T] \quad (4.106)$$

where $\Theta_{\text{ROT}} = h^2/(8\pi^2Ik)$. For homonuclear diatomic molecules of integer spin

$$q_{\text{NS,ROT}} = \left[\frac{1}{2} g(g + 1) \right] \sum_{J=0,2,4..}^{\infty} (2J + 1) \exp[-J(J + 1)\Theta_{\text{ROT}}/T] \\ + \left[\frac{1}{2} g(g - 1) \right] \sum_{J=1,3,5..}^{\infty} (2J + 1) \exp[-J(J + 1)\Theta_{\text{ROT}}/T] \quad (4.107)$$

and, finally, for heteronuclear diatomics

$$q_{\text{NS,ROT}} = g_{\text{A}} g_{\text{B}} \sum_{J=0}^{\infty} (2J+1) \exp[-J(J+1)\Theta_{\text{ROT}}/T] \quad (\text{heteronuclear}) \quad (4.108)$$

where $\Theta_{\text{ROT}} = h^2/(8\pi^2Ik)$.

For the case where the temperature is large and $\Theta_{\text{ROT}} \ll T$, which is the high temperature or classical limit, the sums over even and odd rotational quantum numbers become equal because the important terms in the sum involve large values of J . Therefore

$$\begin{aligned} \sum_{J=0,2,4..}^{\infty} (2J+1) \exp[-J(J+1)\Theta_{\text{ROT}}/T] &= \sum_{J=1,3,5..}^{\infty} (2J+1) \exp[-J(J+1)\Theta_{\text{ROT}}/T] \\ &= \frac{1}{2} \sum_{J=0,1,2..}^{\infty} (2J+1) \exp[-J(J+1)\Theta_{\text{ROT}}/T] \\ &= \frac{1}{2} \frac{T}{\Theta} = \frac{1}{2h^2} q_{\text{ROT,CLASSICAL}} \end{aligned} \quad (4.109)$$

Thus the factor 1/2 in Equation 4.109, above, arises naturally in the high temperature (classical) limit and is just the reciprocal of the symmetry number of the homonuclear diatomic molecule.

Examples: We now consider examples for $I = 0, 1/2$, and 1.

(A) For $I = 0$, as it is for ^{16}O , ^{18}O and many other nuclei including ^4He , ^{12}C , ^{32}S , ^{34}S , etc, $g = (2I + 1) = 1$. Using Equations 4.107 and 4.109 we obtain

$$\begin{aligned} q_{\text{NS,ROT}} &= \sum_{J=0,2,4..}^{\infty} (2J+1) \exp[-J(J+1)\Theta_{\text{ROT}}/T] \\ &= \frac{1}{2} \sum_{J=0,1,2..}^{\infty} (2J+1) \exp[-J(J+1)\Theta_{\text{ROT}}/T] = \frac{1}{2h^2} q_{\text{ROT,CLASSICAL}} \end{aligned} \quad (4.110)$$

(B) For $I = 1/2$ as it is for H, ^{13}C , ^{19}F , etc., $g = (2I + 1) = 2$. Using Equation 4.110,

$$\begin{aligned} q_{\text{NS,ROT}} &= \sum_{J=0,2,4..}^{\infty} (2J+1) \exp[-J(J+1)\Theta_{\text{ROT}}/T] \\ &\quad + 3 \sum_{J=1,3,5..}^{\infty} (2J+1) \exp[-J(J+1)\Theta_{\text{ROT}}/T] \end{aligned} \quad (4.111)$$

which using Equation 4.109 reduces at high temperature to

$$q_{\text{NS,ROT}} = \frac{4}{2} \frac{T}{\Theta} = \frac{1}{2h^2} q_{\text{ROT,CLASSICAL}} = \frac{1}{sh^2} q_{\text{ROT,CLASSICAL}} \quad (4.112)$$

because from Equation 4.108 in the high temperature limit for distinguishable (classical) particles

$$q_{\text{NS,ROT}} = g_A g_B \frac{T}{\Theta} = 4 \frac{T}{\Theta} \quad (4.112a)$$

For H_2 with its small moment of inertia the rotational level spacing is significant compared to kT even at room temperature and above. The two terms in Equation 4.110 thus refer to hydrogen molecules with significantly different physical properties. The first term on the right stemming from the combination of anti-symmetric nuclear spin and symmetric rotational wave functions refers to para hydrogen, while the second derived by combining symmetric nuclear spin and anti-symmetric rotational wave functions refers to ortho hydrogen. Note the ratio of statistical weights in the classical high temperature limit is $(\text{ortho/para})_{\text{HYDROGEN}} = 3/1$, while at very low temperature the para form predominates. The ortho/para notation follows the rule $\text{ortho/para} = (\text{larger statistical weight})/(\text{smaller statistical weight})$.

(C) For $I = 1$, as it is for D, ${}^6\text{Li}$, ${}^{14}\text{N}$ and other atoms, $g = (2I + 1) = 3$. From Equation 4.107

$$q_{\text{NS,ROT}} = 6 \sum_{J=0,2,4,\dots}^{\infty} (2J + 1) \exp[-J(J + 1)\Theta_{\text{ROT}}/T] + 3 \sum_{J=1,3,5,\dots}^{\infty} (2J + 1) \exp[-J(J + 1)\Theta_{\text{ROT}}/T] \quad (4.113)$$

which at high temperature reduces to

$$q_{\text{NS,ROT}} = \frac{9}{2} \frac{T}{\Theta} = \frac{1}{2h^2} q_{\text{ROT,CLASSICAL}} = \frac{1}{sh^2} q_{\text{ROT,CLASSICAL}} \quad (4.113a)$$

since from Equation 4.108 in the high temperature limit

$$q_{\text{NS,ROT}} = g_A g_B \frac{T}{\Theta} = 9 \frac{T}{\Theta} \quad (4.114)$$

Notice from Equation 4.113 for $I = 1$ (deuterium) it is the combination of the symmetric nuclear spin with the symmetric rotational functions which has the higher statistical weight. At high temperature $(\text{ortho/para})_{\text{DEUTERIUM}} = 2/1$, and at low temperature the ortho form predominates.

For each of the diatomic examples above, examples which include all possible combinations of symmetric or anti-symmetric nuclear spin wave functions

with symmetric or anti-symmetric rotational wave functions, for nuclei with both half-integer and integer spins, the symmetry number used in the relation relating the classical and quantum mechanical partition functions has been shown to arise naturally by calculating the degeneracies of the wave functions comparing distinguishable and indistinguishable particles.

From the quantum mechanical standpoint the appearance of the factor $1/2 = 1/s$ for the diatomic case means the configurations generated by a rotation of 180° are identical, so the number of distinguishable states is only one-half the classical total. Thus the classical value of the partition function must be divided by the symmetry number which is 1 for a heteronuclear diatomic and 2 for a homonuclear diatomic molecule.

The case of polyatomics, which is considered in more detail below, follows analogously. The point to keep in mind is that the symmetry restricts the number of distinguishable states. The symmetry number is the number of equivalent (indistinguishable) positions into which a molecule can be carried by rigid body rotation. For example $s = 12$ for CH_4 since the molecule can be held by a CH bond and rotated into three equivalent positions, and there are four CH bonds. Similarly for benzene $s = 12$ since there are six indistinguishable positions for rotation about an axis perpendicular to the plane of the molecule (and through its center), and six more when the molecule is flipped over.

The development above, which is similar to that found in many physical chemistry and statistical thermodynamic texts, is modeled closely after Berry et al. (Berry, R. S., Rice, S. A. and Ross, J. *Physical Chemistry*, Wiley, New York (1980)).

4.9.2 *Symmetry Numbers Continued, Comments, Polyatomics*

Proceeding in the spirit above it seems reasonable to inquire why s is equal to the number of equivalent rotations, rather than to the total number of symmetry operations for the molecule of interest. Rotational partition functions of the diatomic molecule were discussed immediately above. It was pointed out that symmetry requirements mandate that homonuclear diatomics occupy rotational states with either even or odd values of the rotational quantum number J depending on the nuclear spin quantum number I . Heteronuclear diatomics populate both even and odd J states. Similar behaviors are expected for polyatomic molecules but the analysis of polyatomic rotational wave functions is far more complex than it is for diatomics. Moreover the spacing between polyatomic rotational energy levels is small compared to kT and classical analysis is appropriate. These factors appreciated there is little motivation to study the quantum "rules" applying to individual rotational states of polyatomic molecules.

For practical purposes the rules for diatomic molecules concerning even and odd J reduce to the statement that for homonuclear diatomic molecules the molecular partition function must be divided by two ($s = 2$), while for heteronuclear diatomic molecules no division is necessary ($s = 1$). The idea of the symmetry number, s ,

goes back to Ehrenfest and Trekel in 1920. If one rotates a symmetric vibrationless molecule around some axis in such a way that the only difference between the original position of the molecule with respect to this axis system is identical to the original except that the (artificial) numbering of equivalent atoms will have changed, then the point where the rotated molecule is located cannot be regarded as a new point in phase space, since the molecule is indistinguishable from that same molecule before it was rotated. Thus, as in the discussion on phase space in Section 4.7, integration over all arrangements in phase space without restriction results in overcounting. Consequently the integral has to be multiplied by 1/2 or divided by 2 to compensate.

If (for a polyatomic) there are additional rotations that take the molecule into itself, then each rotation creates another point in phase space which in the quantum world is equivalent to the original point. Thus if there are s rotations that take the molecule into itself (including the identity “leave it alone” operation E of group theory) then one must divide the phase space integral by s . Spectroscopists and others usually designate the symmetry number as σ . In isotope chemistry, however, the symmetry number is referred to as “ s ” following the convention set by Bigeleisen and Mayer. Division by s is required even if the summation over individual quantum levels is replaced by integration (a procedure that is often used to obtain the high temperature limit for rotational partition functions). There is a large amount of evidence based on agreement between theoretical and experimental thermodynamic quantities which shows this procedure is valid.

How does one determine the symmetry number? As illustrated in the section above it is equal to the number of rotations that take the molecule into itself. Another and very attractive method is based on the use of group theory. Students who have taken a course in inorganic chemistry have been introduced to group theory. If the reader is uncomfortable with this topic the next few paragraphs can be skipped, especially since this method of finding molecular symmetry numbers need not to be used for finding the ratios of symmetry numbers, s_1/s_2 , required to understand isotopomer fractionation.

Use will be made of the character table for the point group of symmetry operations which take the defining points of the group into each other. All that we require from the character table is the number of rotations in the point group. For example, for methane the point group T_d consists of 24 elements including E the identity or “leave it alone” operation, 8 threefold rotation axes ($8C_3$), 3 twofold rotation axes ($3C_2$), 6 planes of reflection (6σ), and 6 fourfold rotation axes followed by a reflections in planes perpendicular to these axes ($6S_4$). Including the E operation there are twelve elements in the rotation subgroup. Thus the symmetry number for methane CH_4 is 12. The point group for CH_3D is C_{3v} . Including the E operation there are three rotational operations in this group and the symmetry number of CH_3D is 3. Herzberg’s well known text “Infrared and Raman Spectroscopy” has a list of symmetry numbers for various molecules; this table can easily be reproduced from the character tables included in the book. The same information is available in many other places.

4.9.3 *The Determination of Relative Symmetry Numbers for Isotopomers*

As already noted in considering the chemistry of isotopes one has no need for absolute symmetry numbers but only ratios of symmetry numbers. In the following the principles of a method to calculate such ratios will be presented and then applied to show that symmetry number factors do not lead to either depletion or enrichment of isotopes in the classical regime. The method is based on a simple formula due to Mayer and Mayer (reading list, 1st Ed). To appreciate their approach one must recognize that some molecules have several, Λ , minima of identical energy in their Born–Oppenheimer electronic energy surface. Identical molecules in one minimum or the other cannot be distinguished from one another. However, continuing with our example, methane has two minima, and substitutions of three of the protons in each minima by entities X, Y, Z forms CHXYZ molecules which are alike in most ways, but do have different optical properties. Polarized light passing through a solution of one or the other type rotates its plane of polarization in equal but opposite directions. The two types are mirror images of each other. All this is part of elementary organic chemistry and will not be pursued here. If a molecule contains n_1 atoms of kind 1, and n_2 atoms of kind 2 then $\prod_i n_i!$ permutations of these atoms are possible and would lead to different configurations of the molecule if the atoms were distinguishable. However, if the symmetry number is s , only $\prod_i \frac{n_i!}{s}$ of these configurations are different since each configuration can be transformed into s new configurations by rotation. This leads to a simple formula which relates Λ the number of identical electronic minima and s the symmetry number

$$\Lambda = \prod_i \frac{n_i!}{s} \quad (4.115)$$

The numerator in this expression is the number of ways of forming RX_n from n X atoms: if the X atoms are distinguishable, and s is the number of rotations which take the molecule into itself. For methane, symmetry point group T_d , $n = 4$, $n! = 24$ and $s = 12$. The ratio in Equation 4.115 is $24/12$. Thus there are 24 methanes (assuming distinguishable hydrogens) but there are two types, “a” and “b” of 12 molecules each, with type “a” not being able to rotate into type “b” and vice versa. They are mirror images. The $\Lambda = 2$ minima lead to the phenomenon of optical isomerization for the substituted methanes.

One can rewrite Equation 4.115 to yield a formula for the symmetry number

$$s = \prod_i \frac{n_i!}{\Lambda} \quad (4.116)$$

and using Equation 4.83

$$q_{\text{classical}} = (1/s)(1/h^{3N}) \int e^{-H/kT} \prod_N dq_j dp_j = \frac{\Lambda(1/h^{3N}) \int e^{-H/kT} \prod_{N_j} dq_j dp_j}{\prod n_i!} \quad (4.117)$$

keeping in mind that N is the total number of atoms in the molecule (here indexed j) and n_i is the number of equivalent atoms (5 and 4 in the case of CH_4).

Equation 4.117 makes complete sense. One of the first things one learns in dealing with phase space integrals is to be careful and not over-count the phase space volume as has already been repeatedly pointed out. In quantum mechanics equivalent particles are indistinguishable. The factor $\prod n_i!$ is exactly the number of indistinguishable permutations, while Λ accounts for multiple minima in the BO surface. It is proper that this factor be included in the symmetry number. Since the BO potential energy surface is independent of isotopic substitution it follows that Λ is also independent of isotope substitution and cannot affect the isotopic partition function ratio. From Equation 4.116 it follows

$$\frac{s_1}{s_2} = \frac{(\prod n_i!)_{\text{ISOTOPOMER1}}}{(\prod n_i!)_{\text{ISOTOPOMER2}}} \quad (4.118)$$

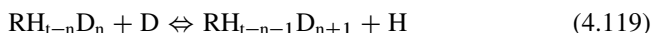
No detailed symmetry analysis is needed. Let us take a quick look at an example and calculate the symmetry number ratio for $\text{CH}_3\text{D}/\text{CH}_4$. For CH_3D $n_1 = 3$, $n_2 = 1$ and $\prod n_i! = (3!)(1!) = 6$ while for CH_4 $n_1! = 4! = 24$, there is no n_2 . Thus $s_{\text{CH}_3\text{D}}/s_{\text{CH}_4} = 6/24 = 1/4$

4.9.4 More Comments, Symmetry Numbers Do Not Lead to Isotope Enrichment

Isotope effects on equilibria have been formulated earlier in this chapter in terms of ratios of $(s_2/s_1)f$ values, referred to as reduced isotopic partition function ratios. From Equation 4.80, we recognize that the “true” value of the isotope effect is found by multiplying the ratio of reduced isotopic partition function ratios by ratios of s_2/s_1 values. Using Equation 4.116 one now knows how to calculate s_2/s_1 from ratios of factorials. Note well that symmetry numbers only enter when a molecule contains two or more identical atoms. Also note that at high temperature $(s_2/s_1)f$ approaches unity so that the high temperature equilibrium constant is the symmetry number factor.

In the following an explicit mathematical proof is presented to show that symmetry numbers factors do not lead to isotope enrichment. That result should come as no surprise since the factor on the right hand side of Equation 4.118 can be identified as

just the relative number of ways of forming the two isotopomers from a bath of the isotopic atoms. It is just a statistical factor. It cannot lead to isotopic enrichment. The proof proceeds as follows. Consider H and D substitution in a parent compound RH_t which has t identical H atoms. Consider the hypothetical equilibrium in which an H/D isotopomer of RH_t dissociates completely into atoms. It will be shown that the high temperature ratio of isotopic atom mole fraction H/D for the isotopic atoms, $p/(1-p)$, is exactly equal to this ratio in the isotopomer mix of RH_t molecules, RH_t , RH_{t-1}D , $\text{RH}_{t-2}\text{D}_2$, etc. Once this proof is given, the same proof applies to another molecule MH_u and its isotopomers. Consequently, if you have two sets of isotopomers, RH_t and MH_u , and both are in equilibrium with a reservoir of H and D atoms, then they must be in equilibrium with each other. The following proof is for two isotopes, the extension to three or more isotopes is left as an exercise for any reader who decides that such a proof is necessary. Consider the high temperature systems where all (s_2/s_1) f values are unity. Consider all isotopomers of RH_t in equilibrium with each other and with all the atoms that make up the respective molecular systems, in particular H and D atoms. Remember that, for D/H atomic species, not only is the (s_2/s_1) f value equal to unity but so is s_2/s_1 . Consider then the following family of isotopic exchange reactions at equilibrium



with $n = 0, \dots, t$. The equilibrium constant for this isotopic exchange equilibrium is given by

$$K = \frac{\frac{s_2}{s_1} f \left(\frac{\text{RH}_{t-n-1}\text{D}_{n+1}}{\text{RH}_{t-n}\text{D}_n} \right)}{\frac{s_2}{s_1} f \left(\frac{\text{D}}{\text{H}} \right)} \quad (4.120)$$

The symmetry number factors are derived from the reduced isotopic partition function ratio of the RH_t species.

$$\text{Symmetry number factor} = \frac{s_2}{s_1} = \frac{(t-n)!n!}{(t-n-1)!(n+1)!} = \frac{t-n}{n+1} \quad (4.121)$$

In terms of concentrations of species indicated by $[\]$'s (these may be pressures for gas phase equilibria), the high temperature equilibrium constant is given by

$$K = \frac{t-n}{n+1} = \frac{[\text{RH}_{t-n-1}\text{D}_{n+1}] [\text{H}]}{[\text{RH}_{t-n}\text{D}_n] [\text{D}]} \quad (4.122)$$

Thus,

$$(t-n) [\text{RH}_{t-n}\text{D}_n] = (n+1) [\text{RH}_{t-n-1}\text{D}_{n+1}] [\text{H}] / [\text{D}] \quad (4.123)$$

Applying Equation 4.123, one finds

$$\begin{aligned} {}^{(t)}[\text{RH}_t] &= [\text{RH}_{t-1}\text{D}][\text{H}] / [\text{D}], \quad (n = 0); \\ (t-1) [\text{RH}_{t-1}\text{D}] &= 2 [\text{RH}_{t-2}\text{D}_2][\text{H}] / [\text{D}], \quad (n = 1); \end{aligned} \quad (4.123a)$$

etc. for $n = 2, 3, \dots, t-1$.

The H/D ratio in the RH_t isotopomers is given by

$$(\text{H}/\text{D})_{\text{RH}_t} = \frac{t[\text{RH}_t] + (t-1)[\text{RH}_{t-1}\text{D}] + (t-2)[\text{RH}_{t-2}\text{D}_2] + \dots}{1[\text{RH}_{t-1}\text{D}] + 2[\text{RH}_{t-2}\text{D}_2] + 3[\text{RH}_{t-3}\text{D}_3] + \dots} \quad (4.124)$$

If one substitutes Equations 4.123a into 4.124, one immediately finds the interesting result that the $[\text{H}]/[\text{D}]$ ratio in the isotopomers of $\text{RH}_{t-n}\text{D}_n$ is exactly equal to the ratio $[\text{H}]/[\text{D}]$ in the gas phase atomic species. We have thus demonstrated that proper consideration of symmetry numbers leads to the result that the RH_t species have $[\text{H}]/[\text{D}]$ ratios exactly the same as those for the atomic species in the high temperature limit. QED.

4.10 Further Remarks on Temperature Dependence of $(s/s')f$: Limiting Forms: An Example

In Section 4.8, Equations 4.78, 4.79 and Table 4.1 develop the connections between the harmonic oscillator rigid rotor partition function and isotope chemistry as expressed by the reduced partition function ratio, RPF_R = $(s/s')f$. RPF_R is defined in Equation 4.79 as the product over oscillators of ratios of the function $[u \exp(-u/2)/(1 - \exp(u))]$

$$(s/s')f = \prod [u \exp(-u/2)/(1 - \exp(u))] / [u' \exp(-u'/2)/(1 - \exp(u'))] \quad (4.79)$$

Here, for convenience, we have employed the (prime/unprimed) notation introduced in Section 4.8 as substitute for $[(\text{subscript}_1 = \text{light}) / (\text{subscript}_2 = \text{heavy})]$. The prime always refers to the more lightly substituted isotopomer. For purposes of simplicity we now limit attention to the diatomic case where there is but one oscillator.

Figure 4.2 plots $[u \exp(-u/2)/(1 - \exp(u))]$ for primed and unprimed oscillators (and their ratio, $(s/s')f$ for $s = s'$) over a broad range of temperature for the case $u = u'/2^{1/2}$. The example is thus a good approximation for diatomic H/D substitution, i.e. H_2/D_2 or HBr/DBr , etc. since for harmonic oscillators $u'/u = v'/v = (\mu/\mu')^{1/2}$. [Recall $\mu_{AB} \sim (M_A M_B) / (M_A + M_B)$ so $\mu_{\text{HH}} \sim 1/2$, $\mu_{\text{DD}} \sim 1$, $\mu_{\text{HB}} \sim 0.988$, and $\mu_{\text{DB}} \sim 1.951$, and to sufficient accuracy $u'/u \sim 2^{1/2}$ in both cases.] The plots each decay exponentially from their value of unity at infinite temperature ($u = hv/kT = 0$) approaching zero at very low temperature.

At high temperature Equation 4.95 shows the limiting behavior of $(s/s')f$ as it decays to its value of unity at infinite temperature

$$(s/s')f = 1 + \Delta u^2/24 + \dots \quad (4.95)$$

and Fig. 4.3 compares the complete equation (Equation 4.79) with the high temperature limiting form, Equation 4.95, for our example, $u = u'/2^{1/2}$.

Finally in this section we turn our attention to the calculation of the isotope exchange equilibrium constant



The vibrational frequencies and rotational constants are given in Table 4.2. To good enough approximation $u = u'/2^{1/2}$ for both the H_2/D_2 and HI/DI pairs. Also

$$K = [(s/s')f(\text{H}_2/\text{D}_2)] / [(s/s')f(\text{HI}/\text{DI})]^2 \quad (4.126)$$

At all but very high temperatures it is necessary to employ the complete equation because the vibrational frequencies for all these molecules are quite high. (Notice at room temperature $u(\text{H}_2) \sim 21$, and $u(\text{HI}) \sim 11$). Harmonic oscillator rigid rotor calculated equilibrium constants are shown in Fig. 4.4. As expected the low temperature limiting value, while bounded, is significantly different from unity. At extremely high temperature Equation 4.95 applies and the isotope exchange constant is

$$\begin{aligned} K &= 1 + (1/24)(1-1/2^{1/2}) (v^2(\text{H}_2) - v^2(\text{HI})) (hc/k)^2/T^2 + \dots \\ &= 1 + 3.55 \times 10^5/T^2 + \dots \end{aligned} \quad (4.127)$$

That result is included in Fig. 4.4. For precise comparison with experiment harmonic oscillator rigid rotor results should be corrected for the effects of nonclassical rotation and anharmonicity. In the region of the maximum (Fig. 4.4) these corrections (see Appendix 4.2), which are temperature dependent, lower the calculated results by several percent. The spectroscopic data employed for the calculation reported in Fig. 4.4 are shown in Table 4.2.

Table 4.2 Spectroscopic properties needed to calculate K_{eq} for Equation 4.125, $\text{H}_2 + 2\text{DI} = \text{D}_2 + 2\text{HI}$ (Herzberg, *G. Spectra of Diatomic Molecules, 2nd Ed.*, Van Nostrand-Rheinhold, New York 1950)

Molecule	ω_e/cm^{-1}	$\omega_e x_e/\text{cm}^{-1}$	B_0/cm^{-1}	σT
H_2	4405.3	125.3	59.3	85.4
D_2	3117.1	63.0	29.9	43.0
HI	2309.5	39.7	6.5	9.3
DI	1640.2	20.0	3.3	4.7

Herzberg uses ν and ω to symbolize observed (anharmonic) and harmonic vibrational frequencies, respectively.

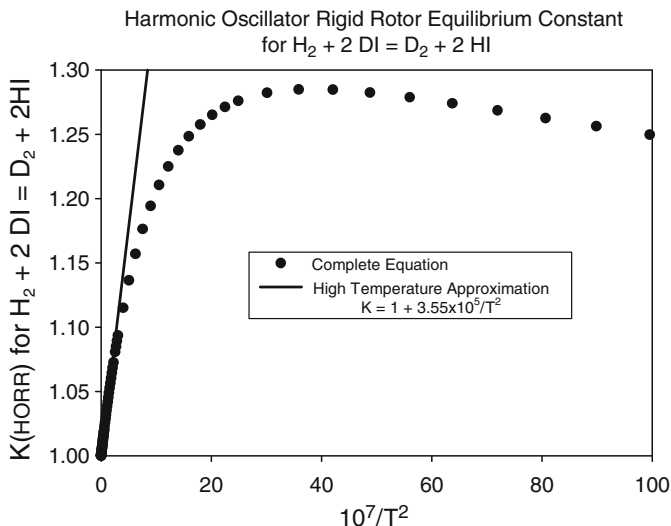


Fig. 4.4 Harmonic oscillator rigid rotor equilibrium constant for $\text{H}_2 + 2 \text{ DI} = \text{D}_2 + 2 \text{ HI}$

4.11 Transition State Theory of Isotope Effects

Isotope effects on rates (so-called kinetic isotope effects, KIE's) of specific reactions will be discussed in detail in a later chapter. The most frequently employed formalism used to discuss KIE's is based on the activated complex (transition state) theory of chemical kinetics and is analogous to the theory of isotope effects on thermodynamic equilibria discussed in this chapter. It is thus appropriate to discuss this theory here.

4.11.1 Fundamentals of Transition State Theory

The idea that an activated complex or transition state controls the progress of a chemical reaction between the reactant state and the product state goes back to the study of the inversion of sucrose by S. Arrhenius, who found that the temperature dependence of the rate of reaction could be expressed as $k = A \exp(-\Delta E^*/RT)$, a form now referred to as the Arrhenius equation. In the Arrhenius equation k is the forward rate constant, ΔE^* is an energy parameter, and A is a constant specific to the particular reaction under study. Arrhenius postulated thermal equilibrium between inert and active molecules and reasoned that only active molecules (i.e. those of energy $E_0 + \Delta E^*$) could react. For the full development of the theory which is only sketched here, the reader is referred to the classic work by Glasstone, Laidler and Eyring cited at the end of this chapter. It was Eyring who carried out many of the



[Historical Vignette 4.3] Henry Eyring (1901–1981) was born on a ranch in the Mormon community of Colonia Juarez, Mexico, then educated at the Universities of Arizona and California, Berkeley. After a short stay at the University of Wisconsin, Eyring was awarded a National Research Council fellowship at the Kaiser Wilhelm Institute in Berlin. His chief collaboration there was with Michael Polanyi. Together with Polanyi he carried out the first quantum mechanical calculation of the potential energy surface for the reaction $\text{H} + \text{H}_2 = \text{H}_2 + \text{H}$. This, at the time, turned out to be a formidable problem, but by introducing clever and intuitive approximations a surface was produced. In due course it led to Eyring's most important scientific contribution: the development of the notion of the activated complex and transition state theory. Eyring spent the years 1932–1946 at Princeton University, moving in 1946 to the University of Utah as Dean of the Graduate School. His efforts over the next 35 years established that institution as a major research university. Eyring was a prolific and highly energetic scientist, and a writer with wide interests. He reported on early calculations of vapor pressure isotope effects, developed the significant structures (statistical thermodynamic) theory of condensed phases, produced a theory of optical rotary dispersion, etc. In addition to his scientific activities, Eyring was an influential member of the hierarchy of the Mormon Church. In that role he wrote extensively on the interface between science and religion. Eyring had a compelling personality. He was a master of communicating ideas and traveled widely, giving many talks. (Pencil sketch courtesy of N. Van Hook 2009)

early studies of this approach to kinetics and his name is often associated with the theory (Historical Vignette 4.3). The term “transition state theory” as an alternate to “activated complex theory” was coined by M. Polanyi and M. G. Evans.

In Chapter 2, we discussed the Schrödinger equation for the ground state of a stable molecule. We made use of the Born–Oppenheimer approximation to separate the electronic motion from the nuclear motion and then considered the solutions which express the electronic energy of the system as a function of the nuclear configuration. The electronic Schrödinger equation contains a Hamiltonian operator that is made up of terms corresponding to the kinetic energy of the electrons and a potential energy term which describes all the electrostatic interactions among the electrons and the atomic nuclei. The electronic energy is calculated as a function of nuclear configuration and for a stable molecule one finds a minimum energy which corresponds to the equilibrium nuclear configuration of the molecule. Since the equilibrium configuration corresponds to an energy minimum, the first derivatives

of the electronic energy with respect to distortion from that configuration are zero. However, the second derivatives are positive (the energy increases away from the minimum). The electronic energy for nuclear configurations sufficiently far from the minimum corresponds to the electronic dissociation energy into products. Within the Born–Oppenheimer approximation, the electronic energy as a function of nuclear configuration is the isotope independent potential energy surface for nuclear motion.

Consider now a chemical reaction



The Born–Oppenheimer approximation applies here just as it does for a single molecule. Calculate the electronic energy as a function of nuclear configuration. The problem is shown schematically in Fig. 4.5. Corresponding to certain configurations

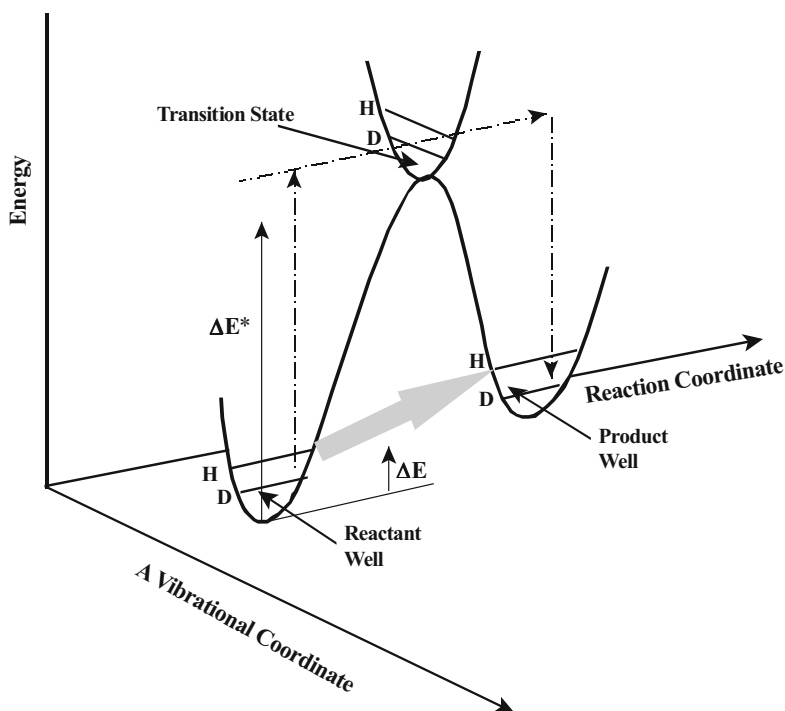


Fig. 4.5 Schematic projection of the energetics of a reaction. The diagram shows the Born–Oppenheimer energy surface mapped onto the reaction coordinate. The barrier height ΔE^* has its zero at the bottom of the reactant well. One of the $3n - 6$ vibrational modes orthogonal to the reaction coordinate is shown in the transition state. H and D zero point vibrational levels are shown schematically in the reactant, product, and transition states. The reaction as diagrammed is slightly endothermic, $\Delta E > 0$. The semiclassical reaction path follows the *dash-dot arrows*. Alternatively part of the reaction may proceed by tunneling through the barrier from reactants to products with a certain probability as shown with the *gray arrow*

of the nuclei, there will be non-interacting molecules A and B; for other configurations there will be non-interacting molecules E and F. Presumably as one brings A and B together, the electronic energy will rise.

Depending on whether the reaction considered is endo- or exo-ergic, the electronic energy of E and F is higher or lower than the energy of A and B. Independent of whether the reaction is endo- or exo-ergic, there will be an energy barrier between reactants and products and this barrier gives rise to the activation energy for the reaction. The electronic energy as a function of nuclear configuration for the molecules A and B (and E and F) as in the case of a single molecule is the isotope independent potential energy for nuclear motion in the Born–Oppenheimer approximation. If one plots paths in coordinate space leading from reactants to products, one has to surmount the energy barrier, but there is will be one path that leads to the minimum barrier (like a “minimum effort” path, or “pass” across a mountain range) and the top of this minimum path corresponds to the nuclear configuration of the transition state. The transition state is the maximum on the minimum energy path from reactants to products. At the transition state, the electronic energy of the system does have zero first derivatives with respect to nuclear distortion. The second derivatives, however, have to be such that the electronic energy increases for all nuclear distortions except the one which corresponds to the direction of moving the transition state either back to reactants or forward to products.

As already noted, in the Born–Oppenheimer approximation, the nuclear motion of the system is subject to a potential which expresses the isotope independent electronic energy as a function of the distortion of the coordinates from the position of the transition state. An analysis of the motions of the N-atom transition state leads to three translations, three rotations (two for a linear molecule), and $3N - 6$ ($3N - 5$ for a linear transition state) vibrations, one which is an imaginary frequency (e.g. $\nu = 400i \text{ cm}^{-1}$ where $i = \sqrt{-1}$), and the others are real vibrational frequencies. The imaginary frequency corresponds to motion along the so-called reaction coordinate and is referred to as ν_L^\ddagger where the (\ddagger) symbol refers to the transition state. The curvature in this coordinate is negative (concave), while curvatures in the other $3N - 5$ ($3N - 4$) dimensions are positive (convex). Reaction 4.128 thus proceeds as follows. The reactants are assumed to be in thermal equilibrium with the transition state



with AB^\ddagger referring to transition state. The equilibrium constant is designated K^\ddagger . Then

$$K^\ddagger = [AB^\ddagger] / [A][B] \quad (4.130)$$

where the brackets [] refer to concentration. The N^\ddagger atomic transition state is taken to have the following degrees of freedom: three translations, three (2) rotations, $3N^\ddagger - 7$ ($3N^\ddagger - 6$) vibrational frequencies corresponding to the $3N^\ddagger - 6$ ($3N^\ddagger - 5$) real frequencies obtained for the transition state from the analysis of the second derivatives, and the last corresponding to the motion of the transition state across the energy barrier. This last degree of freedom is often assumed to be a translational

motion of an effective mass m^* moving in a one-dimensional box of length δ . The equilibrium constant for the gas phase reaction is formulated in terms of partition functions for the reactants and for the transition states (with the transition state degrees of freedom noted above). The transition state is assumed to decompose with equal probability to either reactants or products. The motion which corresponds to decomposition is the one-dimensional translation with effective mass m^* referred to above. Its velocity is calculated from a one-dimensional Maxwell–Boltzmann distribution, and the rate of decomposition obtained by combining the velocity with the length δ of the transition state. Finally a transmission coefficient κ is introduced to account for quantum mechanical effects in the translational motion (tunneling or reflection through or at the barrier); in practice κ is either replaced by unity or by the Wigner or Bell tunneling corrections (see reading list). Tunnel corrections are discussed in more detail in Section 6.3.

4.11.2 Introduction of the Partition Functions

Let us now put all of this together to obtain a numerical value of the rate constant k for the chemical reaction. Note that chemists always use the symbol k for the rate constant. Elsewhere in this chapter and in other chapters, we also use k for Boltzmann's constant. Whenever there is a possibility of confusion, we will use k_B for Boltzmann's constant. The rate constant is defined by the relation

$$-\frac{d[A]}{dt} = k[A][B] \quad (4.131)$$

where the left-hand side is the time rate of disappearance of concentration of A. In terms of the transition state theory of the previous section, $-d[A]/dt$ is given by the equilibrium concentration of transition state $[AB^\ddagger]$ multiplied by the rate of decomposition of the transition state, r , and by κ the probability in the forward direction (to products) rather than the reverse (to reactants).

Then

$$-\frac{d[A]}{dt} = r[AB^\ddagger]\kappa \quad (4.132)$$

With use of Equation 4.130, we obtain

$$= -\frac{d[A]}{dt} = rK^\ddagger\kappa[A][B] \quad (4.133)$$

and obtain an expression for the rate constant k in terms of the equilibrium constant K^\ddagger

$$k = rK^\ddagger\kappa \quad (4.134)$$

This equation contains the factor r , the rate of decomposition of the transition state which depends on the effective mass m^* , and κ , neither of which is simple to estimate. However, the statistical mechanical expression for K^\ddagger also contains m^* and δ in the one-dimensional translational partition function corresponding to translation along the reaction coordinate. Combining the factor r above with the one-dimensional translational partition function for motion across the barrier, one obtains (see references at the end of the chapter) the simple result

$$r = \frac{k_B T}{h} \quad (4.135)$$

where k_B is Boltzmann's constant, T is temperature and h is Planck's constant. All reference to m^* and δ has disappeared. One then obtains for the rate constant

$$k = \frac{k_B T}{h} K' \kappa \quad (4.136)$$

K^\ddagger has been replaced by K' to indicate that the statistical mechanical expression for the partition function contains only $3N^\ddagger - 7$ ($3N^\ddagger - 6$, if linear) real vibrational frequencies, and that there is no contribution in the partition function corresponding to the imaginary frequency. The parameter κ is dominated by the tunneling correction. The Wigner tunneling correction, which is only correct for small tunneling and therefore only appropriate in the case of heavy atom isotope effects, is given by

$$\kappa = 1 + \frac{h^2}{24} \frac{|\nu_L^\ddagger|^2}{(k_B T)^2} = 1 + \frac{|u_L^\ddagger|^2}{24} \quad (4.137)$$

Equation 4.137 is only valid for $(u_L^{\ddagger 2}/24) \ll 1$. Remember that ν_L^\ddagger is the imaginary transition state frequency and $u_L^\ddagger = h\nu_L^\ddagger / k_B T$. A more complete discussion of tunnel corrections, including tunnel corrections for light atom isotope effects (e.g. H/D) is given in Chapter 6.

Returning to Equation 4.136 we see the isotope effect on the rate constant is then given by

$$\frac{k_1}{k_2} = \frac{K_1' \kappa_1}{K_2' \kappa_2} \quad (4.138)$$

where 1 and 2 refer, as usual, to reactions involving different isotopomers (say A_1 and A_2 as reactants in Equation 4.128 and their corresponding isotopomer transition states $A_1 B^\ddagger$ and $A_2 B^\ddagger$). To sum up, the calculation of the kinetic isotope effect requires a calculation of an isotope effect on an equilibrium constant K' for

the equilibrium between reactants and transition state. The prime indicates that the contribution of one degree of freedom in the transition state, the one corresponding to translation along the reaction coordinate has been considered separately, and the corresponding imaginary frequency ν_L^\ddagger in the transition eliminated as a vibrational degree of freedom (although, caveat, it will be seen that this frequency reappears in the final expression for the isotope effect when the Teller–Redlich Product Rule is applied).

The partition function ratios needed for the calculation of the isotope effect on the equilibrium constant K_1^\ddagger will be calculated, as before, in the harmonic-oscillator-rigid-rotor approximation for both reactants and transition states. One obtains in terms of molecular partition functions q

$$\frac{K_1^\ddagger}{K_2^\ddagger} = \frac{(q_{A_2} q_B / q_{A_1} q_B)}{\left(q'_{A_2 B^\ddagger} / q'_{A_1 B^\ddagger} \right)} = \frac{(q_{A_2} / q_{A_1})}{\left(q'_{A_2 B^\ddagger} / q'_{A_1 B^\ddagger} \right)} \quad (4.139)$$

Equation 4.139 has been written for the case where the isotopic substitution is on reactant molecule A only. Therefore the q_B ratio in the numerator cancels. The partition function ratio q_{A_2}/q_{A_1} in the numerator can be replaced by isotopic ratios of translational, rotational, and vibrational partition functions as in Equation 4.76. However, in the denominator one has to be careful to remember that the isotopic partition ratio involves the q' functions which contain only $3N^\ddagger - 7$ (for a linear transition state $3N^\ddagger - 6$) vibrational frequencies, one vibration, ν_L^\ddagger , having been replaced by a translation along the reaction coordinate which was included in the factor $k_B T/h$ (then eliminated when the isotopic ratio of rate constants was introduced). Thus

$$\frac{q'_{A_2 B^\ddagger}}{q'_{A_1 B^\ddagger}} = \frac{s_1^\ddagger}{s_2^\ddagger} \frac{M_2^{\ddagger \frac{3}{2}}}{M_1^{\ddagger \frac{3}{2}}} \frac{\left(I_{A_2}^\ddagger I_{B_2}^\ddagger I_{C_2}^\ddagger \right)^{\frac{1}{2}}}{\left(I_{A_1}^\ddagger I_{B_1}^\ddagger I_{C_1}^\ddagger \right)^{\frac{1}{2}}} \frac{(3N^\ddagger - 6)}{3N^\ddagger - 7} \prod_i \left(\frac{1 - e^{-h\nu_{i1}^\ddagger/kT}}{1 - e^{-h\nu_{i2}^\ddagger/kT}} \right) e^{\frac{1}{2} h \sum_i^{(3N^\ddagger - 6)} (\nu_{i1}^\ddagger - \nu_{i2}^\ddagger)/kT} \quad (4.140)$$

Equation 4.140 is the exact analogue of Equation 4.76 for a stable molecule except there is one less vibrational degree of freedom. It must now be noted that the derivation of the Teller–Redlich Product Rule, applies equally well to a transition state as to a stable molecule. Thus, when the Teller–Redlich Product rule is introduced into the expression for q_2/q_1 of a transition state, the ratio of vibrational frequencies includes the isotopic ratio of the imaginary frequencies in the transition state. One can then write for transition state isotopic ratios, analogously to Equation 4.78

$$\frac{s_2^\ddagger q_2^\ddagger}{s_1^\ddagger q_1^\ddagger} = \frac{\nu_{2L}^\ddagger}{\nu_{1L}^\ddagger} \prod_i^{3N^\ddagger} \left(\frac{m_{2i}^\ddagger}{m_{1i}^\ddagger} \right)^{\frac{3}{2}} \prod_i^{3N^\ddagger-7} \frac{u_{2i}^\ddagger}{u_{1i}^\ddagger} \left(\frac{1 - e^{-u_{1i}^\ddagger}}{1 - e^{-u_{2i}^\ddagger}} \right) e^{(u_{1i}^\ddagger - u_{2i}^\ddagger)} / 2 \quad (4.141)$$

Finally, one defines a reduced partition function ratio for the transition state as

$$\left(\frac{s_2}{s_1} \right) f^\ddagger = f^\ddagger = \prod_i^{3N^\ddagger-7} \frac{u_{2i}^\ddagger}{u_{1i}^\ddagger} \left(\frac{1 - e^{-u_{1i}^\ddagger}}{1 - e^{-u_{2i}^\ddagger}} \right) e^{(u_{1i}^\ddagger - u_{2i}^\ddagger)} / 2 \quad (4.142)$$

This equation for the reduced isotopic partition function ratio of a transition state differs from that for a normal stable molecule only in that one frequency, the imaginary frequency of the transition state ν_L^\ddagger , is missing from the expression.

Having now considered the isotopic ratio in the denominator on the right hand side of Equation 4.139, one has no difficulty with the numerator (which refers to the isotopomer reactant molecules), to obtain

$$\frac{k_1}{k_2} = (\text{symmetry number factor}) \frac{\nu_{1L}^\ddagger}{\nu_{2L}^\ddagger} \frac{\left(\frac{s_2}{s_1} f \right) (A_2/A_1)}{\left(\frac{s_2}{s_1} f^\ddagger \right) (A_2 B^\ddagger / A_1 B^\ddagger)} \frac{\kappa_1}{\kappa_2} \quad (4.143)$$

It should be emphasized that the symmetry number ratio (s_2/s_1) f is entered as a multiplier of (s_2/s_1) f so that the symmetry number factors which lead to no isotopic enrichment in themselves are left out. To obtain the complete isotope effect one has to multiply the above expression by symmetry number ratios so that the symmetry number ratios in front of the f expressions are removed. So the symmetry number factor in Equations 4.143 and 4.144 is given by

$$\frac{\left(\frac{s_1}{s_2} \right) (A_1/A_2)}{\left(\frac{s_1}{s_2} \right) (A_1 B^\ddagger / A_2 B^\ddagger)} \quad (4.144)$$

4.11.2.1 Further Details: The MMI \times EXC \times ZPE Formalism

Combining Equations 4.77, 4.140 and 4.145 we obtain a useful expression for the isotopic rate ratio

$$\begin{aligned}
 \left(\frac{k_1}{k_2}\right) (\text{SymmetryNumberFactor})^{-1} &= \left(\frac{M_1^\ddagger M_2}{M_2^\ddagger M_1}\right)^{3/2} \left(\frac{I_{A_1}^\ddagger I_{B_1}^\ddagger I_{C_1}^\ddagger}{I_{A_2}^\ddagger I_{B_2}^\ddagger I_{C_2}^\ddagger} \times \frac{I_{A_2} I_{B_2} I_{C_2}}{I_{A_1} I_{B_1} I_{C_1}}\right)^{1/2} \\
 &\times \prod_i^{3N^\ddagger-7} \frac{1 - e^{-u_{i2}^\ddagger}}{1 - e^{-u_{i1}^\ddagger}} \prod_i^{3N-6} \frac{1 - e^{-u_{i1}}}{1 - e^{-u_{i2}}} \\
 &\times \prod_i^{3N^\ddagger-7} \frac{e^{u_{i2}^\ddagger/2}}{e^{u_{i1}^\ddagger/2}} \prod_i^{3N-6} \frac{e^{u_{i1}/2}}{e^{u_{i2}/2}} \quad (4.145)
 \end{aligned}$$

which can be mnemonically represented as

$$\text{KIE} = \text{MMI} \times \text{EXC} \times \text{ZPE} \quad (4.146)$$

The MMI (mass moment of inertia), EXC (excitation factor), and ZPE (zero point energy) terms are defined on successive lines of Equation 4.145. For reactions involving heavier isotopes the effects are no longer concentrated in the ZPE term and it is convenient to apply the Teller–Redlich product rule (Section 3.5.1) and eliminate the moments of inertia by using Equations 4.79, 4.79a, and 4.141, thus obtaining an equivalent relation

$$\begin{aligned}
 \left(\frac{k_1}{k_2}\right) (\text{SymmetryNumberFactor})^{-1} &= \frac{v_{L(1)}^\ddagger}{v_{L(2)}^\ddagger} \prod_i^{3N^\ddagger-7} \frac{u_{i(1)}^\ddagger}{u_{i(2)}^\ddagger} \prod_i^{3N-6} \frac{u_{i(2)}}{u_{i(1)}} \\
 &\times \prod_i^{3N^\ddagger-7} \frac{1 - e^{-u_{i2}^\ddagger}}{1 - e^{-u_{i1}^\ddagger}} \prod_i^{3N-6} \frac{1 - e^{-u_{i1}}}{1 - e^{-u_{i2}}} \\
 &\times \prod_i^{3N^\ddagger-7} \frac{e^{u_{i2}^\ddagger/2}}{e^{u_{i1}^\ddagger/2}} \prod_i^{3N-6} \frac{e^{u_{i1}/2}}{e^{u_{i2}/2}} \quad (4.147)
 \end{aligned}$$

Equation 4.147 is mnemonically written as $\text{KIE} = \frac{v_{L(1)}^\ddagger}{v_{L(2)}^\ddagger} \times \text{PDT} \times \text{EXC} \times \text{ZPE}$ where PDT (product factor), EXC and ZPE are defined on successive lines. The leading term is of course the ratio of imaginary frequencies along the reaction coordinate.

4.11.3 Comments

4.11.3.1 The Wigner Correction

The Wigner correction for tunneling has been given by Equation 4.137. This is valid only if $u_L^\ddagger/24$ is small compared to unity (see Figs. 4.2 and 4.3). It is only rarely useful for studying primary kinetic isotope effects involving isotopes of hydrogen. Other methods of dealing with large tunneling corrections will be discussed in Chapter 6.

4.11.3.2 The High Temperature Limit

The importance of understanding isotope effects in the high temperature (classical) limit has been stressed before. In the limit of infinite temperature, the reduced isotopic partition function ratios all go to unity and κ_1/κ_2 also goes to unity. The kinetic isotope effect becomes

$$\lim_{T \rightarrow \infty} \left(\frac{k_1}{k_2} \right) = \frac{v_{1L}^\ddagger}{v_{2L}^\ddagger} (\text{symmetry number factor}) \quad (4.148)$$

It has been previously noted that the first quantum correction to the classical high temperature limit for an isotope effect on an equilibrium constant is interesting. Each vibrational frequency makes a contribution $\phi(u)$ to RPFR and this contribution can be expanded in powers of u with the first non-vanishing term proportional to $u^2/24$, the so called first quantum correction. Similarly, for rates one introduces the first quantum correction for the reduced partition function ratios, includes the Wigner correction for κ_1/κ_2 and makes use of relations like Equation 4.103 for small x and small y , to find a value for the rate constant isotope effect (omitting the non-interesting symmetry number term)

$$\frac{k_1}{k_2} = \frac{v_{1L}^\ddagger}{v_{2L}^\ddagger} \left[1 + \frac{1}{24} \left(\frac{h}{kT} \right)^2 \left[\sum_i^{3N-6(5)} (v_i^2(A_1) - v_i^2(A_2)) - \sum_i^{3N^\ddagger-6(5)} (v_i^2(A_1B^\ddagger) - v_i^2(A_2B^\ddagger)) \right] \right] \quad (4.149)$$

The vibrational sum rule (Equation 4.99) applies to transition states even when one of the frequencies is imaginary (and v_i^2 is negative for that frequency). In that case one finds for k_1/k_2 , with omission of the symmetry number factor, the analogue of Equation 4.105 for the exchange equilibrium constant

$$\frac{k_1}{k_2} = \frac{v_{1L}^\ddagger}{v_{2L}^\ddagger} \left(1 + \frac{1}{24} \left(\frac{h}{kT} \right)^2 \left(\frac{1}{m_1} - \frac{1}{m_2} \right) [(f_{xx} + f_{yy} + f_{zz})_A^* - (f_{xx} + f_{yy} + f_{zz})_{AB^\ddagger}^*] \right) \quad (4.150)$$

As written Equation 4.150 applies to the case of a single isotopic substitution in reactant A with light and heavy isotopic masses m_1 and m_2 , respectively. Equation 4.150 shows that the first quantum correction (see Section 4.8.2) to the classical rate isotope effect depends on the difference of the diagonal Cartesian force constants at the position of isotopic substitution between the reagent A and the transition state. While Equations 4.149 and 4.150 are valid quantitatively only at high temperature, we believe, as in the case of equilibrium isotope effects, that the claim that isotope effects reflect force constant changes at the position of isotopic substitution is a qualitatively correct statement even at lower temperatures.

4.11.3.3 Remarks

The use of reduced isotopic partition function ratios to study kinetic isotope effects was first undertaken by Bigeleisen; this work was corrected and elaborated by Bigeleisen and Wolfsberg. References are cited at the end of this chapter. Application of the equations developed above to specific chemical reactions will be found in Chapter 10, where other theoretical approaches will also be presented.

It is appropriate to make a few general comments about Equation 4.143 without considering specific chemical reactions. The factor $\nu_{1L}^\ddagger / \nu_{2L}^\ddagger$ on the left, is the high temperature isotope effect and can be shown to be equal to or larger than unity supposing 1 and 2 refer to light and heavy isotopes, respectively. The more interesting term is the one expressing the ratio of isotopic partition function ratios of reactant divided by the corresponding isotopic partition function ratio of the transition state. With the heavy/light notation specified above, each of the reduced isotopic partition function ratios will be equal to or larger than unity so $(s_1/s_2)_f$ values tend to be larger for larger force constants (i.e. stronger bonding). With $1/2 = \text{light/heavy}$ one expects $k_1 > k_2$ when the transition state is less tightly bonded (lower force constants at the position of isotopic substitution in the transition state than in the reactant). On the other hand, if the transition state is more tightly bonded than the reactant, as would be the case if the isotopic reactant is an atom, one expects k_1/k_2 to be less than unity. This situation is referred to as an inverse rate isotope effect. Experimentally observed kinetic isotope effects tend to follow these expectations.

4.12 The Development of Modern Methods to Calculate Reduced Isotopic Partition Function Ratios

In earlier sections of this chapter we learned that the calculation of isotope effects on equilibrium constants of isotope exchange reactions as well as isotope effects on rate constants using transition state theory, TST, requires the evaluation of reduced isotopic partition function ratios, RPF_R's, for ordinary molecular species, and for transition states. Since the procedure for transition states is basically the same as that for normal molecular species, it is the former which will be discussed first.

4.12.1 *The Calculation of $(s/s')f$ for Normal Molecular Species*

From the formulae discussed above, especially in Sections 4.5 and 4.6 and Table 4.1, we know that calculation of RPF_R's requires knowledge of the equilibrium geometry of the molecule, the principal moments of inertia, and the $3N - 6$ ($3N - 5$ for linear molecules) normal mode vibrational frequencies of the isotopic molecules involved. Vibrational frequency data from infrared and Raman spectroscopic measurements are available for a great many compounds. Similarly data from rotational spectroscopy (mainly in the microwave region) has enabled the calculation of equilibrium geometries and moments of inertia. So, off hand, the obvious procedure for calculating $(s/s')f$ would seem to be the substitution of experimentally observed values into the formulae derived for the reduced isotopic partition function ratios (see Table 4.1). This has proved to be an entirely unsatisfactory procedure. Except for diatomic and other small molecular systems, it has usually been impossible to observe all the normal mode vibrational frequencies of all the isotopic molecules required. Furthermore the precision of vibrational frequency measurements is often insufficient to represent isotopic frequency shift data at the precision required to calculate useful RPF_R values. Moreover the observed frequencies are obviously anharmonic, and uncertainties in the corrections needed to produce sets of harmonic frequencies are troubling. For these reasons, beginning in thirties, and continuing almost to the present day, a minor cottage industry developed which made use of isotopes and experimental spectroscopy to find the set of isotope independent force constants which a given number of isotopomers share within the framework of the Born–Oppenheimer approximation. Such work became the subject of many Ph.D. theses in physical chemistry. The calculations were usually carried in terms of valence coordinates with use of the GF matrix technique (see Chapter 3). That set of force constants can then be employed to calculate a self consistent set of harmonic frequencies for all isotopomers and thence high precision frequency shifts and RPF_R's. Also, early on, such calculations allowed the development of useful generalizations concerning the nature of chemical bonding. For example, on the one hand, they showed that force constants for CH bond stretching while approximately the same from molecule to molecule, were not strictly transferable from a CH bond in one molecule to a CH bond in another, or for that matter even in the same molecule. On the other hand, the approximate sameness gave chemists an idea of the magnitudes of various constants so that one was able to guess at frequencies for a given set of molecules and the isotope effects on these frequencies without recourse to experimental spectral data. It goes without saying that the majority of such work was carried out in the harmonic approximation. The main computational labor in the vibrational calculations involves the diagonalization of matrices, a procedure which has already been discussed (Chapter 3). The size of these matrices can be as large as the number of normal coordinates ($3N - 6$ by $3N - 6$ for a non-linear N atomic molecule) unless advantage can be taken of molecular symmetry. For historical interest it should be mentioned that the diagonalization of a 4×4 matrix using of a mechanical calculator of the type available during the 1930s, 1940s and 1950s, took 30 min to 1 h of labor, and the effort increased exponentially with size to the

point where it was impractical for matrices larger than, say, 8×8 . This situation started to change in the mid 1950s with the advent of digital computers, although even then diagonalizations of large matrices were still a long way off. Thus, one of the authors (MW) approached Wallace Givens, a mathematician from Oak Ridge who was visiting the Courant Institute at New York University, to ask whether it was possible to diagonalize a matrix as large as 40×40 . Givens replied that he had an algorithm for carrying out such a calculation and would ask a student to write the necessary program. So, we were able to carry out calculations for non-symmetric molecules containing as many as 13 atoms. The matrix diagonalization program “worked” and is still being used; it is known as the Givens routine.

The fast digital computer revolutionized methods for deducing force constants from observed vibrational spectra. In particular, J. H. Schachtscheider and R. S. Snyder (reading list, Chapter 3), wrote a program based on the GF matrix method and used their programming suite to study the spectra of all the lower alkanes. They generously made their program available to one of the authors (MW) around 1960. Prior to about 1960 many theoretical studies on isotope effects had dealt with the equations of isotope effects calculating RPF_R's by employing a limited number of terms from the Bernoulli expansion (Section 4.8.2). Unfortunately that series does not converge except at higher temperatures. Consequently many interpretations of isotope effect data devolved into simple qualitative rationalizations. Very few actual calculations of molecular frequencies were carried out for the numerical evaluation of RPF_R's, and then only for quite small molecules. However, these early studies did lead to the conclusion that isotope effects are very sensitive to the change in force constants at or near the position of isotopic substitution; that is force constant changes between reactants and products for isotope effects on an equilibrium constant, or between reactant and transition state for isotope effects on a rate constant.

With the availability of the new computer programs and access to digital computers of appropriate power, it became possible to carry out calculations of frequencies of larger molecules, to calculate isotope effects on these frequencies, and thence RPF_R's and isotope effects on equilibrium constants and on rate constants. The molecular force fields chosen for such calculations were deemed reasonable based on the force fields that had been obtained by vibrational spectroscopists from fitting experimental spectral data to obtain force constants. The idea then was to study the relationship between force constant changes (reactant to product, or reactant to transition state) and the calculated isotope effects. In the mid-1960s Marvin J. Stern joined MW in this endeavor (see reading list, Chapter 10). They wrote a subroutine THERMO which was added to the Schachtscheider/Snyder programs and enabled the calculation of isotope effects using the known molecular geometry and valence coordinate force constants as input. THERMO was made available to many people in the isotope community. In short order a number of such programs were developed and became widely available. Thus, computers were beginning to change our understanding of isotope effects by the late 1960s. However, much bigger changes in computational ability were taking place at this time. The computer program packages for the calculation of the electronic structures of molecules which were briefly discussed in Chapter 2, in particular the Gaussian program of John Pople,

were beginning to become available to the chemical community. By the late 1970s these programs enabled the calculation of normal mode vibrational frequencies of molecules using Cartesian coordinate force constants derived from the electronic calculations (see Chapter 3).

In the mid 1980s M. Saunders at Yale University and his students had undertaken the experimental study of an H/D isotope effect and had also carried out Gaussian calculations on that equilibrium. The Gaussian output included Cartesian force constants and normal mode frequencies of the molecules. His question then was how to best use THERMO to calculate a theoretical value of the isotope effect. The answer was to take the subroutine THERMO out of the modified Schachtschneider/Snyder program and create a new free standing program which was called QUIVER. As input QUIVER requires the equilibrium geometries of the relevant molecules, the atomic masses, and the Cartesian force constants calculated by the Gaussian part of the program. Quiver then calculates frequencies and RPFR's at the desired temperatures. An improved program THERMISTP developed in 2008 in connection with a study of a steric deuterium isotope effect in 1,1,3,3-tetramethylcyclohexane is available from M. Saunders (see reading list). Any detailed discussion of either the underlying experiments or of the theory is beyond the scope of this chapter; the paper is recommended reading for those who are interested. An even newer version of this program, THERMIE, which includes anharmonic corrections to the zero-point energies is available from M. Wolfsberg.

4.13 Corrections to the Bigeleisen–Mayer Equation: The Nuclear Field Shift Effect

Several corrections to the Bigeleisen–Mayer equation have been mentioned in sections above or are treated in the appendices. The most important of these is the correction for anharmonicity (Appendix 4.A2). The zero point energy of an anharmonic vibration is $ZPE/hc = G_0 + \omega_e/2 - \omega_e x_e/4 + \dots$ (ω_e is the harmonic vibrational frequency). Both G_0 and $\omega_e x_e$ are mass dependent. In the harmonic approximation $ZPE/hc = \omega_e/2$. Anharmonic zero point corrections to BM ($G_0 - \omega_e x_e/4$), are only important for vibrations involving light atoms. They account for changes of at most 1% or so in logarithmic fractionation factors calculated for exchange between molecular species containing H, D or T. Two other corrections arise from the use of the Born–Oppenheimer approximation. The first of these, the adiabatic correction (see especially Fig. 2.1 and surrounding text), arises from the coupling between electronic and nuclear motion. This correction, also, is only important for reactions involving hydrogen isotopomers. It amounts to a small percentage of observed H, D, T fractionation factors, and for heavier atoms is completely negligible because it scales proportionally to $\delta M/M^2$. The second BO correction arises from a shift in electron energy states in an atom or molecule due to the perturbation of those electrons by high charge density at the nucleus (e.g. electrons in s atomic orbitals) with the nuclear charge. This, the field shift correction,

thus depends on nuclear size and shape. Since the electron is bound more strongly to the smaller (lighter) nucleus with its higher charge density, the ground state of the heavier isotopomer will lie higher than the one for the lighter isotopomer. This is opposite to the ordering of the zero point energies associated with molecular vibrations.

Although nuclear field shifts in electronic spectra of isotopomers have been known since the 1920s it was not suspected that the effects were large enough to affect thermodynamic isotope effects until the late 1980s. At that time Fuji and coworkers reported anomalies in separation factors (see Chapter 5) for the (uranium-IV/uranium-VI) red-ox exchange reaction between ^{238}U and other lighter uranium isotopes (^{232}U , ^{233}U , ^{234}U , ^{235}U and ^{236}U). They employed a chromatographic technique using an ion exchange resin (see Chapter 8). For example for the $^{235}\text{U}/^{238}\text{U}$ pair

$$^{235}\text{U}(\text{IV})_{\text{aq}} + ^{238}\text{U}(\text{VI})_{\text{resin}} = ^{238}\text{U}(\text{IV})_{\text{aq}} + ^{235}\text{U}(\text{VI})_{\text{resin}} \quad (4.151)$$

Figure 4.6 plots separation coefficients for various pairs, $^i\text{U}/^{238}\text{U}$, against mass number, and compares these separation factors with the calculated vibrational (Bigeleisen–Mayer) and field shift contributions. Interestingly the coefficients for the odd/even ($^{233}\text{U}/^{238}\text{U}$ and $^{235}\text{U}/^{238}\text{U}$) separations lie significantly above the correlation lines for the even/even ($^{234}\text{U}/^{238}\text{U}$ and $^{236}\text{U}/^{238}\text{U}$) separations. According to the Bigeleisen–Mayer formalism all the separation factors should scale proportionally to the mass difference ($^{238}\text{U} - ^i\text{U}$). The anomaly lies well outside the experimental error. It was Bigeleisen (1996) who demonstrated the ($^i\text{U}/^{238}\text{U}$) separation factors can be written as the sum of vibrational (BM) and field shift contributions.

$$\ln(\alpha_i) = a(\text{hc}/k\text{T}) fs_i + b[(1/24)(\text{hc}/k\text{T})^2 \delta m_i / (238m_i)] = \ln(\alpha)_{\text{fs}} + \ln(\alpha)_{\text{BM}} \quad (4.152)$$

The first term on the right hand side of Equation 4.152 is due to the field shift. Here fs_i is the field shift of the i th isotopomer for a particular reference line (the 5028 Å line in the atomic spectrum of ^{238}U). Also “ a ” is a theoretically calculated isotope independent scaling factor. The second term is the Bigeleisen–Mayer vibrational contribution. Here ($\delta m_i = m_i - 238$) is negative, and b is the isotope independent difference in the vibrational force constants for the redox reaction $\text{U}(\text{IV}) = \text{U}(\text{VI})$. The comparison between calculation and experiment is shown in Fig. 4.6. The agreement is quantitative. It is interesting and important that the field shift and BM contributions are of opposite sign. For this heavy metal system the field shift makes the largest contribution to the separation factor. The vibrational contribution leads to a preference for the heavier isotope in the $\text{U}(\text{VI})$ species, while the larger field shift effect prefers the heavy isotope in the $\text{U}(\text{IV})$ species. The net effect is a preference of the heavy isotope in $\text{U}(\text{IV})$. The anomalous odd/even behavior is due to the fact that the ^{233}U and ^{235}U isotopomers have nuclear quadrupole moments,

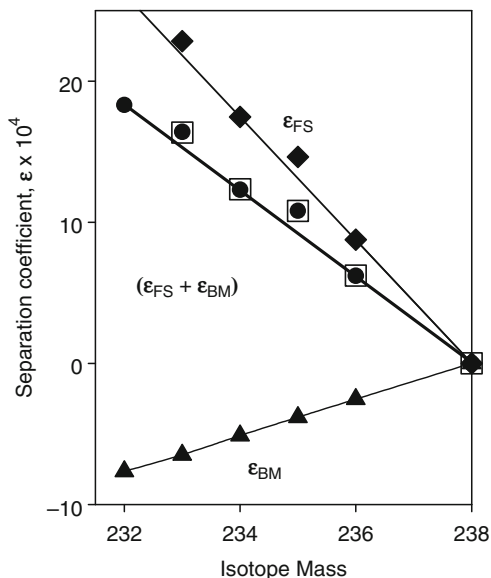


Fig. 4.6 Chromatographic separation factors for various uranium isotopes vs. ^{238}U as a function of mass at 433 K. $\epsilon = \ln[(^{238}\text{U}/^i\text{U})_{\text{IV,aq}}/(^{238}\text{U}/^i\text{U})_{\text{VI,resin}}]$. The field shift (FS) and vibrational (BM) contributions are of opposite sign. *Triangles* = calculated vibrational (Bigeleisen–Mayer) contribution, *diamonds* = calculated FS contribution, *circles* = measured effects, *open squares* = calculated effects. Note that agreement between calculation and experiment is quantitative. The correlation lines are drawn through even/even data points only (Data from Bigeleisen, J., *J. Am. Chem. Soc.*, **118**, 3676 (1996))

the even mass isotopomers do not. Consequently the field shift does not scale proportionally to mass difference. Field shift contributions to redox separation factors have been observed for other metal systems.

4.A1 Appendix: The Connection Between the Equilibrium Constant, Its Isotope Effects, and Pressure or Concentration Ratios: Corrections for Nonideality

It is useful to keep in mind that the equilibrium constant is defined in terms of the difference in standard state free energies between products and reactants. Thus, for the reaction written in Equation 4.36 we obtained Equation 4.50, essentially by thermodynamic definition,

$$\Delta G^0 = -RT \ln K_P \quad (4.50)$$

As a convenience we restricted attention to a mixture of ideal gases, used Equation 4.47, $\mu_i = \mu_i^0 + RT \ln(P_i/P_i^0)$, recognizing $\sum \nu_i \mu_i^0 = \Delta \mu_i^0 = \Delta G^0$ and $\sum \nu_i \mu_i = \Delta \mu_i = \Delta G = 0$, to conclude $\Delta G^0 = -RT \ln K_P$ where

$K_P = \prod (P_i/P_i^0)^{\nu_i}$. Ordinarily the standard state pressures, P_i^0 , refer to the ideal gas at unit pressure, in which case one can write $K_P = \prod (P_i)^{\nu_i}$. The ν_i are stoichiometric coefficients with (+) being understood for products and (–) for reactants.

For real gases, which fortunately or unfortunately are the only ones which can be studied in the laboratory, it may be necessary to deal with the effects of nonideality. This is most conveniently done by introducing the fugacity function f_i as a thermodynamic analogous pressure. By this strategy all thermodynamic equations calling for partial pressures, P_i , of an ideal gas remain exact for nonideal gases if f_i is substituted for P_i . The fugacity is so defined that $f_i \rightarrow P_i$ as $P_i \rightarrow 0$ and the gas approaches ideality. Fugacities are readily calculated from real gas properties given the equation of state for the gas. In any case, proceeding, for the real gas we write $\mu_i = \mu_i^0 + RT \ln(f_i/P_i^0)$ to replace $\mu_i = \mu_i^0 + RT \ln(P_i/P_i^0)$ (Equation 4.47). For most purposes it is convenient to introduce a further quantity, the activity coefficient γ , defined as $f_i = \gamma_i P_i$. The activity coefficient is the factor by which the fugacity differs from the actual pressure of the gas. These substitutions lead directly to Equation 4.A1.1 replacing Equation 4.50.

$$\Delta G^0 = -RT \ln K_f \quad (4.A1.1)$$

with

$$K_f = \prod (f_i/P_i^0)^{\nu_i} = \prod (\gamma_i P_i/P_i^0)^{\nu_i} = [\prod (P_i)^{\nu_i}] [\prod (\gamma_i)^{\nu_i}] = K_P K_\gamma \quad (4.A1.2)$$

Obviously these considerations carry over to the isotope effects on the equilibrium constant. Thus, using subscripts 1 and 2 to refer to the lighter and heavier isotopically substituted equilibrium reaction, one obtains

$$\begin{aligned} \delta \Delta G^0 / RT &= (\Delta G_1^0 - \Delta G_2^0) / RT = -\ln(K_{f1}/K_{f2}) \\ &= -[\ln(K_{P1}/K_{P2}) + \ln(K_{\gamma 1}/K_{\gamma 2})] \end{aligned} \quad (4.A1.3)$$

Equation A1.3 shows that isotope effects calculated from standard state free energy differences, and this includes theoretical calculations of isotope effects from the partition functions, are not directly proportional to the measured (or predicted) isotope effects on the logarithm of the isotopic pressure ratios. Rather they must be corrected by the isotopic ratio of activity coefficients. At elevated pressures the correction term can be significant, and in the critical region it may even predominate. Similar considerations apply in the condensed phase except the fugacity ratios which define K_f are replaced by activity ratios, $a_i = \gamma_i X_i$ and $a_i = \gamma_i C_i$, for the mole fraction or molar concentration scales respectively. In either case corrections for nonideality, $\prod (\gamma_i)^{\nu_i}$, arising from isotope effects on the activity coefficients can be considerable. Further details are found in standard thermodynamic texts and in Chapter 5.

For isotope effects on equilibrium constants in both gas and condensed phase the take-home lesson is there is no direct proportionality between measured isotope effects on logarithmic concentration or pressure ratios and isotopic differences in

the standard state free energy differences. The corrections can be appreciable at high pressure in the gas phase, and in the condensed phase for solutions which show significant departures from Raoult's or Henry's Laws (depending on the choice of standard state), see section 5.10 for examples.

4.A2 Corrections to the Rigid Rotor Harmonic Oscillator Approximation in the Calculation of Equilibrium Constants

Calculations of isotope effects and isotopic exchange equilibrium constants based on the Born–Oppenheimer (BO) and rigid-rotor-harmonic-oscillator (RRHO) approximations are generally considered adequate for most purposes. Even so, it may be necessary to consider corrections to these approximations when comparing the detailed theory with high precision high accuracy experimental data.

The BO approximation, which assumes the potential surface on which molecular systems rotate and vibrate is independent of isotopic substitution, was discussed in Chapter 2. In the adiabatic regime, this approximation is the cornerstone of most of isotope chemistry. While there are BO corrections to the values of isotopic exchange equilibria to be expected from the adiabatic correction (Section 2.4), these effects are expected to be quite small except for hydrogen isotope effects.

The RRHO approximation is a widely used stratagem for the convenient and straightforward calculation of vibrational and rotational contributions to the partition function (Section 4.6.1, Table 4.1). The main corrections to RRHO arise from vibrational anharmonicity and from the explicit consideration of rotational vibrational interaction. In the room temperature region by far the largest contributor to the corrections is the effect of anharmonicity on the zero point energy (the ground state) of vibration. So far as experiment is concerned there are only a few polyatomic molecules for which spectroscopic analysis has been detailed enough to permit the definition of complete sets of harmonic and anharmonic vibrational force constants, and until recently (see Section 4.12) this prohibited anharmonic corrections to (s/s') and isotopic exchange equilibrium constants for all but the simplest cases (i.e. usually diatomic molecules). As earlier noted, however, there now exist computer programs which enable one to calculate reduced isotopic partition function ratios (s/s') with the anharmonic corrections to the zero-point energies included using force constants directly calculated from a quantum chemistry program package (see Section 2.5.2).

To illustrate application of corrections to RRHO the following section briefly discusses the work of one of the coauthors on equilibria involving diatomic molecules.

4.A2.1 Corrections to RRHO: Diatomic Molecules

Wolfsberg has shown the vibrational contribution to the energy of a diatomic molecule is properly written

$$E_n/hc = G_0 + \omega_e(n + 1/2) - \omega_e x_e(n + 1/2)^2 + \text{higher order terms} \quad (4.A2.1)$$

where ω_e is the harmonic frequency (cm^{-1}) and n is the vibrational quantum number, $n = 0, 1, 2$, etc. The constant term, G_0 can be expressed in terms of the parameters of the anharmonic potential V

$$V = (1/2)k(r - r_e)^2 + a(r - r_e)^3 + b(r - r_e)^4 + \dots \quad (4.A2.2)$$

$$G_0 = (21/2)\gamma + (1/2)\delta \quad (4.A2.3)$$

Here r_e is the equilibrium internuclear distance of the diatomic oscillator and k is the harmonic force constant. Also $\gamma = -ha^2/[48(2\pi)^6 c^5 \omega_e^4 \mu^3]$, $\delta = 3hb/[4(2\pi)^4 c^3 \omega_e^2 \mu^2]$, $\omega_e x_e = -90\gamma - 2\delta$, and μ is the oscillator reduced mass $1/\mu = (1/m_1 + 1/m_2)$. Notice, because ω_e is proportional to $\mu^{-1/2}$, that both γ and δ are proportional to $1/\mu$ and are therefore isotope dependent.

At ordinary temperatures for most diatomic molecules in the gas phase only the $n = 0$ term needs to be considered. Excitation into upper levels is small or negligible. The zero point energy through second order is

$$E_0/hc = G_0 + \omega_e/2 - \omega_e x_e/4 \quad (4.A2.4)$$

and the correction for anharmonicity is $(G_0 - \omega_e x_e/4)$. Values of G_0 and $\omega_e x_e/4$ for isotopic hydrogens and a few diatomic hydrides are presented in Table 4.A2.1.

It is instructive to calculate the anharmonic correction to the zero point energy contribution to fractionation factors for isotope exchange equilibria involving hydrogen and deuterium. For example consider the exchange



The ZPE contribution is $[(\omega_e/2)_{\text{HD}} + (\omega_e/2)_{\text{OH}} - (\omega_e/2)_{\text{H}_2} - (\omega_e/2)_{\text{OD}}] = 106 \text{ cm}^{-1}$ and the anharmonicity correction is substantial, $[G_0 - \omega_e x_e/4]_{(\text{HD} + \text{OH} - \text{H}_2 - \text{OD})} = 6.3 \text{ cm}^{-1}$. The ZPE contribution to the isotope exchange equilibrium constant is

Table 4.A2.1 G_0 , $\omega_e/2$ and $\omega_e x_e/4$ (all in cm^{-1}) for isotopically substituted hydrogens and some hydrides (Wolfsberg, M., *Adv. Chem.* **89**, 185, (1969))

Species	$\omega_e/2$	G_0	$\omega_e x_e/4$	$(G_0 - \omega_e x_e/4)$
H ₂	2198	9.2	30.2	-21.0
HD	1795	6.9	22.7	-15.8
D ₂	1554	4.6	15.1	-10.5
HCl	1495	1.5	13.0	-11.5
DCl	1071	0.8	6.7	-5.9
HBr	1325	0.8	11.3	-10.5
DBr	943	0.4	5.7	-5.3
OH	1868	10.7	8.5	2.2
OD	1359	5.3	4.2	1.1

$e^{-hc106/kT} = e^{-152/T} = 0.602$ at 300 K and the anharmonicity correction factor is $e^{-9.1/T} = 0.970$ at 300 K, an approximate 3% correction. As a second example consider



From Table 4.A2.1 we obtain $\text{ZPE} = -21 \text{ cm}^{-1}$ which contributes $e^{30.2/T} = 1.11$ at 300 K, while the anharmonicity correction through second order is $[G_0 - \omega_e X_e/4]_{(\text{HD}+\text{HBr}-\text{H}_2-\text{DBr})} = [-1.9 - (-1.9)] = 0 \text{ cm}^{-1}$, i.e. offsetting corrections of $e^{2.7/T}$ and $e^{-2.7/T}$, and is fortuitously negligible.

Isotope effects on anharmonic corrections to ZPE drop off rapidly with mass and are usually neglected. The ideas presented above obviously carry over to exchange equilibria involving polyatomic molecules. Unfortunately, however, there are very few polyatomics on which spectroscopic vibrational analysis has been carried in enough detail to furnish spectroscopic values for G_0 and $\omega_e X_e$. For that reason anharmonic corrections to ZPE's of polyatomics have been generally ignored, but see Section 5.6.3.2 for a discussion of an exception; also theoretical (quantum package) calculations of anharmonic constants are now practical (see above), and in the future one can expect more attention to anharmonic corrections of ZPE's.

Reading List

- Bell, R. P. Tunnel effect corrections for parabolic potential barriers, *Trans. Far. Soc.* **55**, 1 (1959).
- Bigeleisen, J. Nuclear size and shape effects in chemical reactions. Isotope chemistry of the heavy elements, *J. Am. Chem. Soc.*, **118**, 3676 (1996).
- Bigeleisen, J. and Ishida, T. Application of finite orthogonal polynomials to the thermal functions of harmonic oscillators. I. Reduced partition function of isotopic molecules, *J. Chem. Phys.* **48**, 1311 (1968). Ishida, T., Spindel, W. and Bigeleisen, J. Theoretical analysis of chemical isotope fractionation by orthogonal polynomial methods, in Spindel, W., ed. *Isotope Effects on Chemical Processes. Adv. Chem. Ser.* **89**, 192 (1969).
- Bigeleisen, J. and Mayer, M. G. Calculation of equilibrium constants for isotopic exchange reactions, *J. Chem. Phys.* **15**, 261 (1947).
- Bigeleisen, J. and Wolfsberg, M. Theoretical and experimental aspects of isotope effects in chemical kinetics, *Adv. Chem. Phys.*, Vol 1., I. Progogine, Ed. Interscience, NY (1958).
- Glasstone, S., Laidler, K. J., and Eyring, H. *The Theory of Rate Processes*, McGraw Hill, New York (1941).
- Herzberg, G. *Molecular Spectra and Molecular Structure, II Infrared and Raman Spectra of Polyatomic Molecules*, D. Van Nostrand, New York (1945).
- Ishida, T. and Fujii, Y. Enrichment of isotopes, in Kohen, A., Limbach, H. H., eds. *Isotope Effects in Chemistry and Biology* CRC, Taylor & Francis, Boca Raton, FL (2006), Chapter 2, pp 41–87.
- Mayer, J. E. and Mayer, M. G. *Statistical Mechanics*, 1st Ed., 2nd Ed., Wiley, New York (1940, 1977).
- McQuarrie, D. *Statistical Mechanics*, Harper Collins, New York (1976).
- Saunders, M., Wolfsberg, M., Anet, F. A. L. and Kronja, O. A steric deuterium isotope effect in 1, 1, 3, 3 tetramethyl cyclohexane, *J. Am. Chem. Soc.* **129**, 10276–10281 (2007). Program THERMISTP is available from M. Saunders, Chemistry Department Yale University, New Haven, CT 06520. Program THERMIE is available from M. Wolfsberg, Department of Chemistry, University of California, Irvine, Irvine, CA 92717.

- Waldmann, L. The theory of isotope separation by exchange reactions. *Naturwissenschaften* **31**, 205 (1943).
- Wigner, E. Crossing of potential thresholds in chemical reactions. *Z. Phys. Chem. B*, **19**, 203 (1932).
- Wolfsberg, M. Comments on selected topics in isotope theoretical chemistry, in Kohen, A. and Limbach, H. H., eds. *Isotope Effects in Chemistry and Biology*, CRC Taylor & Francis, Boca Raton, FL (2006), Chapter 3, p. 89.
- Wolfsberg, M. Correction to the effect of anharmonicity on isotopic exchange equilibria in; Isotope Effects in Chemical Processes, in Spindel, W., ed. *Adv. Chem. Ser.* **89**, 185 (1969).
- Wolfsberg, M. and Kleinman, L. I. Corrections to the Born–Oppenheimer approximation in the calculation of isotope effects on equilibrium constants, in Rock, P. A., ed. *Isotopes and Chemical Principles, ACS Symposium Ser.* **11**, 64 (1975).

Chapter 5

Condensed Phase Isotope Effects; Isotope Effects in Non-ideal Gases

Abstract Isotope effects on the PVT properties of non-ideal gases and isotope effects on condensed phase physical properties such as vapor pressure, molar volume, heats of vaporization or solution, solubility, etc., are treated in some thermodynamic detail. Both pure component and mixture properties are considered. Numerous examples of condensed phase isotope effects are employed to illustrate theoretical and practical points of interest.

5.1 Introduction

In this chapter we will discuss IE's on the PVT properties of non-ideal gases, then in more detail treat IE's on condensed phase physical properties like vapor pressure, molar volume, heats of vaporization or solution, solubility, etc. Some of these properties (e.g. the vapor pressure isotope effect, VPIE) are of great practical interest because they form the basis for isotope separation processes (e.g. distillation, solvent extraction, etc.). Of equal interest, however, is the fact that IE's of non-ideal gases (virial coefficient isotope effects, VCIE's), and condensed matter isotope effects (CMIE's), are closely related to the intermolecular forces governing both gas phase clustering and condensation. To understand this more clearly we will compare standard state free energy differences between average condensed phase molecules (for the VPIE) or average gas phase dimers, trimers, etc. (for VCIE), on the one hand, and the dilute ideal-gas phase reference on the other. The comparison will show that the two effects share a common origin.

5.2 Thermodynamic Formalism

We begin with a discussion of the vapor pressure isotope effect (VPIE). To do so we compare the equilibria between condensed and vapor phase for samples of two isotopomers. At equilibrium, condensed(c) = vapor(v), the partial molar free energies, $\mu(v)$, and $\mu(c)$, of the two phases are equal; this, in fact, is the thermodynamic

definition of equilibrium. Hence $\mu'(c) = \mu'(v)$ and $[\mu'(v) - \mu'(c)] = 0$. Similarly for the other isotopomer, $\mu(c) = \mu(v)$ and $[\mu(v) - \mu(c)] = 0$. Combining

$$[\mu'(v) - \mu'(c)] - [\mu(v) - \mu(c)] = [\mu'(v) - \mu(v)] - [\mu'(c) - \mu(c)] = 0 \quad (5.1a)$$

and rewriting

$$\delta\Delta\mu = 0 \quad (5.1b)$$

Here the prime symbolizes the lighter isotope. Also upper case Greek Δ is used for the isotopic difference (primed – unprimed), and lower case Greek δ for the phase difference (vapor – condensed). The sections which follow further develop Equation 5.1 in order to arrive at more practical expressions involving measurable quantities.

5.2.1 The Vapor Phase Reference

As is customary we select the ideal vapor at unit pressure, P° , as the standard state. The partial molar free energy (chemical potential) of the vapor, $\mu(v)$, is

$$\mu_i(v) = \mu_i^\circ(v) + RT \ln(P/P^\circ) + RT \ln(f/P) \quad (5.2)$$

P is the total pressure and f is the fugacity. The ratio f/P expresses the deviation of the gas from ideality (see Appendix 4.1). For the ideal gas reference state $f^\circ = P^\circ = 1$. The correction for vapor non-ideality may be further expressed as:

$$RT \ln(f/P) = \int (V(v) - RT/P) dP \quad (5.3)$$

The integral in Equation 5.3 extends from 0 to P , $V(v)$ is the vapor volume of the real gas, and RT/P is the vapor volume for the ideal gas. At low enough pressures $V(v)$ can be obtained from the virial equation of state, which in the pressure expansion is $PV(v)/(RT) = 1 + BP + CP^2 + \dots$. Therefore from Equation 5.3, $V(v) = (RT/P)[1 + BP + CP^2 + \dots]$, and

$$\ln(f/P) = BP + CP^2/2 + \dots \quad (5.4)$$

B and C are second and third virial coefficients. The partial molar free energy of the vapor phase neglecting higher order terms is thus

$$\mu_i(v) = \mu_i^\circ(v) + RT [\ln(P) + BP] \quad (5.5)$$

In Equation 5.5 $\mu_i^\circ(v)$ is the standard state partial molar free energy of the vapor, P is the observed vapor pressure, and BP is a first order correction for vapor nonideality.

5.2.2 The Condensed Phase

The chemical potential for the condensed phase is defined

$$\mu_i(c) = \mu^{\circ}(c) \quad (5.6)$$

Here $\mu^{\circ}(c)$ is the standard state chemical potential of condensed fluid in equilibrium with the vapor at the vapor pressure P , and the temperature of the measurement.

5.2.3 The Vapor Pressure Isotope Effect, Separated Isotopes

Thermodynamic analysis of VPIE data for separated isotopes (see, e.g., Figs. 7.18a and b) proceeds by equating partial molar free energies in condensed and vapor phases for each isotope. Using Equations 5.1, 5.5 and 5.6 one obtains

$$RT \ln(P_i'/P_i) = -[(\mu^{\circ}(v) - \mu^{\circ}(c))' - (\mu^{\circ}(v) - \mu^{\circ}(c))] - RT(B'P' - BP) \quad (5.7)$$

or

$$\ln(P'/P) = \text{VPIE} = -\delta\Delta(\mu^{\circ})/RT - (B'P' - BP) \quad (5.8)$$

This is a simple and important result. It equates VPIE to the isotopic difference of standard state free energies on phase change, plus a small correction for vapor phase nonideality, here approximated through the second virial coefficient. Therefore Equation 5.8 is limited to relatively low pressure. As T and P increase third and higher virial corrections may be needed, and at even higher pressures the virial expansion must be abandoned for a more accurate equation of state.

In making comparisons with theoretical model calculations it is convenient to express $\ln(P'/P)$ using Helmholtz free energy differences, $\delta\Delta A^{\circ}$, because A° (and hence $\delta\Delta A^{\circ}$) is straightforwardly connected to the partition function, Q , $A = -RT \ln Q$, ($\delta\Delta A = -RT \delta\Delta \ln Q$ and $\delta\Delta A^{\circ} = -RT \delta\Delta \ln Q^{\circ}$). From the thermodynamic identity $A = \mu - PV$ we obtain $\delta\Delta(\mu^{\circ}) = \delta\Delta A^{\circ} - [(P'V' - PV)_{\text{v}} - (P'V' - PV)_{\text{c}}] = \delta\Delta A^{\circ} + (P'V' - PV)_{\text{c}}$ where V' and V are condensed phase molar volumes (in the ideal vapor reference state $(P'V_{\text{v}}')^{\circ} = (PV_{\text{v}})^{\circ} = RT$ and $\Delta(PV)_{\text{v}}^{\circ} = 0$). Thus

$$\ln(P'/P) = \text{VPIE} = -\delta\Delta A^{\circ}/RT - (B'P' - BP) + (P'V' - PV)_{\text{c}}/RT \quad (5.9)$$

and

$$\ln(P'/P) = \text{VPIE} = \ln(Q_{\text{v}}'Q_{\text{c}}/Q_{\text{v}}Q_{\text{c}}') - (B'P' - BP) + (P'V' - PV)_{\text{c}}/RT \quad (5.10)$$

In Equation 5.10 and subsequently we have dropped the superscript “ \circ s” from the Q 's in order to simplify the notation.

5.2.3.1 The Corrective Terms: Simplification of Equation 5.10

It is useful to comment on the relative contributions of the last two terms on the right hand side of Equations 5.9 and 5.10. These correction terms both scale proportionally with pressure $(B'P' - BP) = B'P'(1 - BP/(B'P'))$ and $(P'V' - PV)_c/RT = (P'V'/(RT))_c(1 - PV/(P'V'))_c$. As we will see in later sections $\ln(P'/P)$ typically varies between -0.005 and -0.015 per H/D substitution for hydrocarbons but is positive and much larger for hydrogen bonded materials. At temperatures not too close to critical, the condensed phase molar volume isotope effect, $MVIE = \ln(V'/V)$ is typically 0.001 or so per D and $\ln(B'/B)$ about the same or a little larger, say 0.002. Thus for typical values of $V_c \sim 50 \text{ cm}^3/\text{mol}$ and $BRT \sim 50 \text{ cm}^3/\text{mol}$ one estimates at a vapor pressure of 1 bar, say around 300 K, $(V'/(RT))_c(1 - PV/(P'V'))_c \sim (2 \times 10^{-3})(0.01) \sim 2 \times 10^{-5}/\text{bar}$, and $B'(1 - BP/(B'P')) \sim (2 \times 10^{-3})(0.01) \sim 2 \times 10^{-5}/\text{bar}$. Each correction amounts to more than 1% of $\ln(P'/P)$ and cannot be neglected in high precision work. Of course as temperature falls, and the vapor pressure drops, the corrections become less and less important, and at low enough pressure they can be neglected. Also for H/D effects in hydrogen bonded systems and for heavy atom isotopomer pairs ($^{12}\text{C}/^{13}\text{C}$ or $^{16}\text{O}/^{18}\text{O}$ for example) the relative corrections are appreciably smaller. In any case, at low enough pressures Equations 5.9 and 5.10 simplify

$$\ln(P'/P) = \text{VPIE} = -\delta\Delta A^0/RT = \ln(Q_v'Q_c/Q_vQ_c') \quad (5.11)$$

Equation 5.11 is important. It relates the experimentally observed vapor pressure ratio to the theoretically important isotope effects on the free energy differences and/or partition function ratios. This equation encapsulates the essential physics of the vapor pressure isotope effect and, as we shall see, provides a path for its theoretical interpretation in terms of molecular structure and dynamics via the partition function ratios.

5.2.4 Fractionation Factors

Now consider the phase equilibrium of a mixture of isotopes (see Fig. 7.18c for example) with isotopic analyses for each phase carried out under equilibrium conditions. Labeling the isotopomers in the two component case as primed and unprimed, as before, the fractionation factor, α and $\alpha'' = 1/\alpha$, are defined

$$\alpha = (y/y')/(x/x') \text{ and } \alpha'' = 1/\alpha = (y'/y)/(x'/x) \quad (5.12)$$

x and y denote mole fractions (for liquid/vapor fractionation y refers to vapor, and x to liquid). We first consider the case where the condensed phase solution is ideal in the Raoult's law sense.

This should certainly be a good approximation as the isotopomers are quite similar, one to the other. Even so we will improve on it later when we consider (the quite small) nonideality of isotopomer solutions and their excess thermodynamic properties. For Raoult's law solutions

$$y' = P'/P_{\text{tot}} = x'P^{o'}/P_{\text{tot}} \text{ and } y = P/P_{\text{tot}} = xP^o/P_{\text{tot}} \quad (5.13)$$

where $P^{o'}$ and P^o are the vapor pressure of the pure separated components, and P_{tot} is the vapor pressure over the solution, $P_{\text{tot}} = (P' + P) = (x'P^{o'} + xP^o)$. From Equation 5.13

$$y'/y = x'P^{o'}/(xP^o) \text{ or } \alpha'' = (y'/y)/(x'/x) = P^{o'}/P^o \quad (5.14)$$

and

$$\ln(\alpha'') = \ln(P^{o'}/P^o) \sim \text{VPIE} \quad (5.15)$$

A more careful analysis taking into account vapor nonideality through the second virial coefficient and the isotope effect on condensed phase molar volume yields Equation 5.16

$$\ln \alpha'' = -\delta\Delta A^o/RT + (B - B') P_{\text{tot}} + P_{\text{tot}}(\Delta V_c)/RT \quad (5.16)$$

An important attribute of Equation 5.16 is that the pressure exerted on both phases, P_{tot} , is common to both isotopomers. The important difference between Equations 5.16 and 5.9 is that the isotopic vapor pressure difference ($P' - P$) does not enter the last two terms of Equation 5.16 as it does in Equation 5.9. Also isotope effects on the second virial coefficient $\Delta B/B = (B' - B)/B$ and the condensed phase molar volume $\Delta V/V$ are significantly smaller than those on $\Delta P/P \sim \ln(P'/P)$. Consequently the corrections in Equation 5.16 are considerably smaller than those in Equations 5.9 and 5.10, and can sooner be neglected. Thus to good approximation $\ln(\alpha'')$ is a direct measure of the logarithmic partition function ratio $\ln(Q_v'Q_c/Q_vQ_c')$, provided the pressure is not too high, and assuming ideality for the condensed phase isotopomer solution. For nonideal solutions a modification to Equation 5.16 is necessary.

$$\ln \alpha'' = -\delta\Delta A^o/RT + \ln(\gamma'/\gamma) = \ln(Q_v'Q_c/Q_vQ_c') + \ln(\gamma'/\gamma) \quad (5.17)$$

where γ' and γ are activity coefficients in the condensed phase. Commonly fractionation experiments are carried out with the rare isotopomer at high dilution. Under those conditions the isotope present at high concentration (taken here as the unprimed one) can be assumed to be ideal in the Raoult's law sense even though the rare isotopomer (primed) is not. Equation 5.17 reduces to a particularly simple result,

$$\ln \alpha'' = -\delta\Delta A^o/RT + \ln(\gamma') = \ln(Q_v'Q_c/Q_vQ_c') + \ln(\gamma') \quad (5.18)$$

The last term may be significantly different from zero and should not be neglected (see Section 5.8 for further discussion of this point)

5.3 Reprise: Remarks Concerning the Partition Functions: The Relation of VPIE to Condensed Phase Molecular Properties and Vibrational Dynamics

The standard state Helmholtz free energy difference, $\delta\Delta A^\circ$, was introduced in Equations 5.9 and 5.11 to show the connection between VPIE and molecular structure and dynamics. Molecular properties are conveniently expressed using standard state canonical partition functions for the condensed and vapor phases, Q_c° and Q_v° ; remember $A^\circ = -RT \ln Q^\circ$. The Q 's are $3nN$ dimensional, n is the number of atoms per molecule and N is Avogadro's number. For convenience we have now dropped the superscript "o's" on the Q 's. The "o's" specify standard state conditions, now to be implicitly understood. For VPIE and α'' respectively, not too close to the critical region,

$$\ln(P'/P) = \text{VPIE} = \ln(Q_v'Q_c/Q_vQ_c') - (B'P' - BP) + (P'V' - PV)_c/RT \quad (5.10)$$

$$\ln \alpha'' = \ln(Q_v'Q_c/Q_vQ_c') + \ln(\gamma') \quad (5.18)$$

These equations are important. They connect VPIE and $\ln(\alpha'')$, both measurable properties, with basic theoretical ideas. The last two terms in Equation 5.10 and the last term in Equation 5.18 are generally small compared to the leading term. They are often neglected. The ratio of Q 's in the leading term expresses VPIE or fractionation factor as the isotope effect on the equilibrium constant for the process $\langle Q \rangle_{\text{CONDENSED}} = \langle Q \rangle_{\text{IDEAL VAPOR}}$. It remains true, of course, that condensed phase Q 's are complicated and difficult to evaluate. Except for especially simple systems (e.g. monatomic isotopomers) approximations are required for further progress.

5.3.1 Application to Polyatomics

When treating polyatomics it is convenient to define an average molecular partition function, $\ln \langle Q \rangle = (\ln Q)/N$, for an assembly of N molecules. In the dilute vapor (ideal gas) this introduces no difficulty. There is no intermolecular interaction and $\ln \langle Q \rangle = (\ln Q)/N = \ln(q)$ exactly (q is the microcanonical partition function). In the condensed phase, however, the Q 's are no longer strictly factorable. Be that as it may, continuing, and assuming $\ln \langle Q \rangle = (\ln Q)/N$, we are led to an approximate result which is superficially the same as Equation 5.10,

$$\ln(P'/P) = \text{VPIE} = \ln(\langle Q_v' \rangle \langle Q_c \rangle / \langle Q_v \rangle \langle Q_c' \rangle) - (B'P' - BP) + (P'V' - PV)_c/RT \quad (5.19)$$

Equation 5.19 relates the molecular energy states of the primed and unprimed isotopomers in condensed and vapor phase to VPIE. The correction terms account for the difference between the Gibbs and Helmholtz free energies of the condensed phase, and vapor nonideality. The comparison is between separated isotopomers at a common temperature, each existing at a different equilibrium volume, V' or V , and at a different pressure, P' or P , although $\Delta V = (V' - V)$ and $\Delta P = (P' - P)$ are small. Still, because condensed phase Q 's are functions of volume, $Q = Q(T, V, N)$, rigorous analysis requires knowledge of the volume dependence of the partition function, and thus MVIE, since the comparisons are made at V' and V . That point is developed later.

As we saw in Chapters 3 and 4 the Q ratio in Equation 5.19 is equivalent to the ratio of reduced partition functions (RPFR's), $(s/s')f_i = (\langle Q \rangle / \langle Q' \rangle)_{\text{qm}} / (\langle Q \rangle / \langle Q' \rangle)_{\text{cl}}$ (s and s' are symmetry numbers, qm = quantum mechanical, cl = classical)

$$\ln(P'/P) = \text{VPIE} = \ln(f_c/f_g) - (B'P' - BP) + (P'V' - PV)_c/RT \quad (5.20)$$

At low enough temperatures, say at or below the normal boiling temperature, $\sim 0.7 T_{\text{CRITICAL}}$, the last two terms in Equation 5.20 are small, and to good approximation low temperature VPIE data can be used to define the reference state condensed phase isotopic partition function ratio, i.e. $\ln(f_c/f_g) \sim \ln(P'/P) = \text{VPIE}$.

5.3.2 *What Happens When Molecules Interact or Condense? A Simplified Physical Picture*

Our interest is in the connection between the intermolecular forces that cause condensation and/or gas phase molecular clustering and thermodynamics. To set the stage consider the following simple model:

Of the $3n$ coordinates needed to describe an n -atom molecule, three are used for center of mass motion, three describe angular displacement (rotation, hindered rotation, or libration) (two if the molecule is linear, 0 if monatomic), the remaining $3n-6$ ($3n-5$, if linear, $3n-3 = 0$, if monatomic) describe atom-atom displacements (vibrations). In some cases it may not be possible to separate translation cleanly from rotation and vibration, but when the separation can be made it is a convenience. Elementary treatments assume

$$\langle Q \rangle = (\langle Q_{\text{TRANS}} \rangle \langle Q_{\text{ROT}} \rangle \langle Q_{\text{VIB}} \rangle) \quad (5.21)$$

Now consider the energy of interaction of an isolated pair as the center to center distance, R , changes. In the transfer from dilute to non-ideal gas (dimer), or to the condensed phase, important changes occur in all degrees of freedom. This is diagrammed in Fig. 5.1 which shows the shifts in intermolecular potential energy

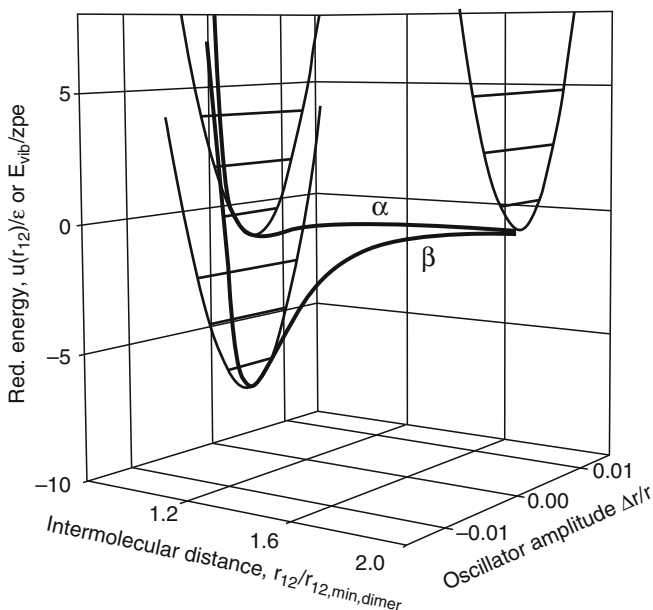


Fig. 5.1 A schematic projection of the $3n$ dimensional (per molecule) potential energy surface for intermolecular interaction. Lennard–Jones potential energy is plotted against molecule–molecule separation in one plane, the shifts in the position of the minimum and the curvature of an internal molecular vibration in the other. The heavy upper curve, α , represents the “gas–gas” pair interaction, the lower heavy curve, β , measures condensation. The lighter parabolic curves show the internal vibration in the dilute gas, the gas dimer, and the condensed phase. For the CH symmetric stretch of methane (3143.7 cm^{-1}) at 300 K, RT corresponds to 8% of the oscillator zpe, and 210% of the LJ well depth for the gas-gas dimer (Van Hook, W. A., Rebelo, L. P. N. and Wolfsberg, M. *J. Phys. Chem. A* **105**, 9284 (2001))

and internal vibrational potential energy for a single vibration, as the molecules approach each other along $R_{\text{INTERMOL}} = R_{12}$. A similar diagram applies for each of the $(3n - 6)$ vibrations. In Fig. 5.1 the upper path shows transfer from dilute gas to complexed (dimerized) vapor. This path is used to describe the virial coefficient isotope effect (VCIE). The lower path refers to condensation and accounts for VPIE. Thus, the upper path $u(R_{12})$ represents the *pair* intermolecular potential energy, the lower one shows the average potential that a single molecule feels when embedded in the field of $(N - 1)$ neighboring molecules. The interaction is with c nearest neighbors (and $(N - c - 1)$ more distant neighbors). The increase in number accounts for the significantly deeper and sharper well for condensation. In the process the intermolecular potential energy shifts to lower energy, and, *of at least equal importance*, the curvature in the vibrational dimension, r , is perturbed. Increased curvature on condensation corresponds to a blue shift (shift to higher frequency), decreased curvature to a red shift (shift to lower frequency). Many examples of such

shifts, albeit small, have been spectroscopically identified. External motions are also quantized. These correspond to blue shifts because $(\partial E_{\text{POT}}/\partial R_{12}) = 0$ in the ideal gas, and is positive in the condensed phase. To sum up, within the precision of the Born–Oppenheimer approximation, properly calculated potential energy surfaces (PES's) are isotope independent, but quantization of the kinetic energies of the various motions on the surface, vibrational energy for example, is isotope dependent because of isotopic differences in mass and mass distribution.

In Fig. 5.1 we see that the intermolecular interactions accounting for VCIE (upper curve) and VPIE (lower curve) differ not in kind, only in degree. The well depth for gas–gas interaction is available from analysis of the virial coefficient of the parent isotopomer, that for the condensed phase can be obtained by combining the energy of vaporization and the zero point energies of the condensed and ideal vapor phases.

5.4 VPIE's in Monatomic and Polyatomic Systems: Approximate Vibrational Analysis

An estimate of the VPIE of monatomics can be obtained from the first quantum correction using the Wigner high temperature approximation (appropriate because the level spacing in the quantized intermolecular well is small compared to the thermal energy, $h\nu/kT \ll 1$, see Chapters 3 and 4)

$$\ln(f_c/f_g) \sim (1/24)(h/kT)^2 \langle \nabla^2 U \rangle (\mu' - \mu) \quad (5.22)$$

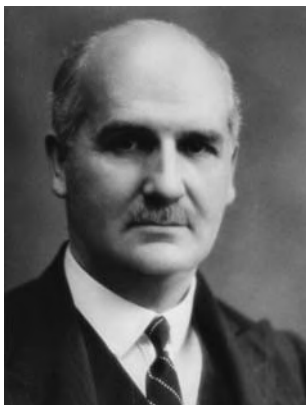
$\langle \nabla^2 U \rangle$ is the mean square force and μ' and μ are reduced masses. In the harmonic approximation,

$$\ln(f_c/f_g) \sim 3(1/24)(hc/kT)^2 \nu_{\text{TR}}'^2 (1 - \mu'/\mu) \quad (5.23a)$$

ν_{TR}' is the harmonically approximated value of the three equivalent lattice translational frequencies. An Einstein frequency distribution has been assumed in Equation 5.23. It is interesting that the earliest treatment of the VPIE by F. A. Lindemann (see Chapter 1) used the more realistic Debye frequency distribution, $N(\nu) = a\nu^2$ for $0 < \nu < \nu_{\text{max}}$ and $N(\nu) = 0$ for $\nu > \nu_{\text{max}}$. The constant of proportionality, a , can be evaluated from the constraint that the total number of lattice vibrations (per mole) is $3N_{\text{Avagadro}}$. (The Einstein approximation assumes a set of $3N$ frequencies all equal to a single constant value.) Lindemann's use of the Debye distribution leads to an expression analogous to Equation 5.23a (Historical Vignette 5.1)

$$\ln(f_c/f_g) \sim (9/5)(1/24)[(\theta'/T)^2 - (\theta/T)^2] \quad (5.23b)$$

where θ , the Debye characteristic temperature, is $\theta = (hc/k)\nu_{\text{max}}$.



[Historical Vignette 5.1] Frederick A. Lindemann (1st Viscount Cherwell) (1886–1957) was an English physicist who became an influential scientific adviser to the British government during World War II, and a close associate of Winston Churchill. Lindemann was educated in Germany at Darmstadt and later took his Ph.D. in 1910 at Berlin studying under Walter Nernst. On his return to England he took a position at Oxford University, then spent the war years 1914–1918 at the Royal Aircraft Establishment. He developed a mathematical theory of aircraft spin recovery, and to prove it, learned to fly, testing the theory on himself; the method is still used. Prior to his development spinning an aircraft was almost invariably fatal. In 1919 Lindemann was appointed professor at Oxford and director of the Clarendon Laboratory. Lindemann was one of the first people to suggest that in the solar wind particles of both polarities, protons as well as electrons, come from the sun. His major contribution to isotope science was his development of the first theory of the vapor pressure isotope effect, see Chapter 1 (Photo credit: M. Bradbury, Oxford University)

Table 5.1 compares VPIE's obtained from Equation 5.23a with experiment for several monatomic liquids at their melting and boiling points. The sign and magnitude of VPIE, and its temperature dependence, are predicted within a reasonable, albeit crude, approximation. Later we will outline more sophisticated calculations which yield quantitative agreement with experiment.

Now compare the VPIE's observed for inert gases (Table 5.1), small (a few tenths percent or less) and "normal" ($P' > P$), with some hydrocarbon/deutero-carbon effects also in Table 5.1 (methane and benzene as typical examples). The H/D effects are larger in magnitude (a few percent), but inverse ($P' < P$). For these isotopomer pairs the small positive IE from quantization of the motion in the LJ translation–rotation potential well is overridden by larger negative contributions from zero point energy (ZPE) shifts in the internal modes (see Fig. 5.1). The shape of the vibrational potential surface has changed on condensation. Most often for hydrocarbons the curvature of the vibrational well at its minimum is less in the condensed phase than in the gas; the frequency is red-shifted. Also, for most internal modes excitation to upper vibrational states is negligible because the potential wells for internal vibrations are very deep. For example the potential well for the CH stretch in methane is more than 50 times deeper than the LJ well which describes condensation. The zeroth vibrational level in the vibrational well lies about $20 RT_B$ above the minimum in the potential, the first excited level about $60 RT_B$, and thermal excitation is inconsequential (T_B is

Table 5.1 Prediction of VPIE's for two rare gases and nitrogen using a crude oscillator model (Equation 5.23). Comparison with experiment at the melting point, T_M , and boiling point, T_B , and with experimental VPIE's for two hydrocarbons (Van Hook, W. A. Condensed matter isotope effects, in Kohen, A. and Limbach, H. H., Eds. *Isotope Effects in Chemistry and Biology*, CRC, Boca Raton, FL (2006))

System	ν'/cm^{-1}	Calc. VPIE (Equation 5.23)		Experimental VPIE	
		at T_M	at T_B	at T_M	at T_B
$^{36}\text{Ar}/^{40}\text{Ar}$	47	0.0068	0.0063	0.0062	0.0055
$^{80}\text{Kr}/^{84}\text{Kr}$	32	0.0009 ₃	0.0008 ₆	0.0010	0.0008
$^{14}\text{N}_2/^{15}\text{N}_2$	48	0.010	0.007	0.006	0.003
CH_4/CD_4	—	—	—	-0.014	-0.027
$\text{C}_6\text{H}_6/\text{C}_6\text{D}_6$	—	—	—	-0.028	-0.025

the boiling temperature). The contribution of this mode to the energy is accurately described using the ZPE approximation. The relative widths of the wells are important because width determines amplitude. At the zeroth level the vibrational width is about one percent of the LJ width at RT_B . The CH bond vibrates many times (35 or so), but with small amplitude, during the time the molecule is executing one relatively slow motion of larger amplitude in the LJ potential well.

5.4.1 Dispersion Forces, Frequency Shifts on Condensation, and the VPIE

It is apparent from the discussion above, and will become increasingly obvious in later sections of this chapter, that the VPIE in polyatomic systems is a consequence of the changes in the vibrational frequencies which occur on condensation. These in turn can be expressed in terms of a set of isotope independent vibrational force constants. For non-polar systems the frequency shifts are invariably to the red, and this explains the tendency to inverse vapor pressure isotope effects. The isotope effect on the van der Waals attractive force (inverse sixth power dispersion force) was first discussed by Baertschi and Kuhn (reading list) in terms of the Drude model. They came to the conclusion that this explains the inverse VPIE's commonly observed. The nature of the dispersion force isotope effect was reinvestigated by Wolfsberg (reading list) who presented a thorough quantitative treatment of the problem using second order perturbation theory. He showed the effect of the intermolecular interaction was to generally lower the diagonal force constants of the internal vibrations due to dipole-induced dipole terms, thus leading to the observed effects. The analysis does not apply to directionally specific dipole-dipole, ion-dipole, or hydrogen-bond type interactions which can result in large blue shifts of specific frequencies and positive (normal) vpie's (like, e.g., those observed for $\text{H}_2\text{O}/\text{D}_2\text{O}$).

5.4.2 Polyatomic Systems in Approximation: The Cell Model

Using harmonic oscillator partition functions to describe both internal and external modes, the logarithmic Q ratios introduced above, $\ln(Q_g'Q_c/Q_gQ_c') = \ln(Q_c/Q_c') + \ln(Q_g'/Q_g)$, become

$$\ln(Q_c/Q_c') = \left[\sum [u_i \exp(-u_i/2)/(1 - \exp(-u_i))]_c / [u_i' \exp(-u_i'/2)/(1 - \exp(-u_i'))]_c \right]_{3n} \quad (5.24a)$$

and

$$\ln(Q_g'/Q_g) = - \left[\sum [u_i \exp(-u_i/2)/(1 - \exp(-u_i))]_g / [u_i' \exp(-u_i'/2)/(1 - \exp(-u_i'))]_g \right]_{(3n-6)_{\text{int}}} \quad (5.24b)$$

In the condensed phase the sum is over all $3n$ frequencies, but in the ideal vapor phase the six external (zero) frequencies do not contribute to the IE's, the sum is over the remaining $3n - 6$ internals. For condensed rare gases the harmonic assumption is highly approximate, and this is also true for the lattice modes of polyatomics. However as molecular size increases the relative contribution of the external modes becomes less and less important relative to internals.

Numerical evaluation of Equation 5.24 requires a self consistent set of $3n$ condensed phase and $3n - 6$ vapor phase frequencies for both members of the isotopomer pair. These are best calculated from the known molecular geometry, masses, and mass distributions using an isotope independent force field consistent with spectroscopically observed gas phase frequencies and frequency shifts on condensation (see Chapter 3). It is dangerous to directly substitute observed frequencies and frequency shifts for each of the isotopomers being compared into Equation 5.24 because spectroscopic experimental error accumulates and may result in large errors on calculated VPIE's. Moreover in most cases the entire set of frequencies and frequency shifts on isotope substitution and/or phase change are not experimentally known. The recommended procedure is based on the FG matrix treatment of vibrational dynamics (Chapters 3 and 4). Computer programs to obtain RPFR and VPIE from information on molecular geometry, atomic masses, and force constants are available have been discussed in the literature (see reading list).

5.4.2.1 Remarks on Spectroscopic and Thermodynamic Precision

To illustrate Equations 5.24a and 5.24b we consider the contribution of a single vibrational mode to VPIE. Comparing CH and CD stretching modes for a typical hydrocarbon at room temperature (300 K) ($\nu_{\text{CH}} \sim 3,000 \text{ cm}^{-1}$ in the gas, red shifting $\sim 10 \text{ cm}^{-1}$ on condensation), we approximate RPFR as

$$\ln(\text{RPFR}_i) = -(1/2)(hc/(kT))(\nu_v - \nu_c)(1 - (G_i/G_i')^{1/2}) = -0.0064 \quad (5.25)$$

In Equation 5.25 the ratio of G matrix elements has been obtained using a “diatomic approximation” ($G_i/G'_i = [(1/12) + (1/2)]/[(1/12) + (1/1)]$). Although in the gas phase the frequency of each isotopomer can be measured to high precision, say $\pm 0.05 \text{ cm}^{-1}$ or better, such precision is impossible in the liquid because of inherent broadening caused by intermolecular forces. Except in special cases band centers cannot be located to better than $\sim \pm 0.5 \text{ cm}^{-1}$, that limit is imposed by the nature of the liquid state. There is an identical uncertainty for each isotopomer, so spectroscopic precision is about

$$\delta \ln(\text{RPFR}_i) / \ln(\text{RPFR}_i) \sim [2 \times 0.05^2 + 2 \times 0.5^2]^{1/2} / [10(1 - 1/2^{1/2})] \sim 0.25 \quad (5.26)$$

and for this particular mode the uncertainty is $\delta \ln(\text{RPFR}_i) \sim (0.25)(0.0064) \sim \pm 0.0016$. To compare, VPiE measurements, on the other hand, are routinely carried out with a precision of $\delta \ln(P'/P) \sim \pm 1 \times 10^{-4}$, better in favorable cases. This is equivalent in our example to $\delta \ln(\text{RPFR}_i) / \ln(\text{RPFR}_i) \sim 1 \times 10^{-4} / 6.4 \times 10^{-3} \sim 0.015$. Thus, for this mode, the thermodynamic precision of measurement of RPFR is more than an order of magnitude better than that calculated from spectroscopic differences. On the other hand real molecules have many vibrational frequencies and VPiE is a complicated sum with contributions from all of them. The example above is oversimplified. It is clear that the best physical understanding will be achieved from an interactive approach which employs both spectroscopic and thermodynamic information. In that process isotope independent force fields are employed to calculate gas frequencies and gas-to-liquid frequency shifts, which, on the one hand, are consistent with the spectroscopic data, and on the other with measured IE's.

5.4.3 A Further Approximation: The AB Equation

It is often useful to have an approximate relation for VPiE's, especially when complete vibrational analysis is impossible. The AB approximation serves that purpose, and sometimes gives more physical insight than do detailed, but very complicated calculations using Equation 5.24. It is based on the observation that ordinarily condensed phase vibrations fall in two groups; the first containing the high frequencies, $u_i \gg 1$ (most often the internal modes, $u_i = hc\nu_i/kT$), where the zero point (low temperature) approximation is appropriate, and

$$\ln(f_c/f_g)_B = B/T = (1/2)(hc/(kT)) \sum [(\nu_{i,c}' - \nu_{i,c}) - (\nu_{i,g}' - \nu_{i,g})]_{\text{high freqs}} \quad (5.27)$$

The second group contains the low frequencies, $u_i < 1$, which are to be treated in the high temperature approximation. This, we have seen, accounts for excitation into upper levels by expanding $\ln(s/s')f$ in even powers of u (see Chapter 4)

$$\ln(s/s')f_i = \sum [(-1)^{j+1} b_{2j-1} \delta u_i^{2j} / ((2j)2j!)]_{\text{low freqs}} \quad (5.28)$$

Reorganizing and dropping higher order terms

$$\ln(f_c/f_v) = A/T^2 + B/T \quad (5.29)$$

with B defined in Equation 5.30 and

$$A = (1/24)(hc/k)^2 \sum [(v_{i,c}'^2 - v_{i,c}^2) - (v_{i,g}'^2 - v_{i,g}^2)]_{\text{low freqs}} \quad (5.30)$$

The A defined in Equation 5.30 is not to be confused with the Helmholtz free energy. Should the A frequencies be limited to the external hindered translations and rotations, $v_{i,g}' = v_{i,g} = 0$, and this is an additional simplification. In some molecules, however, there are isotope sensitive low lying internal modes (often internal rotations or skeletal bends). In that cases both terms in Equation 5.30 contribute.

A is generally positive and predicts ($P' > P$). B results from the shifts in internal force constants on condensation. An increased force constant on condensation leads in the direction of a normal VPIE, a decrease towards an inverse effect ($P' < P$). Keep aware of the different temperature dependences. At low enough temperature A/T^2 must predominate. The IE is normal and proportional to $1/T^2$. At intermediate temperatures the B term, which can be positive, but more often is negative (see Section 5.4.1), may dominate. This accounts for the commonly observed crossover to inverse IE's. At higher temperatures yet, both terms decay to zero. The temperature dependence of VPIE can thus be complicated.

Our development has assumed temperature independent force constants. In real liquids, however, there is a small temperature dependence of frequencies and force constants due to anharmonicities, lattice expansion, etc. The incorporation of these effects into the theory is treated in later sections.

5.5 Non-ideal Gases: Virial Coefficient Isotope Effects

Rationalization of virial coefficient isotope effects follows similarly to that for the VPIE. In classical statistical thermodynamics the virial coefficient is given by,

$$B = -2\pi N \int [\exp(-\phi_2(r)/kT) - \exp(-\phi_1(r)/kT)] r^2 dr \quad (5.31)$$

In this equation $\phi_2(r)$ is the potential of interaction between two molecules and $\phi_1(r)$ is the one molecule potential function, $\exp(-\phi_1(r)/kT) = 1$. The coordinate, r , specifies interparticle distance and the integral extends from zero to infinity. Statistical arguments (see, e.g., Rice 1967) show that Equation 5.31 can be replaced with

$$B = (2/3)\pi\sigma^3 - K(T) \quad (5.32)$$

$2K(T)$ is the probability of finding two particles closer than they would be in a random distribution (i.e. it is the probability of pair formation, the factor 2 occurs because it takes two particles to form one pair). K is the equilibrium constant for pair formation and has units of volume. The first term $b_0 = (2/3)\pi\sigma^3$ is the volume excluded by the short range repulsive part of the potential and is isotope independent. The VCIE is therefore associated with the isotope effect on $(B - b_0)$ and can be written

$$\begin{aligned}\ln(K/K') &= -\ln(K'/K) = \ln(f_p/f_g^2) = -\ln[(B-b_0)'/(B - b_0)] = (-VCIE) \\ &= A_p/T^2 + B_p/T\end{aligned}\quad (5.33)$$

Subscript ‘‘p’’ refers to pair formation, the minus sign is explained by the fact that K refers to the equilibrium, two monomer (gas) = one pair, but the vapor pressure equilibrium is written, condensed phase = ideal gas monomer. In analogy with Equations 5.25 and 5.28 A_p and B_p are given as $A_p = (1/24)(hc/k)^2 \sum[(\nu_{i,p}'^2 - \nu_{i,p}^2) - (\nu_{i,g}'^2 - \nu_{i,g}^2)]_{\text{low freqs}}$ and $B_p = (1/2)(hc/(kT)) \sum[(\nu_{i,p}' - \nu_{i,p}) - (\nu_{i,g}' - \nu_{i,g})]_{\text{high freqs}}$. In the ordinary case the sum in the expression for A is over the six external modes of the dimer and $\nu_{i,g}'^2 = \nu_{i,g}^2 = 0$. In the B term the sum extends over the $2(3n - 6)$ internal modes of the dimer, n is the number of atoms in the monomer. As for VPIE, A_p is positive. B_p , however, involves the sum of dimer–monomer isotopic frequency differences, and as in Equation 5.27, can be either positive or negative. If the net frequency shift for internal modes is to the blue, the A and B terms are both positive and reinforce one another. The IE is positive and large. More often the net shift in internal frequencies is to the red, B is negative, and at some temperatures B/T may be, and often is, larger in magnitude than A/T^2 . In that case the isotope effect is negative (although at low enough temperature A/T^2 must predominate and the IE is positive).

It is interesting to compare the magnitude of VCIE and VPIE, and this is done for several compounds of interest in Table 5.2. Unfortunately VCIE data are extraordinarily difficult to obtain at high precision and only rarely are available at temperatures where direct comparison with VPIE is possible. The discussion in Section 5.3.2, considered together with Fig. 5.1, leads to the conclusion

Table 5.2 A and B parameters for fits to $[-VCIE]$ and VPIE for selected molecules (per deuterium substitution) (Van Hook, W. A., Rebelo, L. P. N. and Wolfsberg, M. *J. Phys. Chem. A* **105**, 9284 (2001) RPF = $A/T^2 + B/T$)

	Virial coefficient IE's			Vapor pressure IE's		
	A_{VCIE}/n_D	B_{VCIE}/n_D	Range(K)	A_{VPIE}/n_D	B_{VPIE}/n_D	Range(K)
CH ₄ /CD ₄	233 ± 40	−2.34 ± 0.21	110/300	258	−2.89	90/120
C ₂ H ₆ /C ₂ D ₆	53 ± 23	−0.74 ± 0.08	210/520	140	−2.86	115/200
NH ₃ /ND ₃	2630 ± 124	−5.43 ± 0.34	298/473	5320	−12.2	218/273
H ₂ O/D ₂ O	4277	−6.14	473/723	16900	−35.2	273/423

n_D = number of D atoms substituted.

that $|-VCIE/VPIE| = \ln(f_p/f_g^2)/\ln(f_c/f_g)$, A_{VCIE}/A_{VPIE} , and B_{VCIE}/B_{VPIE} are all significantly less than unity (at temperatures well removed from crossovers between positive and negative IE's) and this is verified by the available data, $\ln(f_p/f_g^2)/\ln(f_c/f_g) = 0.4 \pm 0.2$, $A_{VCIE}/A_{VPIE} = 0.4 \pm 0.2$, and $B_{VCIE}/B_{VPIE} = 0.3 \pm 0.2$. The large uncertainties are primarily due to experimental uncertainty in the VCIE data.

5.6 Further Discussion of VPIE's

5.6.1 Representative Effects, Especially H/D Effects and Solvent Dependence

Figure 5.2 shows VPIE's per atom D for a few organic compounds and for water and ammonia. H/D VPIE's range from 10% *per D* normal for H₂O/HOD at 273 K (the freezing point of H₂O, the effect in ice is even larger), to 1.6% inverse for CH₃CCH/CH₂DCCH at 160 K. The temperature dependence of VPIE also varies widely (from $\partial \ln(P'/P)/\partial(1/T) = -110$ K for HOD at 273 K, to 1.3 K for CH₂DCCH at 160 K). D for H substitution at hydrogen bonds results in large normal VPIE's with large negative temperature coefficients (e.g. HOD/H₂O). Contributions to VPIE from the large hindered lattice modes of hydrogen bonded molecules far outweigh the red-shifts observed in their internal frequencies on condensation, even though such strongly associated molecules usually show larger red-shifts in internal modes than do nonassociated ones. For example, for water there is a net red-shift of ~ 280 cm⁻¹ for internal OH stretching frequencies on condensation, but that is more

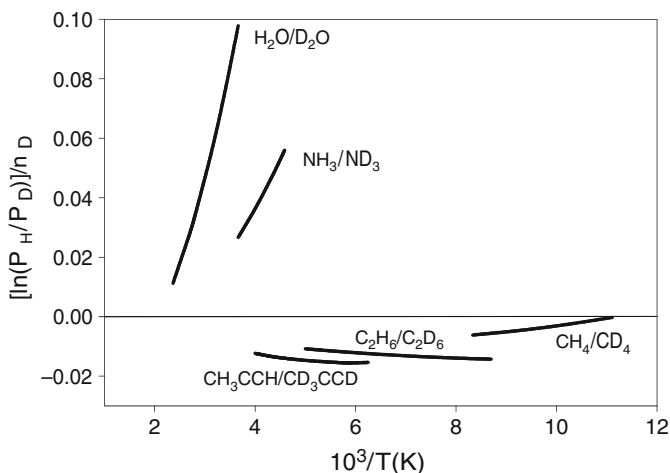


Fig. 5.2 H/D vapor pressure isotope effects (per atom D) for some representative compounds

than compensated by the appearance of three blue-shifted librational modes (each in excess of 500 cm^{-1}) and three hindered translations ($\sim 160\text{ cm}^{-1}$). Large phase frequency shifts are also observed for other condensed phase associated molecules, for example at amino or alcoholic hydrogens. On the contrary D for H substitution at methyl, methylene, or phenyl, groups is different. It is characterized by much smaller shifts, even when the D/H sites are found in molecules which contain NH_2 , OH, etc. associated functional groups. This is because the isotopically substituted site is not directly involved in the hydrogen bonding or other association.

Since VPIE is determined by intermolecular forces, significant changes should occur when one varies the condensed phase environment. This is nicely shown in Table 5.3 which compares RPFR's for $\text{H}_2\text{O}/\text{D}_2\text{O}$ and $\text{C}_6\text{H}_6/\text{C}_6\text{D}_6$ at 306 K (obtained from VPIE's of pure waters or benzenes, or from Henry's law coefficients, K_{H} and K_{D} respectively, for the dilute solutions of H_2O or D_2O in benzene, or C_6H_6 or C_6D_6 in water or heavy water). In the hydrocarbons water is monomeric and nonassociated, or nearly so. For $\text{H}_2\text{O}/\text{D}_2\text{O}$ in benzene the IE is about 1.4% inverse, very different indeed from the VPIE of pure water which is 13% normal at this temperature. The IE on the free energy of transfer between water and the dilute solution in benzene, $\Delta\delta G^{\text{TRANS}} = RT[\ln(K_{\text{H}}/K_{\text{D}}) - \ln(P_{\text{H}}/P_{\text{D}})]$, is dramatic; it is consequent to large changes in both internal and lattice frequencies on transfer from the hydrogen bonded to the nonpolar medium (K_{H} and K_{D} are Henry's law constants for H_2O and D_2O at high dilution in C_6H_6 , respectively). Less strongly associated

Table 5.3 Solute and solvent solubility isotope effects for (benzene–water) solutions at 306.2 K obtained from IE's on Henry's Law coefficients, K_{I} and K_{II} . [Isotope effects on free energies of transfer, ideal gas to solution in the limit of infinite dilution] (Dutta-Choudhury, M., Miljevic, N. and Van Hook, W. A. *J. Phys. Chem.* **86**, 1711 (1982))

(A) – Water-rich solutions				
	Solute	Solvent(s)	Solute effects $\text{RPFR} = \delta\Delta\mu^{(*,o)}$ $\text{RT} = \ln(K_{\text{I}}/K_{\text{II}})$	Solvent effects $\text{VPIE} = \delta\Delta\mu^0$ $\text{RT} = \ln(P_{\text{I}}^0/P_{\text{II}}^0)$
I	C_6H_6	H_2O		
II	C_6H_6	D_2O	–0.088	
I	C_6D_6	H_2O		
II	C_6D_6	D_2O	–0.109	
I	C_6H_6	H_2O		
II	C_6D_6	H_2O	0.061	
I	C_6H_6	D_2O		
II	C_6D_6	D_2O	0.040	
I	H_2O	H_2O		
II	D_2O	D_2O		0.131
(B) – Benzene-rich solutions				
I	H_2O	C_6H_6		
II	D_2O	C_6H_6	–0.014	
I	C_6H_6	C_6H_6		
II	C_6D_6	C_6D_6		–0.027

molecules also show large isotope effects on free energies of transfer. Table 5.3 includes IE data on reduced transfer free energy, this time for C_6H_6 or C_6D_6 from the pure hydrocarbon to H_2O (or D_2O). The table shows that $RPFR_{(C_6H_6/C_6D_6)}$ increases markedly (from $\sim -2.7\%$ to 6.1%) on transfer from the pure hydrocarbon liquid to the Henry's law reference state (infinite dilution) in H_2O . Moreover there is a solvent IE on this process. The isotope effect on the transfer free energy to D_2O lies about 2% below that for H_2O .

Another interesting example of solvent effects on isotopic vapor pressure ratios is shown by hydrocarbon/alkylamine solutions. Logarithmic activity ratios of NH_2/ND_2 -ethylamines in n-butane, $\ln[P(CH_3NH_2)/P(CH_3ND_2)] \sim RPFR$ (for $0 < x(\text{amine}) < 1$) are reported in Fig. 5.3. The IE falls smoothly from the large normal effect with a large temperature dependence at $x(\text{amine}) = 1$ characteristic of hydrogen bonded systems, to a much smaller inverse effect with a small temperature dependence at $x(\text{amine}) = 0$. The behavior is the one expected as the strong directionally dependent hydrogen bonding between amino groups is progressively diminished on dilution with butane.

The thermodynamic connection between IE's on gas solubility, infinite dilution Henry's law constants, and transfer free energy IE's, implies that gas-liquid chromatography should be a convenient way to study solvent effect IE's. That in fact is the case, and many authors have reported on chromatographic isotope separations and on the interpretation of the separation factors in terms of the transfer free energy IE's (Section 8.5).

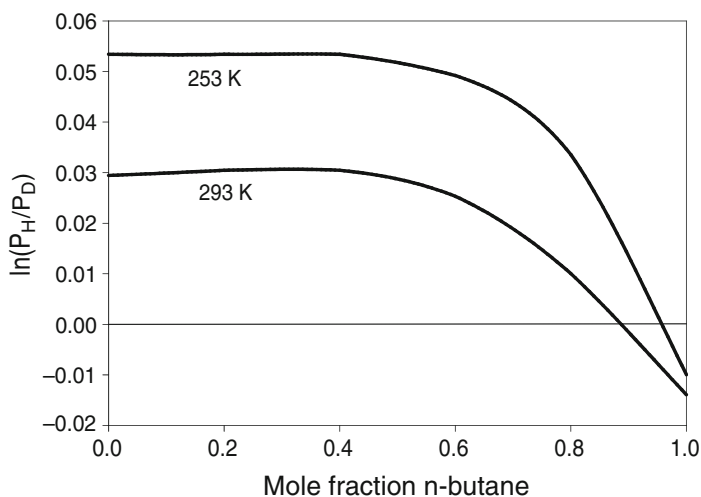


Fig. 5.3 Concentration dependence of the vapor pressure ratios of $C_2H_5NH_2$ and $C_2H_5ND_2$ dissolved in liquid n-butane at two temperatures (Data of Wolff, H. and Hopfner, A. *Ber. Buns. Ges. Phys.Chem.* **69**, 710 (1965))

5.6.2 *Interpretation of VPIE Using Model Calculations: Preliminary Remarks*

In simplest outline the harmonic oscillator cell model (HOCM) for condensed phase IE's outlined in Section 5.4 begins with spectroscopic analysis of the gas phase parent molecule to define a set of isotope independent harmonic force constants. These are combined with experimentally observed frequency shifts on condensation for each of the $3n$ normal modes to generate condensed phase force constants. The double set of force constant and force constant shifts describing the phase change is used to generate complete sets of harmonic frequencies for each isotopomer of interest in each phase, and thence reduced partition function ratios. The criterion of success is that the calculated RPF_R's agree with those obtained from observed VPIE's for each pair over a reasonably wide range of temperature. Thus the process generates sets of harmonic force constants consistent on the one hand with observed frequencies and frequency shifts, and on the other with thermodynamically measured VPIE's. Broadly speaking HOCM has proven successful, and examples discussed in Section 5.7 illustrate that point. Even so, improvements to the procedure outlined above are sometimes possible. The most important are corrections for the contributions of anharmonicity, especially for lattice modes, and dielectric corrections to observed condensed phase frequencies and frequency shifts (Sections 5.6.3 and 5.6.4).

5.6.3 *Anharmonic Corrections*

5.6.3.1 *Lattice Anharmonicity and the Pseudo-harmonic Approximation*

A realistic look at the potential functions used to describe intermolecular vibrational modes shows the commonly used harmonic approximation to be no better than "rough-and-ready." Best fit harmonic potentials for lattice modes approximately coincide with more realistic potentials (like LJ-6/12) only at or very near the bottom of the potential curves, and thus it is no surprise that strictly harmonic oscillator IE calculations only agree with experiment over narrow temperature ranges (see, e.g., Figs. 3.1 and 5.1). The harmonic model does not properly account for thermal expansion of the lattice, nor for the shifts in frequency associated with lattice expansion. These effects, however, can be treated empirically by introducing a set of volume dependent "best fit" lattice harmonic oscillator force constants. The method follows an approach introduced many years ago by Gruneisen and generally known as the pseudo-harmonic approximation. In Gruneisen notation, $\Gamma_i = -(d \ln \nu_i / d \ln V)_T = -(1/2) d \ln(f_i) / d \ln V$. Γ_i is the Gruneisen constant for the frequency of interest ν_i , and f_i is the harmonic force constant. Also, $\Gamma_i = -d \ln \nu_i / d \ln V = -(d \ln \nu_i / dP)(dP / d \ln V) = (d \ln \nu_i / dP) / \kappa$. Here κ is the isothermal compressibility, $\kappa = -(d \ln V / dP)_T$. This relation is useful because there is much more experimental information available on the pressure dependence of vibrational frequencies than on their volume dependence. [For lat-

tice translational modes of monatomics an additional semiempirical relation was proposed by Gruneisen, $\Gamma_{tr} = \alpha V / (\kappa C_V)$. Here α is the coefficient of thermal expansion, $\alpha = (\partial \ln V / \partial T)_P$ and typically, Γ_{tr} is about 2. For rotation/libration modes and internal vibrations, however, Γ_i may be significantly different from 2, for internal modes very much different (much smaller), and so far as these motions are concerned the Gruneisen formalism is best described as a completely empirical approach which accounts for vibrational anharmonicities caused by lattice expansion.] In the pseudoharmonic formalism the temperature dependences of the various normal mode frequencies arise only indirectly, i.e. through the temperature dependence of the volume. Anharmonic corrections for lattice modes can be important. For example in the ethylene/deutero-ethylene system it was found the lattice translational and rotational force constants decreased $\sim 15\%$ and 40% respectively between 104 and 180 K. One expects (and finds) that changes in the volume dependent pseudo-harmonic internal force constants are relatively much smaller than are the changes in lattice force constants (the internal modes are stiffer and much less sensitive to intermolecular coupling). For ethylene/deuteroethylene the CH stretching constant decreases only 0.15% between 104 and 180 K, bending force constants change about 2% over that temperature range.

5.6.3.2 Anharmonicity: Internal Modes, Effect of Zero Point Anharmonicity

It is interesting to compare lattice mode pseudoharmonic corrections to VPIE with zero point anharmonic corrections to RPFPR for high frequency internal modes (Appendix 4.2). In making the connection between thermodynamic and optical experiments it is important to recall that infra-red or Raman spectroscopic measurements of vibrational frequencies (in the region, say, $600 < \nu(\text{cm}^{-1}) < 4,000$) do not measure ZPE itself, but rather the energy difference between the zeroth and first levels, $\delta E(0, 1)$. With the curvature of PES thoroughly understood it is possible to calculate ZPE from $\delta E(0, 1)$ but only for those relatively few diatomic and polyatomic isotopomer pairs for which complete vibrational analysis has yielded harmonic frequencies and first-order (and very rarely second-order) anharmonic contributions to ZPE. Vibrational analysis for the vast majority of polyatomics has been limited to the harmonic approximation, and RPFPR for these molecules must be calculated using effective harmonic oscillator frequencies and frequency shifts on condensation. (As noted in Appendix 4.2, however, it is now possible to use standard quantum chemistry packages to estimate anharmonic corrections to ZPE's and RPFPR's).

As an isotopomer pair of interest gets larger and/or heavier, either by accumulating mass in the form of heavier atoms, or by adding more atoms, the relative contribution of the external degrees of freedom, the lattice modes, to RPFPR decreases. Massive molecules have small hindered translation and librational frequencies, $\nu^2(\text{tr}) \sim 1/M$ and $\nu^2(\text{lib}) \sim 1/I$, and the contribution to RPFPR drops off rapidly with mass. If at constant mass one increases the number of bonds, the change in M and I is modest, but the number of internal oscillators increases rapidly ($dN(\nu) \sim 3dn$, N the number of oscillators, n the number of atoms). Thus the relative contribution of B in Equation 5.29 grows at the expense of A .

To illustrate the anharmonic contribution to RPF_R from a particular high frequency mode treated in the ZPE approximation, for example a CH/CD stretch, we recall the oscillator energy neglecting G_0 is expressed

$$E = hc\omega(v + 1/2) - hc\omega x_e(v + 1/2)^2 + hc\omega y_e(v + 1/2)^3 \dots \dots \dots] \quad (5.34)$$

In Equation 5.34 ω is the harmonic frequency, v the vibrational quantum number, and x_e and y_e the first and second anharmonicity constants (mass dependent, $\omega'x'_e/(\omega x_e) = X'/X = \mu/\mu'$, μ , and μ' are vibrational reduced masses). The ZPE($v = 0$) contribution to RPF_R through first order is thus

$$\ln(f_c/f_v)_{CH/CD} = (hc/kT) \{ [(\omega'_c - \omega_c)/2 - (\omega'_v - \omega_v)/2] - [(X'_c - X_c)/4 - (X'_v - X_v)/4] \} \quad (5.35)$$

The “best fit” harmonic approximation, on the other hand, gives

$$\ln(f_c/f_v)_{CH/CD} = (hc/kT) \{ (v'_c - v_c)/2 - (v'_v - v_v)/2 \} \quad (5.36)$$

where v_i is the “best fit” fundamental frequency, $v_i = \omega_i - 2X_i$. The anharmonicity correction to RPF_R is expressed by the difference.

$$\delta \ln(f_c/f_v) = (3/4)(hc/kT)[1 - \mu'/\mu]\delta X' \quad (5.37)$$

where $\delta X'$ is the shift in the anharmonic constant X' on condensation. Harmonic oscillator frequencies, anharmonic constants, and phase frequency shifts are available for chloroform (among other molecules) which we consider as an example (Table 5.4). For $CHCl_3/CDCl_3$ the H/D VPIE is dominated by the contribution of the CH(CD) stretching mode to the ZPE (B) term ($v' = 3,033 \text{ cm}^{-1}$, $\Delta v' = 14 \text{ cm}^{-1}$, $X'_{\text{vap}} = 62$). Vibrational analysis of the VPIE data near room temperature shows that X' decreases by about 4% on condensation. The 0.6 cm^{-1} uncertainty in this thermodynamic estimate ($\delta X' = -2.6 \pm 0.6 \text{ cm}^{-1}$)_{VPIE} is less than the uncertainty in the spectroscopic value ($-1.3 \pm 2 \text{ cm}^{-1}$)_{SPEC}. The results indicate that

Table 5.4 Gas phase frequencies and frequency shifts on condensation, and anharmonicity constants for $CHCl_3$ and $CDCl_3$ in cm^{-1} (Jancso, G., Jakli, Gy. and Fetzer, C. Z., *Naturforsch.* **38a**, 184 (1983))

		Gas phase frequencies		$\nu_{\text{GAS}} - \nu_{\text{LIQ}}$		$\delta \Delta \nu$
ν_1	CH(CD) stretch	3033.2	(2265.0)	14.0	(10.0)	4
ν_2	Sym CCl_3 stretch	675.0	(652.6)	5.6	(5.9)	-0.3
ν_3	Sym CCl_3 bend	363.4	(357.6)	-1.8	(-2.0)	0.2
ν_4	HCCl (DCCl) bend	1219.1	(910.8)	3.0	(4.8)	-1.8
ν_5	Antisym CCl_3 stretch	773.5	(742.2)	3.9	(1.8)	2.1
ν_6	Antisym CCl_3 bend	261.7	(261.3)	0.1	(0)	0.1
X_1	Anharmonicity cons.	-61.5	(-33.6)	-2.6	(-1.3)	-1.3

intermolecular forces in liquid chloroform make the CH stretch for this molecule more nearly harmonic than in the vapor. In the absence of information on anharmonic constants (the ordinary situation for polyatomics) vibrational analysis of VPIE follows Equation 5.36 and one expects some deterioration in the agreement between spectroscopically observed and thermodynamically calculated phase frequency shifts.

5.6.4 Corrections for the Dielectric Effect

There is an additional complication in comparing thermodynamically observed and spectroscopically calculated RPF_R's. The intermolecular forces which we conventionally describe in terms of changes in effective well depth and shape parameters, and in this way account for condensed matter isotope effects, also affect spectral band shapes, centers of gravity, spectral intensities, and related spectroscopic properties. For high intensity IR bands, shape corrections for condensed phase interactions are substantial; in the spectroscopic literature they are referred to as "dielectric corrections". Dielectric corrections take account of the difference between the effective electric field of a light wave acting on a molecule in a condensed medium, and the average electric field in that medium. The two are different because of the absorption of part of the radiation. Neglect of the dielectric corrections affecting condensed phase band shapes and frequency assignments can lead to large errors in RPF_R's derived from spectroscopic measurements. For IR intense bands dielectric corrections can amount to 10 cm⁻¹ or more. Table 5.5 gives a few values. Bearing in mind that typical spectroscopic precision in the condensed phase is

Table 5.5 Some dielectric shifts for intense IR frequencies of pure liquids (Maessen, B. and Wolfsberg, M. *Z. Naturforsch.* **38a**, 191 (1983))

Substance	Frequency	cm ⁻¹	Dielectric shift (Δν/cm ⁻¹)	10 ³ Intensity/ (cm ² mol ⁻¹)
CO		2143	1.3	2.7
CO ₂	ν ₂	667	2.6	6.2
	ν ₃	2349	11.6	27.4
CS ₂	ν ₂	397	0.4	1.4
	ν ₃	1535	10.3	36.8
SO ₂	ν ₂	518	4.0	5.2
	ν ₁	1151	1.6	2.1
	ν ₃	1362	10.9	14.1
CH ₄	ν ₄	1306	1.3	2.7
	ν ₃	3019	1.2	2.3
C ₆ H ₆	ν ₄	673	2.5	13.1
	ν ₁₃	1486	0.2	0.9
	ν ₁₂	3080	0.4	2.0

$\sim \pm 0.5$ to $\pm 1.0 \text{ cm}^{-1}$, the corrections are significant. They cannot be ignored when making accurate comparisons between spectroscopically calculated and thermodynamically observed RPFR's for molecules with intense IR bands.

5.6.4.1 Example, VPIE of Carbon Disulfide

CS_2 is a symmetric linear molecule with carbon at the center. There are five external (three hindered translations and two librations) and four internal modes, the symmetric and antisymmetric stretches and the doubly degenerate bend. The spectrum is available for both phases (Table 5.6). The inverse carbon VPIE is large (-0.0018 at 250 K, -0.0013 at 325 K), the sulfur IE is positive and much smaller (0.0003 at 250 K, 0.0002 at 325 K). Because carbon lies at both center of mass and center of symmetry there is no carbon IE on the symmetric stretch nor on libration. The $^{12}\text{C}/^{13}\text{C}$ effect is a sum of IE's for hindered translation, degenerate bending, and asymmetric stretching, but the isotope dependence of translation and bending modes is small. These motions cannot explain the unusually large carbon VPIE, nor the fact that it is inverse. The predominant contribution is from the antisymmetric stretch, ν_3 , but the 13 cm^{-1} phase shift in this frequency calculated from the VPIE does not agree with the spectroscopically observed (uncorrected) frequency shift of 27 cm^{-1} . The difference is far outside the combined thermodynamic and spectroscopic uncertainty, which is no more than $\sim \pm 2 \text{ cm}^{-1}$. It seems clear that the appropriate phase frequency shift to employ in thermodynamic calculations is the one corrected for the dielectric effect. For chloroform the corrected frequency shift has been variously estimated by spectroscopists to lie between 10 and 15 cm^{-1} in good agreement with the thermodynamic value (13 cm^{-1}), and the theoretical estimates (Table 5.6).

Most theoretical interpretations of condensed phase IE's have depended heavily on spectroscopic measurements of ZPE shifts to define limits on parameter assignments (force constant shifts). It is therefore a matter of some importance to determine the magnitude of dielectric corrections to be applied to such shifts. Fortunately dielectric corrections are larger than typical spectroscopic uncertainties in phase frequency shifts only for very intense IR bands, and therefore dielectric corrections are very often unnecessary.

Table 5.6 Calculated and observed frequency shifts on condensation for CS_2 (Jancso, G. and Van Hook, W. A. *Can. J. Chem.* **55**, 3371 (1977))

Frequency	Degeneracy	$(\nu_g - \nu_l)_{\text{OBS}}/\text{cm}^{-1}$	$(\nu_g - \nu_l)_{\text{CALC}}/\text{cm}^{-1}$
ν_1	1	5.2	5.2
ν_2	2	5.5	5.5
ν_3	1	27.1 ^a (10–15) ^{b,c}	13.1
ν_{tr}	3	-52	-52
ν_{libr}	2	-70	-70

^aObserved.

^bAfter spectroscopic correction for dielectric effect.

^cTheoretical dielectric correction (Table 5.5) = 10.3 cm^{-1} .

5.7 Some Examples

To illustrate the principles developed in earlier sections we consider VPIE's for some thoroughly studied systems.

5.7.1 Example #1: Monatomic Systems Reconsidered; Accurate Calculations

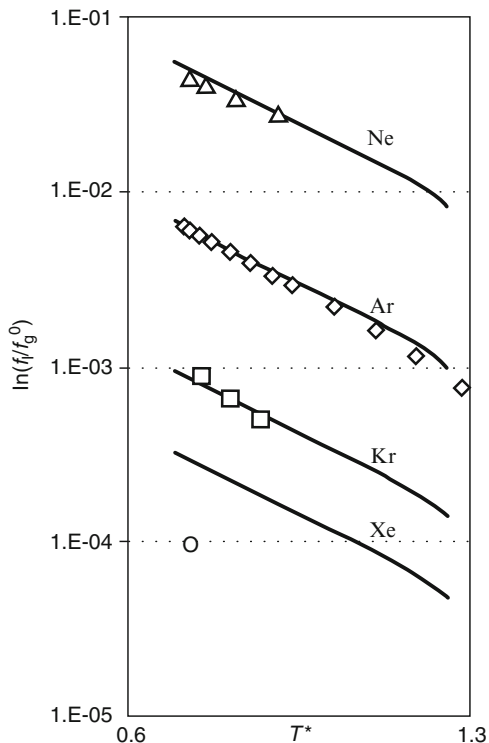
Precise intermolecular potentials are available for monatomic He, Ne, Ar and Xe. This permits accurate calculations of the VPIE's of these gases, their mixtures, and rare gas isotopomer mixtures. To begin, we are reminded that the mean intermolecular potential energy, $\langle U \rangle$, and mean force constant $\langle \nabla^2 U \rangle$ can be obtained from the pair correlation function of the fluid, $g(r)$,

$$\langle U \rangle = 4\pi\rho \int g(r) u(r)r^2 dr \quad (5.38)$$

$$\langle \nabla^2 U \rangle = 4\pi\rho \int (g(r)\partial/\partial r)(r^2\partial u(r)/\partial r)dr \quad (5.39)$$

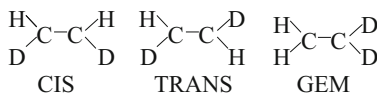
In Equations 5.38 and 5.39 $u(r)$ is the intermolecular potential, r is the intermolecular distance, ρ the number density, and the integrals extend ($0 < r < \infty$). Integral equation theory can be used to calculate $\langle \nabla^2 U \rangle$ across a broad range of density (using a reduced Lennard–Jones potential). This approach is an alternative to computer simulation which is more lengthy and expensive. Figure 5.4 compares calculated RPF_R's with experiment. The input parameters (well depth, ϵ , and size parameter, σ .) for each species are completely defined in terms of the observed critical properties for each of the fluids. The agreement with experiment is remarkably good, especially considering that the VPIE's span several orders of magnitude. At any specific reduced temperature ($T^* = kT/\epsilon$), RPF_R scales very nearly as $[(\Delta m/m^2)/(\sigma^2\epsilon)]$. The excess free energies, G^E , and activity coefficients, $\ln \gamma^\infty$, of isotopomer mixtures scale as $[(\Delta m/m^3)/(\sigma^4\epsilon)]$ and $[(\Delta m/m^3)/(\sigma^4\epsilon^2)]$, respectively. Since, in turn, the product $(\sigma^2\epsilon)$ for the rare gases is linearly dependent on mass, m , then RPF_R is directly proportional to the isotopic mass difference and inversely proportional to m^3 , while $\ln(\gamma)$ is inversely proportional to m^5 . Thus the excess free energy of isotopic mixtures of rare gases vanishes rapidly as one proceeds down Group VIII of the periodic table from helium through argon to, say, radon. Although the LJ potential is only approximate, it turns out to be an excellent choice to represent IE's in rare gas systems. The thermodynamic properties are described with a single master (reduced) equation. Theory and experiment are in satisfactory agreement.

Fig. 5.4 Theory and experiment compared for VPIE's of rare gases (*points* = experiment, *lines* = calculation, *triangles* = $^{20}\text{Ne}/^{22}\text{Ne}$, *rhombs* = $^{36}\text{Ar}/^{40}\text{Ar}$, *squares* = $^{80}\text{Kr}/^{84}\text{Kr}$, *circle* = $^{130}\text{Xe}/^{136}\text{Xe}$) (Reused with permission from Lopes, J. N. C., Padua, A. A. H., Rebelo, L. P. N. and Bigeleisen, J. J. *Chem. Phys.* **118**, 5028 (2003). Copyright 2003, American Institute of Physics)



5.7.2 Example #2: VPIE's of Ethylene Isotopomers

Vapor pressures of C_2DH_3 , *cis*-, *trans*-, and *gem*- $\text{C}_2\text{D}_2\text{H}_2$, $\text{C}_2\text{D}_3\text{H}$ and C_2D_4 , and $^{12}\text{C}^{13}\text{CH}_4$, have been measured at high precision



and theoretically interpreted (see Fig. 5.5). VPIE's for the liquids are inverse, but there is a large positive discontinuity on freezing, and VPIE for solid C_2D_4 is positive (0.0376 at 104 K, the melting point) and increases even more as temperature drops.

Ethylene was one of the first systems subjected to detailed vibrational analysis using HOCM modified to account for lattice anharmonicity. Agreement with experiment is excellent (Fig. 5.5). The differences in the VPIE's of the equivalent isotopomers *cis*-, *trans*-, and *gem*-dideuteroethylene (Fig. 5.6) are of considerable interest since they neatly demonstrate the close connection between molecular structure and isotope chemistry. The IE's are mainly a consequence of hindered rotation in the liquid (moments of inertia for *cis*-, *trans*-, and *gem*- $\text{C}_2\text{D}_2\text{H}_2$ are slightly

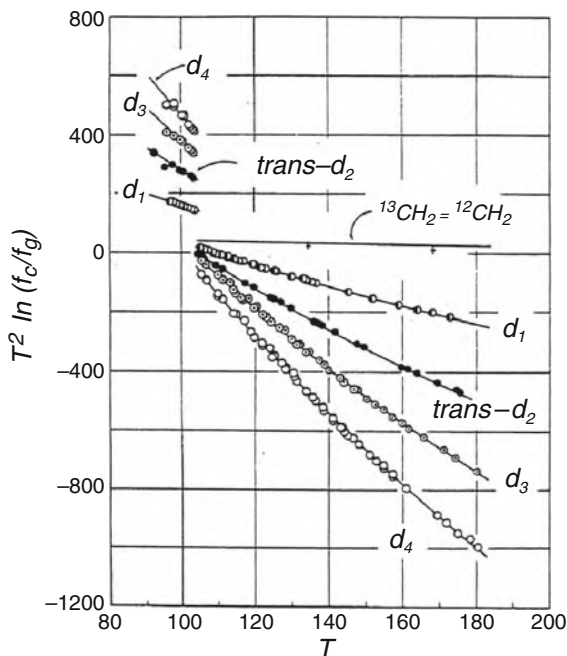


Fig. 5.5 Plot of $T^2 \ln(f_c/f_g) = T^2 \ln(f_c/f_v)$ for some isotopically substituted ethylenes. The *solid lines* are theoretically calculated from the isotope independent force field in Table 5.7 (Reused with permission from Bigeleisen, J., Fuks, S., Ribnikar, S. V., and Yato, Y., *J. Chem. Phys.* **66**, 1689 (1977). Copyright 1977, American Institute of Physics)

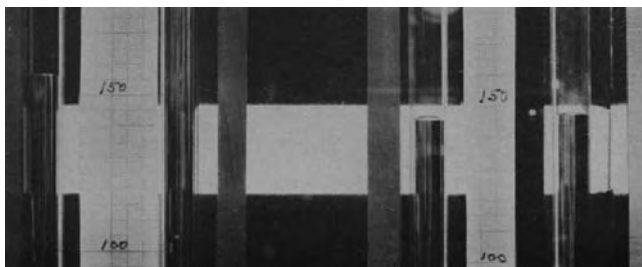


Fig. 5.6 Vapor pressure differences between equivalent isotopic isomers of dideuteroethylene. The three mercury levels shown (*left to right*) measure the vapor pressures of ordinary ethylene C_2D_4 , *trans*-ethylene-1,2 d_2 , and *cis*-ethylene-1,2 d_2 . The vapor pressure of *gem*-ethylene-1,1 d_2 is very similar to the *cis*-isotopomer and is not shown in this photograph (Bigeleisen, J., *Science* **147**, 463 (1965))

different), but superposed on that effect is an additional ZPE contribution caused by coupling between the hindered rotational modes in the liquid and certain internal vibrations. An interesting feature of IE calculations using comprehensive vibrational analysis is that contributions from individual frequencies can be sorted out and

Table 5.7 The contribution of various motions to $T^2 \ln(f_c/f_v)$ in the ethylene/deuteroethylene system at 104 K. Values in K^2 . (Reused with permission from Bigeleisen, J., Fuks, S., Ribnikar, S. V. and Yato, Y. *J. Chem. Phys.* **66**, 1689 (1977). Copyright 1977, American Institute of Physics)

	d_1	Trans- d_2	Cis- d_2	Gem- d_2	d_3	d_4
Hindered-tr	62	84	92	111	134	153
Libration	433	801	830	833	1120	1408
C = C stretch	53	123	106	72	122	113
C-H stretch	-411	-814	-803	-749	1255	-1102
CH ₂ bend	1268	1497	1065	293	-1103	578
CH ₂ wag(in pl)	-1222	-1425	-981	-205	-1162	-743
(out of pl)	86	395	-186	20	161	50
Torsion	-133	-423	131	-114	-206	-64
Non-classical- rot(vap)	4	8	8	8	11	13
Total	142	247	262	269	333	406
Experiment	145	249	262	267	334	407

considered separately even though the net IE must be calculated from a complicated linear combination of all 3N motions. For deuteroethylenes Table 5.7 shows the most important contributions to VPIE are from the external hindered rotations and the internal CH/CD stretching modes.

5.7.3 Example #3: VPIE's of Benzene Isotopomers; Excess Pressures of Isotopomer Solutions

High precision VPIE's for C_6H_5D , *ortho*-, *meta*-, and *para*- $C_6H_4D_2$ and C_6D_6 are available between the normal melting and boiling points, as are data on the excess free energy of mixing (small and positive) for C_6H_6/C_6D_6 , the $^{13}C/^{12}C$ effect at the boiling temperature, VPIE's and MVIE's for C_6H_6/C_6D_6 across the entire LV coexistence range, triple to critical points, and isothermal compressibility IE's between 288 and 313 K. HOVM calculations show good agreement with spectroscopic information and reproduce the observed subtle deviations from the law of the mean in the series D_1, D_2, \dots, D_6 , and the VPIE's between equivalent isomers *ortho*-, *meta*-, and *para*- $C_6H_4D_2$. For liquid benzenes the lattice mode (A/T^2) contribution is relatively small. At the triple point hindered translation and rotation contribute about 3% and 5% of total VPIE, respectively; at the boiling point only 2-3%. That is not enough to rationalize the anharmonic contribution to VPIE (by applying Gruneisen theory to these external frequencies). A better approach invokes condensed phase volume dependent pseudo-harmonic CH/CD stretching modes. With (df_{CH}/dV) obtained from VPIE of one isotopomer pair, and using the experimentally observed molar volume isotope effect, one calculates $\mu^E = 1.8 J/mol$ for the excess free energy of isotopomer mixing in the low temperature

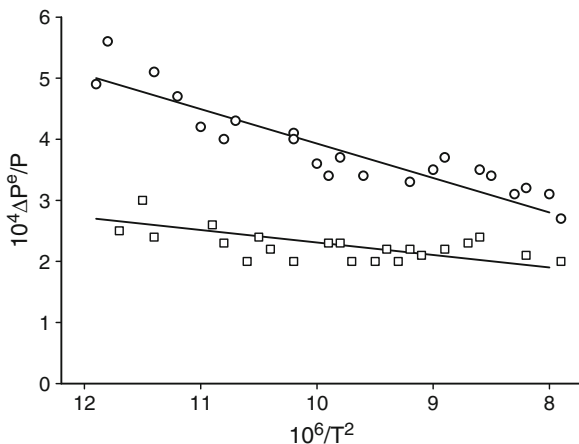


Fig. 5.7 Excess pressures of equimolar solutions of *per*-protio and *per*-deuterobenzene and of *per*-protio and *per*-deuterocyclohexane. $\Delta P = (P_{\text{SOLUTION}} - [0.5P^\circ(\textit{per} - \textit{protio}) + 0.5P^\circ(\textit{per} - \textit{deutero})])$. The upper line refers to cyclohexane ($\text{C}_6\text{H}_{12}/\text{C}_6\text{D}_{12}$) solutions, the lower to benzene ($\text{C}_6\text{H}_6/\text{C}_6\text{D}_6$) (Redrawn with permission from Jakli, Gy., Tzias, P., and Van Hook, W. A. *J. Chem. Phys.* **68**, 3177 (1978). Copyright 1978, American Institute of Physics)

fluid $[(0.5 \text{C}_6\text{H}_6 + 0.5 \text{C}_6\text{D}_6)]$, see Fig. 5.7] in good agreement with experiment, $2.1 \pm 0.3 \text{ J/mol}$. The agreement furnishes strong support for the theoretical development (Section 5.8) correlating molar volume isotope effects and excess free energies of solutions of isotopomers.

5.7.4 Example #4: Water

It is instructive to illustrate the use of Equations 5.19 and 5.29 using a simplistic 3-atom model calculation for water. Even though it is well established that the condensed phase structure of water is complicated and involves the coordinated motions of many molecules coupled through a constantly fluctuating hydrogen bond network, the fundamentals of the VPIE are represented reasonably well by the simplified model.

The principal features of water VPIE's are illustrated in Fig. 5.8 which compares VPIE's for water isotopomers from well down in the solid-vapor part of the phase diagram to near 400 K. For $\text{H}_2\text{O}/\text{D}_2\text{O}$ and $\text{H}_2^{16}\text{O}/\text{H}_2^{18}\text{O}$ high precision data from VPIE or LVFF, respectively, are available all the way to the critical point. VPIE's in the solid, and in the liquid not too far from the melting point, are normal and unusually large. At 273.15 K for $\text{H}_2\text{O}/\text{D}_2\text{O}$, $\ln(P'/P)_{\text{SOLID}} = 0.242$ and $\ln(P'/P)_{\text{LIQ}} = 0.204$. Such large effects are consequent to the large vibrational frequency shifts which occur on the condensation of a freely rotating and translating vapor molecule to the librationaly hindered and hydrogen-bonded condensed phase. Although the OH/OD stretching modes red shift significantly on condensation, that change is more than compensated by the very large and isotope sensitive blue shift in external frequencies.

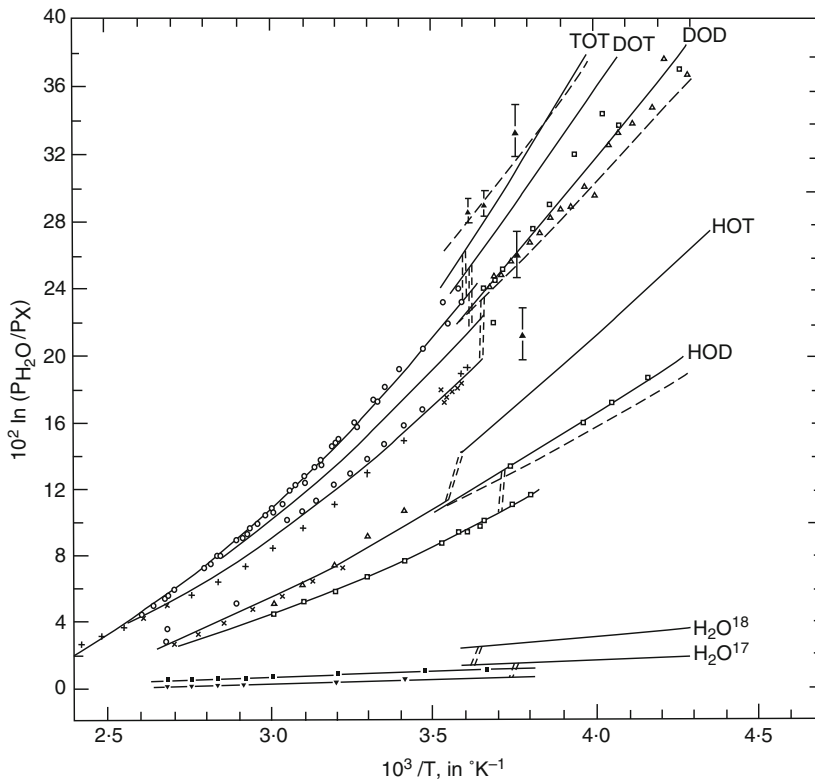


Fig. 5.8 VPIE's of Waters and Ices. The points are experimental from various sources. The lines are calculated using an isotope independent harmonic force field consistent with spectroscopic information (Van Hook, W. A. *J. Phys. Chem* **72**,1234 (1968))

The temperature coefficient of VPIE is also unusually large. For $\text{H}_2\text{O}/\text{D}_2\text{O}$ VPIE (normal at low temperature) falls steeply from 0.204 at the triple point to 0.051 at the boiling point, continues to drop as it crosses into the inverse VPIE region at 494 K, and still falls, albeit more slowly, all the way to the critical point of H_2O , 647.2 K, where it is -0.024 . Within experimental error $\ln(\alpha)$ is zero at that temperature. The interpretation of these temperature dependences is straightforwardly connected with the loss of hydrogen bonding as temperature increases. At high enough temperature, H-bonding has essentially disappeared, and the librational frequencies have all but vanished. Near T_C the most important contribution to IE is from the red-shifted OH/OD stretches. Thus, in this region the interpretation is similar to that of a hydrocarbon or other van-der-Waals bonded fluid. Table 5.8a shows observed and calculated frequencies and frequency shifts for room temperature water and VPIE's calculated from a harmonic isotope independent force field (Table 5.8b) chosen to be consistent with the spectroscopic phase frequency shifts

Table 5.8a Gas phase frequencies and observed and calculated gas–ice (173 K) and gas–liquid (213 K) frequency shifts for H₂O and D₂O. Values in cm⁻¹ (Van Hook, W. A. *J. Phys. Chem* **72**, 1234 (1968))

	H ₂ O		D ₂ O	
Gas to solid at 173 K				
ν_{GAS}	$(\nu_{\text{GAS}} - \nu_{\text{ICE}})_{\text{OBS}}$	$(\nu_{\text{GAS}} - \nu_{\text{ICE}})_{\text{CALC}}$	$(\nu_{\text{GAS}} - \nu_{\text{ICE}})_{\text{OBS}}$	$(\nu_{\text{GAS}} - \nu_{\text{ICE}})_{\text{CALC}}$
Internal modes				
3755.8	375.8	375.9	363	368.3
3656.7	506.7	506.5	277	274.8
1594.6	-55.4	-55.4	-31.7	-43.1
Librations ^a				
	-840	-843.6		-596.8
	-770	-772.9		-557.7
	-660	-666.7		-501.2
Hindered				
	-250	-275		-261
Translations ^a				
	to	-275		-260
	-300	-275		-258
Gas to liquid at 313 K				
ν_{GAS}	$(\nu_{\text{GAS}} - \nu_{\text{LIQ}})_{\text{OBS}}$	$(\nu_{\text{GAS}} - \nu_{\text{LIQ}})_{\text{CALC}}$	$(\nu_{\text{GAS}} - \nu_{\text{LIQ}})_{\text{OBS}}$	$(\nu_{\text{GAS}} - \nu_{\text{LIQ}})_{\text{CALC}}$
Internal modes				
3755.8	125.8	125.8	126.1	92
3656.7	206.7	206.6	156.5	150.4
1594.6	-50.4	-50.6	-46.7	-38.0
Librations ^a				
	-450	-500.0		-371.7
	to	-496.5		-358.0
	-600	-495.4		-353.6
Hindered ^a				
	-150	-162.2		-153.7
Translations ^a				
	to	-162.2		-153.5
	-175	-162.2		-154.0

^aBroad spectral features. Approximate center reported.

of H₂O and D₂O. VPIE's for various water isotopomers calculated from this force field are those shown in Fig. 5.8 as the solid lines.

In treating mixtures of isotopes in aqueous systems one must consider disproportionation, H₂O + D₂O = 2 HOD, at the same time recognizing that a pure sample of HOD cannot be obtained in bulk. Careful consideration of data on vapor pressures and freezing and boiling points of H₂O/HOD/D₂O mixtures leads to the conclusion that $\ln [P(\text{H}_2\text{O})/P(\text{D}_2\text{O})] / \ln [P(\text{H}_2\text{O})/P(\text{HOD})] = 1.91 \pm 0.02 (273 < T/\text{K} < 473)$ and is essentially independent of HOD concentration. In first approximation one would expect a ratio of two, which is the value predicted by the law of the geometric mean, but that law does not properly account for the interactions between internal and external modes, large and important in water because of hydrogen bonding.

IE's on some of the other properties of water are shown in Table 5.9. Many properties (like the enthalpies of phase change, triple points, etc.) are closely related to VP and can be interpreted similarly. Molar volume isotope effects are interesting and are discussed in Chapters 12 and 13. In the low temperature liquids

Table 5.8b Isotope independent gas, liquid and solid force fields for water. Units are mdyn/A for stretches and mdyn – A/rad² for bends (Van Hook, W. A. *J. Phys. Chem* **72**, 1234 (1968))

	Gas	Liquid (313 K)	Solid
OH stretch	8.4543	7.7470 ^a	6.6435
HOH bend	0.6994	0.7448 ^a	0.7520
Stretch–stretch	–0.1002	–0.2705	–0.3577
Stretch–bend	0.2272	0.2371	0.2371
Stretch–libration		–0.0234	–0.0480
Bend–libration		0.0072	0.0086
Translations		0.2789 ^a	0.8020
Libration 1		0.0896 ^a	0.1625
Libration 2		0.1705 ^a	0.4858
Libration 3		0.2575 ^a	0.6249

^aThese constants are temperature dependent. $df(st) = 2.8 \times 10^{-3}$ mdyn/(A deg) equivalent to the observed $dv(OH)/dT = 0.696 \text{ cm}^{-1}/\text{deg}$; $df(bend) = -0.052 \times 10^{-3}$ mdyn A/(rad² deg) equivalent to the observed $dv(HOH)/dT = -0.061 \text{ cm}^{-1}/\text{deg}$. For the external librations and translations $df(ext)/f(ext) = -0.0041 T + 1.2839$

Table 5.9 IE's on some of the thermodynamic properties of isotopic waters (Jancso, G. and Van Hook, W. A. *Chem. Rev.* **74**, 689 (1974))

	HOH	DOD	TOT	H ₂ ¹⁸ O	H ₂ ¹⁷ O
t(triple)/°C	0.0	3.82	4.49	0.38	0.21
(t(boil) – 100)/°C	0.0	1.42	1.51	0.15	0.08
VPIE crossover (c.o.)/°C	–	220.9	190	no c.o.	no c.o.
Critical properties					
T _C '/K	647.1				
ln(T _C '/T _C)		0.0050			
P _C '/MPa	22.06				
ln(P _C '/P _C)		0.0180			
ρ _C '/(mol/m ³)	17.9				
ln(ρ _C '/ρ _C)		0.0056			
Relative enthalpy (L _x – L _{H₂O})					
0°C (J mol ^{–1})	–	1750	1960	67	38
100°C (J mol ^{–1})	–	810	1210	46	25
δH _{FUS} (J mol ^{–1}), 0°C	6010	5960			
(J mol ^{–1}), 3.82°C	–	6280			
C _p / (J mol ^{–1} K ^{–1}), 25°C	75.3	84.3			
C _v / (J mol ^{–1} K ^{–1}), 25°C	74.5	83.7			
10 ⁶ κ _T /atm ^{–1} , 25°C	45.3	46.6			

molar volumes are in the order TOT > DOD > HOH > HH¹⁸O. These inverse isotope effects have been ascribed to librational motion in the hydrogen bonded condensed phase. The center of mass and center of interaction (about which the molecule librates) do not coincide and translation–rotation coupling must be taken into account. The center of mass moves progressively away from the oxygen in the

series ^{18}OHH , ^{16}OHH , ^{16}ODD , ^{16}OTT and this explains the ordering in the low temperature liquids. At higher temperatures MVIE falls off to more negative values due to ever increasing isothermal compressibility (unbounded at T_C). Near T_C this fixes the order of isobaric molar volumes as $\text{TTO} > \text{DDO} > \text{HH}^{18}\text{O} > \text{HH}^{16}\text{O}$ and the ordering of critical temperatures as $\text{HH}^{16}\text{O} > \text{DDO} > \text{TTO}$.

Numerous model calculations correlating aqueous VPIE's using simple harmonic or *pseudo*-harmonic cell models have been reported (see Fig. 5.8 and Table 5.8 for an ultra-simple version). Such calculations show the importance of the librational hydrogen bonded modes and the stretch–libration interaction in determining VPIE for D or T substitution.

5.8 Excess Free Energies in Solutions of Isotopes: Connections Between VPIE, the Liquid Vapor Fractionation Factor, α , and RPF

The pseudo-harmonic cell model leads straightforwardly to the idea that the excess free energies of isotopomer mixtures correlate with the isotope effect on the molar volumes of the pure isotopomers (MVIE's). An excess thermodynamic property Y^E is just the difference between the value of that property for the real (nonideal) solution and the corresponding ideal solution, $Y^E = Y - Y^{\text{ideal}}$. MVIE's are discussed in Chapters 12 and 13. We begin by expanding the Helmholtz free energy about the equilibrium volumes, $V^{o'}$ or V^o , to obtain an expression for the contribution of ΔV to the excess Helmholtz free energy

$$A^E(V) = xx' (V' - V) [(dA/dV) - (dA'/dV)] \\ + (1/2) xx' (V' - V)^2 [x (d^2A'/dV^2) + x' (d^2A/dV^2)] + \dots \quad (5.40)$$

Here x and x' are isotopomer mole fractions in the binary mixture. Remembering $x' = 1 - x$, differentiating to obtain partial molar free energies (and using the thermodynamic relations $\mu^E(V) = A^E(V) - x' (dA^E(V)/dx')$ and $\mu^{E'}(V) = A^E(V) + x' (dA^E(V)/dx')$ one finds expressions for the excess partial molar free energies, $\mu^E(V)$ and $\mu^{E'}(V)$. In the high dilution limit, an important case of practical interest, the excess chemical potential of the trace isotopomer, say the unprimed one, is

$$\mu^{\infty,E} = (V^{o'} - V^o) [(dA/dV) - (dA'/dV)] + (1/2) (V^{o'} - V^o)^2 \left[\left(\frac{d^2A'}{dV^2} \right) \right]; x' \rightarrow 1 \quad (5.41)$$

The development to this point has been rigorous but difficulties arise as simplifications are introduced. Early authors continued by discarding the first term in Equation 5.40 since $V^o \sim V^{o'}$ and $[(dA/dV)_T = P \sim (dA'/dV)_T = P']$, and identified $(d^2A/dV^2)_T$ with $1/(\kappa V)$, κ the isothermal compressibility. Then $\mu^{\infty,E} = (V^{o'} - V^o)^2 / (2\kappa V^o)$. Since $\text{RPF} = -\delta\Delta A^o/RT$ and RT

$\ln(\gamma) = \mu^E$, at this level of approximation $\ln(\gamma) = V(\Delta V/V)^2/(2\kappa RT)$. At low enough temperature compressibility IE's can be neglected, and

$$\ln(\alpha) = \text{RPFR} - (V^{o'} - V^o)^2/(2\kappa RTV^o) \quad (5.42)$$

Although Equation 5.44 was long used to convert liquid vapor fractionation factors (LVFF's = α) to RPFR's it was more recently argued that identification of $\ln(\gamma)$ with $V(\Delta V/V)^2/(2\kappa RT)$ seriously underestimates the contribution of internal modes (i.e. the high frequency motions). These frequencies make negligible contribution to κ , but do contribute to the free energy. An improved method calculates the free energy of mixing in a two step process (Prigogine 1957) – (1) compress or dilate each separated component to the molar volume of the solution, and (2) mix at constant volume, assuming the free energy change in step (2) is zero. In terms of HOVM the free energy change in first step (1) is

$$-RT \ln(\gamma) = - \int (dA/dV)dV = -RT \int \Sigma [(d \ln(Q_i) / dv_i)(dv_i/dV)dV]_{3n \text{ freqs}} \quad (5.43)$$

The integral is from V to V' . With Equation 5.43 the disadvantage of the slowly converging Taylor series (Equation 5.40) is avoided and the contributions of internal modes properly evaluated. Also apparent differences between RPFR obtained via VPIE or LVFF can be successfully rationalized, and the excess free energies in concentrated solutions of isotopomers, one in the other, interpreted. Examples are given in Table 5.10.

Table 5.10 Excess IE's of some isotopomer solutions

System	T/K	x'	$(10^4 \ln \gamma)^a$	$G^E/(J/mol)$	$H^E/(J/mol)$	Ref.
$^{36}\text{Ar}/^{40}\text{Ar}$	84	0	-3	—	—	c, d
	90	0.5	—	0.015	0.12	d
CH_4/CD_4	100	0.5	—	0.57	1.3	c, d
HCl/DCl	170	0.5	—	0.66	2.1	c
$\text{H}_2\text{S}/\text{D}_2\text{S}$	190	0.5	—	-0.92	—	c
$\text{C}_6\text{H}_6/\text{C}_6\text{D}_6$	298	0.5	—	0.58	1.1	c
$c\text{-C}_6\text{H}_{12}/c\text{-C}_6\text{D}_{12}$	298	0.5	—	1.08	3.1	c
$\text{H}_2\text{O}/\text{D}_2\text{O}$	305	1	-8	—	—	c
	278–363	0.5	—	0 ^b	0 ^b	c, e
$\text{H}_2^{18}\text{O}/\text{H}_2^{16}\text{O}$	305	1	4	—	—	c
Polybutadiene-h/-d	296	—	9	—	—	c
Polystyrene-h/-d	300	—	4	—	—	c

^aActivity coefficient of the more dilute species ^{36}Ar , HDO, or H_2^{18}O .

^bBut recall the complication introduced by the disproportionation equilibrium $\text{H}_2\text{O} + \text{D}_2\text{O} = 2 \text{HDO}$ and its IE, $\ln(P_{\text{HOH}}/P_{\text{DOD}}) / \ln(P_{\text{HOH}}/P_{\text{HOD}}) = 1.92 \pm 0.02$.

^cJancso, G., Rebelo, L. P. N., and Van Hook, W. A. *Chem. Rev.* **93**, 2645 (1993).

^dCalado, G. et al. *Phys. Chem. Chem. Phys.* **2**, 1095 (2000); *J. Chem. Phys.* **100**, 4582 (1994).

^eJancso, G. and Jakli, Gy. *Aust. J. Chem.*, **33**, 2357 (1980).

5.8.1 Excess Free Energies and Demixing in Isotopomer Solutions, Further Discussion

It is interesting to explore the possibility of phase separation in solutions of isotopomers. Phase separation is a straightforward consequence of solution non-ideality. In regular solution theory the total excess free energy is expressed, $G^E = x'\mu'^E + x\mu^E = xx'\chi$. In first approximation the Flory–Huggins parameter χ is independent of temperature and concentration, and the thermodynamic conditions for the initial liquid–liquid phase separation from symmetrical mixtures, and certainly mixtures of isotopomers are the example par excellence of symmetrical mixtures, are $x = x' = 0.5$ and $\chi/RT = 2$. For $\chi/RT > 2$ there is incomplete mixing, i.e. phase separation. Typically, IE's on the excess free energy, now expressed in terms of the parameter χ , are inversely proportional to the temperature raised to some power, and directly proportional to the total isotope and phase frequency shift, $\Delta\delta\nu$. It follows that liquid–liquid demixing of isotopomers will be enhanced at very low temperature, or, should one be restricted to higher temperature because the solution freezes, to molecules with many (isotopically substituted) oscillators. The first case is realized for $^3\text{He}/^4\text{He}$ and H_2/D_2 mixtures, the second by polymer/polymer mixtures.

It has been long established that $^3\text{He}/^4\text{He}$ liquid mixtures phase separate at temperature below 0.9 K. (see Fig. 5.9), and the theoretical explanation for this, first advanced by Prigogine, has been outlined above. Similarly, mixtures of solid $^3\text{He}/^4\text{He}$ (formed at elevated pressure) and mixtures of solid H_2/D_2 both phase separate, but liquid mixtures of H_2 and D_2 do not, although they do show appreciable nonideality. No other “small molecule” isotopomer mixtures phase separate, but

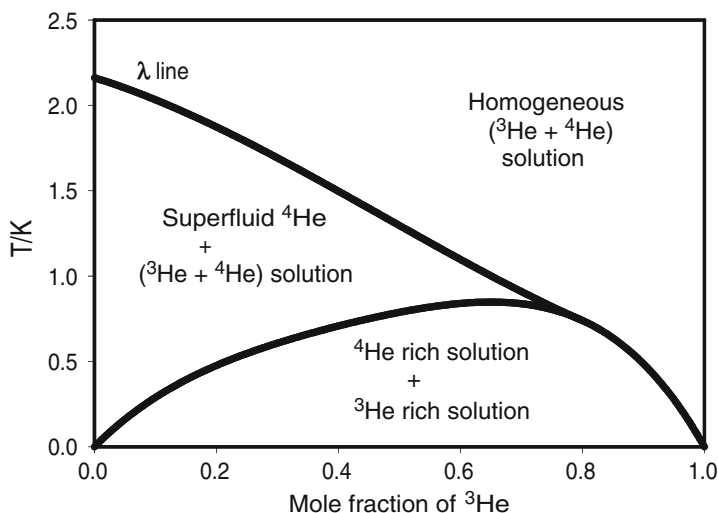


Fig. 5.9 Phase separation in $^3\text{He}/^4\text{He}$ liquid mixtures

in polymer mixtures, the excess free energy of mixing is sufficiently large (for long enough chains) that binary mixtures of perprotio and perdeutero polymers can, and do, phase separate. The reason, of course, is that the total excess free energy of the isotopomer mixture is proportional to the number of oscillators with D for H substitution, and that number in turn is proportional to chain length. H/D phase separation has been observed in polystyrene(H/D), polybutadiene(H/D), and polyethylene–polypropylene(H/D) mixtures. The explanation proceeds by writing the Helmholtz excess free energy of the solution, A^{ex} , as

$$A^{ex} = \phi_H \phi_D (N \Gamma_i r_i / 2) (\Delta V / V) (u_H - u_D) \quad (5.44)$$

In Equation 5.44, ϕ_1 and ϕ_2 are volume fractions of isotopomers H and D, N is the number of monomer units per molecule, r_i the number of H/D substituted bonds per monomer, Γ_i the Gruneisen coefficient, $\Gamma_i = -\partial \ln(u_i) / \partial \ln(V)$, for the effective frequency (which, for these polymers is the CH(CD) stretch), $\Delta V / V$ is the molar volume isotope effect, and the u_i 's are reduced frequencies, $u_i = h\nu_i / kT$. The thermodynamic conditions for phase separation are $\phi_H = \phi_D = 0.5$, and

$$(N \Gamma_i r_i / 2) (\Delta V / V) u_H \left(1 - (\mu_H \mu_D)^{1/2} \right) \geq 2 \quad (5.45)$$

The μ 's are reduced masses for the CH(CD) oscillators. For polybutadiene, $r_i = 6$, and the critical polymerization number for H/D demixing is 1.2×10^3 monomer units.

5.9 The Isotope Effect on T_{CR} for the Superconducting/Resistive Transition in Metals

Figure 5.10 shows old and very important data on the isotope dependence of the critical temperature for the superconducting/resistive transition in metallic mercury at liquid helium temperatures. T_{CR} is inversely proportional to the square root of atomic mass. These data are especially interesting because if electrical conduction in mercury were purely electronic, there would be no dependence upon nuclear mass. It is remarkable that an electrical phenomenon like the transition to zero resistivity involves a purely mechanical property of the lattice. It indicates that lattice vibrations are part of the superconducting process. This was an important clue in the Nobel Prize winning development of the BCS (Bardeen–Cooper–Schrieffer) theory of superconductivity because it was the first direct evidence for interaction between the electrons and the lattice. In ordinary superconductors lattice vibrations (phonons) push electrons into pairs, which form a superconducting condensate. Lighter isotopes lead to higher phonon frequencies (in first order ν is proportional to $1/M^{1/2}$) and correspondingly higher transition temperatures. This lattice vibration type of isotope effect is not found in Type-II superconductors (for example high

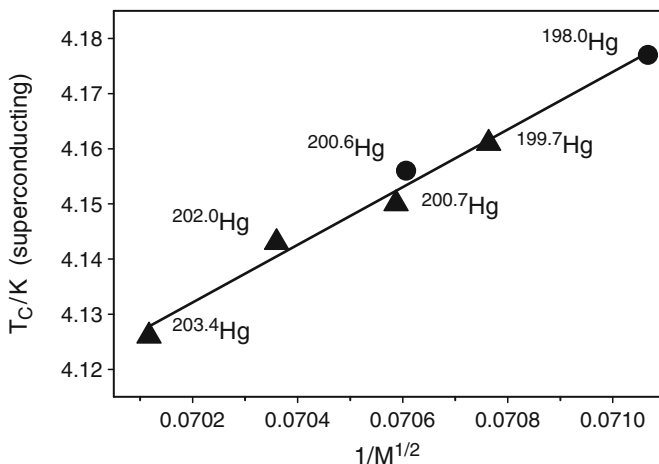


Fig. 5.10 The mass dependence of the critical temperature of the superconducting/resistive transition in isotopically enriched samples of mercury (*Triangles*: Reynolds, C. A., et al. *Phys. Rev.* **78**, 487 (1950). *Circles*: Maxwell, E., *Phys. Rev.* **78**, 477 (1950))

T_{CR} cuprates), whose superconductivity depends on subtle, phonon-free coupling between electrons. It is interesting that the highest known temperature Type-I superconductor, MgB_2 , shows a much larger isotope effect than does mercury ($T_{CR}(Mg^{11}B_2) = 39.2$ K, $T_{CR}(Mg^{10}B_2) = 40.2$ K).

5.10 Isotope Effects on Solubility

5.10.1 Liquid–Liquid Equilibria: Two Component Systems

Isotope effects on the mutual solubility of liquids have been widely studied (see Section 7.5.4). Consider a binary mixture, components 1 and 2, which phase separates into two solutions in equilibrium, the first (A) richer in component 1, the second (B) in component 2. Focusing on component 2, the one isotopically substituted, its standard state in A is most conveniently expressed using the Henry's Law standard state (infinite dilution), but in B, the standard state is more reasonably the pure liquid (Raoult's Law). In gross approximation, then, the transfer free energy is that from the Raoult to Henry standard state. Remember, however, that in their standard states, solutions are by definition ideal, while in contrast the very observation of liquid–liquid demixing is *prima facie* evidence of nonideality. Thus, proper understanding of isotope effects on liquid–liquid equilibria (or liquid–liquid demixing) requires a marriage of the theory of condensed phase isotope effects with theories which treat the excess free energy of nonideal solutions, G^E . For example using the Guggenheim or modified Flory–Huggins theories to describe critical

immiscibility, one relates the isotope shift in the UCST and/or LCST, ΔT_c , with G^E model parameters. (UCST and LCST, the upper and lower critical solution temperature, respectively, are those temperatures above or below which, respectively, the solution is homogeneous at all concentrations).

$$-\Delta T_c/T_c = \delta\Delta\mu_2/\chi RT_c \quad (5.46)$$

Here, χ is the isotope-independent value of excess free energy interaction parameter that triggers phase separation (χ varies between 2 for strictly symmetrical mixtures, and 0.5 for solutions of infinitely long polymers dissolved in small molecule solvents). Also $\delta\Delta\mu_2$ is the isotope effect on the partial molar free energy of transfer from reference state to solution. In using μ to symbolize both partial molar free energy (or chemical potential) and reduced mass (as in Equation 5.45) we are following widely employed standard notations. Ordinarily the distinction between one or the other use will be clear from the context. The development leading to Equation 5.46 establishes the relation between the isotope shift on UCST and/or LCST with the isotope dependent normal mode frequency shifts which occur on transfer from the reference state to solution.

5.10.2 Small Molecule Solutions Including Aqueous Systems

For small molecules dissolved in water (or alcohols or amines) deuteration on the solvent enlarges the two-phase region(s) (either lowering LCST, raising UCST, or both (Section 7.5.4)). The effects are substantial; it is common to observe isotope dependent temperature shifts as large as 10 or 20 K, or even more. If one assumes that it is hydrogen bonding which is predominantly responsible for UCST IE's, then, one expects (and observes) a significant decrease in ΔT_c as T_c increases. For H_2O/D_2O solutions the typical ~ 25 K isotope shift on UCST observed at 270 K becomes negligible at 470 K. The importance of hydrogen bonding can also be appreciated by comparing ΔT_c for methanol/ cyclohexane mixtures for H/D substitution on the alcoholic group (where there is an increase UCST of about 4 K) with the effect for substitution at the methyl group, or in the cyclohexane (which leads to a decrease in T_c of ~ 0.3 K/atom replaced). In another interesting example UCST demixing envelopes describing the H/D IE's for (nitromethane + pentanol), Fig. 5.11, and (nitromethane + isobutanol) solutions were determined. For these solutions the T_c shifts are small (1.4 K and less) but in all cases it was found that deuteration leads to the enlargement of the limited miscibility region.

At temperatures well below UCST, solubilities of hydrocarbons in water or water in hydrocarbons drop to very low values. The solutions are very nearly ideal in the Henry's law sense, and the isotope effects on solubility can be directly interpreted as the isotope effect on the standard state partial molar free energy of transfer from the Raoult's law standard state to the Henry's law standard state. Good examples include the aqueous solutions of benzene, cyclohexane, toluene,

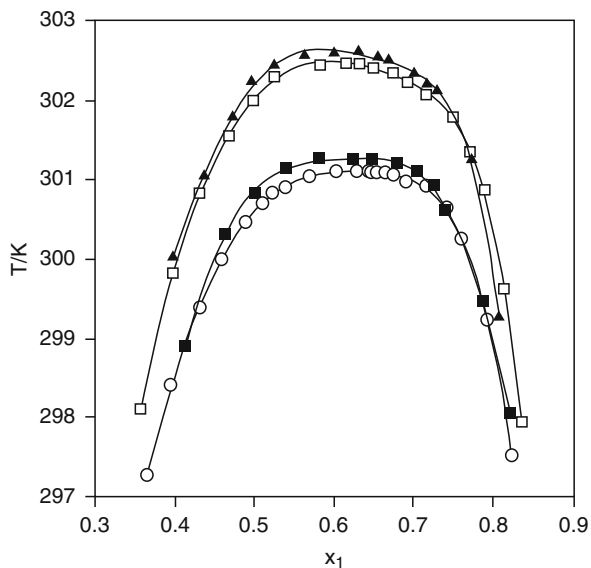


Fig. 5.11 Phase diagrams for UCST demixing of variously deuterated nitromethane(1) + pentanol(2) solutions. *Open circles* = $(\text{CH}_3\text{NO}_2 + n\text{-C}_5\text{H}_{11}\text{OH})$; *solid squares* = $(\text{CH}_3\text{NO}_2 + n\text{-C}_5\text{H}_{11}\text{OD})$; *open squares* = $(\text{CD}_3\text{NO}_2 + n\text{-C}_5\text{H}_{11}\text{OH})$; *solid triangles* = $(\text{CD}_3\text{NO}_2 + n\text{-C}_5\text{H}_{11}\text{OD})$ (Milewska, A. and Szydłowski, J. *J. Chem. Eng. Data* **44**, 505 (1999))

and tetrachloromethane where both solute and solvent isotope effects around room temperature have been studied. Results for benzene/water solutions are found in Table 5.3 and have been discussed in Section 5.6.1. The data are complete enough to deduce both the shift in the position of the benzene PES on phase change and the change in shape of its isotope sensitive vibrations.

A dramatic isotope effect on the solubility diagram has been reported for solutions of 3-methylpyridine + water (H/D). At atmospheric pressure a 70 K ($T_{\text{UCST}} - T_{\text{LCST}}$) closed-immiscibility-loop is observed for (3-methylpyridine + D_2O) and the immiscibility gap is modestly pressure dependent (Fig. 5.12). Viewed on the (p,T) projection, the phase diagram shows a characteristic “hour-glass” shape. On addition of H_2O , however, the gap shrinks, becomes more and more pinched at the waist, and at 21 wt % D_2O it disappears completely as the phase diagram changes from this “hour-glass” to a shape that resembles the UCST/LCST configuration in the (T,x) plane – two immiscible domes, an upper and a lower. With continued addition of H_2O , holding (3-methylpyridine + water) at the critical concentration, the upper and lower immiscible branches move further and further apart, until finally at high enough $\text{H}_2\text{O}/\text{D}_2\text{O}$ (17 wt % D_2O) the low-pressure branch is no longer present at atmospheric pressure, dropping below the $P = 0$ isobar. For (3-methylpyridine + H_2O) the miscibility gap between the upper and lower branches amounts to ~ 160 MPa. The phenomenon corresponds to an impressive pressure shift of hundreds of atmospheres merely upon (H/D) solvent isotope substitution.

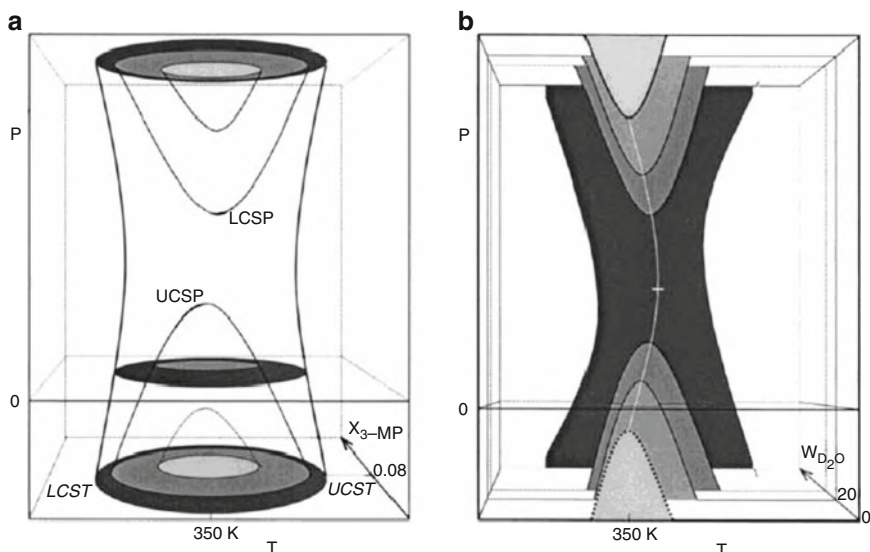


Fig. 5.12 Two different 3-D representations of the phase diagram of 3-methylpyridine plus water(H/D). **(a)** T-P-x(3-MP) for three different H₂O/D₂O concentration ratios. The inner ellipse (light gray) and corresponding critical curves hold for $(0 < W(\text{D}_2\text{O})/\text{wt}\% < 17)$. Intermediate ellipses stand for $(17(\text{D}_2\text{O})/\text{wt}\% < 21)$, and the outer ellipses hold for $(21(\text{D}_2\text{O})/\text{wt}\% < 100)$. There are four types of critical lines, and all extrema on these lines correspond to double critical points. **(b)** Phase diagram at approximately constant critical concentration 3-MP ($x \sim 0.08$) showing the evolution of the diagram as the deuterium content of the solvent varies. The white line is the locus of temperature double critical points whose extrema (+) corresponds to the quadruple critical point. Note both diagrams include portions at negative pressure (Visak, Z. P., Rebelo, L. P. N. and Szydowski, J. J. *Phys. Chem. B.* **107**, 9837 (2003))

Very large isotope effects like those shown in Fig. 5.12 seem to be limited to the hypercritical regions of phase diagrams, i.e. not too far from thermodynamic divergences of the type $(dP/dT)_c = \infty$ or $(dT/dP)_c = \infty$ (i.e. pressure-double critical points (p-DCP) or temperature-double critical points (T-DCP), respectively).

5.10.3 IE's on Solubility of Gases in Liquids, Chromatographic IE's

There is a good deal of data which compares the solubilities of H₂ and D₂ in various solvents, but by far the most extensive information on gas solubility IE's compares gas solubilities in H₂O and D₂O (Table 5.11). The solubility of D₂ is considerably higher than H₂ in all solvents investigated (Table 5.12). The isotope effect increases sharply as temperature falls (although not shown in Table 5.12). The isotope effect increases sharply as temperature falls (although not shown in Ta-

Table 5.11 H₂O/D₂O solvent isotope effects on gas solubility. Thermodynamics of transfer at 298.15 K, $\Delta Y^* = Y(\text{H}_2\text{O}) - Y^*(\text{D}_2\text{O})$ (Scharlin, P. and Battino, R. *J. Solut. Chem.* **21**, 67 (1992). *Fluid Phase Equilib.* **94**, 137 (1994))

Solute	$\Delta G^*/(\text{J}\cdot\text{mol}^{-1})$	$\Delta H^*/(\text{kJ}\cdot\text{mol}^{-1})$	$T\Delta S^*/(\text{kJ}\cdot\text{mol}^{-1})$
⁴ He	210	2.62	2.41
Ne	163	2.06	1.90
Ar	180	0.24	0.06
Kr	145	-0.18	-0.32
H ₂	546		
D ₂	597	0.23	-0.37
N ₂	159	0.88	0.72
O ₂	231	0.24	0.01
CH ₄	144	1.84	1.70
C ₂ H ₆	123	1.86	1.74
C ₃ H ₈	147	1.72	1.57
CCl ₂ F ₂	124	1.81	1.69
CClF ₃	505	-4.08	-4.58
c-C ₄ F ₈	971	-9.74	8.77
CF ₄	111	5.81	5.69
SF ₆	221	2.05	1.83

Table 5.12 Ratio of solubilities of H₂ and D₂ in various solvents (Rabinovich, I. B. *Influence of isotopy on the physicochemical properties of liquids*. Consultants Bureau, New York, 1970)

Solvent	T/K	$x(\text{D}_2)/x(\text{H}_2)$
H ₂ O	292	1.027
NH ₃	240	1.029
SO ₂	293	1.033
Ar	87	1.165
N ₂	67	1.297
CH ₄	112	1.084
CS ₂	298	1.020
Octane	308	1.020
Benzene	308	1.027

^a x = mole fraction of gas in the saturated solution at the Henry's Law limit.

ble 5.12), but the economics of using these differences to extract D₂ or HD from their mixtures with H₂ are unfavorable compared with distillation. Solute solubility isotope effects are small for substitution at non-hydrogenic positions. The aqueous solvent isotope effects reported in Table 5.11 are the result of careful gas solubility measurements covering the range (288 < T/K < 318). Thermodynamic analysis yielded standard state free energies, and Van't Hoff enthalpies, entropies and heat capacities of transfer.

The extension of the ideas presented in Sections 5.8 and 5.10 to the theoretical treatment of isotope separation by gas chromatography is straightforward. The isotope effects observed in chromatography are governed by the isotopic ratio of Henry's Law constants (for gas-liquid separations), or adsorption constants (for

Table 5.13 Solvent isotope effects on solubility of selected electrolytes in H₂O and D₂O, ΔL , % = 100 (L_H - L_D) / L_H. L_H and L_D are moles anhydrous salt per 55.508 mol H₂O and D₂O, respectively (Rabinovich, I. B. *Influence of isotopy on the physicochemical properties of liquids*. Consultants Bureau, New York, 1970)

Salt	T/K	L _H	ΔL , %
NaCl	293	6.13	6.7
NaBr(2 aq)	293	8.89	1.5
NaBr	323	11.38	3.3
NaI(2 aq)	293	11.26	1.9
NaI	373	20.1	1.7
KCl	293	4.61	9.8
KBr	298	5.75	1.1
KI	298	8.90	9.2
BaCl ₂ (2 aq)	298	1.78	13
BaCl ₂	398	3.01	9.3
HgCl ₂	298	0.27	25
PbCl ₂	298	0.039	36
Na ₂ SO ₄ (10 aq)	298	1.96	1.6
Na ₂ SO ₄	323	3.26	1.2
LiF	298	0.1	-13
LiCl	298	13	-2

gas–solid separations), and gas chromatography has been widely used for isotope separation and for the rapid and convenient analysis of mixtures of isotopomers (see Section 8.5 for discussion and examples).

5.10.4 Solubility of Ionic Solids in H₂O/D₂O

Concentrations of aqueous electrolyte solutions are conventionally expressed using the aquamolality scale (L = moles salt per 55.508 mol solvent (1,000 g for H₂O)). Some typical solubilities (298.15 K) are listed in Table 5.13. Almost all salts are less soluble in D₂O than in H₂O. For those salts whose solubility increases with temperature, which is the ordinary behaviour, the isotope effects decrease with temperature. Writing the standard state partial molar free energy of pure solid salt as $\mu_{(\text{SALT})}^\circ$ and its standard state in solution as $\mu_{(\text{H or D})}^\circ$ we have on comparing the saturated solutions in H₂O and D₂O,

$$\mu_{(\text{SALT})}^\circ = \mu_{(\text{H})}^\circ + RT \ln(\gamma_{\text{H}} L_{\text{H}}) = \mu_{(\text{D})}^\circ + RT \ln(\gamma_{\text{D}} L_{\text{D}}) \quad (5.47a)$$

and, keeping in mind that the activity coefficients are a function of concentration, we obtain

$$-(\mu_{(\text{H})}^\circ - \mu_{(\text{D})}^\circ) = RT [\ln(L_{\text{H}}/L_{\text{D}}) + \ln(\gamma_{\text{H}}/\gamma_{\text{D}})_{\text{LD}} + \int (\text{d} \ln \gamma_{\text{H}}/\text{d}L_{\text{H}}) \text{d}L_{\text{H}}] \quad (5.47b)$$

The integral extends from L_H to L_D. Equation 5.47b demonstrates that the solvent solubility IE offers a convenient way to determine the IE on the standard state partial molar free energy for the salt provided the concentration dependence of its activity coefficient in one solvent, most likely H₂O, is available at high concentration.

The largest solubility isotope effects are found for sparingly soluble salts. For example, lead chloride and potassium bichromate are 36% and 33.5% more soluble in H₂O than D₂O at 298.15 and 278.15 K, respectively. For the more soluble salts, NaCl and KCl, the values are 6.4% and 9.0%. Interestingly LiF and LiCl.aq have inverse effects of 13% and 2%, respectively. Recall that lithium salts are commonly designated as “structure makers”. Almost all other electrolytes are “structure breakers”.

Further Reading

- Baertshi, P. and Kuhn, W. Dampfdruckunterschiede isotoper Verbindungen. (Infrarot-Anteil der Dispersionswechselwirkung als Ursache für grössere Flüchtigkeit der schweren Molekel-spezies) *Helv. Chim. Acta* **40**, 1084 (1957).
- Bigeleisen, J. Statistical mechanics of isotope effects on the thermodynamic properties of condensed systems. *J. Chem. Phys.* **34**, 1485 (1961).
- Jancso, G. and Van Hook, W. A. Condensed phase isotope effects (especially vapor pressure isotope effects). *Chem. Rev.* **74**, 689 (1974).
- Jancsó, G., Rebelo, L. P. N. and Van Hook, W. A. Isotope effects in solution thermodynamics: excess properties in solutions of isotopomers. *Chem. Rev.* **93**, 2645 (1993).
- Prigogine, I. *The Molecular Theory of Solutions*, North Holland, Amsterdam (1957).
- Rabinovich, I. B. *Influence of Isotopy on the Physicochemical Properties of Liquids*, Consultants Bureau, New York 1970.
- Rice, O. K. *Statistical Mechanics, Thermodynamics and Kinetics*, W. H. Freeman. San Francisco, CA (1967), Ch. 8.
- Van Hook, W. A. Condensed matter isotope effects, in Kohen, A. and Limbach, H. H., eds. *Isotope Effects in Chemistry and Biology*, Taylor & Francis, CRC, Boca Raton, FL (2005), p 119.
- Van Hook, W. A. and Rebelo L. P. N. Isotope effects on solubility, in T. Letcher, T., ed., *Developments and Applications in Solubility*, Royal Society of Chemistry, Cambridge (2007)
- Wolfsberg, M. Isotope effects on intermolecular interactions and isotopic vapor pressure differences. *J. Chemie Physique* **60**, 15–22 (1963)

Chapter 6

Kinetic Isotope Effects Continued: Variational Transition State Theory and Tunneling

Abstract Some of the successes and several of the inadequacies of transition state theory (TST) as applied to kinetic isotope effects are briefly discussed. Corrections for quantum mechanical tunneling are introduced. The bulk of the chapter, however, deals with the more sophisticated approach known as variational transition state theory (VTST).

6.1 Introduction: Transition State Theory, Variational Transition State Theory, and Tunneling

To begin we are reminded that the basic theory of kinetic isotope effects (see Chapter 4) is based on the transition state model of reaction kinetics developed in the 1930s by Polanyi, Eyring and others. In spite of its many successes, however, modern theoretical approaches have shown that simple TST is inadequate for the proper description of reaction kinetics and KIE's. In this chapter we describe a more sophisticated approach known as variational transition state theory (VTST). Before continuing it should be pointed out that it is customary in publications in this area to use an assortment of alphabetical symbols (e.g. TST and VTST) as a short hand tool of notation for various theoretical methodologies.

6.1.1 Transition State Theory

In conventional transition state theory (TST) (see Chapter 4) the first approximation for the thermal rate constant k is given:

$$k = \frac{k_B T}{h} \frac{q^\ddagger(T)}{q^R(T)} \exp(-V^\ddagger/k_B T) \quad (6.1)$$

where k_B is the Boltzmann constant, T is the temperature, q^\ddagger and q^R are molecular partition functions of the transition state(\ddagger) and the reactant (R), and V^\ddagger is the

potential energy difference between reactants and the transition state measured at the minima of their respective vibrational wells (i.e. the reaction barrier height). This expression can be improved by introduction of the transmission coefficient, k_{TRANS} , which is usually further divided into three parts:

$$k_{\text{TRANS}} = \Gamma(T)g(T)\kappa(T)k^{\ddagger} \quad (6.2)$$

In Equation 6.2 $\Gamma(T)$ is equal to unity in classical TST, $g(T)$ is a measure of the deviation from the assumption that reactant molecules are locally equilibrated, and $\kappa(T)$ describes the contribution from non-classical transmission through the barrier. $\kappa(T)$ is usually dominated by tunneling but also includes nonclassical reflections.

For reactions in which energy transfer is fast enough to maintain an equilibrium population of the reactant states, $g(T)$ is approximately equal to unity and only the remaining two factors of the transmission coefficient need to be considered. Unfortunately, ordinary TST is not capable of correctly describing quantum effects. In particular the term, $\kappa(T)$, which accounts for non-classical transmission often plays a critical role, especially in enzyme catalyzed reactions. The proper inclusion of such quantum effects requires a more general theory. One such theory, variational transition state theory (VTST) developed by Truhlar and coworkers (reading list), optimizes the location of the surface which divides reactants from products, placing it so that the forward flux is minimized. Inclusion of tunneling, however, requires substantially more information about the energetic landscape of the reaction than is necessary to describe this same reaction within the simpler TST formalism. As a consequence VTST calculations are more tedious and time consuming. Furthermore, it is sometimes hard to separate the discussion of the theory from its practical implementation.

6.2 The Basics of Variational Transition State Theory and How It Differs from Conventional Transition State Theory

6.2.1 *The Dividing Surface for the Reaction*

Consider, as an example of a gas phase reaction, the reaction of a diatomic molecule with an atom



In principal one can calculate the electronic energy as a function of the Cartesian coordinates of the three atomic nuclei of the ground state of this system using the methods of quantum mechanics (see Chapter 2). (In subsequent discussion, the terms “coordinates of nuclei” and “coordinates of atoms” will be used interchangeably.) By analogy with the discussion in Chapter 2, this function, within the Born–Oppenheimer approximation, is not only the potential energy surface on which the reactant and product molecules rotate and vibrate, but is also the potential

surface on which the reaction takes place. It is being assumed here that the chemical reaction occurs on the ground electronic surface; that is, the reaction is adiabatic with respect to electronic energy. (Under appropriate conditions, one can extend the ideas here to consider reactions of molecules in electronically excited states.) Potential energy surfaces for reactions of type 6.3 are illustrated in Fig. 6.1. On these surfaces, there exists a region which corresponds to a rotating-vibrating reactant molecule AB far removed from its reaction partner C and therefore not interacting

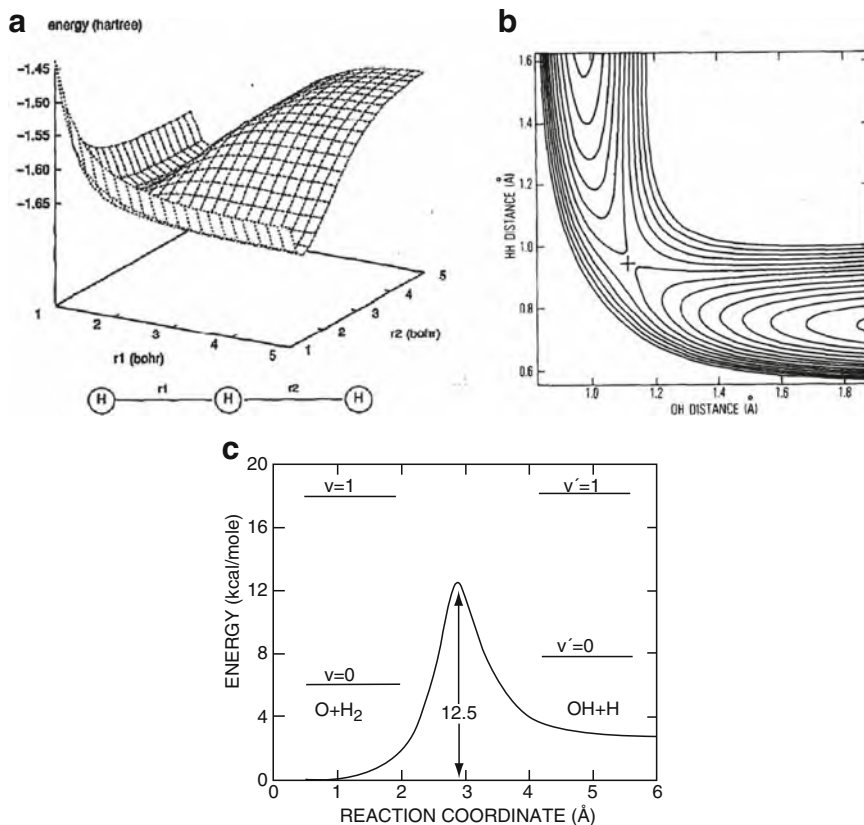


Fig. 6.1 Representations of potential energy surfaces for collinear reactions. (a) *Upper left*. 3D diagram of the collinear reaction $\text{H} + \text{H}_2 = \text{H}_2 + \text{H}$. Binding energy is plotted along the vertical (z) axis. The axes in the plane of the paper show the r_1 and r_2 axes (Diedrich, D. L. and Anderson, J. B., *J. Chem. Phys.* **100**, 8089 (1994)). (b) *Upper right*. 2D projection of a 3D potential surface, this time for the collinear reaction $\text{O} + \text{H}_2 = \text{OH} + \text{H}$. The shape is analogous to that shown in Fig. 6.1a. The saddle point is marked by “+” and occurs at $\text{O}-\text{H} = 1.118 \text{ \AA}$ and $\text{H}-\text{H} = 0.953 \text{ \AA}$. The contours show lines of constant energy and the plateau at the *upper right* corresponds to the separated atoms $\text{O} + \text{H} + \text{H}$. (c) Schematic diagram of the energy along the minimum energy path MEP in Fig. 6.1b. The transition state for ordinary TST is located at the maximum. Also indicated are energy levels of the zeroth and first vibrations of product and reactant (Figure 6.1b and c are from Johnson, B. R. and Winter, N. W., *J. Chem. Phys.* **66**, 4116 (1977))

with it. This region corresponds to the reactant side of Equation 6.3. Likewise, there exists another region of space which corresponds to non-interacting product species A and BC (the product side). In order to move on this surface from the low energy region corresponding to separated reactants to the low energy region corresponding to separated products, one has to surmount a potential energy barrier. The position in space corresponding to the minimum in that energy barrier is a saddle point on the potential energy surface and is the transition state of the reaction in the conventional transition state theory (TST) discussed in Chapter 4. An analysis of the potential surface at the transition state shows that the first derivatives of the potential with respect to displacements of the Cartesian coordinates of the atomic nuclei must all vanish. The second derivatives (force constants) can, however, be obtained. With the use of the methods discussed in Chapter 3, one finds the vibrational frequencies of the transition state; for an N-atomic transition state there are $3N^\ddagger - 7$ real vibrational frequencies ($3N^\ddagger - 6$ for a linear system) and one imaginary frequency. The word ‘imaginary’ means that the frequency is a number multiplied by the square root of -1 , or ‘i’ (see any algebra text). The imaginary frequency corresponds to motion along the minimum energy pathway (MEP), see Fig. 6.1c. It corresponds to motion leading to decomposition (either to reactants or products) of the transition state and is referred to as an ‘unbound’ motion as it displays negative (concave) curvature. The real frequencies, on the other hand, correspond to actual bound vibrations in directions ‘perpendicular’ to the MEP. In conventional transition state theory, the imaginary frequency is referred to as ν_L^\ddagger . The superscript double dagger, refers to the transition state. Also, in TST (Chapter 4), one assumes that in a normal reaction the transition state is in chemical equilibrium with reactants and its concentration can be calculated from the chemical equilibrium constant corresponding to the reaction between the reactants and transition state. The equilibrium constant K_r^\ddagger is usually evaluated by the methods of statistical mechanics using the partition functions of the transition state and reactants. As pointed out in Chapter 4, at this point in the TST derivation, there has been no consideration yet of the partition function corresponding to motion along the MEP, nor has there been consideration of the rate of decomposition of the transition state to yield products. Such considerations (Chapter 4) lead to a multiplicative factor $k_B T/h$ in the expression for the rate constant, where k_B refers to Boltzmann’s constant. One then obtains for the rate constant k of the reaction (Chapter 4, Equation 4.135, compare with Equation 6.1)

$$K = (k_B T/h) K_r^\ddagger \quad (6.4)$$

Using the well known relation between an equilibrium constant and the standard state free energy change for the reaction, $\Delta G^\circ = -RT \ln K$, one can re-write this equation as

$$K = k_B T/h \exp(-\Delta G_r^\ddagger / k_B T) \quad (6.5)$$

ΔG_r^\ddagger is known as the free energy of activation.

In TST, one recognizes that the saddle point is the locus of the equilibrium configuration of the transition state. In calculating the partition function of the transition state, one considers the real frequencies corresponding to the potential energy at the saddle point to be the frequencies of the transition state. As already noted, these frequencies are “perpendicular” to the MEP. Thus the vibrational motions of the TST transition state take place on the surface perpendicular to the MEP. Note that in an N dimensional space an $(N - 1)$ dimensional object in that space can be referred to as a surface. Thus, in conventional TST, the $(N - 1)$ dimensional surface perpendicular to the MEP at the saddle point is referred to as the transition state of the reaction. Moreover, in TST, it is assumed that once the system gets to the transition state it either proceeds to products or returns to reactants, and the probability of going forward or backward is taken to be the same. In that case one arrives at the $k_B T/h$ factor above. Thus, it is reasonable to describe the transition state in TST as the “dividing surface” of the reaction (dividing reactants from products). This idea was tested as described below.

6.2.2 *The Minimum Energy Path*

Given the definition of the geometry of the transition states in TST as the highest energy point in the minimum energy pathway from reactants to products, the formal definition of MEP is as follows. The MEP is, in one direction, the path of steepest descents from the transition state to reactants while, in the other direction, it is the path of steepest descents from transition state to products. For reasons which will not be discussed here, the formal definition of MEP includes the statement that the pathway is expressed in mass scaled Cartesian coordinates of the position of the atoms (introduced in Chapter 3, e.g. x_i is replaced by $x'_i = \sqrt{m_i} x_i$). This simplifies the dynamics of the system in classical mechanics. The computer programs mentioned in Chapter 2 which enable the calculation of Born–Oppenheimer potentials for molecular vibrations can also be used to calculate the potential energy surface for a chemical reaction and thence MEP. In the Gaussian computer program, the MEP is referred to as the intrinsic reaction coordinate (IRC).

6.2.3 *Classical Trajectory Calculations*

With the advent of large digital computers in the late 1950s, workers started doing calculations on collisions between molecules, using potential energy surfaces, which were usually derived empirically. They studied chemical reactions by numerically solving the Newtonian (classical) equations of motion of molecules moving on these surfaces. Such calculations are known as (classical) trajectory calculations. One of the first chemical reactions studied in this way was the reaction



which can be studied in the laboratory making use of the two modifications of H_2 known as ortho and para hydrogen, and also by using deuterium substitution. As expected, the calculations predicted that if the reacting partners had sufficient energy then reaction could take place. For the calculations one interesting observation was that after reaching the transition state, the atom-molecule system often passed back and forth repeatedly from the reactant to the product side of the dividing surface. Thus, it was reasoned that a theory like TST which assumes that the transition state proceeds to either reactants or products with equal probability will lead to a calculated rate constant which may grossly overestimate the rate of the reaction. In fact, these considerations lead to the conclusion that TST will lead to a rate constant which is an upper limit to the true rate constant calculated by classical mechanics. Furthermore it can be demonstrated that there exists a dividing surface for which there will be no “recrossings” and, with the use of this dividing surface as the transition state, the calculated classical mechanical rate constant would be the correct one.

6.2.4 The Differences Between TST and VTST

The considerations introduced in the sections above led to the idea of variational transition state theory. The basic idea of VTST is to find a dividing surface which leads to a higher free energy of activation and thus to a lower rate constant. Within classical mechanics this dividing surface must lead to fewer recrossings to reactants and consequently to a “better” transition state for calculating the rate constant. While these ideas arose from classical mechanics, it has since been assumed that the idea of finding a transition state with a higher free energy of activation leads to a better prediction of a rate constant in the real “quantum mechanical world” than does the use of the transition state of conventional transition state theory. Here “quantum mechanical world” means that the equilibrium constant or the corresponding free energy of activation, is calculated with the use of partition functions based on quantum mechanical energy levels. It should be noted that, prior to the studies leading to VTST, it had been thought that the assumption of equilibrium which exists between reactants and transition state was a very bold assumption which should be seriously questioned; this assumption is no longer regarded as a weak point of the theory. Indeed, after finding the dividing surface yielding the highest free energy of activation, the main problem which remains in transition state theory is the effect of quantum mechanics on motion along the reaction path. This will be referred to as the “tunneling” problem in this book.

Note that the formula for the rate constant in VTST is exactly the same as in TST (compare Equations 6.1, 6.4 and 6.5). In TST the dividing surface is defined by the saddle point in the Born–Oppenheimer electronic energy surface (the maximum along the MEP from reactants to products), while in VTST it is defined as that surface which leads to the minimum value of the rate constant. In both approaches the dividing surface separates product space from reactant space. The assumption in VTST is that a given transition state in equilibrium with reactants will pass through

the dividing surface only once, going either towards products or reactants with equal probability. A dividing surface which gives rise to a lower rate constant should correspond more closely to a transition state with fewer recrossing and therefore be closer to the transition state required by the theory.

6.2.5 *Locating Dividing Surfaces*

Dividing surfaces are usually assumed to be perpendicular to the MEP (i.e., that is motion on the dividing surface involves no motion along the MEP) because this assumption saves much computational time. For the dividing surface of TST this result is automatically obtained because the normal mode coordinate of the frequency ν_L^\ddagger is along the MEP, and therefore is perpendicular to the normal mode coordinates corresponding to the real frequencies of the TST transition state. The situation is not so simple in VTST where it is necessary to locate the dividing surface by some kind of search algorithm. The dividing surfaces to be tested are first characterized by the distance s from the highest point on the MEP, which, remember, locates the TST surface. (It is convenient to use a plus or minus sign to indicate whether the VTST test surface lies farther towards products or reactants than does the TST surface). The potential function at that value of s is analyzed to produce the unique projection which contains no motion along MEP and thus defines a proper dividing surface.

Early in the development of VTST calculations on simple three atom systems compared rates obtained by exact classical dynamics with conventional TST and VTST, the same potential energy surface and classical partition functions being used throughout. These calculations confirmed the importance of eliminating the “recrossing phenomenon” in VTST. While TST yielded very much larger rate constants than the exact classical calculations, the VTST calculations yielded smaller rate constants, but never smaller than the exact classical values.

6.2.6 *Quantum Mechanical VTST*

Of course, one is not really interested in classical mechanical calculations. Thus in normal practice the partition functions used in TST, as discussed in Chapter 4, are evaluated using quantum partition functions for harmonic frequencies (extension to anharmonicity is straightforward). On the other hand rotations and translations are handled classically both in TST and in VTST, which is a standard approximation except at very low temperatures. Later, by introducing canonical partition functions one can direct the discussion towards canonical variational transition state theory (CVTST) where the statistical mechanics involves ensembles defined in terms of temperature and volume. There is also a form of variational transition state theory based on microcanonical ensembles referred to by the symbol μ . Discussion of VTST based on microcanonical ensembles μ VTST is beyond the scope of the discussion here. It is only mentioned that in μ VTST the dividing surface is

variationally chosen to minimize the number of rotational-vibrational states. The variational rate constant involves Boltzmann averaging over the ro-vibrational energy E . There is a different dividing surface for each energy E . Although this method does tend to give lower (better) rate constants than the CVTST approach, it can be very time consuming and consequently is seldom employed.

There is a third quantum mechanical VTST which is easier to use than CVTST or μ VTST. In this method, all reactant states with energy below the threshold for reaction (i.e. the energy corresponding to the ground state of conventional transition state theory) are handled by the microcanonical approach, but these states give zero rate of reaction. Those reactant states having energies above threshold are handled by the canonical theory. At each temperature an optimized surface is determined for these reactant states to minimize their contribution to the rate. This approach is called improved canonical variational theory (ICVT). It yields rate constants intermediate between the microcanonical approach and the full canonical approach. In tests of the variational transition state theory, this approach is often the method which is used when comparing with exact quantum mechanical calculations.

One must recognize that TST is much simpler conceptually than VTST. Thus, there is one transition state in TST and that is located at the maximum energy on the MEP (the saddle point). In VTST the dividing surface is temperature dependent since the partition functions and consequently the free energy of activation are temperature dependent.

6.2.7 *Isotope Effects, Comments*

In considerations of isotopic molecules, the potential surface itself is isotope independent in both TST and VTST. This follows from the Born–Oppenheimer approximation of quantum mechanics (Chapter 2). However, in all variational approaches, the position of the variational transition state on the Born–Oppenheimer surface will be isotope dependent, as will, then, the force constants of the transition state. Thus the Teller–Redlich product rule which led to many simplifications in the discussion of isotope effects on molecular partition functions in Chapter 4, is no longer operative in any of the various VTST's. As a consequence when one looks at the isotope effect on a rate constant k_1/k_2 in VTST, the expression will, unlike the final TST expression of Chapter 4, explicitly contain ratios of moments of inertia of isotopic transition states as well as an energy factor involving the energy differences of the isotopic dividing surfaces along the MEP. Additionally, the force constants from which the vibrational frequencies of the isotopic transition states are calculated, and the geometries of the non-vibrating non-rotating transition states differ. However, the contribution to the isotope effect from the reactants can still be expressed in terms of the isotopic partition function ratio $(s_2/s_1)^f$ as in Chapter 4. It is probably well to emphasize again that the electronic energy surface, the Born–Oppenheimer surface, on which the reaction takes place is isotope independent. The MEP, the path of steepest ascent from reactants to the isotope independent transition

state of TST and the path of steepest descent from this transition state to products, is isotope independent. Transition state surfaces are defined in terms of s , the distance from the maximum of the MEP to where the MEP is cut by the dividing surface. For TST, there is one dividing surface, independent of which isotopomer reactant(s) is considered and also the temperature, $s = 0.0$. In VTST the s value for the transition state depends on both the temperature and the isotopic constitution of the reactant(s). The value of s is determined by finding that path which leads to the highest value of the free energy of activation which depends not only on the contribution from the electronic energy which is isotope independent, but also on contributions from the vibrations, rotations and translations which are isotope dependent.

6.3 Tunneling

In classical mechanics, the total energy minus the potential energy is the kinetic energy and kinetic energy cannot be negative. It is well recognized, on the other hand, that quantum mechanics permits a system to have negative kinetic energy. Thus, while a potential “hill” or “barrier” will stop a classical system whose energy is less than the barrier height, a quantum system can “penetrate” the barrier. The phenomenon is referred to as tunneling and is extensively discussed in most introductory quantum mechanics texts. Thus, a quantum system undergoing a chemical reaction as in Equation 6.3 can react even if the total energy of the molecular system is lower than the saddle point energy.

It is well understood that the probability of tunneling decreases as the deficit of energy for classical passage increases; also tunneling probability decreases as the length of the tunneling path increases; important from the point of view of isotope effects is the fact that a light particle has a higher tunneling ability than a heavy particle. Thus, R. P. Bell proposed the study of H/D kinetic isotope effects for this purpose because he realized that the heavy isotope of hydrogen would have a lower tunneling probability than would the lighter isotope (see Historical Vignette 6.1).

In both TST and VTST, quantum mechanical tunneling is introduced into the rate constant expression as a correction factor usually referred to as κ . A short discussion of κ which is used largely with TST is presented in Section 6.3.1. Tunneling has been explored much more thoroughly in connection with VTST and this work will be discussed later.

6.3.1 Tunneling in TST

In the discussion of TST in Chapter 4 tunneling was introduced as a multiplicative correction factor to the TST rate constant. TST tunneling is usually discussed in one of three approximations. In first order (for small tunneling), Wigner has shown the correction is given by the $u^2/24$ law

$$\kappa = 1 - u^{\ddagger 2}/24 + \dots \quad (6.7)$$



[Historical Vignette 6.1] **R. P. Bell** (1907–1996) read for a chemistry degree at Balliol College, Oxford during 1924–1928. Between 1928 and 1932 he worked in Copenhagen with the great Danish physical chemist J.N. Bronsted. When he was ready to leave Bronsted remarked that although he had spent less time than usually required to earn a Ph.D. his work was of high quality and he should write a dissertation. Bell declined, saying that he had no need for a Ph.D. degree; throughout his working life he gloried in being simply Mr. Bell. Bell learned to speak Danish while in Copenhagen. During World War II, he monitored Danish radio broadcasts for messages from the resistance. He was also involved with smuggling Niels Bohr out of Denmark during the war. Mr. Bell's great contribution to science was the study of proton transfer reactions and the elucidation of the nature of acids and bases in solution. His work combined high-powered theory with ingenious and innovative experimentation. On the theoretical side he was one of the first (1933) to use quantum theory to predict that when a proton reacts it might tunnel through the energy barrier rather than go over the top. He also pioneered studies in which a hydrogen atom is replaced with the heavier isotope deuterium. He made early measurements of polarizability and dipole moment isotope effects. After a long association with Balliol College at Oxford, he left for Sterling University where he became the first professor of chemistry in 1967. He retired in 1975 (Photo credit: Ramsey & Muspratt, Oxford)

u^\ddagger is the reduced (imaginary) frequency describing the curvature at the top of the barrier, $u^\ddagger = h\nu^\ddagger/kT$. In the Bell approximation the barrier is assumed to be given by a truncated (and inverted) parabola (Fig. 6.2a), $V(s) = V^\ddagger - k^\ddagger s^2/2$, where s is the displacement from the transition state along the MEP, and k^\ddagger is the force constant corresponding to the imaginary frequency which describes the decomposition of the transition state. The harmonic assumption is defended purely on the grounds of convenience; it leads to an exactly soluble quantum mechanical expression with the following results for the reflection and transmission probabilities, R and T respectively

$$R = 1/(1 + \exp(2\pi\varepsilon)); \quad T = 1/(1 + \exp(-2\pi\varepsilon)) \quad (6.8)$$

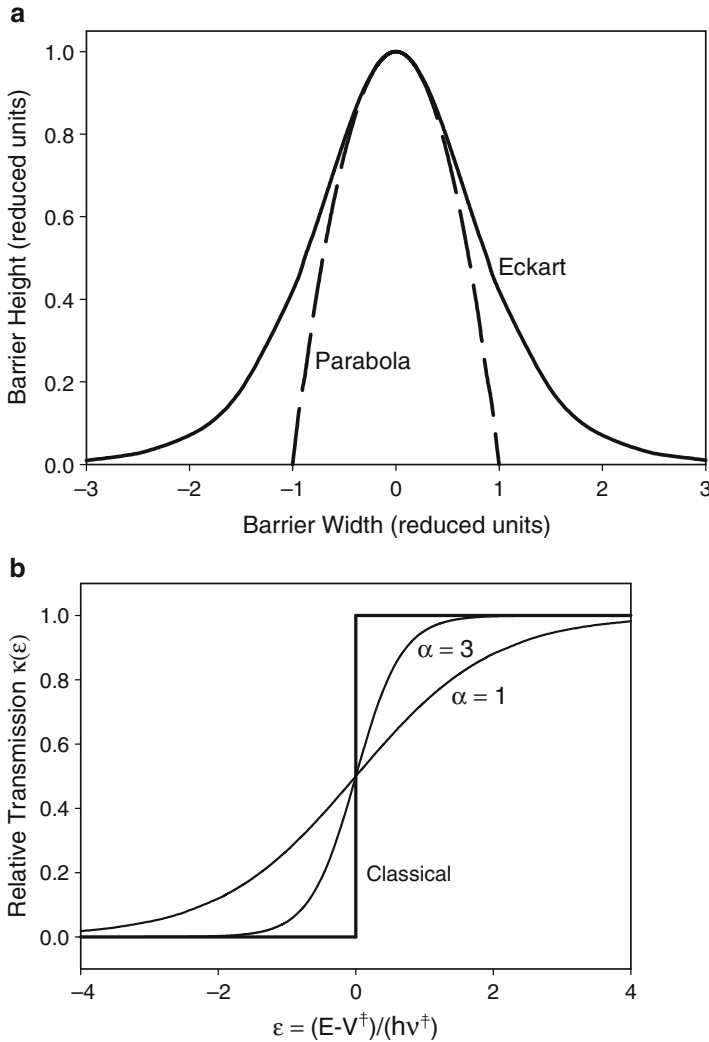


Fig. 6.2 (a) Bell (parabolic) and Eckart barriers, both widely used in approximate TST calculations of quantum mechanical tunneling. (b) Transmission probability (Bell tunneling) as a function of energy for two values of the reduced barrier width, α

In Equation 6.8, $\epsilon = (E - V^\ddagger)/(2\pi h\nu^\ddagger)$, $\nu^\ddagger = (k^\ddagger/\mu^\ddagger)^{1/2}/(2\pi)$, and μ^\ddagger is the reduced mass of the system motion along MEP. Details are available in most introductory quantum mechanics texts. T is plotted as a function of reduced energy in Fig. 6.2b for several values of the reduced barrier width $\alpha = V^\ddagger/(2\pi h\nu^\ddagger)$. The figure shows that tunneling becomes less important as α increases; that is as barrier height and thickness, or particle mass increases. In fact only very light particles are capable of significant tunneling so we expect these corrections to be important only

for proton, hydride ion, or hydrogen atom transfer reactions. Also since H tunnels more readily than D or T we expect its rate constant to be larger than it would be without tunneling and the ratios k_H/k_D and k_H/k_T to be substantially larger. Multiplication of the values plotted in Fig. 6.2b by the Boltzman factor gives the distribution of transmitted systems as a function of energy.

A second widely used approximation uses the more smoothly shaped Eckart barrier (Fig. 6.1), which for a symmetric barrier may be expressed as $V = V^\ddagger \text{sech}^2(x) = V^\ddagger [2/(e^x + e^{-x})]^2$ where $x = \pi s/a$ with s a variable dimension proportional to the displacement along MEP, and “ a ” a characteristic length. Like the Bell barrier the Eckart potential is amenable to exact solution. The solutions are similar and tunnel corrections can be substantial. In both the Bell and Eckart cases one is implicitly assuming separability of the reaction coordinate (MEP) from all other modes over the total extent of the barrier, and this assumption will carry through to more sophisticated approaches.

6.3.1.1 Tunneling on Potentials of Arbitrary Shape

The simplest way to extend the approach above is to recognize that the tunneling exponent, $\pi\varepsilon$ in Equation 6.8 above, can be identified with the magnitude of the semi-classical action integral between the classical turning points

$$\phi = -\pi\varepsilon = (1/(2\pi\hbar)) \int |p(s)|ds = (1/(2\pi\hbar)) \int (2\mu[V(s) - E])^{1/2} ds \quad (6.9)$$

The integrals extend from $-s_0$ and $+s_0$ lying at the edges of the barrier. For the truncated parabola the solution reduces to Equation 6.8. Note that the tunneling corrections introduced in Sections 6.3.1 and 6.3.1.1 can be used either with TST or with VTST.

6.3.2 Tunneling in VTST

6.3.2.1 Jacobi Coordinates: The Skew Angle in Three Center Collinear Reactions

Before discussing tunneling in VTST where the discussion will focus on multidimensional tunneling, it is appropriate to consider the potential energy surface for a simple three center reaction with a linear transition state in more detail. The reaction considered is that of Equation 6.3. The collinear geometry considered here is shown in Fig. 6.1a; it is in fact true that for many three center reactions the transition state can be shown to be linear. The considerations which follow apply to a one-dimensional world where the three atoms (or rather the three nuclei) are fixed to a line. We now consider this one-dimensional world in more detail. The Born–Oppenheimer approximation applies as in Chapter 2 so that the electronic energy of

the ABC system is the potential energy surface for the nuclear motion of the atoms. From considerations introduced in Chapter 3, there will be three degrees of freedom for motion of the nuclei in the collinear direction. The first of these is the translational motion of the center of mass with no change in the internuclear distances; the other two lead to changes in the internuclear distance(s). As in Chapter 3, these two degrees of freedom can be chosen as linear combinations of valence coordinates, most conveniently r_{AB} and r_{BC} or their displacement from some set values. The kinetic energies and corresponding momenta are expressed in terms of time derivatives of these coordinates. The interest is in the relative motions of nuclei with respect to each other during a reaction. The most useful coordinate system is one that has no cross terms in the kinetic energy for the internuclear motions and recipes exist for constructing such coordinate systems. Moreover, such generalized coordinates (known as Jacobi coordinates) can always be “mass scaled” which means that only one mass value appears in the final kinetic energy expression rather than two diatomic molecule reduced masses. Among the advantages of the use of Jacobi coordinates for internuclear motions is the fact that the classical kinetic energy can be easily transformed into the corresponding kinetic energy in quantum mechanics (eventually the quantum kinetic energy is needed for the tunneling problem) and, additionally, even for purely classical studies there is considerable simplification in the equations of motion. For the three atom system, a well known set of two mass-scaled Jacobi coordinates X and Y is pictured in Fig. 6.3, with Y the BC distance r_{BC} and X the distance from A to the center of mass of BC,

$$X = r_{AB} + \gamma r_{BC}, \quad \gamma = m_C / (m_B + m_C) \quad (6.10)$$

$$Y = r_{BC} \quad (6.11)$$

The coefficients of the two velocity terms corresponding to these coordinates can be derived fairly easily from the rules for constructing the G matrix elements (Chapter 3) but the details will not be given here. The kinetic energy is

$$2T = (m_B m_C / (m_B + m_C)) \dot{Y}^2 + ((m_A (m_B + m_C) / (m_A + m_B + m_C)) \dot{X}^2 \quad (6.12)$$

where the dots denote time derivatives (velocities). While Equation 6.12 has not been derived here, it is comforting to realize that the coefficient of the first velocity is just the reduced mass of a diatomic BC molecule while the coefficient of the second term is the reduced mass of A vibrating against B–C. This form of the kinetic energy still does not satisfy. What is desired is a coordinate system in which both coordinates correspond to the same mass. Such a coordinate system is also known as an iso-inertial coordinate system. This is accomplished by appropriate mass scaling. Thus, introduce x and y ,

$$x = Xy = \epsilon Y \text{ with } \epsilon = (m_B m_C M / m_A \{m_B + m_C\}^2)^{1/2} \text{ and } M = m_A + m_B + m_C \quad (6.13)$$

The kinetic energy then becomes

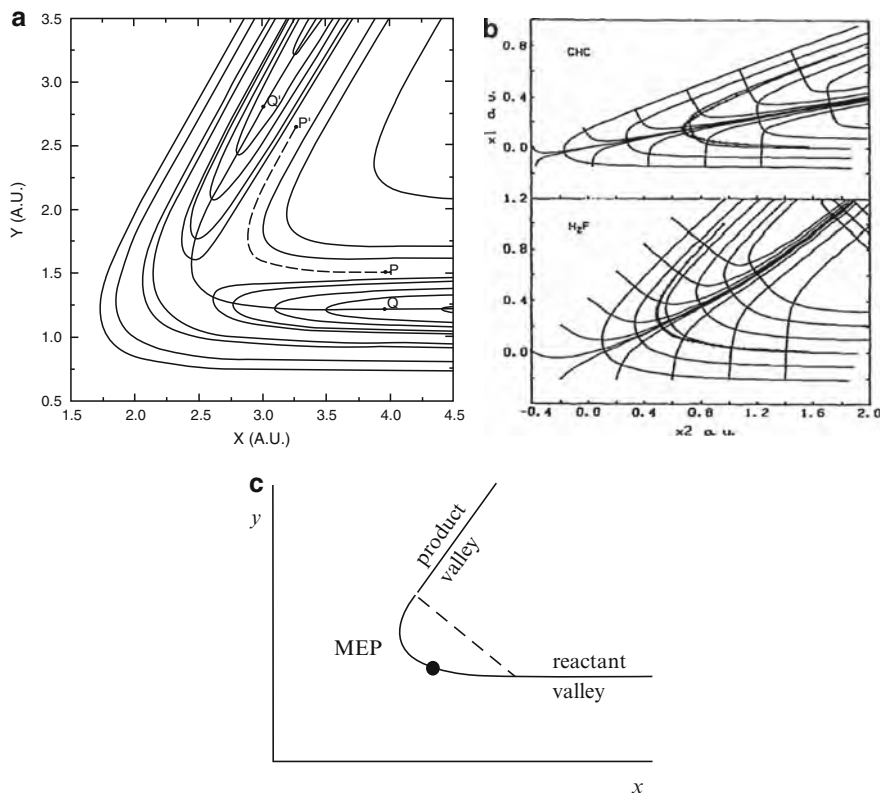


Fig. 6.3 Skewed coordinate potential surfaces for some hydrogen transfer reactions. (a) Top $\text{HH} + \text{H} = \text{H} + \text{HH}$. (b, upper) $\text{CH} + \text{C} = \text{C} + \text{HC}$. (b, lower) $\text{HF} + \text{H} = \text{H} + \text{FH}$. (c) $\text{CIH} + \text{Cl} = \text{Cl} + \text{HCl}$ (schematic). The mass dependence of the skew angle is apparent. The MEP's are indicated as the line QQ' in Fig. 6.3a and the heavier lines in Fig. 6.3b. The path in Fig. 6.3a marked PP' is discussed later in the text, as is the corner cutting path in Fig. 6.3c shown as the *dotted line* (Figure 6.3a is from Marcus, R. A. and Coltrin, M. E., *J. Chem. Phys.* **67**, 2609 (1977); Figure 6.3b and c are From Agmon, N., *Chem. Phys.* **76**, 203 (1983))

$$2T = (m_A(m_B + m_C)/M)((dx/dt)^2 + (dy/dt)^2) = \mu((dx/dt)^2 + (dy/dt)^2) \quad (6.14)$$

By the introduction of the (x, y) coordinate system, one has reduced the problem to the motion of a particle of mass μ in a two-dimensional rectilinear space (x, y) . Thus, the problem of the collision between an atom and a diatomic molecule in a collinear geometry has been converted into a problem of a single particle on the potential energy surface expressed in terms of the coordinates x and y rather than the coordinates r_{AB} and r_{BC} . The coordinates x and y which transform the kinetic energy to diagonal form in such way that the kinetic energy contains only one (effective) mass are referred to as mass scaled Jacobi coordinates.

6.3.2.2 The Skew Angle: Transformation Between the (r_{AB} , r_{BC}) and (x , y) Coordinates

It is interesting to compare potential energy diagrams in the “natural” (r_{AB} , r_{BC}) coordinates with the equivalent diagrams in mass scaled Jacobi coordinates. Figure 6.1 diagrams potential energy as a function of internuclear distance for collinear ABC systems. The MEP path $A + BC$ to $AB + C$ is shown by extrema in the contour lines in the valleys parallel to the two axes (Figs. 6.1a and b), and the top of the energy barrier (saddle point) which corresponds to the activated complex in ordinary transition state theory is marked by (+) in Fig. 6.1b. The solid lines in Fig. 6.1b represent contours of constant energy and are projections onto a plane from a three-dimensional figure (Fig. 6.1a) in which energy is plotted perpendicular to the plane of the page. Although the TST transition state (+) is at a maximum along MEP, it is at a minimum in the direction perpendicular to the reaction coordinate and a group of atoms at that point can vibrate in the direction perpendicular to MEP without dissociation, although vibration parallel to MEP leads to immediate dissociation. On the other hand the ordinary diatomic molecules BC and AB in the $A + BC$ and $AB + C$ trenches to the upper left and lower right of the diagram can vibrate in all directions without flying apart because they are surrounded on all sides by a potential energy barrier.

Although diagrams like Fig. 6.1 are especially convenient to illustrate the qualitative features of TST and VTST, the solution of the equations of motion in (r_{AB} , r_{BC}) coordinates is complicated due to cross terms coupling the motions of the different species. It is for that reason we introduced mass scaled Jacobi coordinates in order to simplify the equations of motion. So, one now asks what does the potential function for reaction between A and BC look like in these new mass scaled Jacobi coordinates. To illustrate we construct a graph with axes designated r_{AB} and r_{BC} within the (x , y) coordinate system. In the x , y space lines of constant y are parallel to the x axis while lines of constant x are parallel to the y axis. The r_{AB} and r_{BC} axes are constructed in similar fashion. Lines of constant r_{BC} are parallel to the r_{AB} axis while lines of constant r_{AB} are parallel to the r_{BC} axis. From the above transformation, Equations 6.10 to 6.13

$$r_{BC} = y/\varepsilon \quad (6.15)$$

$$r_{AB} = x - \gamma y/\varepsilon \quad (6.16)$$

From Equation 6.15, constant r_{BC} corresponds to constant y (because ε depends only on mass and is constant for any particular reaction) so constant r_{BC} corresponds to a line parallel to the r_{AB} axis (which is also parallel to the x axis). From Equation 6.16,

$$y = (\varepsilon/\gamma)x - (\varepsilon/\gamma)r_{AB} \quad (6.17)$$

This shows that constant r_{AB} transforms to straight lines in x , y space of slope ε/γ parallel to the r_{BC} axis. Lines parallel to r_{AB} axis intersect lines parallel to the r_{BC} axis at an angle which will be called β , generally not equal to 90° .

Table 6.1 Skew angles for collinear reactions of interest: $AB + C = ABC = A + BC$

Reaction	m_A	m_B	m_C	M	γ	ϵ	Skew angle β
HH + H = H + HH	1	1	1	3	0.500	0.866	60.0
DH + H = D + HH	2	1	1	4	0.500	0.707	54.7
HD + H = H + DH	1	2	1	4	0.333	0.942	70.5
HH + D = H + HD	1	1	2	4	0.667	0.942	54.7
HD + D = H + DD	1	2	2	5	0.500	1.118	65.9
DH + D = D + HD	2	1	2	5	0.667	0.913	53.9
DD + H = D + DH	2	2	1	5	0.333	0.745	65.9
DD + D = D + DD	2	2	2	6	0.500	0.866	60.0
HCl + Cl = H + ClCl	1	35	35	71	0.500	4.213	83.2
ClH + Cl = Cl + HCl	35	1	35	71	0.972	0.234	13.5
ClCl + H = Cl + HCl	35	35	1	71	0.028	0.234	83.2

$$\tan \beta = (\epsilon/\gamma) = (m_B M / m_A m_C)^{1/2} \quad (6.18)$$

To summarize, there exists a rectangular x, y coordinate system corresponding to the motion of a particle of mass $\mu = m_A(m_B + m_C)/M$ on a plane. This particle is subject to the potential function $V(r_{AB}, r_{BC})$ of the collinear three particle ABC system. When plotted in (x, y) space the r_{AB} and r_{BC} coordinate axes define an angle β (the skew angle) with respect to each other. The motion of the single particle describes exactly the motion of the collinear ABC system in classical mechanics. This was recognized by Eyring and his coworkers in the early 1930s. They further recognized (and this is important although quite straightforward) that the analogy of the motion of a particle of mass μ in the (x, y) plane applies not only to the classical mechanical problem but also to the problem in quantum mechanics.

Table 6.1 illustrates the calculation of skew angles for some reactions of interest. Figure 6.3a through c shows $V(x, y)$ plots for several examples of collinear A + BC reactions.

Keep in mind that both classically and quantum mechanically the mechanics of a system is governed by the potential shown in the skewed diagram for a given mass scaling. One realizes that the skewing of the axes might have a significant effect on the dynamics, in particular the tunneling. This conjecture will be validated in the following section.

6.3.3 Tunneling in Three Center Collinear Reactions

Tunneling in VTST is handled just like tunneling in TST by multiplying the rate constant by κ . The initial tunneling problem in the kinetics was the gas phase reaction $H + H_2 = H_2 + H$, as well as its isotopic variants with H replaced by D and/or T. For the collinear reaction, the quantum mechanical problem involves the two coordinates x and y introduced in the preceding section. The quantum kinetic energy operator (for a particle with mass μ) is just

$$2T = -\frac{\hbar^2}{2\mu} \left(\frac{\partial^2}{\partial x^2} + \frac{\partial^2}{\partial y^2} \right) \quad (6.19)$$

The potential energy is illustrated in Fig. 6.3a. While one can in principle calculate the “exact” quantum mechanical Born–Oppenheimer surface, the figure presents a semi-empirical surface constructed to yield the exact spectral properties of reactants and products and the correct “activation energy” (taken as the difference in energy between the energy (potential) in the reactant valley ($x = \infty$) and the maximum of the MEP (minimum energy pathway).)

The tunneling factor is defined from a knowledge of the quantum mechanical transmission coefficient $\Gamma(E)$ which gives the probability that the system with given relative kinetic energy of reactants E in a given initial quantum state in the reactant valley ends up in the product valley. This quantum mechanical value must then be averaged over states using the appropriate Boltzmann factor to yield the quantum mechanical transmission coefficient for the reaction at a given temperature T . The corresponding classical transmission coefficient is calculated by Boltzmann averaging the classical $\Gamma(E)$. The classical $\Gamma(E)$ is zero if the kinetic energy is lower than the activation energy for the surface and is unity if the kinetic energy is larger than this activation energy (Fig. 6.2b). The tunneling factor κ is set equal to the ratio of the temperature averaged quantum transmission coefficient and the corresponding classical transmission coefficient.

While the quantum mechanical tunneling problem can readily be solved exactly for the three atom collinear problem and even for the corresponding three-dimensional case, the general problem is still very difficult mathematically. Hence, one looks for a simpler solution. The problem is solved by using a semi-classical approach known as the WKB method. (For details, see the references at the end of the chapter.) This method involves the evaluation of the quantity referred to in classical mechanics as the action integral along the tunneling path designated here as s , as shown in Equation 6.9. The integral needs only to be evaluated along the quantum mechanical tunneling path where E is less than V , with s_1 the starting point of the tunnel motion and s_2 the exit, so that the integral is an imaginary quantity. R.A. Marcus and M.E. Coltrin in their study of the $H + H_2$ reaction looked for the path which maximizes tunneling. This is the path that minimizes the imaginary action integral, and they found that this path does not follow the MEP but is displaced in a direction perpendicular to MEP by an amount equal to the maximum classical displacement during the zero-point quantum vibration. This path is shown as the line PP' in Fig. 6.3a. The transmission coefficient calculated by Marcus and Coltrin for path PP' was found to closely match the presumably correct value obtained by the full quantum mechanical treatment for two different empirical potential energy surfaces. The use of the MEP as the tunneling pathway gives rise to considerably lower transmission coefficients. These points are illustrated in Fig. 6.4. The Marcus–Coltrin path is shorter than the MEP path. The shorter path comes at the expense that the instantaneous values of $V-E$ are higher than they are for MEP, an effect which lowers the tunneling probability but the shorter path raises the tunneling probability. The Marcus–Coltrin pathway balances these two factors in such

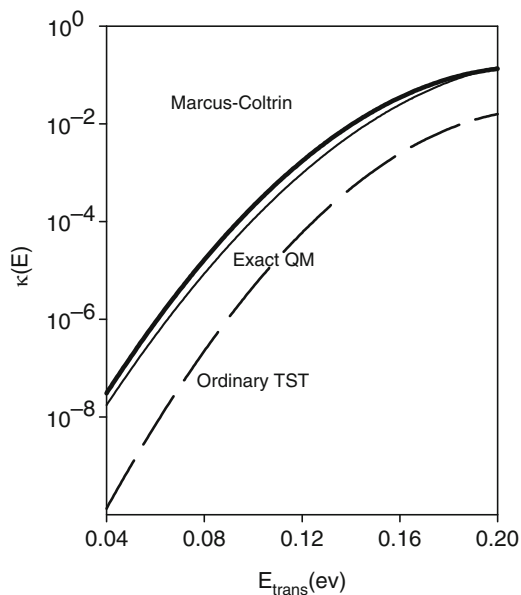


Fig. 6.4 Plot of reaction probability vs. initial translational energy for the $\text{H} + \text{HH} = \text{HH} + \text{H}$ reaction for a certain empirical potential energy surface (the Porter–Karplus surface). Curves (reading down) are shown for the path shown as PP' in Fig. 6.3a. (marked Marcus–Coltrin), the exact quantum mechanical result for the Porter–Karplus surface (marked Exact QM), the usual TST result calculated for the MEP, QQ' (Fig. 6.3a) (The data are from Marcus, R. A. and Coltrin, M. E., *J. Chem. Phys.* **67**, 2609 (1977))

fashion to maximize tunneling. In classical mechanics, the principal of least action may be employed to study mechanics without using Newton’s laws explicitly. In using the semi-classical formulation of tunneling the principal of least action has been extended to a quantum situation where the action is imaginary. As seen in Fig. 6.3a, the Marcus–Coltrin tunneling path is located on the concave side of the MEP path; the phenomenon is sometimes referred to as “corner cutting”. It is noted that for the $\text{H} + \text{HH}$ reaction considered here, the tunneling factor κ has been found at 300 K to vary between 3 and 6 depending on the empirical surface used for the calculation.

Because of the success of the Marcus–Coltrin tunneling path for $\text{H} + \text{H}_2$, the same procedure was applied to other collinear three center reactions including



Here it was found that the tunneling factor κ is very close to unity. However this result is uncertain because the magnitude of κ is sensitive to the choice of the potential energy surface which is not as well established for reaction 6.20 as it is for 6.6. For that matter, learning whether a given reaction rate is significantly influenced by tunneling either on the basis of theory or experiment is not a trivial problem as will be pointed out in further discussion.

At this point, it is important to compare Fig. 6.3a and c for the hydrogen atom transfers $\text{HH} + \text{H} = \text{H} + \text{HH}$ and $\text{ClH} + \text{Cl} = \text{Cl} + \text{HCl}$. The skew angles are 60.0° and 13.6° , respectively. Keep in mind that, with the introduction of the mass scaled coordinate systems x , y these problems each correspond to the motion of a mass point in two dimensions, albeit the potential functions acting on the mass point are indeed different. For the first case, $\text{HH} + \text{H} = \text{H} + \text{HH}$, the Marcus–Coltrin least action pathway for tunneling gives results in good agreement with the complete QM calculations, as illustrated in Fig. 6.4. The question is whether that is necessarily correct in the second case, $\text{ClH} + \text{Cl} = \text{Cl} + \text{HCl}$, given the different geometries of the potential functions for the two cases. For example the straight line pathway leading directly between reactant and product indicated in Fig. 6.3c is an attractive alternative. This path is much shorter than the Marcus–Coltrin path, but the potential “hill” through which the particle must pass is much higher – the new path is much further from MEP. The calculation of $\phi(E)$, Equation 6.9, leads to the conclusion that the new tunneling path is indeed the proper one to use for the reaction $\text{ClH} + \text{Cl} = \text{Cl} + \text{HCl}$. Thus, was born the idea of two possible tunneling pathways: small curvature tunneling (SCT) which refers to the Marcus–Coltrin path and large curvature tunneling (LCT) which refers to the straight line path of Fig. 6.3c. While these ideas come from considering low and high skew angle situations, the recommendation is not to base the usage of these two tunneling paths on the skew angle, but rather to carry out the calculation of the transmission coefficient for each molecular energy E by both methods and to chose that method which gives rise to the smaller value of $\phi(E)$ (Equation 6.9). This method is known as the μ OMT method where MT stands for multidimensional tunneling, O stands for optimized, and μ stands for microcanonical ensemble (as a reference to individual molecular energies). The other recommended method which gives rise to the “best” pathway but which is also the most time consuming method is to find the path yielding the smallest value of $\phi(E)$ for each E , referred to as the LAT (least action tunneling) method.

It should be emphasized that the tunneling calculations are usually carried out as a function of initial kinetic energy E so the total energy of the reacting system is then fixed. It is assumed that during the tunneling-process the quantized internal motions (rotations and vibrations) adjust adiabatically to the motion along the reaction coordinate with no sudden jumps in quantum states. In the alphabet soup of naming various aspects of variational transition state theory, a capital letter A often refers to the fact that adiabaticity is assumed.

6.4 Tests of Variational Transition State Theory (Including Tunneling)

6.4.1 Collinear Three Center Reactions

There exist a fairly large number of numerical tests of VTST (including tunneling) for three center reactions, the tests being the comparison with exact quantum me-

chanical calculations on the same reactions using identical potential energy surfaces. Most of these comparisons have been made for collinear reactions; a smaller number have been made for full three-dimensional space. Table 6.2 shows a few of these tests. The entries in Table 6.2 present the ratio of the VTST result to the exact quantum mechanical calculations for the same reaction. What is indeed remarkable is how close the ICVT/ μ OMT result (best expected result from a variational transition state theory among those listed) is to the exact result. In fact, in the comparisons of the exact versus transition state theory from which Table 6.2 was abstracted, the average percentage error for 48 different cases (including both collinear and 3D calculations) at 300 K was 24%, which is extremely good agreement for theoretical kinetic calculations. The TST and ICVT results without accounting for tunneling tend to be quite unsatisfactory but, in this context, it must be remembered that the

Table 6.2 Tests of Variational Transition State Theory by Comparing with Exact Quantum Calculations (Extracted from Allison, T. C. and Truhlar, D. G. *Testing the accuracy of practical semiclassical methods: variational transition state theory with optimized multidimensional tunneling*, in Thompson, D. L., Ed. *Modern methods for multidimensional dynamics computations in chemistry*, World Scientific, Singapore 1998, pp 618–712. This reference quotes results on many more reactions and BO surfaces over broad temperature ranges.) The numbers in the table are ratios of the results of the approximate calculation to the quantum calculation, all at 300 K

Reaction	Surface	Ratios (approximate/quantum)				
		TST	ICVT	$\frac{\text{ICVT}}{\text{SCT}}$	$\frac{\text{ICVT}}{\mu\text{OMT}}$	k_{QUANTUM}
H + HH' \rightarrow HH + H'	PK2-collinear	0.12	0.12	0.77	0.93	3.15(1)
D + HH \rightarrow DH + H	TK-collinear	0.39	0.32	1.00	1.05	7.24(0)
H + DD \rightarrow HD + D	TK-collinear	0.47	0.42	1.25	1.28	3.17(-1)
D + DD \rightarrow DD + D	TK-collinear	0.43	0.43	1.19	1.22	5.54(-1)
H + FF \rightarrow HF + F	JOT-II-collinear	0.70	0.70	0.96	0.97	2.28(3)
D + FF \rightarrow DF + F	JOT-II-collinear	0.85	0.83	0.99	1.00	1.42(3)
Cl + HCl \rightarrow ClH + Cl	BCMR-collinear	0.50	0.33	0.35	0.83	1.16(1)
Cl + DCl \rightarrow ClD + Cl	BCMR-collinear	0.37	0.30	0.36	0.71	2.16(0)
H + HH' \rightarrow HH + H'	PK2-3dim	0.05	0.05	1.06	1.23	7.99(-16)
H + HD \rightarrow HH + D	PK2-3dim	0.06	0.05	0.69	0.83	2.00(-16)
H + DH \rightarrow HD + H	PK2-3dim	0.08	0.08	1.38	1.45	1.10(-16)
D + HH \rightarrow DH + H	PK2-3dim	0.06	0.06	0.69	0.80	1.40(-15)
Cl + HCl \rightarrow ClH + Cl	BCMR-3dim	0.26	0.26	0.30	1.06	5.20(-16)
Cl + DCl \rightarrow ClD + Cl	BCMR-3dim	0.30	0.30	0.41	1.02	7.93(-17)

TST = conventional Transition State Theory, ICVT = Improved Canonical Variational Transition state theory, ICVT/SCT = ICVT/Small Curvature Tunneling, ICVT/ μ OMT = ICVT/Microcanonical Optimized Multidimensional Tunneling.

The various Born–Oppenheimer surfaces are: PK2 = Porter, R. N. and Karplus, M. *J. Chem. Phys.* **40**, 1105 (1964); TK = Truhlar, D. G. and Kupperman, A. *J. Chem. Phys.* **52**, 3841 (1970); JOT-II = Jonathon, N., Okuda, S., and Timlin, D. *Mol. Phys.* **25**, 466(E) (1973); BCMR = Bondi, D. K., Connor, J. N. L., Manz, J. and Romelt, J. *Mol. Phys.* **50**, 467 (1983).

The units of k are cm molecule⁻¹ s⁻¹ for the collinear calculations and cm³ molecule⁻¹ s⁻¹ for the three dimensional calculations, the figures in parentheses denote multiplicative powers of ten.

Table 6.3 Tests of variational transition state theory by comparing with exact quantum calculations; isotope effects at 300 K. The numbers in the table are ratios of rate constants for the two selected reactions

Reaction	Surface	Ratios: ($k_{\text{UPPER}}/k_{\text{LOWER}} = k_{\text{H}}/k_{\text{D}}$)				
		TST	ICVT	$\frac{\text{ICVT}}{\text{SCT}}$	$\frac{\text{ICVT}}{\mu\text{OMT}}$	$\frac{\text{EXACT}}{\text{QUANTUM}}$
H + HH' → HH + H'	PK2-collinear					
D + HH → DH + H	TK-collinear	1.33	1.63	3.34	3.85	4.35
H + DD → HD + D	TK-collinear					
D + DD → DD + D	TK-collinear	0.62	0.56	0.60	0.60	0.57
H + FF → HF + F	JOT-II-collinear					
D + FF → DF + F	JOT-II-collinear	1.33	1.36	1.56	1.56	1.61
Cl + HCl → ClH + Cl	BCMR-collinear					
Cl + DCI → CID + Cl	BCMR-collinear	7.25	5.90	5.22	6.27	5.37
H + HH' → HH + H'	PK2-3dim					
H + HD → HH + D	PK2-3dim	3.33	4.00	6.14	5.92	4.00
H + DH → HD + H	PK2-3dim					
D + HH → DH + H	PK2-3dim	0.10	0.10	0.16	0.14	0.08
Cl + HCl → ClH + Cl	BCMR-3dim					
Cl + DCI → CID + Cl	BCMR-3dim	5.68	5.68	4.80	6.81	6.56

See footnotes to Table 6.2.

reactions all involve motions of H or D atoms where one would expect tunneling to be more important than it is in reactions involving motions of heavier atoms. For the reaction Cl + HCl, LCT leads to much better agreement with the exact result than SCT. On the other hand, for the reaction of Cl + HBr (not listed in Table 6.1) which has an even smaller skew angle ($\beta = 11.6^\circ$) than Cl + HCl ($\beta = 13.6^\circ$), SCT and LCT lead to very similar results. In fact, for many cases, LCT and SCT tunneling results are very similar. Without tunneling, TST results tend to be larger than ICVT results.

Table 6.3 lists a few H/D isotope effects ($k_{\text{H}}/k_{\text{D}}$) for some of the examples listed in Table 6.2. It is noted with some regret that the errors in the isotope effects ($k_{\text{H}}/k_{\text{D}}$) calculated by ICVT/ μ OMT are about the same as the errors reported for k_{H} in Table 6.1. One might have hoped to see some cancellation of error when calculating isotope effects.

Further Reading

Allison, T. C. and Truhlar, D. G. *Testing the accuracy of practical semiclassical methods: variational transition state theory with optimized multidimensional tunneling*, in Thompson, D. L., Ed. *Modern methods for multidimensional dynamics computations in chemistry*, World Scientific, Singapore (1998), pp. 618–712.

Marcus, R. A. and Coltrin, M. E. *A new tunneling path for reactions such as $H + H_2 = H_2 + H$* . *J. Chem. Phys.* 67, 2609 (1977).

Truhlar, D. G. *Variational transition state theory and multidimensional tunneling for simple and complex reactions in the gas phase, solids, liquids, and enzymes.* in Kohen, A. and Limbach, H. H., Eds. *Isotope Effects in Chemistry and Biology*. CRC Press/Taylor & Francis, Boca Raton, FL (2006), pp. 579–619.

Chapter 7

Instrumentation and Experimental Techniques

Abstract In this chapter we discuss practical techniques and instrumentation used in experimental measurements of kinetic and equilibrium isotope effects. After describing methods to determine IE's on rate constants, brief treatments of mass spectrometry and isotope ratio mass spectrometry, NMR measurements of isotope effects, the use of radio-isotopes, techniques to determine vapor pressure and other equilibrium IE's, and IE's in small angle neutron scattering are presented.

7.1 Experimental Determination of Kinetic Isotope Effects

Choosing a method to determine isotope effects on rate constants, and selecting a particular set of techniques and instrumentation, will very much depend on the rate and kind of reaction to be studied, (i.e. does the reaction occur in the gas, liquid, or solid phase?, is it 1st or 2nd order?, fast or slow?, very fast or very slow?, etc.), as well as on the kind and position of the isotopic label, the level of enrichment (which may vary from trace amounts, through natural abundance, to full isotopic substitution). Also, does the isotopic substitution employ stable isotopes or radioactive ones, etc.? With such a variety of possibilities it is useless to attempt to generate methods that apply to all reactions. Instead we will resort to discussing a few examples of commonly encountered strategies used to study kinetic isotope effects.

The illustrations used in this chapter usually employ first order reactions and unit stoichiometry. Generalization to more complicated cases is straightforward but sometimes tedious.

7.1.1 *The Non-competitive or "Direct" Method*

Conceptually, the simplest way to measure a kinetic isotope effect (KIE) is to use a non-competitive method, in which two separate kinetic runs are carried out, each starting with a different isotopomer of the reactant. The rate constants for both species are determined and the kinetic isotope effect (KIE) is the ratio of the two rate constants. This procedure is frequently referred to as "the direct method".

Consider a simple first order reaction $S \rightarrow P$:

$$-d[S]/dt = d[P]/dt = k[S] \quad (7.1)$$

The time dependence of accumulation of product P ([P]) depends on the initial concentration of substrate (reactant), S ($[S_0]$):

$$[P] = [S_0](1 - e^{-kt}) \quad (7.2)$$

The subscript indicates the beginning concentration ($t = 0$), k is the rate constant, and t is time. Introducing the fraction of reaction f ,

$$f = [P]/[S_0] = 1 - e^{-kt} \quad (7.3)$$

and using subscripts L, for the light, and H, for the heavy isotopomer, equations can be written for each isotopomer:

$$[P_L] = [S_{0L}](1 - \exp(-k_L t)) \quad (7.4)$$

$$[P_H] = [S_{0H}](1 - \exp(-k_H t)) \quad (7.5)$$

where k_L and k_H are the corresponding first-order rate constants. After rearrangement:

$$e^{-k_L t} = 1 - [P_L]/[S_{0L}] = 1 - f_L \quad (7.6)$$

$$e^{-k_H t} = 1 - [P_H]/[S_{0H}] = 1 - f_H \quad (7.7)$$

Taking logarithms and dividing, we obtain an expression for KIE in terms of the ratios of concentrations of product to substrate:

$$\text{KIE} = k_L/k_H = \ln(1 - [P_L]/[S_{0L}]) / \ln(1 - [P_H]/[S_{0H}]) \quad (7.8)$$

This non-competitive method has several practical limitations. Since the ordinary precision of determination of rate constants, $(\delta k_L/k_L)$ or $(\delta k_H/k_H)$, is on the order of a few percent, the method is limited as a practical matter to large, primary kinetic isotope effects, generally of hydrogen. This, because deuterium, the common heavy isotopomer for hydrogen, is available at $\sim 100\%$ abundance at reasonable cost, and for hydrogen KIE's are usually large enough to constrain the relative error, $\delta(k_L/k_H)/(k_L/k_H)$, to acceptable values.

One disadvantage of the non-competitive method is the necessity to synthesize samples of isotopically pure (or at least highly enriched) reactants, and this can be tedious and expensive. Since light and heavy isotopomers are very often obtained using different synthetic pathways (in order to optimize isotopic yield), they may carry different impurities or different concentrations of the same impurity. Therefore it is necessary to meticulously purify both samples before running experiments. In this

context, remember that highly enriched radioactive compounds (e.g. compounds fully titrated in a specific position) not only require special handling and safety measures, but often undergo spontaneous auto-radiolysis to yield chemically polluted samples which may show anomalous isotopic fractionation. Even when the rates of reaction of stable isotopes are being compared, results obtained from non-competitive experiments should be treated with caution because the two reactions are inevitably carried out under slightly different conditions. Non-competitive measurements are especially risky when the reaction is prone to catalysis. The separate syntheses of isotopomers may result in different trace amounts of catalytic impurities, in which case the measured ratio of rate constants will reflect differences caused by the impurities. The measured isotope effect can then be seriously in error. Similarly, the pollutant may turn out to be an inhibitor – this situation is commonly encountered for enzyme-catalyzed reactions. To some extent such problems may be investigated and minimized by mixing the isotopomers in different proportions and studying the isotope effect as a function of composition.

7.1.1.1 Mixing Studies and Non-competitive KIE's

If we denote the rate constant for the light isotopomer as k_L , that for the heavy one as k_H , and the rate constant for a mixture of isotopomers of mole fraction x of the heavier isotope as k_x , then (k_L/k_H) is related to the observed isotope effect, (k_x/k_H) , by:

$$k_L/k_H = [(k_x/k_H) - x]/(1 - x), \text{ for } x \neq 1 \quad (7.9)$$

Equation 7.9 assumes a linear dependence of k_x on mole fraction, x , which is reasonable provided that neither isotopomer sample contains trace amounts of catalytic impurities or inhibitors. That assumption met, the deviation from Equation 7.9 affords a reasonably sensitive test for the experimental validity of non-competitive KIE data.

As a practical matter it is sometimes impossible to make studies across the entire range of composition ($0 < x < 1$) because the criterion of 100% enrichment is either too difficult or too expensive to meet. Sometimes, particularly for solvent isotope effects, the linear dependence employed in the derivation of Equation 7.9 is not obeyed, and the deviation from linearity can be employed to elucidate some details of the reaction mechanism given sufficient information on the x dependence of k_x , and the absence of trace catalytic impurities. For studies of H_2O/D_2O solvent isotope effects the approach, called “proton inventory”, has been widely employed. It is discussed in more detail in Section 11.4.3.

7.1.1.2 Comment

In spite of the limitations of direct non-competitive measurements of KIE, their use is sometimes unavoidable. For example, when information on the KIE of the V_{max} parameter for an enzymatic reaction is required, non-competitive kinetic runs using

isotopically different molecules must be employed. This is because the different isotopomers which would be present simultaneously in a common reaction mixture can act as competitive inhibitors to each other.

7.1.2 Simultaneous Non-competitive Measurements

A partial resolution to some of the problems with the non-competitive technique is to carry out the reactions of the separated isotopomers at the same time, and under the same conditions, but in different containers (say in a common thermostat). In this fashion one can directly compare isotopic differences as the reactions progress. For example, if the concentration of product or substrate can be followed spectrophotometrically, one might use a two-beam instrument with the two samples placed next to each other. The photometric signal, then, is proportional to the difference in the absorption, A , of light and heavy species, and therefore to the difference in their concentrations, (provided the experiment is carried out in a region where the Lambert–Beer law is valid, and the molar extension coefficients are equal for both isotopomers), see Fig. 7.1.

Introduction of Equations 7.6 to 7.8 defines KIE in terms of the fractions f_L and f_H :

$$\text{KIE} = k_L/k_H = \ln(1 - f_L)/\ln(1 - f_H) \quad (7.10)$$

Rearranging:

$$f_H = 1 - (1 - f_L)^{1/(k_L/k_H)} \quad (7.11)$$

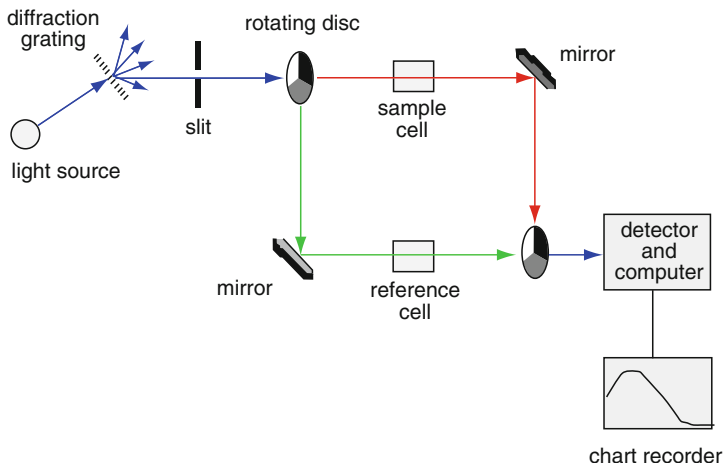


Fig. 7.1 Spectrophotometric simultaneous non-competitive measurement of KIE. In this technique the reaction mixture containing the reference isotopomer is placed in the reference cell and the mixture with the other isotopomer in the sample cell (at identical concentrations). The two cells are placed in a common thermostat (www.chemguide.co.uk)

Table 7.1 Isotopic differences in reaction progress as a function of f_L , (simultaneous non-competitive measurement of isotope effects)

k_L/k_H	1.01	1.05	1.1	2
f_L	Δf			
0	0	0	0	0
0.1	0.000939	0.004527	0.008662	0.048683
0.2	0.001769	0.008546	0.016394	0.094427
0.3	0.002476	0.011991	0.023069	0.136660
0.4	0.003042	0.014774	0.028520	0.174597
0.5	0.003443	0.016779	0.032521	0.207107
0.6	0.003645	0.017840	0.034747	0.232456
0.7	0.003598	0.017702	0.034700	0.247723
0.8	0.003213	0.015931	0.031512	0.247214
0.9	0.002306	0.011588	0.023285	0.216228
1	0	0	0	0
$f_{L,max}$	0.634	0.641	0.650	0.750

and, using $\Delta f = (f_L - f_H)$,

$$\Delta f = (f_L - f_H) = (1 - f_L)^{1/(k_L/k_H)} - (1 - f_L) \quad (7.12)$$

provided the initial concentrations are equal. At both beginning and end of the reaction $\Delta f = 0$. The deviation from zero during the course of the reaction depends only on KIE. It reaches its maximum at

$$f_{L,max} = 1 - (k_L/k_H)^{(k_L/k_H)/(1-k_L/k_H)} \quad (7.13)$$

whence Δf_{max} is easily obtained using Equation 7.12. Examples for KIE's varying between 1.01 and 2 are given in Table 7.1 and illustrated in Fig. 7.2.

7.1.3 KIE's of Enzyme Catalyzed Reactions by Isotope Perturbation

The protocol described in Section 7.1.2 involves isotopic competition, but with the different isotopomers held in separate containers. Equations 7.10 to 7.13 apply equally well to a type of competition experiment known in biochemistry as the perturbation method for determining KIE's of reversible enzyme catalyzed reactions. The perturbation method differs from simultaneous non-competitive measurements in several important ways. One begins by mixing equilibrium concentrations of substrate and product but with one component (substrate or product) at a different isotopic composition than the other. Thus, the mixture is in chemical, but not isotopic equilibrium. At this stage no enzyme is present and the interconversion is

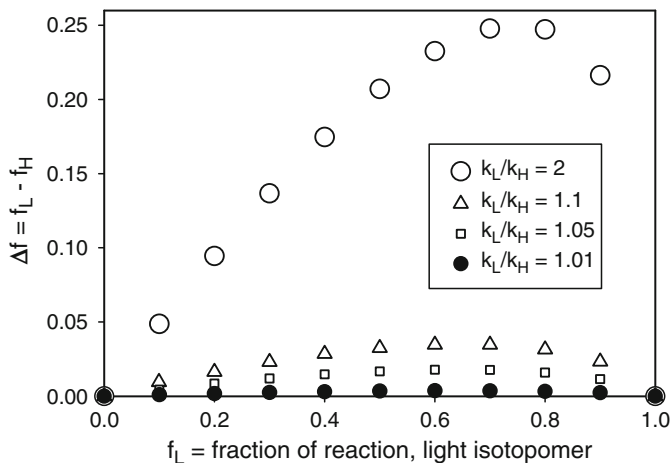


Fig. 7.2 Differences in reaction progress of light and heavy isotope as a function of the fraction of reaction (simultaneous non-competitive measurement of isotope effects)

proceeding at a negligible rate. Later, when the enzyme which catalyzes interconversion is added, the system acts to redistribute the isotopes and as a consequence moves away from chemical equilibrium. After sufficient time, however, the system returns to chemical equilibrium and at the same time comes to isotopic equilibrium. If the initial move from chemical equilibrium can be observed, for example by following the concentration change of one of the reactants spectrophotometrically, then curves identical to those shown in Fig. 7.2 are obtained. The KIE can be obtained from the time-to-maximum using Equation 7.13.

For heavy atom isotope effects (which are usually smaller than 1%) the maximum difference predicted by Equation 7.13 is small (Table 7.1) and special care must be taken. For example, in the equilibrium perturbation method, the maximum deviation corresponding to a heavy-atom KIE of a percent or so is comparable to the change that would be observed by warming the UV cell by holding it briefly in one's fingers when adding enzyme, then returning it to the thermostat (at, say, 25°C). To avoid such errors devices are available which automatically deliver and mix enzyme without otherwise perturbing the conditions of the experiment.

7.1.4 Competitive Measurements of KIE's

7.1.4.1 Double Labeling

In the discussions above we assumed the isotopomers being compared were in different containers. However, separate determinations of rate constants are also possible in a common container in the same solution. This obviously eliminates

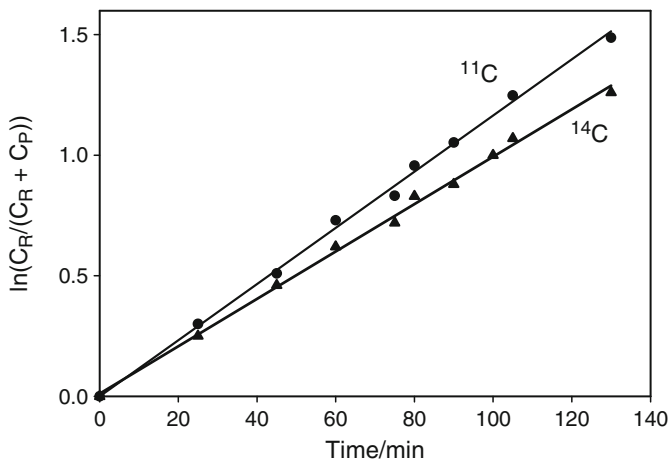


Fig. 7.3 Kinetic plots for ^{11}C and ^{14}C in the reaction of labeled methyl iodide with *N,N*-dimethyl-*p*-toluidine in methanol at 30°C . (C_R is the count rate (cpm) for the reactant fraction and C_P the count rate for product fraction) (After Axelsson, B. S. et. al. *J. Am. Chem. Soc.* **109**, 7233 (1987))

errors introduced by differences in impurities, concentrations, temperature control, etc. An interesting implementation of this method uses reactant labeled with two different radioisotopes, the first being the one for which the isotope effect is to be measured, while the second is placed at a remote location in the molecule which does not show an isotope effect (see Sections 7.2.2.2 and 11.5.3). Double isotope labeling experiments are best performed using beta-emitters that differ in maximum energy, e.g., ^{32}P and T , T and ^{14}C or ^{35}S , and ^{32}P and ^{14}C or ^{35}S . The remotely labeled site serves only as a tracer, for example for double labeling with ^{14}C and remotely labeled T , the observed $\text{KIE} = k_{\text{T}}/k_{14}$ is equivalent to the isotopic ratio of interest, $\text{KIE} = k_{12}/k_{14}$. The virtue of this method is that it takes full advantage of the convenience of radiochemical analysis. More details are found later in the chapter.

A slightly different example is the separate determination of rates of reaction of ^{11}C and ^{14}C labeled methyl iodide with *N,N*-dimethyl-*p*-toluidine as illustrated in Fig. 7.3. Again the method takes advantage of the convenience of radiochemical analysis. If, as likely, the KIE of interest is k_{12}/k_{14} , it can be obtained to sufficiently good approximation by applying a modified Swain–Schaad rule, $\ln[k_{12}/k_{14}]/\ln[k_{11}/k_{14}] = [(12/14)/(11/14)]^{1/2}$ obtained from the law of the geometric mean (see Section 10.5).

7.1.4.2 Competitive Studies with Single Labeling

The most frequently used type of competitive study measures relative rates with both isotopomers present in the same solution. Instead of measuring individual

concentrations the concentration ratios are determined. Defining the isotopic ratio of products, R_P , as:

$$R_P = [P_H]/[P_L] \quad (7.14)$$

the initial isotopic ratio of substrate, R_{0S} , as

$$R_{0S} = [S_{0H}]/[S_{0L}] \quad (7.15)$$

and rewriting f_H in terms of f_L and the R 's:

$$\begin{aligned} f_H &= [P_H]/[S_{0H}] = ([P_H]/[S_{0H}])/([P_L]/[S_{0L}]) \cdot ([P_L]/[S_{0L}]) \\ &= ([P_H]/[P_L])/([S_{0H}]/[S_{0L}]) \cdot ([P_L]/[S_{0L}]) = (R_P/R_{0S})f_L \end{aligned} \quad (7.16)$$

using Equation 7.10, we obtain:

$$k_L/k_H = \ln(1 - f_L)/\ln(1 - f_L R_P/R_{0S}) \quad (7.17)$$

Similarly:

$$k_L/k_H = \ln(1 - f_L)/\ln[(1 - f_L)R_S/R_{0S}] \quad (7.18)$$

Equations 7.17 and 7.18 show that KIEs can be obtained by comparing isotopic ratios of reactant or product with the initial isotope ratio of reactant as the reaction progresses.

7.1.4.3 Approximations to Equations 7.17 and 7.18

Frequently, one of the isotopes is present only in trace quantities (usually the heavier isotope) and the overall fraction of reaction, f , reduces to f_L to good approximation. If this is not the case Equations 7.17 and 7.18 can be easily rewritten in terms of f or f_H instead of f_L . By the same token, with one isotopomer present in trace amounts (the commonly occurring case) the probability of reaction between two labeled molecules is very low, and formal second and higher order kinetics can be approximated using the first-order kinetic expressions developed above.

Two further approximations are of interest. When the fraction of reaction is small (as a practical matter, say $f < 0.1$, more conservatively $f < 0.05$) the right-hand-side of Equation 7.17 can be simplified using:

$$\ln(1 + x) \approx x \quad (7.19)$$

and at the early stages of reaction:

$$k_L/k_H \approx -f_L/(-f_L R_P/R_{0S}) = R_{0S}/R_P \quad (7.20)$$

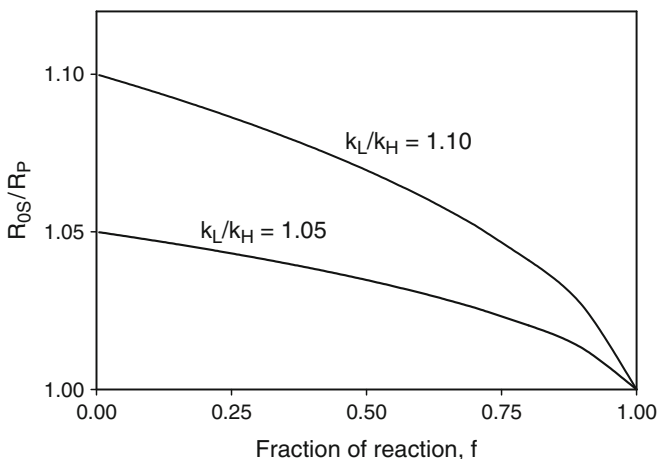


Fig. 7.4 Time dependence of isotopic ratios in product during single label competitive KIE studies

R_{0S}/R_P is shown as a function of f in Fig. 7.4

$$R_{0S}/R_P = [f/1 - f]^{1/(k_L/k_H)} \quad (7.21)$$

for KIE's equal to 1.05 and 1.1. The isotope effect is fully expressed by R_{0S}/R_P at the beginning of the reaction and then becomes gradually obscured as reaction progresses and R_{0S}/R_P falls off toward unity. Thus it is best to measure isotopic product ratios in the very early stages of reaction.

Alternatively, one may elect to rewrite Equation 7.18:

$$\ln R_S = [1/(k_L/k_H) - 1] \ln(1 - f_L) + \ln R_{0S} \quad (7.22)$$

because it may be convenient to measure the isotopic ratio of the remaining reactant, R_S , as the reaction progresses, and then obtain KIE from the slope of linear dependence of $\ln R_S$ on $\ln(1 - f_L)$. The intercept can be used to test the quality of the measurements. It should be equal to the logarithm of the initial isotopic ratio of reactants, $\ln R_{0S}$.

Figure 7.4 shows the initial ratio of isotopic ratios R_{0S}/R_P corresponds to KIE. In contrast, R_S/R_{0S} varies between unity at the beginning of the reaction to infinity at completion.

$$R_S/R_{0S} = (1 - f)^{1/(k_L/k_H) - 1} = (1 - f)^{[(k_H/k_L) - 1]} \quad (7.23)$$

Equation 7.23 is plotted in Fig. 7.5 for KIE's of 1.05 and 1.1 (compare with Fig. 7.4). Note that $R_S/R_{0S} = \text{KIE}$ at a particular value of f_L (conveniently labeled as f_{KIE}), after which it continues to increase.

$$f_{\text{KIE}} = 1 - (k_L/k_H)^{(k_L/k_H)/(1 - k_L/k_H)} = 1 - (k_L/k_H)^{[1/((k_H/k_L) - 1)]} \quad (7.24)$$

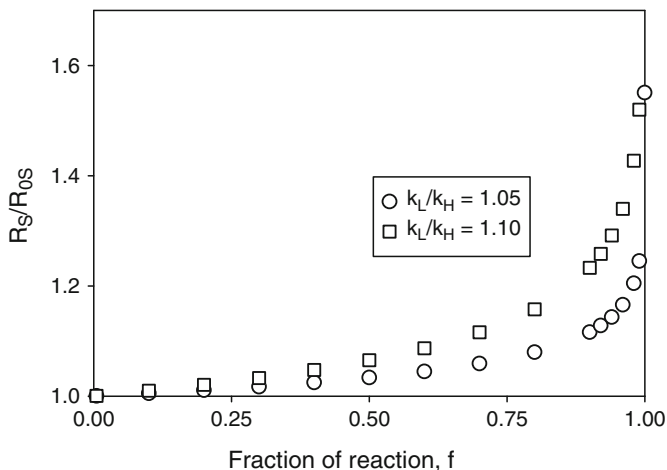


Fig. 7.5 Time dependence of isotopic ratios in measurements of substrate compositions

Table 7.2 Solutions to Equation 7.24

(k_L/k_H)	1.001	1.01	1.1	1.2	1.5	2	4
$(1 - f_{KIE})$	0.37	0.37	0.35	0.33	0.30	0.25	0.16

For KIE's in the range ($1 < \text{KIE} < 4$) f_{KIE} varies between 0.63 and 0.85 (see Table 7.2). Note the similarities between Equations 7.24 and 7.13. As a reaction progresses beyond f_{KIE} the ratio R_S/R_{0S} is said to “overexpress” KIE. Measurements in this region may be convenient from an experimental point of view since the difference between R_S and R_{0S} is large, and this allows better precision for the determination of KIE, all else remaining the same. It should be noted, however, that large overexpressions are only achieved at very high conversions where error in the determination of f_L becomes the dominating factor.

7.1.5 Error Analysis

When measuring KIE using isotope analysis for the product (Equation 7.17) three quantities are determined experimentally; f_L , R_{0S} and R_P . For measurements of KIE using substrate (reactant) analysis (Equation 7.18) the corresponding quantities are f_L , R_{0S} and R_S . All these measurements, of course, are subject to experimental error. Equation 7.25 expresses the relative error of KIE in terms of the errors in these three experimental quantities:

$$\frac{\sigma_{k_L/k_H}}{k_L/k_H} = \sqrt{A^2 \left(\frac{\sigma_f}{f}\right)^2 + B^2 \left[\left(\frac{\sigma_{R_f}}{R_f}\right)^2 \left(\frac{\sigma_{R_0}}{R_0}\right)^2 \right]} \quad (7.25)$$

Table 7.3 Expressions for A and B, Equation 7.25

	A	B
Substrate	$\frac{(k_L/k_H - 1) \cdot f}{1 - f \ln(1 - f)}$	$\frac{(k_L/k_H)^2}{\ln(1 - f)}$
Product	$\frac{f}{\ln(1 - f)} \left(\frac{k_L/k_H \cdot R_P/R_{0S}}{1 - f \cdot R_P/R_{0S}} - \frac{1}{1 - f} \right)$	$\frac{f}{\ln(1 - f)} \left(\frac{k_L/k_H \cdot R_P/R_{0S}}{1 - f \cdot R_P/R_{0S}} \right)$

In Equation 7.25, σ is the standard deviation, R_f the isotope ratio corresponding to the fraction of reaction, f , of either substrate (R_S) or product (R_P). Expressions for A and B are given in Table 7.3. R_0 is the isotope ratio in the starting material. Obviously, for simple reactions the isotope composition of the product after full conversion (R_{1P}) is equal to the isotope composition of the initial substrate (R_{0S}). The dependence of A and B on the progress of the reaction is illustrated in Fig. 7.6:

Figure 7.6 confirms that the error of measurement of KIE's determined by following the progress of reaction by product analysis increases to unacceptable values for f larger than ~ 0.8 . This is not surprising, since R_P approaches R_{0S} as f approaches 1. Experiments based on Equation 7.17 should be carried out at low fractions of reaction. On the other hand, for experiments based on substrate analysis, the largest error is introduced at low fractions of reaction. This is because at early stages the isotopic composition R_S is close to R_{0S} . Thus when experiments are based on Equation 7.18 measurements at both very early and very late stages of reaction should be avoided.

Equations 7.17 and 7.18 have been developed assuming that the fraction of reaction for the light isotopomer (f_L) is the one monitored. Frequently, however, the chemical (overall) fraction of reaction:

$$f = [P]/[S_0] = ([P_L] + [P_H])/([S_{0L}] + [S_{0H}]) \quad (7.26)$$

is measured, i.e., total chemical concentrations are monitored rather than those of individual isotopic species. The difference between f and f_L is negligible when one isotope is present in trace amounts, or when its natural abundance is low. Otherwise an appropriate correction should be included. Introduction of isotopic ratios R_{0S} and R_P and rearrangement of Equation 7.26 yields the correction which is needed when both isotopomers are present in similar abundance:

$$f_L = f(1 + R_{0S})/(1 + R_P) \quad (7.27)$$

In some cases the progress of reaction may be followed by monitoring the heavier isotope. For example, one might study a carbon-13 kinetic isotope effect competitively by monitoring the progress of reaction using radioactive carbon-14, or follow a deuterium kinetic isotope effect using tritium. Table 7.4 illustrates the error that is introduced when Equation 7.17 is used without correction (i.e. assuming $f_{14} = f_{12}$ or $f_T = f_H$). In constructing Table 7.4 we have assumed ^{13}C and ^{14}C kinetic isotope effects of 1.05 and 1.10, and a deuterium KIE of 3 with the tritium effect calculated from Swain–Schaad rule (Chapter 10). As seen in Table 7.4, deviation from the true

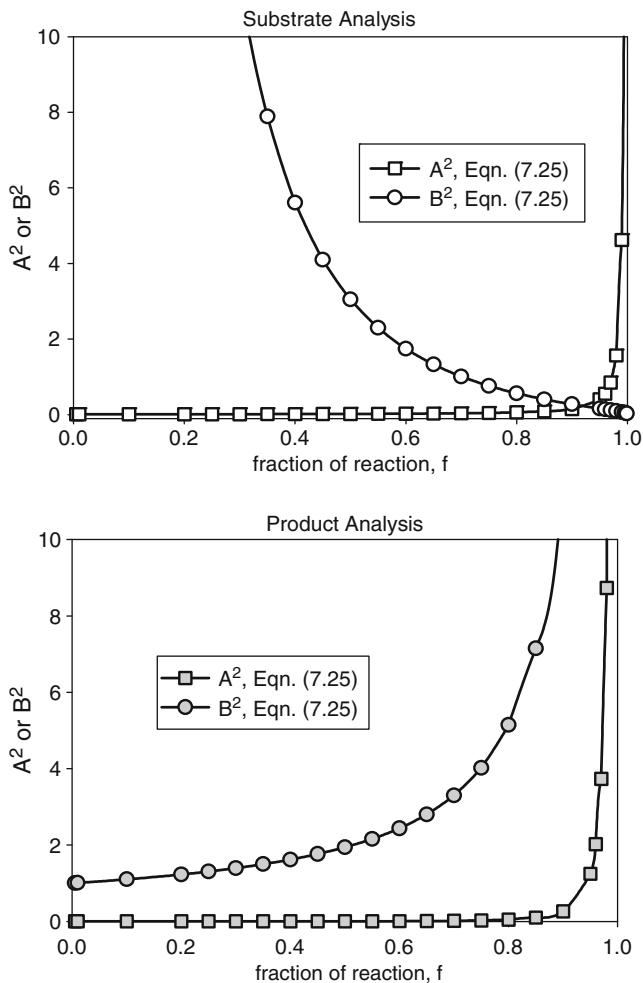


Fig. 7.6 Dependence of factors A^2 and B^2 , Equation 7.25, on the progress of reaction for $k_L/k_H = 1.1$. *Top* = substrate analysis. *Bottom* = product analysis

Table 7.4 Corrections to KIE's necessitated by substituting heavy atom monitors of progress of reaction (^{14}C for ^{12}C , or T for H)

Progress	k_{12}/k_{13}	k_H/k_D
0.1	1.0498	2.92
0.2	1.0495	2.83
0.3	1.0492	2.74
0.4	1.0488	2.64
0.5	1.0483	2.53
0.6	1.0477	2.41
0.7	1.0469	2.26
0.8	1.0457	2.09
0.9	1.0437	1.86
True effect	1.0500	3.00

value of the carbon isotope effect using the heavy-atom monitor is negligible as far as $f \sim 0.4$. If, however, measurements are carried out at higher conversion a correction is recommended. For hydrogen isotope effects the differences are larger and corrections may be needed even at low conversions.

While competitive methods to determine KIE's are free from errors due to differences in reaction conditions (impurities, temperature, pH, etc.) they do require access to equipment that allows high precision measurements of isotope ratios. The selection of an appropriate analytical technique depends on the type of the isotope and its location in the molecule. For studies with stable isotopes the most commonly used technique (and usually the most appropriate) is isotope ratio mass spectrometry (IRMS).

7.2 Mass Spectrometry and Isotope Ratio Mass Spectrometry

7.2.1 Whole Molecule Mass Spectrometry

In its ordinary configuration mass spectrometry separates ions according to their mass-to-charge (m/z) ratio, the ions having previously been formed by electron bombardment or other methods. Since methods of ionization are usually powerful enough to break chemical bonds, or to excite molecules to high-energy unstable states, the result at the detector is a mixture of ions of the parent molecular mass together with the (perhaps many) ion fragments formed in high energy decomposition processes. The dominant ions are singly charged. They form a spectrum that relates ion intensity (population) to mass. That spectrum is characteristic for chemical compounds subjected to a particular ionization technique, and is widely used for qualitative and quantitative analysis.

The most widely used method for ionization is electron impact (EI). In an EI source the sample is placed in the path of an electron beam. Although many newer kinds of ion sources have been developed, EI is the method commonly used in classical isotope-ratio mass spectrometers (IRMS), i.e. mass spectrometers designed for precise isotopic analysis. In this type of spectrometer the ions, once formed, are electrostatically accelerated, and then ejected through a slit into a magnetic field held perpendicular to the ion trajectory. In the magnetic sector part of the instrument the particles are deflected in an arc described by:

$$m/z = B^2 r^2 / 2V \quad (7.28)$$

B is the magnetic field intensity, r is the radius of the ion path, and V is the accelerating potential. In analytical mass spectrometers either B or V is varied systematically so that ions of different m/z are sequentially focused on the collector and the spectrum recorded. Such "whole molecule mass spectrometers" have been employed occasionally for isotope ratio measurements but their use is restricted to samples

where the relative abundances are not too different, say ($0.1 < (I/I') < 0.9$). I' and I are ion beam intensities at the collector. Isotopomer pairs (at natural abundance) well suited for measurements using whole molecule mass spectrometers are those of chlorine and bromine. Most isotopomer pairs of common interest, however, contain much smaller quantities of the less common isotopomer (at natural abundance) and need to be enriched for analysis with whole molecule mass spectrometers (Tables 7.5 and 9.1).

Apart from the need for isotopic enrichment and synthesis there are other problems in applying “whole molecule mass spectrometry” to measure isotope ratios. Assume, for example, that we want to determine isotopic composition of chlorine from the spectrum of chlorobenzene presented in Fig. 7.7. The peaks at 114 and

Table 7.5 Isotopomer pairs of lighter elements commonly used in isotope effect studies

Element	Isotope	Natural abundance (%) or half-life	Standard isotope ratio or energy
Hydrogen	H (^1H)	99.985	
	D (^2H)	0.015	SMOW (H_2O): 0.015576
Carbon	T (^3H)		β^- 0.018 MeV
	^{11}C		12.43 years
	^{12}C	98.9	20.42 min
	^{13}C	1.10	β^+ 0.95 MeV
Nitrogen	^{14}C		5730 years
	^{14}N	99.634	
	^{15}N	0.366	PDB ($\text{CaMg}(\text{CO}_3)_2$): 0.0112372
Oxygen	^{15}N		air (N_2) 0.003676
	^{15}O		1.97 min
	^{16}O	99.762	β^+ 1.64 MeV
Fluorine	^{17}O		0.038
	^{18}O	0.200	SMOW (H_2O): 0.000372
	^{18}F		SMOW (H_2O): 0.0019934
	^{19}F	100	1.87 h
Phosphorus	^{19}F		β^+ 0.65 MeV
	^{31}P	100	
Sulfur	^{32}P		14.30 days
	^{32}S	95.02	
	^{33}S	0.75	
	^{34}S	4.21	IAEA (AgS): 0.00794442
	^{35}S		IAEA (AgS): 0.0449832
Chlorine	^{35}S		87.1 days
	^{36}S	0.02	β^- 0.17 MeV
	^{35}Cl	75.77	IAEA (AgS): 0.000000554
	^{36}Cl		301,000 years
	^{37}Cl	24.23	β^- 0.72 MeV
			SMOC (NaCl): 0.32453

SMOW = Standard Mean Ocean Water; IAEA(AgS) = International Atomic Energy Agency (silver sulfide); SMOC = Standard Mean Ocean Chloride

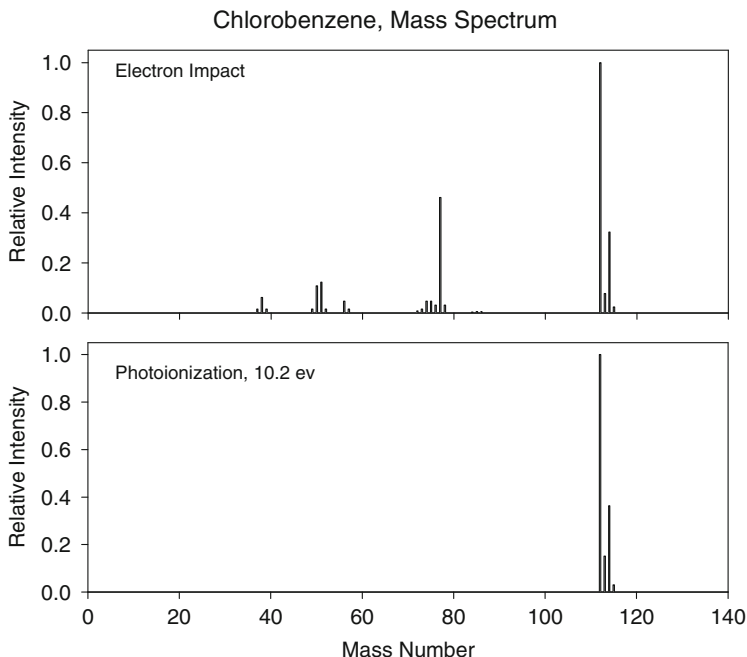


Fig. 7.7 Mass spectra of chlorobenzene. *Top*: electron impact: (Data from <http://webbook.nist.gov/chemistry>). *Bottom*: photoionization at 10.2 eV. (Data from Tonakura, K., Nakamura, T. and Koshi, M. *Anal. Sci.* **19**, 1109 (2003)) (See Table 7.6 for assignments)

112 m/z correspond to $^{12}\text{C}_6^1\text{H}_5^{37}\text{Cl}$ and $^{12}\text{C}_6^1\text{H}_5^{35}\text{Cl}$, respectively. Relative abundances are approximated by relative intensities. In order to gain maximum resolution and spectral clarity in ordinary mass spectrometry each peak is focused as sharply as possible (high intensity narrowly distributed around a given m/z). An unfortunate consequence is that slight imprecisions in focusing can result in substantially different intensities as one moves from the peak maximum slightly to one or the other side. This is not a big problem in routine mass spectrometry but can be crucial when precise measurements of intensity ratios are required.

A second problem in whole molecule mass spectrometry is that fluctuations in ion current may introduce substantial errors. Recall that ions of different m/z are not measured simultaneously in whole molecule mass spectrometry. If the ion current is not stable (and it commonly fluctuates in EI sources), then after first peak (say $m/z = 112$ in our example) is measured, and instrumental parameters are changed in order to focus the next peak ($m/z = 114$) on the collector, the ion current of this second peak may no longer correspond to that existing at the time the first peak was measured. One can try to switch the detector from peak to peak more rapidly but that shortens the collection time for each peak, fewer ions will be counted, and errors in counting statistics will increase. Normally this problem is dealt with by statistical

averaging over repetitive determination of isotopic ratios (as many as several thousand times) optimizing the ratio of the counting time devoted to each peak and the time required to switch from peak to peak.

A third source of error is associated with the fragmentation pattern caused by dissociation of the molecular ions formed in the source region of the spectrometer. Under severe conditions these processes may proceed with substantial isotopic fractionation, and this obscures the measurements of isotopic composition at the collector. To some extent careful standardization of the instrumental conditions may ensure that errors from fragmentation are systematic, and thus cancel (at least to some extent). Alternatively, softer ionization methods can be used to prevent most or all of the fragmentation. The bottom spectrum in Fig. 7.7 illustrates this approach; it shows the mass spectrum of chlorobenzene obtained by photoionization. Only the parent molecular ions are observed. It should be kept in mind, however, that softer ionization usually yields smaller ion currents; and consequently statistical counting errors increase.

Finally there are problems caused by background contamination in the spectrometer. Background peaks, while always present, need to be minimized by appropriate cleaning, degassing, and pumping to ensure their intensity is small or negligible compared to the sample ion current. More importantly, however, in whole-molecule mass spectrometry, part of the background is introduced by the fragmentation of the molecular-ion under investigation, and cannot be avoided. In our example, chlorobenzene, four main peaks with the relative intensities listed in Table 7.6 are detected. The peak at $m/z = 112$ corresponds to the molecule containing all light isotopes. The major component of the peak at $m/z = 113$ is due to $^{12}\text{C}_5^{13}\text{C}^1\text{H}_5^{35}\text{Cl}$ but there is a contribution from heavy hydrogen, $^{12}\text{C}_6^1\text{H}_4^2\text{H}^{35}\text{Cl}$, which can be neglected because the natural abundance of deuterium relative to protium is two orders of magnitude smaller than that of ^{13}C relative to ^{12}C (Table 7.4). Since chlorobenzene contains six carbon atoms the relative intensity of $m/z = 113$ is about 6.6% (since $^{13}\text{C}/^{12}\text{C} \sim 0.011$). Contributions to $m/z = 114$ from double labeling of ^{13}C and D, i.e. $^{12}\text{C}_4^{13}\text{C}_2^1\text{H}_5^{35}\text{Cl}$ ($0.011^2 \sim 1.2 \times 10^{-4}$), $^{12}\text{C}_6^1\text{H}_3^2\text{H}_2^{35}\text{Cl}$ ($(1.5 \times 10^{-4})^2 \sim 2.2 \times 10^{-8}$), and $^{12}\text{C}_5^{13}\text{C}^1\text{H}_4^2\text{H}^{35}\text{Cl}$ ($(0.011)(1.5 \times 10^{-4}) \sim 1.3 \times 10^{-6}$), can be neglected. Thus if the isotopic analysis of chlorine is to be determined for

Table 7.6 Relative intensities of parent-ion peaks of chlorobenzene

Peak	Major isotopic composition	Relative intensity
112	$^{12}\text{C}_6^1\text{H}_5^{35}\text{Cl}$	100
113	$^{12}\text{C}_5^{13}\text{C}^1\text{H}_5^{35}\text{Cl}$	6.6
114	$^{12}\text{C}_6^1\text{H}_3^{37}\text{Cl}$	33
115	$^{12}\text{C}_5^{13}\text{C}^1\text{H}_3^{37}\text{Cl}$	2.2

chlorobenzene the ratio of peak intensities at 114 and 112 m/z can be safely used. If, however, the isotope effect for hydrogen is required, say by comparing reactions of singly deuterated and *per*-protio-chlorobenzene, it would be necessary to employ highly enriched $C_6^1H_5^2HCl$ to marginalize the 6.6% background at $m/z = 113$ coming from heavy isotopes of carbon.

To avoid the kind of problems which trouble whole-molecule mass spectrometry it is better to use instrumentation especially designed for high precision measurements of isotope ratios; isotope-ratio mass spectrometry (IRMS).

7.2.2 Isotope-Ratio Mass Spectrometry

To secure the highest possible precision in isotope ratio measurements mass spectrometers of special design are employed. An important feature of these instruments is that only gaseous samples are used. This permits a slow constant flow of sample from the inlet system into the ionization chamber and minimizes variations in ion current. The sample remains in the inlet system for a long time, thus careful instrument tuning can be performed methodically during the measurements. Hydrogen gas is used for measurements of hydrogen IE's, carbon dioxide for carbon and oxygen IE's, nitrogen gas for nitrogen IE's, methyl chloride for chlorine IE's, and sulfur dioxide or sulfur hexafluoride for sulfur IE's.

Unlike ordinary mass spectrometers, the goal of peak focusing in IRMS is broad peaks with wide flat tops. This allows peaks to be centered on the detectors during measurements and ensures that small inaccuracies in focusing do not affect the ion current. A typical peak shape for CO_2 measurements is shown in Fig. 7.8.

Another important feature of IRMS is the provision of a dual inlet system which permits the operator to alternate the gas flowing into the ionization chamber between

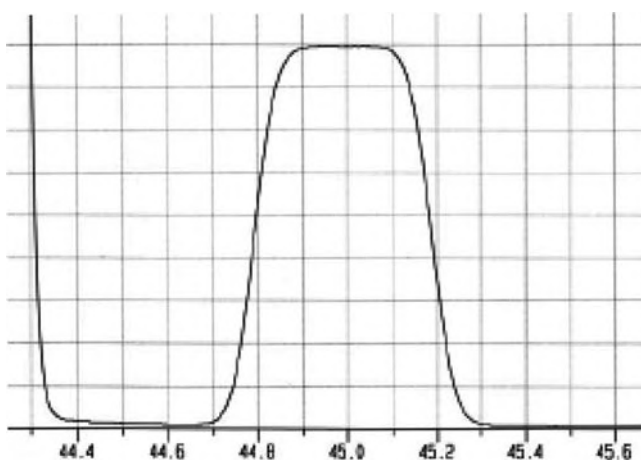


Fig. 7.8 Peak shape in IRMS of carbon dioxide (www.monitorinstruments.com)

the sample and an appropriately chosen standard. Thus two isotopic ratios are measured in rapid sequence, R_{ST} the standard, and R_{SA} the sample. The isotopic composition of the sample is then reported as a δ -value, i.e., the relative difference between the isotopic compositions of the sample and the standard. The δ -value (Chapter 9), usually expressed in units of “per-mil” (‰), is defined:

$$\delta = [(R_{SA} - R_{ST})/R_{ST}] \cdot 1000 = (R_{SA}/R_{ST} - 1) \cdot 1000 \quad (7.29)$$

Also, since ratios of isotopic ratios are commonly used to report isotope effect data (see Equations 7.17 and 7.18 for example), the actual numerical value of the abundance ratio of the standard is not important since it drops out from the final equation expressing the isotope effect:

$$R_{P/S}/R_{O/S} = (1000 + \delta_{P/S})/(1000 + \delta_{O/S}) \quad (7.30)$$

Commonly used interlaboratory standards are discussed in Section 9.1.2 and listed in Tables 7.5 and 9.1.

Small variations in apparent isotope ratio are observed when inlet pressure changes. Therefore IRMS dual inlet systems are equipped with bellows mechanisms (Fig. 7.9) so that inlet pressures of both sample and standard can be adjusted to be the same. Furthermore, small systematic changes, if any, in the measured isotope ratio as the measurement progresses are compensated by appropriate interpolation. Both these corrections are handled automatically by the software which controls the modern IRMS.

Because the molecular masses of the sample gases used in IRMS are small it is possible to use small magnetic sectors. Unlike routine mass spectrometers, many IRMS's are equipped with an array of detectors permanently located in the paths of

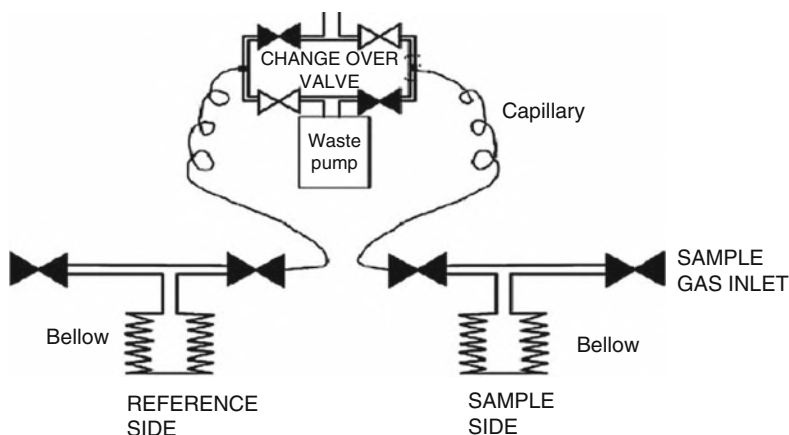
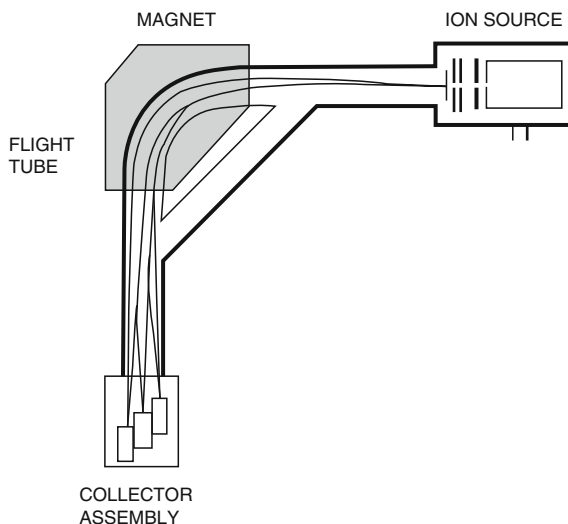


Fig. 7.9 Dual inlet system for IRMS (Ghosh, P. and Brand, W. A. *Int. J. Mass Spectrom.* **228**, 1 (2003))

Fig. 7.10 Detector geometry in IRMS (Ghosh, P. and Brand, W. A. *Int. J. Mass Spectrom.* **228**, 1 (2003))



desired ions (Fig. 7.10). Alternatively, a universal collector located at fixed geometry, usually comprising three Faraday cups, allows measurement of all isotopomer pairs of principal interest (however, a separate additional detector is necessary for studies on hydrogen since the curvature for hydrogenic ions is substantially different than those of the heavier gases. In either case it is unnecessary to sweep the magnetic, B , or electric, V , accelerating potentials.

Ordinarily electrical amplification is used to compensate for differences in isotope abundances in the gas being measured. Thus, for carbon dioxide all three Faraday collectors are used with relative signal amplification at $m/z = 44$, 45 , and 46 of 1: 91: 500 (since the normal abundance ratios $^{12}\text{C}/^{13}\text{C} \sim 91$, and $^{16}\text{O}/^{18}\text{O} \sim 500$). The amplified signals from all three detectors are thus comparable in intensity. Because of this feature, however, IRMS should only be used on gases with isotope composition close to natural abundance. Enriched material should not be used without careful recalibration since there is no guarantee of a linear response of electric signal to ion current for widely different isotope ratios.

As in whole molecule mass spectrometry, peak intensities in IRMS must be corrected for contributions from other isotopomer pairs. For example, using CO_2 as the analyte, three intensities are measured for carbon isotopic analysis because the contribution at $m/z = 45$ is the sum of $^{13}\text{C}^{16}\text{O}_2$ and $^{12}\text{C}^{16}\text{O}^{17}\text{O}$. The contribution from ^{17}O can be calculated from the one at $m/z = 46$ ($^{12}\text{C}^{16}\text{O}^{18}\text{O}$) taking the intensity ratio $^{17}\text{O}/^{18}\text{O} = 0.038/0.200 \sim 0.2$; the contributions at $m/z = 46$ from $^{13}\text{C}^{16}\text{O}^{17}\text{O}$ and $^{12}\text{C}^{17}\text{O}^{17}\text{O}$ are negligibly small. Similarly, for the measurement of sulfur isotope ratios using SO_2 as analyte the oxygen isotopic composition must be known in order to be able to deconvolute the $m/z = 66$ peak into its principal components, $^{34}\text{S}^{16}\text{O}_2$ and $^{32}\text{S}^{18}\text{O}^{16}\text{O}$. In order to avoid this complication SF_6 has

replaced SO_2 in many laboratories. The electron impact spectrum of SF_6 has its most intense peak at $m/z = 127$ corresponding to SF_5^+ . Isotope signals at 128, 129, and 131 m/z , can be used without correction to obtain ^{33}S , ^{34}S , and ^{36}S abundances, respectively, since natural fluorine is monoisotopic. An additional advantage of using SF_6 is that it is not strongly adsorbed on the walls of the spectrometer, and does not react with moisture or mercury. Thus sample-to-sample background and memory effects are negligible.

7.2.2.1 Sample Preparation

IRMS is a powerful technique because of its high precision which is typically $\sim 0.01\%$ but may be as good as $\sim 0.001\%$. The relative errors of IRMS isotopic ratios (σ_R/R) are usually much smaller than errors introduced by inaccuracies or imprecision in sampling, sample preparation, kinetic measurements, etc. and can frequently be ignored. Typically these latter errors sum to $\sim 0.05\%$ to $\sim 0.2\%$. A drawback, however, is that IRMS can be straightforwardly applied only to gaseous samples, most often carbon dioxide or nitrogen. For example, in studies on carboxylation and decarboxylation carbon dioxide can be isolated from the reaction mixture, purified, and used directly for IRMS analysis. This happy situation is, however, rather the exception than the rule, and usually conversion of a specific atom or atoms within the reactant or product molecule into an IRMS appropriate gas is required. That is usually not an easy task, and numerous methods have been elaborated that are usually specific to particular reaction systems. A more general approach, suitable for use on a wide variety of compounds, employs oxidation/reduction trains yielding nitrogen and carbon dioxide as gaseous products. Such systems usually contain several catalytic oxidation and/or reduction tubes which operate at high temperature. They are now available from many vendors and can be connected in-line with the IRMS instrument. Combustion trains can be coupled with chromatography to perform both molecular separation and isotope analysis directly. A typical set up is diagrammed in Fig. 7.11.

An important criticism of the use of combustion trains is that combustion is not site specific, that is all atoms in the analyte end up in the gas transferred to the IRMS. For studies of carbon isotope effects this is invariably CO_2 . The question is especially important for carbon isotope analysis because analyte molecules of interest usually contain several different kinds of carbon atoms and therefore combustion methods average or dilute the IE's of interest. Should site specific isotope ratios be required another method of sample preparation (usually much more tedious) is necessary. Combustion methods, however, are frequently used to study nitrogen and sulfur IE's because many organic molecules are singly substituted with these atoms. Obviously, oxygen isotope effects cannot be determined using combustion trains because external oxygen is employed. Rather some type of pyrolytic sample preparation is required.

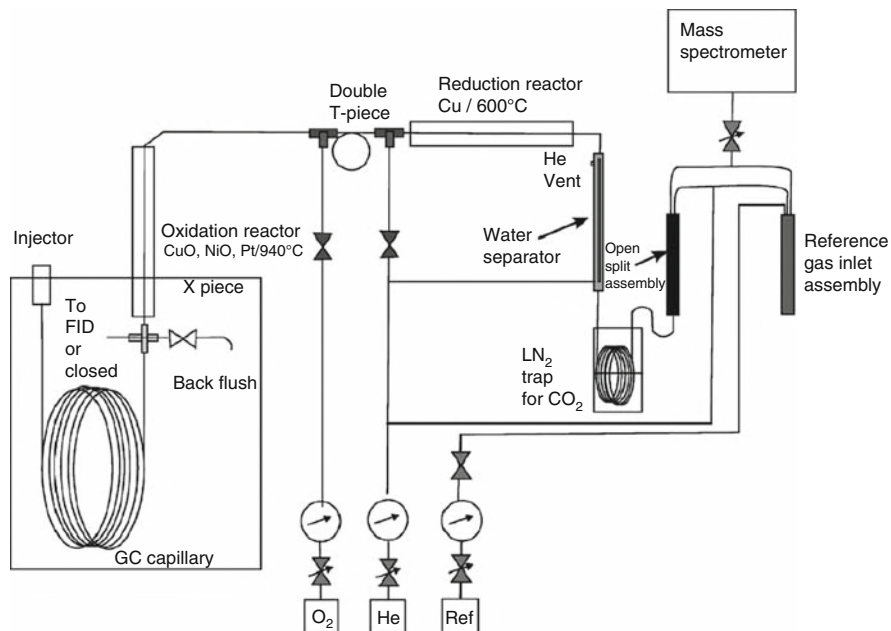


Fig. 7.11 On-line GC-combustion unit for isotope ratio determinations (Ghosh, P. and Brand, W. A. *Int. J. Mass Spectrom.* **228**, 1 (2003))

7.2.2.2 Remote Labeling for IRMS of Oxygen and Nitrogen IE's

An alternative way to obtain oxygen IE's is to take advantage of multiple isotope effects (see Sections 7.1.5 and 7.4). The method relates the isotopic composition of the atom of interest located at a specific position to an IE of another atom in the same molecule. The approach is called *remote labeling*. Remote labeling experiments are best explained using an example. Consider the *p*-nitrophenol anion:

Measuring the oxygen isotope ratio at the phenolic position is not an easy task. However, measurement of the nitrogen isotope ratio is straightforward, and one can use the on-line combustion – isotope ratio mass spectrometer setup (Fig. 7.11) to obtain $\delta^{15}\text{N}$ at high precision. The two compounds illustrated in Fig. 7.12 need to be synthesized. The structure on the left is 100% isotopically substituted with both ^{15}N and ^{18}O . That on the right is substituted with ^{14}N and ^{16}O . These molecules are then mixed. When using IRMS it is best to mix in a ratio close to natural abundance for nitrogen (Table 7.5), this is the so-called “pseudo-natural abundance”, which minimizes background errors. If the isotope composition were very different from natural abundance a small contamination of the sample from an external source, atmospheric air for example, would result in a large change in the $\delta^{15}\text{N}$ value. In the mixture every molecule that contains ^{14}N also contains ^{16}O , and similarly those containing ^{15}N also contain ^{18}O . Thus $\delta^{15}\text{N}$ for the gaseous sample of nitrogen obtained from the combustion line simultaneously reports the isotopic composition of

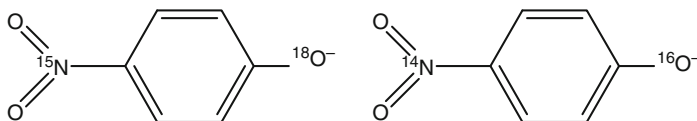


Fig. 7.12 Isotopically substituted *p*-nitrophenol anions

both nitrogen and phenolic oxygen. The nitrogen site is therefore called the “reporting” position although some years ago it was denoted the “remote” position, thus the name of this technique – “remote labeling.”

Two experiments are carried out. First KIE is determined for the reporting position (i.e., k_{14}/k_{15}), and then the same experiment is repeated using pseudo-natural abundance mixture. These measurements yield $k_{14,16}/k_{15,18}$ which is nicely approximated by Equation 7.31:

$$k_{14,16}/k_{15,18} = k_{14}/k_{15} \cdot k_{16}/k_{18} \quad (7.31)$$

Comparison of the results allows calculation of k_{16}/k_{18} . Obviously there are drawbacks to this procedure. The major one is the necessity of a costly and tedious isotopic synthesis of labeled materials. Optimally those compounds should be as close as possible to 100% enriched. This can seldom be achieved and using partially enriched samples requires substantial corrections to the raw data and increases experimental uncertainty. A rule of thumb used in remote labeling experiments is that the remote (reporting) position should be reasonably far from the reaction center (the phenolic oxygen in the present example). For the case where there is no isotope effect at the reporting site (e.g. no ^{15}N -KIE), the “double-label experiment” leads directly to the isotope effect of interest. This is more probable when the reporting site is remote, (i.e. well isolated from the reaction coordinate).

Although the multiple isotope method is most frequently used with stable isotopes (for example studies of oxygen KIE's in biophosphates used ^{15}N at a remote nitro group, or ^{13}C on a remote carboxy group, as reporting isotopes), the technique is not restricted to stable isotopes; radioisotopes have been used as reporting sites for stable isotopes. In a practical sense this is the only method that allows the measurement of isotope effects for elements that have only one stable isotope (e.g. fluorine and phosphorus). In these cases doubly radiolabeled material is used (see Section 7.4).

7.2.2.3 Cavity Ring-Down Spectroscopy

Zare and coworkers (2009) have recently discussed a continuous flow ring down spectroscopy system integrating chromatographic separation, a catalytic combustor, and an isotopic $^{13}\text{C}/^{12}\text{C}$ optical analyzer which conveniently yields $\delta^{13}\text{C}$ values at a precision nearing that for IRMS. A modification yields δD and $\delta^{15}\text{N}$ values.

7.3 NMR Measurements of Isotope Effects; Isotope Effects on NMR Spectra

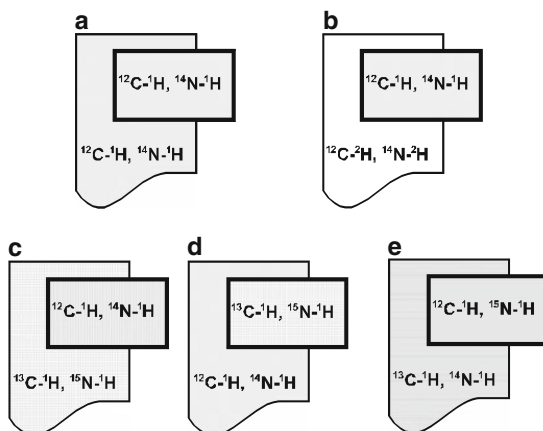
NMR (Nuclear Magnetic Resonance) is arguably the most widely used instrumental method in chemistry. Isotope substitution affects NMR spectra in several ways, each of which extends the usefulness of the NMR technique. In discussing IE's on NMR spectra it is important to distinguish between three areas. The first has its origin in the differences of the nuclear magnetic properties of isotopes. For example, the nuclear magnetic spins of ^{16}O , ^{17}O , and ^{18}O are 0, $5/2$, and 0, and for ^{12}C and ^{13}C are 0 and $1/2$ spin units, respectively. Thus neither ^{12}C , ^{16}O , nor ^{18}O show an NMR spectra, but ^{13}C and ^{17}O do. Similarly the nuclear spins of ^1H , $^2\text{H(D)}$, and $^3\text{H(T)}$ are $1/2$, 1 and $1/2$, in that order. Isolated atom NMR frequencies relative to $^1\text{H} = 100$ are D = 15.4, T = 106.7, $^{13}\text{C} = 25.1$ and $^{17}\text{O} = 13.6$. Changes in NMR spectra due to such magnetic differences are extremely useful. For example judicious substitution of H by D removes signals of the replaced proton(s) from the ^1H spectrum and collapses (simplifies) the multiplet pattern due to much smaller coupling with the D nuclei. The $^2\text{H(D)}$ spectrum is shifted far down field and does not interfere with that part of the spectrum due to unsubstituted ^1H . Similarly ^{13}C enrichment splits resonances of the $^{13}\text{C}/^1\text{H}$ coupled protons in the ^1H spectrum. However these magnetic isotope effects in NMR, although important and interesting, are peripheral to our interests. The second kind of NMR isotope effect is consequent to the effect of isotopic mass differences on NMR spectra, for example differences in chemical shielding or coupling constants caused by isotopic differences in vibrational frequencies and rms amplitudes. Such rovibrational NMR IE's are analogous to other types of kinetic and equilibrium IE's described in other chapters. They are discussed in Chapter 12. The third area of interest is the exploitation of NMR as a widely available analytical tool to employ for measurements of IE's.

7.3.1 *Isotope Labeling in NMR Investigations of Molecular Structure*

An excellent example of the use of isotope labeling in NMR spectroscopy is in its application to studies of protein structure and protein–ligand interaction. Such studies are of prime importance for drug screening and drug design. Consequently this field of research has been supported by drug companies.

An important difficulty in NMR studies of protein–ligand interaction is the spectral complexity including (but not limited to) overlap of the ligand and protein resonances. If the protein–ligand binding is relatively weak, and the rate of exchange is fast compared to the various NMR timescales, the observed spectrum will be the weighted average of the spectra of the free and bound states, and will reflect changes induced by the binding. However for tight binding (slow exchange) separate spectral peaks will be observed for free and bound ligands. Information concerning the binding can only be obtained from the spectrum of the bound state which will probably

Fig. 7.13 The use of NMR isotope labeling to select signals from either ligand (small box) or protein (large box) for studies on drug interaction (After Roberts, G. C. K., *DDT (Drug Discovery Today)* **5**, 230 (2000))



overlap the protein spectrum. This problem can be overcome straightforwardly by judicious labeling with stable isotopes such as ^{13}C , ^{15}N , and/or ^2H (D), together with “isotope editing” experiments. Even when exchange is fast, isotope labeling can be helpful. The idea is a simple one and consists of nothing more than isotope substitution on either protein or ligand in order to either shift, enhance, or eliminate that part of the spectrum, and in that way to deduce structural information. Isotope effects on the structure, if any, are ignored. The scheme is outlined in Fig. 7.13. The use of isotopically enriched growth media to prepare labeled recombinant proteins in bacteria or yeast is now commonplace, and is even possible for proteins produced in mammalian cells. It is very often more convenient to label the protein instead of the smaller ligand (drug) molecule.

A simple extension of the technique outlined in Fig. 7.13 is chemical shift mapping. In its simplest form it is based on two-dimensional heteronuclear correlation measurements. For (^1H - ^{15}N) correlations, for example, one obtains a two-dimensional NOE (Nuclear Overhauser Effect) spectrum containing one cross peak for each amide in the protein at a position characterized by its ^1H and ^{15}N chemical shifts. The spectrum therefore contains one signal for each amino acid residue plus additional signals from the side chains of asparagine and glutamine. Once the ligand is introduced, the signals characterizing the binding site will change position according to the change in structure. Addition of a second or third isotope label allows extension of the correlation patterns to three or more dimensions. Again, isotope effects on the structural parameters are ignored. A few of the many possible labeling patterns are illustrated in Fig. 7.14.

7.3.2 Rovibrational NMR Isotope Effects

The second kind of NMR isotope effect has its origin in the mass differences between isotopes. In NMR mass effects show up as isotopic differences in NMR shielding constants and coupling constants. Their theoretical rationalization is

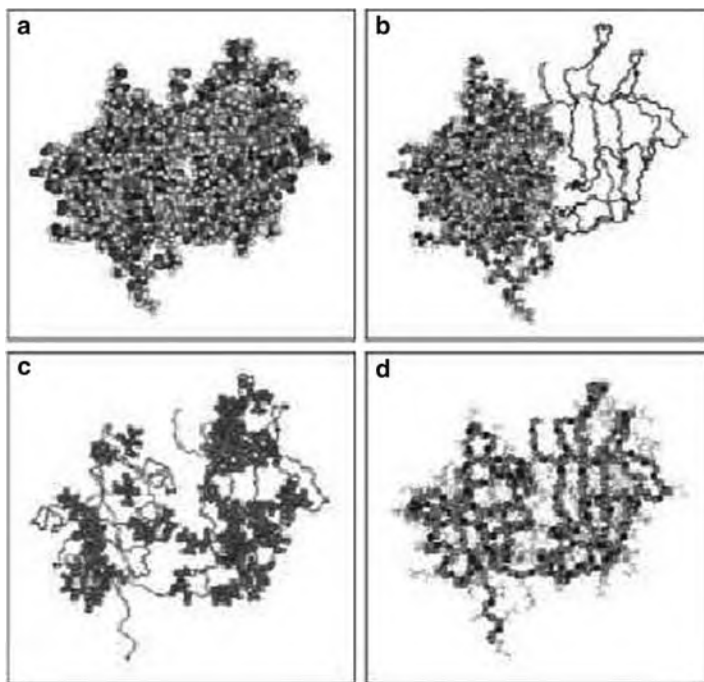


Fig. 7.14 Some different NMR isotope labeling strategies: (a) global protein labeling (^{15}N , ^{13}C , ^2D); (b) domain specific labeling (most useful for large targets); (c) amino acid specific labeling; (d) position specific labeling (non-exchangeable protons substituted by deuterons) (Reprinted with permission from Heller, M. and Kessler, H, *Pure Appl. Chem.* **73**, 1429 (2001))

fundamentally rotational–vibrational (rovibrational) in origin, and most theoretical treatments begin by introducing the effective change in molecular geometry and molecular wave functions due to IE's on vibrational averaging.

The rovibrational origin of NMR isotope differences in chemical shifts is a consequence of the fact that more lightly substituted atoms show larger amplitude motions than the heavier (see Section 12.4 for a more thorough discussion). Consequently isotopic substitution alters the magnetic shielding about the substituted nucleus (a primary isotope effect), and changes shielding at other (nearby) nuclei (a secondary isotope effect). For example one might measure an H/D primary isotope effect on the ^1H and ^2H (D) chemical shifts for methane, $\sigma(^1\text{H})$ and $\sigma(^2\text{H})$, and compare that result with the isotope effect on the chemical shift at hydrogen due to $^{13}\text{C}/^{12}\text{C}$ substitution at the carbon atom (a secondary isotope effect). It makes no sense to speak of a primary isotope effect on the carbon chemical shift because ^{12}C has zero nuclear magnetic moment. Similarly the nuclear spin coupling due to the spin-spin magnetic interaction between the ^{13}C and ^1H , or ^{13}C and ^2H nuclei can be formally expressed as either primary or secondary isotope effects, but isotope effects on coupling constants are extremely small. Table 7.7 reports some NMR chemical shifts and coupling constants for isotopically substituted methane, and these results are compared with rovibrational theory in Section 12.4.2.1.

Table 7.7 Isotope effects on NMR spectra of isotopically substituted methane

	Screening constants (chemical shift)	Coupling constants
Proton NMR ^a	¹ Hσ (ppb) ^c	
¹² CH ₄	0 (Reference)	
¹² CH ₃ D	14.9	
¹² CH ₃ D ₂	29.7	J _{HD} = -1.93 Hz
¹² CHD ₃	44.2	J _{DD} = -0.29 Hz
¹² CD ₄	-	
¹³ C NMR ^{a,b}	¹³ Cσ (ppb)	
¹³ CH ₄	0 (Reference)	
¹³ CH ₃ D	187	
¹³ CH ₃ D ₂	385	J _{13CH} = 125 Hz
¹³ CHD ₃	579	J _{13CD} = 19.2 Hz
¹³ CD ₄	774	

^aAnet, F. A. L. and O'Leary, D. J. *Tetrahedron Lett.* **30**, 2755 (1989). Measurements at ~500 MHz

^bAlei, M. and Wageman, W. E. *J. Chem. Phys.* **68**, 783 (1978) Measurements at ~25.2 MHz

^cppb = parts per billion

The NMR theory of rovibrational averaging successfully explains the general empirical trends observed for NMR chemical shift isotope effects. (1) Substitution with a heavier isotope shifts the NMR signal of a neighboring nucleus to lower frequency (greater shielding). (2) The isotope shift decreases with distance. (3) The isotope shift is largest where the fractional mass change is greatest. Thus shifts on substitution of ¹³C for ¹²C, or ¹⁸O for ¹⁶O, are proportionally smaller than ²H(D) for ¹H.

Chemical shift isotope effects of non-exchanging or slowly exchanging atoms or groups provide an excellent method for assigning NMR signals. An example is shown in Fig. 7.15a which reports ¹³C NMR of dry partially deuterated glycerol dissolved in DMSO-d₆. The compound was prepared by placing DMSO-h₆ in a 1:1 H₂O/D₂O mixture then drying so that half the hydroxyl is now OH and half OD. In the proton decoupled ¹³C spectrum the carbons within three bonds of a D are shifted upfield by an isotope effect and their signals are split. The central carbon (C(2), left side Fig. 7.15a), at 74 ppm experiences one β shift (next nearest neighbor interaction) and two γ shifts (next-next nearest neighbor interactions), while the terminal carbons (right side) only experience one β shift. The extreme left hand line of each carbon signal arises from molecules containing only OH, and the extreme right from those containing only OD. The triplet signals for the terminal carbons result from the 1:2:1 mixture of terminal hydroxyls, (OH)₂, (OH,OD), (OD)₂. Isotope shifts like these provide a useful diagnostic tool, but, unfortunately, they are quite small and the method is only useful with high field instruments.

A second example of a study exploiting chemical shift isotope effects is shown in Fig. 7.15b which reports ¹H, ²H and ¹⁹F low temperature NMR spectra of the

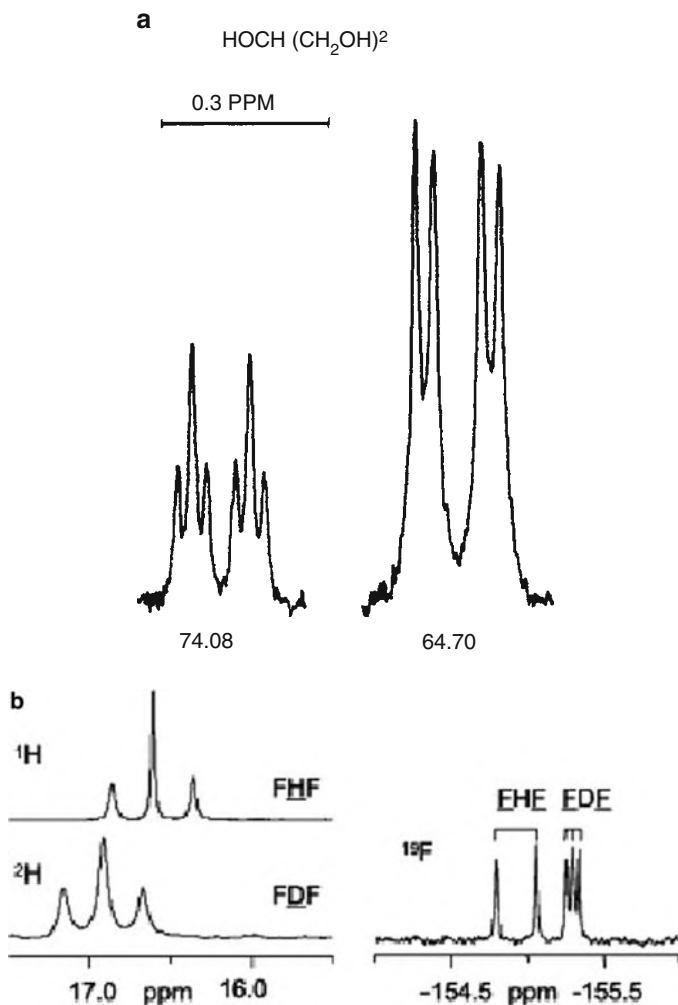


Fig. 7.15 (a) ¹³C NMR resonances of a dry DMSO-d₆ solution of glycerol containing equal number of OH and OD groups (see text). Reuben, *J. J. Am. Chem. Soc.* **107**, 1756 (1985). (b) ¹H, ²H and ¹⁹F NMR spectra of a solution containing partially deuterated (C₄H₉)₄N⁺ (FL)_nF⁻ dissolved in CDF₃/CDF₂Cl at 130 K. The deuterium fraction was about 0.5. Note the H/D primary isotope effect on the chemical shift (*left hand side*) and the isotope effect on the splitting of the ¹⁹F NMR signal (*right hand side*) (Reprinted with permission from Shendarovich, G., Limbach, H. H., et al. *Phys. Chem. Chem. Phys.* **4**, 5488 (2002), copyright 2002, Royal Society of Chemistry)

(FLF)⁻ (L = H or D) anion in low temperature solutions of (C₄H₉)₄N⁺ (FL)_nF⁻. The authors were able to determine zero-, one-, and two-bond, H/D isotope effects on hydrogen and fluorine NMR chemical shifts for the series n = 1 to n = 3, and to relate the observed spectra to H/D isotope effects on the hydrogen bond geometries. Isotope effects on spin-spin L-F and F-F coupling ¹³C constants were reported.

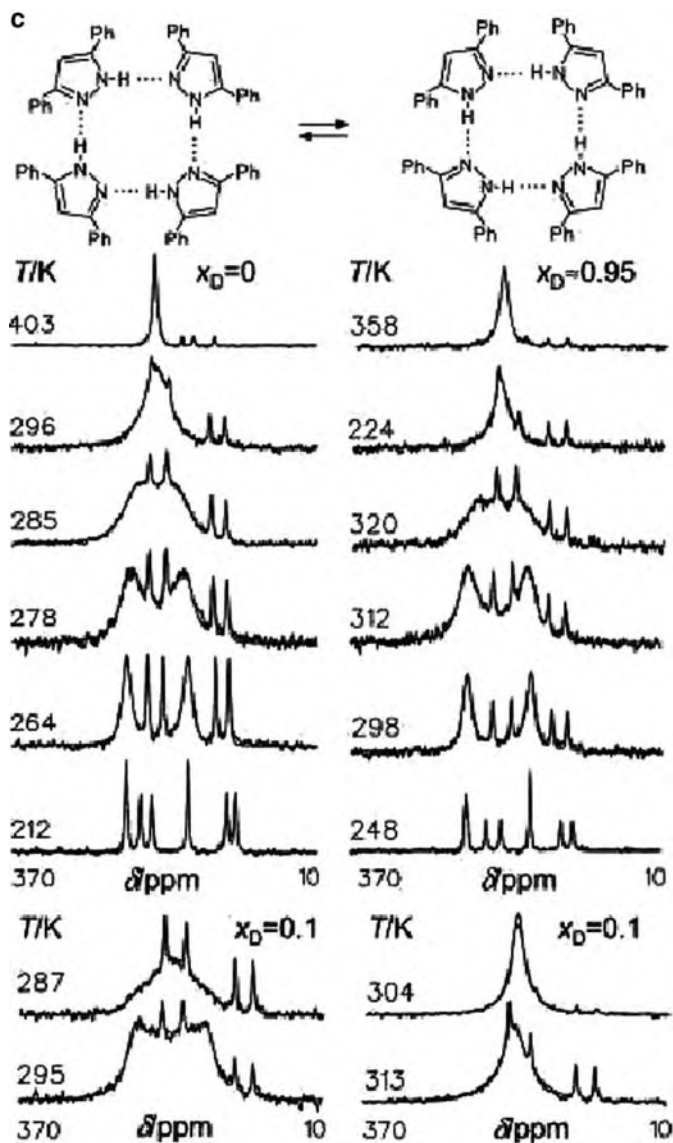


Fig. 7.15 (continued) (c) Superposed experimental and calculated 30.41 MHz (7 T) ^{15}N NMR spectra of ^{15}N enriched DPP at different temperatures and deuterium fractions x_D in the mobile sites. The four sharp lines with temperature dependent positions stem from a small quantity of ^{15}N labeled tetramethyltetraaza-[14]annulene reference in a separate capsule (Klein, O., Limbach, H. H., et al. *J. Am. Chem. Soc.* **126**, 11718 (2004))

7.3.2.1 NMR Studies of Fast Exchange IE's

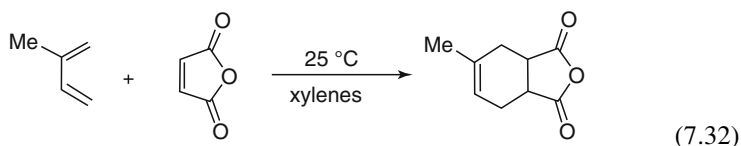
For NMR studies of hydrogen bonding, complex formation, and fluxional or conformational equilibrium the situation is more complicated. When the exchange occurs at a fast rate on the NMR timescale, only an average spectrum is observed with averaged values of nuclear shielding. Often, however, the populations of the equilibrating states show marked temperature or medium dependences and when the exchange rate is slowed to rates comparable to the NMR time constants the peaks broaden, then split. Line shape analysis can be used to deduce the kinetics and KIE's of the exchange process. The example shown in Fig. 7.15c reports H/D isotope effects on the cyclic hydrogen-bond exchange in the tetramer of ^{15}N labeled polycrystalline 3,5-diphenylpyrazole (DPP). For this study solid state ^{15}N NMR methods were employed. The H/D labeling was restricted to the hydrogen bonding (N-H ... N) positions. Rate constants for the cyclic H or D exchange (Fig. 7.15c) were measured on the millisecond timescale by line shape analysis of the doubly labeled ^{15}N compounds. The Arrhenius curves are nonlinear and indicate tunneling at low temperatures.

7.3.3 *NMR as an Analytical Tool; NMR Measurements of Carbon IE's*

The third area in our brief review of NMR focuses on the fact that modern NMR technology can provide both quantitative and position-specific information on isotope fractionation, and this without an elaborate work up of the reaction mixture. Compare such results with those of IRMS where laborious selective degradation (carefully avoiding isotope fractionation) into small molecule analytes (like CO_2) is required before isotope analysis can even begin. As an example we consider the application of NMR analysis to certain carbon KIE's. Until recently NMR measurements of $^{12}\text{C}/^{13}\text{C}$ fractionations near natural abundance (1.1%) were unreliable. Uncertainties caused by low natural abundance of ^{13}C coupled with the inherently low precision of NMR integrations of peak intensity nearly equal or even exceed the KIE being measured. The resolution of this difficulty takes advantage of the fractional enrichment of slower (isotopically heavier) molecules remaining in the reactant mixture at high conversion (i.e. the overexpression of isotopic fractionation at high conversion, see Equations 7.23 and 7.24 and Fig. 7.4). For example at a fraction of reaction, $f = 0.99$, for $\text{KIE} = 1.05$, beginning with natural abundance material, the $^{13}\text{C}/^{12}\text{C}$ ratio in the remaining substrate is 1.25, which is sufficiently large to permit precise measurement using ^{13}C NMR. In addition to careful NMR measurements the method also requires high precision analysis of the fraction of reaction, because at high conversion the dependence of R_S/R_{0S} on f is very steep (Fig. 7.5). Studies using both ^2H and ^{13}C NMR have been reported but the former

are handicapped because the low natural abundance of $^2\text{H}(\text{D})$, 0.02%, makes an initial isotope enrichment of starting material advisable.

As an example of this technique we consider $^{12}\text{C}/^{13}\text{C}$ isotope effects in the Diels–Alder condensation of isoprene and maleic anhydride (Equation 7.32). The terminal carbons of isoprene carbons are numbered 1 and 4, the methyl substituted carbon is number 2. The reaction proceeds via a concerted and slightly asynchronous mechanism.



After reaction to $f = 0.989$ the reaction was stopped and unreacted isoprene analyzed for isotope enrichment. The methyl group was selected as an internal standard under the assumption it remains unchanged during reaction because it is not involved in either bond breaking or bond making. Results are shown in Table 7.8 and clearly demonstrate that only the terminal CH_2 groups of isoprene are involved in the rate limiting step. In agreement with theoretical calculations based on Gaussian 94 the experiments suggest the methyl group introduces a small asynchronicity into the transition state.

Although natural abundance NMR analysis of KIE's offers great potential for studying reaction mechanisms there are limitations. Relatively large amounts of material are required because sufficient unreacted starting material must be recovered for NMR analysis at fractions of reaction approaching unity. The reactions to be studied must be irreversible, and the mechanism must not change as the reaction proceeds. On the other hand, the advantage of using natural abundance material and avoiding labeling steps and/or isotope synthesis is appealing. Also NMR measurements are insensitive to impurities as long as their signals do not overlap with those of the measured compound. Finally and most powerfully, NMR analysis allows the determination of isotope effects on several (or many) positions in a single sample without necessitating laborious site-specific degradation. Since, however, a

Table 7.8 NMR measurements of $^{12}\text{C}/^{13}\text{C}$ fractionation of unreacted isoprene undergoing reaction 7.32 (Singleton, D. A. and Thomas, A. A.; *J. Am. Chem. Soc.* **117**, 9357 (1995))

Carbon atom	Isotope fractionation	$k(^{12}\text{C})/k(^{13}\text{C})$ from Equation 7.23
CH_3	[1.000]	[1.000] assumed
1	1.103(11)	1.022(3)
2	1.005(9)	1.001(2)
3	0.999(15)	1.000(3)
4	1.077(14)	1.017(2)

Standard deviations in parentheses.

point of reference is necessary for each position, the NMR signal from a reference atom expected to undergo little or no isotope fractionation has to be selected as an “internal standard”. Thus all kinetic isotope effects measured by NMR carry a small systematic error corresponding to the KIE, if any, at the reference site. This problem may be minimized by referencing the measurement to an external standard or to a far-distant site introduced by chemical derivatization.

7.4 Radioisotopes

Isotope effect studies using radioisotopes are sometimes convenient. Some elements, fluorine and phosphorus for example, have only one stable isotope, and the determination of isotope effects for them is only possible with radioisotopes.

An interesting way to determine IE's using radioactivity is by comparing rates of reaction for a particular compound labeled (on separate samples) with two different radioisotopes. A good example might be the determination of an $^{11}\text{C}/^{14}\text{C}$ kinetic isotope effect, taking advantage of the very large difference in the half lives of these two species (20.4 min and 5,730 years, respectively, Table 7.5). The reaction is started by mixing the ^{11}C substrate, immediately after its preparation, with previously synthesized ^{14}C substrate and other reactants as required. Samples are withdrawn at convenient intervals, separated into reactant and product fractions by chromatography, and the total radioactivity (^{11}C plus ^{14}C) obtained by liquid scintillation counting. After decay of the ^{11}C activity (typically overnight), the sample is counted again to obtain the ^{14}C activity. ^{11}C radioactivity is calculated from the difference after correction for radio-decay. The advantages of this simple and straightforward analytical technique, however, scarcely overbalance the enormous synthetic and handling problems connected with the preparation of materials labeled with short-lived isotopes like ^{11}C .

An alternative approach takes advantage of the different decay energies of radioisotopes. Figure 7.16 shows an example where $^3\text{H(T)}$, ^{14}C , and ^{32}P , activities are simultaneously counted by taking advantage of the difference in their decay energies. The separate kinetics for each isotope are followed in appropriate (energy specific) channels of the liquid scintillation counter (LSC). Obviously for measurements of isotope effects in the absence of double radio-labeling for each element the reaction rates of the stable isotopes (^1H , ^{12}C , or ^{31}P in the present example) must be determined by another technique.

7.4.1 Errors

In LSC measurements precautions are required to avoid impurities which may cause scintillation quenching. Since radioactive decay is random and is described with the Poisson distribution, the standard deviation for a given count, C , is equal to $C^{1/2}$.

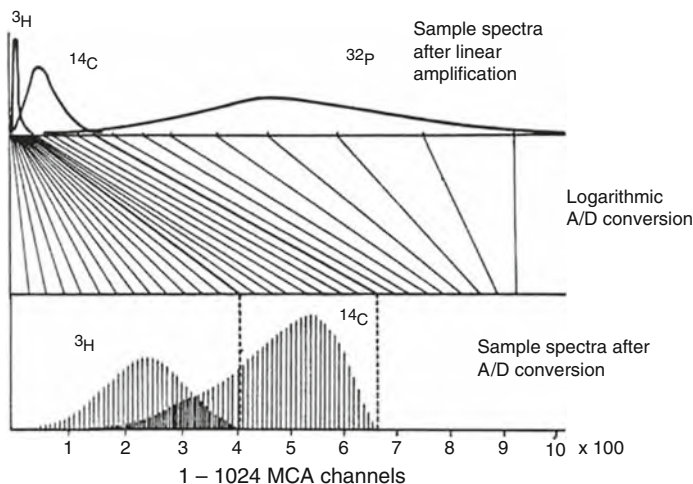


Fig. 7.16 Separate radioisotope counting using LSC spectrometry from LKB Instruments (Manual 1214/1219, LKB Australasia)

Thus the counting rate should be sufficiently high to ensure a precision sufficient for isotope effect measurements; a target precision of 0.1% is obtained for total counts of $\sim 10^6$. Radiolabeled material used for isotope effect measurements usually has counting rates of $\sim 15,000$ counts per minute (cpm). To achieve 0.1% precision such samples must be counted for 8 h or more. More often counting time is limited to several cycles of about 10 min each with a commensurate increase in the statistical error.

The most frequently used combination of radioisotopes in double labeling experiments is tritium and ^{14}C . Ideally the ratio of the activities in the corresponding channels (Fig. 7.16) should be high enough to insure the carbon counts in the tritium channel are negligible compared to tritium counts. Usually this is not achieved and a correction must be applied.

7.5 Equilibrium Isotope Effects

7.5.1 Fractionation Measurements

The experimental determination of isotope fractionation factors on chemical equilibria is completely analogous to the methods used for measuring kinetic isotope effects. In brief this amounts to quenching an equilibrated mixture, separating reactant from product, and analyzing either or both by IRMS, spectroscopy, chromatography, NMR or some other technique of convenience. Equilibrium isotope effects, broadly speaking, are usually smaller than kinetic isotope effects. Thus, the demands on experimental precision are somewhat greater, but the essentials of the analytical procedures and instrumentation remain the same.

7.5.2 Studies Using Separated Isotopes

7.5.2.1 Vapor Pressure Isotope Effects

The vapour pressure isotope effects (VPIE) is a particularly important equilibrium measurement because it directly compares isotope effects on free energies in the condensed phase to those in the dilute gas reference state. VPIE's are generally small, typically no larger than a percent or so per H/D atom substituted, for heavier isotopomer pairs as small as a few parts in 10^4 , and it is advisable to employ difference methods. Exacting attention to temperature control, transducer stability and sensitivity, and to chemical and isotopic purity is necessary. Figure 7.17a is a schematic diagram of a typical apparatus used to measure VPIE's at high precision. This particular configuration was employed in studies of VPIE's of deuteromethanes and solutions of protio- and deuterio- methanes, including measurements of the excess free energies of solution (straightforwardly obtained from measurements of excess vapor pressures). Figure 7.17a specifically refers to an experiment to measure pressure differences between CH_4 and CD_4 (and/or CH_4/CD_4 mixtures) using the right-hand and left-hand pressure transducers, respectively. It is possible to monitor, simultaneously, the two differences (double differential method) and, thus, to obtain excess vapor pressures with unprecedented precision. The transducers are differential capacitance manometers. The three sample cells are contained in a common massive and well thermostatted copper block ($\sim \pm 0.001$ K) which is surrounded by an adiabatic shield, and temperature differences between the samples are held to 0.1 mK or less. The total pressure of CH_4 is measured with the quartz spiral manometer shown at the lower center. Other kinds of pressure measuring devices can and have been used, replacing the differential capacitance and/or quartz spiral manometers. The transducers are thermostatted at a higher temperature than the sample block in order to prevent condensation outside the sample cells. The temperature of the copper block is read with a resistance thermometer. Gas handling lines and other necessary auxiliaries are not included in the diagram.

The precision obtained in measurements of this kind is impressive. It is illustrated for our example (CH_4/CD_4) in Table 7.9 and amounts to a few parts in 10^5 on the total pressure, equivalent to a few parts per thousand on VPIE (which scales approximately as $\ln(P'/P) \sim (\Delta P/P)$). Of course for excess free energy IE's in mixtures of isotopomers, or for VPIE's of heavier isotopomer pairs, both markedly smaller, the relative error is commensurately larger. Thus for the excess free energy of CH_4/CD_4 mixtures at 100 K, which is at most 0.6 J/mol (equivalent to $\Delta P/P = 7 \times 10^{-4}$), the relative error increases to $\delta(\Delta P/P)/(\Delta P/P) \sim 6 \times 10^{-2}$. Similarly the VPIE for $^{36}\text{Ar}/^{40}\text{Ar}$ at 100 K amounts to $\Delta P/P = 0.0041$, and the precision of measurement, $\delta(\Delta P/P)/(\Delta P/P) \sim 1 \times 10^{-2}$, compares favorably with that obtained from single stage fractionation measurements employing high precision IRMS for analysis (see below).

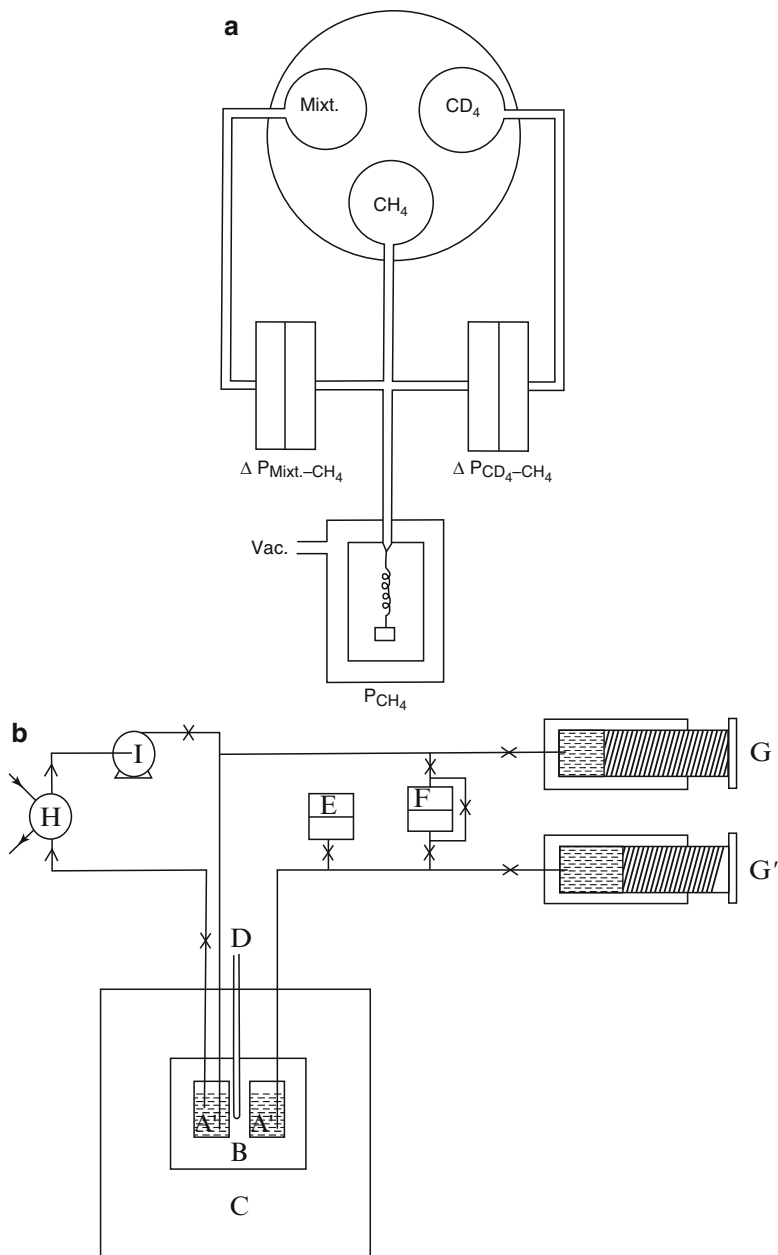


Fig. 7.17 (a) Double differential apparatus used for VPIE measurements (see text) (Jancso, G., Rebelo, L. P. N. and Van Hook, W. A. *Chem. Rev.* **93**, 2645 (1993)). (b) Differential PV apparatus for isotope effect studies (see text) (Kooner, Z. and Van Hook, W. A.. *J. Phys. Chem.* **90**, 4860 (1986))

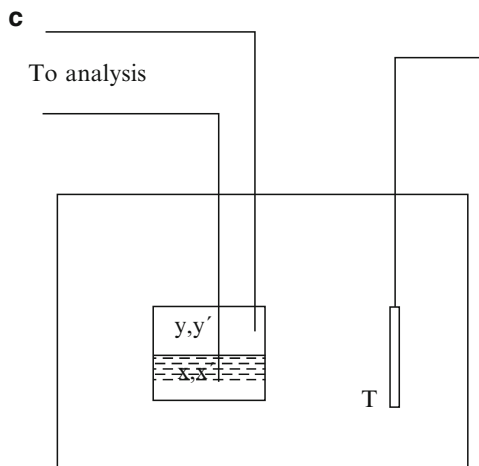


Fig. 7.17 (continued) (c) A one plate liquid–vapor isotope fractionation experiment (Jancso, G., Rebelo, L. P. N. and Van Hook, W. A. *Chem. Rev.* **93**, 2645 (1993))

Table 7.9 Precision of measurement for CH_4/CD_4 VPIE's at three temperatures (Calado, J. C. G. et al. *J. Phys. Chem.* **93**, 3355 (1989))

T/K	P(CH_4)/kPa	$\Delta\text{P}/\text{P}$	$\delta(\Delta\text{P}/\text{P})$	$\delta(\Delta\text{P}/\text{P})/\Delta\text{P}/\text{P}$
95.06	20.006	0.01602	4×10^{-5}	2.5×10^{-3}
105.25	57.739	0.02456	4×10^{-5}	1.6×10^{-3}
121.53	213.42	0.03172	2×10^{-5}	0.6×10^{-3}

$\Delta\text{P}/\text{P} = [\text{P}(\text{CH}_4) - \text{P}(\text{CD}_4)]/\text{P}(\text{CH}_4)$

7.5.2.2 PVT Isotope Effects for Liquids, Vapors, and VPIE at LV Equilibrium

A somewhat different PV apparatus is shown schematically in Fig. 7.17b. Two closely matched stainless steel vessels of nominal volume 25 cm^3 are mounted in a massive copper block contained in a high precision thermostat ($\sim \pm 1 \text{ mK}$) over the range ($25 < t/^\circ\text{C} < 300$). Samples are loaded into the cells from a pair of carefully matched high pressure screw injectors, and pressure and differential pressure transmitted to the transducers through those same lines. During a VPIE measurement the cells are kept nearly full of liquid to minimize the amount of material in the vapor phase, which is important for experiments on solutions. The screw injectors are precision machined from stainless steel and permit the amount of material in the cells and pressure measuring network to be obtained to $\sim \pm 10^{-3} \text{ cm}^3$. The absolute pressure of one cell and the differential pressure between cells are measured by zero-displacement quartz oscillator transducers. For solution measurements the material in the cell is mixed using a low-volume, high-pressure pump of the kind used

in liquid chromatography. An injection valve is included in the loop so that aliquots of solute can be added to the solution. For molar volume and compressibility studies the degassed samples are fed from the screw injectors to the measuring cells. As the cells fill the pressure jumps abruptly from the equilibrium vapor pressure to a higher value. Continued injection of liquid allows the liquid phase compressibility to be determined, and the intersection between the steep and flat parts of the curve defines the amount of liquid required to just fill the cell and permits calculation of the orthobaric liquid molar volume. This general design permits measurement of isotope effects on vapor pressure, and liquid and vapor phase molar volumes, compressibilities, and thermal expansivities, and vapor phase virial coefficients.

7.5.3 *Liquid–Vapor Isotope Fractionation Measurements*

Figure 7.17c schematizes a one plate liquid–vapor isotope fractionation (LVIF) experiment designed to measure the concentration ratio of two isotopomers in each of two coexisting phases, for example liquid (x/x') and vapor (y/y'). The LVIF factor is $\alpha = (y/y')/(x/x')$, x and x' , and y and y' , are liquid and vapor mole fractions respectively. The temperature is measured with a resistance thermometer, T , and liquid and vapor samples are removed through capillary tubing for IRMS (or some other kind of) analysis. The demands on sample purity, vacuum integrity, and temperature stability are less stringent for LVIF measurements than they are for VPIE. It is important to ensure good equilibrium between phases (i.e. adequate boil-up) while at the same time scrupulously guarding each phase from contamination with the other (i.e. from splash). This becomes increasingly difficult as pressure drops, and as a general rule LVIF measurements at pressures less than, say, 10–50 kPa are impractical. At higher pressures experimental precision for LVIF is principally determined by statistical uncertainty in the IRMS analysis. At low enough pressure $\ln \alpha \sim \text{VPIE}$ plus a small correction. Thermodynamic expressions for the correction are developed in Chapter 5.

7.5.4 *Isotope Effects on Liquid–Liquid Equilibria*

Liquid–liquid (LL) miscibility is an important topic with impact on separation and extraction processes. In particular, it is one of the central topics in polymer science because the physical properties of polymer solutions and blends depend sensitively on phase equilibria in the mixture. Figure 7.18a diagrams the effects of molecular weight, pressure, and/or isotope (H/D) substitution on LL phase diagrams of polymer/solvent systems showing both upper and lower branches (see Chapter 5). By lowering pressure, increasing solvent D/H ratio, or increasing solute MW one decreases miscibility in the sequence “dotted – solid – dashed – dash-dot”. The kind of instrument employed to map such phase diagrams is schematized in Fig. 7.18b.

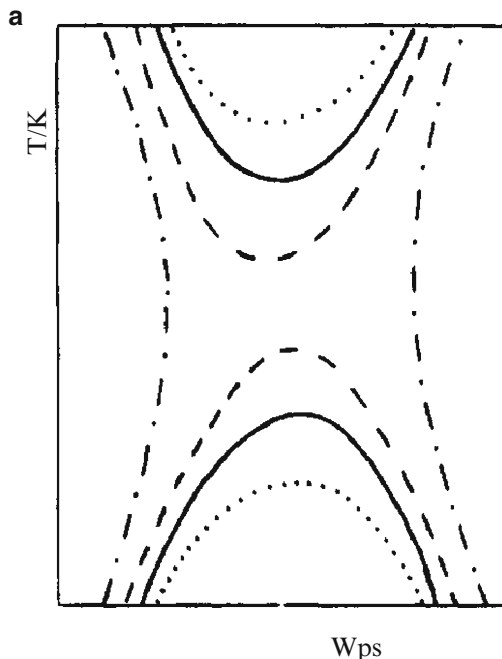


Fig. 7.18 (a) Schematic showing effects of molecular weight and/or pressure and/or H/D substitution on LL demixing phase diagrams with both upper and lower branches. Temperature is plotted vs. concentration W_{ps} , (weight fraction). By lowering pressure, increasing solvent D/H ratio or raising solute MW the miscibility decreases in the succession shown by the *dotted* – *solid* – *dashed* – *dash-dot* lines. The areas below the lower, and above the upper, *dotted*, *solid*, and *dashed* lines represent two phase regions, the areas between those same lines are one phase regions. The area between the *dashed-dotted* lines is a two phase region (Luszczyk, M., Rebelo, L. P. N. and Van Hook, W. A. *Macromolecules* **28**, 745 (1995))

Demixing transitions (cloud points) are detected optically. Light from a 5 mW He–Ne laser is transmitted through an optical cable and enters the thermostatted pressure cell through a sapphire window. The transmitted light at 180° nominal geometry exits via a second sapphire window into the central portion of a bifurcated optical cable to a light dump. Scattered light falls on the outer portion of the optical cable (180°) or onto a separate cable (90°) and is fed to silicon photodiode detectors. The experiment begins in the homogeneous region (toward the center of Fig. 7.18a). By raising or lowering pressure, or raising or lowering the thermostat temperature, one moves from the central one phase region into one or the other of the two phase regions, all the while monitoring transmitted and scattered light intensity, temperature and pressure. It is rather more convenient and certainly more efficient to vary pressure (isothermally) than it is to vary temperature (isobarically). The macroscopic manifestation of the formation of a daughter phase in a phase transition is solution turbidity (the so-called cloud-point). Thus, at the phase transition, scattered light intensity increases dramatically and transmitted intensity falls. Plots of scattering

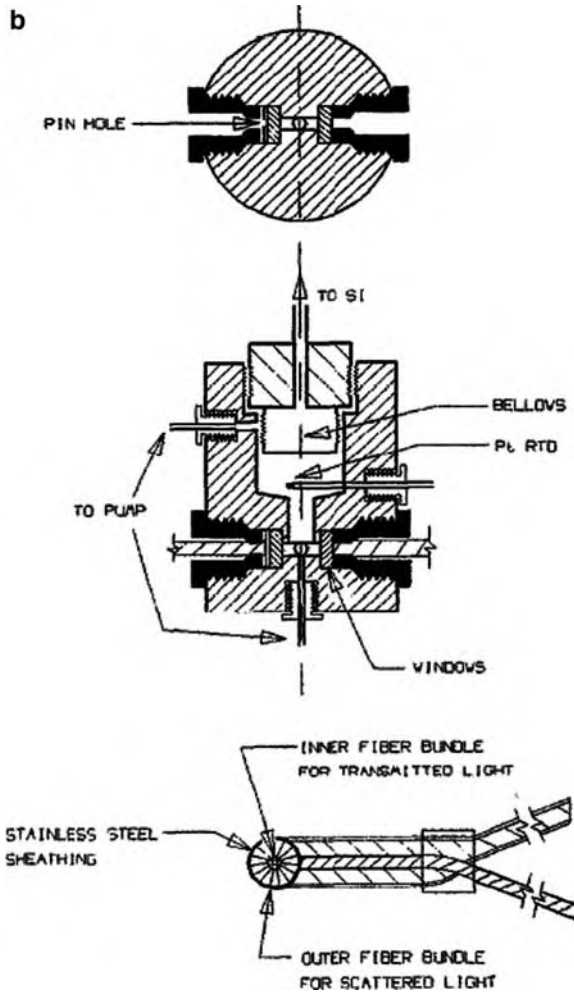


Fig. 7.18 (continued) (b) High pressure cell for detection of LL demixing by light scattering (Reused with permission from Szydłowski, J., Rebelo, L. P. N. and Van Hook, W. A. *Rev Sci. Ins.* **63**, 1717 (1991))

intensity define the cloud point and operational spinodal using the Debye theory of light scattering.

7.5.4.1 Demixing of Polymer Blends

The kinetics of polymer/polymer demixing are many orders of magnitude slower than those for polymer/solvent demixing. In a typical instrument used to study blend demixing a polymer film supported on a thin glass cover slip is placed in a thermostatted pressure cell (Fig. 7.18c). The sample is annealed for some hours well

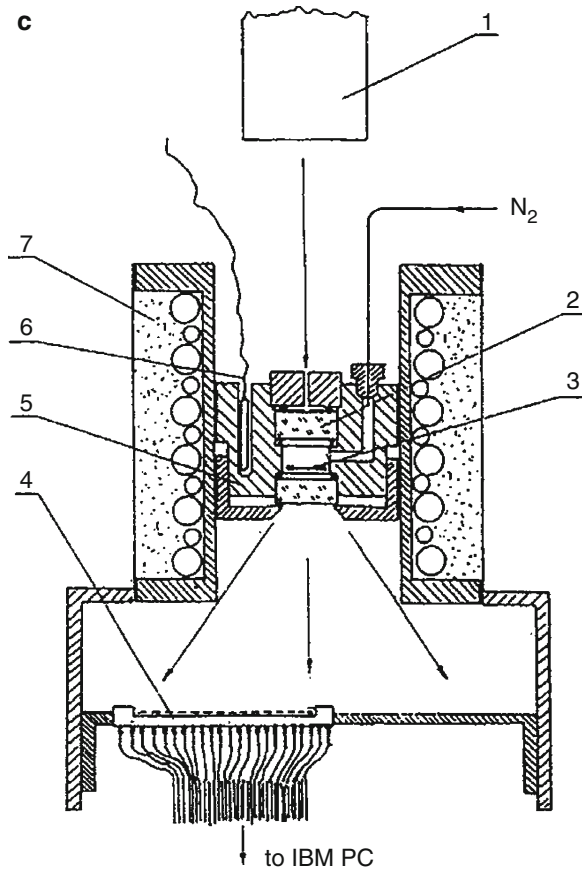


Fig. 7.18 (continued) (c) Light scattering apparatus used to detect polymer–polymer demixing 1 – HeNe laser, 2 – sapphire window, 3 – polymer film, 4 – photodiode array, 5 – copper block, 6 – resistance thermometer, 7 – temperature controlled jacket, (Reproduced with permission from Zywockinski, A., et al. *J. Polymer Sci. Polym. Phys.* **33**, 595 (1995))

above the glass temperature and in the homogeneous part of the phase diagram. Once the pressure has been set to a predetermined value using compressed nitrogen, the oven is reset to the desired quench temperature. This requires several minutes, a negligible time compared to the 10–70 h usually required to complete the phase transition. Scattered light from an He–Ne laser enters the cell, then exits through the lower sapphire window and falls on a photodiode array. Scattering intensity is thus recorded as a function of time and angle at the chosen pressure and temperature, and the effects of isotope substitution and pressure analyzed using the Cahn–Hilliard theory for spinodal decomposition.

7.6 H/D Isotope Effects and Small Angle Neutron Scattering

Isotope substitution is an important technique which is widely used in neutron scattering studies of the thermodynamic and structural properties of polymer solutions. The reason lies in the large difference in the coherent scattering length for slow (thermal) neutrons of the proton ($b_H = -0.374 \times 10^{-12}$ cm) and the deuteron ($b_D = 0.667 \times 10^{-12}$ cm). As a consequence to this large IE, judicious isotope substitution on solute or solvent permits the various contributions to the net scattering to be sorted out. In this fashion the intermolecular particle–particle correlation length, ξ and the intramolecular radius of gyration R_g can be deconvoluted. A good example is the use of the high concentration isotope label method to study polystyrene solutions at the concentration for liquid–liquid critical demixing. The coherent scattering intensity, $I(Q, x)$, for an incompressible mixture is

$$I(Q, x) = KnN^2S_s(Q) + LnN^2S_t(Q) \quad (7.33)$$

The functions $S(Q)$ are known as structure factors and contain information on the correlation lengths. Subscripts “s” and “t” correspond to scattering from a single chain and to total scattering, respectively, n is the number density of polymer molecules and N the degree of polymerization. Also Q , the scattering vector, is given by $Q = 4\pi \sin \theta/\lambda$. Here 2θ is the scattering angle and λ the neutron wave length, which for these studies was 0.48 nm and is commensurate with the size of the monomer unit. The value of isotope effect studies lies in the fact that K and L can be “tuned” by adjusting the H/D ratio, $x/(1 - x)$, in polymer or solvent.

$$K = (b_H - b_D)^2x(1 - x); L = (b_Hx + b_D(1 - x) - b_{Sol})^2 \quad (7.34)$$

In Equation 7.34 b_H , b_D and b_{Sol} are the coherent scattering lengths of the protiated and deuterated monomers and the solvent, respectively. The point of interest is that L can be adjusted to zero or nearly zero by varying the H/D ratio. For example $L = 0$ at $x = 0.214$ for polystyrene-h (PSh) and PSd mixtures dissolved in deuterioacetone. Under those conditions $I(Q, x) = KnN^2S_s(Q)$ and the measurement can be used to deduce the single particle correlation length (radius of gyration), R_g . Later measurements at $x = 1$ or some other value yield the total scattering intensity at non-zero L , and permit calculation of $S_t(Q)$ and ξ using Equation 7.33. In deuterated cyclohexane or other solvents, somewhat different isotope ratios obtain, but the procedure is analogous. An example of the results is shown in Fig. 7.19a which compares the radius of gyration (single particle correlation length) and the particle–particle correlation, ξ , for a solution of polystyrene ($M_w = 5.3 \times 10^5$) in cyclohexane-d₁₂ at several pressures in the vicinity of liquid–liquid critical demixing. As temperature falls, ξ rises steadily from ~ 109 Å at the Flory θ point, and eventually diverges at the critical demixing temperature, T_{CR} . Notice the pressure dependence of T_{CR} . The single particle correlation, R_g , on the other hand, holds steady at the value characteristic of unperturbed Gaussian chains. It is invariant with both P and T , and remains unchanged through the critical transition.

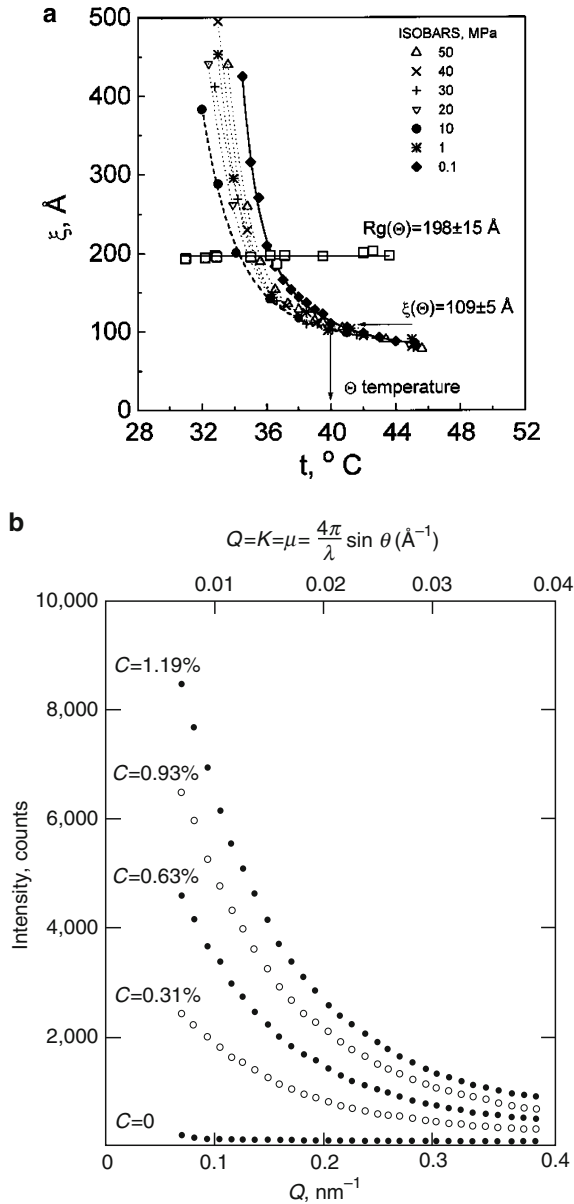


Fig. 7.19 (a) Results of neutron scattering measurements using the high concentration isotope label technique. Particle–particle correlation, $\xi_p(T)$, for polystyrene-h ($M_w = 5.3 \times 10^5$) in cyclohexane-d at different pressures. The single particle correlation, $R_g(P,T)$, of PS-h chains in a solution of (h + d)PS is also shown (*open squares*). R_g measured over the pressure range $0.1 < P/\text{MPa} < 50$ (Melnichenko, Y., Wignall, G., Van Hook, W. A., Szydowski, J., Wilczura, H. and Rebelo, L. P. N. *Macromolecules* **31**, 8436 (1998)). (b) Results of neutron scattering measurements using low concentration isotope labeling. Intensity vs. Q for various concentrations of polymethylmethacrylate-h (PMA-h) dissolved in PMA-d (Reprinted from Kirste, R. et al. *Polymer* **16**, 120 (1975))

A second example illustrates the use of low concentration isotope labeling to enhance contrast and scattering intensity in neutron scattering. The scattering intensity per unit sample volume of an isotopic solution of polymers (no third component solvent) at low concentration of h or d, can be shown to be proportional to the product ($c_h c_d$). The only effect of varying the concentration of deuterated, c_d , or protiated, c_h , species is to vary the scattering intensity from that of the background. An example is shown in Fig. 7.19b. At low enough concentrations Zimm analysis can be employed to deduce R_g . It is good practice to confine labeling levels using the low concentration technique to less than 10% or so to avoid complications from the effects of nonideality and demixing in H/D solutions of polymers at high concentration.

Further Reading

- Buncel, E. and Lee, C. C., Eds. *Isotopes in Organic Chemistry. Vol. 22 Isotopic Effects*, Elsevier, Amsterdam, 1984.
- Higgins, J. S. and Benoit, H. C., *Polymers and Neutron Scattering* Oxford Science Publications, Oxford, 1994.
- Mason, J., Ed. *Multinuclear NMR*, Plenum, New York, 1987.
- Matsson, O., *Isotope Effects for Exotic Nuclei*, in A. Kohen and H.H. Limbach, Eds. *Isotope Effects in Chemistry and Biology*, CRC Press/Taylor & Francis, Boca Raton, FL, 2005.
- Sergeyev, M. M., *Isotope Effects on Spin-Spin Coupling Constants: Experimental Evidence*, in P. Diehl et al., Eds. *NMR Basic Principles and Progress, Vol 22*, Springer Verlag, Berlin, 1990.
- Zare, R. N. et al., *High Precision Optical Measurements of $^{13}\text{C}/^{12}\text{C}$ Isotope Ratios in Organic Compounds at Natural Abundance*. Proc. Natl. Acad. Sci. **106**, 10928, 2009.

Chapter 8

Isotope Separation

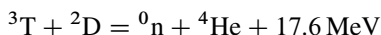
Abstract Isotope effects are small and separation of mixtures of isotopes is correspondingly difficult. The theory of isotope separation is reviewed and necessary terminology introduced. Practical methods of isotope separation are discussed focusing on the fundamentals of multistage processes and cascade design. We discuss the use of distillation, chemical exchange, gaseous diffusion, thermal diffusion, centrifugation, electromagnetic fields, and laser processes for the separation of isotopes from natural abundance feeds. Numerous examples are treated.

8.1 Introduction

We have seen that isotope effects on the properties of atoms and molecules are usually small, and this is true for all except the lightest elements. Consequently separation of single isotopes from mixtures of isotopes or isotopomers is tedious and difficult. The difficulty is compounded by the fact that the desired isotope is often present at low or very low concentration in the starting material (normally a naturally occurring fluid, ore, or mineral). Even so, the nuclear properties of certain separated isotopes are enough different from their sisters to justify the (usually enormous) expense of preparing isotopically pure or nearly pure materials. Three important examples follow:

- (1) The fission cross section of ^{235}U on bombardment with slow neutrons is many orders of magnitude larger than for the other naturally occurring isotopes of uranium. Large amounts of energy are released in controlled (reactor) or uncontrolled (bomb) fissions. These facts account for the enormous worldwide investment in the enrichment of ^{235}U from natural abundance (0.72%) to reactor ($\sim 3\text{--}6\%$ or so) or bomb grade ($\sim 90\%$) material. Commonly employed methods have included gaseous diffusion, centrifugation, and laser isotope separation (LIS).
- (2) Separation of ^6Li from natural abundance (7.4%) feed to synthesize ^6LiD (an important component of the fuel used in hydrogen fusion weapons (hydrogen bombs)). This, because the (n,T) cross section for ^6Li is much larger than that of ^7Li , so production of tritium is much enhanced in the triggering explosion.

The tritium so produced goes on to fuse with deuterium:



The classical method for lithium isotope separation employed chemical exchange between lithium amalgam and an aqueous solution of lithium hydroxide.

- (3) Less ominously, consider the enrichment of ${}^{18}\text{O}$ (natural abundance = 0.20%) and ${}^{17}\text{O}$ (0.04%) by distillation of water (${}^{16}\text{O} = 99.76\%$). A major and rapidly growing use of highly enriched ${}^{18}\text{O}$ water is for synthesis of ${}^{18}\text{F}$ radio-pharmaceuticals by cyclotron bombardment, ${}^{18}\text{O}(\text{p}, \text{n}){}^{18}\text{F}$. ${}^{18}\text{F}$ substituted compounds are used in positron emission tomography (PET scanning) techniques in medical diagnostics (the radiopharmaceutical being preferentially adsorbed on the tumor surface or other organ of interest).

In each of the examples above isotope separation involves the processing of large amounts of feedstock, at high reflux, through many, many separative stages. This accounts for the high cost of these and most other separated isotopes. For example, during peak production in the US, on the order of $\$10^9$ worth of ${}^{235}\text{U}$ was enriched per year from the natural abundance level (0.7%) to between 1.5% and 4% for use in power reactors, or to higher enrichment for military purposes. Again, at its peak, worldwide production of deuterium (>99%) from water or other natural abundance feedstocks (0.015%) was on the order of many tons per year. Such production rates demanded large scale and expensive industrial installations.

The first attempt at isotope separation was made just after World War I by Aston and Lindemann who employed a multistage laboratory scale gas–solid adsorption process to partially separate neon isotopes (Chapter 1). Since that time many different processes have been used to separate isotopes on laboratory, pilot plant, or industrial scale. Some of these are listed in Table 8.1. They include (for U) gaseous diffusion, gas centrifugation, thermal diffusion, electromagnetic separation, laser based methods, and various vapor expansion processes. Because the physico-chemical properties of ${}^{235}\text{U}$ and ${}^{238}\text{U}$ are very nearly the same, the enrichment per separative unit (stage) is small (except for certain electromagnetic or laser based methods), and it is necessary to multiply the single stage effect in a cascade. For lighter isotopes (D from H, ${}^6\text{Li}$ from ${}^7\text{Li}$, ${}^{13}\text{C}$ from ${}^{12}\text{C}$, etc.) separation

Table 8.1 Some methods of isotope separation

Gas centrifuge	Electromagnetic
Chemical exchange	Electromigration
Chromatography	Ion exchange
Gaseous diffusion	Mass or sweep diffusion
Thermal diffusion	Membrane pervaporation
Distillation	Supersonic nozzle expansion
Photochemical and laser methods	Electrolysis
Exchange distillation	

factors are larger, and the list of practical processes broadens to include chemical exchange, distillation, electrolysis, and similar methods. Even then, however, production of highly enriched material requires many partial separations carried out over and over in multistage processes termed cascades. So far as the basic theory of cascade design is concerned, the particular process or type of separating unit is irrelevant. Once a given separation process has been selected, the design of the individual unit completed, and the separation per stage established, the problem of isotope separation reduces to an understanding of cascade design.

8.2 Theory of Cascades: Terminology

The relationships between separative units, stages, and the cascade are outlined in Fig. 8.1. An individual separative unit in an isotope separation plant might be a single plate in a distillation or chemical exchange column, a single gas centrifuge, a laser or electromagnetic separator, a membrane diffusion unit, etc. The choice of a particular type of unit depends on the nature of the feed and its isotopic composition, the enrichment factor, energy demand per unit of separative work, the amount of material to be refluxed, and, of course, economic considerations.

A number of separative units operating in parallel, all taking feed of identical composition, and discharging partially enriched product and partially depleted waste streams comprise a stage. A single unit may suffice for a stage, but more often several units or many units are required. Because the separation per stage is almost

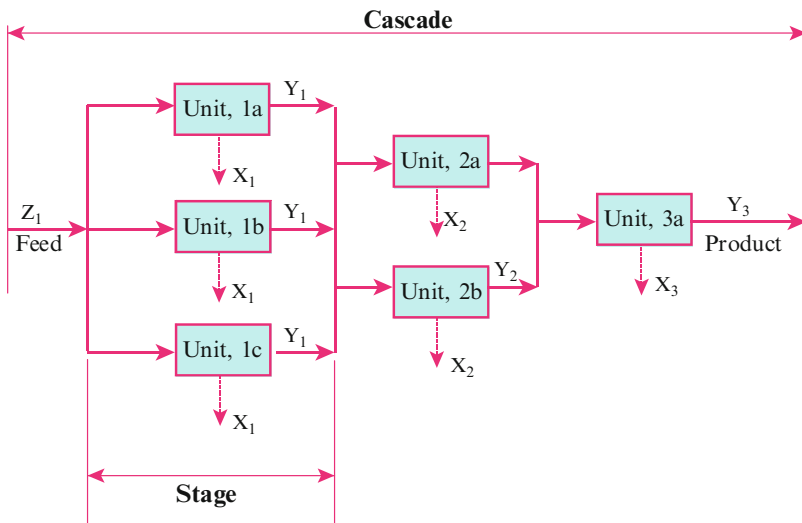


Fig. 8.1 Distinctions between separative units, stages, and cascades. The cascade in this diagram is tapered (See text for further clarification)

always smaller than the total desired enrichment, stages are connected in series; the resulting assembly is called a cascade. A cascade with the same number of units in each stage is “squared-off”; one in which the number of units per stage decreases as the product (or waste) end is approached is “tapered”. Stages may also be characterized as “ideal” or “non-ideal”. An ideal stage processes the feed stream to yield product and waste in equilibrium with each other. Since from thermodynamics we know it is the equilibrium condition which minimizes free energy, the ideal stage operates at the highest possible efficiency. To illustrate these points we begin with a discussion of the historically important separation of uranium isotopes by gaseous diffusion.

8.2.1 Gaseous Diffusion of UF_6

The obvious first step in the design of an isotope separation process is to select a carrier molecule which is well suited for handling in the cascade. For uranium the compound of choice is UF_6 . Although corrosive, UF_6 is reasonably volatile (at 56°C its vapor pressure is 1 atm). Also important is that fluorine has only one stable isotope so the isotopic mass difference ($^{238}\text{U} - ^{235}\text{U}$) is cleanly preserved in the UF_6 carrier. In the following paragraphs we illustrate the general features of isotope separation cascades using the specific example of UF_6 gaseous diffusion because of its historical importance. Later, other methods which have been or are being used to separate uranium isotopes will be briefly described (principally centrifuge and laser based processes).

The separation factor, r , in an isotope separation process is the ratio of the relative concentration of desired isotope in the product, p , to its relative concentration in the feed, f . Denoting the feed to the i 'th stage, the i 'th section of an overall plant, or the i th overall plant, as Z_i mol/s of isotope with an isotope fraction z_i , yielding product at a rate of Y_i mol/s of analysis y_i , and waste at a rate of X_i mol/s and isotope analysis x_i , we have for a two isotope feed

$$r = (y'/y)_p / (z'/z)_f = (y'/(1 - y'))_p / (z'/(1 - z'))_f \quad (8.1)$$

The primed or unprimed symbols refer to isotope fractions. The single stage separation factor for infinitesimal product removal ($y_i/z_i \sim 0$), $(r_i)_0$, is given the symbol “ α ”. The i 's index the stage number. Most often α is close to unity and it is convenient to define the isotope enrichment factor (the single stage enrichment factor), ε , between the i 'th and $(i + 1)$ 'th stage

$$\varepsilon = \alpha - 1 = (r_i^{i+1})_0 - 1 \quad (8.2)$$

To reasonable approximation ε , α and $(r_i^{i+1})_0$ are independent of stage number. In naturally occurring uranium the mass of the primed isotope, ^{235}U , is 235, the unprimed, 238, and $x'/(1 - x') = 0.0072$. For enrichment to 90% ^{235}U

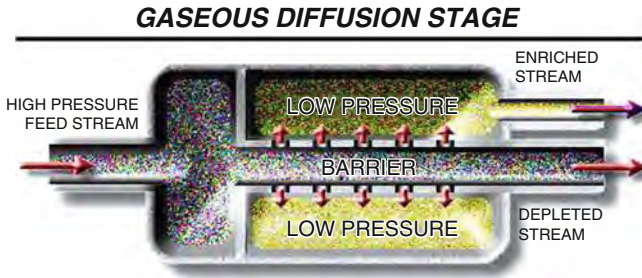


Fig. 8.2 Gaseous diffusion cell for uranium enrichment, schematic (<http://www.globalsecurity.org>)

$$r = (y'/(1 - y'))_p / (z'/(1 - z'))_f = (0.9/(1-0.9)) / (0.0072/(1-0.0072)) = 1241$$

For ideal gaseous diffusion of UF_6 through a porous yet restrictive barrier (see Fig. 8.2), Graham's law yields

$$\alpha = (M/M')^{1/2} = ((238 + 6 \times 19)/(235 + 6 \times 19))^{1/2} = 1.00429$$

which holds when the fraction of gas which has diffused is small. If the fraction which passes the barrier is appreciable a diminution due to back diffusion and other effects is expected. For half the gas diffusing $(r - 1) \sim \ln(2)(\alpha - 1)$.

8.2.2 Types of Separations: Cascades

8.2.2.1 Simple and Countercurrent Cascades

In a simple cascade the feed to any given stage, say the i 'th, is the product (heads) taken from the previous, $(i - 1)$ 'th, stage. The $(i - 1)$ 'th waste (tails) is discarded as it has insufficient value to be worth reprocessing. Thus, successive stages process progressively smaller amounts in the ratio of product to waste flows, Y_i and X_i , now defined as the cut, θ_i , $\theta_i = Y_i/X_i$. In a simple cascade it is impossible to obtain a high recovery of the desired component because of losses in the tails (waste) stream. A simple cascade can only be used when the feed is abundant and cheap, for example natural water fed to a deuterium separation plant, and even then is only practical for plants with a limited number of stages. (The overall product, P , to waste, W , ratio for a simple cascade of " i " stages is θ^i . Thus, for example, a 20 stage plant shows $P/W \sim 10^{-6}$ for $\theta = 0.5$ and $\sim 10^{-20}$ for $\theta = 0.1$.)

The countercurrent (recycle) cascade (Fig. 8.3) is much more useful because by reprocessing the waste stream a larger fraction of the desired isotope is recovered. In a recycle cascade the i 'th stage is fed by a mixture of the product, $Y_{(i-1)}$ from the $(i - 1)$ 'th, and the waste, $X_{(i+1)}$ from the $(i + 1)$ 'th, stage. A distillation column

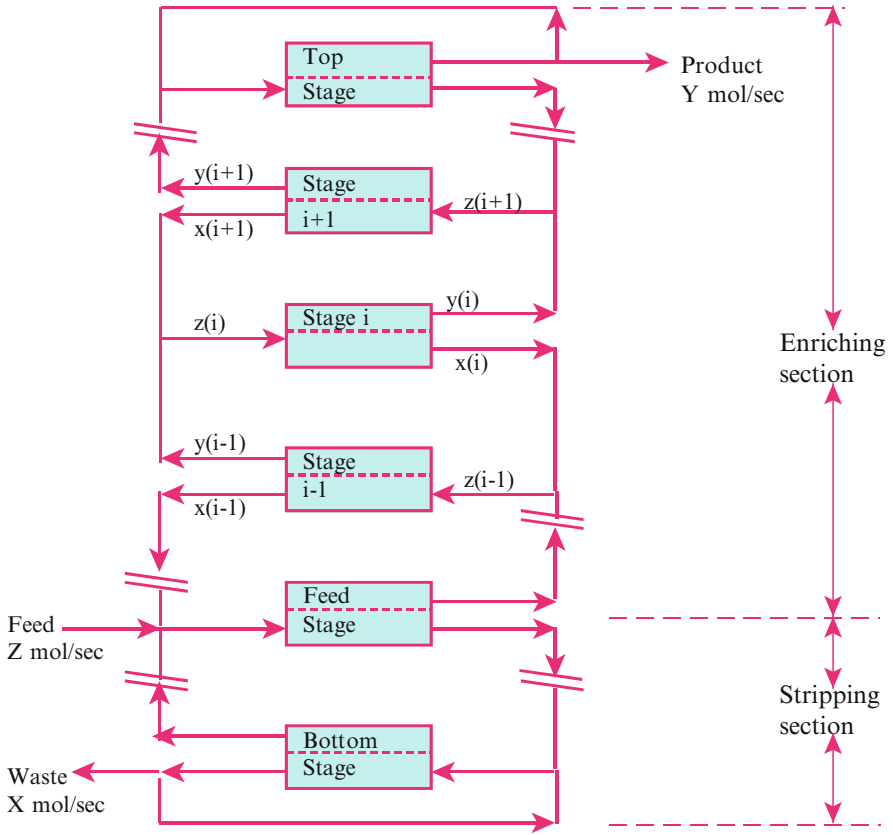


Fig. 8.3 Isotope separation stages arranged in a countercurrent cascade. The cascade in this diagram is squared off

is a good example. The feed is introduced somewhere near the middle of the cascade. The portion between feed and final product is the “enriching” section, and that between feed and final waste the “stripping” section. The enriching section is essential to give the desired product, the stripping section serves only to reduce the amount of feed required per unit amount of product. The countercurrent streams moving from final product or waste back towards feed point are known as “reflux”. Obviously the sum of the product and waste withdrawal rates must equal the feed rate. The total processing rate, however, is much larger because the countercurrent reflux streams are being continually processed and reprocessed. Thus,

$$(y_i - x_{i+1}) = (y_p - y_i)/(X_{i+1}/P) \tag{8.3}$$

In Equation 8.3 y_p is the product analysis at the last stage and P is the product withdrawal rate, and X_{i+1} is the waste withdrawal at stage $(i + 1)$. The ratio (X_{i+1}/P) is

the reflux, which for a simple countercurrent cascade is independent of stage number (i.e. the cascade is squared off). Notice that y_i and x_{i+1} approach each other as X_{i+1}/P approaches infinity, which happens at total reflux. At total reflux the number of stages, n , required for any specified overall separation is a minimum and is given by the Fenske equation (1932)

$$n_{\text{MIN}} = \ln[(y_p/(1 - y_p))/(x_w/(1 - x_w))]/\ln \alpha \quad (8.4)$$

Equation 8.4 shows n_{MIN} increases as the specified separation is increased or as α decreases, and in fact n_{MIN} approaches infinity as α falls to unity. Because in many cases α is near unity the minimum number of stages for isotope separation can be very large. Continuing with the example of ^{235}U gaseous diffusion, producing 90% enriched product, rejecting 0.3% tails, from 0.7% feed with $\alpha = 1.0043$, one finds $n_{\text{MIN}} \sim 1870$. Of course, at total reflux no product is withdrawn, it is all held in the cascade as inventory, and the cascade is serving no useful purpose. At practical levels of production many more stages are required.

At total reflux the concentration differences on successive stages are at their maximum but as production begins and reflux decreases these concentration ratios decrease. They reach unity (no enrichment) at minimum reflux. Materials balance considerations lead to Equation 8.5.

$$[n_{(i+1)}/P]_{\text{MIN}} = y_p[(\alpha x_{(i+1)} + 1 - x_{(i+1)}) - \alpha x_{(i+1)}]/[(\alpha - 1)x_{(i+1)}(1 - x_{(i+1)})] \quad (8.5)$$

When α lies close to 1 the minimum reflux ratio is large, but since x_i varies with stage number so does $[n_{(i+1)}/P]_{\text{MIN}}$. At the feed point in a ^{235}U plant enriching to 90% ^{235}U , $(n_f/P)_{\text{MIN}}$ is 29,100, but at the product end of the cascade it approaches zero.

A practical isotope separation plant can operate at neither minimum reflux (where the separation is zero, but the rate of production is high), nor at minimum number of stages (where the rate of production is zero, but the separation is high). A compromise is required. Since optimum reflux varies with stage number it is customary to employ tapered cascades for isotope separation. This results in marked savings in material hold-up, and in plant size and investment.

8.2.2.2 The Ideal Cascade

An ideal cascade is tapered to give minimum interstage flow and thus minimum operating cost. In the ideal cascade the product stream from the $(i+1)$ 'th stage is mixed with the waste stream from the $(i-1)$ 'th stage to feed the i 'th stage. Obviously the two streams being mixed should have the same isotopic analyses, otherwise separative work has been used to no good purpose. Materials and isotope balances show the number of stages in an ideal cascade is twice the minimum number of stages at total reflux, less one. Tapering in the stripping and enriching sections has been described by [Benedict et al. \(1981\)](#) (Historical Vignette 8.1). Optimal tapering is sensitive to α



[Historical Vignette 8.1] Manson Benedict (1907–1998). BS Cornell 1928, Ph.D. 1935 MIT. During World War II while working for the M. W. Kellogg Co. Benedict helped plan and set up the gaseous diffusion plant for uranium separation at Oak Ridge, TN. For this important effort, and for many other imaginative contributions to the development of the nuclear reactor, and to reactor safety, he was awarded the 1972 Fermi Medal of the US Department of Energy. In 1951 Benedict became a professor of nuclear engineering at MIT and developed a program which led to the establishment of the Department of Nuclear Engineering in 1958. He was lead author of the influential text, “Nuclear Chemical Engineering” (see the bibliography at the end of this chapter for a complete citation). (Photo credit: Nuclear Engineering Department, MIT)

and r . For our illustration (^{235}U separation with $y_P = 0.9$, $x_W = 0.003$, $z_F = 0.007$, and $\alpha = 1.0043$) 1 mol of product requires 213.6 mol of feed and yields 212.6 mol of depleted tails (waste). The number of stages is twice the minimum less one, or 3738, with 410 stages in the stripping section, and 3328 enriching. The interstage flow at the feed point, $i = 410$, is enormous, $Y_{410}/P = 58229$, but decreases rapidly as one moves away from the feed in either direction. Figure 8.4 is a schematic representation of the cascade. Height and width are proportional to stage number and interstage flow respectively. Capital cost and operating energy demand are approximately proportional to total interstage flow. With feed, product, and waste analyses specified, the plant size (and cost) diverges to infinity proportionally to $1/(1 - \alpha)^2$ and it is therefore of utmost importance to select a separation process with the largest possible α . Still, α remains small for many isotope separations and this accounts for the enormous capital and operating costs of isotope separation plants. An important point to keep in mind is that the cost of enrichment by any combination of processes is essentially determined by the base of the cascade. For example in a heavy water plant using the GS scheme (*vide infra*) concentrating D from 0.015% to 15% followed by distillation to obtain the final enrichment (99.8 atom%) almost all the separative work occurs in the GS exchange process, less than 1% is needed in the distillation. For gaseous diffusion about 42×10^6 mol of UF_6 must be processed for every mole of 90% $^{235}\text{UF}_6$ product, even though only 213.6 mol of feed are supplied. Thus on average each mole of feed is refluxed $\sim 2 \times 10^5$ times. It is difficult

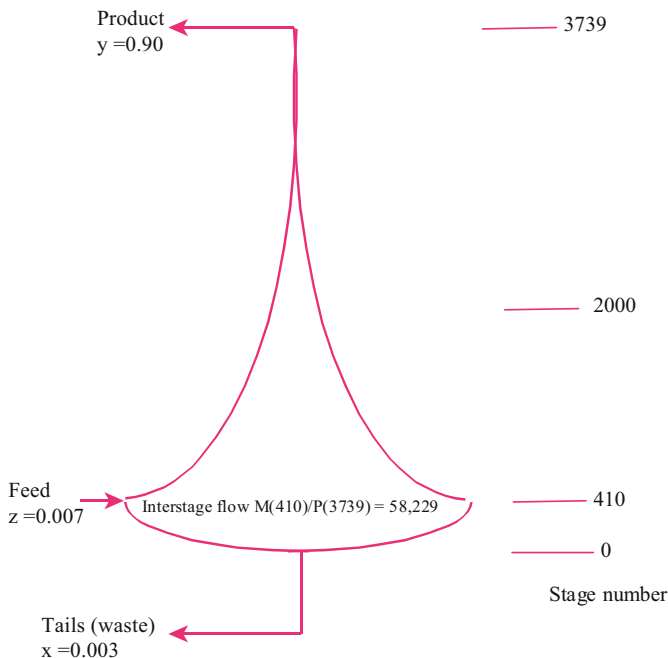


Fig. 8.4 Ideal cascade for uranium enrichment. The height of each section is roughly proportional to the number of stages in that section and the width at any stage to the amount of material being processed in that stage (Modified from Spindel in Rock, P. A., ACS Symposium Series 11. *Isotopes and Chemical Principles* 1975)

to appreciate the enormous scale of the operation required to produce the quantities of ^{235}U thought needed at the height of the cold war. The gaseous diffusion plant at Oak Ridge (now closed, see Fig. 8.5) required construction of one of the largest industrial facilities in history, while the Portsmouth, Ohio plant (also now closed) covered 93 acres, but had a floor area nearly three times larger.

8.2.2.3 Equilibrium Time

Due to high reflux demand separation plants can have inventories corresponding to many days of normal production. Equation (8.6) is an approximate relation for time to first production, t_p . The behavior is similar to that for plant size, i.e. t_p increases linearly with residence time per stage, h , but diverges toward infinite time proportionally to $1/(1 - \alpha)^2$.

$$t_p = [8h/(1-\alpha)^2] \{ [(y_p - 2y_p z_F + z_F)/(y_p - z_F)] \ln[(y_p - z_F)/(z_F(1 - y_p))] - 2 \} \quad (8.6)$$

For the 90% ^{235}U example, taking $h = 1$ s, $t_p \sim 30$ days. For squared-off cascades t_p is longer because more enriched material is required in the upper stages.



Fig. 8.5 The K-25 Gaseous Diffusion Plant at Oak Ridge, TN is no longer operational. This photograph conveys some sense of the extremely large scale of this operation (Photo credit. US Department of Energy and Knoxville News Sentinel, Oct. 17, 2004)

Long time to production implies the necessity for safe-guards against stage-to-stage remixing in the event of power failure or other problems. For example in distillation a power failure may cause the column to drain and isotopes to remix in the boiler. One must begin again at considerable cost.

8.2.3 Further Discussion of Gaseous Diffusion: Separative Work

Although many details of uranium diffusion plants remain classified even at this late date, certain features are obvious. (a) The high and low pressure sides of the cells are divided by a membrane which must have small pores ($\sim 10\text{--}100\text{ nm}$) to obtain isotope separation, but the total membrane must be porous enough to permit the processing of large volumes of gas. Moreover, the membranes must have good thermal, mechanical (to withstand the pressure difference across the cell), and chemical stability (since UF_6 is highly corrosive). The cells and tubing in the plant are therefore principally nickel and teflon to avoid corrosion. (b) To transport large volumes of gas and maintain proper pressure differences across membranes a gaseous diffusion plant requires a large number of pumps. A large cooling capacity is required to remove the heat of compression. Thus isotope separation by gaseous diffusion involves a large energy input to accomplish the work of compression and cooling

required at each stage. It was likely the ever increasing cost of energy which resulted in DOE's decision to replace the gaseous diffusion process for uranium enrichment using alternative methods with lower energy demand (see below).

In any uranium separation process the work of enrichment increases rapidly with ^{235}U content in the product. Because the price of natural uranium varies widely with time and location (and fluctuating government subsidies) it is useful to distinguish between the price of the feed and the value added by the separative process. For example, the purchaser himself might provide the feed and then pay only for the separative work required to make the desired product. Separative work is defined in Equation 8.7.

$$\text{Separative work} = WV(x_W) + PV(x_P) - FV(x_F) \quad (8.7)$$

Here W, P and F are the amounts of waste, product, and feed, respectively, and the $V(x_i)$'s are the separation potentials of waste, product and feed, respectively.

$$V(x_i) = (2x_i - 1) \ln(x_i/(1 - x_i)) \quad (8.8)$$

Most often W, P and F are chosen to have units of mass (x_i , as always, is isotope fraction), in which case separative work has the dimension of mass and can be thought of as the mass flow rate multiplied by the time required to yield a given quantity of product. The cost of isotope separation is then obtained by assigning a cost to one separative work mass unit (kgSW or SWU).

8.3 Practical Isotope Separation: Some Examples

The selection of an isotope separation process including the design of the separative units and the cascade depends principally on engineering and economic considerations. One must consider the amount of product which is desired, choose the starting material, consider energy demand, etc. It comes as no surprise, then, that many different methods have been used for isotope separation. Some of these have been listed in Table 8.1 and a few are discussed in more detail in the material which follows.

While the single-stage factor α is the best single measure of separative ease, a process cannot be chosen or optimized on that basis alone. Engineering concerns, convenience, and safety are also important. Even for a given isotope there is no single best method, but experience has shown electromagnetic separations to be the most versatile way to produce small or moderate quantities of isotopes of moderate to heavy mass. For light isotopes the simplest and most inexpensive method is the thermal diffusion column (Clusius and Dickel 1938) for small to moderate amounts of product. For large scale separation of light elements, distillation, chemical exchange, or exchange distillation are best, and for large scale separations of heavy isotopes (notably uranium) gaseous diffusion and (more recently) centrifu-

gation have been used, as have processes based on laser technology. Examples are given in the balance of this chapter.

8.3.1 Electromagnetic Separation

Electromagnetic separators (large scale mass spectrometers, also known as “Calutrons” because they were first developed at the California University Cyclotron Laboratory) were used during the Manhattan project in the early 1940s to separate ^{235}U in kilogram quantities. Positive ion species were generated in an ion source and electrically accelerated through a potential difference, V . In the process positive ions of charge q acquire kinetic energy $qV = Mv^2/2$, so ions of masses, M and M' , but identical charge, show a velocity ratio $v'/v = (M/M')^{1/2}$. Next the ions are further accelerated, this time magnetically by a field perpendicular to the plane in which they move, and are deflected in a circular path of radius R .

$$R = Mv^2/qBv = (2VM/q)^{1/2}/B \text{ so } \Delta R/R = 1/2(\Delta M/M) \quad (8.9)$$

B is the magnetic field strength and, as always, Δ denotes an isotopic difference. Equation 8.9 shows that isotopes of different masses will move in paths with radii $R'/R = (M'/M)^{1/2}$. For a 180° sector like that in Fig. 8.6 the two isotopes are separated linearly by

$$\Delta R = (V/(2MqB^2))^{1/2} \Delta M \quad (8.10)$$

Collectors are placed at the focal points. At sufficiently high vacuum genuinely large separation factors are obtained in electromagnetic separators (high resolution in the language of the mass spectroscopist), but this important advantage is offset by sev-

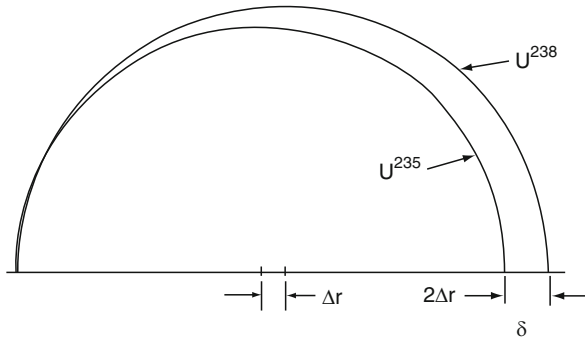


Fig. 8.6 The principle underlying electromagnetic separation of isotopes. Electrostatically accelerated ions enter at the *left*. A magnetic field perpendicular to the plane of the paper causes the circular orbits shown in the sketch (See text for further detail)



[Historical Vignette 8.2] Ernest O. Lawrence (1901–1958) was born in 1901 in Canton, SD. He was educated at the Universities of South Dakota and Minnesota, and at Yale (Ph.D. Physics 1925), and was appointed to the faculty of The University of California, Berkeley in 1928. Two years later he became a Full Professor. In 1926 he was appointed Director of the University’s Radiation Lab (now the Lawrence Berkeley National Laboratory), a position he held until his death.

In 1929 Lawrence invented the cyclotron, which instrument played (and still plays) an important role in nuclear physics. That work led directly to the award of the Nobel Prize in Physics for 1939, just one of his many honors. During World War II E. O. Lawrence made vital contributions to the development of the atomic bomb holding several high-level appointments in the Manhattan Project. He played an influential role in the decision to develop and later employ electromagnetic methods for uranium isotope separation (Calutrons) during the early 1940s. (Photo credit <http://wikipedia.org>, public domain)

eral difficulties. First, the feed must be chemically treated to provide compounds of appropriate volatility and chemical purity. More importantly, electromagnetic processes have inherent high loss. Typically only a small fraction of feed is ionized and extracted through the electrical accelerating slits. There are scattering losses in the beam, and space charge effects result in high loss and degradation of separation factors as ion current increases. Additionally, and most tellingly, the cost of the electrical energy needed to generate the large magnetic fields involved was unacceptably high under mid twentieth century conditions because Calutron technology predated the development of superconducting magnets. These factors have worked against the use of electromagnetic separation for large scale isotope production, although the method is well suited for producing small quantities (milligram to gram) of separated isotopes for research and specialized medical purposes (Historical Vignette 8.2).



Fig. 8.7 The PSP Superconducting Ion Cyclotron Resonance Isotope Separator. The large tank holding the superconducting magnetic is ~ 15 m long \times 2 m diameter (Reprinted from Bigelow, T. S. et. al. *Nucl. Instr. Methods Phys. Res. B* **241**, 652 (2005), copyright 2005 with permission from Elsevier)

8.3.1.1 The Plasma Separation Process

A good example of a modern method for electromagnetic isotope separation is the plasma separation process (PSP) (Fig. 8.7). The separator uses a large and uniform cylindrically shaped magnetic field (~ 1 m diameter \times ~ 15 m long) generated by a solenoidal superconducting magnet (~ 2 T). The magnet is contained in a super-insulated vacuum Dewar held at ~ 4.5 K using liquid helium. Source and collector assemblies lie at opposite ends of the high vacuum chamber. Microwave energy is injected into the source region at a frequency resonant with free electrons contained there. The electrons gain energy by cyclotron heating and maintain the plasma concentration by impacting and ionizing argon gas atoms continuously injected into the chamber at a suitable pressure. Positive argon ions in the source plasma collide with the negatively biased source plate with sufficient force to sputter neutral metal atoms from the plate. The vaporized metal atoms are rapidly ionized by the cyclotron energized electrons in the source zone. The sputtered ions are trapped in the magnetic field and drift toward the collector along helical paths. In the central region of the drift field a microwave antenna is excited with an Ion Cyclotron Resonant Frequency (ICRF) chosen to be resonant with a particular isotope from the source material. ICRF excited ions exit the antenna region with a wider orbit than the unexcited off-resonant ions. The collector plate is designed to take advantage of the orbital differences. Source and collector plates are periodically removed for product removal and refurbishing.

The principal advantage of PSP lies in its large enrichment factor (for example Pd^{102} can be enriched from 0.5% natural abundance to $\sim 80\%$ in just one pass) at useful efficiencies (typically $\sim 15\%$ of sputtered atoms end at the collectors) and relatively modest energy cost. These advantages are principally due to advances in superconducting magnet technology which permit the generation of uniform high-strength magnetic fields over large volumes at low energy cost. The result is the production of grams per day of highly enriched isotopes at reasonable cost. The PSP facility at Oak Ridge, TN was operated by the TheragenicsTM Corporation for about 10 years ending in 2005. Materials enriched by PSP include Pd^{102} , and selected isotopes of nickel, molybdenum, gadolinium, dysprosium and erbium. The palladium isotope was used to generate radioactive Pd^{103} by bombardment. Pd^{103} , in turn, is encapsulated in “rice sized” implantation seeds used for radio-treatment of prostate cancer. Certain of the other isotopes mentioned above are employed in the nuclear power industry in specialty applications (for example Gd enriched in Gd^{157} , which has a huge neutron cross section, can be used as a burnable poison to extend fuel rod life in nuclear reactors, Gd^{160} is employed in high sensitivity scintillation neutron detectors, and Er^{170} can be neutron activated to yield the radioactive Eu^{171} which is a useful energy source for remote application, e.g. “nuclear battery”). Another versatile facility used in the electromagnetic preparation of small amounts of high mass isotopes is the ISOLDE online isotope separator located at the European accelerator facility, CERN.

8.3.2 Thermal Diffusion of Gases

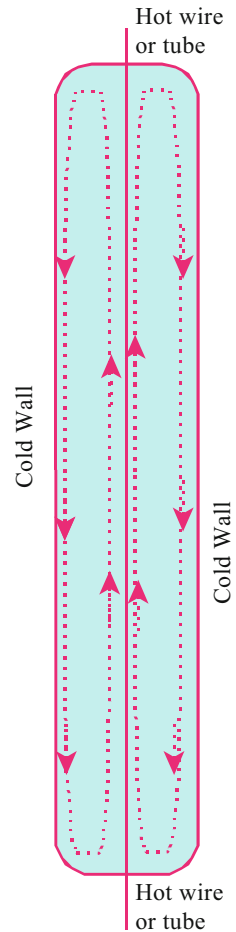
When a gas mixture is subjected to a temperature gradient, diffusion occurs establishing a separation, θ .

$$\ln \theta = g \ln(T_2/T_1) \quad (8.11)$$

The thermal diffusion factor, g , can be calculated from the kinetic theory of gases if the intermolecular potential is known. To good approximation, g is proportional to $(m - m')/(m + m')$. It vanishes for gases with an inverse sixth power intermolecular attractive potential. If the power is greater than six the lighter isotope moves preferentially to higher temperature, and if less than six it moves to lower temperature. Although g is small for mixtures of isotopes ($\sim 10^{-2}$) Clusius and Dickel (1938) developed an elegant countercurrent apparatus which multiplies the elementary effect. A Clusius–Dickel thermal diffusion column is shown schematically in Fig. 8.8, and Fig. 8.9b is a photograph of a Clusius–Dickel cascade. In these columns an electrically heated wire or tube held along axis of a cylinder with a refrigerated wall establishes thermal diffusion in the radial direction. The consequent mass gradient induces convection. Hotter molecules near the center rise and those at the wall fall. The countercurrent flow enhances the elementary separation factor many times (Historical Vignette 8.3).

For practical separations a number of individual columns, each about 3 m long, are connected in a cascade, Fig. 8.9b. Figure 8.9a diagrams a four stage cascade of

Fig. 8.8 A hot wire thermal diffusion column, schematic



11 columns used to separate argon isotopes (Mound Laboratories USDOE, or one of its commercial heirs, Isotec Corp. or Cambridge Isotopes Inc.). The fractionations at different points in the cascade, and the feed, waste, and production rates are indicated (notice that ^{38}Ar concentrates in the middle of the cascade, which in this example is operated without a stripping section). Thermal diffusion dissipates large amounts of power and is primarily used for laboratory scale separations. Results illustrating the versatility of the method are given in Table 8.2.



[Historical Vignette 8.3] Klaus Clusius (1903–1963) received the Dr. Ing. degree from the Breslau Technische Hochschule in 1928. After study abroad he took faculty positions at Göttingen, Würzburg and Munich (where he was department head), finally joining the University of Zurich as Director of the Physikalisch-Chemisches Institut (1947–1963). Clusius made important contributions to low temperature physical chemistry including early specific heat measurements on para-hydrogen, the first measurements of the λ -transitions in liquid ^4He and solid deuteromethanes, and measurements of the thermodynamic properties of a great number of atoms and molecules and their isotopomers. However he is best known for his development (with G. Dickel) of the thermal diffusion cascade, Fig. 8.9, which resulted in production of useful quantities of rare isotopes. (Photo credit: Archives of the Institute of Physical Chemistry, University of Zurich)

8.3.3 Large Scale Separations and Energy Demands

Earlier sections have pointed out that almost any pair of isotopes can be separated on a small scale by thermal diffusion or electromagnetic methods. For large scale separations, however, enormous amounts of material must be processed and energy consumption and cascade design become controlling. Table 8.3a lists the approximate upper limits of single stage separation factors for H/D, $^{12}\text{C}/^{13}\text{C}$, and $^{235}\text{U}/^{238}\text{U}$. Earlier we saw that ϵ values of a few tenths percent or so, lead to reflux ratios at the feed point of 10^4 or greater. The cost of processing and reprocessing such an enormous amount of material and the associated energy demand controls the choice of separative method. To illustrate, we return to the gaseous diffusion of UF_6 . In the separative unit gas diffuses from high to low pressure through a porous membrane. The upper limit of the separation factor is $(\alpha - 1) = \epsilon = \ln[(M'/M)^{1/2}] = 4.3 \times 10^{-3}$, and the optimized cut for the ideal cascade is $\theta = 0.5(\epsilon \ll 1)$. The minimum reflux energy is therefore the work of ideal recompression, $RT \ln 2 = 1.9 \times 10^3 \text{ J mol}^{-1}$ at 333 K. The actual compression is not isothermal and warms the gas by about 5% which increases the compressor bill from ~ 1.9 to $\sim 2.0 \text{ kJ mol}^{-1}$ of gas processed. If, roughly, the equipment operates at 50% of ideal efficiency, the energy cost increases to $\sim 4 \text{ kJ mol}^{-1}$. For uranium

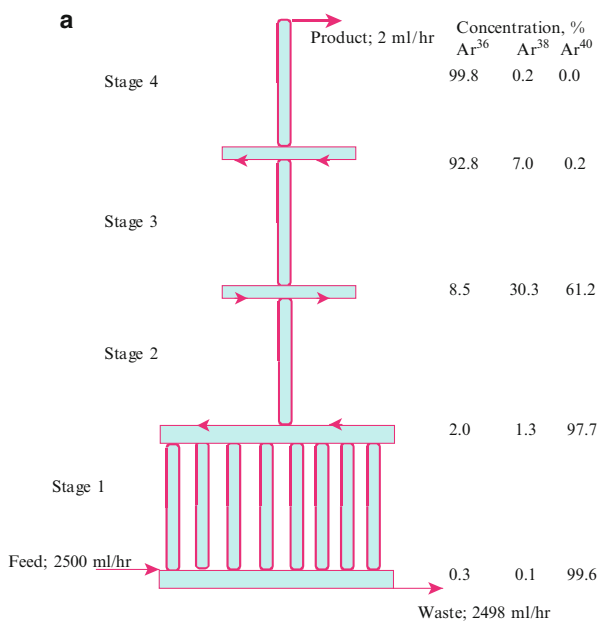


Fig. 8.9 (a) A four stage thermal diffusion cascade for argon isotope separation (Modified from Spindel, W. *ACS Symp. Ser.* **11**, 82 (1975)). (b) The thermal diffusion cascade operated by K. Clusius and collaborators at the University of Zurich during the 1950s (Photo credit: Archives of the Institute of Physical Chemistry, University of Zurich)

Table 8.2 Isotopes separated by K. Clusius and coworkers by thermal diffusion (Clusius, K. and Dickel, G., *Naturwissenschaften* **26**, 546 (1938); Clusius, K. and Starke, K., *Z. Naturforsch.* **4A**, 549 (1949))

Year	Isotope	%Abundance	Sepn. factor	Final purity
1939	³⁵ Cl	75.7	53	99.4
1939	³⁷ Cl	24.3	775	99.6
1942	⁸⁴ Kr	57.1	45	98.3
1942	⁸⁶ Kr	17.5	940	99.5
1950	²⁰ Ne	90.5	210	99.95
1950	¹⁵ N	0.37	135,000	99.8
1953	¹³ C	1.09	45,000	99.8
1955	¹³⁶ Xe	8.9	810	99.0
1956	²¹ Ne	0.275	96,500	99.6
1959	¹⁸ O	0.204	200,000	99.75
1959	³⁸ Ar	0.064	9,750,000	99.98
1960	²² Ne	9.21	12,500	99.92
1962	³⁶ Ar	0.37	3,300,000	99.99

enrichment about 4.2×10^7 mol of UF₆ are processed per mole of 0.9 fraction ²³⁵U product. Thus reflux energy demand is $\sim 17 \times 10^{10}$ J mol⁻¹ of product. A calculation based on a 1972 estimate for the most efficient plant then operating more than doubles that, yielding $\sim 45 \times 10^{10}$ J mol⁻¹. In 1975, at or near the peak of production, installed gaseous diffusion capacity for ²³⁵U was $\sim 3.2 \times 10^5$ mol year⁻¹ (Spindel 1975), requiring $\sim 4,500$ MW of processing energy. Of course at any given time a large fraction of the separative capacity was not being used, or was only being used for partial enrichment (from 0.7% to 3.5% or 4% as required for fueling nuclear power plants). However even the scaled down energy demand was enormous. It certainly contributed to the decision to phase out gaseous diffusion.

It is interesting to compare the reflux energy required for gaseous diffusion with that for distillation. In an ideal distillation column heat is required only at the boiler, and extracted only at the condenser. In between there are many separating units (plates or stages) where vapor is continually condensing and liquid continually evaporating. The heat of vaporization is identically the negative of the heat of condensation and in a perfectly adiabatic column the intermediate stages do not contribute to energy demand. For example, a well designed laboratory distillation column has ~ 100 plates (stages) and is 1 or 2 m in length. The energy cost per stage is $\sim 1\%$ of the heat of vaporization, and the reflux cost is several tens, rather than several thousands of joules per mole processed. When chemical exchange is compared with distillation, the reflux energy increases by about a factor of ten, i.e. it is now proportional to a heat of chemical reaction rather than a heat of vaporization. The height equivalent per theoretical plate (HETP) also increases, and energy demand per stage rises from several tens to several hundreds of joules per mole processed.

We now appreciate the reasons for the high cost of enriched uranium. The single stage separation factors are low, as is the natural abundance. This leads inexorably

Table 8.3a Approximate upper limits of separation factors using different methods ((Van Hook, W. A. in Vertes, A., Nagy, S. and Klencsar, Z., Eds., *Nuclear Chemistry*, Kluwer, Dordrecht 5, 177 (2003))

Method	H/D	$^{12}\text{C}/^{13}\text{C}$	$^{235}\text{U}/^{238}\text{U}$
Chemical exchange	3	1.02	1.001
Distillation	1.05–1.7	1.01	1.0000
Gaseous diffusion	1.2	1.03	1.004
Centrifuge, 250 m s ⁻¹	1.01	1.01	1.026
750 m s ⁻¹	1.11	1.11	1.34

Table 8.3b Some H/D separation factors for distillation (Van Hook, W. A. in Vertes, A., Nagy, S. and Klencsar, Z., Eds., *Nuclear Chemistry*, Kluwer, Dordrecht 5, 177 (2003))

Compound	T/K	P/kPa	Sepr. factor
Hydrogen	24	250	1.5
Methane	112	100	1.0036
Ammonia	239	100	1.036
Water	378	120	1.024

to a high reflux demand and a large number of stages. Additionally the historically practical processes have a large reflux cost, and the result is an extremely expensive product. The economic decision to replace gaseous or thermal diffusion with centrifuge or laser based separations, technically more difficult, and with a much higher cost per stage, can now be appreciated. These methods have larger or much larger single stage separation factors and consequently require exponentially smaller reflux.

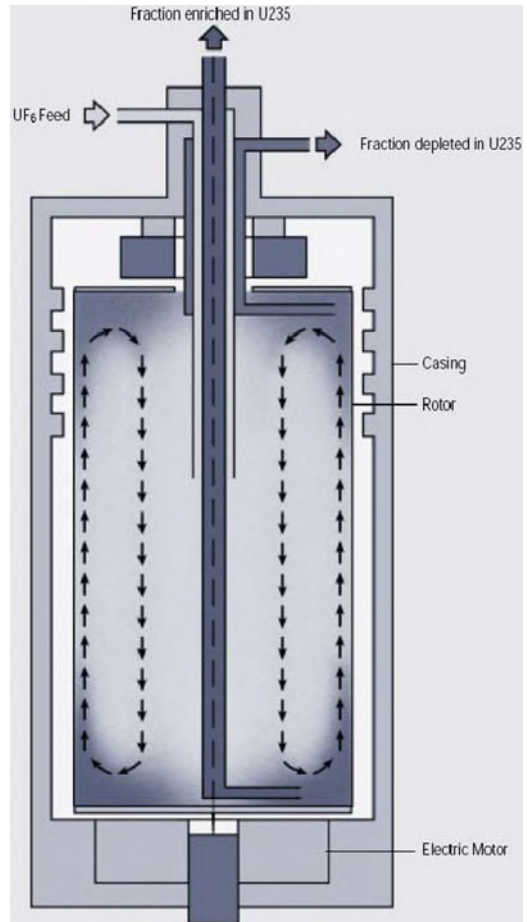
8.3.4 Centrifuge Based Separations

The use of centrifuges for isotope enrichment was suggested by Lindemann and Aston as early as 1919, but success required the development of vacuum centrifuges in the late 1930s. The rotors in such devices are suspended in vacuum chambers and gas is introduced and withdrawn through metal capillaries. Introductory discussions have been given by London (1961) and Benedict et al. (1981).

In a centrifugal field the energy per mole at a distance r from the axis is $M(\omega r^2)/2$. M is molecular weight and ω angular velocity. The ratio of partial pressures for two isotopomers (primed and unprimed) at the wall, r_w , and on the axis, r_0 , yields the elementary separation factor.

$$\alpha[(p'(r_w)/p(r_w))/(p'(r_0)/p(r_0))] = \exp[(M' - M)(\omega r_w)^2/(2RT)] \quad (8.12)$$

Fig. 8.10 Schematic of a single centrifuge unit showing the flow of the depleted and the enriched streams (www.urenco.com)



Equation 8.12 shows that α is function of the mass difference, $(M' - M)$, in contrast to most other methods where the separation factor depends on the ratio of masses, or the ratio raised to some power. In a modern centrifuge UF_6 gas is subject to centrifugal accelerations which are thousands of times greater than gravity. Consequently pressures at the outer radius are millions of times those at the axis, and at the highest possible speeds the ^{235}U concentration at the center can be 20% or more larger than at the periphery. Also a longitudinal countercurrent flow of UF_6 is induced by the density gradient and a series of rotating baffles and scoops multiplies the enrichment. In the centrifuge unit diagramed in Fig. 8.10 gas enriched in ^{235}U at the center flows upward and that enriched in ^{238}U at the outside flows down. By making the unit sufficiently long the difference between isotope concentration ratios, top to bottom can be many times greater than that between axis and outer wall. This results in large single stage separation factors and implies, for example, that on

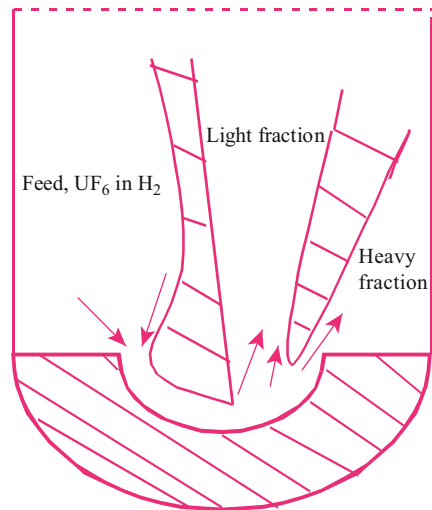


Fig. 8.11 Separation hall with centrifuges at the Gronau Enrichment Plant, Germany (Photo credit. www.urenco.com)

the order of tens of stages should be required to enrich uranium from 0.72% natural abundance to 3% (reactor grade) rejecting 0.2% tails. In comparison a gaseous diffusion plant under these specifications requires ~ 1300 stages. Though many fewer stages are required a very large number of centrifuges are needed to produce the quantity of enriched uranium required by the electrical power industry (Fig. 8.11).

The single stage separation factors of present day centrifuges are limited by the material strength of the rotor and its length. The practical limits are set by the need to avoid combinations of length, radius, and speed at which the rotor experiences resonant vibrations. Dynamic computer control with resonant damping may be used to advantage. Estimated values for present day centrifuges are: length 1.5–3 m., radius 0.25–0.5 m., rotational speed $75\text{--}100 \times 10^3$ rpm. Centrifuge separation plants require $\sim 2\text{--}3\%$ of the power of like-sized gaseous diffusion plants. In spite of the mechanical complexity of individual units and their limited lifetime, mass production constrains capital cost and present day centrifuge operation has a significantly lower enrichment cost than large scale gaseous diffusion. Performance has increased by a factor of more than 25 since 1980. At present large scale plants are operating in Russia, in Western Europe, and in the United Kingdom, and ground was recently broken in New Mexico for a 1.5 billion dollar separation plant to serve future US needs. An unfortunate consequence of the lowered cost of centrifuge separations has been unwanted nuclear proliferation in Iran, North Korea, and perhaps elsewhere.

Fig. 8.12 Schematic cross section of a supersonic nozzle isotope separator of radial design (Modified from Becker, E. W. *Uranium Enrichment*, Villani, S., Ed. Springer-Verlag, Berlin, 1979 with permission)



8.3.5 Aerodynamic Isotope Separation

The basic idea of aerodynamic isotope separation is illustrated in Fig. 8.12. Feed gas consisting of a mixture of the material of interest (e.g. UF_6) diluted with lighter gas (say H_2 or He) at a total pressure of ~ 2.5 kPa is fed through a slit into a region of much lower pressure. The light carrier gas enhances the centrifugal force thus generated. The flow in the forward direction is supersonic. Because of kinetic-molecular effects a certain fraction of gas, θ , diverges from the feed jet (~ 0.05 mm) enriched in the lighter isotope, while the rest of the jet passes through a second and somewhat wider “skimming” slit (~ 0.2 mm). The radial design sketched in Fig. 8.12 yields significantly larger separations than do simple “straight-through” aerodynamic separators. Still, the high proportion of carrier gas required in proportion to UF_6 process gas results in high specific-energy consumption (compressor cost) and substantial requirements for removal of waste heat.

8.4 Distillation and Exchange Distillation: The Large Scale Production of Deuterium

The extraction of deuterium from natural water feed forms an excellent case study of the application of large scale distillation and exchange distillation to isotope separation. The principal historical demand for deuterium has been as heavy water, D_2O , for use in certain nuclear reactors. Deuterium is an excellent neutron moderator, and more importantly, it has a low absorption cross section for slow neutrons. Therefore a reactor moderated and cooled with D_2O can be fueled with natural uranium thus avoiding the problems of uranium isotope enrichment. This was the

route chosen by Atomic Energy of Canada for its nuclear electric power program. Their CANDU (CANadian-Deuterium-Uranium) reactors require approximately 0.8 t D₂O per megawatt, and cumulative Canadian production exceeds 11,000 t. American production ended in 1981 after production of ~7,000 t. That heavy water had been mostly used as a moderator in reactors breeding plutonium from uranium fuel. The U.S., and most nuclear power programs worldwide, presently use pressurized normal water reactors. There are no large scale commercial uses of deuterium except as a moderator in power production or breeder reactors. Deuterium and tritium are used in nuclear weapons, but weapons production continues to decline, and hopefully will someday end. In spite of large stockpiles, 1945 to present, the total amount of deuterium contained in nuclear weapons should not amount to any significant fraction of world production. Finally, although deuterium is widely employed in scientific research, that use does not consume any large fraction of the available stock.

The very low D/H natural abundance ratio (0.015% = 150 ppm) is responsible for the high cost of heavy water. Materials balance requires a minimum of $\sim 7 \times 10^3$ mol feed per mol of product, and that increases even more for reasonable values of tails analysis (in some plants the feed/product ratio has reached nearly 4×10^4). At peak Canadian production, ~ 800 t year⁻¹, this amounted to feeds of $\sim 3 \times 10^7$ t year⁻¹. Clearly that figure demands a cheap and easily accessible feed (i.e. water), or alternatively, requires deuterium production to be parasitic on some large industrial process, for example the production of NH₃ for fertilizer, or petrochemical processing.

Table 8.4 contains a list of some processes adaptable to heavy water production (and brief comments). Distillation, while the simplest method, is prohibitively expensive (except for low temperature distillation of H₂/HD) because the α values (separation factors) are too small. Small α implies inordinately high reflux, and large capital investment. Although α for water electrolysis is high (and reflux cost correspondingly smaller), and this method was used in an historically important Norwegian plant beginning in the 1930s and operated by Germany during part of

Table 8.4 Possible processes for heavy water production (Rae, H. K., Ed., *Separation of hydrogen isotopes*, ACS Symp. Ser. **68**, 134 (1978))

Process	Remarks
Distillation	Size excessive, except for H ₂ /HD
Chemical exchange	Most promising
Diffusion	Barrier or membrane cost excessive. High energy demand
Electrolysis	Energy cost too high
Gravitational	Energy cost too high
Adsorption	High adsorbent volume
Biological	Excessive volume
Crystallization	Impractical on large scale
Photochemical	Promising if selectivity approaches 10 ⁴

World War II (until incapacitated by the Allies in a series of famous commando and bombing raids), high energy demand ordinarily makes electrolysis too expensive. Even so, water electrolysis followed by upper stage distillation of HD/H₂ was used in a modestly sized Indian plant (~14 t year⁻¹ D₂O). Also several larger plants (~65 t year⁻¹), parasitic to ammonia synthesis and fertilizer production, and based on ammonia distillation or catalytic ammonia/hydrogen exchange have been employed, especially in the French nuclear program. In view of the enormous quantities of methane which are processed in the petroleum and natural gas industries it is unfortunate that the separation factor for distillation of CH₃D/CH₄ (the VPIE) is unattractively small (see Chapter 5).

Of the other processes in Table 8.4, most have high energy or large capital cost per separative work unit (SWU). Laser and photochemical methods continue to be investigated but have not proven economical for H/D separation, even on small scale. The most promising methods are the ones based on chemical exchange; H₂S + HDO = HDS + H₂O, or H₂ + HDO = HD + H₂O, or H₂ + NH₂D = HD + NH₃. These equilibria have large separation factors which are pronounced functions of temperature. This allows the design of dual temperature processes which provide efficient thermal reflux and decided cost advantage. Other exchange processes employ chemical reflux, which is normally much more expensive (since the cost of large amounts of low-grade thermal energy is typically less than that of recycling large amounts of bulk chemicals).

Because of the very large enrichments required in heavy water production, cascades taper markedly. In the upper stages the relative advantage of chemical exchange over water distillation vanishes. Most heavy water plants carry out the last portion of the enrichment by distillation (from 20% or 30% D to 99.85%). Accordingly both exchange and distillation will be briefly treated below. First, however, to clarify the important distinction between chemical and thermal reflux we treat an example of isotope separation using chemical reflux.

8.4.1 *An Aside: Monothermal Isotope Exchange with Chemical Reflux; ¹⁵N Enrichment*

In 1958 Taylor and Spindel described the enrichment of ¹⁵N (99.8%) from natural abundance feed (0.365%) using chemical exchange,

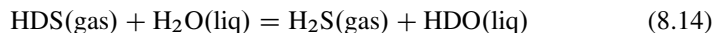


This uncatalyzed reaction occurs at an acceptable rate at room temperature (298 K), $\alpha = (15/14)_{\text{aq}}/(15/14)_{\text{gas}} = 1.055$. The value calculated from spectroscopic data is 1.096 (Chapter 4), so parasitic bleed to species other than NO(g) and HNO₃(aq) is indicated (the chemistry shown in Equation 8.13 is oversimplified). In the exchange aqueous acid trickles down through a packed column countercurrent to a rising NO stream. A two column cascade was employed in which 4% of the acid flow is

shunted to the upper stage, and the remaining 96% reduced to NO by reaction with SO₂ and recycled. Depleted NO from the lower section is mixed with air and water to generate a waste HNO₃(aq) flow. To sum up, a refluxed nitric acid feed is separated into enriched nitric acid product and slightly depleted nitric acid waste, while converting SO₂(g) and air to H₂SO₄(aq). The minimum ratio of H₂SO₄ to ¹⁵N is one and one-half times minimum reflux. For 99.8% ¹⁵N product generated from 0.365% feed, and $\alpha = 1.055$, $n(\text{SO}_2) = (3/2)[(y_P - z_F)/z_F][\alpha/(\alpha - 1)] = 7930$. This is a high reflux requirement. The cost of the $\sim 8 \times 10^3$ mol SO₂ per mole of product is partly offset by the fact that H₂SO₄ is more valuable than SO₂. (But remember that H₂SO₄ is an inexpensively priced commodity chemical, and the value added may not be a significant fraction of process cost.) Also, even though the cascade is tapered, the amount of SO₂ required is unchanged from the “squared-off” cascade because reflux demand is proportional to inter-stage flow at the feed point. The principal advantage of tapering is that it results in a lower holdup of ¹⁵N, and less time to production.

8.4.2 Dual Temperature Exchange: The GS Process for Deuterium Enrichment

To avoid the high cost of chemical reflux the dual temperature H₂S/H₂O exchange was independently suggested by Geib (1946) and Spevack (1957) (GS). The method exploits the fact that the equilibrium constant for isotope exchange is temperature dependent. The scheme is illustrated in Fig. 8.13. To carry out the exchange



feed (H₂O) is introduced at the top of a cold tower and equilibrated against an H₂S gas stream in a countercurrent multiplate column. D concentrates in the liquid phase and builds toward its maximum at the bottom of the cold tower. The essential distinction between the GS process and standard chemical reflux, is that in the GS process the reflux is carried out thermally. The hot tower serves as refluxer for the cold tower. At the top of the cold tower, an intermediate point in the plant, the D analysis of the gas stream, u_g , is set by equilibration against cold feed, the separation factor is α_C , $\alpha_C = [z_F/(1 - z_F)]/[u_g/(1 - u_g)]$. Next, that cold-equilibrated gas is introduced to the bottom of the hot tower where it re-equilibrates with the waste flow, $\alpha_H = [x_W/(1 - x_W)]/[u_g/(1 - u_g)]$. The symbols have been defined in earlier sections. The overall separation is $S = \alpha_C/\alpha_H$. Both the hot and cold towers contain many plates (stages), so S is larger than it would be for single equilibrations at each temperature. If the isotope abundance in the feed is small, the fraction extracted can be approximated as $(1 - \alpha_H/\alpha_C)$. For the GS process (hot tower = 138°C, $\alpha_H = 1.80$; cold tower = 32°C, $\alpha_C 2.32$) the recovery of deuterium is 0.22 fraction.

The large industrial scale GS plant (100 kg h⁻¹, ~ 700 t year⁻¹, 99.8% D₂O product) operated by Ontario Hydro at Bruce Ontario for more than 20 years was

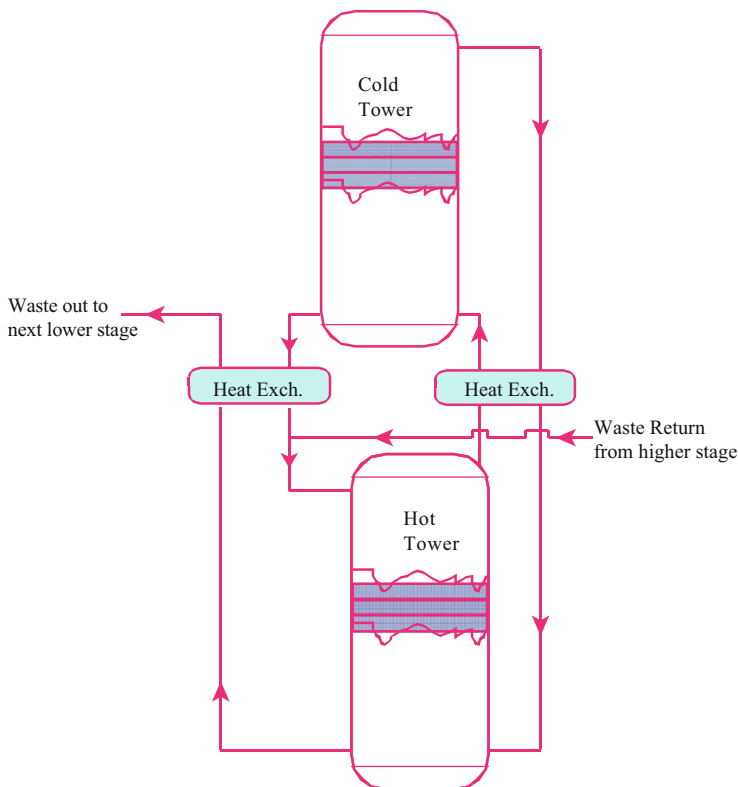


Fig. 8.13 Schematic diagram of one stage of a GS dual temperature chemical exchange system (Modified from Bigeleisen, J., *Adv. Chem. Ser.* **89**, 1 (1969))

decommissioned in 1998 after cumulative production was judged to meet Canada's future heavy water needs. The Bruce plant (Fig. 8.14) was the largest on record. The GS section consisted of three stages of hot/cold towers with a total enrichment from natural abundance to 20% D₂O. Distillation was used for the final enrichment to 0.998 fraction heavy water. Each GS tower contained a hot and cold section. Deuterium was carried forward to the second and third stages in the gas phase. Deuterium not extracted was returned to waste (Lake Huron) after removal of H₂S (i.e. there is an H₂S stripper to satisfy environmental regulations, but there is no deuterium stripping). The plant tapered markedly between towers 1 and 2, and 2 and 3. Since deuterium recovery increases with α_C/α_H one supposes the hot tower should run at as high a temperature as possible, and the cold tower as low as possible, and this would be so in the absence of complications. The rather surprising choice, ($30 < t_C/^\circ\text{C} < 32$), was dictated by the necessity to avoid precipitation of the solid hydrate H₂S–H₂O which occurs below 30°C. The optimum upper temperature ($130 < t_H/^\circ\text{C} < 140$) was determined by balancing the improvement with increasing t_H against higher heating costs.



Fig. 8.14 Aerial view of the Bruce D₂O plant (now decommissioned) (www.sno.phy.queensu.ca/sno)

We close discussion of the GS process with the comment that it is dangerous. A GS plant requires a very large inventory of highly toxic H₂S employed at elevated temperature and pressure in a corrosive environment. The safety of operating personnel and of the population in the area surrounding the plant is a major concern.

8.4.3 Other Exchange Reactions for Deuterium Enrichment

H/D separation factors for some exchange reactions involving hydrogen are shown in Fig. 8.15. Those with the highest separation factors also have the largest temperature dependences. Although the GS process has one of the smaller separation factors of those shown, it has proven to be the most practical large scale industrial method for D enrichment. That is because the kinetics of the exchange are favorable, even without catalyst. That fact, combined with the further advantage that the feed (water) is abundant and cheap, accounts for its importance. Even so, careful attention has been paid to the other equilibria which have the advantage of much larger separation factors. To that end the French have developed a low temperature process based on an amide catalyzed NH₃/HD exchange at low temperature ($\alpha \sim 8$ at the boiling point of ammonia). Enrichment plants parasitic to Haber–Bosch ammonia synthesis have been operated in France and India.

8.4.4 Distillation

Distillation is a countercurrent process which maintains liquid–vapor equilibrium, usually in a vertical column containing packing, thin wetted walls, or bubble-cap

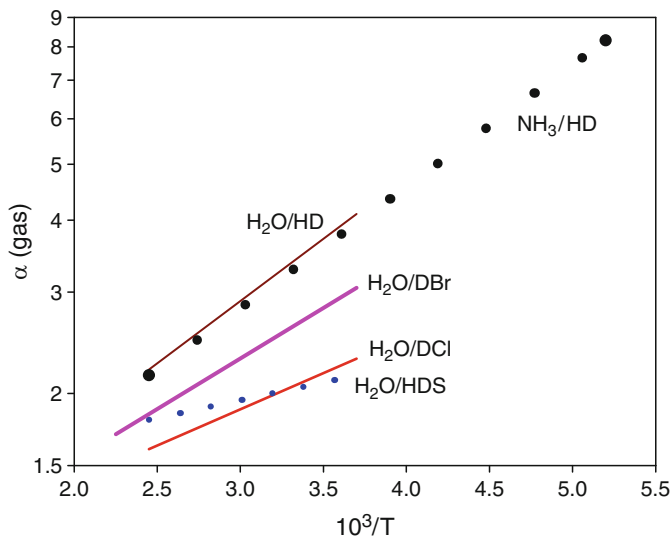


Fig. 8.15 Semilog plot of H/D liquid–gas separation factors for some chemical equilibria (After Bigeleisen, J., *Adv. Chem Ser.* **89**, 1, 1969)

plates. In this fashion the ascending vapor condenses, mixes and equilibrates with descending liquid, and re-evaporates many times as it works its way up the column. Each equilibration defines an ideal plate or stage. The single stage separation factor for distillation is given by the vapor pressure isotope effect. Because solutions of isotopomers are nearly ideal in both liquid and vapor, separation factors in isothermal distillation columns are virtually independent of enrichment (plate number), and the analysis of the distillation process is simplified. (In large scale plants, on the other hand, there may be an appreciable pressure drop along the column which causes a change in boiling temperature. In such cases α can no longer be assumed to be independent of plate number.) For many separations the desired enrichment may not be possible with a single column and it is necessary to use several columns in series. This can be a convenience since it permits the plant to be tapered at column interconnections.

The properties of a fractionating column which are important for isotope separation are (1) the throughput or boil-up rate which determines production; (2) HETP (height equivalent per theoretical plate) which determines column length; (3) the hold-up per plate which determines plant inventory and time to production; (4) the pressure drop per plate which should be as small as possible. The choice of a particular column is invariably a compromise between these factors. The separation in a production column is of course less than it would be at total reflux (no product withdrawal). The concentration at any point in the enriching section can be calculated from the transport equation (see, e.g., London 1961)

$$wC_p = BC(1 - C)(\alpha - 1) - Bh(dC/dM) + wC \quad (8.15)$$

where B is the boil-up rate at a point a distance M along the column, C the isotope concentration at this point, w the withdrawal rate, α the separation factor, and h the HETP. A voluminous literature concerning the design of columns, packings, and staging is available.

Power consumption in distillation is an important consideration. In the ideal limit, as for any separative process, it is only necessary to introduce an amount of energy equivalent to the entropy of mixing,

$$q_{\text{REV}} = T\Delta S_{\text{MIX}} = RT[z_F \ln(z_F) + (1 - z_F) \ln(1 - z_F)]. \quad (8.16)$$

In practice, however, many inefficiencies exist. To approach ideality the column would have to be lengthened to infinity (for complete separation), the boil-up rate varied according to plate number, the pressure drop made infinitesimally low, and isotope re-mixing completely eliminated. This is impossible. If, instead, we assume the column itself is perfectly adiabatic so that boil-up energy is supplied only in the pot (stage 1) and removed only at the top (head), then $1/[z_F(\alpha - 1)]$ moles are boiled and re-condensed. Taking the heat of vaporization of a liquid as typically $\sim 10RT_B$ (Trouton's rule) the quantity of heat put into the boiler and extracted from the condenser is $q \sim 10RT_B/[z_F(\alpha - 1)]$ per mole. For example consider $^{14}\text{N}_2/^{14}\text{N}^{15}\text{N}$ distillation with $\alpha = 1.0038$, $T_B = 78\text{K}$, and $z_F = 0.0074$, in which case $q \sim 2.3 \times 10^8 \text{ J mol}^{-1} \text{ }^{14}\text{N}^{15}\text{N}$. This contrasts with the value of $\sim 28 \text{ J mol}^{-1}$ for the perfectly reversible process (Equation 8.16). The difference is striking.

Even though the energy demand in distillation is many times the minimum reversible separation energy, it is still small compared to the energy demand of most irreversible processes (such as gaseous diffusion). On the laboratory scale power costs are usually low compared to equipment and operating costs. As the size of operations increases, however, power costs become proportionally more important (because they rise approximately in proportion to production, but other costs increase more slowly). Eventually it becomes economic to consider staged columns with vapor recompression and heat exchange. In favorable cases energy demand can be reduced significantly, perhaps by a factor of as much as ~ 10 .

8.4.5 Specific Examples, Isotope Separation by Distillation

Commercial scale distillation plants have been or are being operated for the separation of the following isotopes: (1) D by exchange distillation of hydrogen, water, or ammonia; D and T by cryogenic distillation of hydrogen, (2) ^{10}B by distillation of BF_3 or exchange distillation of BF_3 :ether complexes; (3) ^{13}C by distillation of carbon monoxide; (4) ^{15}N by distillation of NO; (5) ^{17}O and ^{18}O by distillation of water, CO or NO; (6) ^{22}Ne by distillation of neon; (7) ^{36}Ar by distillation of argon. There may be others not listed.

Single stage factors, $\alpha = P'/P$, are given to good approximation by the VPIE's although there may be minor corrections for excess free energies of mixing (Chapter 5). Also to good approximation, $\ln \alpha = A/T^2 + B/T$ (Chapter 5). While A is always positive, B can be either positive or negative. Most often it is advantageous to distill at as low a temperature as possible (except when B is negative and large, as it is for H/D VPIE's of hydrocarbons). Of course as temperature drops, so does vapor pressure, and at low enough temperature throughput falls to unacceptable values. It is impractical to design isotope production plants, even on a laboratory scale, for vapor pressures less than 0.01 MPa (0.1 bar).

8.4.5.1 Hydrogen

Distillation of hydrogen for deuterium production is attractive because of the large vapor pressure isotope effect $(P(\text{H}_2)/P(\text{HD}) = 1.7$ at 21K). The production of D by distillation of hydrogen (parasitic to Haber–Bosch ammonia production) has been employed on a moderate scale, but high concentrations of nitrogen and other impurities in ammonia synthesis gas introduce complications. A special problem which occurs in the distillation of hydrogen is the need to minimize the conversion of ortho to para hydrogen. At room temperature the ortho/para ratio is close to 3, but that ratio drops rapidly with temperature, and at the boiling point (20 K) it is essentially zero. The heat of reaction, ortho \rightleftharpoons para, releases about 1.5 times the heat of vaporization. This would significantly increase power consumption if allowed to occur. The ortho/para reaction is catalyzed by paramagnetic and ferromagnetic materials, including oxygen and most steels, and these materials must be excluded from the low temperature portions of the equipment.

8.4.5.2 Carbon Monoxide

One method which can be used to produce ^{13}C is by the cryogenic distillation of CO. CO is easy to distill. Its vapor pressure curve closely follows that for N_2 and liquid nitrogen can be used as a convenient refrigerant. At the boiling point of nitrogen, 77.4 K, $(\alpha - 1)$ for $^{12}\text{C}^{16}\text{O}/^{13}\text{C}^{16}\text{O}$ is 0.0078 and for $^{12}\text{C}^{16}\text{O}/^{12}\text{C}^{18}\text{O}$ is 0.0057. At 72 K the vapor pressure is ~ 0.25 bar and the α values are 0.0096 and 0.0070. The increased separation factor makes it worthwhile to operate at reduced pressure. The triple point of CO (68 K, 0.15 bar) establishes the lower limit of the operating temperature. Natural abundances of ^{13}C and ^{18}O are 1.1% and 0.2%, respectively.

An early CO distillation pilot plant described by Johns (in London (1961), reading list), used a two section vacuum insulated column packed with wire gauze rings. The upper section was 5.2 m long with a diameter of 3.2 cm, the lower 4.6 m \times 1.9 cm. The column contained about 600 plates. An intermediate boiler re-evaporated part of the downward flowing liquid at the junction. This plant accumulates product in the liquid and enriches toward the bottom. Enriched CO (0.4 g day⁻¹ of $\sim 65\%$ ^{13}C and 0.05 g day⁻¹ of $\sim 5\%$ ^{18}O) was withdrawn from the bottom

of the column and converted to CH_4 and H_2O . Arrangements were made to isolate the different sections of the column in the event of power failure; the isotope inventory (holdup) corresponded to about 2 months of production. This technology has been successfully scaled up to commercial size and Spectra Gases Inc. has operated large CO distillation columns at Los Alamos National Laboratory.

8.4.5.3 Isotope Enrichment by Distillation of Nitrous Oxide or Water

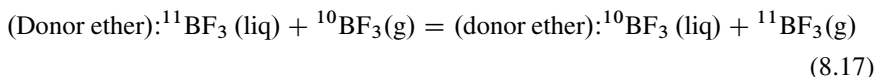
Beginning in the early 1960s MacInteer and coworkers at Los Alamos described production of ^{18}O , ^{17}O , and ^{15}N by low temperature distillation of NO. Separation factors for NO are some three to five times larger than for other diatomic molecules with similar boiling points. The abnormally large α values are due to the formation of dimers, almost completely associated in the boiling liquid, but completely dissociated in the vapor. We have seen that large α leads to marked increases in efficiency of isotope separation. It reduces the number of plates required for a specified enrichment, the time to production, and capital and operating costs. In the case of NO, however, these advantages are partly offset by the relatively high cost of the feed material, and its chemical instability and toxicity. Nonetheless the Los Alamos facility operated successfully for many years before it was shutdown in the mid-1980s. However Spectra Gases Inc. has announced plans to refurbish and restart the unit for production of heavy oxygen isotopes. World demand for ^{18}O has increased markedly in recent years because of its use in the synthesis of ^{18}F radio-pharmaceuticals by cyclotron bombardment, $^{18}\text{O}(\text{p}, \text{n})^{18}\text{F}$. ^{18}F substituted compounds, in turn, are used for positron emission tomography (PET scanning) in medical diagnostics (the radio-pharmaceutical being preferentially adsorbed at the tumor site of interest).

An alternative and more widely used technique for ^{18}O production is via water distillation. The separation factors are much smaller than they are for NO, and the number of plates required, the time to production, and the energy demand and capital costs commensurately larger, but cost of feed, ease of handling, and safety concerns favor water distillation. Production columns are located in the United States, Israel, Russia and other countries. The Israeli plant has the advantage of using already partially enriched Dead Sea water as feed.

8.4.6 Exchange Distillation: ^{10}B Enrichment

^{10}B is a powerful neutron absorber and has been employed in reactor control rods, neutron detectors, and other applications. Cascades based on exchange distillation of boron-ether complexes have usefully large α 's and were used for $^{10}\text{B}/^{11}\text{B}$ isotope separation by the US DOE. Exchange distillation takes advantage of the fact that condensed phase/vapor phase separation factors can be enhanced (as compared to liquid/vapor α 's) by association/dissociation equilibria in one or the other phase. At the normal boiling point (173 K) the VPIE for

BF_3 , $\ln \alpha \sim \ln[\text{P}(^{10}\text{BF}_3)/\text{P}(^{11}\text{BF}_3)] = -0.0075$, is sufficiently large to permit useful separation by distillation. Compare this effect, however, with association-dissociation constants for reactions of the type



which lie between 0.01 and 0.02 at 298 K. A distillation plant based on the larger separation factor, and operating at a more convenient temperature, obviously promises (and delivers) superior performance.

8.4.7 Liquid–Liquid Exchange: Lithium Enrichment

Enriched ^6Li is combined with deuterium to make ceramic-like ^6LiD parts for the secondary stages of thermonuclear weapons. During the 1950s and 1960s the US, Russia and other nations separated sufficient quantities of ^6Li for their then massive weapons programs. The US COLEX (Column Exchange) process was based on the IE on transfer of Li between an aqueous solution of LiOH and a lithium-mercury amalgam. ^6Li has a greater affinity for Hg than does ^7Li . In the COLEX process the amalgam was prepared using natural abundance lithium, and then agitated in contact with a natural abundance LiOH solution. The rare ^6Li isotope concentrates in the amalgam. A countercurrent flow of amalgam and hydroxide solution was passed through a cascade to obtain the desired enrichment. Enriched ^6Li was separated from the heads amalgam and the mercury recovered and mixed with natural abundance feed for recycling.

The COLEX units operated between 1955 and 1963. Approximately 24 million pounds of mercury were employed and, unfortunately, a good deal was lost through waste, accidental spills, and evaporation. In fact, about 2 million pounds have not been accounted for. The process discharged approximately a quarter million pounds into the surface waters in the vicinity of the plant, and much of this remains in the bottom sediments of the watershed.

8.5 Chromatography

Chromatography is a separation process which exploits exchange between a stationary phase and a mobile fluid phase. It differs from distillation or liquid–liquid extraction which employ two mobile phases. If the moving phase is a vapor or a vapor carried in a stream of permanent gas, and the stationary phase is a supported liquid film, one has gas–liquid chromatography; alternatively if the stationary phase is an absorptive solid, one has gas–solid chromatography. Similarly if the moving phase is a solution at low concentration in a liquid solvent or a high density super-critical fluid, we have liquid or super-critical fluid chromatography,

as appropriate. In still another modification, the stationary phase might be an ion-exchange resin and the moving phase an aqueous (or non-aqueous) solution. Clearly, any or all of these chromatographic techniques can be adapted to isotope separation.

An essential feature of chromatography is that it offers multiple equilibrations between the mobile and stationary phases. By straightforward analogy with distillation where the single stage separation factor is given by VPIE, one defines the single stage chromatographic factor in terms of the equilibrium distribution coefficient between mobile and stationary phases. This accounts for one great advantage of chromatography, i.e. the possibility of tailoring the separation factor to fit the problem (within limits) by varying the chemical nature of the stationary phase, the solvent for the mobile phase, the temperature, etc. Another advantage is that chromatographic columns contain large numbers of theoretical plates (in excess of 10^6 in gas chromatography, 10^5 or more for liquid elution chromatography). Therefore complete or substantially complete enrichments are possible even when separation factors are small. Still, this advantage is offset by serious difficulties. In chromatography a small amount of adsorbate (the mixture of isotopes in our case) is placed on the first plate, or the first few plates, then washed through the column using an eluent mobile phase. The more strongly adsorbed isotope lags the less strongly adsorbed one(s). As elution proceeds, separation increases, but so do band widths. The technical problem is to adjust conditions to optimize separation for given band broadening.

Throughout any chromatographic process it is easy to see that not all plates are carrying out separative work. In fact separation is only happening at the front and rear of the moving band. At any given instant, most of the column is empty. A direct comparison between the number of plates in chromatography, where there are a very large number of plates, but only a few of them are working at any given time, and the number of plates in reflux distillation, where there are far fewer plates, but all are working, is inappropriate. It can even be misleading. Another important difficulty in chromatography is that band broadening and other diffusive inefficiencies increase dramatically (and nonlinearly) with column loading. The result, except in special cases, is that it is difficult to scale-up chromatographic separations to produce useful amounts of separated isotopes. Most often chromatography is better suited to the analysis of mixtures of isotopes, than it is to production enrichment.

8.5.1 Gas Chromatography

To illustrate consider gas chromatography. Figure 8.16 shows an idealized plot of detector response vs. time. Here t_0 is the time lapse between injection and elution of inert material, and t_1 and t_2 are retention times for the isotopomers of interest. For difficult separations $t_1 \sim t_2 \gg t_0$. The resolution, R , is related to the band widths, $R = (t_2 - t_1)/(2w)$, and the number of plates (assumed to be the same for both isotopomers) is, $n = 4(t/w)^2$. The separation factor is $\alpha = t_2/t_1$, and the

Henry's Law constant for the equilibrium is $K_H = (V_c/V_g)((t/t_0) - 1)$. V_c and V_g are the volumes of condensed and vapor phases in the column (i.e. for gas-liquid chromatography, V_c is the volume of the liquid film on the supported packing or open tubular wall, and V_g the volume of void space, respectively). If the column is in the linear range (small loading) the resolution is,

$$R^2/t = (1/16)(V_g/V_c)(C/K_H)((\alpha - 1)/\alpha)^2 \quad (8.18)$$

C is an apparatus constant. Usually C , α , and K_H are temperature dependent, but α and K_H more so than C . Also $\ln(\alpha)$ behaves analogously to VPIE and normally increases as temperature falls according to $1/T$ or $1/T^2$ (Chapter 5), while K_H typically increases exponentially as temperature falls. These two criteria conflict so far as the best choice of temperature is concerned, and for good separations it is necessary to determine the optimum compromise. With α and K_H set by the selection of operating system and temperature, resolution is proportional to V_g/V_c . For maximum resolution the vapor volume is increased by electing open tubular columns, i.e. wetted wall columns with minimal liquid loading, and therefore minimal capacity.

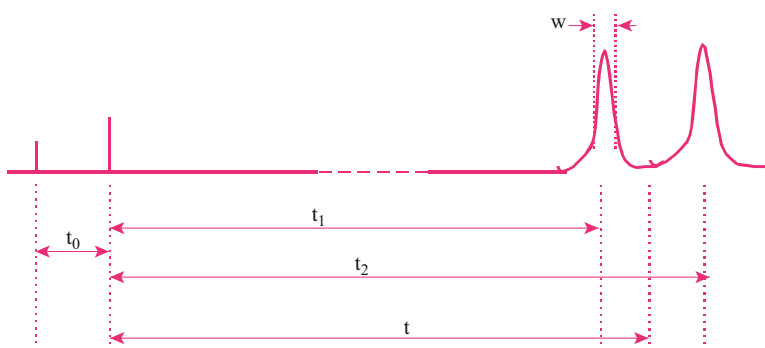
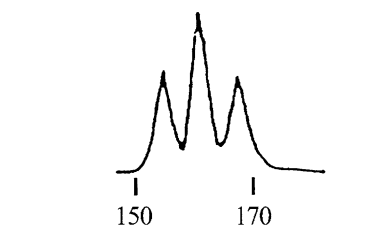


Fig. 8.16 An idealized gas chromatogram. The ordinate shows detector response, the abscissa is time

Fig. 8.17 Gas chromatographic separation of deuterio-acetylenes at 195 K. Elution, left to right in minutes, is in the order C_2H_2 , C_2HD , C_2D_2 (Reprinted from Phillips, J. and Van Hook, W. *A. J. Chromatography* **30**, 211 (1967), copyright 1967, with permission from Elsevier)



Examples of gas chromatographic isotope separation are shown in Figs. 8.17 and 8.18. Figure 8.17 shows the gas chromatographic separation of the three protio/deutero-acetylenes. The separation is interesting, especially because ordinary syntheses lead to a disproportionated mixture of C_2H_2 , C_2HD , and C_2D_2 . Pure C_2HD can only be obtained by separation of the ternary mixture. Distillation is not possible because the triple point lies above 1 atm, and the compressed gas is not only dangerous (it tends to detonate), but polymerizes except when dilute. The authors attempted to scale-up the separation, but resolution deteriorated with column loading and the method is impractical except for isolation of very small amounts of C_2HD .

Significant differences in gas-liquid chromatographic separation factors are obtained by varying the polarity of the liquid loading or column substrate (and hence the strength of the gas-condensed phase interaction), as well as the temperature. Careful attention must be paid to both factors when optimizing chromatographic separations. Figure 8.18a shows separation of some H/D-n-alkanes at high resolution using an open tubular liquid film capillary column. It nicely demonstrates the power of gas chromatography for small scale (analytical) separations. Figure 8.18b shows RPLC (reversed phase liquid chromatography) plots for separations of a selection of H/D hydrocarbons. For these separations the mobile phase is a dilute solution of the hydrocarbons in a methanol/water mixture. The stationary phases are surface bound and coated $-Si-O-R$ groups. Again, complete quantitative separations are possible on an analytical scale.

8.5.2 Redox Ion Exchange Chromatography

The use of anion-exchange resins for isotope separation of uranium (pilot plant scale) is an interesting example of applied liquid elution chromatography. Japanese workers studied anion redox reactions of the U(IV)–U(VI) couple and developed a process to separate uranium isotopes. They used Ti(III) and Fe(III) as the reducing and oxidizing reagents respectively and fine tuned the process to enable recovery and recycling of those reagents. Recycle is an obvious requirement for practical implementation. In a typical set of experiments a 0.1 M U(VI) solution in 3.6 M HCl was fed to a column packed with a porous strongly basic anion exchanger supported on 50 μm porous silica beads to form a uranium adsorption band. The band was then eluted with a solution containing 3.5 M HCl, 0.6 M U(IV), a reducing reagent, and 1 M Fe(II) which is a catalyst for the U(VI)–U(IV) exchange. A cyclic process using two 1 m columns was employed with intermittent addition of the red-ox reagents after each band pass. After a total migration of ~ 192 m, the uranium band, now 1.4 m long was extracted from the column and fractions collected for elemental and isotope ratio analysis. It is interesting to note that the data (amply confirmed with many additional experiments on uranium and other heavy metals) show the temperature dependence and the odd/even mass ratios of isotope exchange fractionation factors for these heavy metals differ significantly from the predictions of the

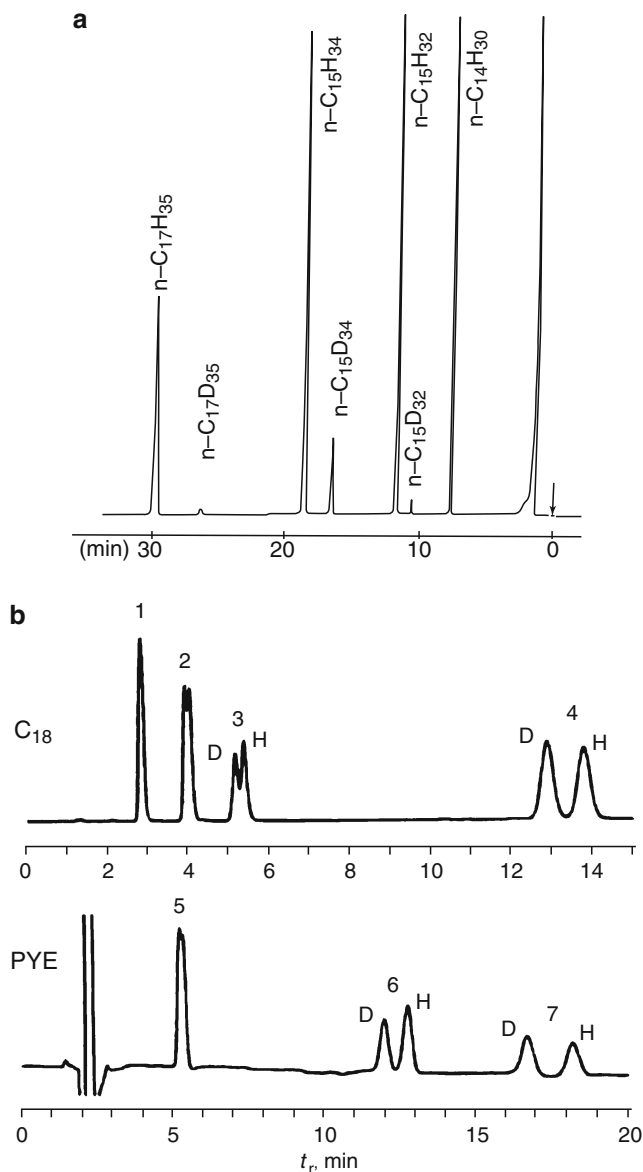


Fig. 8.18 (a) High resolution gas chromatographic separation of some perprotio/perdeutero hydrocarbons at high resolution using an open tubular fused silica column at 413 K, $\sim 1.5 \times 10^5$ theoretical plates (Reprinted from Matuchka, M. *Chromatographia* **27**, 552 (1989), copyright 1989 with permission from Springer Science and Business media). (b) Liquid chromatographic H/D separations in a 70% methanol/water mobile phase for seven isotopomer pairs with surface bound $-\text{Si}-\text{O}-\text{C}_{18}\text{H}_{37}$ and $-\text{Si}-\text{O}-\text{PYE}$ (PYE = pyrene) stationary phases. 1 –Benzene- h_6/d_6 ; 2 –toluene- h_8/d_8 ; 3 –naphthalene- h_8/d_8 ; 4 –anthracene- $\text{h}_{10}/\text{d}_{10}$; 5 –cyclohexane- $\text{h}_{12}/\text{d}_{12}$; 6 –n-octane- $\text{h}_{18}/\text{d}_{18}$; 7 –dodecan-1-ol- $\text{h}_{25}/\text{d}_{25}$ (Thornton, E. R. et. al. *J. Am. Chem. Soc.* **125**, 13836 (2003))

vibrational Bigeleisen–Mayer theory of isotope effects (Chapter 4). That observation is of considerable theoretical importance, and was later shown to be due to the contribution of heavy element nuclear isotope field shifts to the reduced partition function ratios. As explained in Section 4.12 the field shifts are consequent to the interaction of electrical nuclear anisotropy (i.e. isotope dependent nuclear dipole and quadrupole moments) with the electronic part of the wave function evaluated at the nucleus. The field shifts, which only contribute significantly at high atomic number, introduce a new mechanism for understanding the unusual temperature dependences and mass dependence of isotope effects on exchange equilibria of heavy elements.

8.6 Photochemical and Laser Isotope Separation

The idea of using selectively absorbed radiation to cause isotope separation is an old one. In 1922 Hartley and his coworkers proposed the synthesis of HCl from a mixture of H₂ and Cl₂ where only one Cl₂ isotopomer would be photoexcited, the idea being that isotopomer would go on to react preferentially. The experiment, using white light filtered through natural chlorine, failed, but only because the reaction involves a scrambling chain mechanism, a fact not appreciated in 1922. A later photochemical experiment succeeded in separating mercury isotopes by exciting gas phase Hg atoms with light from an isotopically enriched mercury arc. That experiment succeeded because mercury has a relatively simple spectrum with widely separated lines.

The essential conditions for photochemical isotope separation are: (1) a significant isotope shift in the absorption spectrum of the element or compound being irradiated (i.e. an isotope shift which is larger than the band width of the incident radiation); (2) rapid reaction of the excited species leading to some atom or molecule readily separable from the mixture; (3) a light source with spectral band narrow enough to excite only one isotopic species, and intensity large enough to carry out the excitation efficiently. It was the invention of the laser which provided a convenient source of intense radiation of narrow band width and made photochemical isotope separation practical. The first laser isotope separation (on bromine) was reported in 1967 (Tiffany, Moos and Schawlow, 1967). Since then vigorous development work has been carried out, and small scale separations have been reported for many elements. An enormous literature dealing with the theoretical and experimental aspects of laser based separations is available. We will make no effort to treat this material in detail, contenting ourselves with simply outlining the conceptual basis of laser isotope separation.

8.6.1 Outline of a Laser Isotope Separation Scheme

It is convenient to divide ordinary LIS schemes into five parts. (1) Preliminary exchange of the “working” molecule with bulk feed. Usually it will not be possible to

apply LIS directly to cheap bulk feed (e.g., water or methane for H/D separation), and the desired isotope must be chemically exchanged into a “working” molecule. If the desired isotope is rare it is important the working material be recyclable. Although this step involves conventional chemistry, its cost may dominate the overall process. (2) Selective excitation: the working molecule is laser irradiated with a frequency which excites only the desired species. (3) Excited state molecules are converted to a new isotopically enriched species (molecules, free radicals, ions, etc.). (4) Capture before the excited species converts and loses enrichment by decay or exchange. (5) Final conversion of the secondary species to useful chemical or physical form.

Note, it is only in step (2), above, that laser physics is involved. Nonetheless in the overall LIS process each and every step is important, and may be critical in determining whether the overall separation scheme is economical. In step (2) it may be advantageous to employ long wave length lasers which have relatively good efficiency and low energy cost per photon. An important parameter is the photon efficiency, ϵ , which gives the fraction of absorbed photons which yield excited species containing the desired isotope. This is approximately

$$\epsilon = 1/[1 + 1/(\delta S)] \quad (8.19)$$

S is the selectivity of photon absorption under the particular experimental conditions, and δ is the relative abundance of the desired isotope. Equation 8.19 shows, for example, that S values on the order of 10^3 are required before more than about 10% of photons are used to excite D in natural abundance H/D mixtures ($\delta \sim 1.5 \times 10^{-4}$). The selectivity required for uranium separation is less because $\delta(^{235}\text{U}) > \delta(\text{D})$. In fact according to Equation 8.19 it is only about 15, but that number is misleading because the density of spectroscopic states for molecules containing heavy atoms (or for the isolated atoms themselves) is orders of magnitude larger than for lighter molecules. Hence the spectroscopic requirements are much more difficult. Practical LIS schemes usually involve the absorption of more than one photon. It is convenient to refer to energy level diagrams like those in Fig. 8.19.

Provided laser fluence is sufficiently high, a species will absorb enough photons to decompose if the pulse is sufficiently short so that collisions (which lead to deactivation) do not occur during the pulse. As the molecule absorbs photons it is said to be “pumped” up the excitation ladder. In the low energy region the density of states is small and radiationless processes leading to de-excitation are slower than pumping. In this region the states are isotopically well separated, and with proper frequency tuning the desired isotope is preferentially excited. As pumping continues the level spacing decreases (in vibrational spectroscopy because of anharmonic effects, for example), and the laser becomes increasingly “off-resonance”. This results in a drop or “bottle-necking” in pumping efficiency, but once this intermediate region is passed the level density increases dramatically as dissociation is approached, and pumping efficiency again increases. However, near dissociation the level density for undesired species is also high, and in this region pumping does not lead to isotope discrimination, only to dissociation. Also, the high density of states near dis-

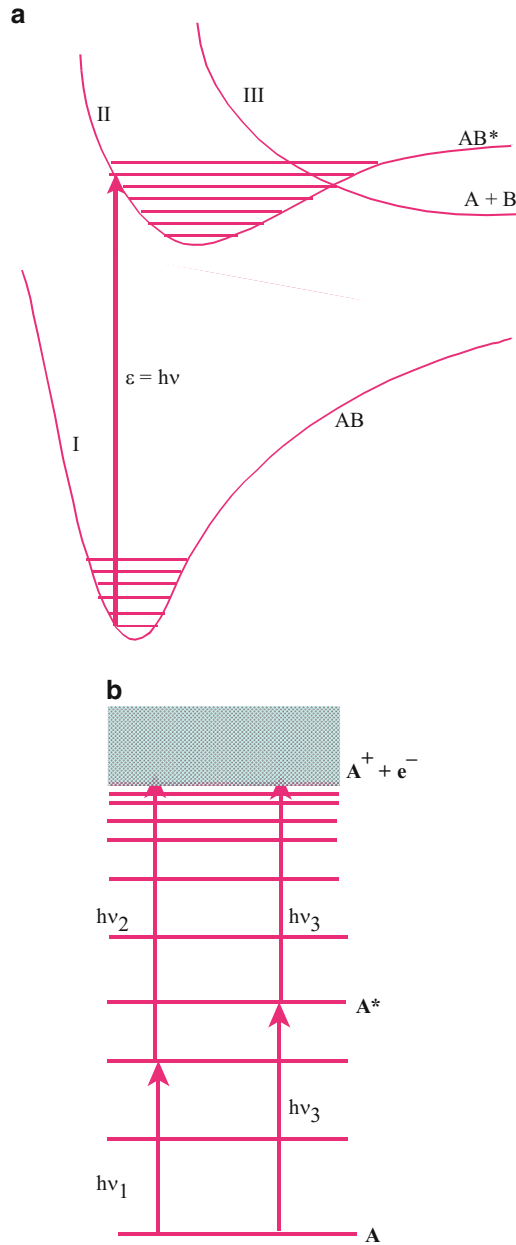


Fig. 8.19 Schematic energy level diagrams showing possible LIS schemes. In each case the level scheme for just one isotope is shown. (Van Hook, W. A. in Vertes, A. *Handbook of Nuclear Chemistry* **5**, 177 (2003)). (a) One photon molecular photodissociation using a single laser. (b) Two photon photoionization using lasers of the same (*right*) or different (*left*) frequencies

sociation leads to an increase in the efficiency of radiationless decay and exchange which may cause isotopic scrambling or recycling to the ground state. Short pulse lasers of high fluence are necessary for efficient separations.

8.6.2 LIS of Deuterium

The ideas above can be illustrated with the multiphoton dissociation of fluoroform, CHF_3 , one of the many LIS schemes which have been proposed for H/D enrichment. Certain of the vibration/rotation bands of CHF_3 , CDF_3 , and CTF_3 are spectroscopically well separated and selective excitation of the heavier isotopomer is practical. For $\text{CDF}_3/\text{CHF}_3$ the selectivity is greater than 2×10^3 when a CO_2 laser is tuned to the ν_5 R branch near 980 cm^{-1} . Dissociation occurs primarily via the reaction, $\text{CDF}_3 \rightleftharpoons \text{CF}_2 + \text{DF}$. Enrichments as high as 2×10^4 have been reported and there is little or no anharmonicity bottle-necking. Because of the high cost of CHF_3 , recycling would have to be incorporated into any practical process. A possibility is the exchange, $\text{CHF}_3 + \text{HDO} \rightleftharpoons \text{CDF}_3 + \text{H}_2\text{O}$, but without a catalyst the reaction is too slow to be practical. The overall economics of LIS H/D enrichment will be determined by the details of the feedstock and exchange reaction selected.

An alternative LIS scheme is one in which a vibrationally excited molecule reacts preferentially with another species. An example is the hydrogen halide/olefin addition reaction, $\text{DX}^* + \text{R}_1\text{R}_2\text{C} = \text{CH}_2 \rightleftharpoons \text{R}_1\text{R}_2\text{CXCH}_2\text{D}$. The scheme involves sequential absorption of several quanta from a CO_2 laser near $5 \mu\text{m}$ to selectively excite DX to a vibrational quantum number of 3 or more. Successful implementation would be expensive because of the highly corrosive nature of halogen acids.

8.6.3 LIS for Uranium

Uranium enrichment using LIS has been exhaustively studied and the conceptual outlines of two different methods can be found in the open literature. These methods are multi-photon dissociation of UF_6 (SILEX, or Separation of Isotopes by Laser Excitation) and laser excitation of monatomic uranium vapor (Atomic Vapor Laser Isotope Separation, or AVLIS). Following an enormous investment, AVLIS was used by the United States DOE in the 1980s and early 1990s, but due to the present oversupply of separated uranium, the plant has been shut down.

8.6.3.1 AVLIS

The spectrum of uranium vapor is complex with more than 3×10^5 lines in the visible region. Still, many of these are sharp and show sufficient isotope separation to permit selective excitation. The basic idea of AVLIS is to irradiate uranium vapor at a concentration around $10^{13} \text{ atoms cm}^{-3}$ (higher concentrations are ineffective

due to collision broadening). The isotope shift $^{235}\text{U}/^{238}\text{U}$ is only $\sim 1/(5 \times 10^4)$ and it is necessary to select a very narrow ^{235}U line, and carry the ionization process out in two steps (because line widths in the ionization region are broad and hence not selective). In the first step ^{235}U is excited from its ground state to a state well below the 6.18 eV ionization potential. That is followed by a less selective absorption into the ionization continuum using a second laser. The ionized uranium atoms are swept to a charged collector. Even though selectivity is high, Benedict, Pigford and Levi writing in 1981 claimed that the charge exchange which occurs during atomic collisions deflects enough ^{238}U to the collector to lower the heads enrichment factor to ~ 10 . At that time the single stage product of $\sim 6\%$ ^{235}U was the highest yet obtained from natural abundance uranium. Presumably enrichments have now improved. Even for the earlier figure, however, nearly complete stripping of ^{235}U was claimed. This is a valuable feature because the feed is expensive. In summary, AVLIS has a sufficient single stage enrichment factor to produce uranium of high enough ^{235}U content to power light water reactors. Furthermore, because AVLIS is an excellent stripper, it can be used to produce 2–3% ^{235}U from the large stockpile of tails now available from earlier gaseous diffusion or gas centrifuge separations. This confers an additional economic advantage.

8.6.3.2 LIS for UF_6 (SILEX)

Although UF_6 has a conveniently high vapor pressure at room temperature, its absorption spectrum is much more complex than the metallic vapor because of the large number of vibration and rotation states superposed on each electronic state. At room temperature these bands are broadened sufficiently to preclude selective absorption. However, if the molecules are cooled the population of thermally excited vib-rot states drops and the spectrum simplifies. At 77 K 69% of UF_6 is in its lowest vibration state, and this increases to 85% at 55 K. However, the vapor pressure is untenably low at such temperatures (7×10^{-3} Pa at 77 K), and equilibrium cooling is out of the question. Still, by cooling in a non-equilibrium expansion nozzle, uranium vapor concentration can be kept at a useful level and LIS is possible. In the first photo-excitation step an infrared long wave length laser selectively excites the $^{235}\text{UF}_6$ molecule in the expansion nozzle to an upper vib-rot state. The excited molecule loses one of its fluorine atoms as it absorbs an ultraviolet photon from a second short wave length laser. The subsequent reaction product precipitates as a fine powder easily separated from the gas.

8.7 Other Isotope Separation Processes

Many other methods for separating isotopes have been described. A partial list includes membrane and membrane pervaporation, thermal diffusion of liquids, mass diffusion, electrolysis and electro-migration, differential precipitation, solvent extraction, biological microbial enrichment, and more. Although not discussed in

this chapter, some are suitable for small scale laboratory separations, and others have been applied on larger scale.

Further Reading

- Avery, D. G., Davies, E., 1973 *Uranium Enrichment by Gas Centrifuge* (London, Mills & Boon, Ltd.)
- Benedict, M., Pigford, M., Levi, H. W., 1981 *Nuclear Chemical Engineering, 2nd Ed.* (New York, McGraw-Hill)
- Cohen, K., 1951 *The Theory of Isotope Separation* (New York, McGraw-Hill)
- Ishida, T., Fujii, Y. 2006 *Enrichment of Isotopes* in Kohen, A., Limbach, H. H. *Isotope effects in Chemistry and Biology* (Boca Raton, FL, CRC Press, Taylor & Francis)
- Kistemaker, J., Bigeleisen, J., Nier, A. O. C., Eds. 1958 *Proceedings of the International Symposium on Isotope Separation* (Amsterdam, North-Holland)
- Klein, E. R., Klein, P. L. Eds. 1979 *Proceedings of the 3rd International Conference on Stable Isotopes* (New York, Academic) p. 175
- London, H., 1961 *Separation of Isotopes* (London, George Newnes)
- Rae, H. K., Ed., 1978. *Separation of Hydrogen Isotopes, ACS Symposium Series 68* (Washington, DC, American Chemical Society)
- Spindel, W. 1969 *Isotope Effects in Chemical Processes, Advances in Chemistry Series 89* (Washington, DC, American Chemical Society)
- Spindel, W., Ishida, T., 1990 *Isotope Separation*, in Lerner, R. G., Trigg, G. L., Eds. *Encyclopedia of Physics* (New York, VCH Publishers) 2nd Ed.
- Van Hook, W. A. 2004 *Isotope Separation*, in Vertes, A., Nagy, S., Klencsar, Z., Eds. Volume 5, p. 177, *Handbook of Isotope Chemistry* (Dordrecht, Kluwer)
- Villani, S., 1979 *Uranium Separation* (Berlin, Springer-Verlag)

Chapter 9

Isotope Effects in Nature: Geochemical and Environmental Studies

Abstract The application of isotope effect studies to problems in geochemistry and geology, meteorology, environmental studies, archeology and paleobotany, food authentication, medical diagnostics and various other practical areas is described using numerous examples.

9.1 Introduction

Ever since the discovery of deuterium nearly 80 years ago measurements of the isotope ratios of naturally occurring materials have provided important information in geochemistry and geophysics, meteorology, evolutionary biology, archeology, and in the applied sciences. For example, comparisons of isotope distributions in co-existing minerals, with those measured on samples equilibrated in the laboratory, or with theoretically calculated ratios, have been used to specify the conditions of formation of the mineral. Similarly, fractionation of the hydrogen and oxygen isotopes of water during natural phase changes (i.e. evaporation, rain, snow, or ice formation), or chemical changes (precipitation of hydrated minerals, biological/ metabolic equilibration, etc.), furnishes considerable information on the nature of those processes. Such information, however, can be hard won. We recall that the natural abundance of many isotopes of interest is very low (Table 7.5), and variations in abundance ratios, while measurable, are even smaller. For example the oxygen isotope ratio in natural waters, $R = {}^{18}\text{O}/{}^{16}\text{O}$, normally lies in the range ($0.0019 < R < 0.0021$), while R for standard mean ocean water (SMOW), the most widely used reference, is 0.00200. Thus a 1% ${}^{18}\text{O}/{}^{16}\text{O}$ IE characterizing some physical or chemical change of interest amounts to a change of about $\Delta R = 0.00200 \times 1.01 - 0.00200 = 0.00002$, i.e. 20 ppm (parts per million). For D/H, $R_{\text{SMOW}} = 1.58 \times 10^{-4}$ and a 1% effect only amounts to $\Delta R = 1.6$ ppm. These are small changes indeed and careful attention to experimental detail and sophisticated instrumentation are required to measure them with sufficient precision and accuracy to distinguish between alternate explanations for observed fractionations.

9.2 Notation and Standards

9.2.1 The Delta, δ , Notation

Because the natural variations in stable isotope abundances are usually very small (see above), and since routine measurements are usually made in an isotope ratio mass spectrometer which compares the relative intensities of the mass resolved beams of the sample with those of some standard material (Section 7.2.2), it is standard practice to report abundance ratios using the dimensionless δ -value notation.

$$\delta_X = 1,000(R_X - R_{STD})/R_{STD} \quad (9.1)$$

The R's refer to isotope ratios, D/H, $^{13}\text{C}/^{12}\text{C}$, $^{18}\text{O}/^{16}\text{O}$, etc. By convention R is the ratio of heavy to light isotope. The factor of 1000 converts to per mil (‰) units. In the case of hydrogen isotope effects $(R_D - R_{STD})/R_{STD}$ is sometimes multiplied by 100 instead of 1000 and reported in per cent (%) rather than per mil, but in this text we use per mil notation almost exclusively.

Example 9.1. A meteoric water sample taken at high latitude and analyzed with ordinary isotope ratio precision might show $\delta\text{D} = (-200 \pm 2)$ and $\delta^{18}\text{O} = (-30 \pm 0.3)\text{‰}$. Using Equation 9.1 we see these are equivalent to $(R_D - R_{STD}) = (31.6 \pm 0.3)\text{‰}$, $R_D = (126.4 \pm 0.3)\text{‰}$; and $(R_{18\text{O}} - R_{STD}) = (-59.7 \pm 0.6)\text{‰}$, $R_{18\text{O}} = (1929.8 \pm 0.3)\text{‰}$, since $R_{STD,D} = 158$ and $R_{STD,O18} = 1989.5\text{‰}$ (Table 9.1). To obtain results of comparable precision by measuring the absolute intensities of the D and H, or ^{18}O and ^{16}O peaks (127.6 and 999,872, or 1930 and 998,070 intensity units, respectively), would have required intensity measurements with a precision of better than a few parts per thousand for each peak, and this for peaks where intensities vary by as much as a factor of 8000. That level of experimental precision is next-to-impossible. The enormous variation in scale between major and minor peaks almost certainly implies significant differences in instrumental sensitivity, calibration settings, etc., when tuning to one or the other. The superiority of the isotope ratio mass spectrometer thus becomes apparent (Section 7.2). In these instruments one compares sample and standard peaks of nearly the same intensity. Thus, when switching from sample to standard, the instrument sensitivity, calibration, scale setting, etc. all remain the same and over-all precision is much improved. It is much more difficult to determine the absolute concentration of a trace isotope than it is to compare the concentrations of that isotope in sample and reference.

9.2.2 Standards

Standards for isotope ratio measurements are chosen for convenience and assigned $\delta = 0\text{‰}$. Ideally, every standard would be homogeneous, easily obtained in the necessary quantity, have an isotope ratio similar to that in the samples being

Table 9.1 A selection from the Table of Light Stable Isotope Standard Reference Materials available from NIST in limited quantity.^a δ values in per mil (‰)

Standard	δD_{VSMOW}	$\delta^{13}C_{VPDB}$	$\delta^{18}O_{VSMOW}$	$\delta^{15}N_{AIR}$	Approx. natural abundance
Vienna standard mean ocean water, VSMOW	0 ^b		0 ^b		D/H = 158 ppm 18/16 = 1990 ppm
Greenland ice sheet precipitation, GISP	-190		-24.8		
Standard light Antarctic Precipitation, SLAP	-428 ^b		-55.5		
Vienna PeeDee Belemnite VPDB		0 ^{b,c}			13/12 = 0.0111
National Bureau of Standards Oil, NBS22-oil		-29.7			
United States Geological Survey 24- Graphite		-16			
National Bureau of Standards limestone, NBS19-limestone		+1.95			
National Bureau of Standards silica, NBS28-silica sand			+9.6		
NGS2 natural gas, petroleum (CH ₄)	-170	-44.8			
NGS2 natural gas, biogenic (CH ₄)	-176	-73.3			
Air				0 ^b	15/14 = 0.00371
International Atomic Energy Agency N1-ammonium sulfate				+0.4	

^aReference samples for Li, B and S are also available.

^bExactly defined reference value.

^cThis material no longer available.

investigated, and be easily processed. The standard of choice for δD and $\delta^{18}O$ measurements is a homogeneous sample of ocean water (standard mean ocean water, SMOW) now entrusted to the International Atomic Energy Agency in Vienna (hence VSMOW). The standard for $\delta^{13}C$ was a sample of limestone (belemnite) from the PeeDee geological formation in South Carolina, (PDB, now VPDB), but that sample is now almost completely used, so other standard limestones are now available from the National Institute of Standards and Technology (NIST) (see Table 9.1).

9.2.3 Conversion from One Standard to Another

To convert a δ value referenced to a given standard (1), to its value when referenced to another (2) multiply by the factor γ ,

$$\gamma = (1000 + \delta X_{\text{STD},2}) / (1000 + \delta X_{\text{STD},1}) \quad (9.2)$$

The δ values are, of course, expressed in per mil (‰). The result is approximately the same as that given by,

$$\delta_2 X = \delta_1 X + (\delta X_{\text{STD},2} - \delta X_{\text{STD},1}) + (\delta_1 X)(\delta X_{\text{STD},2} - \delta X_{\text{STD},1}) / 1000 \quad (9.3)$$

Similarly the fractionation between two samples, say A and B, both referenced to the same standard is,

$$\alpha_{A=B} = (1000 + \delta B) / (1000 + \delta A) \quad (9.4)$$

To good approximation, for δB and $\delta A \ll 1000$,

$$\alpha_{A=B} \sim 1 + (\delta B - \delta A) / 1000 \quad (9.5)$$

because $\alpha_{A=B} = (1000 + \delta B) / (1000 + \delta A) = (1 + \delta B / 1000) / (1 + \delta A / 1000) = (1 + \delta B / 1000)(1 - \delta A / 1000 + \dots) = (1 + \delta B / 1000 - \delta A / 1000 + \text{higher order terms})$. Defining $\Delta_{A=B} = \delta B - \delta A$ we arrive at the simple and very useful result

$$\Delta_{A=B} = 1000(\alpha_{A=B} - 1) \quad (9.6)$$

or

$$\Delta_{A=B} = 1000 \ln \alpha_{A=B} \quad (9.7)$$

since $\ln(1 + x) = x$ for $x \ll 1$.

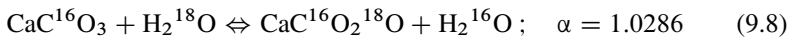
9.2.4 Remarks, Experimental Technique

Differences in isotope abundance between samples are often very small, and sometimes minuscule. Isotope ratio mass spectrometers are generally designed to use gas samples and due care is required in the chemical work up of the raw samples in order to avoid any isotope fractionation. One should select procedures which give 100% chemical yield and also ensure the product gas is thoroughly mixed, because the isotopic abundance of the first aliquot of gas can be significantly different from the last, due to Rayleigh enrichment (Section 9.4). One must avoid contamination by exchange with reagents or extraneous materials and ensure quantitative yields of pure gas. Contamination with impurities having the same

molecular mass as the sample are especially to be avoided (i.e. CO₂ with N₂O, CO with N₂). Typical errors introduced in careful chemical workup sum to 0.05 to 0.2‰.

9.3 Geochemical Temperature Scales

In 1947 Harold Urey, the 1934 Nobel Laureate, recognized that the temperature dependence of the isotope exchange equilibrium between water and calcite (the principal mineral in marine limestones) could be employed as a paleo-thermometer. At 298.15 K the fractionation factor for calcite–water is 1.0286,



which is to say $\delta^{18}\text{O} = +28.6$, provided the calcite was laid down from SMOW. Since the temperature dependence of α was known ($d\alpha/dT \sim -0.23\text{‰ K}^{-1}$), Urey concluded that accurate $\delta^{18}\text{O}$ measurements on ancient marine sediments could be used to determine water temperature at the time the sediment was precipitated. In addition to presupposing development of instrumentation of the necessary precision, this conclusion depended on two important assumptions: (1) the isotope concentration of the ocean has remained constant over time and position, (2) the mineral was deposited in thermodynamic equilibrium with ocean water, and has remained unchanged over long periods of time. The original measurement of the temperature dependence of the reference system was made using samples prepared by slowly precipitating inorganic calcite from aqueous solution at several temperatures (Historical Vignette 9.1).

An interesting study using the calcite thermometer scale examined annual growth patterns in mollusks from the Gulf of California. Figure 9.1 compares incremental shell growth for a single mollusk, and $\delta^{18}\text{O}$ in those growth increments, with water temperature. The data were collected over a 1 year period with growth increments measured on an almost daily basis, and $\delta^{18}\text{O}$ samples taken approximately each week. The data show negative correlation of $\delta^{18}\text{O}$ and positive correlation of growth rate with water temperature. Typically mollusks live for 3–4 years and individual shells show the expected cyclic pattern for $\delta^{18}\text{O}$ and growth rings for the entire 3 or 4 year period. In a related study the authors compared isotope and growth data for modern (living) mollusks with those of older shells taken from middens in the Colorado River delta. The data comprise an important contribution to studies on the environmental effects of closing Hoover Dam (mid 1930s), thereby raising average water temperature and salinity in the study region.

One of the more important applications of the carbonate paleo-temperature scale was to aid our understanding of the climate changes Earth has experienced during the last ~ 3 million years, a period of intermittent glaciation. $\delta^{18}\text{O}$ data from a Caribbean sedimentary core corresponding to the most recent 700,000 years are shown in Fig. 9.2. The repeated variations in $\delta^{18}\text{O}$ of amplitude $\sim 1.6\text{‰}$ and



[Historical Vignette 9.1] Harold C. Urey (1893–1981) was born in rural Indiana and educated at the Universities of Montana and California, Berkeley. Following a study leave in 1924 at the Niels Bohr Institute in Copenhagen, he held professorships at Johns Hopkins and Columbia Universities, and at the Universities of Chicago and California where he ended his career as Professor-at-Large. From 1940 to 1945 he was Director of War Research, Manhattan Project, at Columbia. In 1931 Urey devised a method to concentrate possible heavy hydrogen isotopes by the fractional distillation of liquid hydrogen: this led to the discovery of deuterium and the award of the 1934 Nobel prize. Urey formulated an early statistical mechanical theory of isotope effects. Following World War II he concerned himself with the measurement of paleo-temperatures, investigations into the origin of the planets, and the chemical problems of the origin of Earth. (Photo credit: Urey at the Mass Spectrometer, New York 1940s, courtesy of J. Bigeleisen)

frequency $\sim 10^{-5}$ year $^{-1}$ have been interpreted in terms of the cyclic growth and retreat of Pleistocene ice sheets. The pattern can be modeled by assuming an approximate 5 K temperature change peak-to-trough, or a commensurate shift in the $\delta^{18}\text{O}$ of ocean water consequent to extensive ice cap growth and melting. In either case the observed isotope effects clearly relate to glacial cycles.

A prime criticism of the $\delta^{18}\text{O}$ carbonate paleo-temperature scale is the absence of any independent measure of the isotopic composition in ancient seawater. Therefore isotopic fluctuations in the sediments do not necessarily correlate with changes in temperature alone. Even so, the basic idea remains valid. Many ore deposits contain coexisting mineral pairs which have been formed in equilibrium as judged by independent (non-isotopic) criteria. In such cases the mineral-mineral fractionation values for a given M–N mineral pair, $\Delta = \delta_{\text{N}} - \delta_{\text{M}}$, correlate straightforwardly with the geochemical temperature of mineral formation (it being supposed that the equilibrium is “locked-in” as temperature rapidly falls after the initial ore formation). At the high temperatures of formation of metamorphic or igneous rock deposits the isotope fractionation for many mineral systems closely follows the $1/T^2$ dependence predicted by the high temperature approximation to equilibrium isotope fractionation (see Chapters 4 and 5),

$$\ln \alpha \sim \Delta/1000 \sim A/T^2 \quad (9.9)$$

or

$$T(\text{formation}) = [(1000 A)^{1/2}/\Delta^{1/2}] \quad (9.10)$$

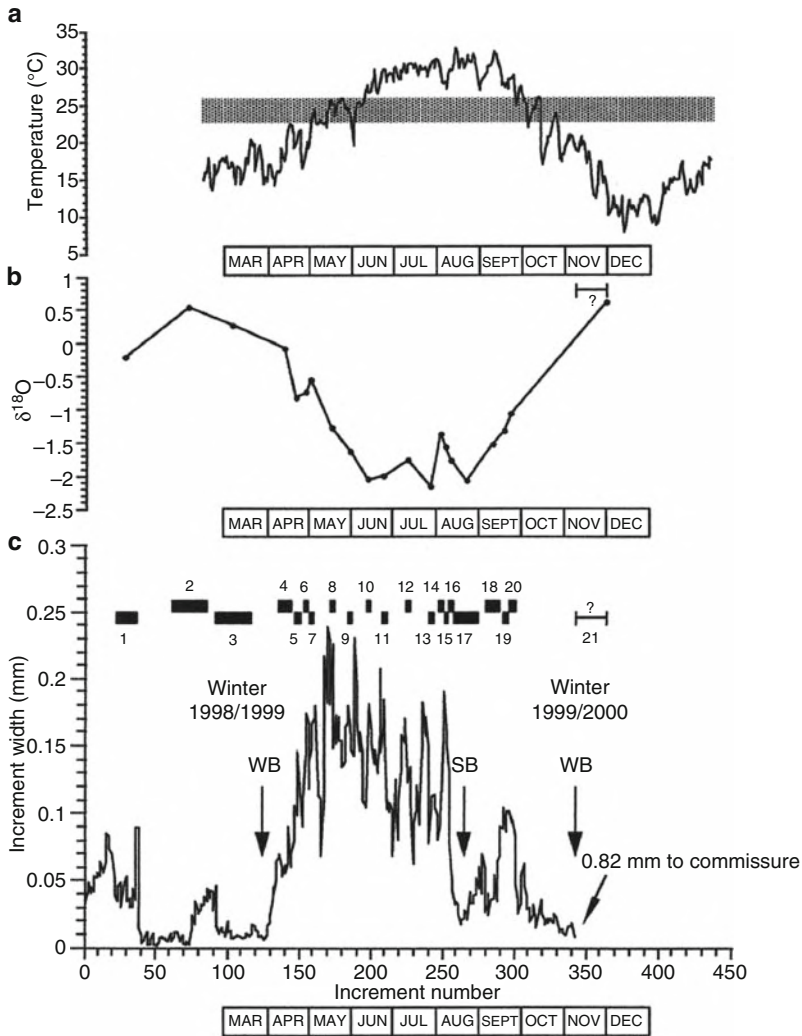


Fig. 9.1 Relation between temperature (a), $\delta^{18}\text{O}$ (b), and daily incremental growth profiles of the mollusk *C. Cortezi* (c). The shaded area in (a) marks the optimum temperature range. In (b) $\delta^{18}\text{O}$ is referenced to (SMOW + 28.6). In (c) WB marks the winter position, and SB the summer growth break. The numbers at the top of (c) locate the samples and rectangular blocks show resolution (Goodwin D. H. et al., *Palios* 16, 387 (2001))

Selected values of $(1000 A)^{1/2}$ for quartz = mineral ^{18}O , and pyrite = mineral ^{34}S equilibria are found in Table 9.2. In other cases, especially at lower temperature, the temperature dependence of IE's on mineral formation may be more complicated and require empirical fits of the form, $\ln \alpha = C_1/T + C_2/T^2$ or $\ln \alpha = C_0 + C_1/T + C_2/T^2$, the C's are empirical least squares fitting parameters.

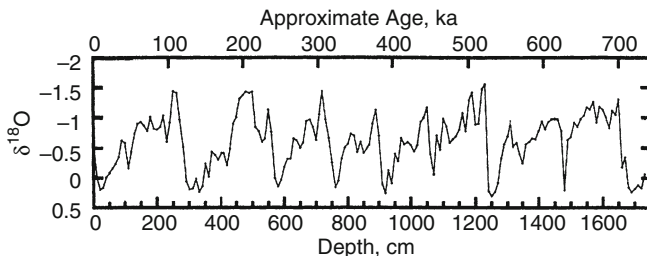


Fig. 9.2 $\delta^{18}\text{O}$ vs. depth for mollusk shells from a 17.4 m-long drilling core from the Caribbean Sea showing systematic variation with time. Each of the saw-tooth patterns lasts $\sim 100,000$ years and correlates with similar patterns at other ocean locations (Reprinted from Emiliani, C. et al. *Earth Planet. Sci. Lett.* **37**, 349 (1978), copyright 1978 with permission from Elsevier)

Table 9.2 Selected ^{18}O and ^{34}S thermometers. (T/K , $\Delta = \delta_N - \delta_M = 1000 \ln \alpha_{NM}$, see Equation 9.10) (Valley et al. *Reviews in Mineralogy* **16**, 1, (1986); Ohmoto and Rye, *Geochemistry of Hydrothermal Ore Deposits* 2nd Ed, p 509. Chacko, T., Cole, D. R., and Horita, J., *Rev. Mineral Geochem.* **43**, 1, (2001))

N	M	$(1000 A)^{1/2}$	Type
Rutile	Quartz	2.3×10^3	$\delta^{18}\text{O}$
Anorthite	Quartz	1.3×10^3	$\delta^{18}\text{O}$
Albite	Quartz	0.5×10^3	$\delta^{18}\text{O}$
Quartz	Calcite	-0.7×10^3	$\delta^{18}\text{O}$
Rutile	Calcite	2.1×10^3	$\delta^{18}\text{O}$
Galena	Pyrite	1.0×10^3	$\delta^{34}\text{S}$
Chalcopyrite	Pyrite	0.7×10^3	$\delta^{34}\text{S}$

9.4 Isotope Hydrology; Rayleigh Fractionation

The use of isotope abundance ratios to refine ideas in earth science is nicely illustrated with studies on natural waters. Water is found almost everywhere on earth. It undergoes phase changes (evaporation, precipitation, freezing, melting), reacts with minerals, and participates in almost all biological processes. Both its hydrogen and oxygen isotopes show large fractionations as these processes occur and provide multiple isotopic records.

The oceans make up $\sim 97\%$ of the hydrosphere and cover $\sim 70\%$ of the earth's surface to an average depth of nearly 4 km. This large reservoir has a surprisingly uniform isotope signature (Table 9.3), showing $\delta\text{D} = 0 \pm 5$ and $\delta^{18}\text{O} = 0 \pm 1\text{‰}$ relative to VSMOW. Larger variations, when they occur, are almost always at the surface and can be assigned to the formation of sea ice, unusually high evaporation from shallow tropical basins, or fresh water riverine influx. The deep waters of the ocean basins show much smaller variations, but have distinctly different values.

Table 9.3 Isotope signatures and reservoir sizes in the hydrosphere (Adapted from Criss 1999)

Reservoir	Volume (%)	$\delta D(\text{‰})$	$\delta^{18}\text{O}(\text{‰})$
Ocean	97.2	0 ± 5	0 ± 1
Glacier, ice caps	2.2	-230 ± 120	-30 ± 15
Groundwater	0.6	-50 ± 60	-8 ± 7
Freshwater streams and lakes	0.02	-50 ± 60	-8 ± 7
Atmospheric water	0.001	-150 ± 80	-20 ± 10

For example deep water samples from the North Atlantic, Pacific, and Antarctic Oceans show $\delta^{18}\text{O} \sim 0.05, -0.15$ and -0.40‰ , respectively.

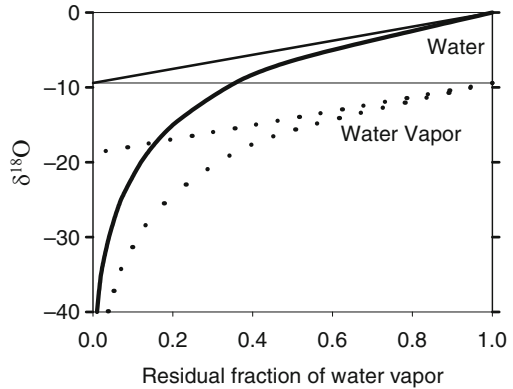
Large changes in the isotope signature of water are associated with condensation, evaporation, or melting. At equilibrium the fractionation between two coexisting phases is a function of the temperature. When water evaporates from the ocean it typically shows $\delta D \sim -80\text{‰}$ and $\delta^{18}\text{O} \sim -9\text{‰}$, less (i.e. more negative) at high latitudes, more (less negative) at lower latitude. No matter the location, however, atmospheric water vapor always has negative δD and $\delta^{18}\text{O}$ relative to SMOW. On condensation from the atmosphere the sign of the fractionation changes. The first rain to fall from a new cloud over the ocean has values of δD and $\delta^{18}\text{O}$ close to 0, and the water which remains in the cloud is systematically depleted in D and ^{18}O . Provided the condensate is continuously stripped from the equilibrating system (i.e. provided the rain falls), the subsequent precipitation has δ values which become more and more negative as the cloud “rains-out”. To sum up, the isotope ratio in the residual cloud changes exponentially according to the fraction of vapor, f , remaining.

$$R = R_0 f^{(\alpha-1)} \quad (9.11)$$

In Equation 9.11 R_0 is the initial isotope ratio of the water comprising the cloud and α is the fractionation factor. This equation was derived by Lord Rayleigh around 1900 to treat single stage enrichment by continuous stripping of vapor from an unreplenished pot. Figure 9.3 shows $\delta^{18}\text{O}$ values for residual vapor and precipitating rain at 300 K calculated from Equation 9.11. Both $\delta^{18}\text{O}$ (residual vapor) and $\delta^{18}\text{O}$ (precipitating rain) fall off dramatically to larger and larger negative values as the fraction of rain-out approaches unity, the difference, $\Delta = \delta^{18}\text{O}(\text{rain}) - \delta^{18}\text{O}(\text{residual vapor})$, remains nearly constant. More realistically, however, as rain-out proceeds the dew-point of the cloud falls and the fractionation factor increases (i.e. becomes more negative, in which case α is a function of the fraction of water vapor which remains), and the changes become even more dramatic than the ones shown by the curved lines in Fig. 9.3.

The straight lines in Fig. 9.3 show $\delta^{18}\text{O}$ for vapor and liquid in a closed system (i.e. where the precipitated liquid remains in contact with residual vapor). As expected from conservation laws $\delta^{18}\text{O}(\text{vapor}, f = 1) = \delta^{18}\text{O}(\text{liq}, f = 0)$ for the closed system. (Conservation laws also predict that $\delta^{18}\text{O}$ for the integrated and thoroughly remixed sample of total rain-out from the open system equals $\delta^{18}\text{O}(\text{vapor}, f = 1)$.)

Fig. 9.3 $\delta^{18}\text{O}$ (water) for liquid and vapor vs. residual fraction of water vapor in open (curved lines) and closed (straight lines) systems during rain-out. The thin line parallel to the abscissa shows $\delta^{18}\text{O}$ for the initial sample of vapor



9.4.1 Fractionation in Hydrology; the Meteoric Water Line

Because the vapor pressure of H_2^{16}O is greater than those of HD^{16}O or H_2^{18}O (Chapter 5) at all temperatures of meteorological interest, $\delta^{18}\text{O}$ and δD for fresh water are always negative with respect to SMOW, and the difference between rain or snow and sea increases as clouds move further inland, or are lifted to higher elevation, or to higher latitude. This pattern is shown for the continental United States in Fig. 9.4. The lightest natural waters globally are observed in snow and ice near the South Pole where $\delta^{18}\text{O}$ values below -50‰ and δD below -450‰ have been reported.

Fractionation data are usually displayed using a three isotope plot (Fig. 9.5). Meteoric waters lie on or close to the correlation line given by Equation 9.12.

$$\delta\text{D} = 8.2 \delta^{18}\text{O} + 10.4 \quad (9.12)$$

Shallow ground-waters follow the same pattern, but waters from deep aquifers, geothermal waters, ice cores, etc. can and do lie well off the line.

9.4.2 Ice Cores

The ice sheets of Greenland and Antarctica are several kilometers thick and preserve a sequential record of high latitude precipitation over tens of thousands of years. This record has been studied by the deep core Arctic and Antarctic drilling programs during the past 30 or more years. An interesting illustration is given by a core drilled at the Russian Station “Vostok” located in the deep Antarctic at high elevation ($78^{\circ}28'\text{S}$, $106^{\circ}48'\text{E}$, 3488 m). The ice sheet at Vostok is about 3.7 km thick and the drill cores sample fossil ice as old as $\sim 350,000$ years. (The present day mean annual temperature is 217 K (-56°C) and the station receives only ~ 2 cm of

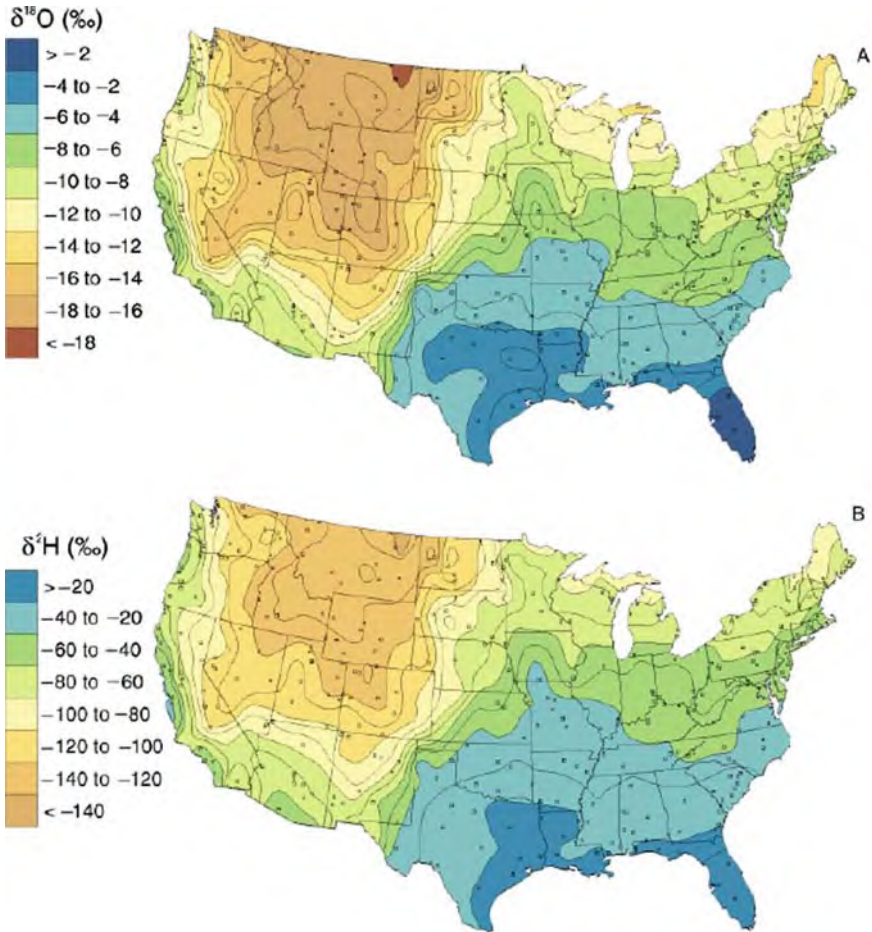


Fig. 9.4 Spatial variations in $\delta^{18}\text{O}$ and δD for river waters in the USA (Reproduced with permission from Kendall, C. and Coplen, J. *Hydrol. Process.* **15**, 1363 (2001). Copyright 2001 from Wiley)

precipitation per year.) The isotopic record of a Vostok core is shown in the upper plot in Fig. 9.6, where it is compared with the $\delta^{18}\text{O}$ data from a carbonate-rich low latitude deep sea core (lower plot). The Vostock data show several sharp saw-toothed climatic cycles. The ice samples corresponding to the glacial maxima are lower than modern precipitation at this location by $\delta\text{D} = \sim 50\text{‰}$ and $\delta^{18}\text{O} = 6\text{‰}$. This suggests that average temperatures during periods of glaciation were about 10 K lower than present day ones. It is interesting that the pattern of the ice core data reflects that of the tropical sedimentary carbonate cores. The $\delta^{18}\text{O}$ saw-tooth pattern occurs at the same intervals, but has smaller amplitude and is of opposite sign. The cy-

Fig. 9.5 $\delta^{18}\text{O}$ and δD values in meteoric waters change with temperature but always lie along the meteoric water correlation line shown in this three isotope plot (Modified from Craig, H. *Science* **133**, 1702 (1961))

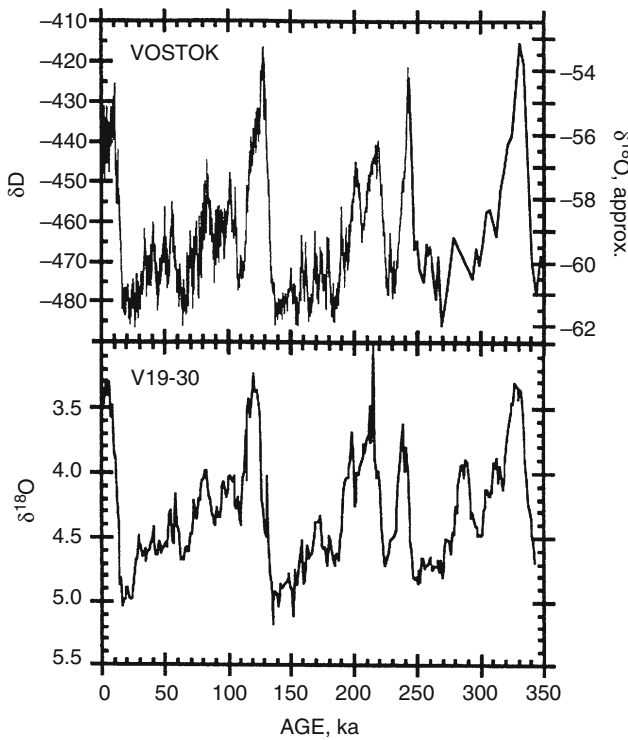
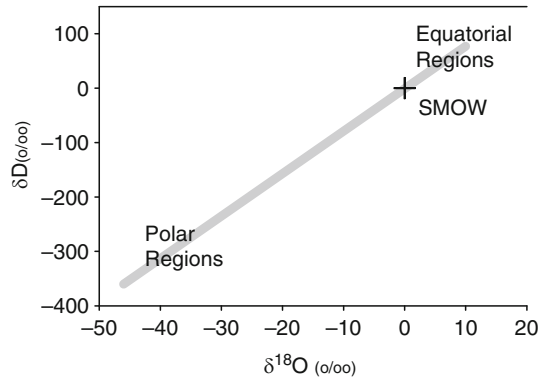


Fig. 9.6 Climate records from the Vostok Antarctic ice core and the tropical carbonate seafloor sediment core V19-30 (Shakleton, N. J. and Pisais, N. *Am. Geophys. Union, Geophys. Mon.* **3**, 303 (1985))

cles represent a combination of the effects of climate change and changes in $\delta^{18}\text{O}$ in seawater caused by the growth or retreat of the polar ice caps.

A second interesting ice core is shown in Fig. 9.7. Here the $\delta^{18}\text{O}$ record preserved in a Greenland core as old as 12,000 years before present (BP) is compared with the

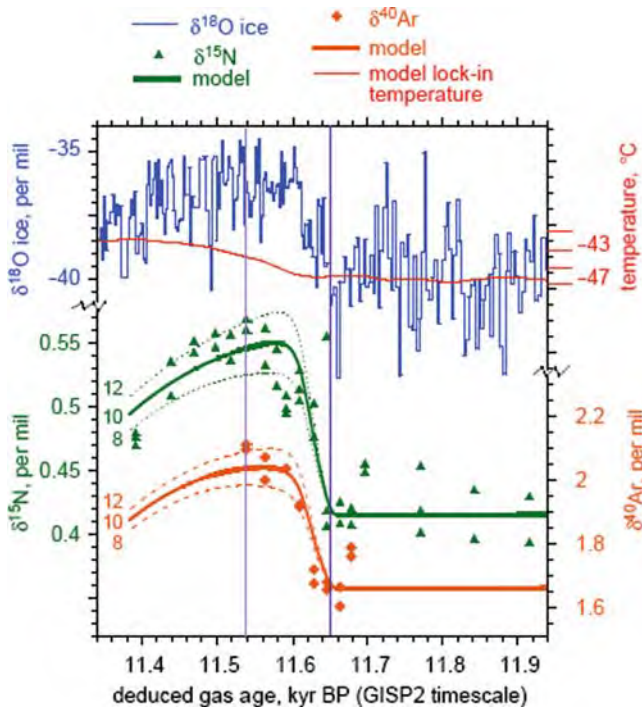


Fig. 9.7 Isotope records of abrupt climate change at the Younger-Dryas/Preboreal transition $\sim 11,600$ years BP taken from Greenland ice core data. The $\delta^{18}\text{O}$, $\delta^{15}\text{N}_2$, and $\delta^{40}\text{Ar}$ isotopic records are plotted from top to bottom (Reprinted from Grachev, A. M. and Severinghaus, J. P. *Quat. Sci. Rev.* **24**, 513 (2005), copyright 2005, with permission from Elsevier)

$\delta^{15}\text{N}_2$ and $\delta^{40}\text{Ar}$ records of gas trapped in the ice. The gas fractionations, referenced to present day air, are consequent to diffusion in (or from) air bubbles trapped in the ice. Gas phase diffusion coefficients are temperature and isotope dependent and provide independent isotope paleo-thermometers. Figure 9.7 clearly shows a “consistent three-isotope, two-pair” demonstration of an abrupt ~ 10 K global warming occurring about 11,600 years BP (the Younger–Dryas transition). The result provides a target for models which attempt to predict the near-future climate of Earth (i.e. global warming models).

9.4.3 Clay Cores: ^{13}C Enrichment in Paleo-Organics

Another example of the use of the isotope fractionation record as an indicator of major geologic change is illustrated in Fig. 9.8. This figure plots $\delta^{13}\text{C}$ values for the organic material extracted from a Maryland clay deposit laid down during the Aptian period of the early Cretaceous geological epoch. This was an eventful time,

geologically speaking. A spike appeared in the already rapid rate of Atlantic Ocean spreading. This for the first time permitted significant mixing of waters above and below the equator and a dramatic increase in sea temperatures. (The increase in sea temperature was presumably caused not so much by equatorial/temperate ocean mixing, as by the volcanic processes associated with mid-ocean continental spreading). The spike in $\delta^{13}\text{C}$ occurring around 117 million years ago and lasting less than 1 million years (marked with the gray arrow, Fig. 9.8) is attributed to the decomposition of deep ocean methane hydrate deposits due to the rise in sea temperature. The data in Fig. 9.8 is similar to trends in early Aptian $\delta^{13}\text{C}$ signals from terrestrial materials sampled in Europe and South America and confirms the $\delta^{13}\text{C}$ excursion as a global signal. The amplitude of the spike can be rationalized by the liberation and oxidation of ~ 129 Gt (gigatons) of C from methane hydrates, which is less than 2% of the methane stored as methane hydrate along the present day continental margins.

9.5 Three Isotope Plots of Terrestrial and Extraterrestrial Samples

Stable isotope analysis of Earth, Moon, and meteorite samples provides important information concerning the origin of the solar system. $\delta^{18}\text{O}$ values of terrestrial and lunar materials support the old idea that earth and moon are closely related. On the other hand three isotope plots for oxygen fractionation in certain meteoric inclusions are anomalous. They show unexpected isotope fractionations which are approximately mass independent. This observation, difficult to understand and initially thought to have important cosmological implications, has been resolved in a series of careful experimental and theoretical studies of isotope fractionation in unimolecular kinetic processes. This important geochemical problem is treated in some detail in Chapter 14.

9.6 Isotope Fractionation by Living or Once Living Organisms

The biological fractionation of isotopes has provided an important tool by which chemists, biochemists and molecular biologists have determined metabolic and genetic pathways (see Chapters 6 and 10–12). Stable isotope pairs of greatest biological interest include D/H, $^{13}\text{C}/^{12}\text{C}$, $^{18}\text{O}/^{16}\text{O}$ and $^{14}\text{N}/^{15}\text{N}$. The range of $\delta^{13}\text{C}$ varies from about -30‰ to $+25\text{‰}$ relative to VPDB, although methane in some natural gases shows values as low as -70‰ and some carbonates in meteorites have been reported in excess of $+60\text{‰}$. In general, however, the reduced carbon found in living and fossilized organisms is isotopically light, but marine carbonates are heavy. Carbonate caps on salt domes, on the other hand, are light ($\sim -36\text{‰}$) and that is evidence they have been formed by oxidation of methane from the petroleum deposits almost always located in the immediate vicinity of the domes. Freshwater

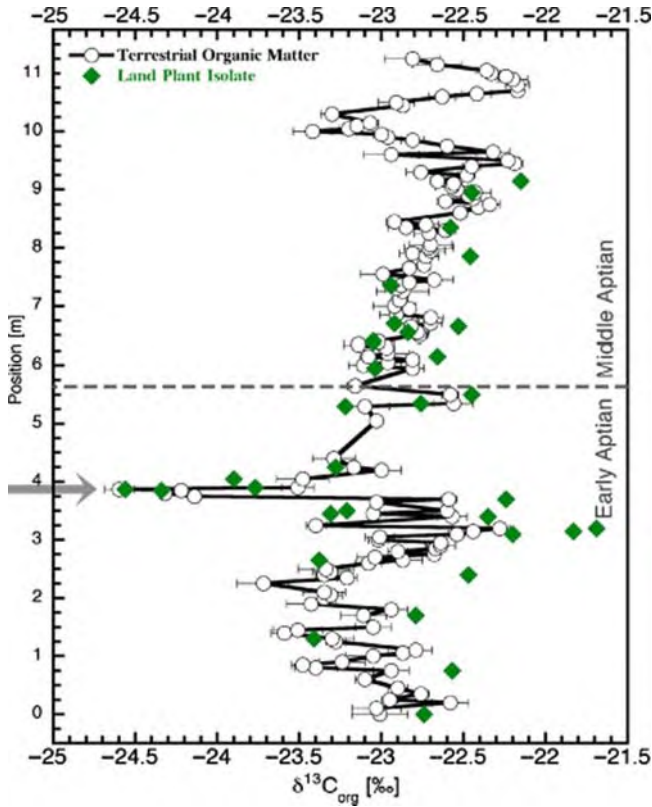


Fig. 9.8 Stratigraphic presentation of $\delta^{13}\text{C}$ values for organic material extracted from the Arundal clay formation, Maryland. *Error bars* reflect the standard deviation for three replicate analyses. The *dashed line* represents the boundary between the early and middle Aptian eras (~ 125 to 112 megayears BP) established from the geological record. The *gray arrow* highlights the isotope shift of interest (Reprinted from Jahren, A. H. et al., *Earth Planet. Sci. Lett.* **236**, 691, (2005), Copyright 2005, with permission from Elsevier)

carbonates are usually light because they are formed from waters charged with CO_2 from the soil, and soil CO_2 is mostly produced from plant respiration and decay. Plant ^{13}C is depleted with respect to the atmosphere.

9.6.1 “We Are What We Eat, \pm a Few per Mil”

The complex biochemical paths in organisms offer many ways to fractionate isotopes by both kinetic and equilibrium processes. It is therefore expected, and is observed, that the different carbon, hydrogen, oxygen and nitrogen atoms in organic residues show compound and atom-site specific isotope fractionations

(Galimov 1985). An outstanding and thoroughly studied example is found in the several distinctly different pathways of photosynthetic carbon fixation by plants. Terrestrial plants using C_3 (e.g. rice, wheat, beets, potatoes, legumes) and C_4 (e.g. maize, corn, sorghum, sugar cane) photosynthetic pathways show different ^{13}C fractionations. In broad terms the photosynthetic process breaks down into at least three different steps, each favoring ^{12}C over ^{13}C : (1) the transfer of CO_2 across cell walls, (2) conversion to intermediate compounds by enzymes, and (3) final synthesis of large organic molecules. The fractionation at each step is kinetically controlled. The distinction between C_3 and C_4 is in the number of carbon atoms found in the products of the initial conversion step. C_4 plants such as maize contain relatively large amounts of carbohydrate and protein and typically show $\delta^{13}C \sim -15\text{‰}$. This compares to the $\sim -25\text{‰}$ found in C_3 plants which contain larger amounts of lignin, cellulose and lipids. Marine plants (including plankton) show $^{13}C/^{12}C$ about 8‰ lower than C_3 plants, most likely because they fix marine HCO_3^- (0‰) rather than atmospheric CO_2 (-7‰). Since, roughly, the degree of isotope fractionation in the plants lying at the base of the food chain is expected to carry over to the animals which consume them, it follows that such isotope ratios can be used to study animal (and human) ecology and archeology (“they are what they eat, ± 1 or 2‰”). That turns out to be the case.

In one interesting study the arrival of maize agriculture from Central America into the lower Illinois valley around AD 1000 was demonstrated by measuring $\delta^{13}C$ of human bone collagen as a function of time (Fig. 9.9). Because of a lack of direct archeological evidence concerning ancient Native American agricultural practice the isotope data helped solve an otherwise intractable problem. This

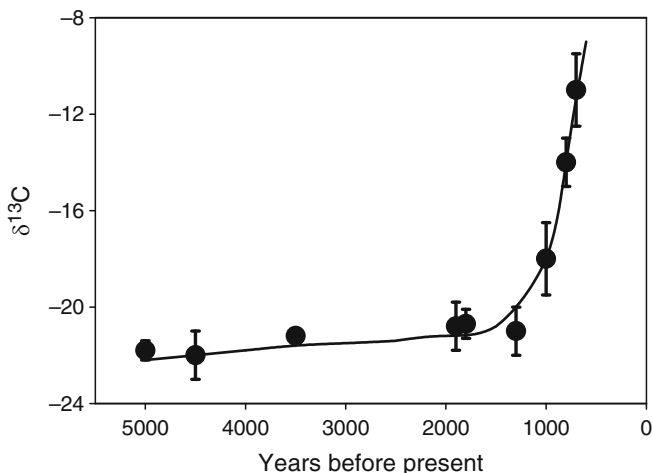


Fig. 9.9 Changes in $\delta^{13}C$ of human bone collagen in the lower Illinois valley prior to AD 800. The data indicate a shift from a C_3 to a C_4 based diet between AD 1000 and 1200 (Van der Merve, *A. Proc. Br. Acad* 77, 247 (1992))

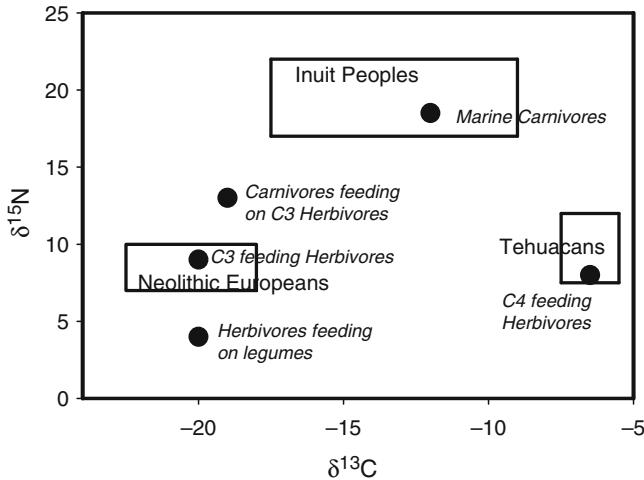


Fig. 9.10 Isotope compositions of plants and of the animals which feed on them (After DeNiro, M. J. *Am. Sci.* 75, 182 (1987))

methodology, extended to include $\delta^{15}\text{N}$ measurements, has been widely applied. Experiments show that with each step up the food chain organisms concentrate ^{15}N . Therefore carnivores have $\delta^{15}\text{N}$ about +3‰ compared to herbivores. In the oceans food chains are longer, and oceanic carnivores may have $\delta^{15}\text{N}$ as much as +10‰ with respect to terrestrial herbivores (see Fig. 9.10).

9.6.2 Isotope Fractionation and Dendrochronology of Bristlecone Pines

Important early measurements of isotope fractionation in ancient organic material were made by Epstein and his students (Historical Vignette 9.2). They reported δD values in bristlecone pines. These plants, found in White Mountains of the southern California desert, are the longest living tree species on earth (~6,000 years). Thus presently living trees are old enough to have sampled the early and mid-Holocene climate which is believed to have been relatively warm. Bristlecone samples can be accurately dated by counting annual growth rings. By measuring δD for the non-exchangeable hydrogen from cellulose extracted from sections of the trunk (thereby avoiding contamination with more recent water) the authors demonstrated that a likely gradual cooling of between 5 and 7 K has occurred in southern California over the past 6,000 or 7,000 years. The observation is consistent with ice core data from Devon Island in the Canadian Arctic. The agreement in the general trend of these two isotopic records suggests that both have recorded global climatic



[Historical Vignette 9.2] **Samuel Epstein** (1919–2001) was born in Kobryn, Poland (now Belarus) and in 1927 moved with his family to Winnipeg, Manitoba. He earned a B.Sc. in Geology and Chemistry from the University of Manitoba, and a Ph.D. in Chemistry from McGill University in 1944. In the late 1940s he worked with Nobel Laureate Harold Urey at the University of Chicago establishing the oxygen isotope paleo-temperature scale. In 1952 Epstein moved to California Institute of Technology to start the geochemistry program. In succeeding years he applied stable isotope chemistry to many aspects of natural science including studies on Pleistocene climatology, glaciology, archeological diets, Greenland and Antarctic ice sheets, the origin of meteorites, tektites and lunar rocks and minerals. His many graduate students and postdoctoral fellows have established their own laboratories all over the world. He exuded a gracious and cordial manner and was particularly adept in showing his interest in and encouragement of the work of younger colleagues, not just in geochemistry, but in all areas of stable isotope science. (Photo credit: Geology Department, California Institute of Technology)

changes. (Neither data set has sufficient temporal resolution to speak to very recent climate changes associated with global warming, i.e. warming effects in the past century, but especially during the past 50 years.)

9.6.3 $\delta^{18}\text{O}$ as a Probe for Storm Patterns

Figure 9.11 shows the oxygen atom isotopic composition in tree rings from long-leaf pines growing in southern Georgia and correlates that data with the historical record of hurricanes in the area. The data extends from around 1855 to 1990 and definitively establishes that wood laid down in hurricane years is isotopically light as compared to the historical average. Clearly the method can be used to extend the record of storms back into earlier history where the documentation of weather events is relatively poor or is missing. Such data is instrumental in establishing patterns of climate change and global warming.

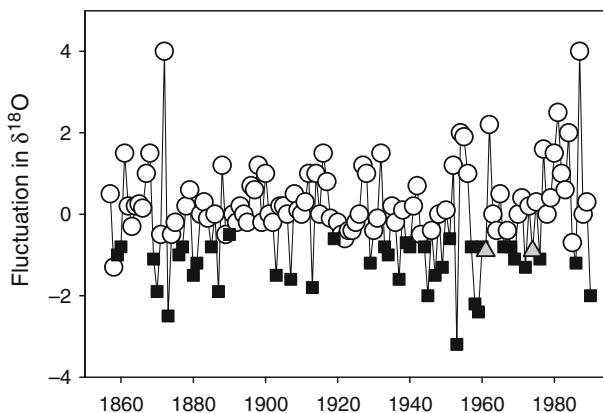


Fig. 9.11 Historical record of $\delta^{18}\text{O}$ in tree rings of long-leaf pine in southern Georgia correlated with the historical record of hurricanes in the area. *Open circles* = no documented tropical storms, *solid squares* = documented storms in area, *shaded triangles* = major tropical storm >400 km from site (Reprinted with permission from Miller, D. L. et al. *Proc. Natl. Acad. Sci.* **103**, 14294 (2006), copyright 2006, National Academy of Sciences, USA)

9.7 Coal, Petroleum and Natural Gas

Petroleum is a naturally occurring complex mixture of mainly hydrocarbons but also containing hetero-compounds with S, N and O, and metal substituted porphyrins. Although most petroleum contains numerous compounds that have been formed directly from biological molecules, its major portion is usually of secondary origin (i.e. decomposition products or products of condensation and polymerization reactions). Stable isotope analysis ($\delta^{13}\text{C}$, $\delta^{18}\text{O}$, $\delta^{15}\text{N}$, $\delta^{34}\text{S}$, δD) is a powerful tool in oil field exploration. Variation in $\delta^{13}\text{C}$ is the most widely studied parameter. Oils are usually depleted 1–3‰ with respect to carbon in their coexisting source rocks. The compounds in a petroleum mixture show characteristic small differences, with ^{13}C increasing from saturated hydrocarbons, through aromatics, to hetero-compounds and asphaltenes. Such information is useful for correlation and mapping purposes.

Coals are formed by high pressure “cooking” of buried ancient plant materials and show variable $\delta^{13}\text{C}$ and δD values. During the coal forming process methane and other light hydrocarbons are liberated, but this has but little effect on the total carbon balance, and little change in $\delta^{13}\text{C}$ is observed with increasing coalification. D/H ratios in coal are usually measured on total hydrogen, even though significant information could be gained by comparing δD of the exchangeable and nonexchangeable fractions. δD usually increases with maturity suggesting some exchange between organic hydrogen and surrounding water during thermal maturation.

About 20% of the World’s natural gas is of biogenic origin. Biogenic methane commonly occurs in recent freshwater or marine sediments and results from various bacterial fermentation processes. Typical $\delta^{13}\text{C}$ for methanes from marine sediments

lie between -110‰ and -60‰ , while those from freshwater sediments are between -65‰ and -50‰ . Thermogenic methane results from deeply buried organic matter subjected to various thermolytic and cracking reactions. Thermogenic methane typically shows $\delta^{13}\text{C}$ in the range -50‰ to -20‰ . Finally abiogenic methane emanating from mid-ocean hydrothermal sources shows very low $\delta^{13}\text{C}$ ($\sim -10\text{‰}$). This kind of data obviously affords a powerful means of discrimination between the different origins of natural gases. Since natural gas as a fuel comprises an ever increasing part of the World's energy consumption such correlations and mappings are economically important.

9.8 Further Examples, Food Authentication

9.8.1 Food Authentication

Natural products such as wine, fruit juices, flavors, oils, and honey are prime targets for fraudulent adulteration because of their high prices. Sophisticated analytical methods (perhaps including isotope abundance measurements) are required to detect whether natural ingredients have been mixed with ones from cheaper synthetic sources. Isotope abundance is markedly different for natural vs. synthetic molecules and these differences can be exploited to detect adulteration. Several examples follow.

9.8.1.1 Fruit and Vegetable Juice

The major adulteration problem in fruit products is addition of sugar. The simplest method of extending a fruit juice is to add inexpensive sugar and dilute with water to rebalance sweetness. Since most juices are extracted from C4 plants ($\delta^{13}\text{C} \sim -15\text{‰}$), and adulterating sugars from corn syrup or cane sugar are from C3 plants ($\delta^{13}\text{C} \sim -25\text{‰}$), the adulterant is easily detected using IRMS. The reference analytical method for authenticating natural strength juices is by determination of D and ^{18}O . European regulations state that values lower than $\delta^{18}\text{O} = 0$ and $\delta\text{D} = -15$ indicate the juice has been watered down.

9.8.1.2 Wines

High quality wines are labeled according to alcoholic content, geographical origin, and year of production. Isotopic fingerprinting makes it possible to determine if there has been dilution with water, the region from which the wine has come (as contrasted to the one from which it is claimed to have come), and the year of production, by using IRMS analysis of the ethanol, sugar and water in the wine.

The EU has installed a data-bank system for all wine producing countries in order to provide reliable proof of the wine's authenticity and origin. One interesting test measures site specific hydrogen isotope ratios at the methyl and methylene groups of the ethanol contained in the wine. It turns out that $\delta D(\text{methyl})$ is representative of the fermentation source (grape, beet, cane or corn sugar), while $\delta D(\text{methylene})$ is mainly representative of the endogenous water (climatic conditions).

9.8.1.3 Alcohols, Acetic Acid (Vinegar)

Alcohol can be produced by anaerobic fermentation of various substrates such as corn, cane, wheat, potatoes, etc. or by chemical synthesis (usually by hydration of petrochemical ethylene). The adulteration of brandy, whiskey, vodka and liquors with synthetically produced ethanol is easily detected with IRMS data for δD and $\delta^{13}C$ (Table 9.4). The matter is important because synthetic alcohol is produced much more cheaply than fermented brandies, whiskeys, etc., but the commercial grade is likely to carry trace amounts of impurities, including carcinogens. Acetic acid is produced by the aerobic fermentation of ethanol to vinegar or by the partial oxidation of synthetic ethanol. Again, marked differences in δD and $\delta^{13}C$ between fermented and synthetic vinegars carry over and permit easy detection of adulteration (Table 9.4).

9.8.1.4 Honey, Maple Syrup

Honey and maple syrup are complex products of high market price ($\delta^{13}C \sim -23\%$). The main source of adulteration is cheap high fructose corn syrup ($\delta^{13}C \sim -13\%$) or cane sugar ($\delta^{13}C \sim -11\%$) and the adulterated product is easily detected at levels as low as 10% or so of added sugar.

Table 9.4 δ values for ethanols and acetic acids from various sources

Origin	δD	$\delta^{13}C$
Alcohol		
Sugar beet	115 ± 2	-27 ± 1
Sugar cane	123 ± 3	-12 ± 1
Corn	122 ± 2	-10 ± 1
Grape	124 ± 2	-27 ± 1
Barley	99 ± 1	
Synthetic	134 ± 1	-31 ± 3
Acetic acid (vinegar)		
Wine	-350 ± 9	-26 ± 1
Cider	-380 ± 7	-27 ± 1
Synthetic	-163 ± 1	-36 ± 5

9.8.2 Athletic ‘Doping’

An interesting illustration of natural product authentication by isotope fractionation is its use in detecting athletic ‘doping’. In the late summer of 2006 the bicyclist Floyd Landis, winner of the Tour de France, was accused of testosterone/epitestosterone (TST/epiTST) doping during the race thus enhancing his performance. The French antidoping lab originally found the athlete’s TST/epiTST ratio to be more than double the ‘normal’ maximum of 4:1. Landis’ claim that this was not due to doping but was a natural fluctuation in his testosterone levels was called into question by the isotope ratio data. His epiTST showed $\delta^{13}\text{C} = -30\text{‰}$, while natural epiTST typically lies at $\delta^{13}\text{C} \sim -24 \pm 1\text{‰}$, and in vitro synthesized epiTST is $\delta^{13}\text{C} \sim -33 \pm 1\text{‰}$. Injection of epiTST is prohibited by sports authorities because its administration will lower the urinary TST/epiTST ratio which is used as a marker of TST administration. This compelling IRMS evidence to the contrary, Landis continued to protest his innocence.

9.9 Stable Isotopes as Tracers in Biological, Agricultural, Nutritional and Medical Research

The use of stable isotopes to trace metabolic processes in plants and animals, including humans, is an important area in isotope science. However the focus of this text is on the understanding of isotopic differences in equilibrium and rate constants (isotope effects), as opposed to the use of isotopes (both stable and radioactive) to follow reaction pathways, metabolic processes, etc. Tracer studies using stable isotopes have a long history. In the 1930s Rittenburg and coworkers fed D-enriched linseed oil to mice and discovered that approximately one-third of the labeled fatty acids were incorporated into the fat tissues of the mice. Later more elaborate studies laid the groundwork for D/H tracer investigations of fat and cholesterol metabolism. Similarly, beginning in the 1940s and 1950s extensive agricultural field investigation using ^{15}N enriched (or depleted) fertilizers or organic residues have allowed agricultural scientists to elucidate the mechanisms of the transformations of N in soils. As a rule of thumb tracer studies ignore isotope effects on equilibrium and rate constants and assume that reaction paths are independent of isotope substitution. Within their frame of reference that approximation seems reasonable, except for studies using heavy hydrogen, where, as we have seen, isotopic differences are often large or very large.

Suggestions for Further Reading

- Abrams, S. A. and Wong, W. W. *Stable isotopes in human nutrition. Laboratory methods and research applications*. CABI Publishing, Cambridge, MA, 2003.
- Criss, R. E., *Principles of Stable Isotope Distribution*, Oxford University Press, New York, 1999.

- Emiliani, C. and Shackleton, N. J. *The Brunhies epoch; Isotopic paleotemperatures and geochronology*. Science **183**, 511–514 (1974).
- Galimov, E.M. *The Biological Fractionation of Isotopes*, Academic, New York, 1985.
- Griffiths, H., Ed. *Stable Isotopes; Integration of Biological, Ecological and Geochemical Processes*, Bios Scientific Publications, Oxford, 1998.
- Hoefs, J. *Stable Isotope Geochemistry*, Springer Verlag, New York, 1973.
- Katz, J. J. and Crespi, H. L. *Isotope Effects in Biological Systems*, in Collins, C. J. and Bowman, N. S. *Isotope Effects in Chemical Reactions*, ACS Monograph #167, Van Nostrand Rheinhold, New York, 1970.
- Kendall, C. and Doctor, D. H. in *Treatise on Geochemistry*, Vol. 5 Drever, J. I., Ed., Elsevier, Amsterdam, 2004.
- Richardson, S. M. and McSween, H. Y., Jr. *Geochemistry, Pathways and Processes*. Prentice Hall, Englewood Cliffs, NJ, 1989.
- Verkouteren, R. M. and Kleindienst, D. B. *Value assignment and uncertainty estimation of selected light stable isotope reference materials*. NIST Special Publication 260–149 (2004).
- Zarzycki, R., Ed. *Stable Isotopes – Some New Fields of Application*, Polish Academy of Sciences, Lodz, 2002.

Chapter 10

Kinetic Isotope Effects on Chemical Reactions

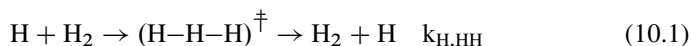
Abstract This chapter describes a number of examples of kinetic isotope effects on chemical reactions of different types (simple gas phase reactions, S_N2 and E reactions in solution and in the gas phase, α and β secondary isotope effects, etc.). These examples are used to illustrate many aspects of the measurement, interpretation, and theoretical calculation of KIE's. The chapter concludes with an example of an harmonic semiclassical calculation of a kinetic isotope effect.

10.1 Introduction

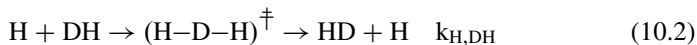
This chapter describes a number of examples of kinetic isotope effects on chemical reactions of different types. These examples will be used to illustrate many aspects of the measurement, interpretation, and theoretical calculation of KIE's. Many of the examples are chosen from the field of organic chemistry. Chapter 11 deals with biochemistry, more specifically with enzyme chemistry.

10.2 KIE's on the "Simplest" Chemical Reaction (Hydrogen Atom + Diatomic Hydrogen)

The hydrogen atom plus hydrogen molecule reaction has been thoroughly studied both theoretically and experimentally (see especially Sections 6.2.3, 6.3 and 6.4). Schematic potential energy surfaces are shown in Fig. 10.1. The diagrams are designed to illustrate the discussion which follows based on transition state theory (TST). More potential surfaces for this reaction are shown in Chapter 6. We begin by considering the two simple identity reactions which proceed on identical potential energy surfaces within the Born–Oppenheimer approximation:

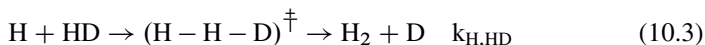


and

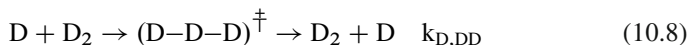
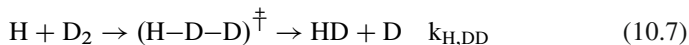
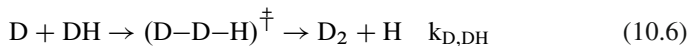


These reactions proceed through symmetrical transition states $[\text{H}\cdots\text{H}\cdots\text{H}]^\ddagger$ and $[\text{H}\cdots\text{D}\cdots\text{H}]^\ddagger$ with rate constants $k_{\text{H,HH}}$ and $k_{\text{H,DH}}$, respectively. The ratio of rate constants, $k_{\text{H,HH}}/k_{\text{H,DH}}$, defines a primary hydrogen kinetic isotope effect. More precisely it should be regarded as a primary deuterium kinetic isotope effect because for hydrogen there is also the possibility of a tritium isotope effect. The term primary indicates that bonds at the site of isotopic substitution the isotopic atom are being made or broken in the course of reaction. Within the limits of TST such isotope effects are typically in the range of 4 to 8 (i.e. $4 < k_{\text{H,HH}}/k_{\text{H,DH}} < 8$).

Complications that arise with this simple reaction are twofold. First, because of the low mass of the hydrogen atom its movement frequently exhibits non-classical behavior, in particular quantum-mechanical tunneling, which contributes significantly to the observed kinetic isotope effect, and in fact dominates at low temperature (Section 6.3). Secondly, in reaction 10.2 protium rather than deuterium transfer may occur:



Note in comparing reactions 10.1 and 10.3 the isotope effect should also be called primary, since the bond to the isotopically substituted atom is being broken, just as it was in Equation 10.2. However in Equation 10.3 the magnitude of the isotope effect will be different than it was in Equation 10.2 since the TS structures $(\text{H}-\text{H}-\text{D})^\ddagger$ and $(\text{H}-\text{D}-\text{H})^\ddagger$ and the newly formed bonds are different (HH in the case of Equation 10.3, HD for Equation 10.2, see Fig. 10.1a). One thus expects $k_{\text{H,HD}}$ to be different from $k_{\text{H,DH}}$ even though both describe primary deuterium isotope effects with a common reference reaction, $k_{\text{H,HH}}$. Furthermore, depending on the experimental conditions one might need to consider other reactions such as:



For these reactions of hydrogen, it is the isotope effect on the high frequency vibrational modes in the diatomic reactant and tri-atomic transition states which dominate in the calculation of the isotope effects using the TS model. Excitation into upper vibrational levels for these high frequency modes is negligible and the zero point energy approximation is appropriate (see Section 4.6.5.2 and Fig. 4.1).

Rate constants comparing reactions 10.1 and 10.4, 10.7 and 10.8 or 10.3 and 10.5 illustrate an interesting point. When the hydrogen (or deuterium) atom attacks the

H₂ molecule, for example (Equations 10.1 and 10.4) (see Fig. 10.1a) the ZPE contribution to the rate ratio is $RT[\ln(k_{H,H_2}/k_{D,H_2})] = -[(ZPE_{HHH} - ZPE_{DHH})^\ddagger - [(ZPE_{HH} - ZPE_{HH}) - (ZPE_H - ZPE_D)]_{\text{REACTANTS}}] = -[(ZPE_{HHH} - ZPE_{DHH})^\ddagger]$ because the atom attack is on a common diatomic (H₂ in this case) and the zero point energies of both attacking atoms, ZPE_H and ZPE_D, are zero. E₀[‡] is the energy difference between the bottom of the transition and ground state potential wells and is isotope independent. Consequently the zero point energy contribution to the isotope effect is expected to be inverse, since there is no zero point energy contribution in the ground state but there is one in the transition state (see Fig. 10.1a). The contribution from tunneling, however, will be in the opposite direction, because H atoms tunnel much more effectively than do D. Consequently, at low temperature where tunneling dominates the isotope effect for this H or D atom transfer is expected to be positive, but at higher temperatures tunneling is damped out and the isotope effect drops off markedly, see Table 10.1.

It is interesting to contrast the rate ratio for reactions 10.1 and 10.4 where either H or D atoms react with H₂ with that for reactions 10.1 and 10.7 where common H atoms react with either H₂ or D₂ (compare Figs. 10.1a and b). In the first case, (k_{H,HH}/k_{D,HH}), there is a ZPE difference in the transition state but not the ground state; consequently the high temperature KIE is inverse. In the second (k_{H,HH}/k_{H,DD}), however, there are zero point energy differences in both the transition and ground states. We expect the vibrational force constants to be smaller in the more loosely bound transition as compared to the ground state. The isotope effects scale with the force constant differences. Consequently $RT[\ln(k_{H,HH}/k_{H,DD})] = -[(ZPE_{HHH} - ZPE_{HDD})^\ddagger - [(ZPE_{HH} - ZPE_{DD}) - (ZPE_H - ZPE_D)]_{\text{REACTANTS}}] = -[(ZPE_{HHH} - ZPE_{HDD})^\ddagger - (ZPE_{HH} - ZPE_{DD})] > 0$ since $(ZPE_{HHH} - ZPE_{HDD})^\ddagger < (ZPE_{HH} - ZPE_{DD})$. The isotope effect calculated by TST is positive and reinforces the positive tunneling contribution (Table 10.1). The term "semi-classical" is often employed when referring to TST calculations because the motion over the barrier is "classical". However the vibrational motion in the other 3N-7 (3N-6) coordinates is treated quantum mechanically, hence the term "semi-classical". Still the term, although in wide use, is a bit misleading since these KIE's, like all vibrational isotope effects are quantum mechanical. Because the term "semi-classical" can be misleading we have chosen not to employ it in this text.

A third example demonstrating the balance between large tunneling effects in VTST, which dominate at low temperature, and TST isotope effects due to vibrational force constant changes between the reactant and corresponding transition state is that for reactions 10.7 and 10.6. For this pair of reactions there is a common transition state (see Fig. 10.1c) and the vibrational contribution to KIE is $RT[\ln(k_{H,DD}/k_{D,DH})] = -[(ZPE_{HDD} - ZPE_{HDD})^\ddagger - [(ZPE_{DD} - ZPE_{DH}) - (ZPE_H - ZPE_D)]_{\text{REACTANTS}}] = -[-(ZPE_{DD} - ZPE_{DH})] < 0$ since $ZPE_{DD} < ZPE_{DH}$. Again, at low temperature where tunneling dominates, the isotope effect for this H or D atom transfer is expected to be positive, but at higher temperatures the relative contribution of the tunneling is damped out and the isotope effect is inverse, $RT[\ln(k_{H,DD}/k_{D,DH})] < 0$.

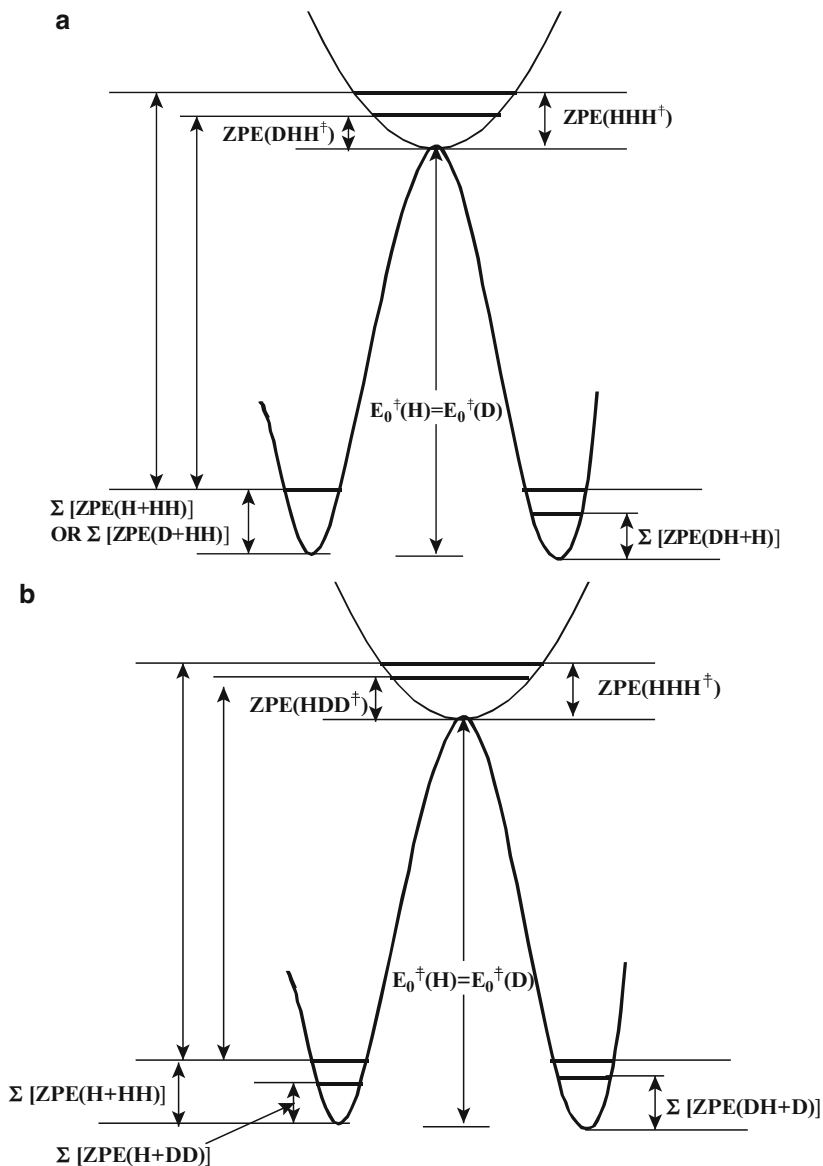


Fig. 10.1 Zero point energy diagrams. (a) An H or D atom attacking an H₂ molecule. The TST isotope effect is negative (inverse, $k_D > k_H$) because there is no zero point isotope effect in the ground state, and tunneling is ignored in the TST approximation. (b) An H atom attacking either an H₂ or D₂ molecule. The isotope effect calculated in the TST approximation is positive (normal, $k_H > k_D$) because the zero point isotope effect in the ground state is larger than that in the transition state.

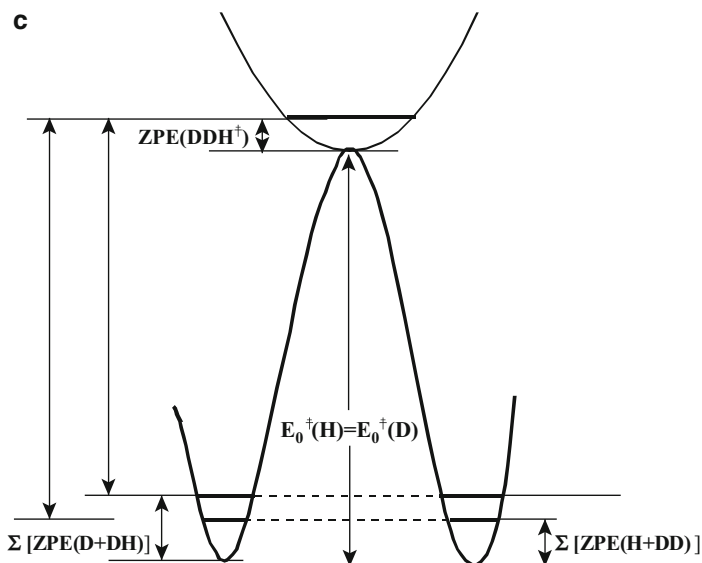


Fig. 10.1 (continued) (c) An H atom attacking D_2 or a D atom attacking HD. The TST isotope effect is negative (inverse) because the zero point isotope effect in the ground state is negative)

Table 10.1 Temperature dependence of some hydrogen isotope effects (After D. G. Truhlar and coworkers)

	$(k_{10.1}/k_{10.7})^a$	$(k_{10.8}/k_{10.7})^a$	$(k_{10.4}/k_{10.7})^b$	$(k_{10.4}/k_{10.7})^c$
	$k_{H,HH}/k_{H,DD}$	$k_{D,DD}/k_{H,DD}$	$k_{D,HH}/k_{H,DD}$	$k_{D,HH}/k_{H,DD}$
T/K	Calculated	Calculated	Calculated	Experiment ^c
200	81	2.4	74	-
300	18	1.7	16	15
400	8.7	1.4	7.9	7.6
800	2.8	1.1	2.7	2.8

^a*J. Chem. Phys.* **59**, 395 (1973).

^b*Phys. Rev. Lett.* **91**, 063201/1–4 (2003).

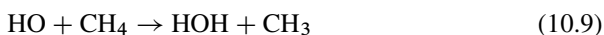
^cRidley, B. A., Schulz, W. R., and Le Roy, D. J., *J. Chem. Phys.* **44**, 3344 (1966).

Table 10.1 shows isotopic rate ratios calculated using variational transition state theory for examples selected from reactions 10.1 through 10.8. The trends shown in the table are those expected from the qualitative discussion above and from examination of Fig. 10.1. The results in the table are in excellent agreement with experiment, and in fact for the last example, $(k_{10.4}/k_{10.7}) = k_{D,HH}/k_{H,DD}$, the agreement is quantitative. Both accurate high precision experimental data and results from exhaustive theoretical analysis have recently become available for these two reactions, $D + HH = DH + H$ and $H + DD = HD + D$. The excellent agreement between theory and experiment is gratifying. In fact, Truhlar and coworkers conclude by remarking, “The list of solved problems in molecular quantum mechanics is very short, e.g. the electronic spectra of the hydrogen and helium atoms

and the vibrational–rotational spectrum of H_2 , H_2^+ , and H_3^+ . Now the thermally averaged $\text{H} + \text{H}_2$ rate constant can be added to the list.” In addition, and as already noted in Chapter 4, values of equilibrium constants for isotopic exchange reactions (including, e.g., $\text{H}_2 + \text{D}_2 = 2\text{HD}$ and $\text{H}_2\text{O} + \text{HD} = \text{HDO} + \text{H}_2$) can be calculated theoretically in very good agreement with experimental observation.

10.3 The Reaction Between Methane and Hydroxyl Radical

A slightly more complicated example, yet one which is useful to illustrate a problem which can occur when analyzing isotope effects is the reaction between hydroxyl radical and methane:



Ideally, comparison of the rate constant for Equation 10.9 with that for the reaction involving mono-deuteromethane:



yields the primary deuterium isotope effect. It should be kept in mind, however, that for mono-deuteromethane the statistical probability of hydrogen atom transfer is three times that for deuterium atom transfer:



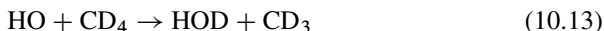
In reaction (10.11) the deuterium isotope effect is a secondary isotope effect, that is one in which the bonding to the isotopically substituted atom is not broken or formed during the course of the reaction. Secondary deuterium isotope effects are generally much smaller than primary ones.

An interesting point to keep in mind when designing experiments to measure isotope effects like those expressed in Equations 10.9 through 10.11 is the dependence of the observed rate ratios on the isotopic composition of the reactants. In principle the true isotope effect should be independent of the isotopic composition; thus the natural abundance experiment should yield the same value of an isotope effect as that measured by experiments using enriched material. On the other hand the observed rate ratios may be significantly different. That point can be illustrated using an example based on the above reactions. First, we assume (arbitrarily) that the true primary deuterium isotope effect ($k_{(10.9)}/k_{(10.10)}$), where subscripts indicate reactions, is equal to 5 and the true secondary deuterium isotope effect ($k_{(10.9)}/k_{(10.11)}$) is 1.3. The values we have selected are typical for reactions of this type. In comparing the rates of reactions 10.9 and 10.10 one must take into account the fact that the OH radical can react with any one of the four H (or D) atoms on the methane or substituted methane. For reaction 10.10 the average rate is simply $k_{(10.10)} = (3k_{(10.11)} + k_{(10.10)})/4$ while for 10.9 the average rate is simply

$4k_{(10.9)}/4$. Therefore the observed rate ratio $(k_{(10.9)}/k_{(10.10)})_{\text{obs}}$ is:

$$\begin{aligned} (k_{(10.9)}/k_{(10.10)})_{\text{obs}} &= 4k_{(10.9)}/(3k_{(10.11)}+k_{(10.10)}) \\ &= 4/[3(k_{(10.11)}/k_{(10.9)}) + (k_{(10.10)}/k_{(10.9)})] \\ &= 4/(3(1.3^{-1}) + 5^{-1}) = 1.6 \end{aligned} \quad (10.12)$$

Compare that figure with the result expected when enriched perdeuterated methane is mixed with unlabeled hydroxyl. The observed isotope effect corresponds to $k_{(10.9)}/k_{(10.13)}$ where:



Using the rule of geometric mean, which states that isotope effects are independent and cumulative we write analogous to Equation 10.12:

$$(k_{(10.9)}/k_{(10.13)})_{\text{obs}} = (k_{(10.9)}/k_{(10.13)})(k_{(10.9)}/k_{(10.11)})^3 = 5 \times (1.3)^3 = 11 \quad (10.14)$$

The observed isotopic rate ratio effect in this case is nearly an order of magnitude larger than the one described by Equation 10.12. This is because the design of the experiment using the fully deuterated species reports simultaneously on both the primary and three secondary deuterium isotope effects, while the earlier experiment yields roughly one-fourth of the primary deuterium isotope effect. (The rule of the geometric mean, which is approximate except in the high temperature limit (Sections 3.5.2 and 4.11.3.2), when applied to the present case is written $[k(\text{CH}_4)/k(\text{CD}_4)] = [k(\text{CH}_4)/k(\text{CDH}_3)]^4 = [k(\text{CH}_4)/k(\text{CD}_2\text{H}_3)]^2$, etc. Thus writing $\ln(\text{KIE}_{\text{D}_4}) = \ln[k(\text{CH}_4)/k(\text{CD}_4)]$ and $\ln(\text{KIE}_{\text{D}_1}) = \ln[k(\text{CH}_4)/k(\text{CDH}_3)]$, etc., we have $\ln(\text{KIE}_{\text{D}_4}) = 4 \ln(\text{KIE}_{\text{D}_1}) = 2 \ln(\text{KIE}_{\text{D}_2}) = (2 \ln(\text{KIE}_{\text{D}_1}) + \ln(\text{KIE}_{\text{D}_2}))$, etc.)

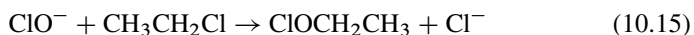
10.4 Further Discussion, Heavy Atom Isotope Effects, Secondary Isotope Effects

For historic and practical reasons hydrogen isotope effects are usually considered separately from heavy-atom isotope effects (i.e. $^{16}\text{O}/^{18}\text{O}$, $^{16}\text{O}/^{17}\text{O}$, etc.). The historic reason stems from the fact that prior to the mid-sixties analysis using the complete equation to describe isotope effects via computer calculations was impossible in most laboratories and it was necessary to employ various approximations. For H/D isotope effects the basic equation $\text{KIE} = \text{MMI} \times \text{EXC} \times \text{ZPE}$ (see Equations 4.146 and 4.147) was often drastically simplified (with varying success) to $\text{KIE} \sim \text{ZPE}$ because of the dominant role of the zero point energy term. However that simplification is not possible when the relative contributions from MMI (mass moment of inertia) and EXC (excitation) become important, as they are for heavy atom isotope effects. This is because the isotope sensitive vibrational frequency differences are smaller for heavy atom than for H/D substitution. Presently

almost every laboratory enjoys access to computer programs which permit detailed calculation of all three terms, MMI, EXC and ZPE. The earliest such programs for machine calculation of KIEs were introduced by Wolfsberg and Stern in the early 1960s (see reading list). The operative distinction between modern day theoretical treatments of hydrogen and heavy-atom isotope effects comes mostly from the appreciation of the fact that H/D and H/T isotope effects frequently include significant contributions from quantum mechanical tunneling that cannot be captured by conventional TST, while heavy atom tunneling is negligibly small and can be ignored.

10.4.1 α -2° Isotope Effects

Secondary hydrogen kinetic isotope effects are further classified as alpha, beta, etc. depending on the distance of the isotopically substituted atom from the bond(s) that is (are) being made or broken (α = 1 bond, β = 2 bonds, etc.). Consider the simple S_N2 reaction between hypochlorite anion and ethyl chloride:



This reaction proceeds via the transition state illustrated in Fig. 10.2. An S_N2 reaction (second order nucleophilic substitution) in the rate limiting step involves the attack of the nucleophilic reagent on the rear of the (usually carbon) atom to which the leaving group is attached. The rate is thus proportional to both the concentration of nucleophile and substrate and is therefore second order. On the other hand, in an S_N1 reaction the rate limiting step ordinarily involves the first order formation of an active intermediate (a carbonium ion or partial carbonium ion, for example,) followed by a much more rapid conversion to product. A sampling of α and β 2° deuterium isotope effects on some S_N1 and S_N2 solvolysis reactions (i.e. a reaction between the substrate and the solvent medium) is shown in Table 10.2. The

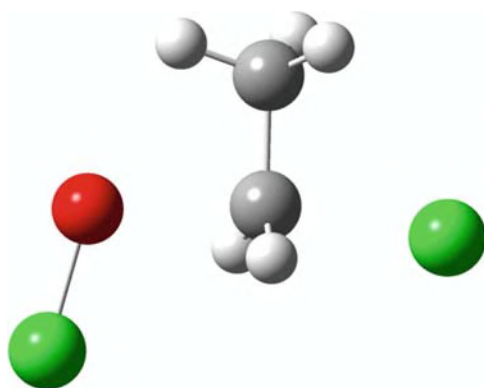


Fig. 10.2 Structure of the transition state of the S_N2 reaction 10.15

Table 10.2 Some 2° deuterium isotope effects mostly on S_N1 reactions(a) Acetolyses of deuterated cyclopentyl tosylates at 50 °C^a

Alkyl tosylate	(k _H /k _D)	ln(k _H /k _D) per D
Cyclopentyl-1-d	1.15	0.14
<i>Trans</i> -cyclopentyl-2-d	1.16	0.15
<i>Cis</i> -cyclopentyl-2-d	1.22	0.20
Cyclopentyl-2,2,5,5-d ₄	2.05	0.18

(b) α-D isotope effects (k_H/k_D) on solvolysis of α-phenylethyl chlorides and bromides in acetone/water or ethanol/water solvents^b

Leaving group	Substituent		
	<i>p</i> -Phenoxy (k _H /k _D)	None (k _H /k _D)	<i>p</i> -Nitro (k _H /k _D)
Cl	1.15	1.15	1.11
Br	1.13	1.12	1.09

(c) Secondary D and primary ¹⁴N/¹⁵N isotope effects on thermolysis of an azo compound^c at 105 °C

Compound	k _H /k _D	k _H /k _D	k ₁₄ /k ₁₅	k ₁₄ /k ₁₅
	Expt	Calc	Expt	Calc
(C ₆ H ₅ (CH ₃)CH(orD)N=) ₂	1.27	1.27	1.023	1.023
ln(k _H /k _D) per D	0.12	0.12		

(d) α-D isotope effects on the S_N2 solvolysis of methyl and ethyl tosylate in water at 25 °C^d

Compound	k _H /k _D
CH ₃ – OTs	0.985
CH ₃ CH ₂ – OTs	1.020

^aStreitwieser, A. et al. *J. Am. Chem. Soc.* **80**, 2326 (1958).^bShiner, V. J. et al. *J. Am. Chem. Soc.* **90**, 418 (1968).^cSeltzer, S. and Mylonakis, S. G. *J. Am. Chem. Soc.* **89**, 6584 (1967); **83**, 2625 (1961); **85**, 14 (1963).^dRobertson, R. E. et al. *Can. J. Chem.* **38**, 222,1505 (1960).

values in the table are typical. Secondary isotope effects for S_N1 solvolysis reactions generally range between 10% and 25% per D. The rationalization originally offered by Streitwieser is generally accepted. In this model the change from sp³ to sp² hybridization at the α-carbon on formation of the carbonium ion transition state is accompanied by changes in force constants and consequently in the vibrational frequencies involving that carbon, particularly in the out-of-plane bending mode, which is significantly red-shifted on the transfer from reactant to transition state thus accounting for the bulk of the isotope effect. These qualitative ideas have been amply confirmed by the machine calculations of Wolfsberg and coworkers (reading list, Stern and Wolfsberg (1968), Shiner et al. (1968)) which show that force constant differences, reactant to transition state, are essential to an understanding of the KIE.

In the S_N2 reaction 10.15 hydrogen atoms on the –CH₂Cl (methylene) group are bonded to the carbon atom that is the center of the nucleophilic attack. This is the

position α to the Cl^- leaving group, and the corresponding isotope effect is the secondary α -hydrogen kinetic isotope effect. The three hydrogen atoms of the methyl group, on the other hand, are separated from the reaction center by a carbon-carbon bond; these positions are β to the leaving group. Similarly, the chlorine isotope effect for ethyl chloride is a primary kinetic isotope effect (the bond to chlorine is broken in the reaction) while that for the chlorine atom in the nucleophile hypochlorite is an alpha secondary ($\alpha - 2^\circ$) kinetic isotope effect.

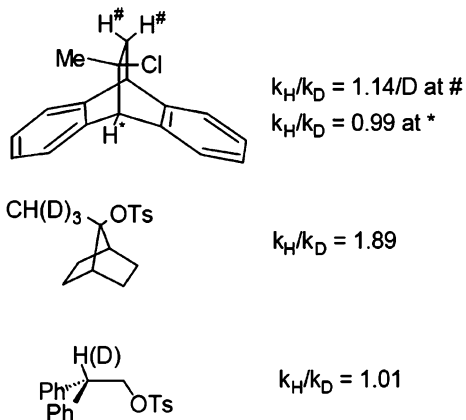
Interestingly, $\text{S}_{\text{N}}2$ reactions do not show significant α - 2° -KIEs. An explanation of the magnitude of typical α -hydrogen KIE's was proposed by Westaway as the so-called "bond strength hypothesis". The hypothesis states that in the formation of an $\text{S}_{\text{N}}2$ transition state the significant changes (and hence larger KIE's) are observed in the weaker of the forming or breaking bonds ($\text{O}\cdots\text{C}$ and $\text{C}\cdots\text{Cl}$, respectively, for reaction 10.15), while the stronger bond will show no or little change (smaller KIE). The relative strengths of the forming and breaking bonds in the transition state are of course not measurable, but can be estimated by assuming they are proportional to the equivalent bond strengths in the reactant and product (which are available from spectroscopic analysis or other methods). Based on this approach, except for identity reactions, it is found that one of the reacting bonds is almost always not significantly altered. This in turn implies that the hybridization of hydrogen atoms alpha to that bond do not significantly differ between reactant and transition state, the corresponding force constant changes are small, and the KIE is expected to be minimal. Similar arguments correlate the magnitude of α - 2° -KIEs with the distance in the transition state between the advancing nucleophile and the leaving group. Loose transition states result in larger isotope effects while tight transition states, in which hydrogen bending is constrained tend to exhibit smaller isotope effects.

10.4.2 β - 2° Isotope Effects

A few examples of β - 2° -KIEs are shown in Fig. 10.3. These effects are markedly dependent on geometry. This is clear from the first example. Deuterium substitution at different β -hydrogen atoms does not lead to the same rate changes for the chloro-solvolysis. That in mind, it is a bit surprising to see that the diphenylethyl derivative shown in the third example does not show much effect upon D-isotope substitution at the β -carbon.

The existence of β - 2° isotope effects is usually rationalized using arguments based on hyperconjugation. A thorough discussion of hyperconjugation is beyond the scope of this book. Briefly, however, if a vacant p-orbital is formed in the substrate during the course of a reaction (as in the formation of a carbocation), and if a hydrogen atom is present at the β -position in a geometry where the C-H bond overlaps with the p (or the developing p) orbital, a stabilizing interaction (denoted as hyperconjugative) is possible. In the limit hyperconjugation can be thought to be a partial cleavage of the β -C-H bond. Because the C-D bond has a lower zero-point energy than does CH, β -C-D bonds will be less effective in stabilizing

Fig. 10.3 Examples of β -2°-KIE's for solvolysis reactions at 318 K (Shiner, V. J. and Humphrey, J. S., *J. Am. Chem. Soc.* **85**, 2416 (1963))



a carbonium ion like species. As a result, the solvolysis rate will be lower in the deuterated derivative. This interpretation assumes that the C–H group is ideally oriented for hyperconjugation with the developing empty p orbital. For this to be valid, the β -C–H bond should be lined up parallel with the developing p-orbital to maximize overlap. Should the two orbitals be orthogonal, there will be no overlap, and isotope substitution will not affect the rate. This is exactly the reason why the “#” positions in the bicyclo[2,2,2] system shown in the first example of Fig. 10.3 displays a normal isotope effect, while substitution at the “*” position shows practically no effect at all. It can be easily seen from a model that the C–H* bond and the empty p-orbital (on loss of Cl^-) are orthogonal. The unusually small β -KIE in the diphenylethyl derivative (Example 3, Fig. 10.3) is a result of an interesting variation in its solvolysis reaction mechanism. Because the carbenium ion formed on loss of tosylate is a primary cation, and since phenyl groups are present at the β -position, the departure of the tosylate group is assisted by phenyl participation (one of the phenyls migrates to form a bridged transition species). Consequently the C–H bond remains almost orthogonal to the developing (empty) p orbital at the adjacent carbon and it is not surprising that there is practically no isotope effect.

10.4.3 Steric Arguments and β , γ ... 2° Isotope Effects

Some distant (i.e. β, γ, \dots) isotope effects have been rationalized using steric arguments. For H/D IE's one recognizes that the C–H vibrational levels lie higher in the potential well and display larger vibrational amplitudes than do the lower lying C–D modes. Also, due to anharmonicity, the equilibrium and mean square bond lengths are slightly shifted from the minimum energy distance. Such effects account for isotope effects on dipole moments, polarizability, NMR shielding coefficients and molar volume (Chapter 12). In any case, the effective bond length is slightly larger for C–H with its larger amplitude of vibration than it is for CD.

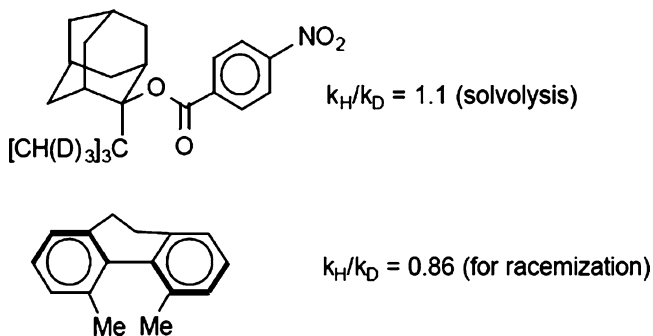


Fig. 10.4 More examples of β - 2° -KIE's. (Top, solvolysis of a *t*-butyl substituted adamantane. Bottom, racemization (loss of optical activity) of a dihydrophenanthrene derivative (Mislow, K., and coworkers, *J. Am. Chem. Soc.* **86**, 1733 (1964))

Consequently it is reasonable to think of CH as slightly larger than CD, and in a crowded environment as more sterically hindered. This can lead to measurable KIE's depending on whether the transition state is less or more sterically encumbered than the ground state. The two examples in Fig. 10.4 demonstrate this idea. If the ground state is more crowded than the transition state (in other words, if strain is relieved upon going to the transition state), the observed KIE will be normal (i.e., >1). This is the case in the solvolysis of the *t*-butyl substituted adamantane shown in the upper example. On the other hand, if the transition state is more crowded, the deuterated isotopomer is more easily accommodated than the protio and the KIE will be inverse (i.e., <1). The racemization of the dihydrophenanthrene derivative (Example 2, Fig. 10.4) is such an example. The molecule is a bit twisted in the ground state due to steric repulsions between the methyl groups. It is therefore chiral. In the transition state of the racemization, however, the molecule is flat, which brings the methyl groups even closer to each other. Since the methyl deuterated derivative has less steric repulsion, the observed KIE is less than unity.

10.4.4 Comment

It is important to point out once again that explanations (rationalizations) of isotope effects which employ arguments invoking hyperconjugation and/or steric effects are completely equivalent to the standard interpretation of KIE's in terms of isotope independent force constant differences, reactant to transition state. In turn, these force constant differences describe isotope dependent vibrational frequencies and frequency differences which are not the same in reactant and transition states. The vibrational frequencies determine the partition functions and partition function ratios in the two states and thus define KIE. The entire process occurs on an isotope independent potential energy surface. This is not to claim that the

hyperconjugation/steric effects do not exist, but rather to argue that it is these effects which cause the force constant and vibrational differences which we in turn employ in the quantitative evaluation of KIE.

10.5 Relative Values for Deuterium and Tritium Isotope Effects: The Swain–Schaad Relation

We will use reaction 10.15 to illustrate two important concepts of kinetic isotope effect studies. The first concerns the relation between isotope effects of different isotopes of the same element, say D and T. We denote the rate constant of reaction 10.15 by k_H and consider isotope effects when one hydrogen in the α -position is substituted by deuterium or tritium:



In reactions 10.16 and 10.17 we label the corresponding rate constants k_D and k_T , respectively. The relationship between k_H/k_D and k_H/k_T is approximately described by the Swain–Schaad equation

$$(k_H/k_T) = (k_H/k_D)^{1.44} \quad (10.18)$$

In deriving Equation 10.18 one assumes that the motions of the H, D, and T can be treated in the ZPE approximation and the only important isotope sensitive motions are the RH, RD, or RT stretching modes which shift significantly on the transfer from reactant to transition state. In the ZPE approximation

$$\ln(k_H/k_D) \sim (\text{ZPE}^\ddagger - \text{ZPE}_R)_H - (\text{ZPE}^\ddagger - \text{ZPE}_R)_D = \Delta\text{ZPE}_H^\ddagger - \Delta\text{ZPE}_D^\ddagger \quad (10.19)$$

For harmonic oscillators recall that the ZPE's, ($\text{ZPE} = (1/2)hc(f/\mu)^{1/2}$), and ZPE differences scale proportionally to $(1/\mu_H)$ and $(1/\mu_D)$, respectively. The μ 's are oscillator reduced masses and f is the isotope independent force constant. Thus, writing equations analogous to Equation 10.19 for tritium substitution, and taking the ratio, we obtain $k_H/k_T = (k_H/k_D)^\chi$ where χ , the Swain–Schaad exponent in the harmonic approximation is expressed

$$\chi = \ln(k_H/k_T) / \ln(k_H/k_D) = (1/\sqrt{\mu_H} - 1/\sqrt{\mu_T}) / (1/\sqrt{\mu_H} - 1/\sqrt{\mu_D}) \quad (10.20)$$

Assuming that the hydrogen, deuterium or tritium vibrates against a carbon atom of mass 12 we have $\mu_X = 12m_X/(12 + m_X) = 0.923, 1.714$ and 2.400 for x equal H, D, and T respectively, so $\chi = 1.43$. Were the hydrogen vibration against infinite

mass the corresponding figures would be 1, 2, and 3, and $\chi = 1.44$. The difference is negligible considering the approximations which have been introduced (Historical Vignette 10.1).

The drastic assumptions involved in reducing the harmonic analysis to the consideration of a single isotopically substituted oscillator in order to obtain Equation 10.20 imply that the result will be most useful for qualitative purposes. In fact, complete $(3n - 6)$ dimensional harmonic TST calculations on numerous different examples of equilibrium and kinetic isotope effects yield a wide range of Swain–Schaad exponents and large deviations of Swain–Schaad exponents from the expected value are often considered as qualitative indicators of either reaction complexity (exponent smaller than 1.44) or intervention of tunneling (exponent larger than 1.44). Even simple reactions, however, exhibit significant deviations from the Swain–Schaad value (see Fig. 10.5). Nowadays, following a suggestion by W. H. Saunders, variants of Equation 10.20 are frequently used in which the common (reference) isotope is one of the heavier isotopes (D or T for the present example), e.g.:

$$(k_H/k_T) = (k_D/k_T)^{3.34} \quad (10.21)$$

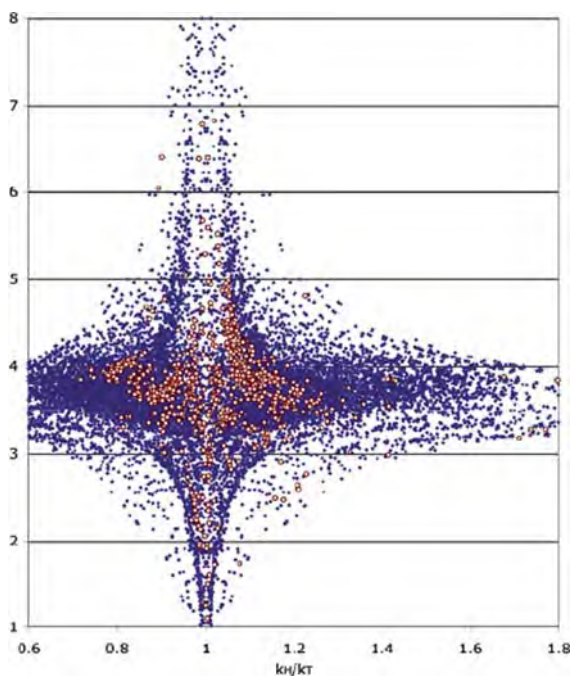


Fig. 10.5 Distribution of exponents, Equation 10.21, for exact harmonic calculated equilibrium and TST kinetic isotope effects (Hirschi, J. and Singleton, D. A., *J. Am. Chem. Soc.* **127**, 3294 (2005))



[Historical Vignette 10.1] C. Gardner Swain (1917–1988) Professor of Chemistry, Massachusetts Institute of Technology made notable contributions to the field of physical–organic chemistry and the investigation of the mechanisms of chemical reactions. His interests focused on nucleophilic reactivities, solvent effects, substituent effects, and the effect of structural changes in reactants on the structure of transition states. He provided one of the first polyfunctional enzyme models. Swain and his students made many contributions to the early development and use of isotope effects to elucidate the mechanisms of important types of organic reactions and transition state structure. (Photo credit: MIT Museum)

Equations analogous to Equation 10.18 have been derived for heavy atom KIEs and validated against experimental data for carbon and sulfur KIEs:

$$\chi = \ln(k_L/k_{H1}) / \ln(k_L/k_{H2}) \quad (10.22)$$

where indexes L, H1 and H2 represent light, first heavy, and second heavy isotopes, respectively. The value of χ is about 1.9 when the mass increments are equal (i.e., $H1 - L = H2 - H1$). Equation 10.22 has been used mostly for carbon KIE's, k_{11}/k_{14} , k_{12}/k_{13} , and k_{12}/k_{14} . Note, however, that some heavy atom isotope effects, e.g., oxygen KIE's (k_{16}/k_{17} vs. k_{16}/k_{18}) deviate substantially (see, e.g., the discussion of mass-independent KIE's in Chapter 14).

10.6 Alternative Reaction Paths, S_N2 and E2: Condensed and Vapor Phase Studies

In the remaining sections of this chapter we will discuss further examples of kinetic isotope effects. The first considers a system in which there is a competition between two mechanisms, S_N2 and E₂ and returns to reaction 10.15. (By E2 we refer to a second order elimination reaction, see Fig. 10.6). In Equation 10.15 the hypochlorite

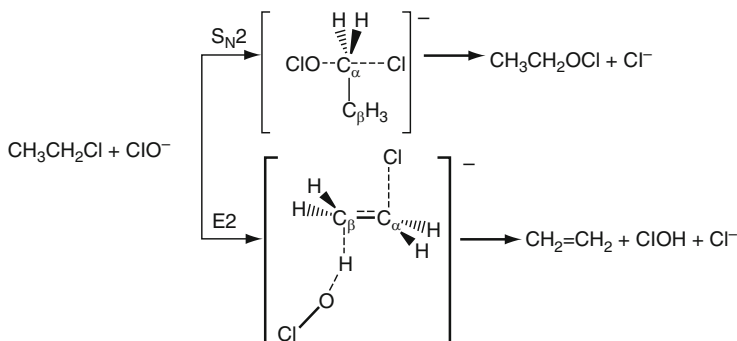


Fig. 10.6 Alternative pathways of reaction between hypochlorite anion and ethyl chloride (Villano, S. M., Kato, S. and Bierbaum, V. M., *J. Am. Chem. Soc.* **128**, 736 (2006))

anion may act as a nucleophile attacking ethyl chloride to form chloride anion and ethyl hypochlorite via the transition state illustrated in Fig. 10.2 and at the top of Fig. 10.6. Alternatively, the hypochlorite anion can abstract a proton from the methyl group eliminating chloride anion to yield ethane and hypochlorous acid. The alternative pathways are illustrated in Fig. 10.6. This particular competition between nucleophilic substitution and base induced elimination has been thoroughly studied in the condensed phase, and more recently in the gas phase. It is interesting to strip away complications introduced by the effects of solvent on the structure and energetics of the reactant ground and the transition states. Studying S_N2 and E2 reactions in the gas-phase allows one to gain insight into the intrinsic features of the reaction path without interference from solvent effects. However, the experiments are inherently difficult and equipment intensive. In broadest outline the technique to study ion-molecule reactions in the gas phase involves the generation of a negative ion by electron bombardment followed by an appropriate series of charge exchange reactions (to yield ClO^- for the example under discussion). The ion of choice passes along a flow tube where once thermalized it reacts with the substrate (ethyl chloride) injected downstream. Ion intensity is measured using a quadrupole mass filter. By this FA-SIFT (flowing afterglow-selected ion flow tube) technique Bierbaum and coworkers have measured reaction rate constants and KIEs for reactions of ClO^- with a series of four alkyl chlorides RCl (R = methyl, ethyl, *i*-propyl and *t*-butyl). The S_N2 /E2 competition, shown in Fig. 10.6 for ethyl chloride, results in substantial changes in the observed KIE's as chain length increases (Table 10.3).

The reaction of ClO^- with methyl chloride can only proceed via the S_N2 process. An inverse KIE of 0.85 is measured (Table 10.3). The reaction with *t*-butyl chloride presumably proceeds via an E2 mechanism (since S_N2 attack on the Cl substituted carbon is blocked) and the observed KIE of 2.31 (Table 10.3) is consistent with that conclusion. The isotope effects for both species are nearly the same as the effects measured in the condensed phase (compare Tables 10.3 and 10.4) and measure the relative contributions of the two paths. The results indicate that the E2 pathway becomes the dominant channel as the substrate becomes more sterically hindered.

Table 10.3 Reaction rate constants ($10^{-10} \text{ cm}^3 \text{ molecule}^{-1} \text{ s}^{-1}$) and deuterium KIEs for the gas phase reaction between RCl and ClO^- around room temperature (Villano, S. M., Kato, S. and Bierbaum, V. M., *J. Am. Chem. Soc.* **128**, 736 (2006))

RCl	k	KIE
CH_3Cl	2.01	
CD_3Cl	2.36	0.85
$\text{C}_2\text{H}_5\text{Cl}$	2.25	
$\text{C}_2\text{D}_5\text{Cl}$	2.27	0.99
<i>i</i> - $\text{C}_3\text{H}_7\text{Cl}$	1.74	
<i>i</i> - $\text{C}_3\text{D}_7\text{Cl}$	1.01	1.7
<i>t</i> - $\text{C}_4\text{H}_9\text{Cl}$	2.33	
<i>t</i> - $\text{C}_4\text{D}_9\text{Cl}$	1.01	2.31

Table 10.4 Deuterium and heavy atom KIEs for methyl and *t*-butyl chloride solvolysis in water at $\sim 350 \text{ K}$

RCl	k(light)/k(heavy)
$\text{CH}_3\text{Cl}/\text{CD}_3\text{Cl}$	0.92 ^a
$^{12}\text{CH}_3\text{Cl}/^{14}\text{CH}_3\text{Cl}$	1.03 ^b
$\text{CH}_3^{35}\text{Cl}/\text{CH}_3^{37}\text{Cl}$	1.01 ^c
<i>t</i> - $\text{C}_4\text{D}_9\text{Cl}/t\text{-C}_4\text{H}_9\text{Cl}$	2.45 ^a

^aRobertson, R. E. and coworkers; *J. Am. Chem. Soc.* **87**, 161 (1965); *Can. J. Chem.* **38**, 222 (1960).

^bBender, M. L. and Buist, G. G. *J. Am. Chem. Soc.* **80**, 4304 (1958).

^cFrisone, G. J. and Thornton, E. R. *J. Am. Chem. Soc.* **86**, 1900 (1964).

It is remarkable that the isotope effects measured for these reactions in the vapor phase are about the same as the solvolysis KIEs measured in aqueous solution.

10.7 KIE's as Probes of Transition State Structure

Based on the early machine calculations of the Brookhaven group (Wolfsberg and Stern, reading list) and somewhat later semiquantitative studies using the BEBOVIB program (Bond-Energy-Bond-Order-VIBration) it has been argued that KIEs provide insight into the structure of the transition state, an entity not amenable to direct experimental scrutiny. At this point we introduce a few concepts from this qualitative description of transition state structure derived from early studies of KIEs. Description of the position of the transition state on the reaction coordinate has been classified into "early", "symmetric" and "late" transition state. Early and late TSs correspond are those that are closer to reactant or product structures, respectively. Since these concepts were first developed to interpret KIE's for $\text{S}_{\text{N}}2$ reactions, the symmetric transition state is defined as one in which the amount of bond formation and bond breakage are equally advanced. Initially it was assumed that the sum of the bond orders of the forming and breaking bond sums to unity. Thus, in an early transition state, a slight weakening of the breaking bond is accompanied by a slightly developed new bond to the incoming nucleophile. The opposite is true for

the late transition state. In either case the sum of the weakened and developing bond orders is unity. Later it was recognized that in many cases the sum of the bond orders of the two reactive bonds does not necessarily add to unity. This brought forward new descriptions of transition states as “loose” or “tight” depending on whether the sum of bond orders is less or greater than unity, respectively. Although modern quantum-chemical calculations show that some of the generalizations made in early interpretations were incorrect (see below), there is no doubt that KIEs are sensitive to a TS structure. While an “absolute” prediction of TS structure from KIE’s alone is unlikely (i.e. without supplementing the discussion with computational analysis), it is generally agreed that the “relative” positions of TS’s on the reaction coordinate for a series of reactions that differ in a substituent or solvent can be elucidated from isotope effect studies. We illustrate this point in the following two examples.

10.7.1 S_N2 Reactions for CN^- Attack on Substituted Benzyl Chlorides

The reaction between benzyl chlorides and tetrabutylammonium cyanide in tetrahydrofuran at 20 °C is illustrated in Fig. 10.7.

Alpha deuterium (d_2), leaving group chlorine $^{35}Cl/^{37}Cl$, and incoming carbon KIE’s for this reaction have been measured for different substituents (R) and compared with high level theoretical calculations (at the B3LYP/aug-cc-pVDZ level, see any modern book on quantum and/or computational chemistry for the description of DFT functionals and basis set symbolism). The results are collected in Tables 10.5 and 10.6. The theoretical calculations indicate that transition states become systematically tighter in the sequence CH_3 to H to Cl (i.e. in the order of increasing values of Hammett constants, σ_p , see any organic text for a complete discussion of Hammett constants, a large positive σ_p implies large electron withdrawing power relative to H, and conversely a large negative value implies high electron releasing power relative to H.). Note that shorter bond length in the transition state has different qualitative meanings for these two bonds; the shorter the C – Cl bond the “earlier” the transition state (closer to reactant structure), while a shorter C – CN bond means a “later” transition state (closer to product structure).

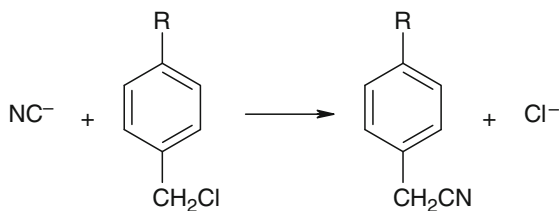


Fig. 10.7 S_N2 reaction between cyanide anion and *p*-substituted benzyl chlorides

Table 10.5 Experimental KIEs for the reaction between cyanide anion and *p*-substituted benzyl chlorides (Westaway, K. C., et al. *J. Phys. Chem. A* **111**, 8110 (2007))

R	α -d ₂	³⁵ Cl/ ³⁷ Cl	¹¹ C/ ¹⁴ C
CH ₃	Not determined	1.00609 ± 0.00014	0.9951 ± 0.0013
H	1.006 ± 0.001	1.00591 ± 0.00004	1.0047 ± 0.0003
Cl	1.012 ± 0.001	1.00537 ± 0.00024	1.0016 ± 0.0025

Table 10.6 Theoretically calculated KIEs and bond lengths in the transition state for the reaction between cyanide anion and *p*-substituted benzyl chlorides (Westaway, K. C., et al. *J. Phys. Chem. A* **111**, 8110 (2007))

R	α -d ₂	³⁵ Cl/ ³⁷ Cl	¹¹ C/ ¹⁴ C	r _{C-Cl} [Å]	r _{C-CN} [Å]
CH ₃ ($\sigma_p = -0.17$)	0.9851	1.00717	0.9838	2.271	2.384
H ($\sigma_p = 0.00$)	0.9812	1.00717	0.9833	2.262	2.378
Cl ($\sigma_p = 0.23$)	0.9788	1.00699	0.9825	2.250	2.370

It is generally observed from quantum-chemical calculations that changes of individual bonds and valence angles by themselves do not necessarily correlate with the “earliness” or “lateness” of the transition state structure. In terms of isotope effects, however, the shorter the C – Cl bond the smaller the chlorine KIE, as might have been expected since it means smaller bond changes along the path from reactant to transition state. Both the calculated and experimental changes are very small for the chlorine effects but the precision of the measurements is sufficient to allow meaningful comparison; the agreement is reasonable. Agreement of the other two measured isotope effects with the calculations is much worse. In the case of the incoming group carbon KIE, this may result from the compensation between the effect on the imaginary vibrations (so-called temperature independent factor given by Equation 4.145) which always favors the light isotope, and the temperature dependent factor which becomes inverse (less than unity) when a new bond is formed to the isotopic atom. Apparently this level of theory overestimates the latter factor. The experimental data are scattered and do not provide clear indication of a particular trend. Theoretical results point to increasingly inverse IE's with shortening of the C – C(N) bond distance. The discrepancy between the measured and observed 2°- α -D KIE's may originate in tunneling that has not been included in calculations. Again, more inverse values of this particular IE correlate with tighter transition states.

10.7.2 Reaction of Substituted Anilines with Methyl Iodide

A second example of the correlation of isotope effects with substituent properties is given by the reaction between *p*-substituted N,N-dimethylanilines and methyl iodide illustrated in Fig. 10.8. 2°- α -D and incoming group nitrogen KIE's are collected in Table 10.7.

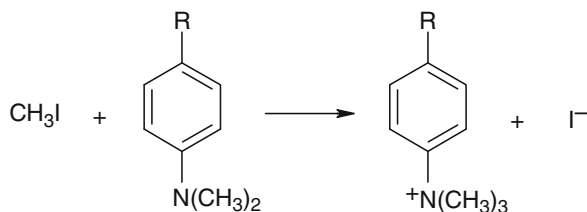


Fig. 10.8 S_N2 reaction between *p*-substituted *N,N*-dimethylanilines and methyl iodide

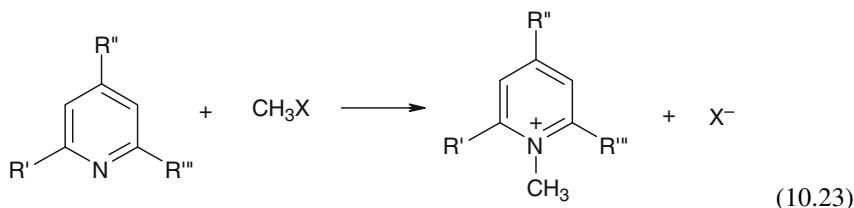
Table 10.7 KIEs on the reaction between *p*-substituted *N,N*-dimethylanilines and methyl iodide in ethanol at 25 °C (Paneth, P., et al. *J. Phys. Org. Chem.* **9**, 35 (1996))

R	$^{14}\text{N}/^{15}\text{N}$	$\text{CH}_3\text{I}/\text{CD}_3\text{I}$
CH_3	1.0036 ± 0.0003	0.927 ± 0.004
H	1.0032 ± 0.0002	0.968 ± 0.004
$\text{C}(\text{O})\text{CH}_3$	0.9989 ± 0.0003	1.143 ± 0.003

In this case the nitrogen KIE changes in the expected way from the normal value for looser transition state to the inverse value for the tighter one, reflecting increased C – N bond formation for the acetyl substituent. This direction of change upon increase in electron-withdrawing strength of the substituent, CH_3 to $\text{C}(\text{O})\text{CH}_3$, is not corroborated by the results obtained for the α -D KIE, which changes in the opposite direction, suggesting loosening of the transition state. These apparently conflicting observations can be explained within the bond strength hypothesis discussed in Section 10.4.1. Qualitatively, the results indicate that overall loosening of the transition state structure does not necessarily mean that all crucial bonds become looser. In the present case the effect of tightening of the C – N forming bond seems to be overbalanced by the loosening of the breaking C – I bond along the series $\text{CH}_3 - \text{C}(\text{O})\text{CH}_3$. (Historical Vignette 10.2)

10.7.3 More on KIE's in Menshutkin Reactions

The reaction shown in Fig. 10.8 belongs to the group of Menshutkin reactions. Many aspects of KIE's on these reactions have been extensively studied. We thus continue using them as examples, choosing first a system to illustrate the effect of steric hindrance on KIE. The effect of the steric hindrance has been explored for quaternizations of lutidines as described by the scheme 10.23:



(10.23)



[Historical Vignette 10.2] Sir Christopher K. Ingold (1893–1970) was influential in shaping modern ideas about physical organic chemistry. His text “Structure and Mechanism in Organic Chemistry” is a cornerstone of modern organic chemistry. Ingold studied at Imperial College, London, and obtained his D.Sc. in 1921. After 6 years as Professor of Organic Chemistry at Leeds University he joined University College, London, where he served as professor, then as head (1937–1961), until his retirement. Professor Ingold was far ahead of his time in applying isotopes to the solution of many problems. His comparisons of rates of racemization and halide-ion isotopic exchange were among the first investigations employing kinetic isotope effects and isotope labeling. Deuterium labeling of benzene was a critical part of Ingold’s spectroscopic work in establishing the structure of benzene. A serious problem which he faced was that neither the isotopes nor the measuring equipment were readily available at the time (1930s), and a major effort was required to enrich stable isotopes and construct the necessary apparatus. Ingold introduced many new scientific terms and concepts (nucleophilic, electrophilic, S_N1 , S_N2 , etc.), terms which are now so widely used their origin has been forgotten. (Photo credit: Chemistry Department, University College London)

where $R' = R''' = \text{CH}_3$ and $R'' = \text{H}$ for 2,6-lutidine (2,6 dimethyl pyridine), and $R' = \text{H}$, $R'' = R''' = \text{CH}_3$ for 2,4-lutidine, and $X = \text{Cl}$, I or CF_3SO_3 . For the reaction involving methyl iodide ($X = \text{I}$) in acetonitrile at 30°C , the carbon KIE for the methyl group transferred to the nitrogen, k_{11}/k_{14} , is 1.220 and 1.189 for 2,6-lutidine and 2,4-lutidine, respectively. Since the substituent effects are essentially the same in both cases the increased value of the carbon KIE has been ascribed to the larger steric hindrance exerted by two methyl groups in close proximity to the nucleophilic center in 2,6-lutidine. An interesting aspect of these results is use of the short-lived ^{11}C isotope (see Sections 7.1.5.1 and 7.4). Although some contribution of tunneling to the increased carbon KIE in the presence of steric hindrance has been postulated (due to coupling of the reaction coordinate with the bending vibrations of the α -hydrogens), the results of theoretical calculations that ascribe this increase to an earlier transition state seems more convincing. The effect of steric hindrance on heavy atom KIE's is not strong. This conclusion is also supported by other heavy atom KIE's on these reactions. Thus, the chlorine leaving group KIE remains practically unperturbed for pyridine ($R' = R'' = R''' = \text{H}$) and 2,6-lutidine react-

Table 10.8 Nitrogen KIEs for reactions of pyridines with methyl trifluoromethanesulphonate ($X = \text{CF}_3\text{SO}_3$) (Kurz, J. L. et al. *J. Phys. Chem.* **90**, 5357 (1986))

Pyridine substituents	Solvent	^{15}N -KIE
$R' = R'' = R''' = \text{H}$	Water	0.9965 ± 0.0006
	1,2-dichloroethane	0.9942 ± 0.0008
	Acetonitrile	0.9946 ± 0.0004
$R' = R''' = \text{H}, R'' = \text{Me}$		0.9937 ± 0.0002
$R' = R''' = \text{Me}, R'' = \text{H}$		0.9941 ± 0.0004

ing with methyl chloride ($X = \text{Cl}$) in bromobenzene at 100°C . The corresponding ^{37}Cl -KIEs are 1.0036 ± 0.0001 and 1.0038 ± 0.0003 , respectively. The same is true for the nitrogen KIE on the incoming group as shown in Table 10.8.

The amine quaternizations (i.e. change in the nitrogen from three to fourfold bonding) discussed above proceed via an $\text{S}_{\text{N}}2$ mechanism. They differ from those discussed earlier by showing a much stronger dependence of reaction rate on solvent polarity. This occurs because instead of charge dissipation on the path from reactant to transition state a strongly polar transition state is formed from neutral reactants. A similar strong dependence on solvent polarity is also observed for decarboxylation processes. Decarboxylation processes are important in biochemistry and in the following sections we will discuss KIEs for one such reaction.

10.7.4 Decarboxylation Reactions

Interpretation of KIEs on enzymatic processes (see Chapter 11) has been frequently based on the assumption that the intrinsic value of the kinetic isotope effect is known. Chemical reactions have long been used as models for catalytic events occurring in enzyme active sites and in some cases this analogy has worked quite well. One example is the decarboxylation of 4-pyridylacetic acid presented in Fig. 10.9. Depending on the solvent, either the zwitterionic or the neutral form dominates in the solution. Since the reaction rates in $\text{D}_2\text{O}/\text{H}_2\text{O}$ solvent mixtures are the same (see Section 11.4 for a discussion of aqueous D/H solvent isotope effects), as are the carbon KIEs for the carboxylic carbon, it is safe to assume that this is a single step reaction. The isotope effects on pK_{a} are expected to be close to the value of 1.0014 determined for benzoic acid. This in mind, changes in the isotope effects have been attributed to changes in solvation.

The solvent dependence of the C, O and N KIEs on the decarboxylation is reported in Table 10.9. The difference between ^{13}C -KIE observed in pure water and dioxane ($1.0636/1.0573 = 1.0060$) exceeds the expected carbon IE on pK_{a} (1.0014, see above) indicating that in an apolar environment the intrinsic value increases. Thus one may expect that the intrinsic KIE for an enzymatic

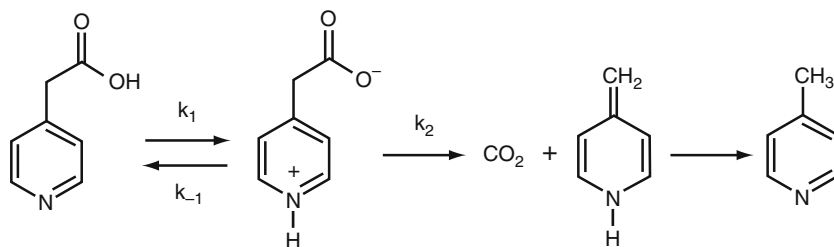


Fig. 10.9 Decarboxylation of 4-pyridylacetic acid

Table 10.9 Heavy atom KIEs on decarboxylation of 4-pyridylacetic acid at 25 °C in water-dioxane solvents (Sicinska, D., Truhlar, D. G. and Paneth, P., *J. Am. Chem. Soc.* **123**, 7683 (2001) and *J. Phys. Chem. B* **106**, 2708 (2002))

% Dioxane (v/v)	¹³ C	¹⁸ O	¹⁵ N
0	1.0573	(0.989) ^a	(1.0077)
25	1.0555	0.995	1.0019
50	1.0598	1.000	0.997
75	1.0605	1.003	0.994
100	1.0636	(1.004)	(0.983)

^aValues in parenthesis are theoretical estimations.

decarboxylation occurring at an hydrophobic active site should be slightly larger than that for the corresponding reaction in water. Alternatively, the difference has been attributed to an earlier transition state in the active site as compared to water. The change in reactant form upon change of polarity of the environment (solvent in the present case or an active site in case of an enzymatic process) is reflected in both oxygen and nitrogen KIEs. The shift of the oxygen KIE to inverse value in water corroborates the conclusion that the transition state is later with longer C – C bond to carboxylic moiety than it is in dioxane (or the gas phase). The increasing value of the nitrogen KIE with increasing water content originates in the large inverse equilibrium isotope effect between the acidic and zwitterionic forms.

10.7.5 Bond Order Dependence of the KIE

It used to be postulated that the magnitude of the alpha-carbon KIE in an S_N2 reaction is an indication of the transition state symmetry. The expectation was that this KIE reaches maximal value for a symmetric transition state and drops back to unity for extremely early or late transition states. That expected behavior is marked by the solid line in Fig. 10.10. However, recent calculations of the nucleophilic substitution of chloride from methyl chloride by a broad variety of nucleophiles

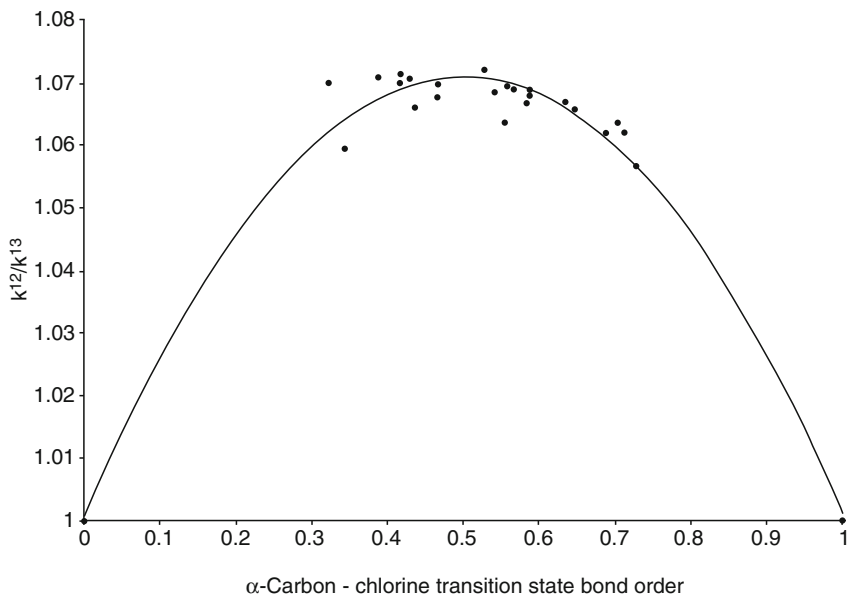


Fig. 10.10 Postulated (*solid line*) and calculated (*points*) α -carbon KIEs for the reaction between methyl chloride and various nucleophiles (Mattsen, O., et al. *J. Org. Chem.* **70**, 4022 (2005))

show that the corresponding KIE values are closely grouped about the average value, 1.065 ± 0.005 (individual points in the figure). While these results actually do not contradict the earlier expectations, they do indicate that the dependence across a wide range of bond orders is flatter than expected and that most of typical nucleophiles are not leading to sufficiently unsymmetrical transition states to observe postulated fall-off in the KIE.

10.7.6 Mechanism of the Diels–Alder Reaction

The Diels–Alder reaction is the best known and most widely used pericyclic reaction. Two limiting mechanisms are possible (see Fig. 10.11) and have been vigorously debated. In the first, the addition takes place in concerted fashion with two equivalent new bonds forming in the transition state (bottom center, Fig. 10.11), while for the second reaction path the addition occurs stepwise (top row, Fig. 10.11). The stepwise path involves the formation of a single bond between the diene (butadiene in our example) and the dienophile (ethylene) and (most likely) a diradical intermediate, although zwitterion structures have also been proposed. In the last step, ring closure results with the formation of a second new carbon carbon bond. Either step may be rate determining.

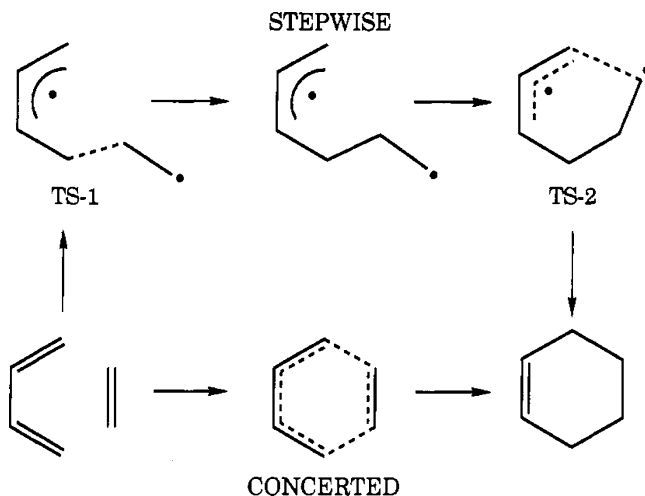


Fig. 10.11 The stepwise and concerted mechanisms for the Diels–Alder reaction between butadiene and ethylene. The reactants (*lower left*) proceed to the product, cyclohexene (*lower right*) either through a two step, two transition state mechanism involving the formation of a diradical intermediate (*top center*), or more directly through the symmetric synchronous transition state (*bottom center*) (Storer, J. W., Raimondi, L., and Houk, K. N., *J. Am. Chem. Soc.* **116**, 9675 (1994))

When deuterium or tritium is substituted for hydrogen on either diene or dienophile secondary isotope effects can be measured. These are expected to be inverse, $k_H < k_D$, in the concerted process because the sp^2 to sp^3 change of hybridization results in a frequency increase in the CH out-of-plane bending modes and consequently an inverse effect (Section 10.4.1). Just the opposite effect is anticipated for certain of the hydrogens on formation of the diradical intermediate. These qualitative predictions have been verified by Houk and coworkers using quantum mechanical *ab initio* calculations with Gaussian 6–31G* basis sets to determine optimal geometry and force constants. These results were then employed to obtain frequencies and thence isotope effects using methods described in Chapter 4 (see also Section 10.8). The calculated transition state geometries and isotope effects at two computational levels are shown in Fig. 10.12.

The experimentally observed secondary KIE's are all inverse (or unity) as expected for a sp^2 to sp^3 hybridization change. The effects vary from 0.93 to 0.99 and are in good agreement with experiment. The KIE's for the stepwise transition state are either inverse or normal depending on the position of the isotope label. As in the case of the concerted mechanism the centers involving sigma bond formation show inverse effects, but normal KIE's (~ 1.10 per D) are predicted at the developing radical center because the out of plane bending constant of the radical is less than that of an alkene. This last observation is in good agreement with measurements on known radical producing reactions which vary between 1.06 and 1.13 per D. For the Diels Alder reaction between butadiene and ethylene, however, all the observed 2° -D isotope effects are inverse, and lie between 0.9 and 1.0 per D.

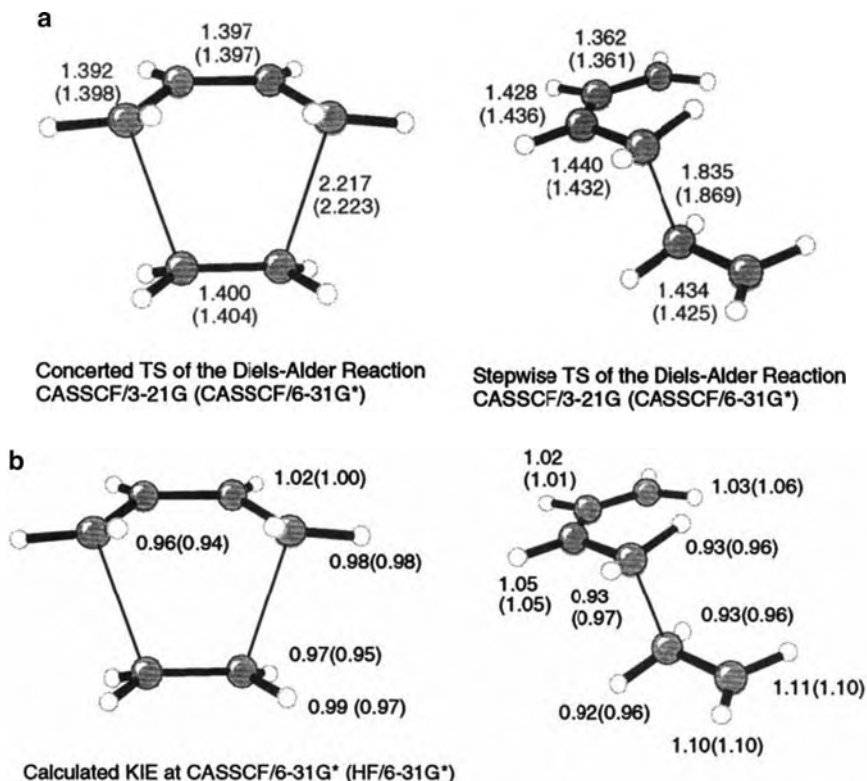


Fig. 10.12 (a) Transition state structures (C–C bond lengths) calculated at two levels for the concerted and step-wise Diels–Alder reaction shown in Fig. 10.11 (Houk, K. N., Gonzalez, J., and Li, Y., *Accts. Chem. Res.* **28**, 81 (1995)). The parenthesized values show results for calculations at a much higher (and much more expensive) level. (b) Calculated secondary deuterium isotope effects, k_H/k_D (per D) for the concerted and stepwise Diels–Alder reactions shown in Fig. 10.11 (Houk, K. N., Gonzalez, J., and Li, Y., *Accts. Chem. Res.* **28**, 81 (1995)). The parenthesized values show results for calculations at a much higher (and much more expensive) level)

The behavior described above has been verified by experiment and calculation on numerous substituted dienes and dienophiles. For example Fig. 10.13 shows results for 2° -D isotope effects on Diels–Alder reactions of 2-methyl-butadiene with cyanoethylene and 1,1-dicyano-ethylene. The calculated and experimental isotope effects are in quantitative agreement with each other and with the results on (butadiene + ethylene). In each case the excellent agreement between calculated and observed isotope effects validates the concerted mechanism and establishes the structure of the transition state as that shown at the bottom center of Fig. 10.11 and the left side of Fig. 10.12a.

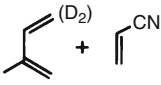
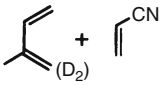
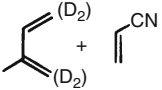
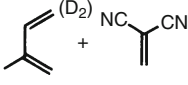
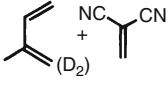
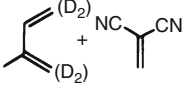
			
Exptl	0.91	0.98	0.89
via concerted TS	0.88	0.98	0.87
via stepwise TS	0.93	1.13	(D ₂) 1.06
			
Exptl	0.79	0.98	0.78
via concerted TS	0.84	0.97	0.81
via stepwise TS	0.90	1.18	1.07

Fig. 10.13 Experimental (*top rows*) and calculated secondary deuterium isotope effects, k_H/k_D (per D) for concerted and stepwise Diels–Alder reactions (Houk, K. N., Gonzalez, J. and Li, Y., *Accs. Chem. Res.* **28**, 81 (1995). The experimental data are due to Gajewski, J. J., et al. *J. Am. Chem. Soc.* **109**, 5545 (1987), **111**, 9078 (1989))

10.8 Remarks

10.8.1 Protocol of Harmonic TST Calculations of Kinetic Isotope Effects

Numerous studies of primary and secondary isotope effects on group transfer reactions (including hydride transfers), acidities, NMR shifts, equilibrium constants, etc. have been reported but are not discussed in this chapter. Reports on extensive theoretical calculations of α - and β - 2° KIE's are available in the literature. As one would expect from the theoretical development presented in Chapters 1 through 4, and the examples already cited in this chapter, the isotope effects are described in terms of vibrational differences consequent to isotope independent force constant changes at the isotopically substituted positions during the transfer from reactant to transition state. That quantitative description replaces more qualitative rationalizations of the IE's in terms of inductive or hyperconjugative electronic effects, or steric effects. These different, better alternate, approaches are equivalent so long as one clearly keeps in mind that the potential energy surface which describes the reaction is isotope independent. It is in that sense that isotope effects are clearly different from substituent effects, because for substituent effects the potential surface differs from one group to another. We conclude with a brief discussion of practical methods for calculation of kinetic isotope effects within transition state theory (TST), employing the Born–Oppenheimer and harmonic oscillator approximations, and following the methods most frequently employed in the literature. One begins by generating an input file of atomic masses and approximate (first guess) coordinates which forms the input for quantum mechanical optimization of the Born–Oppenheimer surface describing the reaction. That process (and the following) must be carried out for both reactants and transition state. The optimization

criterion is that the BO energy be at a minimum with respect to displacement along any of the coordinates chosen to describe the system. The energy surface is probed in the vicinity of the minimum to establish the gradients (which vanish at the minimum) and the force constants. This involves the calculation of the energy at numerous points along each coordinate. A common program of choice for the quantum mechanical optimization is Gaussian03. Still, it is to be noted that the choice of software and quantum mechanical basis set functions is arbitrary and a plethora of other programs and quantum packages, both commercial and distributed free of charge, are available and are capable of performing these tasks. Once the BO surface is optimized the force constant matrix, which is the matrix of second derivatives of the energy with respect to coordinate displacement ($f_{ij} = \partial^2 E_{\text{BO}} / \partial x_i \partial x_j$) is calculated. Many current programs (including Gaussian) employ (a set of $3 \times 3N$) Cartesian coordinates centered on each atom. The Cartesian force constants and the known masses of each atom in each isotopomer are used to calculate the set of $3N$ normal mode frequencies for each of the isotopomers of interest using the methods described in Section 3.3. If, alternatively, one chooses to carry out the calculations employing, say, valence coordinates it becomes necessary to calculate the set of G matrix elements as described in Section 3.4. The normal mode frequencies are then obtained from the diagonalization of the \mathbf{GF} matrix (see the discussion in the neighborhood of Equation 3.43, Section 3.4, and Appendix 3A1.2). In either approach one ends up with a set of normal mode frequencies for each of the isotopomers of interest. These frequencies are then used in Equation 4.79 (sometimes called the complete equation) or its equivalent, Equation 4.77, to calculate equilibrium isotope effects, or in Equation 4.146 to obtain TST kinetic isotope effects. Recall that Equation 4.79 was obtained from Equation 4.77 by replacing isotopic masses and moments of inertia by isotopic frequency ratios using the Teller–Redlich rule (Equation 3.49). Calculations carried out using Equations 4.77 and 4.79 are completely equivalent so long as the quantum mechanically calculated structures are well optimized and the numerical analysis is carried out to sufficient precision. The many examples of theoretically calculated isotope effects described in this chapter (and others), especially in Section 10.7, have employed these general procedures. [For information regarding the programs Gaussian and GaussView see <http://www.gaussian.com>. The program, Isoeff06 (see reading list), which can be used to calculate isotope effects from input frequencies according to the Bigeleisen equation (4.79), may be obtained from the Paneth group. In its present form it accepts output files of frequencies generated using Mopac, Gaussian, GAMESS, or Jaguar computer packages.]

10.8.2 *The TST/VTST Interface*

Most of the calculations discussed in this chapter, and in Chapter 11, have been carried out using the TST model. However the calculations on the hydrogenic molecule-hydrogenic atom reactions reported in Table 10.1, which include

accurate analysis of tunnel corrections (including multidimensional tunneling), have employed the variational transition state theory VTST. Other TST and VTST calculations analyzing KIE's of enzyme catalyzed reactions are presented in Chapter 11 (Sections 11.7 and 11.8). TST was introduced in Chapter 4 and VTST in Chapter 6. The two theories were compared in the later chapter. VTST theory is broader than TST theory, which in fact is a special case of VTST. In VTST the position of the transition state is optimized on the Gibbs free energy surface rather than on the potential energy surface. This difference has important implications for isotope effect calculations. First, the saddle point on the isotope independent (Born–Oppenheimer) potential energy surface that is usually obtained with majority of quantum calculation packages, and which corresponds to the transition state in TST, is not necessarily the transition state in VTST. Second, and even more important for calculations of isotope effects, is the fact that the Gibbs free energy surface is isotope-dependent and thus the position of the transition state may be different for the light and heavy isotopomers. Those differences may be significant for very light atoms (H/D) but for heavier particles are generally small or negligible. Apart from this fundamental difference there is also the practical matter that VTST calculations are far more tedious and expensive, and VTST methods (i.e. packages for computer implementation) are not so widely available as are those for TST.

In the majority of cases, especially for isotope effects on heavy atoms, differences in location of the transition state for two isotopomers are expected to be minimal (proton, hydride or H atom transfer excepted), and one expects that the isotope effects calculated by VTST and TST should be very similar. However, the most pronounced differences between VTST and TST calculations are obtained for so-called “non-classical” effects, tunneling in particular. In principle, advanced multidimensional treatment of tunneling can be incorporated into TST. However, in practice, tunneling is usually approximated in TST calculations using a simple one-dimensional correction based on the imaginary vibration which describes the reaction coordinate (see Section 6.3). Such an approach usually significantly underestimates the tunneling contribution to the isotope effect. In this and the next chapter we do not (have not) elaborate(d) on the type of theory used in calculations, the majority of the results which are discussed are from TST. Those examples where VTST has been employed are carefully specified. To sum up, it seems generally recognized that VTST is a more general and more elegant theory than TST but its application is still not fully tested except for very simple systems, and the implementation of VTST is much more cumbersome. Both approaches are useful (helpful) aids to the interpretation of KIE's and transition state structure.

Reading List

- Anisimov, V. and Paneth, P. *ISOEFF98*. A program for studies of isotope effects using Hessian modifications. *J. Math. Chem.* **25**, 75 (1999).
- Bierbaum, V. M. et al. Deuterium kinetic isotope effects in microsolvated gas-phase E2 reactions. *J. Am. Soc. Mass. Spectrom.* **18**, 1046 (2007); Deuterium kinetic isotope effects in gas-phase SN2 and E2 reactions: comparison of experiment and theory. *J. Am. Chem. Soc.* **128**, 736 (2006).

- Cramer, C. J. *Essentials of Computational Chemistry*, Wiley-VCH, New York, 2004.
- Hengge, A. C., *Secondary Isotope Effects* in Kohen, A. and Limbach, H. H., *Isotope Effects in Chemistry and Biology*, Taylor & Francis, Boca Raton, FL, 2006.
- Matsson, O. and Westaway, K. C. in Bethell, D., Ed. *Advances in Physical Organic Chemistry, Volume 31*, Academic, New York, 1998.
- Melander, L. and Saunders, W. H. *Reaction Rates of Isotopic Molecules*, Wiley, New York, 1980.
- Shiner, V. J., Rapp, M. W., Halevi, E. A. and Wolfsberg, M. *Solvolytic α -deuterium effects for different leaving groups*. *J. Am. Chem. Soc.* **90**, 7171 (1968).
- Stern, M. J. and Wolfsberg, M. *On the absence of isotope effects in the absence of force constant changes*. *J. Chem. Phys.* **45**, 2618 (1966).
- Wolfsberg, M. and Stern, M. J. Validity of some approximation procedures used in the theoretical calculation of isotope effects. *Pure Appl. Chem.* **8**, 225 (1964); Secondary isotope effects as probes for force constant changes. *Ibid.* **8**, 325 (1964).

Chapter 11

Enzymes; Aqueous Solvent IE'S

Abstract This chapter introduces the basic principles used in applying isotope effects to studies of the kinetics and mechanisms of enzyme catalyzed reactions. Following the introduction of algebraic equations typically used for kinetic analysis of enzyme reactions and a brief discussion of aqueous solvent isotope effects (because enzyme reactions universally occur in aqueous solutions), practical examples illustrating methods and techniques for studying enzyme isotope effects are presented. Finally, computer modeling of enzyme catalysis is briefly discussed.

11.1 Introduction

Enzymes are proteins that have evolved to catalyze specific chemical or biochemical reactions that usually do not proceed at a reasonable rate in their absence. Enzymes are extremely specific. The protein alone, called an apoenzyme, may possess biological activity. More frequently, however, enzymes require the presence of additional compounds called coenzymes, prosthetic groups, or cofactors during the reaction. Such compounds may include metal cations, vitamins, NAD(P)^+ , etc. Together with the apoenzyme they form biologically active holoenzymes. Amazingly, rate enhancements of as much as 19 orders of magnitude have been observed for enzyme catalyzed reactions, and thus it is not surprising that mechanisms of enzyme catalysis are being vigorously explored. At the molecular level the mechanism by which enzymatic catalysis is achieved is still debated, although in broad terms there is general agreement that the catalysis is due to destabilization of reactants and/or stabilization of the corresponding transition state in an enzyme/substrate complex.

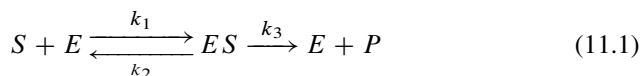
All enzymatic processes are complex reactions that involve more than one step. The substrate first binds to the enzyme, in the second step reaction occurs, and finally products are released from the enzyme. This all happens at a catalytic center in the enzyme which is termed the active site. Enzymes are usually very large molecular systems, and may contain anywhere between several and several hundred aminoacids. The active site is usually buried inside a bulky three dimensional structure that shields the reactant-active site complex from the surrounding bulk phase aqueous solution. It typically contains several aminoacids that are vital for

the reactivity. The remaining parts of the enzyme are believed to serve as nothing more than a frame for the active site. In multiunit and/or multienzyme systems these outer parts also play the role of an anchor which holds the different sections together.

11.2 Some Simple Enzyme Kinetics

11.2.1 Introduction: The Michaelis–Menten Mechanism

The simplest possible enzymatic reaction scheme was proposed in 1913 by Michealis and Menten. They assumed the molecule undergoing reaction (the substrate, S) is adsorbed reversibly on a specific site of the enzyme E to form a complex ES whose decomposition into product P is rate controlling. The scheme resembles that for unimolecular decomposition (see Chapter 14).



The rate constants k_1 and k_2 correspond to forward and reverse binding steps to the enzyme, and k_3 describes the rate of decomposition to product. The essential assumption is that the complex concentration (ES) reaches steady state

$$\frac{d[ES]}{dt} = 0 = k_1[E][S] - k_2[ES] - k_3[ES] \quad (11.2)$$

so

$$[ES] = \frac{k_1[E][S]}{k_2 + k_3} \quad (11.3)$$

The concentration of uncomplexed enzyme is $[E] = [E]_0 - [ES]$ so

$$[E]_0 = [E] \left(1 + \frac{k_1[S]}{k_2 + k_3} \right) \text{ and } [E] = [E]_0 \left(\frac{k_2 + k_3}{k_2 + k_3 + k_1[S]} \right) \quad (11.4)$$

Substitution into Equation 11.3 yields

$$[ES] = \frac{k_1[E]_0[S]}{k_2 + k_3 + k_1[S]} = \frac{[E]_0[S]}{\frac{k_2 + k_3}{k_1} + [S]} = \frac{[E]_0[S]}{K_M + [S]} \quad (11.5)$$

where the Michaelis constant $K_M = (k_2 + k_3)/k_1$. The rate of production of product is

$$RATE = v(\text{velocity}) = \frac{d[P]}{dt} = k_3[ES] = \frac{k_3[E]_0[S]}{K_M + [S]} \quad (11.6)$$

(In the equations describing enzyme kinetics in this chapter, the notation varies a bit from other chapters. Thus v is accepted in the biochemical literature as the symbol for reaction rate while V_{\max} is used for the maximum rate. Furthermore, for simplification frequently V_{\max} is truncated to V in complex formulas (see Equations 11.28 and 11.29). Although at first glance inconsistent, these symbols are familiar to students of biochemistry and related areas. The square brackets indicate concentrations. V_{\max} expresses the upper limit of the rate of the enzyme reaction. It is the product of the rate constant k_3 , also called the turnover number, and the total enzyme concentration, $[E]_0$. The case $v_i = V_{\max}$ corresponds to complete saturation of all active sites. The other kinetic limit, $v_i = (V_{\max}/K_M)[S]$, corresponds to $K_M \gg [S]$, in other words V_{\max}/K_M is the first order rate constant found when the substrate concentration approaches zero:

$$\lim_{[S] \rightarrow 0} v_i = \lim_{[S] \rightarrow 0} \left(-\frac{d[S]}{dt} \right) = \frac{V_{\max}}{K_M} [S] \quad (11.7)$$

Equation 11.6 shows that K_M corresponds to the substrate concentration at which the rate has fallen to half the maximum. The kinetic parameters V_{\max} and V_{\max}/K_M can be obtained by least squares regression of v vs. $[S]$ plots or graphically by linearizing Equation 11.6.

Figure 11.1 illustrates the behavior of Equation 11.6. By the assumption of rapid equilibrium the rate determining step is the unimolecular decomposition. At high substrate composition $[S] \gg K_M$ and the rate becomes zero-order in substrate, $v = V_{\max} = k_3[E]_0$, the rate depends only on the initial enzyme concentration, and is at its maximum. We are dealing with saturation kinetics. The most convenient way to test mechanism is to invert Equation 11.6

$$\frac{1}{v} = \frac{K_M}{k_3[E]_0[S]} + \frac{1}{k_3[E]_0} \quad (11.8)$$

and carry out rate measurements as a function of $[S]$ at constant $[E]_0$. From a plot of $1/v$ vs. $1/[S]$ one recovers k_3 from the intercept and K_M by combining slope and intercept. At the intercept the rate is at its maximum. An artificially constructed example, including isotope effects, is shown in Fig. 11.2 which is an alternative plot of the data in Fig. 11.1. In this case the experiment yields the rate constant for the step of primary interest, which is the rate of catalysis at the enzyme active site. By comparing measurements for, say, H and D labels on the substrate, the enzyme, or both substrate and enzyme, the intrinsic isotope effect, k_{3H}/k_{3D} , is straightforwardly obtained. Unfortunately, for more realistic (more complex) mechanistic paths a clean separation and singling out of the intrinsic isotope effect is often not possible. This point is developed in the material which follows. The plots shown in Fig. 11.2 provide the isotopic ratio of Michaelis constants ($K_{M(H)}/K_{M(D)}$), but there is insufficient information to resolve the individual rate constants k_1 and k_2 or their isotope effects. That requires further and more difficult experiments.

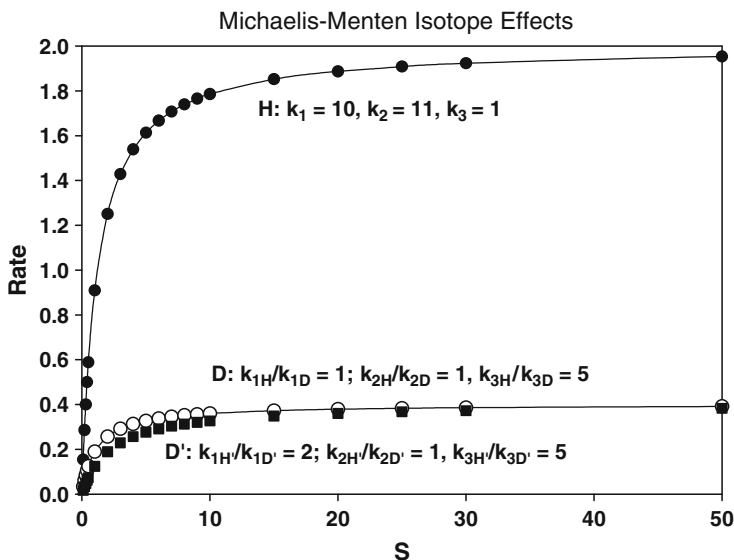


Fig. 11.1 Michaelis–Menten kinetic behavior (Equation 11.6). The rate of product formation for mechanism 11.1 is plotted vs substrate concentration (arbitrary units) for three cases: $[E]_0 = 2$. *Solid circles* (H): $k_{1H} = 10; k_{2H} = 11; k_{3H} = 1$; *open circles* (D): $k_{1D} = 10, k_{1H}/k_{1D} = 1; k_{2D} = 11, k_{2H}/k_{2D} = 1; k_{3D} = 0.2, k_{3H}/k_{3D} = 5$; *solid squares* (D'): $k_{1D'} = 5, k_{1H}/k_{1D'} = 2; k_{2D} = 11, k_{2H}/k_{2D'} = 1; k_{3D} = 0.2, k_{3H}/k_{3D'} = 5$

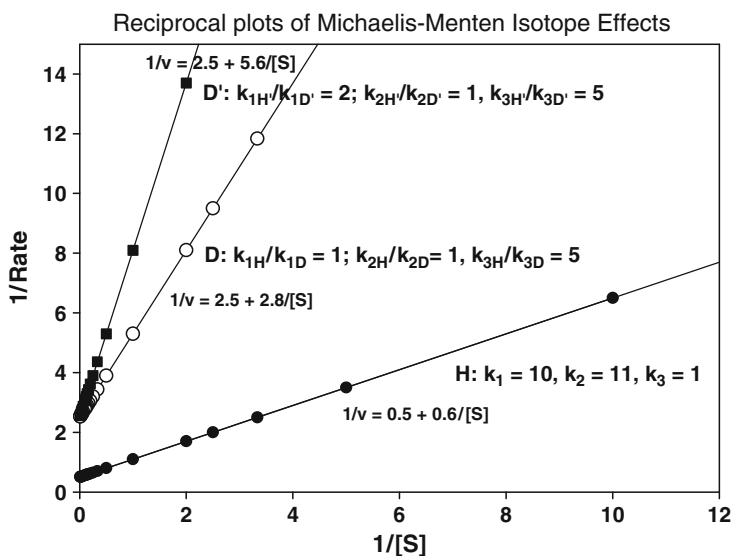
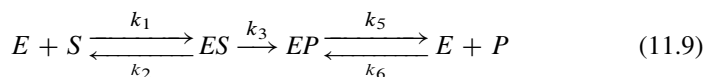


Fig. 11.2 Reciprocal plots of Michaelis–Menten kinetic behavior (Equation 11.8). The reciprocal rate of product formation for mechanism 11.1 is plotted vs reciprocal substrate concentration (arbitrary units) for the three cases specified in the caption of Fig. 11.1

11.2.2 The Incorporation of Product Binding

A more realistic but still relatively simple model of enzyme catalysis includes binding of both substrate and product as described by Equation 11.9. This reaction is characterized by five individual rate constants; k_1 and k_2 , and k_4 and k_5 , correspond to the forward and reverse binding steps of the substrate S and product P to the enzyme E, respectively, while k_3 expresses the irreversible chemical conversion at the enzyme active site:



The overall rate is

$$v = \frac{d[P]}{dt} = k_5[EP] - k_6[E][P]. \quad (11.10)$$

(In Equation 11.9 we reserve the missing rate constant k_4 for an elaboration of the mechanism). Following Briggs and Haldane we make the assumption that the steady-state approximation applies to ES and EP complexes:

$$\frac{d[EP]}{dt} = k_3[ES] - k_5[EP] + k_6[E][P] = 0 \quad (11.11)$$

$$\frac{d[ES]}{dt} = k_1[E][S] - (k_2 + k_3)[ES] = 0 \quad (11.12)$$

Substitution into Equation 11.10 leads to:

$$v = \frac{d[P]}{dt} = -\frac{d[S]}{dt} = k_3[ES] = \frac{k_1 k_3}{k_2 + k_3} [E][S] \quad (11.13)$$

With both intermediates in steady-state, the rate of loss of substrate is equal to the rate of product formation. Also

$$[E]_0 = [E] + [ES] + [EP] = [E] \left(1 + \frac{k_1[S]}{k_2 + k_3} + \frac{\frac{k_1 k_3 [S]}{k_2 + k_3} + k_6 [P]}{k_5} \right) \quad (11.14)$$

Rearrangement of Equation 11.14 and substitution into Equation 11.13 gives:

$$v = \frac{\frac{k_3 k_5}{k_3 + k_5} [E]_0 [S]}{\frac{k_2 + k_3}{k_1} \cdot \frac{k_5 + k_6 [P]}{k_3 + k_5} + [S]} \quad (11.15)$$

When initial rates (v_i) are measured the concentration of product is negligible and

$$v_i = \frac{\frac{k_3 k_5}{k_3 + k_5} [E]_0 [S]}{\frac{k_2 + k_3}{k_1} \cdot \frac{k_5}{k_3 + k_5} + [S]} \quad (11.16)$$

If, as sometimes reasonable, k_5 is much faster than k_3 ;

$$v_i = \frac{k_3 [E]_0 [S]}{\frac{k_2 + k_3}{k_1} + [S]} \quad (11.17)$$

Finally, introduction of the commonly used symbols V_{\max} and K_M yields the Briggs–Haldane rate equation for enzymatic reactions (compare with Equation 11.6)

$$v_i = \frac{V_{\max} [S]}{K_M + [S]} \quad (11.18)$$

where for initial rates we have from Equation 11.15

$$V_{\max} = \frac{k_3 k_5}{k_3 + k_5} [E]_0 = k_{cat} [E]_0 \quad (11.19)$$

$$\frac{V_{\max}}{K_M} = \frac{k_1 k_3}{k_2 + k_3} \quad (11.20)$$

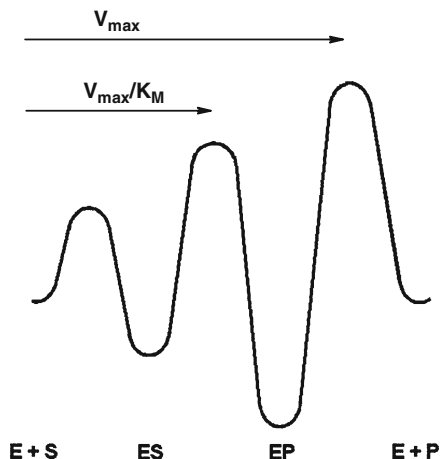
The subscript on k_{cat} in Equation 11.19 abbreviates “catalyzed”. V_{\max} is connected with the rate determining step. For desorption much faster than catalysis, $k_5 \gg k_3$, $V_{\max} = k_3 [E]_0$ which is the result found for the simpler Michaelis–Menten mechanism, Section 11.2.1. If, however, k_5 is commensurate with k_3 the intrinsic catalysis is damped by the weighting function $k_5 / (k_3 + k_5)$. Note that V_{\max} / K_M “sees” events through the first irreversible step as illustrated in Fig. 11.3. The same is true for the isotope effects. These points are discussed in considerable detail by Northrop (see reading list).

When Equations 11.19 and 11.20 are rewritten for isotopic light (L) and heavy (H) species, the isotope effects are obtained by taking ratios, recognizing $[E_{0L}] = [E_{0H}]$:

$$\frac{V_{\max L}}{V_{\max H}} = \frac{k_{3L} k_{5L}}{k_{3L} + k_{5L}} \bigg/ \frac{k_{3H} k_{5H}}{k_{3H} + k_{5H}} \quad (11.21)$$

$$\frac{V_{\max L}}{K_{ML}} \bigg/ \frac{V_{\max H}}{K_{MH}} = \frac{k_{1L} k_{3L}}{k_{2L} + k_{3L}} \bigg/ \frac{k_{1H} k_{3H}}{k_{2H} + k_{3H}} \quad (11.22)$$

Fig. 11.3 Energy diagram for the reaction given in equation 11.1. As usual in diagrams of this sort energy (ordinate) is plotted against progress along the reaction coordinate (See, for example, Northrop, D. B. in Cleland, W. W., O'Leary, M. and Northrop, D. B. (reading list))



or rewriting

$$V_{\max L} / V_{\max H} = \frac{(k_{3L} / k_{3H}) + (k_{5L} / k_{5H}) \cdot (k_{3L} / k_{5L})}{1 + k_{3L} / k_{5L}} \quad (11.23)$$

$$\frac{V_{\max L} / V_{\max H}}{K_{ML} / K_{MH}} = (k_{1L} / k_{1H}) \frac{(k_{3L} / k_{3H}) / (k_{2L} / k_{2H}) + (k_{3L} / k_{2L})}{1 + k_{3L} / k_{2L}} \quad (11.24)$$

11.2.3 A Simpler Notation

Before proceeding to more realistic reaction mechanisms which are usually more complicated than either example above, some simplification in notation is advisable. In chemical kinetics the right hand subscript on the rate constant is traditionally reserved to identify a given step in the reaction scheme, e.g. k_1 . However, that same location is often used, as in the example above, to identify isotopes in kinetic isotope effects, e.g. k_{1L} or k_{1H} . This causes problems when treating more complex reactions. Northrop has suggested a notation now widely used for enzymatic reactions. In this notation the isotope effect is identified using the atomic mass of the heavy isotope only (or its symbol, for hydrogen isotope effects) placed as the left-hand superscript. Thus a nitrogen kinetic isotope effect on the rate constant corresponding to the n th step in the kinetic scheme is represented by $^{15}k_n$ rather than k_{n14}/k_{n15} . Analogously, a tritium equilibrium isotope effect is represented as $^3K(\equiv K_H/K_T)$. The system can be a bit misleading since a single letter, k , is used to represent both isotopic ratios of rate constants and the rate constants themselves. Even so, it is much easier to follow than the traditional notation in complicated cases. Thus Equations 11.23 and 11.24 in the Northrop notation are given as:

$$H_{V_{\max}} = \frac{H_{k_3} + H_{k_5} \cdot (k_{3L}/k_{5L})}{1 + k_{3L}/k_{5L}} \quad (11.25)$$

$$H\left(\frac{V_{\max}}{K_M}\right) = H_{k_1} \frac{H_{k_3}/H_{k_2} + (k_{3L}/k_{2L})}{1 + k_{3L}/k_{2L}} \quad (11.26)$$

or in the even shorter version that will be used throughout this chapter (omitting subscripts on V_{\max} and K_M and remembering that rate constants refer to the lighter species)

$$H_V = \frac{H_{k_3} + H_{k_5} \cdot (k_3/k_5)}{1 + k_3/k_5} \quad (11.27)$$

$$H(V/K) = H_{k_1} \frac{H_{k_3}/H_{k_2} + (k_3/k_2)}{1 + k_3/k_2} \quad (11.28)$$

In studies of isotope effects on enzymatic processes it is frequently assumed that substrate–enzyme binding processes do not introduce isotope fractionation. That assumption is not generally true and some examples of binding isotope effects are shown later in this chapter. However, since ordinarily no changes in covalent bonding are associated with binding, these isotope effects are usually smaller than those on chemical changes and can be neglected in first approximation. For the reaction scheme of Equation 11.9 the following expressions result:

$$H_V = \frac{H_{k_3} + k_3/k_5}{1 + k_3/k_5} \quad (11.29)$$

$$H(V/K) = \frac{H_{k_3} + k_3/k_2}{1 + k_3/k_2} \quad (11.30)$$

11.2.4 The Intrinsic IE, Commitments, and Partitioning Factor

Using the various simplifications above, we have arrived at a model for reaction 11.9 in which only one step, the chemical conversion occurring at the active site of the enzyme characterized by the rate constant k_3 , exhibits the kinetic isotope effect H_{k_3} . From Equations 11.29 and 11.30, however, it is apparent that the observed isotope effects, H_V and $H(V/K)$, are not directly equal to this kinetic isotope effect, H_{k_3} , which is called the intrinsic kinetic isotope effect. The complexity of the reaction may cause part or all of H_{k_3} to be masked by an amount depending on the ratios k_3/k_5 and k_3/k_2 . The first ratio, k_3/k_5 , compares the intrinsic rate to the rate of product dissociation, and is called the ratio of catalysis, $r(=k_3/k_5)$. The second, k_3/k_2 , compares the intrinsic rate to the rate of the substrate dissociation and is called forward commitment to catalysis, $c_f(=k_3/k_2)$, or in short, commitment. The term partitioning factor is sometimes used in the literature for this ratio of rate constants.

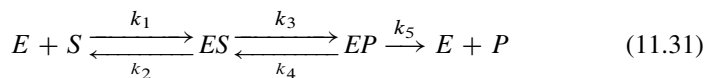
If the overall reaction rate is controlled by step three (k_3) (i.e. if that is the rate limiting step), then the observed isotope effect is close to the intrinsic value. On the other hand, if the rate of chemical conversion (step three) is about the same or faster than processes described by k_5 and k_2 , partitioning factors will be large, and the observed isotope effects will be smaller or much smaller than the intrinsic isotope effect. The usual goal of isotope studies on enzymatic reactions is to unravel the kinetic scheme and deduce the intrinsic kinetic isotope effect in order to elucidate the nature of the transition state corresponding to the chemical conversion at the active site of an enzyme. Methods of achieving this goal will be discussed later in this chapter.

11.3 More Complicated Enzyme Reactions

In the remaining part of our presentation of the formal kinetics of enzyme isotope effects a few more complicated examples will be discussed. The methods developed here should be also useful for unraveling other complicated enzyme reactions, and in reading and understanding the modern literature on isotope effects on enzymatic processes.

11.3.1 Reversible Reaction at the Active Site

We start with the case when chemical conversion at the active site is reversible. By assuming the initial product concentration to be negligible we may neglect the reversibility of product binding:



Using the steady-state approximation for the concentrations of complexes ES and EP:

$$\frac{d[EP]}{dt} = k_3[ES] - (k_4 + k_5)[EP] = 0 \quad (11.32)$$

and

$$\frac{d[ES]}{dt} = k_1[E][S] + k_4[EP] - (k_2 + k_3)[ES] = 0 \quad (11.33)$$

one obtains an expression for the apparent rate constant k_{app} (corresponding to V/K in the development above)

$$v_i = \frac{d[P]}{dt} = k_5[EP] = \frac{k_1 k_3 k_5}{k_2 k_4 \left[1 + \frac{k_5}{k_4} \left(1 + \frac{k_3}{k_2} \right) \right]} [E][S] = k_{app}[E][S] \quad (11.34)$$

Taking ratios of the apparent rate constants for light and heavy species we obtain:

$$\begin{aligned}
 {}^H k_{app} = {}^H (V/K) &= \frac{{}^H k_1 {}^H k_3 {}^H k_5}{{}^H k_2 {}^H k_4} \cdot \frac{1 + \frac{k_5 H}{k_4 H} \left(1 + \frac{k_3 H}{k_2 H}\right)}{1 + \frac{k_5}{k_4} \left(1 + \frac{k_3}{k_2}\right)} \\
 &= {}^H k_1 \cdot \frac{\frac{{}^H k_3 {}^H k_5}{{}^H k_2 {}^H k_4} + \frac{k_5}{k_4} \left(\frac{{}^H k_3}{{}^H k_2} + \frac{k_3}{k_2}\right)}{1 + \frac{k_5}{k_4} \left(1 + \frac{k_3}{k_2}\right)} \quad (11.35)
 \end{aligned}$$

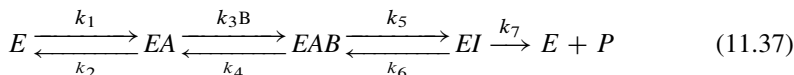
As before, the assumption that binding processes do not introduce appreciable isotope fractionation, i.e., ${}^H k_1 = {}^H k_2 = {}^H k_5$, allows the simplification of Equation 11.35:

$${}^H k_{app} = \frac{\frac{{}^H k_3}{{}^H k_4} + \frac{k_5}{k_4} \left({}^H k_3 + \frac{k_3}{k_2}\right)}{1 + \frac{k_5}{k_4} \left(1 + \frac{k_3}{k_2}\right)} = \frac{{}^H k_3 + \frac{k_3}{k_2} + \frac{{}^H k_3}{{}^H k_4} \frac{k_4}{k_5}}{1 + \frac{k_3}{k_2} + \frac{k_4}{k_5}} = \frac{{}^H k_3 + c_f + {}^H K_{3/4} c_r}{1 + c_f + c_r} \quad (11.36)$$

Equation 11.36 recognizes that ${}^H k_3/{}^H k_4$ corresponds to the equilibrium isotope effect, ${}^H K_{3/4}$ for the step containing rate constants k_3 and k_4 . The rate ratio k_4/k_5 is the commitment for catalysis for the reaction that proceeds from products to substrates, and therefore is called the reverse commitment to catalysis, c_r . Also $c_f = k_3/k_2$ is the forward commitment to catalysis. Since we have assumed that these steps are the only isotope sensitive ones, ${}^H K_{3/4}$ corresponds to the overall equilibrium isotope effect, ${}^H K$.

11.3.2 Ordered Sequential Reactions

Thus far only reactions involving a single substrate have been considered. Most enzymatic reactions have two substrates. Unlike chemical processes, the sequence in which the substrates bind to the enzyme may be important. If two substrates, A and B, bind in a specific order (e.g., A binds first) as illustrated in Equation 11.37 the mechanism is called ordered sequential.



Following a protocol analogous to the one used in developing Equations 11.32 through 11.36, the apparent rate constant and its isotope effects can be calculated:

$$k_{app} = \frac{k_1 k_3 k_5 k_7}{k_2 k_4 k_6 \left\{ 1 + \frac{k_7}{k_6} \left[1 + \frac{k_5}{k_4} \left(1 + \frac{k_3[B]}{k_2} \right) \right] \right\}} \quad (11.38)$$

$${}^H k_{app} = H_{k_1} \cdot \frac{\frac{H_{k_3}}{H_{k_2} H_{k_4}} \frac{H_{k_5} \left(\frac{H_{k_7}}{H_{k_6}} + \frac{k_7}{k_6} \right)}{(1 + k_7/k_6)} + \frac{k_5 k_7}{k_4 (k_6 + k_7)} \left(\frac{H_{k_3}}{H_{k_2}} + \frac{k_3[B]}{k_2} \right)}{1 + \frac{k_5 k_7}{k_4 (k_6 + k_7)} \left(1 + \frac{k_3[B]}{k_2} \right)} \quad (11.39)$$

One important difference between Equations 11.35 and 11.39 is that in the latter case the commitment is a function of the concentration of the second substrate (i.e. the one which binds second and is labeled B in Equation 11.37, while in Equation 11.35 it is not.

Equation 11.39 reduces to 11.35 when steps labeled with rate constants k_5 – k_7 are lumped together and treated as a unit, e.g.:

$$k'_5 = \frac{k_5 k_7}{k_6 + k_7} \quad \text{and} \quad H_{k'_5} = H_{k_5} \cdot \frac{\left(\frac{H_{k_7}}{H_{k_6}} + \frac{k_7}{k_6} \right)}{\left(1 + \frac{k_7}{k_6} \right)} \quad (11.40)$$

Equation 11.40 is a special case of a more general mechanism discussed below in which substrates bind to the enzyme randomly. However, to finish discussion of the sequential ordered mechanism, Equation 11.37, we simplify as before, by assuming that binding processes are isotopically insensitive. Equation 11.39 becomes:

$${}^H k_{app} = \frac{\frac{H_{k_5} \left(\frac{H_{k_7}}{H_{k_6}} + \frac{k_7}{k_6} \right)}{(1 + k_7/k_6)} + \frac{k_5 k_7}{k_4 (k_6 + k_7)} \left(1 + \frac{k_3[B]}{k_2} \right)}{1 + \frac{k_5 k_7}{k_4 (k_6 + k_7)} \left(1 + \frac{k_3[B]}{k_2} \right)} = \frac{H_{k'_5} + \frac{k'_5}{k_4} \left(1 + \frac{k_3[B]}{k_2} \right)}{1 + \frac{k'_5}{k_4} \left(1 + \frac{k_3[B]}{k_2} \right)} \quad (11.41)$$

If $k_3[B]/k_2$ is much larger than unity, then the forward commitment is given by Equation 11.42:

$$c_f = \frac{k'_5 k_3 [B]}{k_4 k_2} \quad (11.42)$$

and depends linearly on the concentration of the substrate which binds second. In this case it becomes possible to vary the commitment by changing initial concentration of B and learn more details, e.g., in a series of experiments with different B concentrations, extrapolation to $[B] = 0$ leads to the value of the intrinsic isotope effect.

isotope effect. A second approach can be illustrated using Equation 11.30. If the experimental value $^H(V/K)$ is known, then, formally speaking, this becomes a single equation involving two unknowns, Hk_3 and $k_3/k_2 (=c_f)$, still assuming that only one step is isotope sensitive. If two kinetic isotope effects of the same element in the same position (e.g. Dk_3 and Tk_3) can be measured, then taking advantage of Section 10.5, the set of three equations can be solved explicitly for all three unknowns:

$$\left. \begin{aligned} ^{H1}(V/K) &= \frac{^{H1}k_3 + c_f}{1 + c_f} \\ ^{H2}(V/K) &= \frac{^{H2}k_3 + c_f}{1 + c_f} \\ ^{H2}k &= (^{H1}k)^\chi \end{aligned} \right\} \quad (11.46)$$

where the Swain–Schaad exponent χ (Section 10.5) depends on the particular kind of kinetic isotope effect. Thus $\chi \sim 1.44$ for H/D/T isotope effects and $\chi \sim 1.9$ for primary heavy atom kinetic isotope effects, thus $^Tk = (^Dk)^{1.44}$. In Section 10.5 it was emphasized that this last result is only a first approximation to be applied to large primary kinetic isotope effects. The value $\chi = 1.37$ has been suggested for secondary effects with tritium kinetic isotope effect of at least 10%.

11.3.5 Multiple Isotope Effects

In the approach above two different isotope effects of the same element substituted at the same position in the substrate have been compared. In similar fashion measurements of isotope effects of different elements on the same reaction can be used:

$$\left. \begin{aligned} ^{H1}(V/K) &= \frac{^{H1}k_3 + c_f}{1 + c_f} \\ ^{H2}(V/K) &= \frac{^{H2}k_3 + c_f}{1 + c_f} \\ ^{H1}(V/K)_{H2} &= \frac{^{H2}k_3 + c_f / ^{H2}k_3}{1 + c_f / ^{H2}k_3} \end{aligned} \right\} \quad (11.47)$$

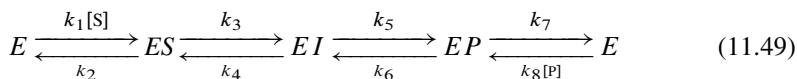
The third equation in Equation 11.47 represents a kinetic isotope effect of the first isotopomer pair measured in the presence of the second (which IE has perturbed the commitment). In order to make the changes in apparent commitment ($c_f / ^{H2}k_3$) sufficiently pronounced, deuterium is usually selected as the second isotope (H2). The first, (H1), on the other hand, is usually a heavy-atom (e.g. ^{13}C , ^{18}O , etc.). Most frequently this approach has been used for carbon kinetic isotope effects in which case Equation 11.47 becomes:

$$\left. \begin{aligned} ^{13}(V/K) &= \frac{^{13}k + c_f}{1 + c_f} \\ ^D(V/K) &= \frac{^Dk + c_f}{1 + c_f} \\ ^{13}(V/K)_D &= \frac{^{13}k + c_f / ^Dk}{1 + c_f / ^Dk} \end{aligned} \right\} \quad (11.48)$$

If the isotope sensitive step is reversible the equations get more complicated and cannot be solved explicitly for the intrinsic isotope effects (unless $c_f = 0$, or the equilibrium isotope effect is unity). The last two equations in Equation 11.48 demonstrate that a normal deuterium kinetic isotope effect diminishes the apparent commitment if both isotopes are present. Thus $^{13}(V/K)$ is smaller than $^{13}(V/K)_D$ when both isotope effects are related to the same step.

11.3.6 Multiple Isotope Effects, Different Steps

It is not always possible to determine intrinsic isotope effects. However, other useful information about the reaction can still be obtained. Above we assumed a single rate determining step sensitive to each isotope substitution. More frequently, however, the isotope sensitivity is found in different steps. Studies with multiple isotope effects can be used to determine the sequence of steps. To illustrate, a more complicated reaction scheme is needed:



As a first example we discuss a mechanism in which the formation of the enzyme–intermediate complex, EI, is sensitive to hydrogen isotopic substitution, while the next step characterized by rate constants k_5 and k_6 exhibits a carbon kinetic isotope effect. Expressions for the three kinetic isotope effects that can be determined experimentally are:

$$\left. \begin{aligned} D(V/K) &= \frac{D k_3 + k_3/k_2 + D K \cdot k_4/k_5 (1 + k_6/k_7)}{1 + k_3/k_2 + k_4/k_5 (1 + k_6/k_7)} \\ {}^{13}(V/K) &= \frac{{}^{13}k_5 + k_5/k_4(1 + k_3/k_2) + {}^{13}K \cdot k_6/k_7}{1 + k_5/k_4(1 + k_3/k_2) + k_6/k_7} \\ {}^{13}(V/K)_D &= \frac{{}^{13}k_5 + k_5/k_4(D k_3 + k_3/k_2)/D K + {}^{13}K \cdot k_6/k_7}{1 + k_5/k_4(D k_3 + k_3/k_2)/D K + k_6/k_7} \end{aligned} \right\} \quad (11.50)$$

Equation 11.51 follows:

$$\frac{{}^{13}(V/K) - 1}{{}^{13}(V/K)_D - 1} = \frac{D(V/K)}{D K} \quad (11.51)$$

A second example (where the step sensitive to carbon isotope substitution precedes the one sensitive to hydrogen substitution) can be treated similarly. If we assume that the conversion of ES to EI in scheme 11.49 (the step involving k_3 and k_4) is characterized by a carbon KIE, while the following step (EI to EP) exhibits an hydrogen KIE, the equations corresponding to Equations 11.50 and 11.51 are:

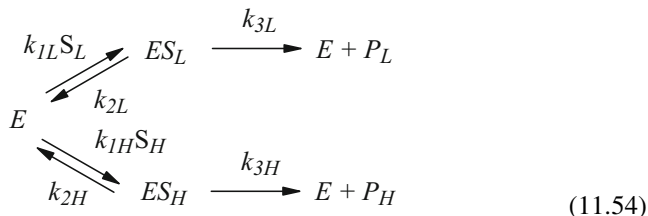
$$\left. \begin{aligned} D(V/K) &= \frac{{}^D k_5 + k_5/k_4(1 + k_3/k_2) + {}^D K \cdot k_6/k_7}{1 + k_5/k_4(1 + k_3/k_2) + k_6/k_7} \\ {}^{13}(V/K) &= \frac{{}^{13}k_3 + k_3/k_2 + {}^{13}K \cdot k_4/k_5(1 + k_6/k_7)}{1 + k_3/k_2 + k_4/k_5(1 + k_6/k_7)} \\ {}^{13}(V/K)_D &= \frac{{}^{13}k_3 + k_3/k_2 + {}^{13}K \cdot k_4/k_5({}^D k_5 + {}^D K \cdot k_6/k_7)}{1 + k_3/k_2 + k_4/k_5({}^D k_5 + {}^D K \cdot k_6/k_7)} \end{aligned} \right\} \quad (11.52)$$

$$\frac{{}^{13}(V/K) - {}^{13}K}{{}^{13}(V/K)_D - {}^{13}K} = D(V/K) \quad (11.53)$$

Equations 11.51 and 11.53 hold for even more complicated mechanisms even though more rate constants enter Equations 11.50 and 11.52. The isotope sensitive steps are not necessarily consecutive. Application of Equations 11.50 through 11.53 is illustrated later in this chapter.

11.3.7 Reversible Competitive Inhibitors

We conclude the discussion of formal kinetics with a practical consideration. When two isotopomers simultaneously present in an enzyme substrate mixture compete for the same active site on the free enzyme E, one can write:



since in the formal sense isotopomers can be regarded as reversible competitive inhibitors. In terms of the steady-state approximation, Equation 11.13 becomes:

$$v_L = \frac{d[P_L]}{dt} = -\frac{d[S_L]}{dt} = k_{3L}[ES_L] = \frac{k_{1L}k_{3L}}{k_{2L} + k_{3L}}[E][S_L] \quad (11.55)$$

$$v_H = \frac{d[P_H]}{dt} = -\frac{d[S_H]}{dt} = k_{3H}[ES_H] = \frac{k_{1H}k_{3H}}{k_{2H} + k_{3H}}[E][S_H] \quad (11.56)$$

The same concentration of free enzyme enters both Equations 11.55 and 11.56. Dividing and introducing Equation 11.20 yields:

$$\frac{v_L}{v_H} = \frac{-d[S_L]/dt}{-d[S_H]/dt} = \frac{d[S_L]}{d[S_H]} = \frac{d[P_L]}{d[P_H]} = \frac{\frac{V_L}{K_L}[S_L]}{\frac{V_H}{K_H}[S_H]} = {}^H(V/K) \frac{[S_L]}{[S_H]} \quad (11.57)$$

Equation 11.57 signifies that when the competitive method is used (i.e., both isotopomers are present simultaneously in the reaction mixture) the experimentally determined kinetic isotope effect corresponds to the isotope effect on V/K regardless of the actual concentration of the substrate. In other words, one cannot measure the isotope effect on V_{\max} using this method even when concentration is much larger than the Michaelis constant K_M .

11.4 Aqueous Solvent Equilibrium and Kinetic Isotope Effects

It is reasonable to expect that isotopic substitution on solvent molecules will affect both equilibrium and rate constants. This is especially true for reactions in aqueous media, many of which are acid or base catalyzed and therefore sensitive to pH or pD. Furthermore H/D aqueous solvent isotope effects often display significant nonlinearity when plotted against isotope fraction of the solvent. The analysis of this effect can yield mechanistic information. The study of aqueous solvent isotope effects is particularly important in enzyme chemistry because enzyme reactions universally occur in aqueous media and are generally pH sensitive.

11.4.1 H_2O/D_2O Solvent Effects on pH (pD) and pK_a

The isotope effect on the acid dissociation constants for H_2O and D_2O has been carefully measured by many workers, most notably Paabo and Bates working at the US Bureau of Standards. Comparing the reactions $2 H_2O = H_3O^+ + OH^-$ and $2 D_2O = D_3O^+ + OD^-$ they found

$$\Delta pK_a = -\log[(D_3O^+)(OD^-)] - (-\log[(H_3O^+)(OH^-)]) = 0.958 \quad (11.58)$$

In other words the acid dissociation constant of ordinary water, $K_a(H_2O) = 1 \times 10^{-14}$, is about ten times larger than that of heavy water, $K_a(D_2O) = 1.10 \times 10^{-15}$. Thus the pH of ordinary water is $pH = -\log((H_3O^+)) = -\log[(1 \times 10^{-14})^{1/2}] = 7.00$ while pD for D_2O is 7.48. This is a significantly large isotope effect and has important consequences.

It is interesting that a plot of ΔpK_a 's vs. $pK_a(H_2O)$ for a series of weak inorganic acids D_3PO_4/H_3PO_4 , $D_2PO_4^-/D_3PO_4^-$, DCO_3^-/HCO_3^- , D_2O/H_2O shows an excellent straight line correlation. This lends credence to the numerical value quoted in Equation 11.58. That correlation is shown in Fig. 11.4. On the other hand, ΔpK_a 's measured on a wide variety of organic acids scatter widely (Fig. 11.4). The correlation for these organic acids is not well established (see the caption to the figure) and many authors choose to approximate the effect by taking the average. For the ~ 100

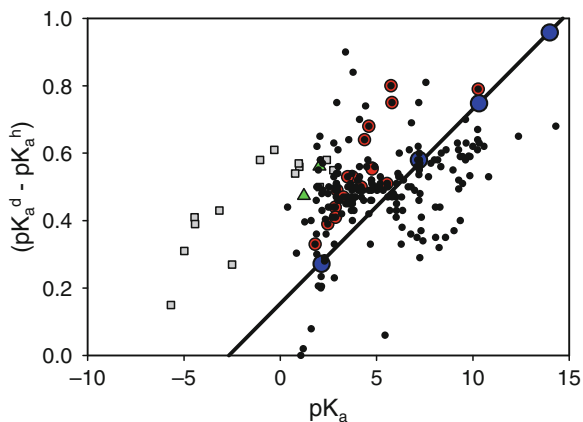


Fig. 11.4 Isotope effect on acid ionization constants. The *heavy line* through the *large circles* correlates data on inorganic weak acids (D_3PO_4 , $D_2PO_4^-$, DCO_3^- , D_2O) due to Paabo, M. and Bates, R. C. (*J. Phys. Chem.* **74**, 706 (1970)), $\Delta pK_a = 0.1537 + 0.0577 pK_a$, $r^2 = 0.9994$. It yields $\Delta pK_a(D_2O) = 0.961$ and $pD(D_2O) = 7.481$. The smaller data points refer to ionization of numerous weak organic acids and have been measured or collected by Li, N. C., Tang, P. and Mathur, R. (*mid-size circles*, *J. Phys. Chem.* **65**, 1074 (1961)), Hogfeldt, E. and Bigeleisen, J. (*squares*, *J. Am. Chem. Soc.* **82**, 15 (1960)), Lowe, B. M. and coworkers (*triangles*, *J. Chem. Soc.:Trans. Far. Soc.* **69**, 1934 (1973); **70**, 362 (1974); **71**, 389 (1975)), or Laughton, P. M. and Robertson, R. E. (*dots*, *Solute-Solvent Interactions*, Coetzee, J. F. and Ritchie, C.D. Eds., Marcel Dekker, NY, 1969). The correlation through these data (not shown), $\Delta pK_a = 0.40 + 0.02 pK_a$, $r^2 = 0.239$, is not reliable. Most authors prefer a simple average $\langle \Delta pK_a \rangle = (0.56 \pm 0.14)$

organic acids plotted in Fig. 11.4 with pK_a 's between 4 and 9, $\langle \Delta pK_a \rangle = 0.5 \pm 0.1$, i.e. on average the deuterated organic acids dissolved in D_2O are only about 30% as dissociated as their protiated sister compounds dissolved in H_2O .

11.4.1.1 An Important Consequence

Many rate constants in aqueous solutions are pH or pD sensitive. In particular, enzyme catalyzed reactions often show maxima in plots of pH(pD) vs. rate. The example in Fig. 11.5 is constructed for a reaction with a true isotope effect, $k_H/k_D = 2$, and with maxima in the pH(pD)/rate dependences as shown by the bell shaped curves. These behaviors are typical for enzyme catalyzed reactions. When the isotope effect is obtained (incorrectly) by comparing rates at equal pH and pD, the values plotted along the steep dashed curve result. If, however, the rate constants at corresponding pH and pD ($pD = pH + 0.5$) are employed, a constant and correct value is obtained, $k_H/k_D = 2$. Thus for accurate measurements of the isotope effects one must control pH and pD at appropriate values ($pD = pH + 0.5$ in our example) using a series of buffers. In proton inventory experiments (see below) buffers should be employed to insure equivalent acidities across the entire range of solvent isotope concentration ($0 < x_D < 1$), x_D is the atom fraction of deuterium $[D]/([H] + [D])$.

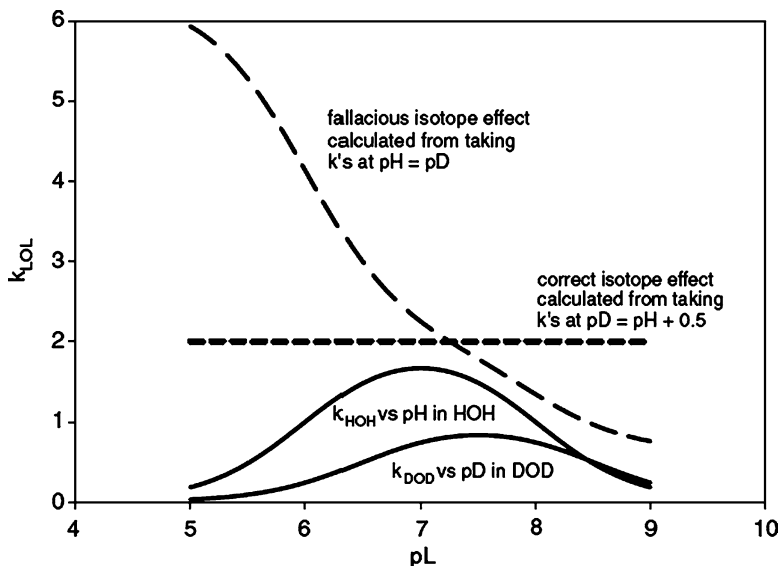
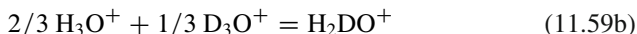


Fig. 11.5 Rate constants in HOH and DOD as a function of pL (two bottom bell shaped curves) for an enzyme catalyzed reaction with three protomeric forms and an isotope effect of 2. L is the H⁺ or D⁺ concentration as appropriate. The steep curve shows the erroneously calculated isotope effect from the rate constants at pH = pD. The correct flat line is calculated taking the IE's at corresponding pL (pD = pH + 0.5) (Schowen, R. L. *J. Label Compd Radiopharm.* **50**, 1052 (2007), with permission Wiley Interscience)

11.4.2 Monoprotic Acid/Base Equilibria in Mixed Solvents

In the discussion which follows it is convenient to have a symbol to represent any one of the three hydrogen isotopes, H, D or T, and L (lyonium or lyate) is widely used for that purpose. Thus in a mixture of H₂O and D₂O the solvent L₂O consists of a mixture of H₂O, D₂O and HDO, and the ion L₃O⁺, could be either H₃O⁺, H₂DO⁺, HD₂O⁺, or D₃O⁺, while OL⁻ represents the two species OH⁻ and OD⁻.



The isotopic abundance of deuterium in the L₃O⁺ ion will differ from that in the water with which it is equilibrated. This is expressed in terms of the fractionation factor *l* which is the ratio of D/H ratios in the lyonium ion and the mixed solvent (water)

$$l = (\text{D}/\text{H})_{\text{L}_3\text{O}^+} / (\text{D}/\text{H})_{\text{L}_2\text{O}} = F_{\text{L}_3\text{O}^+} (1-x) / [(1-F)_{\text{L}_3\text{O}^+} x] \quad (11.60)$$

In this equation $F_{L_3O^+}$ is the fraction D in L_3O^+ and x the fraction D in the solvent.

$$x = ([D_2O] + [HDO])/2 / ([D_2O] + [HDO] + [H_2O]) \quad (11.61)$$

$$F_{L_3O^+} = ([D_3O^+] + 2[HD_2O^+]/3 + [H_2DO^+]/3) / ([D_3O^+] + [HD_2O^+] + [H_2DO^+] + [H_3O^+]) \quad (11.62)$$

The square brackets denote number of moles. With the use of the law of the geometric mean, which in this context implies that the equilibrium constants for reactions 11.59a through c are 4, 9/2 and 9/2 respectively, the mixed isotopomer species can be eliminated and Equation 11.60 reduces to

$$l = ([D_3O^+]/[H_3O^+])^{1/3} \left([H_2O]/[D_2O] \right)^{1/2} \quad (11.63)$$

While not exact, K_{EQ} for reaction 11.59a is actually 3.8 at 298 K, the approximation is sufficiently accurate for our purposes. With this use of the law of the geometric mean a good deal of algebraic complexity is avoided. Notice that l^6 is the equilibrium constant for the reaction $2H_3O^+ + 3D_2O = 3H_2O + 2D_3O^+$.

Similar fractionation factors can be defined for other species. These are ordinarily given the symbol “ ϕ ” in order to reserve “ l ” for solvent fractionation. Thus for an acid dissociation in mixed media, $AL_j + L_2O = L_3O^+ + AL_{j-1}^-$

$$\phi_{AL_j} = F_{AL_j}(1 - x) / ((1 - F_{AL_j})x) \quad (11.64)$$

For the case of an acid AL with a single exchangeable hydrogen Equation 11.64 reduces to

$$\phi_{AL} = [AD](1 - x) / ([AH]x) \quad (11.65)$$

Since the ratio of the acid dissociation constants of a monoprotic acid in pure H_2O to that in the mixed solvent is

$$K^H/K^x = [H_3O^+][AL][L_2O] / ([L_3O^+][AH][H_2O]) \quad (11.66)$$

we can use Equations 11.59 through 11.64 to deduce

$$K^H/K^x = (1 - x + x\phi_{AL}) / (1 - x + xl)^3 \quad (11.67)$$

For pure D_2O ($x = 1$), $K^H/K^D = \phi_{AL}/l^3$. This allows Equation 11.67 to be more usefully written as

$$K^H/K^x = (1 - x + xl^3K^H/K^D) / (1 - x + xl)^3 \quad (11.68)$$

The value of l has been determined by NMR measurements on the mixed solvent as 0.69 ± 0.02 and is not to be interpreted as an independent fitting parameter. With l established, ϕ can be calculated from the acid dissociation constants in pure H_2O and D_2O , and Equation 11.68 interpreted as a zero parameter theoretical prediction of

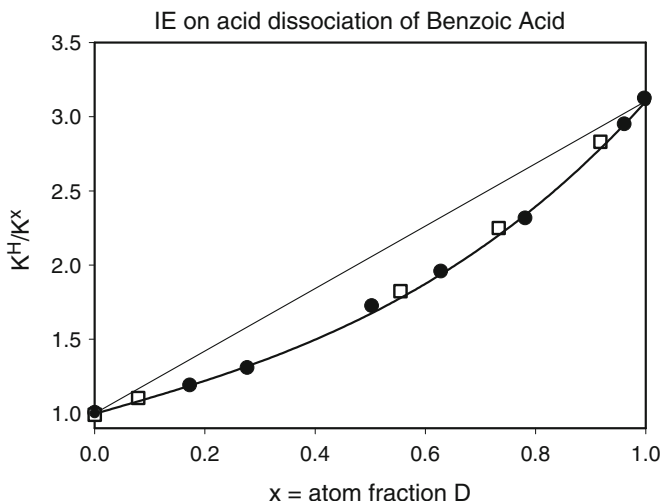


Fig. 11.6 The ratio of acid dissociation constant for benzoic acid C_6H_5COOL as a function of D atom fraction in the solvent. The data are those of Lowe, B. M. and Smith, D. G., *J. Chem. Soc.; Faraday Trans.* **71**, 389 (1975) as determined by EMF (circles) and conductance (squares). The heavy line is the prediction of Equation 11.61 with $l = 0.69$, $\phi = 1.02$ and $pK^H = 4.201$. The lighter line shows the linear approximation

IE's in mixed solvents. The success of the theory is illustrated in Fig. 11.6 using the case of benzoic acid. The agreement between theory and experiment is quantitative.

11.4.2.1 Extension to Dissociation of Polyprotic Acids

For polyprotic acids, $AL_j + L_2O = L_3O^+ + AL_{j-1}^-$, an analogous treatment to the leading to Equation 11.67 gives

$$K^H/K^x = (1 - x + x\phi_{ALi})^j / ((1 - x + xl)^3 (1 - x + x\phi_{AL(i-1)})^{j-1}) \quad (11.69)$$

In pure D_2O ($x = 1$) this becomes $K^H/K^D = \phi_{ALi}^j / (l^3 \phi_{AL(i-1)}^{j-1})$. Consequently the observed value of K^H/K^D can only be used to eliminate one, not both, of the fractionation factors. The other must be considered as an adjustable parameter. That accepted, the available experimental results are consistent with Equation 11.69.

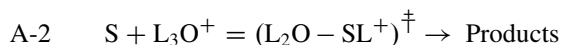
11.4.3 Kinetic Isotope Effects in Mixed Solvents

To calculate the mixed solvent isotope effect on rate constants one applies simple ideas from transition state theory to evaluate the isotope effect on the



[Historical Vignette 11.1] Victor Gold (1922–1985) was born in Vienna but shortly after Hitler's Anschluss emigrated to Britain. He was educated at University and Kings Colleges, London, receiving his graduate degree in 1943. He joined the faculty at Kings in 1944 where he spent his entire career, eventually rising to Head of Department and Dean of Faculty. Gold's most important contribution to isotope science was his development of the field of kinetic solvent isotope effects. He presented generalized expressions for reactions in mixed ($\text{H}_2\text{O}/\text{HOD}/\text{D}_2\text{O}$) solvents and brought forward important ideas on isotope effects in acid/base reactions. (Pencil sketch courtesy of N. Van Hook, 2009)

equilibrium constant between reactant (substrate) and transition state. Several different mechanisms are possible:



For the A-1 mechanism the transition state involves only one hydrogen and the ratio of rate constants follows analogously from Equation (11.67)

$$k^{\text{H}}/k^{\text{x}} = (1 - x + xl)^3 / (1 - x + x\phi^\ddagger) \quad (11.70)$$

where k^{H} is the rate in pure H_2O and k^{x} that in the mixed solvent. Notice Equation 11.70 is similar to the reciprocal of Equation 11.67. That is because the hydronium ion is now being considered as a reactant rather than a product. The single proton fractionation factor for the transition state ϕ^\ddagger can be obtained from the observed rate in pure D_2O , $k^{\text{H}}/k^{\text{D}} = l^3/\phi^\ddagger$. On the other hand if there are multiple hydrogens involved in the transition state the rate ratios are deduced from Equation 11.69. For two protons participating in the transition state

$$k^{\text{H}}/k^{\text{x}} = (1 - x + xl)^3 / \left((1 - x + x\phi_1^\ddagger) (1 - x + x\phi_2^\ddagger) \right) \quad (11.71)$$

where the subscript "1" and "2" refer to the fractionation factors for the two transition state protons. Again, one, but only one, of these may be eliminated by using the observed value of k^H/k^D . Extension to multiple protons participating in the transition state is straightforward.

It is obvious from the discussion that one can take advantage of equations of the type (11.69), and its generalization to multiple sites, to deduce information about the number of protons actively participating in the transition state, see Fig. 11.7.

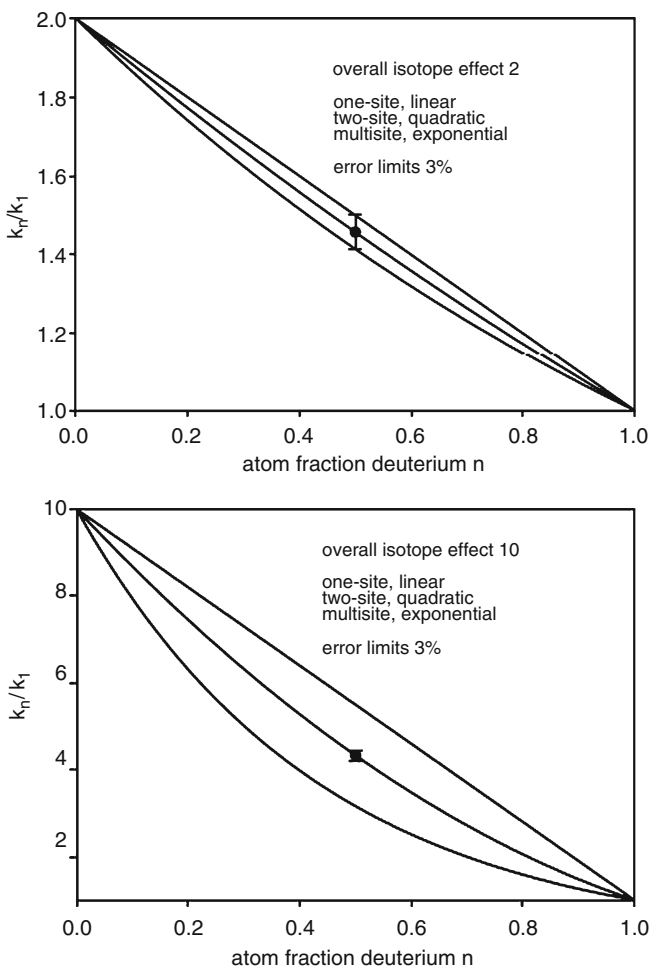


Fig. 11.7 Proton inventory curves (plots of $k(n)/k(H)$ vs. n (or x) = atom fraction D) for overall isotope effects of 2 (*upper plot*) and 10 (*lower plot*). In each, the three curves (reading from *top* to *bottom*) are for single site, two site, and multi-site isotope effects. Error bars of $\pm 3\%$ (*middle curves*) are shown in each case. For $k_0/k_1 = 2$ the technique is unable to distinguish between the curves at this level of precision (3%), but is more than adequate for $k_0/k_1 = 10$ (Schowen, R. L., *J. Label Compd Radiopharm.* **50**, 1052 (2007), with permission Wiley Interscience)

This technique is called the proton inventory method and has been employed with success in studies of enzyme reactions. Numerous examples are cited by Quinn (reading list).

11.5 Examples, Enzyme Catalysis

11.5.1 Decarboxylation KIE's

Carbon kinetic isotope effects on enzyme-catalyzed decarboxylations are among the most intensively studied enzyme reactions. This is because of the central role that carbon dioxide plays in plant metabolism and also because precise kinetic measurements are relatively easy to obtain since the carbon dioxide liberated in the reaction can be immediately analyzed using isotope ratio mass spectrometry.

11.5.1.1 Enzyme Catalysed Conversion of L-Malate to Pyruvate

The practical usefulness of Equations 11.46 through 11.53 has been demonstrated for the malic enzyme catalyzed conversion of L-malate to pyruvate (Equation 11.72). Table 11.1 lists experimentally determined isotope effects for this reaction. Comparison of carbon kinetic isotope effects for protio and deuteromalate substituted at position 2 (the carbon that undergoes sp^3 to sp^2 transition) rules out the possibility that the hydride transfer and the decarboxylation events are concerted. This conclusion follows from Equation 11.48 which, for a concerted reaction, predicts that $^{13}(V/K)$ should be smaller than $^{13}(V/K)_D$, which is opposite to the order observed experimentally.

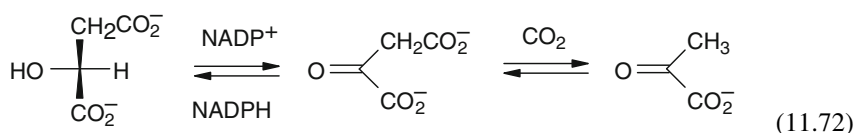
There are two mechanistic possibilities left, either hydride transfer precedes decarboxylation, or vice versa. These two possibilities can be distinguished using Equations 11.51 and 11.53. Within experimental error only Equation 11.51 is consistent with the isotope effect data collected in Table 11.1, thus confirming that the reaction proceeds via a stepwise mechanism with hydride transfer to triphosphate nucleotide ($NADP^+$) and intermediate formation of oxalacetate preceding decarboxylation:

Table 11.1 Isotope effects on malic enzyme catalyzed conversion of L-malate to pyruvate (Hermes, J. D. et al. *Biochemistry* **21**, 5106 (1982))

Isotope effect	Experimental value
$^{13}(V/K)$	1.0302
$^{13}(V/K)_D$	1.0250
$^D(V/K)$	1.47
^{13}K	0.999
DK	1.18



[Historical Vignette 11.2] Frank Westheimer (1912–2007) earned a Ph.D. from Harvard in 1935. On leaving for Columbia University as a National Research Fellow, James Bryant Conant, who had been his research advisor, and was then president of Harvard, asked him what he planned to do next. “I described my research project to him,” Westheimer recalled. “He thought about my answer for a minute, then he said, ‘If you are successful, you’ll be a footnote to a footnote in the history of chemistry.’” Westheimer did the project and it was successful. “Conant was right,” he said. “It was an utterly trivial piece of research. As a result, I decided I would never again undertake research that wasn’t at least potentially important,” and he did not. Westheimer was at the University of Chicago from 1936 to 1953. He returned to Harvard in 1953 as a visiting professor and never left. Until his retirement in 1983, he kept getting good ideas and making seminal discoveries about once every decade. Westheimer was at the forefront of the development of physical-organic chemistry and was one of the early users of isotope effects in the detailed study of reaction mechanisms. In the 1950s he broadened his field of interest to include the study of enzyme reactions and biochemistry. Here too, his pioneering studies had a profound and lasting impact – this time on biological and biochemical processes. (Photo credit: Harvard News Office)



It is historically noteworthy that it was experiments with [2-D]-L-malate that led to the discovery of the equilibrium perturbation method (Section 7.1.4). As can be seen in Fig. 11.8 the perturbation is only a few μmolar although the isotope effect is quite sizable.

11.5.2 Glucose-6-Phosphate Dehydrogenase

As mentioned in Section 11.3.5 for the case where the rate determining step is sensitive to both isotopic species, elucidation of the intrinsic isotope effects is not possible using the equations given thus far (if neither the reverse nor the forward commitment is zero). Even then, however, it is possible to solve for the intrinsic iso-

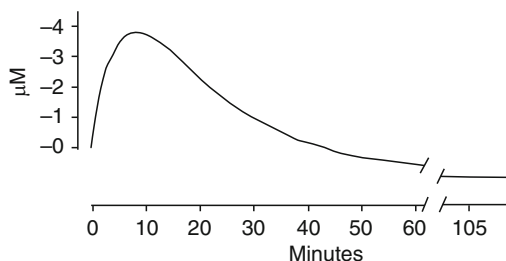
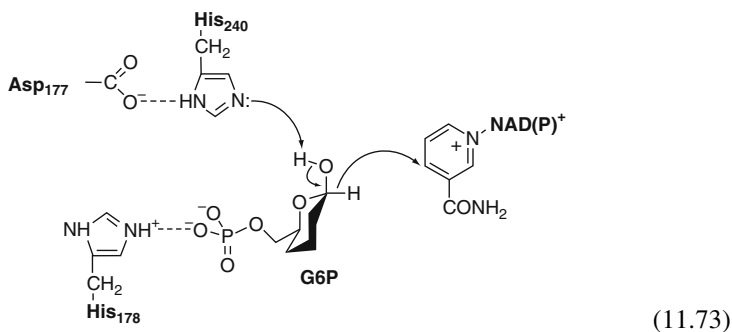


Fig. 11.8 Equilibrium perturbation trace for deuterated L-malate reaction catalyzed by malic enzyme. The equilibrium perturbation technique is discussed in Section 7.1.4. The label on the ordinate, μM has been recalculated from the change in absorbance of TPNH at 340 nm (Schimerlik, M. I., Rife, J. E. and Cleland, W. W. *Biochemistry* **14**, 5347 (1975))

tope effects given additional isotope effect data. One such example is the reaction catalyzed by glucose-6-phosphate dehydrogenase:



Isotope effects on both the carbon and hydrogen of the breaking C-H bond have been measured. However, for this reaction both forward and reverse commitments are sizable so the three equations corresponding to Equation 11.48 have four unknowns; the forward and reverse commitments and two intrinsic isotope effects. Measurements of the secondary deuterium kinetic isotope effect (at position 4 of nicotinamide ring of NAD(P)^+) and the carbon kinetic isotope effect with the secondary position deuterated introduce two additional equations, but only one more unknown:

$$\left. \begin{aligned} {}^{13}(V/K) &= \frac{{}^{13}k + c_f + c_r {}^{13}K}{1 + c_f + c_r} \\ D(V/K) &= \frac{Dk + c_f + c_r D K}{1 + c_f + c_r} \\ \alpha D(V/K) &= \frac{\alpha D k + c_f + c_r \alpha D K}{1 + c_f + c_r} \\ {}^{13}(V/K)_D &= \frac{{}^{13}k + c_f/Dk + c_r {}^{13}K^D K/Dk}{1 + c_f/Dk + c_r D K/Dk} \\ {}^{13}(V/K)_D &= \frac{{}^{13}k + c_f/\alpha D k + c_r {}^{13}K^{\alpha D} K/\alpha D k}{1 + c_f/\alpha D k + c_r {}^{13}K^{\alpha D} K/\alpha D k} \end{aligned} \right\} \quad (11.74)$$

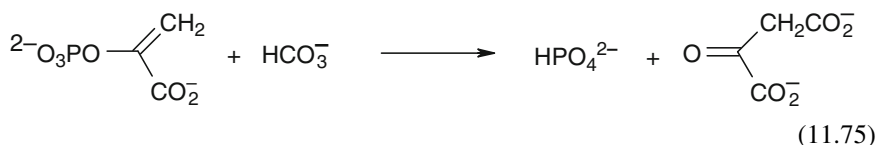
Table 11.2 Observed and intrinsic isotope effects on the glucose-6-phosphate dehydrogenase reaction (Hermes, J. D. and Cleland, W. W. *J. Am. Chem. Soc.* **106**, 7263 (1984))

Isotope effects	Observed		Evaluated intrinsic
	Kinetic	Equilibrium	
$^{13}(\text{V/K})_{\text{D}}$	1.0316		
$^{13}(\text{V/K})_{\alpha\text{D}}$	1.0176		
$^{13}(\text{V/K}), ^{13}\text{K}, ^{13}\text{k}$	1.0165	0.992	1.041 ± 0.002
$^{\text{D}}(\text{V/K}), ^{\text{D}}\text{K}, ^{\text{D}}\text{k}$	2.97	1.28	5.3 ± 0.3
$^{\alpha\text{D}}(\text{V/K}), ^{\alpha\text{D}}\text{K}, ^{\alpha\text{D}}\text{k}$	1.000	0.887	1.05 ± 0.04

Equation 11.74 allows for an explicit solution for all five unknowns. The intrinsic values obtained are listed in Table 11.2 together with the experimental ones. In addition to these intrinsic values of kinetic isotope effects to be used in further analysis of the transition state structure, the commitments were calculated as $c_f = 0.8 \pm 0.3$ and $c_r = 0.5 \pm 0.3$.

11.5.3 Concentration Dependence of KIE; Phosphoenolpyruvate Carboxylase

Another technique for unmasking the intrinsic isotope effect is to study the concentration dependence of the observed kinetic isotope effect (see Section 11.3.2). This is straightforward for reactions with ordered reactant binding. In that case lowering the concentration of the substrate binding in the second step lowers the commitment (see Equations 11.37 through 11.42). Table 11.3 illustrates the dependence on bicarbonate concentration for the bridging oxygen kinetic isotope effect on the phosphoenolpyruvate carboxylase (PEP-C) catalyzed reaction between bicarbonate and phosphoenolpyruvate leading to oxalacetate and inorganic phosphate (O'Leary and Paneth, reading list):



There are several interesting aspects to this study. The dependence on bicarbonate concentration can be described formally by introducing Equation 11.42 into Equation 11.41 and assuming that only the reaction specified by rate constant k_5 is isotope sensitive:

Table 11.3 Kinetic isotope effects on *Zea mays* PEP-C catalyzed reaction at pH 7.5 (O'Leary, M. H. and Paneth, P., *Bioact. Mol.* **3**, 303 (1987). Gawlita, E., Caldwell, W. S., O'Leary, M., Paneth, P., and Anderson, V. E., *Biochemistry*, **34**, 2577 (1995))

[HCO ₃ ⁻] (mM)	¹⁸ O-KIE	[1- ¹³ C]-KIE
200	0.9943	0.9951
8	1.0043	0.9975
2	1.0056	0.9950

$${}^{18}k_{app} = {}^{18}(V/K) = \frac{{}^{18}k_5 + \frac{k_3k_5[\text{HCO}_3^-]}{k_2k_4}}{1 + \frac{k_3k_5[\text{HCO}_3^-]}{k_2k_4}} \quad (11.76)$$

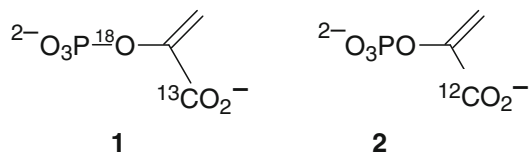
However, although Equation 11.76 gives a qualitative explanation of the change in the observed isotope effect and can be used to calculate the intrinsic oxygen kinetic isotope effect, it suffers from one important criticism. Since ¹⁸k₅ is normal (larger than unity) at high bicarbonate concentration (i.e. when k₃k₅[HCO₃⁻]/k₂k₄ is much larger than the intrinsic isotope effect), the observed isotope effect should be “washed out” to unity. Instead, the limiting observed isotope effect is inverse (less than unity). This was explained by invoking an inverse isotope effect on PEP binding to the enzyme, which leads to a modified expression:

$${}^{18}k_{app} = {}^{18}(V/K) = {}^{18}k_1 \frac{{}^{18}k_5 + \frac{k_3k_5[\text{HCO}_3^-]}{k_2k_4}}{1 + \frac{k_3k_5[\text{HCO}_3^-]}{k_2k_4}} \quad (11.77)$$

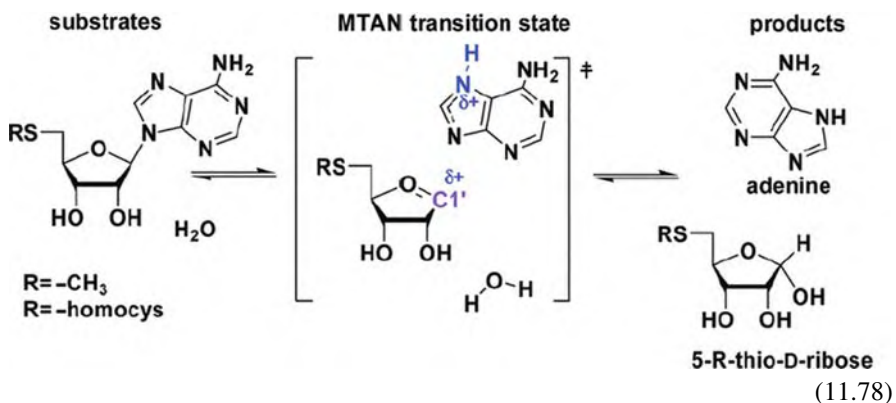
The solution of Equation 11.77 for all unknowns yields 1.013, 0.994, and 0.06 for the intrinsic IE's of ¹⁸k₅ and ¹⁸k₁, and k₃k₅/k₂k₄ [mM], respectively.

Oxygen isotope effects in Table 11.3 were determined with the remote labeling technique (Section 7.2.2.2) using doubly labeled substrate. This permitted straightforward use of high precision isotope ratio mass spectrometry employing CO₂ analysis. Direct measurement of the isotope effect of oxygen in the C-O-P bridge position in phosphoenolpyruvate is not easy. Instead remote label carbon kinetic isotope effects were employed. Two labeled isotopomers 1 and 2 were mixed in pseudo-natural isotopic composition of carbon (1:90). Isotopomer 1 was simultaneously labeled with carbon-13 in the carboxylic carbon and with oxygen-18 in the bridging C-O-P position. Isotopomer 2 was C-13 depleted in carboxylic carbon. Isotope ratios of the phosphoenolpyruvate carboxylic carbon liberated enzymatically thus reported on both the oxygen and carbon isotope effects. In separate

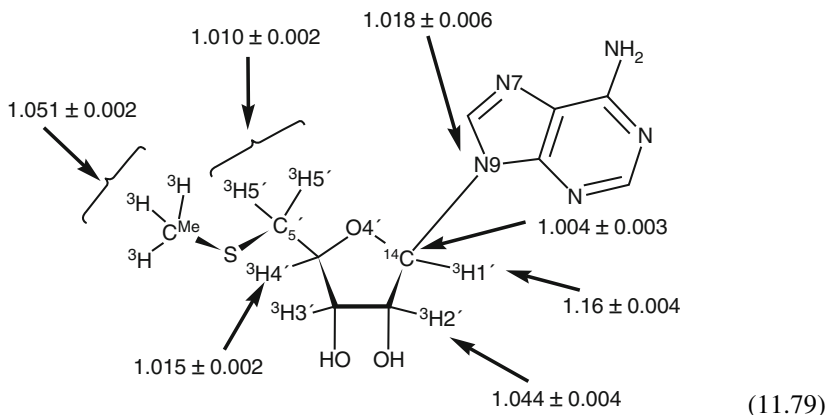
measurements the carbon kinetic isotope effects in the carboxyl position were measured using natural abundance C-13. The two sets of carbon isotope effect data were combined and used to evaluate the oxygen isotope effects.



A sizable isotope effect on $^{18}\text{k}_5$ has been interpreted as an evidence of substantial charge development on the oxygen atom in the transition state. The inverse isotope effect on binding PEP to the enzyme corroborates similar findings for pyruvate kinase and the equilibrium oxygen binding isotope effect determined for oxamate binding to lactate dehydrogenase (also slightly inverse). It is worth noting that binding isotope effects documented in the literature frequently come from studies involving remote labeling. This is not surprising; one usually chooses a site for the reporting atom that is easy for isotopic analysis and which is expected to show little or no isotope effect. The same is true for remote labeling studies using radioactive isotopes. For example, in a recent report on catalysis by methylthioadenosine/*S*-adenosylhomocysteine nucleosidase (MTAN) (Schramm, V. L. et al. *Biochemistry* **44**, 11647 (2005)):



the nitrogen kinetic isotope effect was measured using doubly labeled $[9\text{-}^{15}\text{N}, 5'\text{-}^{14}\text{C}]$ - and $[5\text{-}^3\text{H}]$ - substrates and correcting the observed multiple isotope effect with that determined for the $[5'\text{-}^3\text{H}]$ -, $[5'\text{-}^{14}\text{C}]$ -labeled pair. Assuming the rule of the geometric mean, product analysis yields the desired isotope effect for nitrogen-15. Other isotope effects in Equation 11.78 have been determined using double counting liquid scintillation techniques (see Figure 11.9):



The results in Equation 11.79 show that the reaction 11.78 proceeds via a dissociative ($D_N^*A_N$ or as commonly called S_N1) mechanism with no involvement of either the leaving group or the attacking nucleophile at the transition state. Based on these results a series of transition state analog inhibitors have been designed. This successful practical application of the information regarding the transition state structure gathered from kinetic isotope effect studies resulted in a thousand-fold improvement of the inhibitor binding constant! This type of study is of particular importance in drug design, where the objective is to find a substance of the largest possible bioactivity. Because all pharmaceuticals have some kind of side effects, minimization of the necessary dose is one of the prime objectives, the other being specificity of their action. More details are given later in this chapter.

11.5.4 Other Factors Influencing Commitment

Perturbation of the commitments can be achieved experimentally in several ways. If the rate constants involved in commitment have different activation energies the commitment will change with temperature. Many enzymatic reactions involve proton shuffling and changes in pH can lead to changes of commitment. Of course, formally speaking, this is only one more example of a change in concentration (this time of protons). Other changes may include varying the solvent, e.g., use of D_2O instead of H_2O , the cofactor (metal), the enzyme (e.g., mutations), or the substrates. A few of these approaches are nicely illustrated by the carbon kinetic isotope effects on the orotidine 5'-monophosphate decarboxylase (ODCase) reaction that catalyses conversion of OMP (orotidine 5'-monophosphate) to UMP (uridine 5'-monophosphate), see Equation 11.80. As can be seen from the data in Table 11.4 which refers to *Saccharomyces cerevisiae* enzyme, lowering the pH from its physiological value of 6.8 to 4.0 increases the carbon isotope effect substantially. The change was interpreted as evidence that the chemical step is rate-limiting at low pH and the observed kinetic isotope effect of about 1.05 is thought to be the in-

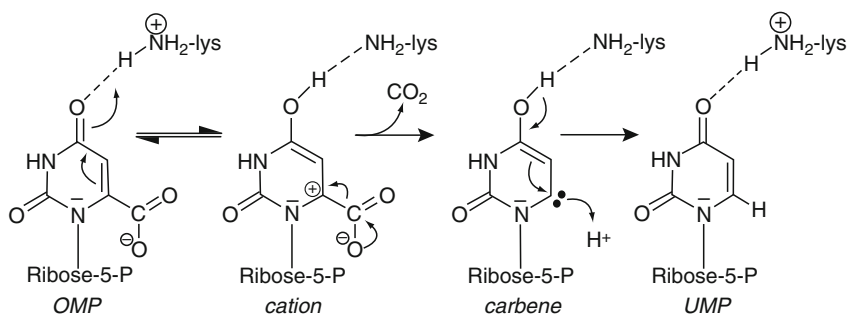
Table 11.4 ^{13}C kinetic isotope effects on the ODCase reaction (Smiley, J. A., Paneth, P., O'Leary, M., Bell, J. B. and Jones, M. E., *Biochemistry* **30**, 6216 (1991))

pH	0 °C/H ₂ O	25 °C/H ₂ O	25 °C/D ₂ O
7.4	–	1.022	
6.8	1.037	1.025	
6.0	–	1.027	
5.4	1.044	1.038	
4.0	1.049	1.051	
7.5 ^a	–	1.043	1.034

^aEhrlich, J. J., Hwang, C. C., Cook, P. F. and Blanchard, J. S., *J. Am. Chem. Soc.* **121**, 6966–6967 (1999).

trinsic value of this isotope effect. Note that similar dependence is observed at 0 °C although the KIE values are different due to temperature dependence of the commitments.

Another way of perturbing the commitments is solvent deuteration. Change of the carbon kinetic isotope effect in the case of *E. coli* enzyme indicates that the proton transfer precedes the decarboxylation step:



The detailed mechanism of this reaction has become the subject of vigorous debate since these isotope effects were first published. It has been chosen for detailed theoretical analysis in several QM/MM studies of enzyme catalyzed reactions.

11.6 Solvent Kinetic Isotope Effects in Enzyme Reactions (See Also Section 11.4)

As a practical matter of cost, studies on solvent isotope effects are usually limited to D/H substituted solvents, although recently a few ^{18}O solvent effects have been measured. Interpretation of enzymatic solvent isotope effects is even more complicated than it is when the isotopic probe is incorporated in the substrate(s). This is because enzyme proteins have many exchangeable protons and, also, this is frequently true for reactants (substrates). Thus the observed isotope effect is the collective result of many different isotopic substitutions, each of which may influence

the reaction in different ways. Another important issue in solvent effects is the fact that hydrogen bonds play an important role in maintaining conformational stability of proteins. Thus one might question if the conformation of the protein is the same in H₂O and D₂O. Furthermore, pK_a values of aminoacids are affected by the isotope composition of the aqueous solvent (see Section 11.4.1 and Fig. 11.4). Each of these factors can be reflected in different reactivity of the corresponding functional groups. The physical properties of water, properties such as viscosity, dielectric constant, specific heat, etc., are isotope sensitive and these differences must be taken into account in the interpretation of solvent KIE data. In spite of these difficulties, however, solvent kinetic isotope effects yield valuable information about reaction mechanisms. This is especially true for the enzyme reactions because of the different mechanistic information embedded in isotope effects on V_{max} and V_{max}/K_M. The basic theory underlying solvent kinetic isotope effects has been provided in Section 11.4; a few additional examples for enzyme reactions follow.

11.6.1 Examples

Table 11.5 lists three examples of solvent isotope effects showing a wide range of values. SrtA transpeptidase catalyzes attachment of surface proteins to the peptidoglycan layer of gram-positive bacteria. The large inverse solvent isotope effect on V/K has been attributed to an equilibrium isotope effect on the interconversion of thiol and thiolate forms of cysteine C184. This conclusion comes from large inverse fractionation factors, 0.55, observed for the sulfhydryl groups in cysteine. The solvent isotope effect on V_{max} is closer to unity (thus “smaller” when the effect is thought of as a deviation from unity) which indicates that a different step, with little or no fractionation is mostly rate-determining. Proton inventories have been measured for this enzyme and the results are presented in Fig. 11.9. The plot of V_{max} in mixed H₂O/D₂O solvents of different deuterium content is linear. This indicates that a single proton is involved in the rate-determining step.

A similar analysis applies to C13S mutated tetrachlorohydroquinone dehalogenase but normal rather than inverse solvent isotope effects are involved. This

Table 11.5 Selected solvent isotope effects on some enzyme catalyzed reactions

Enzyme	D ^{OD} (V/K)	D ^{OD} V
<i>Staphylococcus aureus</i> transpeptidase SrtA ^a	0.57	0.89
<i>Enterobacter cloacae</i> P99 β-lactamase ^b	0.79	1.44
C13S tetrachlorohydroquinone dehalogenase ^c	4.42	2.87

^aFrankel, B. A., Kruger, R. G., Robinson, D. E., Kelleher, N. L. and McCafferty, D. G.. *Biochemistry* **44**, 11188 (2005).

^bAdediran, S. A., Deraniyagala, S. A., Yang, W. and Pratt, R.. *Biochemistry* **35**, 3604 (1996).

^cKiefer, P. M., Jr., McCarthy, D. L. and Copley, S. D.. *Biochemistry* **41**, 1308 (2002).

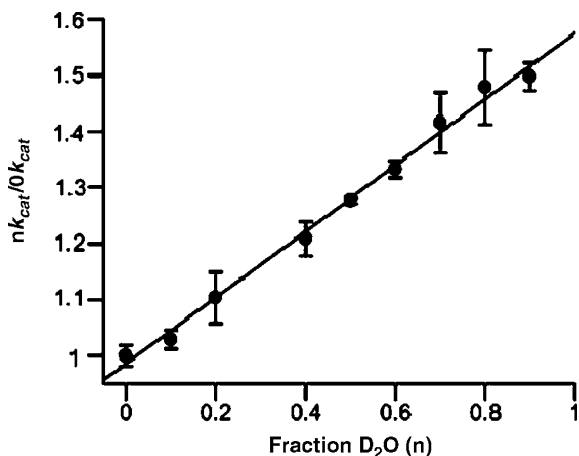
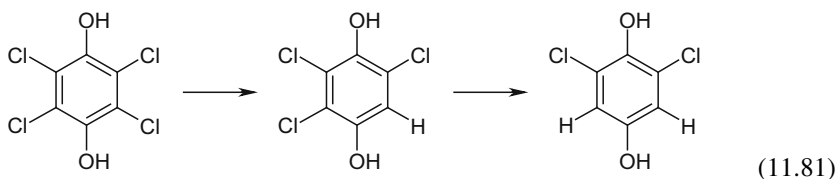


Fig. 11.9 Proton inventory on SrtA catalyzed reaction. The ratio of $k_{\text{CAT}} = K_{\text{M}}$ (Section 11.2, Equations 11.9 through 11.13) measured in a $\text{D}_2\text{O}/\text{H}_2\text{O}$ solvent mixture of mole fraction n D_2O to that measured in H_2O ($n = 0$), is plotted vs. n (Frankel, B. A., et al. *Biochemistry* **44**, 11188 (2005))

dehalogenase enzyme catalyzes the second and third steps in the biodegradation of a pesticide, pentachlorophenol, by *Sphingobium chlorophenolicum*. It uses tetrachlorohydroquinone and trichlorohydroquinone as substrates (see Equation 11.81):



An $\text{S}_{\text{N}}\text{Ar}$ (nucleophilic substitution at aromatic carbon atom) mechanism has been proposed for these reactions. Both nonenzymatic and enzymatic reactions that proceed via this mechanism typically exhibit inverse solvent kinetic isotope effects. This observation is in agreement with the example above since the thiolate form of glutathione plays the role of the nucleophile role in dehalogenation reactions. Thus values of solvent kinetic isotope effects obtained for the C13S mutant, which catalyzes only the initial steps of these reactions, do not agree with this mechanism. Rather, the observed normal solvent isotope effect supports a mechanism in which step(s) that have either no solvent kinetic isotope effect at all, or an inverse effect, and which occur after the elimination step, are kinetically significant and diminish the observed solvent kinetic isotope effect.



[Historical Vignette 11.3] **W. Wallace Cleland** (1930–present) received his A.B. from Oberlin College in 1950 and his M.S. and Ph.D. from the University of Wisconsin-Madison in 1953 and 1955, respectively. After a postdoctoral fellowship spent at the University of Chicago he returned to Madison to join the faculty where he remains and is still actively involved in research. Cleland has devoted a great deal of time to developing and using isotope effect techniques to study enzyme mechanisms, see for example *J. Biol. Chem.* **278**, 51975 (2003). (Photo credit: Biochemistry Department, University of Wisconsin, Madison)

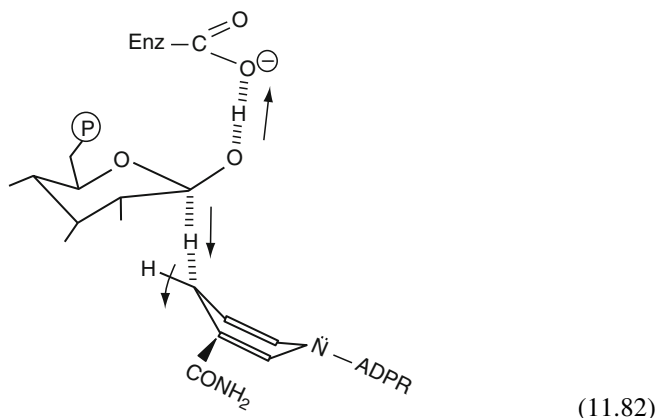
11.6.2 Coupled Motion

Solvent isotope effects can sometimes reveal the effects of coupled motion and tunneling in enzymatic reactions. For example, consider the H/D solvent IE on the set of carbon isotope effects in the reaction catalyzed by glucose-6-phosphate dehydrogenase presented in Table 11.2. The experiments in D₂O yielded an intrinsic value of the primary deuterium kinetic isotope effect $^Dk(D_2O) = 3.7$ (Table 11.6) which differs substantially from the value obtained in H₂O, $^Dk(H_2O) = 5.3$ (Table 11.2). If deuteration of the solvent affected only the commitments, the intrinsic values of the isotope effects in D₂O and H₂O would be identical within experimental error. Thus the large solvent isotope effect on the intrinsic primary hydrogen kinetic isotope effect can be explained in terms of coupled motion of the hydrogen atoms in the transition state and tunneling. This is because the probability of simultaneous tunneling of two or more hydrogens is lower than is the probability of each tunneling separately.

Table 11.6 Observed and intrinsic kinetic isotope effects on the glucose-6-phosphate dehydrogenase reaction in D₂O (Cleland, W. W. in Cook, P. F., Ed., *Enzyme Mechanism from Isotope Effects* CRC Press, Boca Raton FL, 1991. Hermes, J. D. and Cleland, W. W. *J. Am. Chem. Soc.* **106**, 7263 (1999))

Isotope effects	Observed	Evaluated intrinsic
$^{13}(V/K)_D$	1.0242	
$^{13}(V/K)_{\alpha D}$	1.0114	
$^{13}(V/K)$, ^{13}k	1.0110	1.044 ± 0.004
$^D(V/K)$, Dk	1.81	3.7 ± 0.3
$^{\alpha D}(V/K)$, $^{\alpha D}k$	0.98	1.00 ± 0.04

For this reaction the transition state drawn in Equation 11.82 involving simultaneous proton and hydride transfers has been proposed to explain the observed isotope effects.



11.7 Tunneling (See Also Section 11.8)

Not only primary but also secondary hydrogen isotope effects can be indicative of tunneling. The most frequently employed criteria of tunneling are the temperature dependence of kinetic isotope effects and the isotopic ratio of the pre-exponential factors in Arrhenius plots, but the pre-exponential criterion has been shown to be invalid for small secondary isotope effects.

11.7.1 Tunneling in Alcohol Dehydrogenases

Probably the most extensively studied enzymes are those from alcohol dehydrogenase family. One enzyme from this series which has been thoroughly examined both experimentally and theoretically is liver alcohol dehydrogenase (LADH). It catalyzes the reversible conversion of an alcohol to an aldehyde by transferring hydride from substrate to the cofactor (NAD^+):

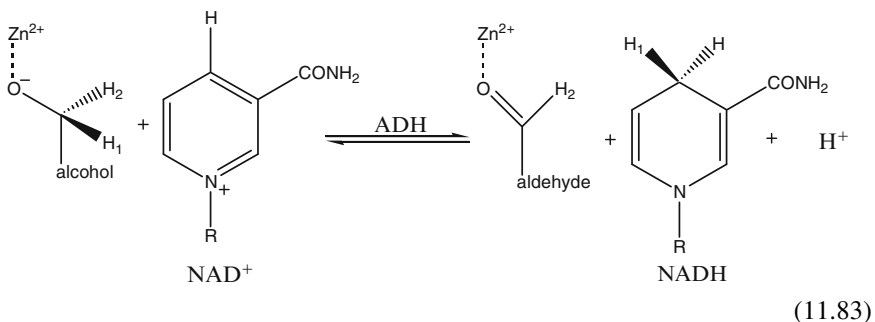


Table 11.7 Primary and secondary KIEs and exponents for the oxidation catalyzed by LADH at 298 K

		Calculated ^a	Experiment ^b
Primary	k_H/k_D		3.8 ± 0.7
	k_H/k_T	7.5	7.1
	k_D/k_T	1.7	1.9 ± 0.01
Secondary	k_H/k_T	1.36	1.33
	k_D/k_T	1.08	1.07
Exponent	α_{prim}	3.6	3.1
	α_{sec}	4.2	4.1

^aCalculated using canonical variational transition state theory VTST (Garrett, B. C. and Truhlar, D. G., *J. Chem. Phys.*, **70**, 1593 (1979); *J. Phys. Chem.*, **83**, 1052 (1979)) with microcanonically optimised multidimensional tunnelling (μ OMT) approximation. (Fernandez-Ramos, A., Ellingson, B. A., Garrett, B. C. and Truhlar, D. G. in *Reviews in Computational Chemistry*, Lipkowitz, K. B. and Cundari, T. R. Eds. Wiley-VCH, Hoboken, NJ, 2007, pp. 125–232.

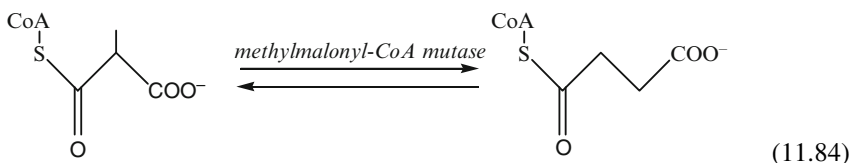
^bCleland, W. W. in Cook, P.F., Ed., *Enzyme Mechanism from Isotope Effects* CRC Press, Boca Raton, FL, 1991.

LADH is a metalloenzyme containing two Zn atoms. One Zn atom plays a structural role, while the other is catalytically important because it interacts with the oxygen atom of both the reactant (alcohol) and the product (aldehyde). The rate of ethanol dehydrogenation using wild-type LADH is limited by the rate of release of product. In contrast the chemical step becomes rate-determining when benzyl alcohol or *para*-substituted benzyl alcohols are used as the substrate, or when hydrophobic residues surrounding the active-site binding pocket are mutated. Primary KIEs observed for the hydride transfer step in various alcohol dehydrogenase transformations of benzyl alcohol and *para*-substituted benzyl alcohols lie in the range $k_H/k_D = 3.2 \pm 0.5$, and $k_H/k_T = 7.4 \pm 0.4$. For secondary KIEs the rate ratios are 1.25 ± 0.05 and 1.35 ± 0.05 , respectively. Rucker and Klinman inferred significant tunneling contributions to the process primarily from two observations. Firstly, the exponent, χ defined as $\chi = \ln(k_H/k_T) / \ln(k_D/k_T)$ from the Swain–Schaad relationship was found to lie at or well above values around 3.3 which W. H. Saunders has suggested is the upper limit in the absence of tunneling. Secondly, the ratio of Arrhenius pre-exponential factors A_H/A_T for the primary KIE was observed to have a value as low as 0.5, whereas a value smaller than 0.6 is considered the lower classical limit. Both observations suggest an appreciable part of the reaction proceeds via tunneling. Calculations summarized in Table 11.7 support that conclusion.

11.7.2 Hydrogen Atom Transfer in Methylmalonyl-CoA Mutase

Historically, the intervention of tunneling has usually been invoked when the observed KIE exceeded limits set by semi-classical theory. A recent example is the hydrogen atom transfer step in methylmalonyl-CoA mutase (MCM) catalyzed

isomerization of methylmalonyl-CoA to succinyl-CoA:



This enzyme belongs to the coenzyme B₁₂-dependent family of enzymes. In the initial, pre-steady-state phase of the reaction two steps occur. The first is homolysis of the Co-C bond present in the AdoCbl, resulting in the reduction of Co(III) to Co(II) and the formation of two radicals, one located on the cobalt atom and the other in the deoxyadenosyl group (Ado). In the following step, the Ado radical abstracts a hydrogen atom from the substrate to generate the substrate radical. These two steps are illustrated in Scheme 11.85. The substrate radical formed in step 2 undergoes rearrangement to product radical. The reabstraction of the hydrogen atom from AdoH group gives the products, and the recombination of the Ado and Cbl radicals completes the catalytic cycle.

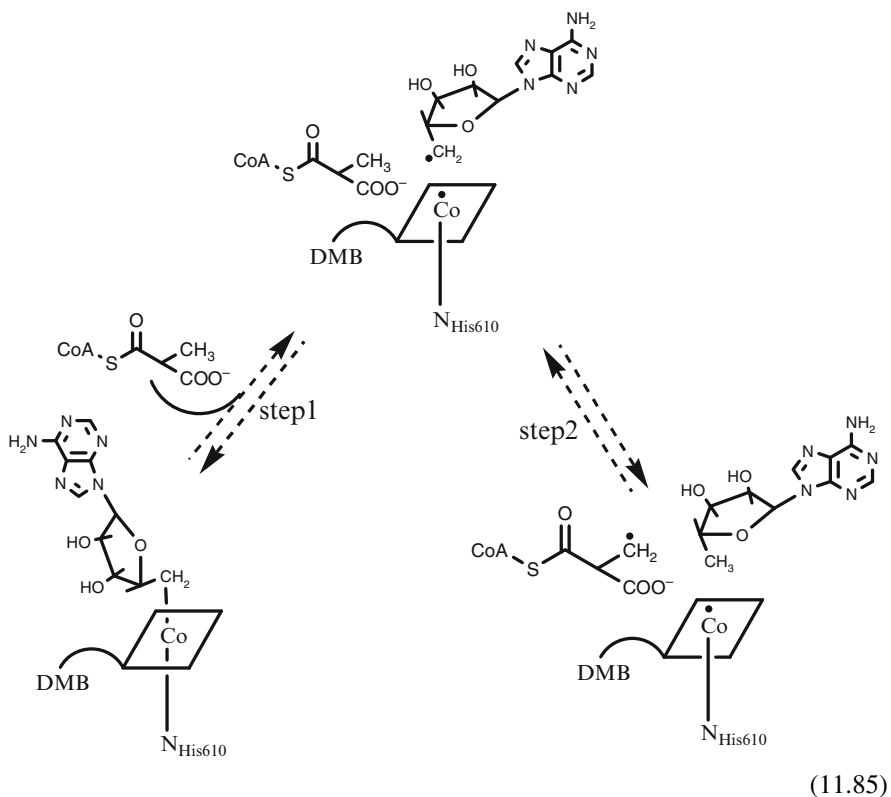


Table 11.8 Primary hydrogen kinetic isotope effects for the pre-steady-step phase of the MCM catalysis (Chowdhury, S. and Banerjee, B. *J. Am. Chem. Soc.*, **122**, 5417 (2000))

T (K)	KIEs
293	35.6
291	37.2
288	39.9
285	42.7
283	43.1
278	49.9

The observed hydrogen kinetic isotope effects on the pre-steady-state phase (Table 11.8) are far above the limit expected in the absence of tunneling (i.e. the semi-classical limit). The two steps are kinetically coupled but theoretical calculations show that homolysis is kinetically silent and the transition state of the hydrogen transfer step is rate controlling so far as the pre-steady-state events are concerned. Furthermore, Arrhenius analysis also shows large deviations from semi-classical behavior: $A_H/A_D = 0.078 \pm 0.005$ and $E_a(D) - E_a(H) = 3.41 \pm 0.07$ kcal/mol. Together, these observations suggest that tunneling is the likely catalytic strategy for the H atom transfer. Again, theoretical calculations support this conclusion.

11.8 Modeling Isotope Effects on Enzyme-Catalyzed Reactions

In the absence of definitive information about the structure of the active site theoretical modeling of enzyme catalyzed reactions is difficult but not impossible. These difficulties are caused by the extremely large size of the enzyme-substrate-solvent system which typically comprises thousands or tens of thousands of atoms so that direct theoretical treatment at the microscopic quantum mechanical level is not yet practical. The computational demand is simply too enormous. As a compromise, a scheme generally referred to as QM/MM (quantum mechanics/molecular mechanics) has been devised. In QM/MM calculations, the bulk of the enzyme-solvent system (i.e. most of the atoms) is treated at a low cost, usually at the molecular mechanics (MM) level, while the more nearly correct and much more expensive quantum level (QM) computation is applied only to the reaction center (active site).

In the molecular mechanics (MM) part of the calculation classical mechanics is employed. The atoms are treated as point charges with an associated mass. Their interactions are typically described by spring-like vibrational motions (representing chemical bonds, and including the associated stretching, bending and internal rotational modes) plus non-bonded interactions using the Lennard–Jones potential. (Electrostatic non-bonded interactions are treated with Coulomb’s law.) The force constants and other parameters required for the calculations are introduced empirically. The most widely used MM packages for modeling enzymes are CHARMM (Chemistry at HARvard Macromolecular Mechanics), AMBER (Associated Model Building with Energy Refinement), and OPLS (Optimized Potentials for Liquid Simulation). Starting from a plausible initially guessed structure, usually based on

the crystal structure deposited in the Protein Data Base (PDB), and a set of particle momenta the program either varies coordinates in searching for minima in the potential energy surface, or allows the system to evolve to the equilibrium structure by following a molecular dynamics trajectory. Time or ensemble averaging follows. The objective of this part of the calculation is to generate a structure which accurately describes the surroundings or "bath" for the active site and thereby defines the boundary conditions for the QM part of the problem.

The MM approach contrasts with the quantum mechanical (QM) part of the modeling which is restricted to the immediate area of the active site and considers either all electrons (or sometimes just outer shell electrons) explicitly in arriving at a first principle evaluation by solving the Schrödinger equation to deduce the local potential energy surface for the active site.

Although a plethora of protocols for QM/MM calculations are now available, only a few have been applied to studies of isotope effects on enzyme-catalyzed reactions. One major limiting factor is the need to diagonalize the Hessian matrix (equivalently the **GF** matrix, see Section 3.4; note the Hessian matrix is a $3N$ dimensional second derivative matrix in mass weighted Cartesian coordinates) in order to obtain a complete set of vibrational frequencies for each isotopic species. When solving the full ($3N \times 3N$) Hessian matrix is not practical due to the very large number of atoms in the enzyme system, approximate techniques and computational shortcuts can be used. The most promising seems to be partial Hessian vibrational analysis. In this approach selected atoms only, beginning with those treated in the QM part, are used for the numerical determination of a Hessian sub-matrix. This method is applied iteratively to an ever increasing set of atoms included in the Hessian determination. This procedure allows one to test for convergence of the vibrational frequencies in the region of interest. An alternative approach is to evaluate the Hessian matrix for the QM part only.

11.8.1 Examples of VTST QM/MM Calculations for Enzyme Reactions

11.8.1.1 Quantum Mechanical Dynamical Effects for an Enzyme Catalyzed Proton Transfer Reaction

The Truhlar group has reported an interesting theoretical study of H/D kinetic isotope effects for conversion of 2 phospho-D-glycerate to phosphoenolpyruvate catalyzed by the yeast enolase enzyme. The proton transfer step (first reaction step in Fig. 11.10) is the rate limiting step and was chosen for theoretical study. The KIE for proton/deuteron transfer is $k_H/k_D = 3.3$ at 300 K.

The isotope independent potential energy surface was evaluated using a mixed quantum mechanics/molecular mechanics (QM/MM) method. The system (N atoms) was partitioned into N_{QM} quantum mechanical atoms and N_{MM} classical mechanical atoms. N_{QM} consisted of the 15 atom substrate (phospho-D-glycerate)

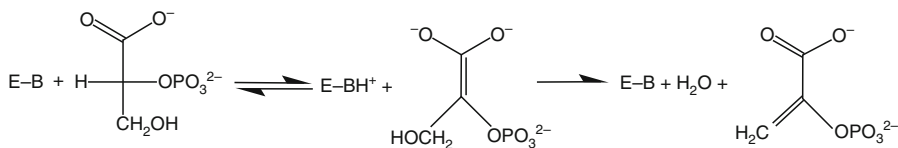


Fig. 11.10 Conversion of phospho-D-glycerate to phosphoenolpyruvate by enzyme (E) catalysis (Alhambra, C., Gao, J., Corchado, J. C., Vill, J. and Truhlar, D. G., *J. Am. Chem. Soc.* **121**, 2253 (1999))

and the $-\text{H}_2\text{N} - \text{CH}_2 - \text{CH}_2 - \text{C}$ portion of the Lys345 (lysine) side chain in the enzyme active site. Thus $N_{\text{QM}} = 25$. The remainder of the system consists of 6934 additional protein atoms plus 1286 crystallographic (enzyme complexed) and 643 bulk water molecules, for a total of 8863 classical atoms. The QM subsystem was described by the semi-empirical AM1 model which was shown equivalent for the present type of reaction to Hartree–Fock (HF) molecular orbital calculations using 6–31+G basis sets.

The HF method (in the older literature known as the self consistent field (SCF) method) is an approximate method for the determination of ground-state wavefunctions and energies of quantum many-body systems. The solutions behave as if each particle (electron, nucleus, etc.) is subjected to the mean field created by all other particles. For molecules, Hartree–Fock is the central starting point for most ab initio quantum chemistry methods. AM1 (Austin Model 1 developed at the University of Texas) is a semi-empirical elaboration based on the neglect of differential overlap integrals, thus reducing the number of integrals to be evaluated. Related methods are PM3 (Parametrized Model #3) and the older MINDO (Modified Intermediate Neglect of Differential Overlap). For large scale calculations inner shell electrons are commonly left out, further reducing the number of integrals to be evaluated and enormously simplifying the calculation. The far fewer integrals which remain are empirically evaluated. Keep in mind, however, that even with these simplifications enormous numbers of integrals remain and the computations described in this chapter require substantial investments in computer power and machine time.

The calculation representing the enzyme reaction given in Fig. 11.10 proceeded in two stages. The system was initialized using the known enzyme crystal structure, followed by a molecular mechanics (MM) simulation of the enzyme/solvent “bath” structure surrounding the active site. The purpose of this step is simply to generate a typical configuration for starting the quantum mechanical (QM) calculation of the active site. The criterion used was that the bath structure chosen should lead to a barrier height and energy of reaction that provides a qualitatively reasonable representation of the experimental situation. For the chosen configuration the secondary atoms were frozen in place and the quantum mechanical calculation optimized the geometry of the primary zone (QM) atoms for three stationary points (reactants, saddle point, products). The results showed a barrier height of 17 kcal/mol and an energy of reaction equal to 2.6 kcal/mol endoergic. The calculated values for the

Table 11.9 Rate constants and KIEs for the conversion of 2-PGA to PEP by enolase at 300 K (see Figs. 11.10 and 11.11)

Theory	$k_H(\text{s}^{-1})$	k_H/k_D
TST ^a	169	4.7
CVTST ^b	129	3.7
CVTST/SCT ^c	214	3.5
“Ordinary” ^d	TST 3.9	1.4
CVTST	3.8	1.3
Experiment	78	3.3

^aTST = transition state theory. The transition state is at the saddle point.

^bCVTST = canonical ensemble variational transition state theory. The location of the transition state is chosen to maximize the free energy of activation in the absence of tunneling.

^cCVTST/SCT denotes CVTST plus a small curvature tunnel transmission (SCT) coefficient.

^dAll vibrations treated by classical mechanics, tunneling and nonclassical reflection are neglected. Alhambra, C. et al. (see Figs. 11.10 and 11.11) employ the term “classical”.

free energies of activation and reaction on this surface are in good agreement with experiment. They correspond to conventional transition state theory.

The Born–Oppenheimer isotope independent potential energy surface calculated with the “bath” atoms frozen in place as outlined in the paragraph above was employed by the authors to compare TST and VTST rate constants and kinetic isotope effects. The results are shown in Table 11.9.

The second column of the table shows that quantum effects (tunneling, etc.) are large, increasing the rate constant by more than an order of magnitude. The authors claim that the fact that the CVTST/SCT rate differs from experiment more than CVTST is probably an indication that the effective barrier used in the calculation is a little low. The last column shows an improvement in the KIE calculated using CVTST. The agreement with experiment is excellent when multidimensional tunneling effects are properly included (CVTST/SCT). The calculated rate constants show that agreement is only possible by going beyond conventional transition state theory. The reason is shown in Fig. 11.11 which compares CVTST geometries for proton and deuteron transfer. Thus, for H^+ transfer the CVT transition state has $r_1 = 1.75 \text{ \AA}$ and $r_2 = 1.12 \text{ \AA}$, but for D^+ transfer r_1 is 1.57 \AA and $r_2 = 1.26 \text{ \AA}$. These deuteron distances differ by less than 0.01 \AA from the values at the saddle point. As a consequence $k_{\text{CVTST}}/k_{\text{TST}} = 0.76$ for H^+ transfer and 0.99 for D^+ transfer. One could say that TST is working reasonably well for D^+ transfer but not at all well for the lighter H^+ species. The CVTST results in Table 11.9 are based on 75 degrees of freedom for the QM atoms moving in the electrostatic and van der Waals fields (MM) of the rest of the enzyme. The treatment is truly multidimensional.

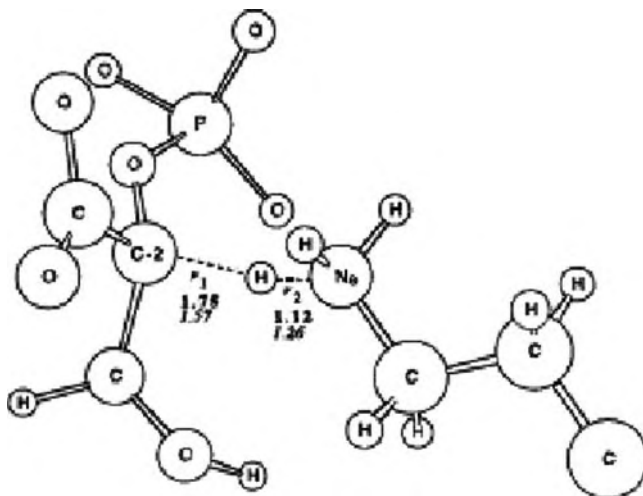


Fig. 11.11 The optimal structure for the quantum mechanical part of the CVT structure for proton transfer. The values of r_1 and r_2 for the proton (*bold*) and deuteron (*italics*) are specified (Alhambra, C., Gao, J., Corchado, J. C., Vill, J. and Truhlar, D. G., *J. Am. Chem. Soc.* **121**, 2253 (1999))

11.8.1.2 Hydrogen Radical Transfer Catalyzed by a Coenzyme B_{12} -Dependent Mutase

These reactions have very large kinetic isotope effects, indicating that they proceed by a highly quantal tunneling mechanism. The kinetic isotope is explained as in Section 11.8.1.1 by using a combined quantum mechanical/molecular mechanical potential. Multidimensional tunneling increases the magnitude of the calculated hydrogen kinetic isotope effect by a factor of 3.6 from 14 to 51. These calculations confirm that tunneling contributions can be large enough to explain even a kinetic isotope effect >50 , not because the barrier is unusually thin but because multidimensional corner-cutting tunneling decreases the distance over which the system tunnels without a comparable increase in either the effective potential barrier or the effective mass for tunneling. Whether or not this is a phenomenon specific to enzyme systems is vigorously debated. An alternative point of view, for example, is put forward by Warshel and collaborators who argue that tunneling in enzymes and in solution is of the same nature. Interested readers should consult appropriate literature as a detailed discussion of the controversy exceeds the objectives of this book.

In a recent paper Truhlar and coworkers applied QM/MM to the title reaction above using methods outlined in Section 11.8.1.1. The isotope effects are in excess of an order of magnitude larger for this H/D radical transfer than they were for the proton/deuteron transfer in Section 11.8.1.1. The calculations employed a QM/MM potential-energy surface with a 45-atom QM part and a 14,833 atom MM part. Rate constants measured under ordinary conditions correspond to an average over fluctuating conformational states of the protein. The present calculations include this average by ensemble-averaging variational transition-state theory (EA-VTST).

Including tunneling increases the rate constant for the unsubstituted (perprotio) case by a multiplicative transmission coefficient κ_H and for the perdeuterated methyl case by κ_D . The KIE increases by κ_H/κ_D . Zero-curvature tunneling (ZCT) is a model in which tunneling occurs along the minimum energy path (MEP). Each MEP actually curves its way through the 135-dimensional primary zone. Tunneling paths on the concave sides of the MEPs increase the tunneling probability because corner-cutting shortens the path (Fig. 6.3c) from reactants to products. Small-curvature tunneling (SCT) allows corner-cutting but only out to approximately the concave turning points of the vibrations transverse to the MEPs (Section 6.4). The large-curvature tunneling (LCT) approximation allows tunneling on paths both near and far from the MEP, even extreme corner-cutting. Finally, microcanonically optimized multidimensional tunneling (μ OMT) variationally selects from among both SCT and LCT paths and further increases the calculated transmission coefficients. The EA-VTST calculations, with quantized vibrations but classical motion along the reaction coordinate, give a KIE at 278 K of 14.3, much smaller than the experimental value of 49.9. These values are compared with the calculations which include tunneling in Table 11.10. That table shows that ZCT gives only a modest increase in the KIE, to 22.0, but that even modest corner-cutting, as in the SCT approximation, approximately doubles the KIE as compared with tunneling along the MEPs. Including extreme corner-cutting, as in either the LCT or μ OMT approximations, yields a KIE that agrees with observation within experimental error.

Table 11.10 shows that ZCT underestimates the effect of tunneling. Thus, the model of tunneling along the MEP is inadequate, and the participation of the other degrees of freedom (other than the progress of the hydrogen atom along the reaction coordinate) is essential to explaining the large KIE. Next we consider the fact that we have different paths for H and D transfer, partly because of corner-cutting. Note that the system will cut the corner only to the extent that this increases the probability of tunneling in isoinertial coordinates, this involves the competition between barrier-raising and path-shortening (refer to Fig. 6.3). Proper multidimensional tunneling methods include these competitions as part of the calculation. In both enzymes and small-molecule reactions corner-cutting tends to increase the KIE. A key factor that

Table 11.10 Transmission coefficients and their effect on KIE for H/D radical transfer at 278 K catalyzed by a coenzyme B₁₂-dependent mutase (Dybala-Defratyka, A., Paneth, P., Banerjee, R. and Truhlar, D. G., *Proc. Natl. Acad. Sci.* **104**, 10774 (2007); Chowdhury, S. and Banerjee, R., *J. Am. Chem. Soc.* **122**, 5417 (2000))

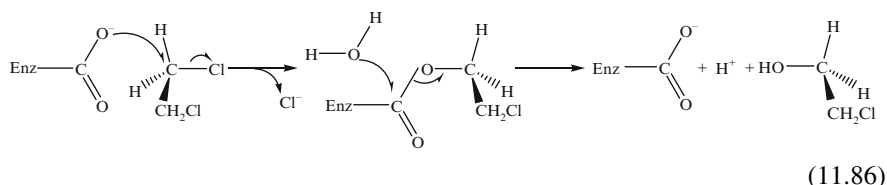
Method	κ_H	κ_D	κ_H/κ_D	KIE
No tunneling	1	1	1.0	14.3
ZCT	13	8.3	1.6	22.0
SCT	79	25	3.2	44.3
LCT	70	19	3.7	52.7
μ -OMT	93	26	3.6	50.5
Experiment				49.9

may appear counterintuitive from some points of view is that although H sees a higher energy along its tunneling path, the tunneling probability is greater because in isoinertial coordinates the path is almost always shorter for H than for D when the reaction is the transfer of a hydrogen, proton, or hydride ion.

11.8.2 QM/MM for Haloalkane Dehalogenase: TST Calculations

For heavy atom isotope effects tunneling is relatively unimportant and the TST model suffices. As an example the dehalogenation of 1,2-dichloroethane (DCE) to 2-chloroethanol catalyzed by haloalkane dehalogenase Dh1A is discussed below. This example has been chosen because the chlorine kinetic isotope effect for this reaction has been computed using three different schemes, and this system is among the most thoroughly studied examples of heavy atom isotope effects in enzymatic reactions.

The haloalkane dehalogenase Dh1A mechanism takes place in two consecutive S_N2 steps. In the first, the carboxylate moiety of the aspartate Asp124, acting as a nucleophile on the carbon atom of DCE, displaces chloride anion which leads to formation of the enzyme–substrate intermediate (Equation 11.86). That intermediate is hydrolyzed by water in the subsequent step. The experimentally determined chlorine kinetic isotope effect for 1-chlorobutane, the slow substrate, is $k(^{35}\text{Cl})/k(^{37}\text{Cl}) = 1.0066 \pm 0.0004$ and should correspond to the intrinsic isotope effect for the dehalogenation step. While the reported experimental value for DCE hydrolysis is smaller, it becomes practically the same when corrected for the intramolecular chlorine kinetic isotope effect (a consequence of the two identical chlorine labels in DCE).



The isotope effect was first modeled using the ONIOM multi layer approach developed by Morokuma and coworkers (reading list). In this method a part of the whole system is selected for detailed quantum mechanical modeling and designated “model” while the whole system is called “real”. The total energy of (E_{ONIOM}) is given by Equation 11.87

$$E_{\text{ONIOM}} = E_{\text{MM}}^{\text{real}} + (E_{\text{QM}}^{\text{model}} - E_{\text{MM}}^{\text{model}}) \quad (11.87)$$

A few points should be clarified. First, the ONIOM approach can be viewed as perturbational, i.e., the whole system is first treated at lower level (molecular mechanics, MM) of theory but since we expect this level to be inadequate for the

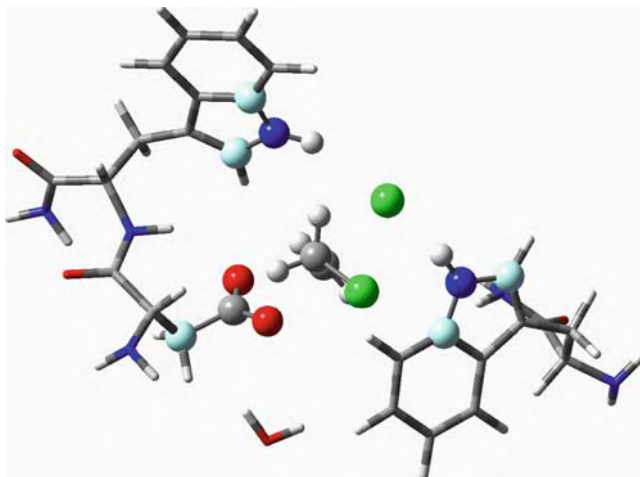


Fig. 11.12 ONIOM model used in calculations of the chlorine KIE on DhIA catalyzed reaction (Lewandowicz, A., Matsson, O., Paneth, P., et al. *J. Am. Chem. Soc.* **123**, 4550 (2001))

description of the reacting center, the energy calculated at the MM lower level of theory is replaced with the energy obtained from the higher order quantum mechanical (QM) level. Second, since in the studies reported here the lower level part of the calculation used a semiempirical Hamiltonian PM3 and the higher level a modified density functional theory (DFT) optimized for frequency calculation, this approach more formally should be classified as QM/QM rather than QM/MM. Thirdly, since the energy of the model part at the higher level is calculated in the absence of the remaining part of the system, the interaction between the two subsets is included only in the lower level calculations – this scheme is called molecular embedding. Following widely accepted nomenclature, the different levels of theory employed in ONIOM calculations are separated with a colon. Thus the results under discussion were obtained at the B1LYP/6–31G(d):PM3 level. In Fig. 11.12, that part of the enzyme/substrate system included in the calculation is presented. The quantum mechanically modeled part is rendered as balls. Atoms substituted by hydrogens in evaluation of the $E_{\text{QM}}^{\text{model}}$ energy component are shown as the darker large balls. The model includes the nucleophile Asp124, DCE and water molecules, and two tryptophans Trp125 and Trp125, which form hydrogen bonds to the departing chloride anion. The influence of the size of the part treated at the highest theoretical level, the choice of basis set, etc. on the calculated chlorine kinetic isotope effect have been studied. The average value from these calculations $k(^{35}\text{Cl})/k(^{37}\text{Cl}) = 1.0065$ is in excellent agreement with the experimentally determined isotope effect.

Another approach to modeling the chlorine kinetic isotope effect of this reaction has been carried out using a true QM/MM scheme.

$$E_{\text{QM/MM}} = E_{\text{QM}} + E_{\text{MM}} + E_{\text{QM-MM}} \quad (11.88)$$

where E_{QM} is the energy of the part calculated at the QM level, E_{MM} is the energy of the part calculated at the MM level, and $E_{QM/MM}$ is the energy of interaction between parts. Since the energy term E_{QM} usually includes polarization caused by the MM part the method is referred to as electrical embedding. The energy of the QM part (see Fig. 11.12) was described using a semiempirical PM3-SRP Hamiltonian (SRP = Specific Reaction Parametrization), i.e., a PM3 Hamiltonian modified to reproduce MP2/6-31+G(d) in the gas phase. The CHARMM force field was used for the MM part. The QM/MM energy can be thus formally written as PM3/CHARMM. The chlorine isotope effect calculated using variational transition state theory was 1.0031. This small value (the experimental value is 1.0065) is typical of the systematic underestimation of chlorine isotope effects using PM3.

The third approach to calculations of the intrinsic chlorine kinetic isotope effect on the Dh1A catalyzed reaction is a combination of the above two methods. In this so called dual level scheme, the QM part is described at two different levels, HL (high level, ab initio or DFT) and LL (low level, usually semiempirical). HL level is used for calculations of the gas phase energy of the QM system while the coupling with the MM part is calculated at the LL level. Due to the close resemblance of this part of the approach to ONIOM it is marked as B3LYP/6-31 + G(d):PM3/OPLS-AA indicating that the unperturbed energy component was calculated at the hybrid DFT level while its PM3 counterpart was polarized by the MM force field. The chlorine kinetic isotope effect was calculated on the QM part that contained Glu56 in addition to the moieties illustrated in Fig. 11.13. The isotope effect was found equal to 1.0071, in very good agreement with the experiment.

The three protocols discussed in this section show that QM/MM techniques available presently are capable of reproducing, and thus hopefully predicting, intrinsic isotope effects, provided that a sufficient part of the enzyme is included

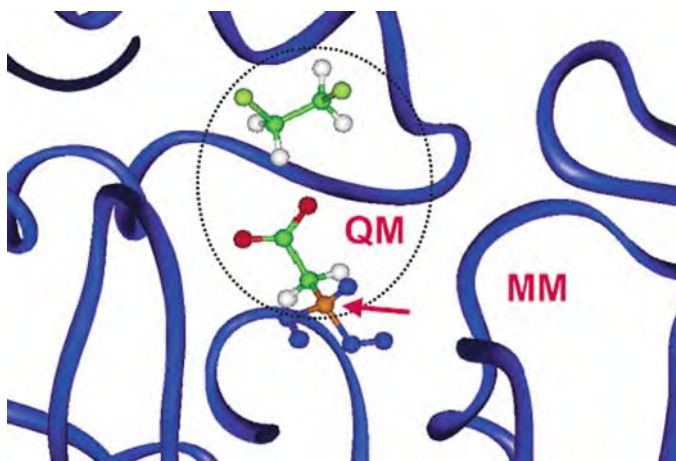


Fig. 11.13 QM/MM model used in calculations of the chlorine KIE on Dh1A catalyzed reaction (Devi-Kesavan, L.S. and Gao, J., *J. Am. Chem. Soc.* **125**, 4550 (2003))

in calculations and that adequate levels of theory are employed. Ever increasing computer power and improvements in computational algorithms allow us to hope that QM/MM calculations will soon become a reliable kinetic tool. Even so calculations on such large systems as enzyme reactions, and especially calculations of subtle quantities like isotope effects, should be performed with the greatest care.

11.8.3 Comment

All of the isotope effect studies on enzymatic systems carry simplifying assumptions, some of which are explicitly mentioned, and some of which are silent and implied. For example, the use of simplified kinetic schemes implies the absence of other isotope sensitive steps than those indicated in the equations used. Careful analysis is always necessary to make sure the assumed kinetic scheme adequately describes the case under consideration. Another assumption often made but not always justified, is the widely invoked hypothesis that changing the system under study by using slow substrates or mutated enzymes does not significantly change the value of the corresponding intrinsic isotope effects. As has been shown in several cases this assumption is not generally true. Thus we conclude this chapter with a general call to use the maximum care possible when studying isotope effects on enzyme catalyzed reactions.

Reading List

- Bell, R. P. *The Proton in Chemistry*, Cornell University Press, 2nd Ed., Ithaca, 1973.
- Cook, Paul F., Ed., *Enzyme Mechanism from Isotope Effects*, CRC Press, Boca Raton, FL, 1991.
- Cook, Paul F. and Cleland, William Wallace, *Enzyme Kinetics and Mechanism*, Garland Science/Taylor & Francis, London, 2007.
- Froese, R. D. J., Morokuma, K. in "Encyclopedia of Computational Chemistry," volume 2, Schleyer, P. von Rague, Ed., Wiley, Chichester, Sussex, 1998, pp. 1244–1257.
- Kresge, A. J. *Pure Appl. Chem.* **8**, 243 (1964).
- Melander, L. and Saunders, W. H., *Reaction Rates of Isotopic Molecules*, Wiley, New York, 1980 (Chapter 10).
- Northrop, D. B. *Determining the Absolute Magnitude of Hydrogen Isotope Effects* in W.W. Cleland, W. W., O'Leary, M., Northrop, D. B. (Eds.) *Isotope Effects on Enzyme-Catalyzed Reactions*, University Park Press, Baltimore, MD, 1976, pp. 122–152.
- O'Leary, M, Paneth, P., *Bioact. Mol.* **3**, 303 (1987).
- Quinn, D. M. *Theory and Practice of Solvent Isotope Effects*, in Kohen, A. and Limbach, H. (Eds.) *Isotope Effects in Chemistry and Biology*, CRC Press, Boca Raton, FL, 2006 (Chapter 41).
- Selected chapters (esp 18 and 23–42) on isotope effects in enzyme research from Kohen, A. and Limbach, H. (Eds.) *Isotope Effects in Chemistry and Biology*, CRC Press, Boca Raton, FL, 2006.

Chapter 12

Isotope Effects on Dipole Moments, Polarizability, NMR Shielding, and Molar Volume

Abstract Although the electronic structure and the electrical properties of molecules in first approximation are independent of isotope substitution, small differences do exist. These are usually due to the isotopic differences which occur on vibrational averaging. Vibrational amplitude effects are important when considering isotope effects on dipole moments, polarizability, NMR chemical shifts, molar volumes, and fine structure in electron spin resonance, all properties which must be averaged over vibrational motion.

12.1 Introduction

Although the electronic structure and the electrical properties of molecules in first approximation are independent of isotope substitution, small differences do exist. These are usually due to the isotopic differences which occur on vibrational averaging. Refer to Fig. 12.1 and its caption for more detail. Vibrational amplitude effects are important when considering isotope effects on dipole moments, polarizability, NMR chemical shifts, molar volumes, and fine structure in electron spin resonance, all properties which must be averaged over vibrational motion. Any such property, P , can be expressed in terms of a Taylor series expansion over the displacements of the coordinates from their equilibrium positions,

$$\langle P \rangle = P_0 + \sum (\partial P / \partial r_i) (r - r_0)_i + (1/2) \sum \sum (\partial^2 P / \partial r_i \partial r_j) (r - r_0)_i (r - r_0)_j + \dots \dots \dots \quad (12.1)$$

In this way one obtains the mean value of P averaged over vibrational motion in terms of mean displacements, mean square displacements, and so on. This approach has been long used to discuss isotope effects on electrical properties of molecules.

12.1.1 Dipole Moments, Polarizabilities and Hyperpolarizabilities

Neutral molecules can be represented as systems of electric charges distributed in space. Positive charge is concentrated in the atomic nuclei, and negative

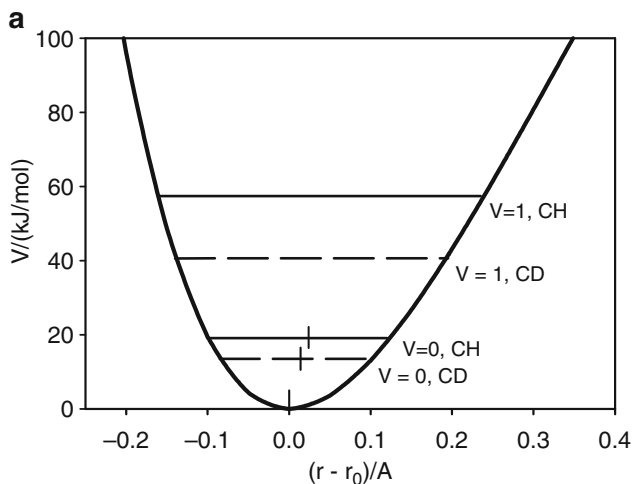


Fig. 12.1 (a) The first two vibrational energy levels for the CH and CD stretching modes compared. The curve shows a Morse potential, $V_{\text{MORSE}} = D_e[1 - \exp(a(r - r_0))]^2$ with $D_e = 397 \text{ kJ/mol}$, $a = 2 \text{ \AA}^{-1}$, and $r_0 = 1.086 \text{ \AA}$. The vertical bars represent ground state vibrationally averaged bond distances, [$\langle r_{\text{CH}} \rangle > \langle r_{\text{CD}} \rangle > r_0$]_{ANH}. Because CH lies higher in the well than CD, its average bond extension is somewhat greater than CD. Since the potential is skewed, bond extension is greater than bond compression. Remember for the harmonic oscillator (HO) the potential curve is parabolic and symmetrical [$\langle r_{\text{CH}} \rangle = \langle r_{\text{CD}} \rangle = r_0$]_{HO}. Very often vibrational amplitude effects are discussed in terms of root mean square amplitudes, $\langle r^2 \rangle^{1/2}$, or mean square amplitudes, $\langle r^2 \rangle = \langle (r - r_0)^2 \rangle$. To good approximation $\langle r^2 \rangle = [h/(8\pi^2 c \mu_r \nu)] [\coth(hc\nu/(2kT))]$ (the relation is exact for the HO). Here c is the speed of light, k the Boltzman constant, ν the oscillator frequency (cm^{-1}) and μ_r its reduced mass

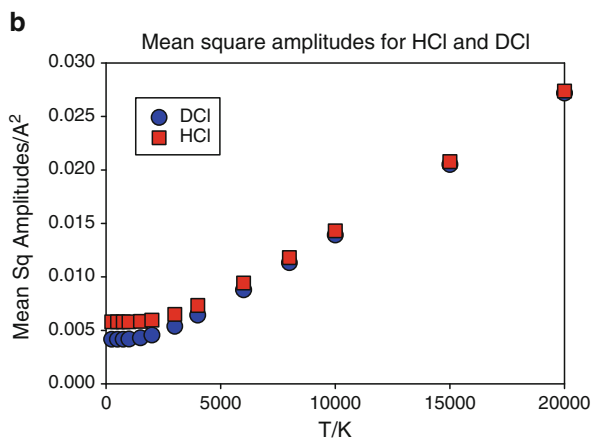


Fig. 12.1 (continued) (b) Mean square amplitudes of hypothetical nondissociating HCl (squares) and DCl (circles) as a function of temperature

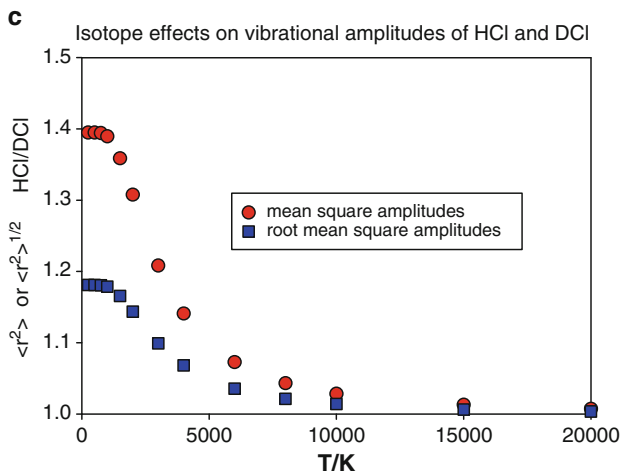


Fig. 12.1 (continued) (c) Isotope effects on mean square amplitudes (*upper curve*) and root mean square amplitudes (*lower curve*) as a function of temperature for hypothetical nondissociating molecules. At low temperatures the molecules are in the ground state and the amplitude is nearly independent of temperature. At higher temperature the vibrational amplitudes increase due to excitation into upper levels (Fig. 12.1) but the ratios drop smoothly to the classical value of unity at very high temperature (Fig. 12.1)

charge is distributed over the entire molecule such that the fractional charge in any incremental volume, $d\tau$, is given in terms of the electronic wave function, $\Psi\Psi^*d\tau / \int \Psi\Psi^*d\tau$. The integral extends over all space. Ordinarily the centers of positive and negative charge do not coincide, and the vectorial distance between them \vec{r} multiplied by the total positive charge, q , defines the electric dipole moment $\mu = \vec{\mu} = q\vec{r}$. The dipole moment is a vector quantity; its direction is usually given from positive to negative. A dipole moment corresponding to charge of one electron (4.8×10^{-10} esu) operating over a distance of 1 \AA (10^{-8} cm) has a dipole moment of 4.8×10^{-18} esu cm = 4.8 Debye (D). In the SI system $1 \text{ D} = 3.334 \times 10^{-30}$ Coulomb meter. Dipole moments and isotope effects on dipole moments for some diatomic and simple polyatomic molecules are shown in Table 12.1.

The discussion to this point has not considered the effect of an externally impressed electric field. When a molecule is placed in an electric field the energetics of the interaction are expressed,

$$\xi(E) = \xi_0 + (\partial\xi/\partial E)_0 E + (1/2)(\partial^2\xi/\partial E^2)_0 E^2 + (1/3!)(\partial^3\xi/\partial E^3)_0 E^3 + \dots \quad (12.2)$$

In Equation 12.2 ξ symbolizes the total energy and E the electric field strength. The subscripts indicate the derivatives are evaluated at $E = 0$. The dipole moment, μ , is given as

$$\mu = - (d/dE)\xi(E) = - (\partial\xi/\partial E)_0 - (\partial^2\xi/\partial E^2)_0 E - (1/2)(\partial^3\xi/\partial E^3)_0 E^2 + \dots \quad (12.3)$$

Table 12.1 Dipole moments, polarizabilities, and isotope effects for some diatomic and simple polyatomic molecules (ground vibrational state values)

	μ_0/D	$\Delta\mu_0/D$	$(\alpha/\text{\AA}^3)^a$	$\alpha(\text{parallel})$ $-\alpha(\text{perpen})$	$\Delta\alpha/\text{\AA}^3$
H ₂	0		0.819	0.314	
HD ^b	0.8×10^{-3}	-0.8×10^{-3}			
D ₂ ^{b,c}	0		0.809	0.299	0.010
¹² C ¹⁶ O ^d	-0.122 ₇		1.95		
¹² C ¹⁸ O ^d	-0.121 ₈	-0.9×10^{-3}			
HCl ^e	1.1085		2.60	0.311	
DCl ^{c,d,e}	1.1033	5.2×10^{-3}			0.006
C ₆ H ₆	0		10.4	-5.6	
C ₆ D ₆ ^c					0.055
C ₆ H ₁₂	0		10.9		
C ₆ D ₁₂ ^f					0.121
NH ₃	1.468		2.22	0.288	
ND ₃ ^{c,g}		-13.5×10^{-3}			0.026
CH ₄	0		2.59		
CH ₃ D ^h	-6.6×10^{-3}	-6.6×10^{-3}			
CHD ₃ ^h	6.8×10^{-3}	6.8×10^{-3}			
CD ₄ ^c	0				0.042
H ₂ O ⁱ	1.848		1.45		
HDO ⁱ	1.845	3×10^{-3}			
D ₂ O ^{c,i}	1.851	-3×10^{-3}			0.011
CH ₃ CCH ^j	0.7806				
CH ₃ CCD ^j	0.7674	13.2×10^{-3}			
CD ₃ CCH ^j	0.7841	-3.5×10^{-3}			
CD ₃ CCD ^j	0.7722	3.4×10^{-3}			
CH ₃ F ^j	1.646				
CD ₃ F ^j	1.647	-1.0×10^{-3}			

^aBridge, N. J. and Buckingham, A. D., *Proc Roy Soc (London)* **A295**, 334 (1966).

^bDrakopoulos, P. G. and Tabisz, G. C. *Phys Rev.* **A36**, 5556 (1987).

^cVan Hook, W. A. and Wolfsberg, M., *Z. Naturforsch.* **49A**, 563 (1994).

^dSee Table 12.2.

^eKaiser, E. W. *J. Chem. Phys.* **53**, 1686 (1970).

^fWieczorek, S. A. Urbanczyk, A. and Van Hook, W. A., *J. Chem. Thermodynamics* **1996**, 28 (1009).

^gScher, C., Ravid, B. and Halevi, E. A., *J. Phys. Chem.* **86**, 654 (1982).

^hQuack, M. et al, *J. Chem. Phys.* **101**, 3588 (1994).

ⁱClough, S. A., Beers, Y., Klein, G. P. and Rothman, L. S., *J. Chem. Phys.* **59**, 2254 (1973).

^jMuenter, J. S. and Laurie, V. W., *J. Chem. Phys.* **45**, 855 (1966).

and is also written as a sum of the permanent (zero field) and induced dipole moments.

$$\mu = \mu_0 + \mu_{\text{INDUCED}} = \mu_0 + \alpha E + (1/2)\beta E^2 + \dots \quad (12.4)$$

In Equation 12.4 μ_0 is the permanent dipole moment, $\mu_0 = -(\partial\xi/\partial E)_0$, α is the polarizability, $\alpha = -(\partial^2\xi/\partial E^2)_0$, β the first hyperpolarizability, etc. At moderate field strengths second order and higher terms are often neglected, so $\mu_{\text{INDUCED}} \sim \alpha E$. Equations 12.2 through 12.4 are simplified. Both the electric field, and the permanent dipole moment are vectors, the polarizability is a second rank tensor, the hyperpolarizability a third rank tensor, etc. A complete description of the interaction is therefore algebraically complex. For diatomic or linear molecules the dipole moment, if it exists at all, has only one component and that is along the bond axis, the polarizability for a linear or diatomic molecule, however, has components both parallel and perpendicular to the bond axis; the rotationally averaged polarizability is $\alpha = (1/3)(\alpha_{\text{parallel}} + 2\alpha_{\text{perpendicular}})$. For polyatomic molecules of threefold or higher symmetry there are parallel and perpendicular components for both the permanent dipole moment and the polarizability. For molecules of lower symmetry the situation is more complex, there may be as many as nine nonzero components of the polarizability, and the reader is referred to specialized treatments. Polarizabilities and isotope effects for some diatomic and simple polyatomic molecules are included in Table 12.1.

12.2 Dipole Moments and Their Isotope Effects

12.2.1 Experimental Methods

Methods for determining permanent dipole moments and polarizabilities can be arbitrarily divided into two groups. The first is based on measuring bulk phase electrical properties of vapors, liquids, or solutions as functions of field strength, temperature, concentration, etc. following methods proposed by Debye and elaborated by Onsager. In the older Debye approach the isotope effects on the dielectric constant and thence the bulk polarization, ΔP , are plotted vs. reciprocal temperature and the isotope effect on the polarizability and permanent dipole moment recovered from the intercept and slope, respectively, using Equation 12.5.

$$\Delta P = \Delta[(\epsilon - 1)/(\epsilon + 2)][M/\rho] = [N/(3\epsilon_0)][\Delta\alpha + \Delta(\mu_0^2)/(3kT)] \quad (12.5)$$

In the equation ϵ is the measured dielectric constant and ϵ_0 the permittivity of the vacuum, M is the molar mass and ρ the molecular density, while $\Delta\alpha$ and $\Delta(\mu_0^2)$ are the isotope effects on the polarizability and the square of the permanent dipole moment respectively. Unfortunately, because the isotope effects under discussion are small, and high precision in measurements of bulk phase polarization is difficult to achieve, this approach has fallen into disfavor and now is only rarely used. Polarizability isotope effects, $\Delta\alpha$, are better determined by measuring the frequency dependence of the refractive index (see below), and isotope effects on permanent dipole moments with spectroscopic experiments.

The second group of techniques includes methods based on microwave spectroscopy and molecular beams. The Stark effect describes the changes in molecular energy levels due to interaction with an external electric field. It can be detected by measuring energy shifts and splittings in the pure rotational spectrum. For example in symmetric top molecules a first order Stark splitting, $\Delta\zeta$, is observed

$$\Delta\zeta = 2\mu KME/[j(j+1)(j+2)] \quad (12.6a)$$

while in linear molecules the splitting is second order (i.e. proportional to E^2)

$$\Delta\zeta = \left\{ \mu^2 / [2(h/2\pi)I] \right\} \left\{ (j(j+1) - 3M^2) / (j(j+1)(2j-1)(2j+3)) \right\} E^2 \quad (12.6b)$$

In Equation 12.6 μ is the permanent dipole moment, h is Planck's constant, I the moment of inertia, j the angular momentum quantum number, and M and K the projection of the angular momentum on the electric field vector or axis of symmetry of the molecule, respectively. Obviously if the electric field strength is known, and the j state is reliably identified (this can be done using the Stark shift itself) it is possible to determine the dipole moment precisely. The high sensitivity of the method enables one to measure differences in dipole moments between isotopes and/or between ground and excited vibrational states (and in favorable cases dipole differences between rotational states). Dipole measurements precise to ± 0.001 D, or better, for moments in the range 0.5–2 D are typical (Table 12.1).

In the molecular beam method one measures the deflection of the beam as it passes through a nonuniform electric field impressed perpendicular to the beam direction. The deflection is a function of the dipole moment but the method suffers from imprecisions introduced by the distribution of molecular velocities in the beam, and from difficulties in controlling and measuring the electric field gradient. A better approach, but one limited to the study of diatomics and linear molecules, uses the molecular beam resonance technique. In this technique the molecular beam passes through two regions of strictly opposed electric field gradients, $\partial E/\partial z$ and $-\partial E/\partial z$, separated from each other by a third region of uniform field, $\partial E/\partial z = 0$. The apparatus design is such that in the end molecules in a specific rotational state converge to a focal point (located as a function of E , $\partial E/\partial z$, and j). The particle detector is located at the focal point. A small high frequency field acting in the middle region induces transitions into states with different orientations of the dipole moment, causing changes in the trajectory. As a result the beam flickers back and forth across the detector. By adjusting the field frequency while measuring particle flux at the detector, the resonance frequency, and thence the dipole moment, is determined at high precision.

12.2.2 *The IE on μ_0 , Discussion*

Some examples of small molecule dipole moment H/D isotope effects are given in Table 12.1. These typically vary from 1 to 10 or more milli-Debyes. A qualitative

rationalization of these IE's advanced many years ago by R. P. Bell is based on the idea that the isotope effect in first approximation is due to the change in mean configuration of the molecule on isotopic substitution. For a diatomic this is given by the IE on vibrational amplitude, for a polyatomic it is a complicated linear combination of the IE on the amplitudes of all the normal modes of vibration. In the diatomic case one obtains

$$\Delta\mu = \mu_H - \mu_D = (\partial\mu/\partial r)_e(\langle r_H \rangle - \langle r_D \rangle) \quad (12.7)$$

It is well established that the average lengths of CH bonds are consistently 0.003 to 0.004 Å longer than the corresponding CD bonds in the ground vibrational state (see Fig. 12.1, its caption, and Section 12.2.3). It remains only to establish the dipole moment derivative, $(\partial\mu/\partial r)$, at the equilibrium bond length. That is available from theoretical calculation or spectroscopic measurement (*via* precise measurements of IR intensities of vibration-rotation bands). Calculations based on Equation 12.7 yield predicted dipole moment IE's in reasonable agreement with experiment.

A schematic curve showing how the dipole moment changes as internuclear distance increases is shown in Fig. 12.2. The figure nicely explains the observation that dipole moment IE's for diatomic molecules can be either normal or inverse depending whether the equilibrium bond length of the diatomic lies to the left (where $(\partial\mu/\partial r)_e > 0$ and consequently $\Delta\mu > 0$) or the right (where $(\partial\mu/\partial r)_e < 0$ and $\Delta\mu < 0$) of the maximum in the plot. The existence of the maximum is readily understandable in qualitative terms. Even though classically the dipole moment

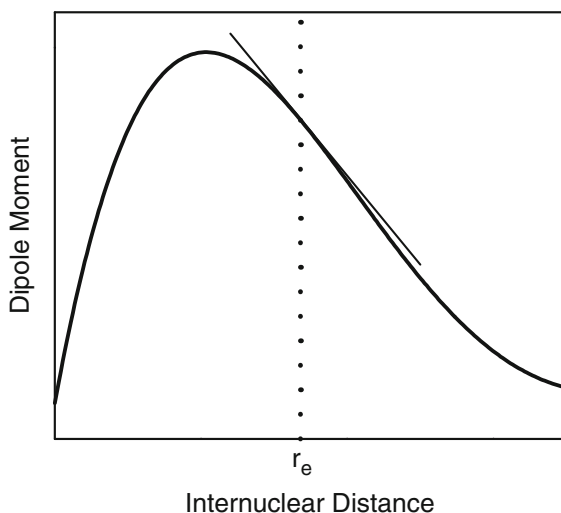


Fig. 12.2 Dipole moment as a function of internuclear distance for a diatomic oscillator. For the case shown r_e is greater than the r value at the maximum of the curve. Consequently $(\partial\mu/\partial r)_e < 0$. The value of $r(\text{max})$ may also be larger than r_e , whence $(\partial\mu/\partial r)_e > 0$ (and this is the case for both CO and HCl). Since the isotope effect [$\langle r_H \rangle - \langle r_D \rangle$] is small one can assume $(\partial\mu/\partial r)_e$ is isotope independent to good approximation

scales linearly with r such is not the case for properly (i.e. quantum mechanically) calculated dipole moments (see Equation 12.10) because the wave function which in the end defines the electronic charge distribution varies markedly and nonlinearly as the diatomic bond length increases.

12.2.3 Dipole Moments for Diatomic Isotopomers

Vibrational amplitude effects for diatomic molecules can be straightforwardly calculated from spectroscopic data. Mean amplitudes and mean square amplitudes for diatomics are expressed in Equations 12.8a and 12.8b (see, e.g. Levine 1975)

$$\langle (r - r_e) \rangle = (1/2)(\alpha_e r_e / (2B_e) + 3B_e r_e / \omega_e) \quad (12.8a)$$

$$\langle (r - r_e)^2 \rangle = r_e^2 B_e / \omega_e \quad (12.8b)$$

In Equation 12.8 B_e is the rotational constant, $B_e = h/(8\pi^2 I)$, (I is the moment of inertia), ω_e is the vibrational frequency, $2\pi\omega_e = (\kappa/\mu)^{1/2}$, (κ the vibrational force constant and μ the reduced mass), r_e the equilibrium bond length (isotope independent to reasonable approximation), and α_e is the vibration-rotation interaction constant

$$\alpha_e = (2B_e^2 / \omega_e) [(2B_e r_e^3 A / \omega_e^2) + 3] \quad (12.8c)$$

The isotope independent constant, A , is proportional to the third derivative of the vibrational potential. [In this section we are following the widely used notation employed by Herzberg and other spectroscopists where ω is the vibrational frequency expressed in cm^{-1} . The actual number of vibrations per second is c times as great, c is the speed of light. In other parts of this text we employ a second convention almost universally used by chemists which represents the vibrational frequency in cm^{-1} by ν rather than ω .] Using Equations 12.8a through 12.8c, and given values of α_e , r_e , and B_e for the reference isotopomer, the constant A is straightforwardly obtained, the isotope effects on α_e , B_e and ω_e evaluated, and zero point mean amplitudes and mean square amplitudes calculated. Results for the isotopomers of hydrogen chloride and carbon monoxide are shown in Table 12.2. The H/D isotope effect on the mean amplitude is about 0.004 A, the $^{35}\text{Cl}/^{37}\text{Cl}$ effects are much, much smaller, $\sim 10^{-4}$ A, and, as expected, carbon and oxygen isotope effects are intermediate. Calculation of the temperature dependence of the anharmonic mean amplitudes and mean square amplitudes is straight forward but tedious. In the harmonic approximation the vibrational contribution to the mean square amplitude is $\langle (r - r_e)^2 \rangle = [h/(8\pi^2 c \mu_r \omega)] [\coth(hc\omega/(2kT))]$ (μ_r is the oscillator reduced mass, c the velocity of light, and from Equation 12.8b to excellent approximation $h/(8\pi^2 c \mu_r \omega) = r_e^2 B_e / \omega_e$). The mean amplitudes and mean square amplitudes in hand, the isotope effect on the dipole moments is calculated from Equation 12.9.

$$\Delta\mu = (\partial\mu/\partial r)_e (\langle (r - r_e)' \rangle - \langle (r - r_e) \rangle) + (\partial^2\mu/\partial r^2) (\langle (r - r_e)^2 \rangle - \langle (r - r_e) \rangle^2) + \dots \quad (12.9)$$

Table 12.2 Isotope effects on permanent dipole moments for isotopomers of CO and HCl (see Section 12.2.3)

Molecule	$\langle(r-r_e)\rangle / \text{\AA}$	$\langle(r-r_e)^2\rangle / \text{\AA}^2$	$\partial\mu/\partial r$	$\partial^2\mu/\partial r^2$	$ \mu(^{12}\text{C}^{16}\text{O}) - \mu(^x\text{C}^y\text{O}) ^a$
$^{12}\text{C}^{16}\text{O}$	0.0041	0.00113	3.10	-0.14	-
$^{13}\text{C}^{16}\text{O}$	0.0039	0.00108			0.0007
$^{13}\text{C}^{17}\text{O}$	0.0037	0.00103			0.0014
$^{12}\text{C}^{17}\text{O}$	0.0042	0.00115			-0.0003
$^{13}\text{C}^{18}\text{O}$	0.0040	0.00110			0.0003
$^{12}\text{C}^{18}\text{O}$	0.0038	0.00106			0.0009
$^{14}\text{C}^{16}\text{O}$	0.0027	0.00079			0.0044
					$ \mu(^1\text{H}^{35}\text{Cl}) - \mu(^x\text{H}^y\text{Cl}) ^b$
H^{35}Cl	0.0159	0.00576	0.925	0.16	-
D^{35}Cl	0.0114	0.00413			0.0044 ₁
H^{37}Cl	0.0158	0.00576			0.0000 ₁
D^{37}Cl	0.0113	0.00412			0.0044 ₃

^aToth, R. A., Hunt, R. H. and Plyler, E. K., *J. Mol. Spec.* **32**, 85 (1969); Muentzer, J. S., *J. Mol. Spectrom.* **55**, 490 (1975); Goorvitch, D., *Astrophys. J. Supp. Ser.* **95**, 535 (1994).

^bKaiser, E. W. *J. Chem. Phys.* **53**, 1686 (1970); Scher, C., Ravid, B. and Halevi, E. A., *J. Phys. Chem.* **86**, 654 (1982).

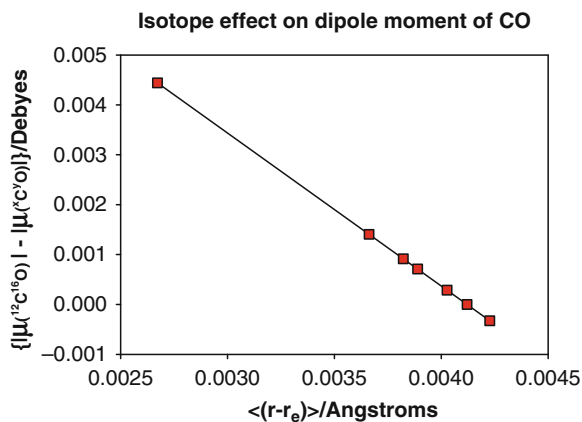


Fig. 12.3 Isotope effects on dipole moment for CO. $|\mu_0(^{12}\text{C}^{16}\text{O}) - \mu_0(^x\text{C}^y\text{O})|$ are plotted vs. the amplitude of the $^x\text{C}^y\text{O}$ isotopomer. Reading from left to right (x,y) values are (14,16), (13,18), (12,18), (13,16), (13,18), (12,16) and (12,17) (see Table 12.2)

assuming, reasonably, that $(\partial\mu/\partial r)_e$ and $(\partial^2\mu/\partial r^2)$ are isotope independent. As usual the prime denotes the more lightly substituted molecule. The derivatives in Equation 12.9 are available from measurements of the absolute intensities of the infrared vibration-rotation bands or from theory. Results are shown in Table 12.2 and (for CO isotopomers) in Fig. 12.3. In CO the dipole moment is oriented $[-\text{CO}^+]$ and by convention is given a negative sign. This accounts for the absolute value notation in Table 12.2 and Fig. 12.3.

12.2.4 Theoretical Approaches

Methods for quantum mechanical calculation of dipole moments and their IE's are well established. The dipole moment for any specified confirmation is defined by the nuclear coordinates of the various atoms \mathbf{r}_i and their charges z_i , plus the electron density at each point in space expressed as a function of the vector \vec{r}_e using the wave function

$$\mu = \left[- \int \psi \vec{r}_e \psi^* d\tau \right]_{\text{ELECTRONS}} + \left[e \sum z_i \mathbf{r}_i \right]_{\text{NUCLEI}} \quad (12.10)$$

Proper attention must be paid to the size and nature of the basis sets employed to evaluate the integral. Isotope effects on μ are small and large basis sets and long running times are needed to insure the necessary precision. Also, many separate calculations are required to establish the dependence of μ on molecular configuration and vibrational amplitude, and the results need to be properly averaged to yield effective dipole moments at thermodynamic equilibrium. A multitude of theoretical calculations of dipole moments are to be found in the literature. As expected, the more thorough and carefully done of these are in reasonable agreement with careful and well done experiments.

12.3 Induced Moments, Polarizability Isotope Effects

12.3.1 The Polarizability

The effect of H/D substitution on refractive index and polarizability was first studied in the 1930s, but even so, 75 years later, IE data are available only for some 25 or 30 compounds. The scarcity of the available data is surprising because an understanding of polarizabilities and polarizability isotope effects (PIE's) is essential when considering the forces between molecules leading to gas imperfection, condensation, and liquid state structure. That is because the attractive term in the intermolecular potential which describes the interaction between nonpolar, non-charged molecules scales with polarizability according to London dispersion theory ([[Historical Vignette 12.1](#)]).

12.3.2 Frequency Dependence

For liquid or gaseous molecules placed in a sinusoidally varying electromagnetic field, i.e. a light beam, the field changes direction many times during a single molecular rotation and molecule fixed permanent dipoles experience only the average field, which is zero. The response of induced dipoles to fluctuating electric fields, however, is essentially instantaneous. Time dependent perturbation theory leads to



[Historical Vignette 12.1] Izrail' Beniaminovich Rabinovich (1914–2001) was born in a small village near Gomel (Belarus). During the Second World War he was head of a laboratory in a military factory, which was engaged in solving problems in the field of metal corrosion and electroplating. In 1950, he started his research on isotope effects on various physicochemical properties of liquids in the Chemistry Department of the State University of Gorky. On the basis of his experimental results – covering more than 150 deuterated compounds – he worked out a semi-quantitative theory of isotope effects. The results were submitted to earn the Doctor of Science degree. They also served to publish the well-known book “Influence of Isotopy on the Physicochemical Properties of Liquids” in Russian (1968), then in English (1970). In addition to his work on isotope effects, he made numerous important contributions to disparate areas of chemistry; many of his results found application in industry and agriculture. He is the author of more than 350 scientific publications. In 2002, he was awarded the State Prize of the Russian Federation. (Adapted from bibliographic notes investigated and translated by Gábor Jancsó, KFKI, Budapest, Hungary, and Jerszy Szydłowski, Warsaw University, Poland. Photo credit: N.N. Smirnova, State University of Nizhny, Novgorod)

Equation 12.11

$$\alpha(\nu) = (2/(3hc)) \sum (\nu_{n0} \mathbf{d}_{0n} \mathbf{d}_{n0} / (\nu_{n0}^2 - \nu^2)) \quad (12.11)$$

In Equation 12.11, ν is the frequency of incident radiation (cm^{-1}), ν_{n0} is the frequency corresponding to the energy difference between ground and excited electronic state, the sum is over all excited states, and \mathbf{d}_{0n} and \mathbf{d}_{n0} are the dipole transition moments between the ground and excited state ($\mathbf{d}_{n0} = \langle n | \mathbf{d} | 0 \rangle = \int \Psi_n \mathbf{d} \Psi_0 \, d\tau$, the Ψ 's are wave functions and \mathbf{d} is the dipole moment operator). At low frequency ($\nu \rightarrow 0$) Equation 12.11 reduces to the static field expression

$$\alpha_0 = (2/3) \sum (\mathbf{d}_{0n} \mathbf{d}_{n0} / (E_{n0})) \quad (12.12)$$

while at very high frequency $\nu^2 \gg \nu_{n0}^2$ the polarizability tends to zero. The polarizability and the refractive index, n , are related by the Lorenz–Lorentz formula

$$(n^2 - 1)/(n^2 + 2) = N\alpha(v)/(3\epsilon_0) = 2N/(9hc\epsilon_0) \sum (\nu_{n0} \mathbf{d}_{0n} \mathbf{d}_{n0}/(\nu_{n0}^2 - v^2)) \quad (12.13)$$

In Equation 12.13, N is the number density of molecules in the beam of radiation (and is thus inversely proportional to the molar volume, V_M), and ϵ_0 is the permittivity of the vacuum. A useful and widely employed method to evaluate the sum in Equation 12.13 leads via the closure approximation to a one-term equation commonly known as the dispersion relation,

$$R = [(n^2 - 1)/(n^2 + 2)] = A/[V_M\{v^{\#2}(1 - v^2/v^{\#2})\}] \quad (12.14)$$

Here, A and $v^{\#2}$ are fitting parameters amenable to physical interpretation using Equation 12.11. The point of present concern is that the isotope effect on polarizability can now be expressed in terms of isotopic differences in refractive index. It follows from Equation 12.14 that a plot of $\Delta R/R = [6n^2/((n^2 - 1)(n^2 + 2))][\Delta n/n]$ vs. v^2 gives an approximately straight line,

$$\Delta R/R = (\Delta A/A - \Delta v^{\#2}/v^{\#2} - \Delta V_M/V_M) - [(\Delta v^{\#2}/v^{\#2})(1/v^{\#2})]v^2 \quad (12.15)$$

Using Equation 12.12 one obtains $(\Delta A/A - \Delta v^{\#2}/v^{\#2}) = (\Delta\alpha_0/\alpha_0)$. We see that precise refractive index differences measured over a reasonable range of wavelengths allow the recovery of the polarizability isotope effect (i.e. the isotope effect on the electric field induced dipole moment), provided the molar volume and its isotope effect are available.

12.3.3 Experimental Methods, Results, Discussion

The method of choice for measurements of refractive index IE's and thence PIE's is differential refractometry. While typical refractive index measurements show precisions between 1 part in 10^4 and 1 in 10^5 , interferometric differential instruments improve that precision by one or two orders of magnitude (i.e. to, say, 1 in $10^{5.5}$ or $10^{6.5}$). For solutions of isotopomers, the refractive index differences between solution (for example a mixture of isotopomers) and reference (usually one or the other pure component) are large enough to give interferograms amounting to many fringes. In the technique of continuous dilution differential refractometry (CDDR) the sample in the solution side of the differential instrument (initially isotopomer-1) is smoothly and continuously diluted, in the end completely replaced, with isotopomer-2, while the reference side remains unchanged (isotopomer-1). The interferogram which results can be straightforwardly deconvoluted and the data plotted using Equation 12.15 to yield the isotope effect on the static polarizability and its dispersion (frequency dependence). Examples of CDDR interferograms are shown in Fig. 12.4.

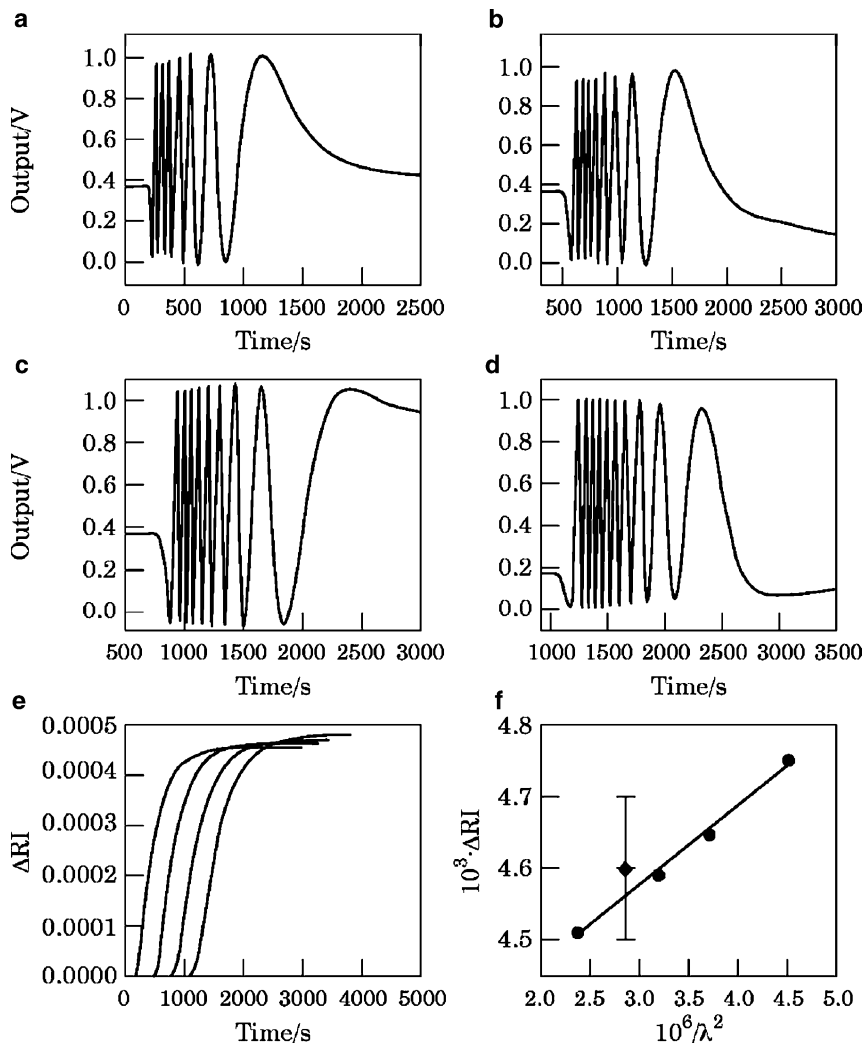


Fig. 12.4 Continuous dilution differential refractometric data for the C_6H_{12}/C_6D_{12} isotopomer pair at 298.15 K. (a) through (d) are interferograms observed at 650, 559, 520 and 470 nm, respectively. (e) shows refractive index differences derived from the interferograms (left to right 650, 559, 520 and 470 nm) and (f) is a dispersion plot of the data. In (f) the interferometric data are compared with the result at 589.3 nm obtained by Abbe refractometry, which nicely illustrates the better precision of CDDR (Reprinted from Wiczorek, S. A., Urbanczyk, A. and Van Hook, W. A., *J Chem. Thermodyn.* **28**, 1009 (1996) copyright 1996 with permission from Elsevier)

PIE's for some representative liquids and gases, mostly at room temperature, are given in Tables 12.1 and 12.3. Both the PIE and MVIE are expected to be approximately additive (e.g. $\Delta\alpha/\alpha(CD_3OD/CH_3OH) \sim \Delta\alpha/\alpha(CH_3OD/CH_3OH) + \Delta\alpha/\alpha(CD_3OH/CH_3OH)$). Typically, these isotope effects each amount to at most a

Table 12.3 CDDR (continuous dilution differential refractometry) least squares parameters, molar volume isotope effects, and derived PIEs for some isotopomer solutions at 298.15K; see Equation 12.15, $\Delta R/R = A + mv^2$ (Wieczorek, S. A., Urbanczyk, A. and Van Hook, W. A., *J. Chem. Thermodyn.* **28**, 1009 (1996))

Isotomers	$10^3 A$	$10^7 m/(nm^2)$	$10^3 \Delta V/V$	$10^3 \Delta \alpha/\alpha$
C_6H_6/C_6D_6	3.273	139.55	2.1	5.4
C_6H_{12}/C_6D_{12}	8.894	122.08	2.2	11.1
$(CH_3)_2CO/(CD_3)_2CO$	6.322	71.25	2.9	9.2

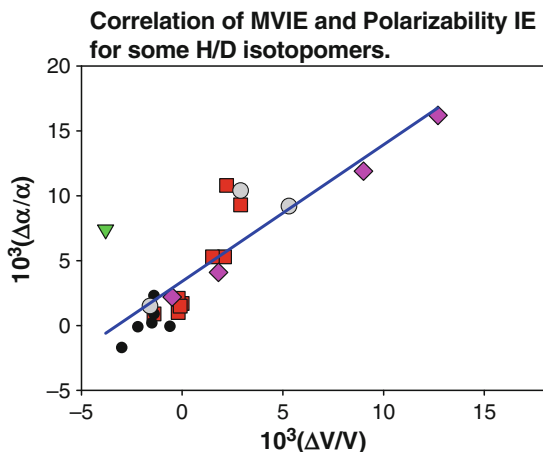


Fig. 12.5 Correlation of molar volume and polarizability isotope effects for some H/D isotopomer pairs. *Squares* = non H-bonded liquids, *small dark circles* = H-bonded liquids (except water), *inverted triangle* = H_2O/D_2O , *large light circles* (left to right; CH_3OH/CH_3OD , CH_3OH/CD_3OD , CH_3OH/CD_3OD), *diamonds* = $\Delta RI/RI$ from gases at 298 K, $\Delta V/V$ from liquids at or below boiling (left to right HCl/DCI , H_2S/D_2S , NH_3/ND_3 , CH_4/CD_4) (Data from *J. Chem. Thermodyn.* **18**, 1077 (1986); **19**, 703 (1987), **19**, 1163 (1987), **28**, 1009 (1996); *Z. Naturforsch* **49a**, 563 (1994); *Russ. Chem. Bull., Int. Ed.* **54**, 1987 (2005); *J. Chem. Phys.* **48**, 1032 (1968)) The equation of the correlating line is $\Delta \alpha/\alpha = 3.41 \times 10^{-3} + 1.05 \Delta V/V$

few parts per thousand per XH/XD bond substituted. Heavy atom PIE's are expected to be significantly smaller but no data are available to confirm that prediction. Figure 12.5 plots the available data for $\Delta \alpha_0/\alpha_0$ of H/D isotopomers (excepting H_2/D_2) vs. the molar volume isotope effects (MVIE's) of the liquids at or below the normal boiling temperatures. The PIE is a molecular property and, except for strongly structured and associated liquids like water (which plots as an outlier in Fig. 12.5), has little or no temperature or phase dependence. Figure 12.5 establishes a crude proportionality between PIE and MVIE. It is significant that the slope of the correlation is \sim unity. Later in this chapter we will see that for liquids well below their critical points one expects a similar crude proportionality between the IE on intrinsic molecular size (thus ultimately on vibrational amplitude IE's) and MVIE. Since PIE also correlates with vibrational amplitude, the correlation is expected. A more detailed analysis would necessitate a complete normal coordinate calculation of the vibrational amplitudes and their isotope effects.

12.4 Isotope Effects on NMR Shielding

12.4.1 Introduction

An enormous literature dealing with isotope effects on NMR parameters has accumulated over the years. As we saw in Chapter 7 this includes studies on chemical shift and coupling constant IE's, the use of isotope labeling for molecular structure determinations, the study of fast exchange processes, and the use of NMR as an analytical tool to measure isotope fractionation. In this section we limit our attention to IE's on chemical shifts (nuclear shielding) due to isotopic differences in averaging of rotation–vibration contributions to molecular properties (rovibrational effects). NMR coupling constant IE's have also been rationalized using rovibrational arguments but such effects are almost vanishingly small and will not be discussed here (but see Section 7.3.2).

An example of an NMR shielding IE is shown in Fig. 12.6. This is a “1-bond” secondary isotope effect because the position of isotope label is immediately adjacent (1-bond removed) to the magnetic probe atom (in this case ^{15}N). The ^{15}N is shifted upfield in excess of 100 parts per billion (0.1 ppm) per neighboring ^{18}O substitution. (Compare these ^{18}O NMR isotope shifts on $[^{15}\text{N}]$ spectra of NaNO_2 solutions (a hundred or so ppb) with the primary and secondary deuterium IE's (on $[\text{H}]$ vs. $[\text{D}]$ resonances, and $[\text{F}]$ resonances, respectively) of the FHF^- and FDF^- moieties shown in Fig. 7.16b, and with the secondary deuterium IE's on the $[\text{C}]$ NMR spectrum of dry glycerol (Fig. 7.16a). 1-Bond deuterium shifts are consistently a few hundred ppb, but heavier atom IE's are smaller. As expected the magnitude of secondary NMR chemical shift IE's falls off dramatically as one moves from 1-bond to 2-bond, 3-bond, etc. substitution. In special cases, however, long range effects likely transmitted through resonance or hyperconjugated structures have been observed. An example of an unusually large 10-bond secondary D shift on a $[\text{F}]$ resonance is shown in Fig. 12.7, but keep in mind that the range of $[\text{F}]$ NMR shifts is unusually large, and these shifts are very sensitive to structural changes and electric field effects.

12.4.2 Application of the Rovibrational Theory

An application of the basic ideas briefly reviewed in Sections 12.2 and 12.3 to NMR shielding has been formulated by Jameson. The isotope effect on the shielding (σ) depends on vibrationally averaged bond lengths and angles according to Equation 12.16

$$\langle\sigma'\rangle - \langle\sigma\rangle = \sum (\partial\sigma/\partial r_i) [\langle\Delta r_i'\rangle - \langle\Delta r_i\rangle] + \sum (\partial^2\sigma/(\partial r_i\partial r_j)) [\langle\Delta r_i'\Delta r_j'\rangle - \langle\Delta r_i\Delta r_j\rangle] + \sum (\partial\sigma/\partial\alpha_{ij}) [\langle\Delta\alpha_{ij}'\rangle - \langle\Delta\alpha_{ij}\rangle] + \dots \quad (12.16)$$

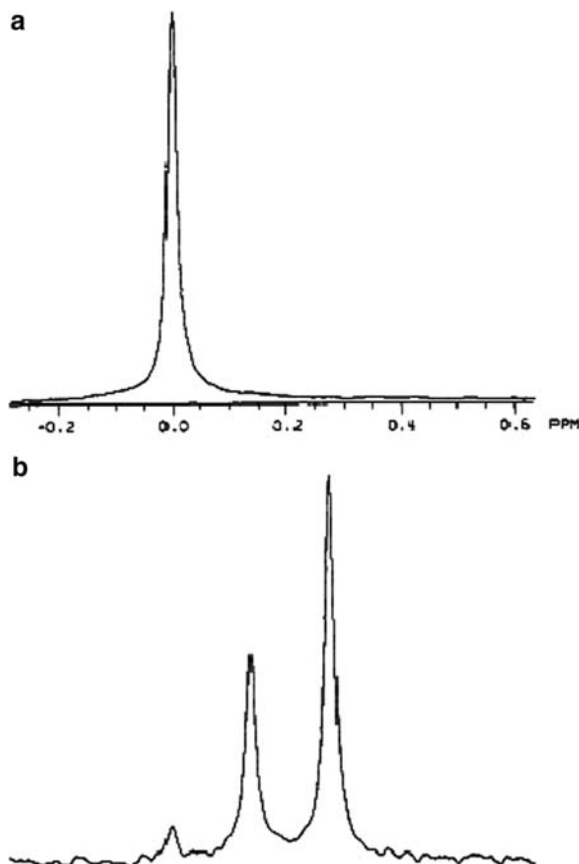


Fig. 12.6 An upfield shift in the NMR signal of the nitrite ion of 0.138 ppm (per ^{18}O) occurs upon substitution of ^{18}O for ^{16}O . (a) Sodium (^{15}N) nitrite (95 atom % ^{15}N) starting material. (b) Silver ($^{15}\text{N}, ^{18}\text{O}_2$) nitrite (95 atom % ^{15}N , 77 atom % ^{18}O). The percentages of the ^{18}O labeled species are 6% $^{15}\text{N}^{16}\text{O}_2$, 33% $^{15}\text{N}^{16}\text{O}^{18}\text{O}$, and 61% $^{15}\text{N}^{18}\text{O}_2$ (Van Etten, R. L. and Risley, J. M., *J. Am. Chem. Soc.* **103**, 5633 (1981))

As is customary the prime refers to the lighter isotope, Δr_i is the averaged change in the i th bond length due to anharmonicity in the stretching vibration, ($\Delta r_i = r_i - r_{i,e}$), and $\Delta\alpha_{ij}$ is the distortion of the angle between bonds i and j . These parameters are available from vibrational analysis given the complete anharmonic potential, while the isotope independent shielding parameters ($\partial\sigma/\partial r_i$), ($\partial^2\sigma/(\partial r_i\partial r_j)$), ($\partial\sigma/\partial\alpha_{ij}$), etc. are most reliably obtained from ab initio quantum mechanical calculation. When values for these derivatives are not available a common strategy is to approximate Equation 12.16 using only the leading term, obtaining ($\partial\sigma/\partial r_i$) by various empirical or semi-theoretical methods.

$$\langle\sigma'\rangle - \langle\sigma\rangle \sim \sum (\partial\sigma/\partial r_i)[\langle\Delta r_i'\rangle - \langle\Delta r_i\rangle] \quad (12.17)$$

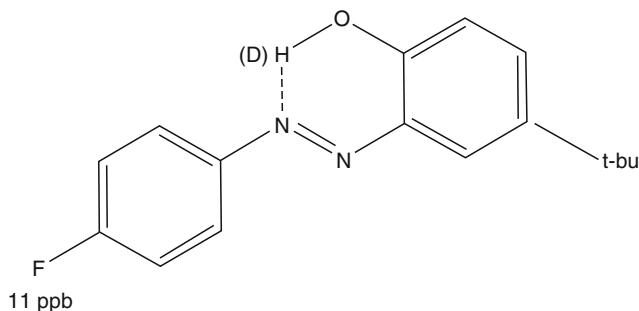


Fig. 12.7 An unusually long range (10-bond) secondary D isotope shift IE on an ^{19}F NMR. The H/D chemical shift isotope effect due to substitution at an OH – N hydrogen bond sited ten bonds away from a para-F is 11 ppb (Hansen, P. E. et al. *Acta Chim. Scandinavia* **51**, 881 (1997))

12.4.2.1 H/D Isotope Effects on ^{13}C NMR of Methane

An excellent illustration of the application of rovibrational theory to NMR shift data, including comparison with experiment is given in Table 12.4. The table compares calculated and experimental isotope effects. The agreement is reasonable although the calculated values are consistently about 20% larger than experiment, probably because the bond length dependence of nuclear shielding, $(\partial\sigma/\partial r_i)$, is overestimated by the choice of Hartree–Fock wave functions used in the calculation. Table 12.4b details first and second order contributions to the isotope effects. Although at first glance the first order contribution of the CH stretch is the most important, and is in apparent agreement with experiment (0.763 viz 0.774 ppm), two of the second order coefficients, σ_{rr} and $\sigma_{\alpha\alpha}$, also make large but nearly offsetting contributions. The widely used approximation quoted as Equation 12.17 is thus not well justified. Rather it works reasonably well in the case of methane because of rough cancellation of the second order terms. That fortunate circumstance cannot generally be expected to carry over to other molecules. Another way to express the zero point IE is to examine the contributions of different normal modes. This is done in Table 12.4c. Notice that the two stretching modes make a positive contribution to the IE but the bending contribution is negative. The largest term is that of the triply degenerate stretching mode. Finally Table 12.4d shows that the effect of thermal excitation into excited vibration-rotation states is modest for the methanes.

12.4.2.2 Larger and More Complicated Molecules

For large molecules it is no longer feasible to carry out the complete anharmonic vibrational analysis implied by Equation 12.16. One is forced to the approximate relation, Equation 12.17, which seems to work pretty well in spite of the criticisms discussed above. Numerous examples abound in the literature. The interested student is referred to the review of Hansen.

Table 12.4a Calculated (Raynes, W. T., et al. *Molecular Physics* **64**, 143 (1988) and experimental (Alej, M. and Wagman, W. E. *J. Chem. Phys.* **68**, 783 (1978) IE's on carbon-13 shielding constants of methane isotopomers at 300 K, $-\langle\sigma'\rangle - \langle\sigma\rangle$ (in ppm)

$\langle\sigma\rangle$	$^{13}\text{CH}_3\text{D}$	$^{13}\text{CH}_2\text{D}_2$	$^{13}\text{CHD}_3$	$^{13}\text{CD}_4$
Calculated	0.250	0.500	0.746	0.992
Experiment	0.187	0.385	0.579	0.774

Table 12.4b Contributions of the different terms in Equation 12.16 to the zero point IE on ^{13}C shielding constants of $^{13}\text{CH}_4$ and $^{13}\text{CD}_4$, $-\langle\sigma'\rangle - \langle\sigma\rangle$ (in ppm)

σ_r (First order)	σ_r (Second order)	σ_{rr}	σ_{rs}	$\sigma_{\alpha\alpha}$	$\sigma_{\alpha\omega}$	σ_{ra}	Total
0.763	0.406	0.453	-0.018	-0.686	0.059	0.001	0.978

Table 12.4c Contributions of different vibrational modes to the zero point IE on ^{13}C shielding constants of $^{13}\text{CH}_4$ and $^{13}\text{CD}_4$, $-\langle\sigma'\rangle - \langle\sigma\rangle$ (in ppm)

Mode	Description	Degeneracy	Isotope shift, $-\langle\sigma'\rangle - \langle\sigma\rangle$
ν_1	Sym. stretch	1	0.047
ν_2	HCH bend	2	-0.014
ν_3	Assym. stretch	3	1.341
ν_4	HCH bend	3	-0.396
Total			0.978

Table 12.4d Temperature dependence of calculated ^{13}C shielding constants of $^{13}\text{CH}_4$ and $^{13}\text{CD}_4$, (in ppm)

T/K	$-\langle\sigma'\rangle - \langle\sigma\rangle$ (in ppm)
0	0.978
300	0.992
500	1.039

12.5 Molar Volume Isotope Effects

Molar volume isotope effects (MVIE's) for some common liquids are given in Table 12.5. The data mostly refer to temperatures between the triple point and the normal boiling point ($T_{\text{TRP}} < T < T_{\text{BP}}$), equivalently ($\sim 0.42 < T_{\text{R}} < \sim 0.6$). At these temperatures, well below the critical point, $T_{\text{R}} = 1$, liquid state molar volumes generally lie within 10% or so of the values in the corresponding solids at the triple point. Also in this temperature range the expansivity, $\alpha = (\partial \ln V / \partial T)_{\text{P}}$, is small and it seems reasonable to assume a model where liquid state molecules, on average, are in contact with one another. For convenience we will label this approach "the mechanical model". At higher temperatures the expansivity and compressibility increase rapidly, the liquid expands dramatically (typically critical volumes are some three or four times molar volumes at T_{TRP}), and the mechanical model becomes inappropriate. Except for $^3\text{He}/^4\text{He}$ MVIE data are only available for H/D substituted molecules, because the effects for heavier isotopomer pairs are too small

Table 12.5 Molar volume isotope effects for some liquids, mostly at or below their normal boiling points (Boiling point is $\sim 0.58 T_C$)

Isotopomer Pair	T	T/T_C'	$10^3 \ln(V'/V)$	Reference
$^3\text{He}/^4\text{He}$	2.00	0.381	326	a
	3.20	0.610	603	
H_2/HD	20.0	0.601	99	a
H_2/D_2	20.0	0.601	182	
	24.0	0.721	204	
HCl/DCl	160	0.493	0.34	b
	240	0.739	-0.89	
$\text{H}_2\text{O}/\text{D}_2\text{O}$	283	0.437	-4.9	a
	323	0.499	-2.6	
	373	0.577	-1.9	
$\text{H}_2\text{S}/\text{D}_2\text{S}$	190	0.509	1.8	b
NH_3/ND_3	200	0.493	9.1	b
CH_4/CD_4	90.4	0.473	11.8	c
	110.6	0.579	11.6	
	120.6	0.631	10.7	
$\text{C}_2\text{H}_4/\text{C}_2\text{D}_4$	120	0.424	4.2	d
	170	0.580	2.7	
$\text{CH}_3\text{OH}/\text{CD}_3\text{OH}$	298	0.581	5.3	e
$\text{CH}_3\text{OH}/\text{CD}_3\text{OD}$	298	0.581	2.9	
$\text{CH}_3\text{OH}/\text{CH}_3\text{OD}$	298	0.581	-1.6	
$\text{C}_6\text{H}_6/\text{C}_6\text{D}_6$	298	0.530	2.3	f
$c\text{-C}_6\text{H}_{12}/c\text{-C}_6\text{D}_{12}$	298	0.539	2.2	f
$(\text{CH}_3)_2\text{CO}/(\text{CH}_3)_2\text{CO}$	298	0.537	2.9	f

^aRabinovitch, I. B., *Influence of Isotopy on the Physicochemical Properties of Liquids*, Consultants Bureau, New York, 1970.

^bStaveley, L. A. K., et al. *J. Chem. Thermodyn.* **19**, 703 (1987), **19**, 703 (1987), **19**, 1163 (1987), **18**, 1067 (1986).

^cGrigor, A. F. and Steele, W. A., *J. Chem. Phys.* **48**, 1032 (1968).

^dBigeleisen, J. et al. *J. Chem. Phys.* **53**, 2869 (1970).

^eIvanov, E. V. and Abrosimov, V. K. *Russ. Chem. Bull., Int. Ed.* **54**, 1987 (2005).

^fKooner, Z. and Van Hook, W. A., *J. Phys. Chem.* **92**, 6414 (1988).

to be conveniently measured using ordinary laboratory techniques. Also, except for H_2/HD , H_2/D_2 and $^3\text{He}/^4\text{He}$, MVIE's only amount to a few parts per thousand, or less, per H/D substitution. Both positive and negative effects are observed for low temperature liquids, but negative values ($\ln(V_H/V_D) < 0$, i.e. $V_D > V_H$) in this temperature region only occur for strongly associated (hydrogen bonded) liquids.

Figure 12.8 shows the temperature dependence of MVIE for three isotopomer pairs (CH_4/CD_4 , $\text{C}_6\text{H}_6/\text{C}_6\text{D}_6$, and $\text{H}_2\text{O}/\text{D}_2\text{O}$). In each case MVIE is relatively flat at low temperature (i.e. $\partial(\ln(V'/V))/\partial T \sim 0$ for ($\sim 0.45 < T_R < \sim 0.6$)) but at higher temperature it drops off rapidly and reaches large negative values as the critical point is approached. MVIE's for $^3\text{He}/^4\text{He}$ and H_2/D_2 , on the other hand, are large and positive (hundreds of parts per thousand) and increase rapidly

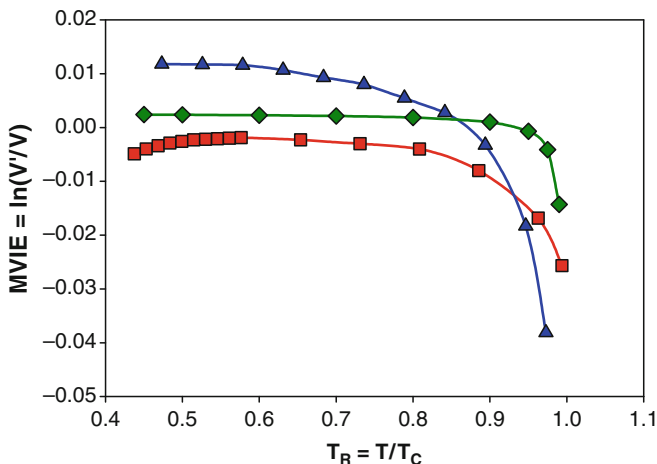


Fig. 12.8 MVIE's as a function of reduced temperature for three isotopomer pairs. Reading down at left, triangles = CH_4/CD_4 , diamonds = $\text{C}_6\text{H}_6/\text{C}_6\text{D}_6$, squares = $\text{H}_2\text{O}/\text{D}_2\text{O}$

with temperature. MVIE's for these ultralight isotopomer pairs and for heavier isotopomer pairs in the expanded liquids (i.e. at elevated temperature) are discussed in Chapter 13. The discussion in this chapter is primarily concerned with the application of the mechanical model to H/D effects for heavier molecules at lower temperatures ($\sim 0.45 < T_R < \sim 0.6$).

12.5.1 The Bartell Mechanical Model for MVIE

The mechanical model assumes that the major part of MVIE for polyatomic molecules at low temperature is due to the isotope effect on the XH/XD vibrational amplitudes. Making use of the well known Van der Waals radii of hydrogen (1.2 \AA (angstrom, $\text{\AA} = 1.2 \times 10^{-8} \text{ cm}$), and taking the isotope effect on CH/CD vibrational amplitude as 0.005 \AA , one finds for benzene (considered to be a disk like molecule), $\Delta V/V = 2\Delta r/r = 2(0.005)/3.7 = 0.0027$ in reasonable agreement with the observed value, 0.0021. Here r is the Van der Waals radius of benzene, and R_{CC} , R_{CH} , and r_{H} are the C – C and C – H bond lengths, and the Van der Waals radius of the hydrogen atom, respectively, $r = [2 \sin(30) R_{\text{CC}} + R_{\text{CH}} + r_{\text{H}} = 1.4 + 1.1 + 1.2 = 3.7 \text{ \AA}]$. Similarly for CH_4/CD_4 , a sphere like molecule, $\Delta V/V = 3\Delta r/r = 3(0.005)/(1.1 + 1.2) = 0.007$ (observed = 0.011).¹ In both cases the predicted MVIE's are in rough agreement

¹ Note: It is interesting to compare the calculation above based on measured interatomic distances and Van der Waals radii with an estimate using thermodynamic data. Using tabulated densities for C_6H_6 and CH_4 of 0.8765 and 0.4256 g/cm^3 , respectively, we find volumes per condensed

with observation, but just as clearly the model is crude and needs refinement. One obvious step in that direction replaces the isotope effect on the CH/CD stretching amplitudes, 0.005 \AA , with a linear combination of properly averaged vibrational amplitudes over all normal modes.

The Bartell mechanical model has also been used to estimate the isotope effect on molar volume due to the over all motion (i.e. hindered translation) of molecules interacting in a Lennard–Jones potential. For $\text{C}_6\text{H}_6/\text{C}_6\text{D}_6$ one finds $\Delta V/V \sim 4 \times 10^{-5}$, about two orders of magnitude smaller than the contribution of the internal modes (and experiment). We conclude that for all but very light molecules this contribution can be neglected.

12.5.2 Hydrogen Bonded Liquids

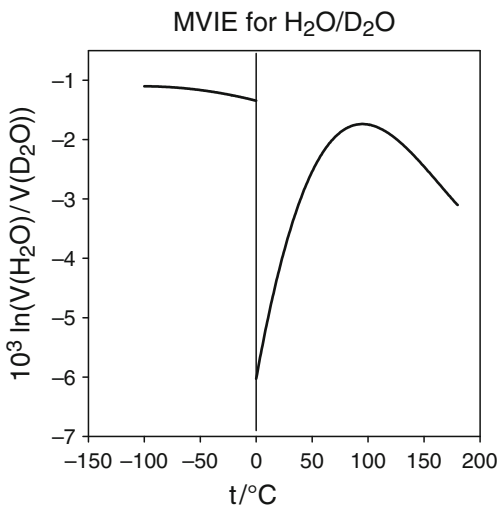
The MVIE for $\text{H}_2\text{O}/\text{D}_2\text{O}$ in both solid and liquid well below T_C is shown in Fig. 12.9. The isotope effects are inverse. In the solid MVIE falls gradually from around -1.2×10^{-3} at -100°C to about -1.6×10^{-3} at the melting point, where it undergoes an abrupt discontinuity. In the liquid at the melting point MVIE is a striking -6.2×10^{-3} but it rises rapidly with temperature, finally going through a maximum of -1.9×10^{-3} near 100°C after which it continues to fall to nearly -30×10^{-3} at the critical point.

The MVIE in both water and ice is complicated by the hydrogen bond network. The inverse isotope effect cannot be understood exclusively in terms of the isotope effect on the OH/OD bond amplitudes (which is necessarily positive, *vide supra*). To begin, consider the ice lattice which is conveniently described in terms of the oxygen positions. Within the Born–Oppenheimer approximation the H/D MVIE is then determined by calculating the H/D isotope effect on the oxygen amplitudes. According to the usual hypothesis the oxygen motions for translation and libration occur about the center of mass, CM, which is isotope dependent for these water isotopomers. The distance from CM to the equilibrium oxygen position for D_2O is

phase benzene or methane molecule of 148 and 62 \AA^3 . Setting the thickness of the benzene disk to $d = 1.2 \text{ \AA}$, (the Van der Waals radius of the hydrogen atom), we find a disk radius of $r = (Vf/\pi d)^{1/2} = 5.0 \text{ \AA}$. Here f is the packing fraction which we take to be that for randomly close packed spheres, 0.64. Other estimates might be 10 or 15% lower. For methane, approximated as spherical, $(4/3)\pi r^3 = Vf$, so $r = 2.1 \text{ \AA}$. As for benzene, the disk approximation was used for ethylene. Summarizing

	$\text{C}_6\text{H}_6/\text{C}_6\text{D}_6$	CH_4/CD_4	$\text{C}_2\text{H}_4/\text{C}_2\text{D}_4$
$r/\text{\AA}$, (estimated from bond lengths)	3.7	2.3	2.7
$10^3 \Delta V/V$, (calculated)	2.7	6.5	3.7
$r/\text{\AA}$, (estimated from liquid density)	5.0	2.1	2.7
$10^3 \Delta V/V$, (calculated)	2.0	7.5	3.7
$10^3 \Delta V/V$ (observed)	2.3	11	4.7

Fig. 12.9 Molar volume isotope effect for $(\text{H}_2\text{O}/\text{D}_2\text{O})_{\text{ICE}}$ (left side) and $(\text{H}_2\text{O}/\text{D}_2\text{O})_{\text{LIQUID}}$ (right side)



almost double that for H_2O . As a consequence the oxygen amplitude due to libration is greater in D_2O than it is in H_2O even though the angular amplitude is greater for H_2O . For centrosymmetric molecules this effect could not lead to the prediction of an inverse contribution to MVIE.

Now consider MVIE in the liquids. Were the isotopic liquids isostructural (like the ices), the MVIE could be estimated as outlined above, but that is not the case. The melting of water is usually described in terms of a partial destruction of the tetrahedral ice lattice to give a partially relaxed liquid structure containing some fraction of molecules in what were interstitial void spaces in the ice lattice. The average coordination increases from 4 in the solid to about 4.4 in the liquid, and there is an $\sim 10\%$ increase in density due to partial destruction of the open ice framework. To interpret the MVIE on melting we assume the HOH lattice is broken apart to a slightly greater extent than the DOD lattice. Hence MVIE falls markedly on melting. As temperature increases, more and more of the residual ice structure is broken, the structures approach each other, and the isotope effect rises to its isostructural value somewhere around 100°C . At higher temperatures yet the effects of thermal expansion dominate and MVIE decays to about -30×10^{-3} at the critical point.

As for water we can expect the MVIEs for other hydrogen bonded systems in low temperature liquids to have an appreciable inverse librational contribution, and this is the case for those alcohols which have been investigated. The data on the isotopic methanols (Table 12.5) confirm this. As expected from the discussion above, the MVIE for OH/OD substitution is negative. Also the isotope effects seem to be approximately additive, $\text{MVIE}(\text{CH}_3/\text{CD}_3) + \text{MVIE}(\text{OH}/\text{OD}) \sim \text{MVIE}(\text{CH}_3\text{OH}/\text{CH}_3\text{OD})$: $5.3 \times 10^{-3} - 1.6 \times 10^{-3} \sim 3.7 \times 10^{-3}$ (observed = 2.9×10^{-3}).

12.5.3 Limitations of the Mechanical Model, the Temperature Dependence

We now return to our discussion of typical (non hydrogen-bonded) liquids. Even at low temperature the thermal expansivity of liquids is not negligible, and MVIE is small (Fig. 12.8). Both $\Delta V/V$ and ΔV itself fall off with temperature, and eventually become negative. Inasmuch as 99% or more of liquid ethylene, benzene, etc. molecules are in the ground vibrational state for internal isotope sensitive frequencies of interest over the range ($\sim 0.45 < T_R < \sim 0.6$), one expects $\Delta V/V$ to be temperature independent according to the mechanical model. Higher order contributions must be invoked to explain the observed temperature coefficient. To complete the analysis it remains to establish the reasons for the significant inverse isotope effect on the expansivity of the high temperature expanded liquids, and therefore in the end on ΔV and $\Delta V/V$. We expect the pseudo-harmonic oscillator cell model (HOCM) to account for the bulk of the effects, at least for temperatures which are not too high. In HOCM the thermal pressure, $(\partial P/\partial T)_V$, which is the ratio of thermal expansivity, $\alpha = (\partial \ln V/\partial T)_P$, and isothermal compressibility, $\kappa = -(\partial \ln V/\partial P)_T$, is given by Equation 12.18 (from the properties of the total differential $(\partial P/\partial T)_V = -(\partial V/\partial T)_P/(\partial V/\partial P)_T = \alpha/\kappa$)

$$\alpha/\kappa = (k/V) \sum \Gamma_i u_i^2 \exp(u_i)/(\exp(u_i) - 1)^2 \quad (12.18)$$

In Equation 12.18, k is the Boltzman constant, the sum is over all $3n$ frequencies, $u_i = h\nu_i/kT$, and the Γ_i are Gruneisen constants, $\Gamma_i = -(\partial \ln \nu_i/\partial \ln V)_T$. The behavior of the thermal pressure can now be deduced. Only the argument in Equation 12.18 is isotope dependent. $\Delta(u_i^2 \exp(u_i)/(\exp(u_i) - 1)^2)$ is negative for all u_i , and decays to 0 for u_i both small and large (Fig. 12.10). The Γ_i are small (of order 10^{-3}) for the large internal frequencies lying to the right of the minimum in Fig. 12.10, but large for the smaller external translational and librational modes (of order unity) lying well to the left of the minimum. As a consequence it is the external modes which make the most significant contribution to the isotope effect on the thermal pressure, and for each given external frequency that contribution becomes smaller and smaller (i.e. less and less negative) as temperature increases (i.e. as u decreases). Thus, in spite of the divergences in the compressibility and expansivity as T_C is approached, the thermal pressure and its isotope effect remain bounded. The details of the behavior of isotope effects on the volumetric properties of fluids at high temperature are thus quite complicated. Application of HOCM in this region is at best highly suspect. The arguments given above have only been developed to further the qualitative understanding of MVIE in high temperature liquids. An alternative and much more convenient approach is *via* the application of corresponding states theory and reduced equations of state (see Chapter 13).

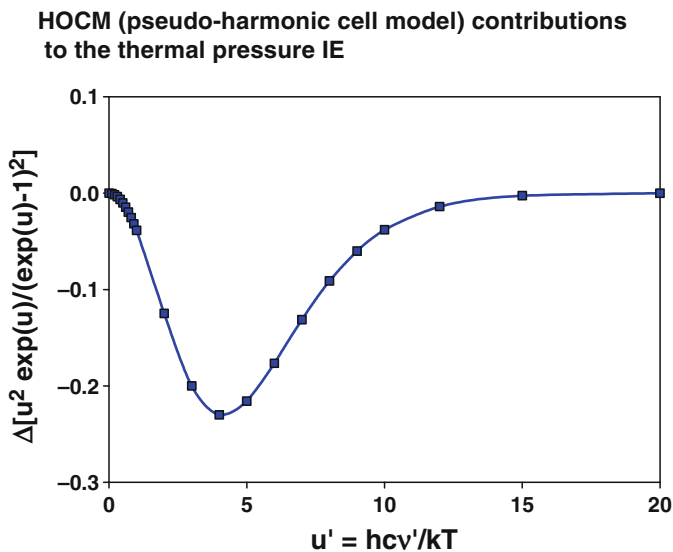


Fig. 12.10 The dependence of $[u_i^2 \exp(u_i)/(\exp(u_i) - 1)^2]$, and thence the contribution to the isotope effect on the thermal pressure, pseudo-harmonic approximation. For purposes of illustration the graph was constructed assuming $u'/u = \nu'/\nu = 2^{1/2}$, approximately the ratio for CH/CD stretching frequencies

Reading List

- Bartell, L. S. and Roskos, R. R., Isotope effects on molar volume and surface tension; simple theoretical model and experimental data for hydrocarbons. *J. Chem. Phys.* **44**, 457 (1966)
- Cyvin S. J., *Molecular Vibrations and Mean Square Amplitudes*, Elsevier, Amsterdam, 1968
- Diehl, P. et al., eds, *Isotope Effects in NMR Spectroscopy*, Vol 22 of *NMR Basic Principles and Progress*, Springer Verlag, Berlin, 1990
- Hansen, P. E., NMR studies of isotope effects of compounds with intramolecular hydrogen bonds, in Kohen, A. and Limbach, H. H., eds, *Isotope Effects in Chemistry and Biology*, Chapter 9, CRC Press, Boca Raton, FL, 2006
- Herzberg, G., *Molecular Spectra and Molecular Structure: I. Spectra of Diatomic Molecules*, Van Nostrand-Rheinhold, New York, 1950
- Jameson, C. J., In Buncl, E. and Jones, J. R., Eds. *Isotopes in the Physical and Biomedical Sciences*, vol.2, Elsevier, Amsterdam (1991), p. 1
- Rabinovich, I. B., *Influence of Isotopy on the Physicochemical Properties of Liquids*, Consultants Bureau, New York 1970
- Van Hook, W. A. and Wolfsberg, M., Comments on H/D isotope effects on polarizabilities. Correlation with virial coefficient, molar volume and electronic second moment isotope effects. *Z. Naturforsch.* **49A**, 563 (1994)

Chapter 13

Reduced Equations of State: Critical Property Isotope Effects

Abstract In corresponding states (CS) theory the PVT properties of fluids are expressed in terms of the critical constants and one or more additional parameters. In this chapter the use of CS theory to correlate isotope effects on the physical properties of fluids is explored.

13.1 Introduction, Corresponding States

In spite of the success of corresponding states (CS) theory in describing the PVT properties of fluids, CS has only been rarely applied so far as isotope effects are concerned. In CS the temperature dependence of the molar volume and the conditions for liquid–vapor coexistence are expressed using the critical properties of the fluid and one or more additional parameters. Therefore in applying CS to isotope effects, quantization, essential to the understanding of thermodynamic IE's, is introduced in terms of the critical property IE's even though reliable critical property IE data are available for only a few isotopomer pairs. CS ignores the subtleties of molecular structure and vibrational properties and therefore cannot be expected to be as useful for rationalization of vapor pressure IE's as it is for molar density IE's. That is because the detailed theory of the VPIE (Chapter 5) shows it to depend on subtle isotopic differences in the vibrational properties of the coexisting vapor and liquid phases. The molar density IE, on the other hand, is a much simpler function of the molecular structure and overall motion in the condensed phase (Chapter 12). To anticipate, one finds this expectation to hold true. Corresponding states fits to vapor pressure IE's are not as good as those to molar density IE's, even after the empirical introduction of an additional isotope dependent parameter.

13.1.1 Equations of State, Corresponding States

In corresponding states, one selects an equation of state (EOS) (e.g., the Van der Waals equation, $P = RT/(V - b) - a/V^2$) containing three or fewer constants (a, b

and R), and uses the mathematical properties of the critical point, [$V(P,T) = f(P, T, R, a, b)$, $(dV(P, T)/dP)_C = 0$ and $(d^2V(P, T)/dP^2)_C = 0$], to express the constants in terms of critical properties P_C , $V_C = 1/\rho_C$ and T_C . The resulting master equation, $V/V_c = f(T/T_c, P/P_c)$, ($V_R = f(P_R, T_R)$), is a reduced equation of state and is universal to the extent that the PVT properties of all substances adequately described by an EOS of the chosen form lie on master curves. One hopes that CS fits to experimental data are accurate and reasonably precise over a wide range of temperature, but no current three parameter EOS satisfies this criterion to anything near experimental accuracy. Rather than abandoning the method, however, many workers have chosen to extend it by adding a fourth empirically chosen system dependent parameter (e.g. the Pitzer acentric factor, ω , selected to force agreement between calculated and observed vapor pressures at $T_R = 0.7$). The extended EOS improves agreement with experiment. The approach has proven enormously useful. To summarize, the three parameters in simple cubic equations of state (e.g. the Van der Waals equation) can be expressed in reduced form in terms of the critical properties alone, but the resulting equations are inadequate so far as fits to experimentally observed molar volumes and vapor pressure are concerned (e.g., see Fig. 13.1). Addition of a system specific fourth parameter improves matters significantly and yields “reasonable” molar volumes and vapor pressures from triple point to critical point.

Commonly encountered cubic equations of state are classical, and, of themselves, cannot rationalize IE’s on PVT properties. Even so, the physical properties of isotopomers are nearly the same, and it is likely in some sense they are in corresponding state when their reduced thermodynamic variables are the same; that is the point explored in this chapter. By assuming that isotopomers are described by EOS’s of identical form, the calculation of PVT isotope effects (i.e. the contribution of quantization) is reduced to a knowledge of critical property IE’s (or for an extended EOS, to critical property IE’s plus the acentric factor IE). One finds molar density IE’s to be well described in terms of the critical property IE’s alone (even though proper description of the parent molar densities themselves is impossible without the use of the acentric factor or equivalent), but rationalization of VPIE’s requires the introduction of an IE on the acentric factor.

13.2 Reference Systems; Critical Property Data for Some Isotopomer Pairs

13.2.1 *The PVT Surface for Isotopomer Pairs*

Extensive PVT data as well as precise values for critical property IE’s are available for $^3\text{He}/^4\text{He}$, CH_4/CD_4 , H_2/D_2 and $\text{H}_2\text{O}/\text{D}_2\text{O}$ and these isotopomer pairs comprise an excellent reference in formulating EOS analysis of PVT IE’s. Critical properties and critical property IE’s for these and a few other selected isotopomer

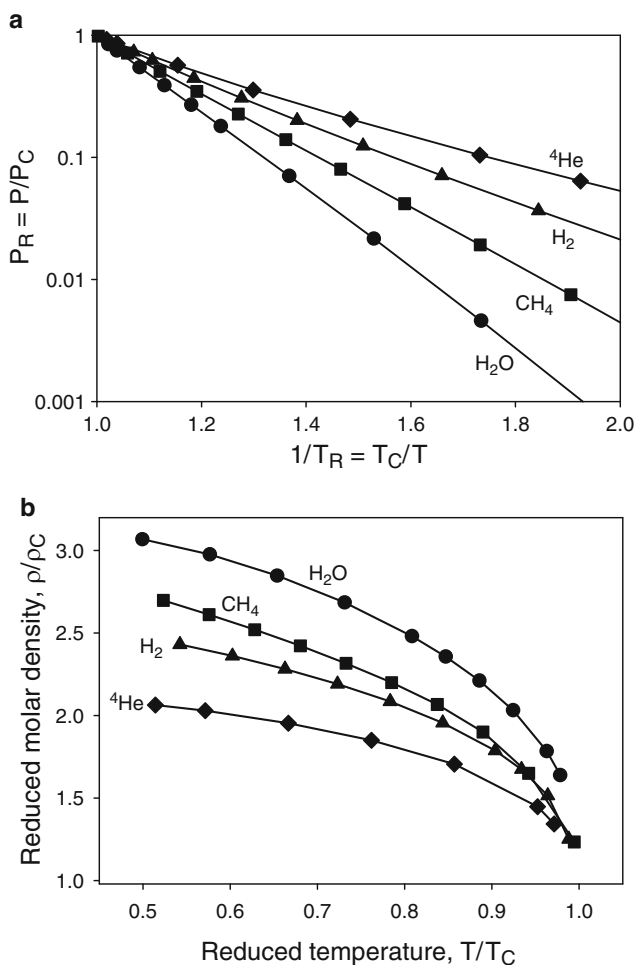


Fig. 13.1 Reduced vapor pressure and molar density vs. reciprocal reduced temperature for H_2O , CH_4 , H_2 , and ^4He . In each case, were simple corresponding states theory adequate, all data would lie on a single master curve. Using extended CS the curves are fit to acceptable precision. (a) (top) = reduced vapor pressures. (b) (bottom) = reduced liquid molar densities

pairs are collected in Table 13.1. Critical property IE's, particularly critical pressure and critical volume IE's are difficult to measure and complete data sets are available for very few pairs.

Figure 13.1a shows reduced vapor pressures and Fig. 13.1b reduced liquid molar densities for the parent isotopomers of the reference compounds. Such data can be fit to acceptable precision with an extended four parameter CS model, for example using a modified Van der Waals equation. In each case the parameters are defined in terms of the three critical properties plus one system specific parameter (e.g. Pitzer acentric factor). Were simple corresponding states theory adequate, the data for all

Table 13.1 Critical properties and critical property isotope effects for some isotopomer pairs

Reference Pairs	$^3\text{He}/^4\text{He}$	H_2/D_2	$\text{H}_2\text{O}/\text{D}_2\text{O}$	CH_4/CD_4
T_C'/K	3.34	33.19	647.096	190.6
P_C'/MPa	0.121	1.315	22.06	4.62
$10^{-3}\rho_C'/(\text{mol}/\text{m}^3)$	13.70	14.94	17.87	10.13
$[P/(\rho RT)]_C'$	0.318	0.319	0.230	0.288
$10^3 \ln(T_C'/T_C)$	-442	-144	5.0	7.4
$10^3 \ln(P_C'/P_C)$	-658	-236	18	-8.6
$10^3 \ln(\rho_C'/\rho_C)$	-236	-148	5.6	-8.1
ω	-0.39	-0.22	0.344	0.008
$10^3 \Delta\alpha/\alpha$	7	23	8	4.7
Ref.	c	c	c	d
Some other pairs ^b	$\text{C}_6\text{H}_6/\text{C}_6\text{D}_6$	$(\text{CH}_3)_2\text{CO}/(\text{CD}_3)_2\text{CO}$	$\text{CH}_3\text{OH}/\text{CH}_3\text{OD}$	HCl/DCl
T_C'/K	562.1	508.1	512.6	324.7
P_C'/MPa	4.89	4.70	8.1	8.47
$10^{-3}\rho_C'/(\text{mol}/\text{m}^3)$	3.86	4.78	8.47	12.3
$\ln(T_C'/T_C)$	2.5	4.2 ^a	4.2 ^a	3.9
$\ln(P_C'/P_C)$	9.2 ^a	12.5 ^a	16 ^a	-3.1
$\ln(\rho_C'/\rho_C)$	5.8 ^a	7.3 ^a	9 ^a	8.2 ^a
ω	0.212	0.309	0.559	0.120
$\Delta\alpha/\alpha$	1.1	1.9	6.7	23
Ref.	e	e	e	f

^aCalculated from correlations in Fig. 13.3 and Equations 13.3 and 13.4.

^bOther isotopomer pairs with information on some critical property IE's include H_2/HD , H_2/T_2 , $\text{H}_2^{16}\text{O}/\text{H}_2^{18}\text{O}$, $\text{H}_2\text{S}/\text{D}_2\text{S}$, $\text{H}_2\text{Se}/\text{D}_2\text{Se}$, NH_3/ND_3 , PH_3/PD_3 , $\text{AsH}_3/\text{AsD}_3$, $^{14}\text{N}_2/^{15}\text{N}_2$, HBr/DBr , HI/DI , $\text{CHCl}_3/\text{CDCl}_3$, $\text{CH}_3\text{COOH}/\text{CH}_3\text{COOD}$, $\text{C}_2\text{H}_4/\text{C}_2\text{D}_4$, and ethyl, *n*-propyl, *i*-propyl, *i*-butyl, *i*-butyl and *s*-butyl alcohols(-OH/-OD)^g.

^cLandolt-Bornstein. *Zahlenwerte und Funktionen*. Springer Verlag, Heidelberg **IV** (1967) 316 and ff, **IV** (1971)632 ff.

^dGrigor, A. and Steele, W. A., *J. Chem. Phys.* **48**, 1032 (1968); **48**, 1038 (1968).

^eKooner, Z. and Van Hook, W. A. *J. Phys. Chem.* **92**, 6414 (1988).

^fHenderson, C., et al., *J. Chem. Thermodyn.* **18**, 1077 (1986).

^gRabinovitch, I. B., *Influence of isotopy on the physicochemical properties of liquids*. Consultants Bureau, New York, 1970.

four substances would lie on a single master curve. Figure 13.1b diagrams the conditions for liquid-vapor coexistence on the (T_R, ρ_R) plane. A (T_R, ρ_R) plot is much preferred to a (T_R, V_R) plot because vapor densities nicely approach zero in the low temperature, low pressure limit. The average density, $(\rho_V + \rho_L)/2$, is called the rectilinear diameter and is approximately linearly dependent on temperature. The vapor pressure curves (Fig. 13.1a), nearly linear in $\ln P_R$ vs $1/T_R$ space, are fit to good precision with quadratic expressions, $\ln P = A + B/T_R + C/T_R^2$. As for the liquid molar densities there is marked system dependence.

13.2.2 IE's of Reference Pairs

The effect of isotopic substitution on the vapor pressure and molar volume of the reference pairs is shown schematically in Fig. 13.2. $P(\text{D}_2\text{O}) < P(\text{H}_2\text{O})$ at low temperature, but as T increases the curves eventually cross, and $P(\text{H}_2\text{O}) < P(\text{D}_2\text{O})$ when the VP curve ends for D_2O at its critical point (21.7 MPa, 643.9 K). The critical point for H_2O is at higher pressure and temperature (22.1 MPa, 647.1 K,

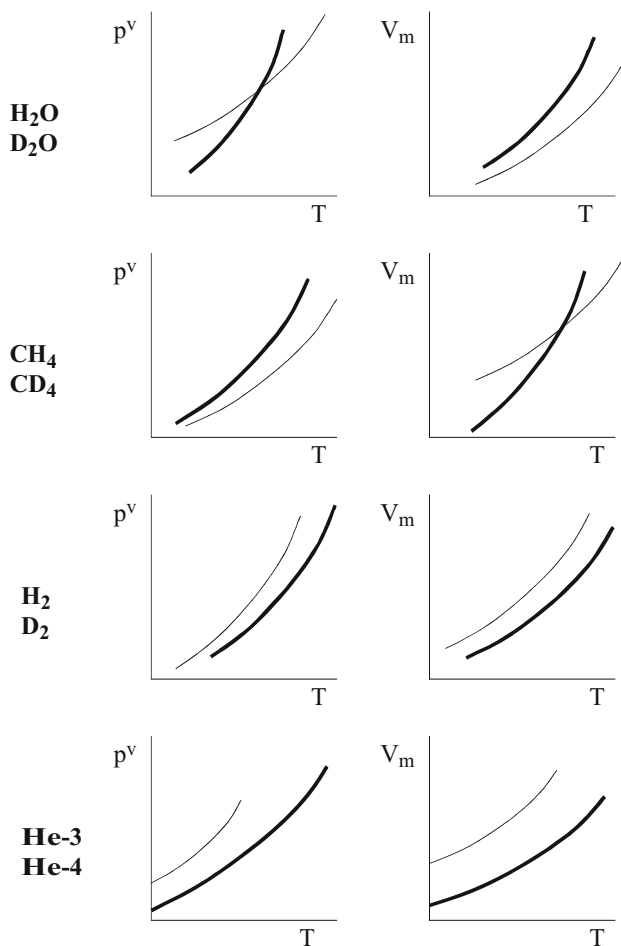


Fig. 13.2 Vapor pressures (P^V, T) and liquid molar volumes (V_m, T) along the orthobaric LV equilibrium line for reference isotopomer pairs, showing their distinctly different behaviors (schematic). The *thicker lines* label the heavier isotopomers. The curves begin at the triple points and end at the critical points (except for He which has no triple point under orthobaric conditions). Not to scale, isotopic differences are exaggerated (Reprinted from Van Hook, W. A., Rebelo, L. P. N. and Wolfsberg, M., *Fluid Phase Equilib.* **257**, 35 (2007), copyright 2007, with permission from Elsevier)

Table 13.1). In the solid $P(\text{CH}_4) > P(\text{CD}_4)$ but the curves cross below the melting point and the vapor pressure IE for the liquids is inverse ($P_D > P_H$). For water and methane $T_C' > T_C$, but for water $P_C' > P_C$ and for methane $P_C' < P_C$. As always, the primes designate the lighter isotopomer. At LV coexistence $\rho_{\text{LIQ}}(\text{D}_2\text{O}) < \rho_{\text{LIQ}}(\text{H}_2\text{O})$ at all temperatures (remember the ρ 's are molar, not mass, densities). For methane $\rho_{\text{LIQ}}(\text{CD}_4) < \rho_{\text{LIQ}}(\text{CH}_4)$ only at high temperature. At lower temperatures $\rho_{\text{LIQ}}(\text{CH}_4) < \rho_{\text{LIQ}}(\text{CD}_4)$. The critical density of H_2O is greater than D_2O , but for methane $\rho_C(\text{CH}_4) < \rho_C(\text{CD}_4)$. Isotope effects are large in the hydrogen and helium systems and $\rho_{\text{LIQ}}' < \rho_{\text{LIQ}}$ and $P' > P$ across the liquid range. $P_C' < P_C$ and $\rho_C' < \rho_C$ for both pairs. Vapor pressure and molar volume IE's are discussed in the context of the statistical theory of isotope effects in condensed phases in Chapters 5 and 12, respectively. The CS treatment in this chapter offers an alternative description.

13.2.3 PVT Isotope Effects and the Modified Van der Waals Equation

In CS one selects an appropriate equation of state (EOS), expresses the parameters in terms of critical properties so far as possible, and fits the result to experimental data to define a minimum set of system specific parameters. A recent example used a modified form of the reduced Van der Waals equation

$$P_R = [4\alpha/(\alpha^2 - 1)][T_R/(V_R - (\alpha - 1)/(\alpha + 1))] - [(\alpha + 1)/(\alpha - 1)]/[V_R^\alpha T_R^\gamma] \quad (13.1)$$

In Equation 13.1 the Van der Waals “a” and “b” parameters are $a = RT_C b^{(\alpha-1)} [4\alpha/(\alpha^2 - 1)][(\alpha - 1)/(\alpha + 1)]^\alpha$ and $b = [(\alpha - 1)/(\alpha + 2)]V_C$, respectively, and α and γ are system dependent parameters selected by numerically fitting Equation 13.1 to PVT data of the parent compounds. That process yields $\alpha = 1.913 - 0.791\omega + 0.969\omega^2$ and $\gamma = 2.44 - 1.06\alpha$. Here ω is the Pitzer acentric factor which has been tabulated for a large number of parent isotopomers, or which can be obtained from their vapor pressures near the normal boiling point. The equation thus reduces to a four parameter representation of the PVT properties of the fluid being fitted (i.e. the three critical properties plus the Pitzer acentric factor). The quality of agreement is satisfactory for the present purpose, calculation and experiment agree to within a few percent. Fits to the unmodified VdW EOS are system independent and display molar density differences, calculated-to-experiment, of 20–50% or even more. The addition of the system dependent acentric parameter improves that by about an order of magnitude.

13.2.4 Reference Systems, Isotope Effects

Molar volume and vapor pressure IE's may be calculated as $f(T_R)$ using critical parameters and their isotope effects (Table 13.1) assuming no IE on the system de-

pendent parameter α , $\Delta\alpha/\alpha = 0$. The results can be compared with ones which force agreement for the VPIE at $T_R' = 0.5$ by ad hoc adjustment of $\Delta\alpha/\alpha$. In either case the agreement between calculated and observed molar density IE's is acceptable. Molar density IE's are not sensitive to $\Delta\alpha/\alpha$, but for vapor pressure IE's setting $\Delta\alpha/\alpha = 0$ is wildly inadequate.

Solutions in hand for the reference pairs, it is useful to write out empirical smoothing expressions for the rectilinear densities, reduced density differences, and reduced vapor pressures as functions of T_R and α , following which prediction of reduced liquid densities and vapor pressures is straightforward for systems where $T_{C'}$ and α (equivalently ω) are known. If, in addition, the critical property IE's, $\ln(T_{C'}/T_C)$, $\ln(P_{C'}/P_C)$, and $\ln(\rho_{C'}/\rho_C)$, are available from experiment, theory, or empirical correlation, one can calculate the molar density and vapor pressure IE's for $0.5 < T_R' < 1$, provided, for VPIE, that $\Delta\alpha/\alpha$ is known or can be estimated. Thus to calculate liquid density IE's one uses the observed IE on T_C , $\ln(T_{C'}/T_C)$, to find $\ln(T_R'/T_R)$ at any temperature of interest, and employs the smoothing relations (or numerically solves Equation 13.1) to obtain (ρ_R'/ρ_R) . Since $(M\rho IE)_R = \ln(\rho_R'/\rho_R) = \ln[(\rho'/\rho_{C'})/(\rho/\rho_C)]$ it follows that $\ln(\rho'/\rho)(M\rho IE)_R + \ln(\rho_{C'}/\rho_C)$. For VPIE's one proceeds similarly, substituting reduced temperatures, critical pressures and $\Delta\alpha/\alpha$ into the smoothing equations to find $\ln(P'/P)_{RED}$ and thence $\ln(P'/P)$, since $\ln(P'/P) = \ln(P_R'/P_R) + \ln(P_{C'}/P_C)$. The approach outlined for molar density IE cannot be used to rationalize the vapor pressure IE without the introduction of isotope dependent system parameters $\Delta\alpha/\alpha$.

13.3 Critical Property Isotope Effects

13.3.1 Experimental Data

Careful literature review reveals only limited data on critical property IE's. A sampling of the few data which are available is found in Table 13.1. Thus, for many systems, calculation of IE's using CS may first require theoretical estimation of critical property IEs and/or empirical correlation of critical property IEs with other properties. Examples are discussed in Section 13.3.2. First, however, two qualitative observations are useful. (1) If in the neighborhood of T_C VPIE is normal, $\ln(P'/P) > 0$, the lighter isotopomer will have a lower critical temperature than the heavier, $T_{C'} < T_C$ (the inequality is opposite for $\ln(P'/P) < 0$). All known systems meet this constraint. For monatomic systems $\ln(P'/P) > 0$ necessarily, so $T_{C'} < T_C$. In contrast, polyatomics generally (but not always), show inverse vapor pressure IE's near T_C , and this is increasingly true for larger molecules. Hence, one expects $T_{C'} > T_C$. (2) The critical pressure IE, ΔP_c , and the critical density isotope effect, $\Delta\rho_c$, should have the same signs, because near T_C the molar density is mainly pressure controlled due to the very large compressibility of the fluid in that region.

13.3.2 Correlations Between Critical Property and Vapor Pressure IE's: $\ln(T_c'/T_c)$ and $\ln(P'/P)$

Figure 13.3 reports a good quality correlation between the critical temperature IE, $\ln(T_c'/T_c)$, and the vapor pressure IE near the critical temperature, say $T_R' = 0.975$. The choice $T_R' = 0.975$ is arbitrary. Other reduced temperatures near $T_R' = 1$ would have served, but at lower T_R' the quality of fit deteriorates. Data for those isotopomer pairs with $T_c' > \sim 50$ K or so (i.e. all pairs except hydrogen and helium), lie close to (0,0). They are plotted using an expanded scale in the insert. The correlation line through the (presumably) more reliable high temperature data [$-0.01 < \ln(T_c'/T_c) < 0.01$] = $-0.0034 - 0.3443 \ln(P'/P)_{0.975}$], is in excellent agreement with the overall correlation in the main figure, $\ln(T_c'/T_c) = -0.0032 - 0.3805 \ln(P'/P)_{0.975}$.

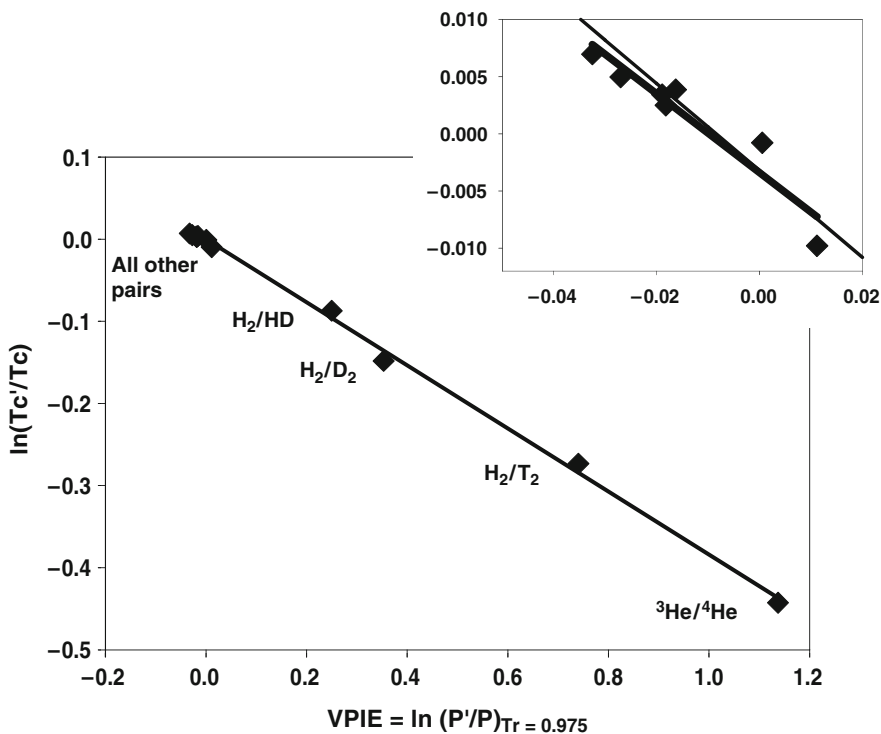


Fig. 13.3 The correlation of $\ln(T_c'/T_c)$ with $\ln(P'/P)$ at $T_R' = 0.975$. The correlation line in the main figure is: $\ln(T_c'/T_c) = -0.0032 - 0.3805 \ln(P'/P)_{0.975}$, $r^2 = 0.998$. The insert enlarges the data near (0,0). In the insert the *heavy line* replots the correlation in the main figure, the *lighter line* shows the correlation through the data in the insert (Reprinted from Van Hook, W. A., Rebelo, L. P. N. and Wolfsberg, M., *Fluid Phase Equilib.* **257**, 35 (2007), copyright 2007, with permission from Elsevier)

Correlating $\ln(P_c'/P_c)$, with vapor pressure data: For isotopomer pairs with the vapor pressure and VPIE established near T_c , a thermodynamic consistency test between $\ln(T_c'/T_c)$ and $\ln(P_c'/P_c)$, and calculation of $\ln(P_c'/P_c)$ from $\ln(T_c'/T_c)$ is possible. The critical pressure of the heavier isotopomer at its critical temperature, $P_c(T_c)$, can be calculated from the lighter, $P_c'(T_c')$, provided the vapor pressure of the lighter between T_c' and T_c , the VPIE, and T_c' and T_c are known. For $T_c < T_c'$

$$\ln(P(T_c)) = \ln(P'(T_c')) + \int (d \ln(P')/dT)dT - \ln(P'/P)_{T_c}. \quad (13.2)$$

Rearranging,

$$\ln(P_c'/P_c) = \ln(P'(T_c')/P(T_c)) = - \int (d \ln(P')/dT)dT + \ln(P'/P)_{T_c} \quad (13.3)$$

The integrals extend over the narrow range, T_c' to T_c . Also $d \ln(P')/dT$ is available to sufficient accuracy from vapor pressure data but is not required at high precision because the range of the integration is short.

Estimating the critical density IE, $\ln(\rho_c'/\rho_c)$: No consistency test is available for $\ln(\rho_c'/\rho_c)$, but for the original Van der Waals equation and the modified VdW equations discussed in this chapter the critical compressibility factors, $Z_c(\text{VdW}) = P_c/(\rho_c RT_c)$, are equal to $3/8$ and $(\alpha^2 - 1)/(4\alpha)$, respectively. In the latter case,

$$- \Delta \rho_c / \rho_c = -\Delta P_c / P_c + \Delta T_c / T_c + [(\alpha^2 + 1)/(\alpha^2 - 1)](\Delta \alpha / \alpha) \quad (13.4)$$

For the unmodified VdW equation $-\Delta \rho_c / \rho_c = -\Delta P_c / P_c + \Delta T_c / T_c$.

13.3.3 Uncertainties in Critical Property IE's

The experimental precision establishing $\ln(T_c'/T_c)$ is almost always better than that for $\ln(P_c'/P_c)$, and very much better than $\ln(\rho_c'/\rho_c)$ (which, in any case, is known for very few isotopomer pairs). Usually $\ln(P'/P)_{T_c}$ is negative and small (a few percent or less), and the first term on the right in Equation 13.4 usually positive and small, ($\ln(T_c'/T_c)$ is most often positive). Consequently the calculated value of $\ln(P_c'/P_c)$ is smaller in magnitude than either of these, and often cannot be reliably established. For isotopomer pairs (excluding hydrogen and helium) the uncertainty is reasonably estimated as $\delta \Delta T_c / T_c \sim 0.001$, except for $\text{H}_2\text{O}/\text{D}_2\text{O}$ which is better known, ~ 0.0005 . Equation 13.3 thus claims $\delta(\Delta P_c / P_c) / (\Delta P_c / P_c) \geq \delta(\Delta T_c / T_c) / \Delta T_c / T_c$. Finally $\delta \Delta \rho_c / \rho_c$ is much, much more difficult to measure and experimental uncertainty here is much higher, say between $\delta \Delta \rho_c / \rho_c = 0.005$ and 0.01 .

Using the correlations in Fig. 13.3 and Equations 13.3 and 13.4, one can estimate $\ln(P_c'/P_c)$ and $\ln(\rho_c'/\rho_c)$ from $\ln(T_c'/T_c)$ and near critical values of VPIE. That information in hand, the modified Van der Waals EOS yields $\ln(\rho'/\rho)$ across the coexistence range ($\sim 0.5 < T_R < 1$). This is a very useful result: few data are available for $\ln(\rho'/\rho)$, except near room temperature, and experimental programs to

expand the data base are difficult, expensive, and tedious to implement. Corresponding states analysis offers an attractive alternative.

13.4 CS Calculations for Some Isotopomer Pairs

The method described above can be applied to isotopomer pairs for which critical property IE data exists or can be estimated. Calculated values of $\ln(\rho'/\rho)$ are insensitive to IE's on the acentric factor, $\Delta\omega/\omega$ (equivalently $\Delta\alpha/\alpha$). The VPIE, on the other hand, is strongly dependent on $\Delta\omega/\omega$. For $^3\text{He}/^4\text{He}$ and H_2/D_2 critical property IE data are complete and $M\rho\text{IE}$ and VPIE are available across the entire liquid range, are one to two orders of magnitude larger, and known to better precision than for other pairs (save perhaps $\text{H}_2\text{O}/\text{D}_2\text{O}$). For heavier pairs critical property IE data are usually incomplete or uncertain, and often data on $M\rho\text{IE}$ and VPIE exist only over a limited temperature range.

13.4.1 The Lighter Pairs

13.4.1.1 $^3\text{He}/^4\text{He}$

Critical property IE's are large. Figure 13.4a compares experimental VPIE's with calculations. On this scale calculation and experiment cannot be distinguished. To find VPIE from the calculated reduced IE's one adds the observed or correlated values for $\ln(P_c'/P_c)$, i.e. $\ln(P'/P) = \ln(P'/P)_{\text{RED}} + \ln(P_c'/P_c)$. The cross-hatched line shows calculated results choosing $\Delta\alpha/\alpha = 0$. For helium the $\Delta\alpha/\alpha$ dependence is small. This observation partly carries over to the hydrogens. It is a consequence of large critical property IE's for these very light molecules. For heavier pairs, however (see below), critical property IE's are smaller, and EOS vapor pressure IE's (but not liquid molar density IE's) are sensitive to $\Delta\alpha/\alpha$. Calculated and experimental liquid molar density IE's for $^3\text{He}/^4\text{He}$ are shown in Figure 13.4(b). The agreement is excellent.

13.4.1.2 Hydrogen

Figure 13.4a shows calculated VPIE's for H_2/D_2 using observed and correlated critical property IE's. The fits are in excellent agreement, superposing on the scale of the figure, and with observation. The cross-hatched line refers to H_2/D_2 choosing $\Delta\alpha/\alpha = 0$. It is in progressively worse agreement with experiment as temperature falls and establishes the need to postulate an isotope dependent α . Figure 13.4b compares calculated and experimental liquid molar density IE data. The agreement is excellent.

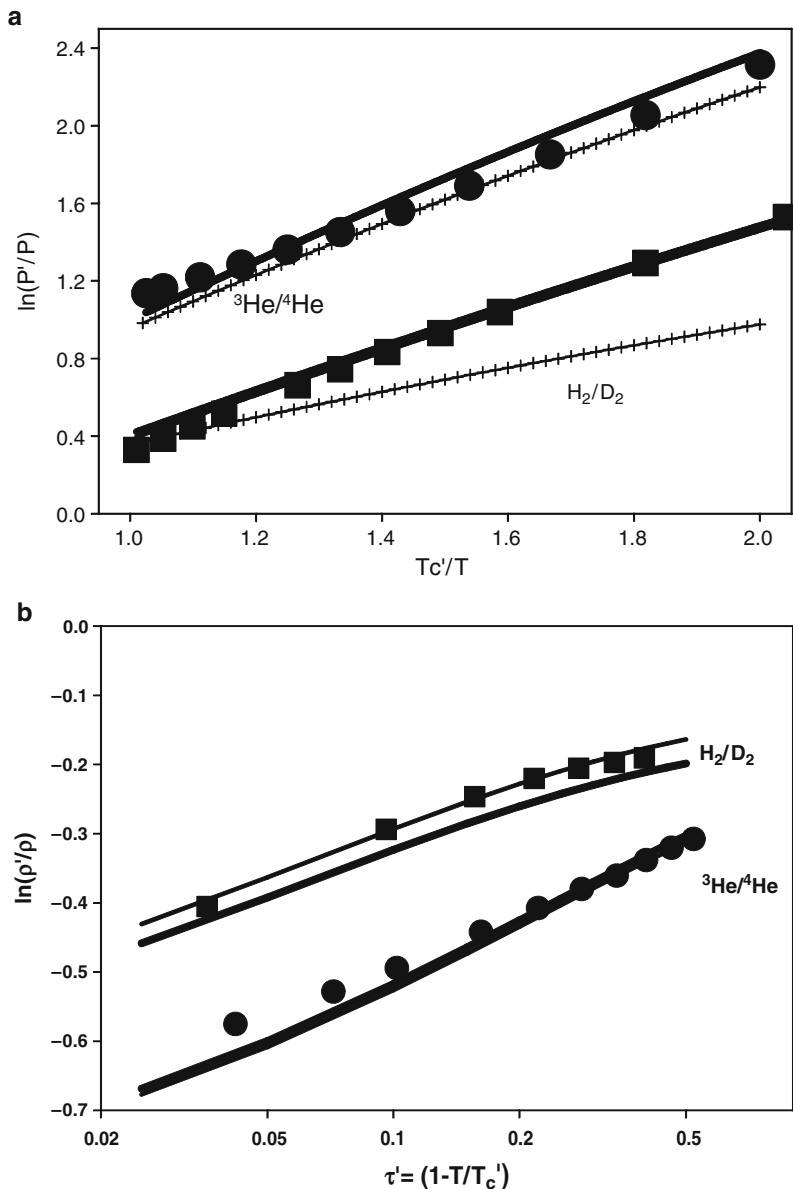


Fig. 13.4 CS calculations for ${}^3\text{He}/{}^4\text{He}$ and H_2/D_2 . Points are experimental, lines calculated. *Heavy lines* use observed critical property IE's and non-zero $\Delta\alpha/\alpha$ (see text). *Lighter lines* employ correlated critical property IE's and non-zero $\Delta\alpha/\alpha$. The *cross-hatched lines* set $\Delta\alpha/\alpha = 0$. (a) (Upper) VPIE's. For ${}^3\text{He}/{}^4\text{He}$ and H_2/D_2 lines based on observed and correlated critical property IE's cannot be distinguished on the scale of the figure. (b) (Lower) molar density isotope effects. For both ${}^3\text{He}/{}^4\text{He}$ and H_2/D_2 *cross-hatched lines* assuming $\Delta\alpha/\alpha = 0$ nearly coincide with the *heavy solid lines* and are not plotted (Reprinted from Van Hook, W. A., Rebelo, L. P. N. and Wolfsberg, M., *Fluid Phase Equilib.* **257**, 35 (2007), copyright 2007, with permission from Elsevier)

13.4.2 VdW1 Parameters for Heavier Pairs

Most data on VPIE's for heavier pairs are at or below the normal boiling point, $T_R \sim 0.7$. Of the critical property IE's, $\ln(T_c'/T_c)$ is the easiest to measure and the most reliably known. Often $\ln(P_c'/P_c)$, and very often $\ln(\rho_c'/\rho_c)$, are unknown or imprecisely known, and $\ln(\rho'/\rho)$ has been measured only at or near room temperature or must be estimated.

13.4.2.1 Water

VPIE's of H_2O/D_2O and LV fractionation factors for H_2O/HOD and $H_2O/H_2^{18}O$ have been carefully measured and thoroughly interpreted over the complete coexistence range. Data for H_2O/T_2O and intermediate isotopomer pairs are limited to lower temperatures. Liquid molar density IE data are complete for H_2O/D_2O . Departures from the law of geometric mean are small and the liquid molar density IE for H_2O/HOD is available to good precision. At low temperature, $\ln(\rho'/\rho)$ for H_2O/D_2O (and presumably for the other water isotopomer pairs) shows a minimum which has been ascribed to H-bonding ("water-structure effects").

Figure 13.5a compares calculated and experimental VPIE's for H_2O/D_2O . Experiment and calculation overlap within the combined uncertainties. The thin line through the small circles in Fig. 13.5a represents VdW1 choosing $\Delta\alpha/\alpha = 0$. It departs radically from experiment, but the corresponding calculated liquid molar density IE's are insensitive to the choice of $\Delta\alpha/\alpha$. Therefore the corresponding states treatment is most useful for analysis of molar density IEs because it avoids the necessity of introducing a fourth isotope sensitive parameter, $\Delta\omega/\omega$ (equivalently $\Delta\alpha/\alpha$).

13.4.2.2 Methane

Figures 13.5a and b include comparisons of CS calculations for CH_4/CD_4 with experiment. The calculated values for $\ln(P'/P)$ lie within 0.01 unit of experiment and within the uncertainty corresponding to the experimental error on T_c IE (± 0.001). Figure 13.5b shows good agreement between CS modified VdW calculations and experiment for liquid molar density IE's.

13.5 Remarks

A CS treatment of liquid phase molar densities, liquid M ρ IE's, and vapor pressures and VPIE's has been described. Quantization, necessary for the proper treatment of thermodynamic isotope effects, was introduced by using measured or correlated IE's on critical temperature, $\Delta T_c = T_c' - T_c$, critical pressure, $\Delta P_c = P_c' - P_c$, and criti-

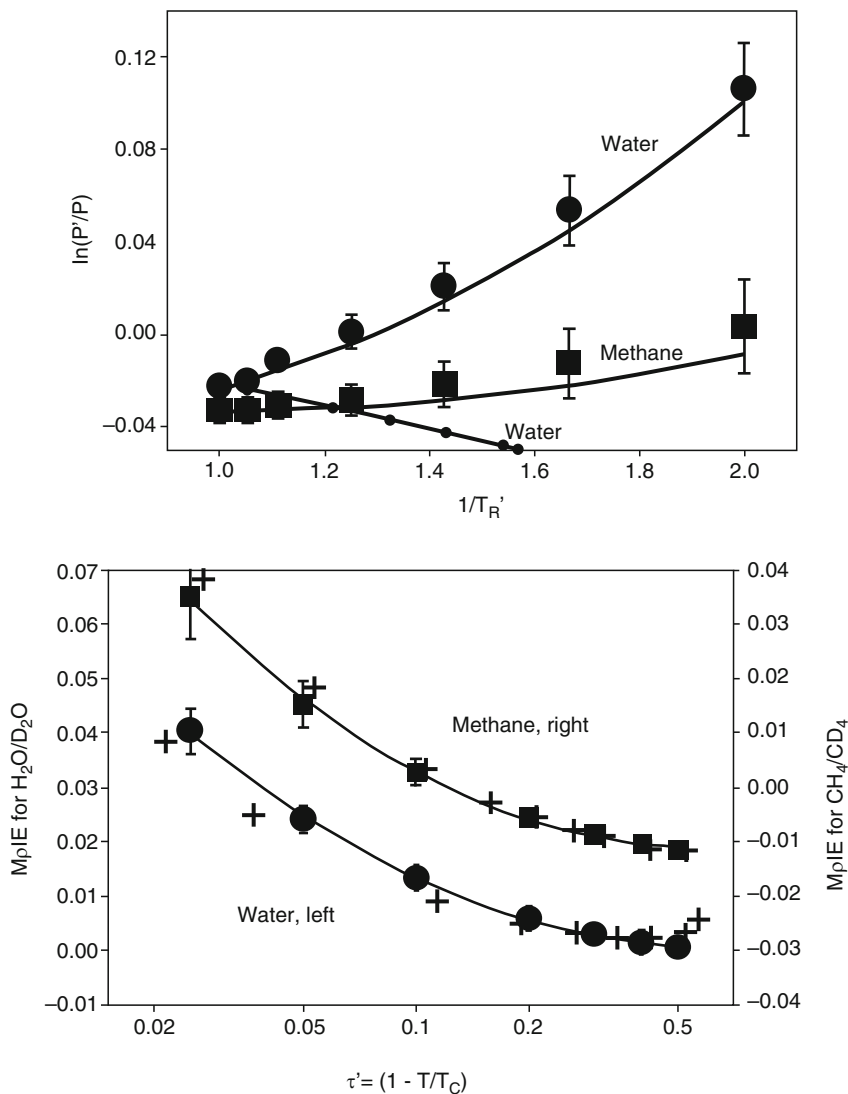


Fig. 13.5 (a) CS calculated VPIE's for H₂O/D₂O and CH₄/CD₄. The *lines* represent experiment, the *points* are calculated using critical point IE's and non-zero $\Delta\alpha/\alpha$ from Table 13.1 The *thin line* through the *small dots* at the bottom shows VdW1 for H₂O/D₂O choosing $\Delta\alpha/\alpha = 0$ Error bars for water are equivalent to an uncertainty in TCIE = 0.0005, and for methane 0.001. (Reprinted from Van Hook, W. A., Rebelo, L. P. N. and Wolfsberg, M., *Fluid Phase Equilib.* **257**, 35 (2007), copyright 2007, with permission from Elsevier). (b) CS calculated liquid molar density IE's of H₂O/D₂O and CH₄/CD₄ compared with experiment. The *heavy black crosses* represent the experimental data. The *large points* and the correlation lines represent calculations using observed critical property IE's and non-zero $\Delta\alpha/\alpha$ from Table 13.1 (Reprinted from Van Hook, W. A., Rebelo, L. P. N. and Wolfsberg, M., *Fluid Phase Equilib.* **257**, 35 (2007), copyright 2007, with permission from Elsevier)

cal density, $\Delta\rho_c = \rho_c' - \rho_c$. For that purpose methods to predict critical property IE's were developed. For most isotopomer pairs some critical property IE's are unknown, so this step is critically important. Calculated liquid $M\rho$ IE's based on critical property IE's alone agree reasonably well with experiment, but rationalization of VPIE's requires a parametric introduction of an IE on the acentric factor. The CS approach is less useful for the description of vapor pressure than liquid molar density IE's. That result is expected because the detailed molecular theory of condensed phase isotope effects (Chapter 5) shows that VPIE is related to subtle isotopic differences on the vibrational frequencies of the coexisting vapor and liquid phases. Liquid molar densities, on the other hand, are a much simpler function of the molecular structure and hindered motion in the condensed phase (Chapter 12). The application of CS theory to PVT isotope effects is particularly useful. This is because complete good quality critical property IE and PVT data are available for only a very few isotopomer pairs, and experimental measurements to generate complete data sets for more pairs are tedious and expensive.

Further Reading

- Hirschfelder, J. O., Curtiss, C. F., Bird, R. B., *Molecular Theory of Gases and Liquids*, Wiley, New York, 1954.
- V. B. Polyakov, V. B., Horita, J., Cole, D. R. and Chialvo, A. A. Novel corresponding-states principle approach for the equation of state of isotopologues: H_2^{18}O as an example. *J. Phys. Chem. B*-**111**, 393 (2007).
- Prausnitz, J. M. *Molecular Thermodynamics of Fluid Phase Equilibria*, Prentice Hall, Englewood Cliffs, NJ, 1969.
- Rabinovitch, I. B. *Influence of isotopy on the physicochemical properties of liquids*. Consultants Bureau, New York, 1970.
- Van Ness, H. C., Abbott, M. M., *Classical Thermodynamics of Nonelectrolyte Solutions*, McGraw-Hill, New York. 1982.
- Van Hook, W. A., Rebelo, L. P. N. and Wolfsberg, M. Isotope effects on VLE properties of fluids and corresponding states: critical point shifts on isotopic substitution. *Fluid Phase Equilib.* **257**, 35 (2007).

Chapter 14

Isotope Effects in Unimolecular Processes: “Mass Independent” Isotope Fractionation and the Ozone Problem

Abstract The theoretical framework needed for interpretation of kinetic isotope effects on unimolecular reactions is reviewed. Application to the satisfactory rationalization of the theoretically puzzling “mass independent isotope effect” observed for oxygen isotope fractionation in extraterrestrial samples is described.

14.1 Introduction: Isotope Effects in Unimolecular Reactions

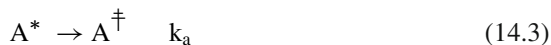
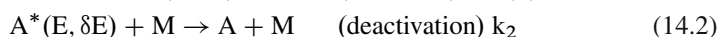
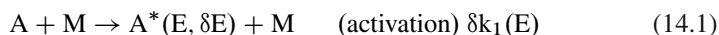
As is implied by the name, a unimolecular reaction is one in which a single molecule of reactant decomposes or rearranges to give rise to product molecules. Ordinary thermal reactions can be modeled by a process which considers the reactant to be in thermal equilibrium with a transition state which then decomposes (rearranges) to give products. One can theoretically describe the process and its isotope effects using transition state theory. For unimolecular reactions, on the other hand, while there is still a transition state, it is not in thermal equilibrium with the reactant except for systems at high pressure. Consequently, a more elaborate theoretical framework is required to understand unimolecular reactions and their isotope effects.

In the following section, the RRKM mechanism for gas phase unimolecular reactions will be introduced and the corresponding theoretical framework, including isotope effects, will be outlined. Subsequent sections will deal with some applications of this theoretical framework to systems which have been studied experimentally.

The last parts of this chapter will deal with the so-called mass independent isotope effects which have been rationalized in recent years to be a consequence of unimolecular processes and which have become one of the most fascinating of present day isotope effect studies.

14.2 The RRKM Mechanism for Unimolecular Gas Phase Reactions

The RRKM mechanism of unimolecular reactions is based on the recognition almost simultaneously by Lindemann (already mentioned in Chapters 1 and 5) and the Danish chemist Christiansen that a unimolecular process in a thermal reaction first requires excitation of the reacting molecule through collision processes. The development of the mechanism is a fascinating story and benefited from the input of a number of distinguished physical chemists, among them Rice, Ramsberger, Kassel, and Marcus whose initials (RRKM) have been used as the name of the theory. For details reference should be made to the book by Holbrook, Pilling, and Robertson which is listed in the suggested additional reading at the end of this chapter. The scheme follows



Here A is the molecule undergoing the unimolecular reaction, $A^*(E, \delta E)$ is a vibrationally/rotationally excited A molecule with excitation energy between E and $E + \delta E$ and A^\ddagger is the transition state which decomposes or rearranges to yield product(s). M is a molecule (or atom) which collides with A and serves to transfer energy to/from A. Under some circumstances, M may be another A molecule. Equation 14.3 is constant energy process between a properly energized A molecule, having sufficient energy E_0 (measured from the ground vibrational state of A to the ground state of A^\ddagger) to form the transition state molecule A^\ddagger . E_0 is sometimes referred to as the activation energy.

The formation of the transition state from the excited molecule is referred to as a microcanonical process, while the formation of the transition state in conventional TST in Chapter 4 and in VTST in Chapter 6 is referred to as canonical process. The terms “microcanonical” and “canonical” in statistical mechanics refer respectively to processes at constant energy and processes at constant temperature.

The rate constants δk_1 , k_2 , k_a , k_3 in the equations above have meaning; for example, Equation 14.1 means

$$-\frac{d[A]}{dt} = \delta k_1(E)[A][M] = \frac{d[A^*(E, \delta E)]}{dt} \quad (14.5)$$

Here [A] is the concentration of A, and t refers to time. $\delta k_1(E)$ is a differential rate coefficient for the reaction in which a molecule is excited to an energy between E and $E + \delta E$. Thus, Equation 14.5 is the equation for the rate of appearance of A^* molecules with energy between E and $E + \delta E$.

In dealing with a complex reaction scheme as the one indicated above, one frequently introduces a so-called “steady state approximation” for reactive intermediates in order to find simplified rate laws (see, for example, Section 11.2). This approximation is usually sufficiently valid to give rise to useful results; most physical chemistry texts discuss and use this application. In the steady state approximation for A^* , one writes

$$\frac{d[A^*(E, \delta E)]}{dt} = \delta k_1(E)[A][M] - k_2[A^*][M] - k_a(E)[A^*] = 0 \quad (14.6)$$

After some rearranging, this equation yields the following result for $[A^*]$,

$$[A^*(E, \delta E)] = \frac{\left(\frac{\delta k_1(E)}{k_2}\right)[A]}{1 + \frac{k_a(E)}{k_2[M]}} \quad (14.7)$$

As for the transition state in the conventional TST of Chapter 4, the transition state A^\ddagger here is in chemical equilibrium with A^* , albeit at constant energy (microcanonical). Also A^\ddagger has one degree of freedom which replaces the imaginary vibration along the reaction path by a translation as is assumed in conventional TST in Chapter 4. This translational motion of the transition state leads to two A^\ddagger species, one corresponding to motion towards products, which will be designated $\overrightarrow{A}^\ddagger$ and the other corresponding to motion back to A^* designated $\overleftarrow{A}^\ddagger$. Each of the two species is equally probable and the total concentration of A^\ddagger is equal to their sum. The steady state assumption for A^\ddagger then yields

$$0 = \frac{d[A^\ddagger]}{dt} = k_a(E)[A^*] - k_3[\overleftarrow{A}^\ddagger] \quad (14.8)$$

$$= k_a[A^*] - \frac{1}{2}k_3[A^\ddagger] \quad (14.9)$$

Consequently,

$$k_a(E)[A^*] = \frac{1}{2}k_3[A^\ddagger] \quad (14.10)$$

and

$$k_a = \frac{1}{2}k_3 \left(\frac{[A^\ddagger]}{[A^*]} \right)_{\substack{STEADY \\ STATE}} = \frac{1}{2}k_3 \left(\frac{[A^\ddagger]}{[A^*]} \right)_{EQ} \quad (14.11)$$

Equation 14.11 explicitly contains the equilibrium assumption of transition state theory, i.e. that the transition state and the excited molecules are in chemical equilibrium.

The unimolecular rate constant k_{uni} is defined

$$\frac{-1}{[A]} \frac{d[A]}{dt} = k_{\text{uni}} \quad (14.12)$$

Appropriate use of Equation 14.12 leads to

$$\begin{aligned} k_{\text{uni}} &= \frac{1}{[A]} \frac{d[\text{products}]}{dt} = \frac{1}{2} k_3 \frac{[A^\ddagger]}{[A]} = k_a(E) \frac{[A^*]}{[A]} \\ &= \frac{k_a(E) \left(\frac{\delta k_1(E)}{k_2} \right) [A]}{1 + \frac{k_a(E)}{k_2 [M]}} \end{aligned} \quad (14.13)$$

It should be noted, and will be further discussed later, that the definition of k_{uni} in Equation 14.13 does not mean that the reaction is a first order reaction. A first order reaction would imply that k_{uni} is independent of concentration. As indicated by Equation 14.13, k_{uni} depends on the concentration of the “third body” M with which A collides for activation and deactivation. For $k_2 [M]$ much larger than k_a , which means high pressure, k_{uni} does indeed become independent of concentration. At low pressure, however, k_{uni} depends on $[M]$ and the overall rate of making products becomes second order, depending linearly on both $[M]$ and $[A]$.

The rate coefficient k_{uni} reflects the unimolecular reaction initiated by exciting reactant molecules to an energy between E and $E + \delta E$. As already noted, there is a minimum excitation energy E_0 required to proceed with reaction, usually called the activation energy, E_0 and all energies from E_0 to ∞ will be assumed to lead to reaction. Thus, the over-all k_{uni} is found by integrating Equation 14.13 to yield

$$k_{\text{uni}} = \int_{E=E_0}^{E=\infty} \frac{k_a(E) \left(\frac{dk_1(E)}{k_2} \right)}{1 + \frac{k_a(E)}{k_2 [M]}} \quad (14.14)$$

In the last equation, δk_1 has been replaced by $dk_1(E)$ for excitation to energies between E and $E + dE$ to indicate that the range of energy can be chosen sufficiently small so that it may be used as a differential.

In the following sections, the rate coefficients $dk_1(E)/k_2$, k_a , and k_3 will be further explored to enable the calculation of k_{uni} and isotope effects thereon from first principles, and the high pressure and low pressure limits of k_{uni} will be explored in more detail.

14.2.1 The Expression for $\delta k_1(E, dE)/k_2$

Equations 14.1 and 14.2 represent the forward and the reverse of the same reaction and it is well known in physical chemistry that the ratio of rate coefficients is the equilibrium constant for the reaction. Thus, for



the equilibrium constant is

$$K_{\text{eq}} = \frac{dk_1(E)}{k_2} \quad (14.16)$$

The reaction described by Equations 14.15 and 14.16 is a thermal system so that the equilibrium constant is given in terms of a ratio of canonical partition functions Q of Chapter 4 with the partition functions for M canceling

$$K_{\text{eq}} = [Q(A^*(E, dE))Q(M)] / [Q(A)Q(M)] = [Q(A^*(E, dE))] / [Q(A)] \quad (14.17)$$

$Q(A)$ is the sum of $\exp(-E_i/kT)$ over all energy states E_i of the A molecule. It will be referred to as Q_2 . For A^* the sum is restricted to those states between E and $E + dE$. Thus

$$Q(A^*(E, dE)) = \left(\sum_E^{E+dE} g_i \right) e^{-E/kT} \quad (14.18)$$

where use has been made of the fact that dE is so small that all the states in the sum in the partition function have the same energy. Thus the exponential term, $e^{-E/kT}$, is multiplied by the sum of the degeneracies g_i of all states in the interval. For a molecule of moderate size the number of states will usually be sufficiently large so that one can talk a density of states $\rho(E)$, i.e. number of states per unit range of energy, and replace $\sum g_i$, the number of quantum states between E and $E + dE$ by $\rho(E) dE$. Thus, the required rate coefficient ratio $dk_1(E, dE)/k_2$ can be written as

$$\frac{dk_1(E, dE)}{k_2} = \left[\rho(E) e^{-E/kT} dE \right] / Q_2 \quad (14.19)$$

14.2.2 Discussion of $k_a(E)$

The rate constant $k_a(E)$ of Equation 14.3 is the rate constant which is calculated by transition state theory. Analogously to the discussion in Chapter 4 of conventional transition state theory, where chemical equilibrium is between reactants and transition state, it will be assumed here that an equilibrium exists between A^* (excited A molecules with vibrational energy E , equal to or larger than E_0 , the minimum

excitation energy required for forming the transition state) and A^\ddagger . There is one very significant difference between the problem addressed here and in Chapter 4. In ordinary TST (Chapter 4) both the reactant species and the transition state were characterized by a common temperature T , but in the present case both the reactant A^* and the transition state A^\ddagger are characterized by the same value of total energy E , measured with respect to the ground state energy of the unexcited A molecule. Since all states of a molecular system corresponding to the same energy should have equal a priori probability at chemical equilibrium, it is quite clear the relative concentrations of A^* and A^\ddagger should be the relative number of energy states of A^* and A^\ddagger accessible at the common energy. It is noted without formal detailed proof that the concept of equilibrium at constant energy means equal a priori probability of all energy states and leads after appropriate Boltzmann ($\exp(-E/kT)$) averaging to the formulation of equilibrium constants at given temperature T in terms of canonical partition functions.

14.2.2.1 Classification of Molecular Energy Levels

In the previous sections there has been discussion of the energy level density and number of energy levels. As in the discussion of Chapters 2 to 4, there is a Born–Oppenheimer potential energy surface for the molecule A and the transition state A^\ddagger which is independent of isotopic substitution within the BO approximation, and which corresponds to the electronic ground state. When the discussion deals with excited states and with counting numbers of states, these states refer to the various rotational, translational, and vibrational states corresponding to the relevant BO potential energy surfaces. The vibrational, rotational and translational energies are isotope dependent as noted in previous discussion. A short discussion of molecular degrees of freedom is appropriate here prior to the presentation of explicit formulae for $k_3(E)$. For more detailed discussion of degrees of freedom in unimolecular reactions, reference should be made to the literature (see Holbrook et al., at the end of the chapter).

As noted in Chapter 3, an N atomic non-linear molecule has three molecular translations, three molecular rotations, and $(3N - 6)$ vibrations. Some of the vibrational motions may actually be hindered internal rotations. An example of an internal rotation is the rotation of the two methyl (CH_3) groups in ethane, C_2H_6 , with respect to each other. In Chapter 4, some justification was given for dealing with these “internal rotations” as though they are vibrations. In counting states for the purpose of unimolecular reactions, for the present it will be assumed that the internal rotations are again handled as though they are vibrations. It is usual to assume that molecular rotations stay in the same quantum states in the transition from A^* to A^\ddagger . Thus, the molecular rotations are taken as “adiabatic” and are not counted in determining relative number of states. The same statement applies to the molecular translations. It is usually assumed that all $3N - 6$ vibrational degrees of freedom are active and therefore included in the number of states which are counted.

One also has to keep in mind that the non-linear transition state A^\ddagger has $3N - 7$ vibrations and one degree of freedom corresponding to the motion along the reaction coordinate which describes the rearrangement in going from A^* to A^\ddagger . As in the transition state theory of Chapter 4, this degree of freedom is taken to have a particle in the box (translational) potential. The corresponding energy levels are very closely spaced. For details reference should be made to the literature. It is well to remember the following formulae for the so-called non-fixed energy (the energy that can be distributed among the active degrees of freedom) in the excited molecule A^* and the corresponding transition state A^\ddagger , referred to as E^* and E^\ddagger respectively,

$$E^\ddagger = E^* - E_0 \quad (14.20)$$

$$E^* = E_v^* \quad (14.21)$$

$$E^\ddagger = E_v^\ddagger + x \quad (14.22)$$

In Equations 14.20 through 14.22, E_v^* refers to the $3N - 6$ vibrational degrees of the excited molecule, E_v^\ddagger refers to the $3N - 7$ vibrational degrees of freedom of the transition state, E_0 is the minimum energy (in excess of the ground state) required for reaction, and x refers to the energy of the particle in the box motion which replaces the imaginary frequency of the transition state.

14.2.3 The Expression for $k_a(E)$

Using the equilibrium assumption of transition state theory the ratio of concentrations of A^\ddagger and A^* can now be expressed as $\left[\frac{A^\ddagger}{A^*} \right] = (\text{number density of states } A^\ddagger \text{ with energy } E^\ddagger) / (\text{number density of states } A^* \text{ with energy } E^*)$

$$\left[\frac{A^\ddagger}{A^*} \right] = \rho(A^\ddagger) / \rho(A^*) \quad (14.23)$$

where the assumption has been made that the numbers of states are a near continuum of energies so that the relative number of states can be represented by the continuous functions $\rho(A^\ddagger)$ and $\rho(A^*)$ expressing the number density of states, ρ , per unit energy.

The only degrees of freedom that contribute to the number of states or to the density of states are the active ones discussed in the previous section. These are the $(3N - 6)$ so-called vibrational states for the N -atomic molecule A^* ($(3N - 5)$ for a linear molecule), and for the transition state A^\ddagger the $(3N - 7)$ active vibrations plus the translational degree of freedom along the reaction coordinate. It is this motion which is substituted for the imaginary frequency of the transition state (again the number of active frequencies is increased by one if the transition state is linear).

Since E_0 , the minimum energy required for E^* in order to react, is usually quite large compared to the vibrational spacing in the reactant, the spacing between the active levels in A^* is small and it makes sense to employ the density of states function $\rho(E_v^*)$ for A^* (i.e. instead of attempting to sum discrete individual states). For the transition state, the relevant energy $E^\ddagger - E_0$ will usually be much smaller than E^* . The degrees of freedom for A^\ddagger include the particle in the box translational motion along the reaction coordinate which replaces the so-called imaginary frequency. The spacing between particles in the box states is small and depends on the length ℓ of the box and reduced mass μ of the transition state. The density of the translational states corresponding to an energy x in the reaction coordinate is

$$\rho_{rc}(x) = 2 \mu \ell^2 / (h^2 x)^{1/2} \quad (14.24)$$

For a derivation of Equation 14.24 reference should be made to the literature (e.g. Holbrook et al. in the suggested reading list). The energy E^\ddagger of the transition state can be thought of being the sum of a vibrational quantum state energy $E_{v_i}^\ddagger$ and a reaction coordinate energy x such that the sum of x and $E_{v_i}^\ddagger$ is equal to E^\ddagger (Equation 14.22). Here x is regarded as a continuous variable because of the close spacing of the reaction coordinate energy levels, and hence one can write for the density of transition state energy levels

$$\rho(E^\ddagger) = \sum_{E_{v_i}^\ddagger=0}^{E_{v_i}^\ddagger=E^\ddagger} P(E_{v_i}^\ddagger) \rho_{rc}(x) \quad (14.25)$$

The sum here is over all vibrational states of the transition state with energy less than E^\ddagger . $P(E_{v_i}^\ddagger)$ here is the number of vibrational states of the transition state with energy $E_{v_i}^\ddagger$ and each term of the sum is subject to Equation 14.22.

It is now proposed to obtain an expression for k_a using Equation 14.11. This equation requires knowledge of the rate constant k_3 in the RRKM scheme. The rate constant k_3 is the inverse of the time required for the particle of mass μ to pass through the transition state, a one-dimensional box of length ℓ . This time is calculated by classical mechanics. For a translational motion with kinetic energy $x = (1/2) \mu v^2$, where v is the velocity, the passage time is ℓ/v and k_3 is

$$k_3 = (2x/\mu)^{1/2} / \ell = (2x/\mu \ell^2)^{1/2} \quad (14.26)$$

By substituting Equations 14.23 through 14.26 into Equation 14.11 one obtains

$$k_a(E^*) = \frac{1}{h} \frac{\sum_{E_v=0}^{E^\ddagger} P(E_v^\ddagger)}{P(E^*)} \quad (14.27)$$

As in the conventional transition state theory Equation 14.27 does not contain any reference to the mass of the reaction coordinate motion or to the length ℓ of the transition state. While some aspects of the derivation have been skipped, it is hoped that the reader understands that the expression in the numerator for the sum of the vibrational energy levels in the transition state arises from Equation 14.25 which applies to the transition state A^\ddagger but not to the excited molecule A^* .

14.2.4 The Pressure Dependence of the Rate Constant k_{uni}

Various rate constants which enter into the expression for k_{uni} , Equation 14.14, have now been discussed. k_{uni} as defined in Equation 14.13 has the appearance of a first order rate constant for the disappearance of A molecules but it is actually only a pseudo first order rate constant since it explicitly depends on the concentration of M, the species involved in the activation and deactivation of A molecules. In the limit of high concentration, $[M] \rightarrow \infty$, k_{uni} reduces to an apparent first order process, $\lim(k_{uni,[M] \rightarrow \infty}) = k_a(E)(\delta k_1(E)/k_2)[A] = k_{1(Apparent)}[A]$, while at low concentration the reduction is to an apparent second order process, $\lim(k_{uni,[M] \rightarrow 0}) = \delta k_1(E)[A][M] = k_{2(Apparent)}[A][M]$.

14.2.4.1 The High Pressure Rate Constant ($[M] \rightarrow \infty$)

In the high pressure limit, the denominator of Equation 14.13 approaches unity ($k_2[M] \gg k_a(E)$) and k_{uni} becomes a truly first order rate constant. After substituting the appropriate expressions for k_a and dk_1/k_2 into the expression for k_{uni} , one obtains (for details see Holbrook et al., reading list)

$$k_{uni} = \frac{kT}{h} \frac{Q^\ddagger}{Q} \quad (14.28)$$

where Q^\ddagger and Q are the vibrational canonical partition function of the transition state A^\ddagger and reactant A, respectively, with the zero of energy of both A^\ddagger and A the ground vibrational state of the reactant A molecule.

The result looks familiar and well it should. Equation 14.28 is just the expression for the rate constant in conventional canonical transition state theory with the assumption that the transition state A^\ddagger is in equilibrium with reactant A. However, Equation 14.28 differs from conventional transition state theory in that the partition function ratio here involves only vibrational partition functions, the rotational partition functions have been omitted. The translational partition functions, which depend only on molecular mass, cancel exactly in the ratio “transition state over reactant”. The absence of the rotational partition functions from Equation 14.28

is puzzling. Its origin lies in the earlier decision to treat the rotational degrees of freedom as adiabatic and has been extensively discussed (argued) in the literature (e.g. Holbrook, reading list).

14.2.4.2 The Low Pressure Rate Constant ($[M] \rightarrow 0$)

From Equations 14.14 and 14.19 the low pressure limit of k_{uni} is

$$\lim(k_{\text{uni}}/M) = \int_{E=E_0}^{E=\infty} dk_1(E) \quad (14.29)$$

$$= k_2 \int_{E=E_0}^{E=\infty} \rho(E)^{-E/kT} dE/Q_2 \quad (14.30)$$

$$= k_2 (Q_2^*/Q_2) \quad (14.31)$$

Q_2^* is the partition function for molecules with energy larger than E_0 , the minimum energy required for reaction.

As pointed out before k_{uni} is a pseudo first order rate constant. Since $k_{\text{uni}}/[M]$ is independent of $[M]$, $k_{\text{uni}}/[M]$ is a second order rate constant at low pressure. It is significant and important for consideration of isotope effects that this second order rate constant for unimolecular reactions depends only on the energy levels of reactant molecules A and excited molecules A^* , and on the minimum energy E_0 required for reaction. It does not depend on the energy levels of the transition state. There will be further discussion of this point in the following section.

14.2.5 Experimental Measurements of Isotope Effects in Unimolecular Reactions and the RRKM theory

The basic idea encapsulated in the mechanism given by Equations 14.1 through 14.4 is that energetically activated molecules A^* are lost either by proceeding on to products via the transition state A^\ddagger , or decay back to unexcited reactant molecules A most likely by a collision induced process. In the simplest analysis conversion of an excited molecule A^* to a non-excited molecule A is taken to be equal to the collision number. In actuality experiments and also theoretical approaches have shown that, for many systems, collisions are “weak”, that is energy is transferred in small steps and multiple collisions are required for complete de-excitation. A crude way of taking into account “weak collisions” is to replace the term $k_2[M]$ in the equation for k_{uni} , Equation 14.13 by $Z\beta_c[M]$ where Z is the collision number and β_c is the “collision efficiency” with $\beta_c = 1$ for strong collisions and $\beta_c < 1$ for weak collisions. However a thorough discussion of “weak collisions” is beyond the scope of this chapter and reference should be made to the literature for more detail, but see Section 14.4.

The term RRKM applies to two types of experimental studies involving isotope effects. In the first molecules are activated by thermal interactions as in Equations 14.1 through 14.4 and the molecules so excited then decompose in a unimolecular reaction. In the second type of study, molecules are excited by chemical interaction to a given energy or a range of energies by a chemical or photochemical process and the molecule so activated decomposes in a unimolecular manner by Equations 14.3 and 14.4 of the RRKM process. It should be noted that the general study of unimolecular reactions is certainly not restricted to the study of isotope effects. Yet, in the present context, our interest is only in isotope effects.

14.2.6 Thermal Activation: Inverse 2°-D-KIE's at Low Pressure

14.2.6.1 Gas Phase Isomerization of Methyl Isocyanide

Our interest in thermally activated unimolecular reactions is in the change of k_{uni} with pressure from the high to the zero pressure limit, and in the pressure dependence of the isotope effect over that range. One particularly interesting study carried out by Rabinovitch and Schneider (reading list) focused on the isomerization of methyl isocyanide, CH_3NC , to methyl cyanide, CH_3CN



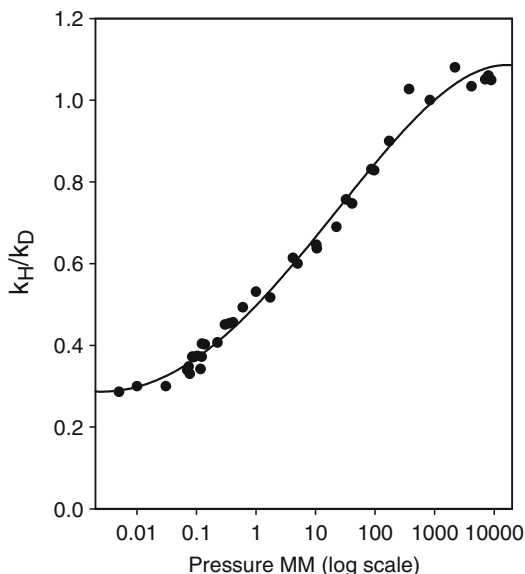
In reactions 14.32 and 14.33 the hydrogen atoms are not involved in any bonds that are being made or being broken in the reaction. The isotope effect is therefore referred to as a secondary α -deuterium isotope effect since the position of isotopic substitution is α to the bond being broken in the rate limiting step (see Chapter 10 for discussion of secondary isotope effects).

The pressure dependence of the isotope effect, $k_{\text{H}}/k_{\text{D}}$, is shown in Fig. 14.1. The isotopic rate ratio decays smoothly from a limiting value just above unity (1.06) at high pressure (10^4 Torr) to ~ 0.3 at 5×10^{-3} Torr. The range of the data thus extends over an impressive range of nearly seven orders of magnitude. As can be seen from the discussion which follows, the behavior is just that expected from application of Equations 14.29 through 14.31, and 14.32, and 14.33. At high pressure the pseudo first order unimolecular rate constant is given by Equation 14.31 and the isotope effect expressed

$$k_{\text{H}}/k_{\text{D}} = (Q^\ddagger/\text{Q})_{\text{H}}/(Q^\ddagger/\text{Q})_{\text{D}} = (Q^\ddagger_{\text{H}}/Q^\ddagger_{\text{D}}) / (Q_{\text{H}}/Q_{\text{D}}) \quad (14.34)$$

The ratios in Equation 14.34 can be calculated using either conventional (Chapter 4) or variational (Chapter 6) transition state theory. In either case one expects a small normal secondary isotope effect (refer to the discussion in Chapter 10) and this is

Fig. 14.1 The pressure dependence of the 2°- α -D isotope effect, k_H/k_D , on the bimolecular isomerization of methyl isocyanide:
 $\text{CH}_3\text{NC} \rightarrow \text{CH}_3\text{CN}$ and
 $\text{CD}_3\text{NC} \rightarrow \text{CD}_3\text{CN}$ at 504 K
 (After Schneider, F. W. and Rabinovitch, B. S., *J. Am. Chem. Soc.* **85**, 2365 (1963))



in good agreement with experimental value $k_H/k_D = 1.06$ observed at 10^4 Torr. With decreasing pressure, k_H/k_D falls off reaching a value of about 0.3 at 0.005 Torr. This fall-off had been expected on the basis of earlier theoretical reasoning by Rabinovitch and coworker based on the zero pressure limiting expression, Equation 14.31,

$$k_H/k_D = [k_{2H}/k_{2D}] [Q_{2D}/Q_{2H}] / [Q_{2D}^*/Q_{2H}^*] = [Q_{2D}/Q_{2H}] / [Q_{2D}^*/Q_{2H}^*] \quad (14.35)$$

where, as a reminder, Q_2 refers to the partition function of the active degrees of freedom (the vibrational ones in the present case) of the reactant, and Q_2^* refers to the partition function of these degrees of freedom with energy equal to or greater than E_0 above the ground vibrational state of the reactant, the energy necessary to reach the transition state. Also k_{2H} and k_{2D} are rate constants for the deactivation reactions, $A_H^*(E, \delta E) + M \rightarrow A_H + M$ and $A_D^*(E, \delta E) + M \rightarrow A_D + M$ (Equation 14.2), which in the strong collision approximation are isotope independent or very nearly so (every collision leads to deactivation). An essential feature of the present example is that we are dealing with a secondary isotope effect (Chapter 10) and it can be assumed that E_0 is the same (or almost the same) for both the CH_3 and CD_3 species. The following theoretical discussion depends on the isotope independence of E_0 .

Numerical evaluation of Equation 14.35 first requires the calculation of the isotopic vibrational partition function ratio in the numerator for the reactant. This can be obtained by applying the methods of Chapter 4 to the relevant H and D vibrational frequencies. The vibrational D/H partition function ratio is larger than unity. The vibrational partition function ratio in the denominator of the right hand side

of Equation 14.35 can be obtained by enumerating the energy levels with values in excess of E_0 . It is, however, well to remember that E_0 is usually sufficiently large and the energy levels sufficiently close to one another to permit one to replace a discrete sum over levels with an integral involving the density of vibrational energy levels $\rho(E_v)$. Then

$$Q^* = \int_{E_0}^{E_\infty} \rho(E_v) \exp(-E_v/kT) dE_v \quad (14.36)$$

Largely in connection with theoretical work on unimolecular reactions, numerical methods have been developed which permit the evaluation of $\rho(E_v)$. The lower vibrational frequencies of the heavy isotopomer lead to the result that the energy level density of the heavier isotopomer is substantially larger than that of the lighter isotopomer and consequently the rate ratio of Equation 14.35 is less than unity. It was the conclusion of Rabinovitch and colleagues that the secondary isotope effect on unimolecular reactions would drop from a small normal isotope effect ($k_H/k_D > 1.0$) at high pressure to an inverse isotope effect ($k_H/k_D < 1.0$) at lower pressure that led Rabinovitch and Schneider to undertake the study on CH_3NC . For details reference should be made to their publication (reading list) where they were able to rationalize the observed low pressure isotope effect, $k_H/k_D \sim 0.3$. This phenomenon was later observed in other systems. The result was a great triumph indicating the validity of the RRKM mechanism. For normal reactions (reactions which are not unimolecular), inverse kinetic isotope effects ($k_{\text{light}}/k_{\text{heavy}} < 1.0$) had always been correlated with the isotope being more strongly “bound” in the transition state than in the reactant (within the framework of conventional transition state theory). For further discussion, see Chapters 4 and 10.

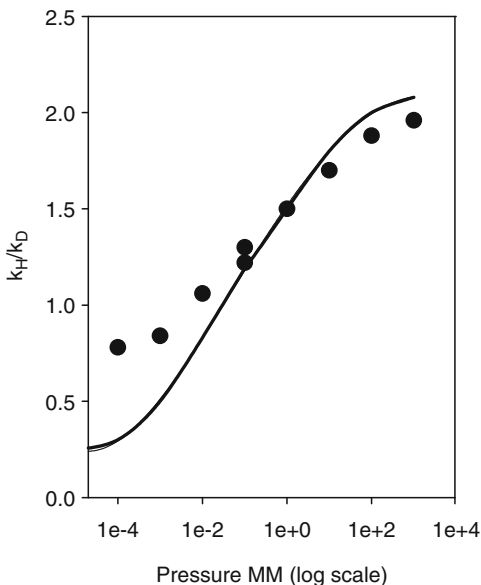
14.2.6.2 Gas Phase Isomerization of Cyclopropane

A second example of an inverse statistical weight isotope effect is that of the secondary H/D KIE on C–C bond rupture during the gas phase unimolecular isomerization of cyclopropane to propene. Theory and experiment are compared in Fig. 14.2 for reactions 14.37 and 14.38.



The isotope effect results from substitution at four α and two β hydrogens. The high pressure limiting KIE obtained from the model calculations, $k_H/k_D \sim 2$, is in good agreement with experiment. The data show a marked fall off with pressure to a limiting inverse effect, $k_H/k_D \sim 0.7$, which while significantly higher than the theoretical value ~ 0.3 , supports the interpretation of an inverse statistical weight isotope effect operative at low pressures. The authors suggest the true low pressure results have been obscured by wall effects.

Fig. 14.2 Pressure dependence of the 2°-D isotope effect, k_H/k_D , on the unimolecular isomerization of cyclopropane at 755 K: $c\text{-C}_3\text{H}_6 \rightarrow \text{C}_3\text{H}_6$ and $c\text{-C}_3\text{D}_6 \rightarrow \text{C}_3\text{D}_6$ (The data are from Blades, A. T., *Can. J. Chem.* **39**, 1401 (1961) and Rabinovitch, B. S. et al., *J. Am. Chem. Soc.* **86**, 2994 (1964). The calculated line is due to Rabinovitch et al.)

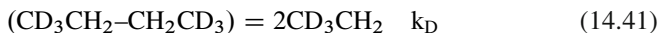
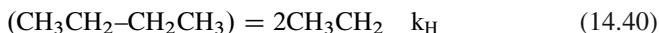


14.2.6.3 Model Calculation of a 2°-β-Deuterium KIE on C–C Bond Rupture

To further illustrate the application of Equation 14.35 (the limiting behavior of the low pressure IE), consider the case when only the external rotations are adiabatic (translations do not contribute to the isotope effect). In this case the ratio of Q 's reduces to a ratio of ratios of moments of inertia, which, provided the structure does not change on passing from active molecules to activated complex, is unity. In this simplified example, the isotope effect reduces to a simple ratio of the number of states and state densities in the activated complex and energized (active) molecules for the light (l) and heavy (h) molecules.

$$k_a^l(E)/k_a^h(E) = \left[\frac{\sum P(E^\ddagger)_l}{\sum P(E^\ddagger)_h} \right] \times [(\rho^*(E)_h/\rho^*(E)_l)] \quad (14.39)$$

Equation 14.39 is relatively simple for a secondary isotope effect because neither E^\ddagger nor E is expected to be isotope dependent for β-H/D isotope effects. To illustrate, Rabinovitch and Setzer (reading list) considered 2,3 C–C bond rupture of *n*-perprotiobutane and 1,4 dideutero-*n*-butane



As in the previous examples both $\sum P(E^\ddagger)$ and $\rho^*(E)$ are larger for the deuterated than the protiated molecule because of the lower vibrational frequencies of the

Table 14.1 Energy dependence of the secondary isotope effect k_H/k_D at zero pressure. Energies in kJ/mol (After Rabinovitch, B. S., Setser, D. W., *Adv. Photochem.* **3**, 1 (1964))

	$(\text{CH}_3\text{CH}_2)_2 = 2 \text{ CH}_3\text{CH}_2$ $(\text{CD}_3\text{CH}_2)_2 = 2 \text{ CD}_3\text{CH}_2$		k_H	k_D
$E - E_0 = E^\ddagger$	$E^\ddagger = 0$ $E_0 = 146$	$E^\ddagger = 0$ $E_0 = 356$	$E^\ddagger = 125$ $E_0 = 146$	$E^\ddagger = 125$ $E_0 = 356$
$\Sigma P(E^\ddagger)_H / \Sigma P(E^\ddagger)_D$	1	1	0.08	0.08
$\rho^*(\epsilon_D) / \rho^*(\epsilon_H)$	14	35	26	48
k_H/k_D	14	35	2	4

deuterated species. Thus $[\Sigma P(E^\ddagger)_H / \Sigma P(E^\ddagger)_D] < 1$ and $[(\rho^*(E)_D) / \rho^*(E)_H] > 1$, but the latter dominates because $\rho^*(E)$ is a continuously increasing function of energy at all energies of interest. $\Sigma P(E^\ddagger)$ is unity at the threshold energy, and relative to $\rho^*(E)$ only increases slowly with energy. These qualitative comments are fleshed out by the model calculations shown in Table 14.1. A large statistical weight isotope effect with strong dependence on both E^\ddagger and E_0 is predicted. The isotope effect is largest when E_0 is high and E^\ddagger low (the difference then being mainly in the $\rho^*(E)$ terms). It is smaller when E^\ddagger is large (since the compensating isotope effect from the $\Sigma P(E^\ddagger)$ term is then at its maximum). The mass dependence of the isotope effect is of secondary concern; it enters only to the extent that the mass effects are correlated with the statistical weight isotope effects.

14.2.7 Primary Isotope Effects

The formalism for treating primary isotope effects on unimolecular processes follows analogously to the development above, once due account is taken of the difference in zero point energies on isotope substitution at the reaction site (which is reflected in an isotopic difference in the threshold energy E_0). For thermal activation the rate ratio in the high pressure limit is straightforwardly obtained from Equation 14.25. For H/D effects

$$(k_H/k_D)_{\text{HIGH P}} = \left[\left(\frac{Q^\ddagger}{Q} \right)_H / \left(\frac{Q^\ddagger}{Q} \right)_D \right] \exp(-\Delta E_0/kT) \quad (14.42)$$

The energy level density is not important in determining the magnitude of the isotope effect at high pressure. At the low pressure limit, again for thermal activation,

$$(k_H/k_D)_0 = (\omega_H/\omega_D) [Q_D^*/Q_H^*] \times \left[\left(\int \rho^*(E_H) \exp(-\Delta E_0/kT) dE \right) / \left(\int \rho^*(E_D) \exp(-\Delta E_0/kT) dE \right) \right] \quad (14.43)$$

where (ω_H/ω_D) is the collision frequency ratio which is close to unity in the strong collision approximation. The partition function ratio refers to the active modes. To exemplify, reconsider the secondary isotope effects of Equation 14.40 and 14.41. In this reaction $E_{0H} \sim E_{0D} \sim 146$ kJ/mol. At 573 K the ratio of integrals in Equation 14.43 is 0.069, the partition function ratio is 4.2 and $(k_H/k_D)_0 = (\omega_H/\omega_D) \times 0.29 = 0.31$. The limiting high pressure ratio is 0.93. Thus at low pressure a large inverse secondary non-equilibrium isotope effect is predicted. Also, as temperature changes both the integral and the partition function ratios change, but in a partially compensating fashion. For example at 473 K the integral ratio is 0.071, $[Q^*_D/Q^*_H] = 3.4$ and $(k_H/k_D)_0 = 0.25$.

14.3 ^{17}O and ^{18}O Enrichment in Terrestrial and Extraterrestrial Samples: “Mass Independent” Isotope Fractionation and the Ozone Problem

14.3.1 Introduction

The equilibrium theory of isotope fractionation developed in earlier chapters has successfully explained the mass dependent fractionations which occur during many processes including chemical exchange, evaporation, condensation, etc. Furthermore we have seen this general approach carries over to those kinetically controlled processes which can be described in the context of absolute rate theory (i.e. where the assumption of a pseudo-equilibrium between activated complex and reactant species is useful). A straightforward consequence of the standard theory is that the ratio of ratios of isotope fractionations can be calculated from the differences in mass and mass distribution of the reacting particles, and this is independent of the particulars of any fractionation process. Thus for a three isotope mixture, say H, D, T or ^{16}O , ^{17}O , ^{18}O the equilibrium theory predicts the ratio of ratio of concentrations $([D]/[H])/([T]/[H])$ or $([^{17}\text{O}]/[^{16}\text{O}])/[^{18}\text{O}]/[^{16}\text{O}]$ to be approximately 0.5. Roughly speaking this is because the mass differences (D–H) or (^{17}O – ^{16}O) are just half those of (T–H) or (^{18}O – ^{16}O). The approximation, ~ 0.5 , results from the fact that a proper understanding entails a complete vibrational analysis of the reacting molecules and this leads to minor corrections to the value 0.5. It was therefore highly surprising to discover that oxygen isotope fractionation for certain inclusions found in meteorites did not follow the expected pattern, but unexpectedly showed $([^{17}\text{O}]/[^{16}\text{O}])/[^{18}\text{O}]/[^{16}\text{O}] \sim 1$, i.e. mass independent fractionation. This surprising and important result is the subject of this rest of this chapter.

Stable isotope analysis of earth, moon and meteorite samples has provided important information concerning the origin of the solar system. Lunar samples returned to earth during the Apollo missions show $\delta^{17}\text{O}$ and $\delta^{18}\text{O}$ enrichment patterns which are virtually identical to those of earth-bound rocks and minerals. On 3-isotope plots like those in Figs. 9.5 and 14.3, a uniform isotope reservoir is represented by a single

point. If that reservoir be subsequently divided, then fractionated by mass dependent processes like those described earlier in this text, the divided parts will lie along a common line. The slope can be calculated from the equilibrium theory of isotope fractionation, or, for kinetically controlled processes from the theory of kinetic isotope effects and transition state theory (Chapter 4) or variational transition state theory (Chapter 6). For oxygen isotope effects that line, generally known as the terrestrial fractionation line (TFL), but occasionally as the earth–moon line, has been experimentally established by measurements on many thousands of samples of oxygen bearing materials and is completely consistent with isotope effect theory. For the three isotope set ^{16}O : ^{17}O : ^{18}O along TFL

$$\delta^{17}\text{O} = m \delta^{18}\text{O} \quad (14.44)$$

with the slope, $m \sim (1-16/17)/(1-16/18) = 0.529$. The approximation sign reminds us for high precision work proper account must be taken of the details of the isotope sensitive vibrations involved in the fractionation process producing each and every analyte sample. The masses used immediately above are atomic masses of the exchanging isotopes and not those of the molecular fragments at the site of isotope substitution. A more detailed treatment (Chapters 3 and 4) includes complete vibrational analysis of the molecules involved in the fractionation process and restricts oxygen mass dependent isotope effects to the range ($0.51 < m < 0.55$). Larger or smaller values are labeled “anomalous” or, more commonly, “mass-independent” isotope effects. The latter term derives from the fact that the anomalous effects of greatest interest are those with $m \sim 1$, i.e. are mass independent (or approximately so).

14.3.2 Oxygen Isotope Fractionation in Earth, Moon, and Meteorite Samples

Equation 14.44 with $m \sim 0.53$ is nicely obeyed by $\delta^{17}\text{O}/\delta^{18}\text{O}$ data for many, many (i.e. the great preponderance of) terrestrial and lunar samples. No other extraterrestrial samples lie on that line, and this observation supports the idea that earth and moon formed in the same region of the solar nebula, and almost certainly represent parts of a single precursor nebular reservoir. Thus, it was surprising in the early 1970s when Clayton discovered that calcium–aluminum oxide inclusions in carbonaceous meteorites showed three isotope plots with $m \sim 1$, i.e. mass independent isotope effects. (Fig. 14.3). Then current thinking assumed that all possible geophysical and geochemical processes produced mass dependent isotope fractionations ($m \sim 0.53$ for oxygen), and large differences from $m \sim 0.5$ most likely reflected the intervention of some nuclear event. The assignment of the earth–moon system to one nuclear reservoir, the precursor of the solar system (or at least of earth and moon), and extraterrestrial meteorites to a second and significantly different nuclear reservoir, would require serious modification of astronomical ideas concerning

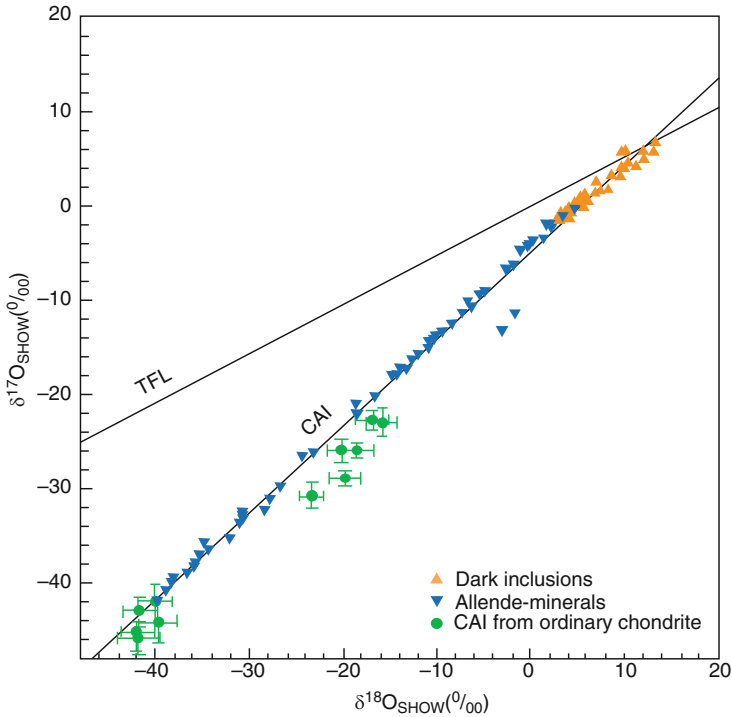


Fig. 14.3 Three isotope plot of calcium-aluminum oxide inclusions in chondrite meteorites compared with the terrestrial fractionation TFL line. For TFL $m \sim 0.5$, the meteoric line shows $m \sim 0.9$ (The data are from Clayton, R. N. et al., *Earth Planet. Sci. Lett.* **34**, 209 (1977); *Geochim. Cosmochim. Acta* **63**, 2089 (1999). Thiemens, M., *Ann. Rev. Earth Planet. Sci.* **34**, 217 (2006))

the early history of the earth/moon/meteorite system. In particular it forced the conclusion that the meteorites had sampled a region or time where or when the “primordial soup” was significantly different than it was when the earth/moon system condensed. It was obviously very important to test the logical necessity of this remarkable conclusion.

14.3.3 Mass Independent Isotope Fractionation in the Laboratory, the Stratosphere, and the Troposphere

The assignment of the earth/moon system to one precursor nebular reservoir, and meteorites to a second, while still logically possible, was shown experimentally to be unnecessary by Thiemens and coworkers (reading list). In the early 1980s these workers studied isotope fractionation during the synthesis of ozone from molecular oxygen in an electric discharge operated at low pressure. The product ozone was

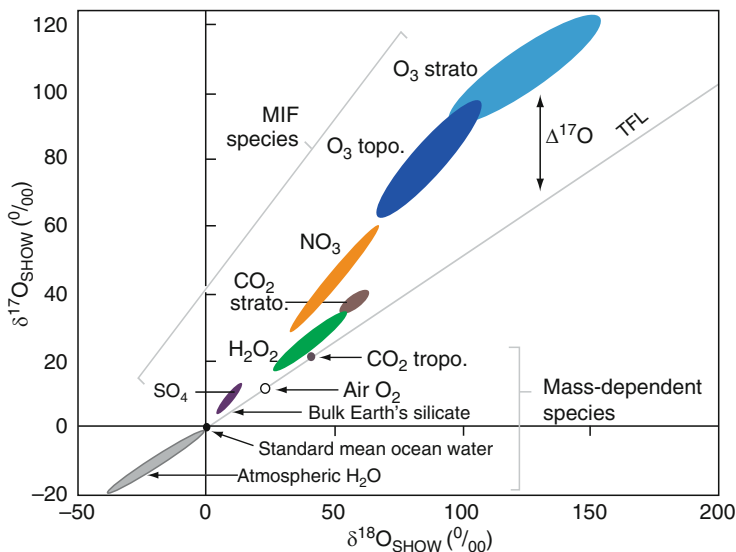


Fig. 14.4 Oxygen isotopic composition of atmospheric species measured to date (After Thiemens, M., *Ann. Rev. Earth Planet. Sci.* **34**, 217 (2006)). For these data, m , Equation 14.31 is approximately $(0.7 < m < 0.9)$ indicating for these materials the fractionation is better described as “anomalous” rather than “mass independent”

found to be equally enriched in ^{17}O and ^{18}O , so $m \sim 1$ in Equation 14.44, rather than the expected mass dependent value, $m \sim 1/2$ (see Fig. 14.4). The slopes of the mass-independent lines in Figs. 14.3 and 14.4 are the same for terrestrial ozone synthesis as they are for the meteorite data. The result leads to the conclusion that the mass independent slope for the meteorite fractionation might have a chemical rather than a nuclear origin (assuming some plausible mechanism which transfers ozone fractionation from the low pressure gas to Ca/Al oxide inclusions in meteorites). The argument was strengthened by the observation that mass independent fractionation (MIF) of ozone was observed not only in electric discharge experiments but also in photochemical ozone production. In each case the fractionation is kinetically controlled (vide infra) during the unimolecular processes which are involved in ozone synthesis. Also, measurements on natural ozone samples collected at high altitude, far into the stratosphere, show mass independent fractionation, not only for ozone but for other oxygen containing molecules (sulfates, nitrogen oxides, and carbon dioxide) (Fig. 14.4). It is important to appreciate that these upper atmosphere fractionations can be transferred from the low pressure gas to aerosol particle surfaces and eventually to precipitated bulk phase solids. For example nitrate MIF's have been observed in samples collected from aerosols, fog, precipitation, soils and stream water, etc. (Fig. 14.5). The magnitude of observed nitrate MIF's suggests a connection to ozone. One possible pathway leading from upper atmosphere ozone to nitric acid is:

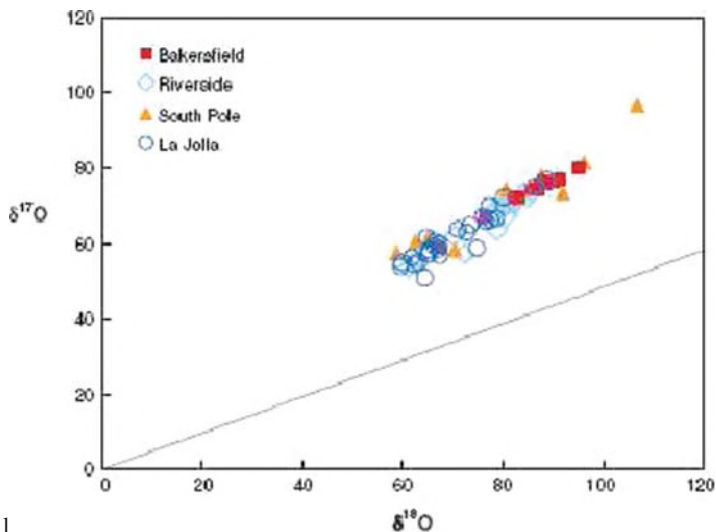
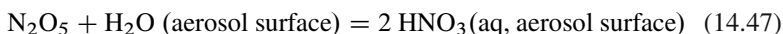
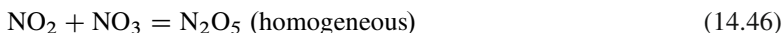
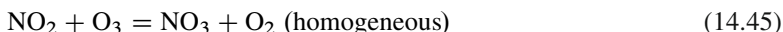


Fig. 14.5 Three isotope plots of oxygen fractionation in nitrate samples from different locations (After Thiemens, M., *Ann. Rev. Earth Planet. Sci.* **34**, 217 (2006)). For these data, m , Equation 14.31, is ~ 0.9 . The expected mass dependent terrestrial fractionation is shown as the *solid line*



In this way aerosol clustering, eventual precipitation, and chemical reaction can account for nitrate MIF's observed in terrestrial or meteoric solids.

14.3.4 MIF's for Ozone from Natural Abundance and Enriched Starting Materials

Figure 14.6 compares measured and calculated isotope fractionations for all 16 possible ozone isotopomers prepared from an enriched oxygen precursor. In this figure ($^{16}\text{O}^{16}\text{O}^{16}\text{O}$, $^{16}\text{O}^{16}\text{O}^{17}\text{O}$, $^{16}\text{O}^{17}\text{O}^{16}\text{O}$, $^{16}\text{O}^{16}\text{O}^{18}\text{O}$, etc. are represented as; 666, 667, 676, 677, 767, 668, 686, 678, 777, 688, 868, 778, 787, 788, 878, and 888). The calculations are those of Gao and Marcus described in sections below. They are in quantitative agreement with experiment. It is interesting that isotope fractionations observed in product ozone for the totally symmetric isotopomers, $\delta^{17}\text{O} = 1000 \ln(777/666)$ and $\delta^{18}\text{O} = 1000 \ln(888/666)$, are negative; they show the heavy isotope to be depleted. Moreover, these totally symmetric effects lie on the mass dependent fractionation line $[\ln(777/666)]/[\ln(888/666)] \sim 0.5$. That

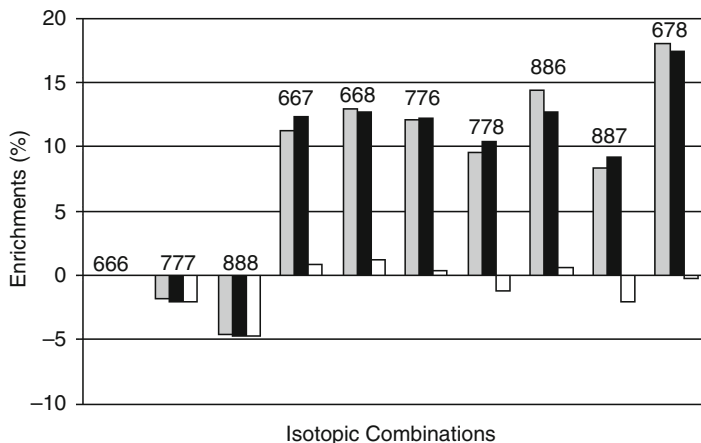
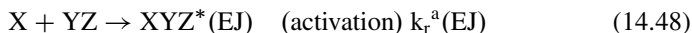


Fig. 14.6 Experimental and calculated enrichments or depletions of all possible ozone isotopomers. The labels 6, 7 and 8 represent ^{16}O , ^{17}O , and ^{18}O respectively. Ozone (gray bars) was produced in well scrambled oxygen mixtures at about 90 mbar and room temperature (Mauersberger et al. *Adv. Atomic Mol. Opt. Phys.* **50**, 1 (2005)). The calculated values (vide infra) are those of Gao, Y. Q. and Marcus, R. A., *J. Chem. Phys.* **116**, 137 (2002) setting the parameter $\eta = 1.18$ (black bars) or $\eta = 1.0$ (white bars). A typical symbol, such as 668, denotes an ozone with the isotopic composition $^{16}\text{O}^{16}\text{O}^{18}\text{O}$ and consists of a mixture of symmetric ($^{16}\text{O}^{18}\text{O}^{16}\text{O}$) and asymmetric ($^{16}\text{O}^{16}\text{O}^{18}\text{O}$) isotopomers (After Gao, Y. Q. and Marcus, R. A., *Science* **293**, 259 (2001))

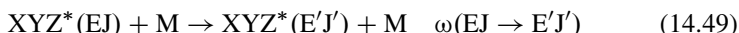
behavior contrasts with $\delta^{17}\text{O}$ and $\delta^{18}\text{O}$ for the scrambled isotopomers, whether symmetric (XYX) or asymmetric (XXY). Note that equal mass symmetric and asymmetric isotopomers are not experimentally distinguished in these measurements. (Thus, for example, the enrichment labeled 668 in Fig. 14.6 is actually the sum of the enrichments for 668 and 686). The scrambled heavy isotopomers are all enriched with respect to the totally symmetric 666, and the magnitudes of the enrichments are larger than are the depletions of the totally symmetric molecules, 777 and 888. They lie nowhere near the mass dependent fractionation line. The pattern shown in Fig. 14.6 does not vary a great deal with the temperature or pressure at which the synthesis is carried out. Moreover it is entirely consistent with experiments on natural abundance starting material, and with samples collected from the upper atmosphere during high altitude balloon flights or rocket sounding experiments. For natural abundance samples, $^{16}\text{O} = 0.9976$, $^{17}\text{O} = 0.0004$, $^{18}\text{O} = 0.0020$, and as a practical matter one need only take into account the isotopomers 666, 676 + 667, and 686 + 668. The next most likely isotopomer, 688 + 868, is only present at trace quantity (i.e. $\sim 0.9976 \times 0.002^2 \sim 4 \times 10^{-6}$, about a factor of 100 less than $(667 + 676) \sim 4 \times 10^{-4}$).

14.4 Theory of Mass Independent Isotope Fractionation of Ozone

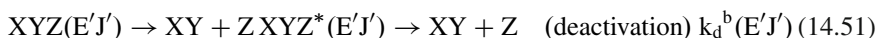
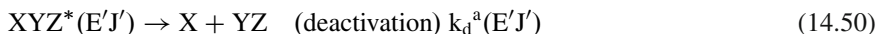
In a series of important papers Marcus and coworkers applied the RRKM (Rice–Ramsberger–Kassel–Marcus) theory of unimolecular reactions to the ozone problem in a successful effort to rationalize the MIF's described above (see Historical Vignette 14.1). The 2002 paper of Gao and Marcus (reading list) considered a kinetic scheme which mildly elaborates that of Equation 14.1



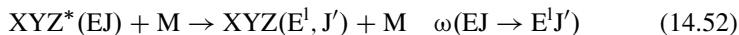
The short-lived activated particle specified by vibration–rotation energy (EJ) most likely undergoes a series of steps which redistribute its internal and rotational energy



but at some point during this process it may dissociate using one of two available paths, a or b,

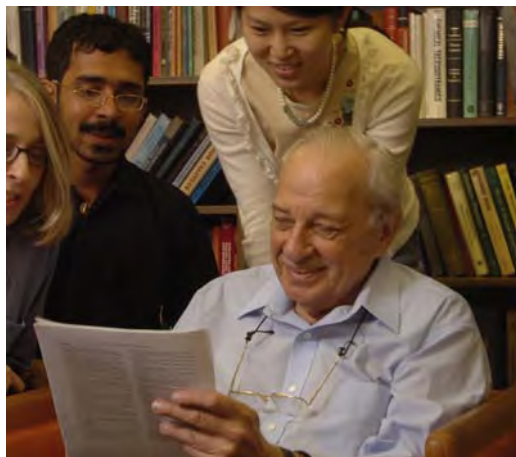


Alternatively, continuing its series of collisions with bath molecules it may deactivate to form a stable ozone molecule



The $k_r^a(E, J)$, $k_d^a(E', J')$, and $k_d^b(E', J')$ are E and J dependent rate constants of the recombination and dissociation reactions, and $\omega(EJ \rightarrow E'J')$ is the rate per unit E of forming XYZ at (E'J') from (EJ) by a third body collision. In Equation 14.52 E^l is any energy sufficiently below the dissociation threshold of ozone to make further reaction highly improbable. In this reaction scheme X, Y, and Z may be any of ^{16}O , ^{17}O , or ^{18}O , and the ozone initially formed is in a high energy state characterized by energy E and total angular momentum J. Obviously the recombination rate constant, k_r , is E and J dependent, and in the end the overall rate of formation of XYZ will involve integrations over the E and J states of product and reactants. For the dissociation of XYZ^* , Equations 14.50 and 14.51 the exit channels a and b are distinguishable for the case $X \neq Z$ and $k_d^a(E'J')$ does not necessarily equal $k_d^b(E'J')$. Obviously, however, for the symmetric case, $X = Z$, the two rate constants are equal.

In the step-ladder scheme described above it is assumed that only a well defined discrete amount of energy, ΔE , is transferred from the activated ozone molecule to the bath per collision, and there is a ladder of M steps which need to be considered. The energy of the lowest step E^l is later varied to ensure the calculated rate constant converges to a finite value. Given the potential energy surface for the reaction Gao



[Historical Vignette 14.1] Rudolf A. Marcus (1923–present) was born in Montreal and educated at McGill University. In 1948 he joined O. K. Rice at the University of North Carolina where he worked on the theory of unimolecular reactions, developing what is now known as RRKM theory (Rice, Ramsperger, Kassel, Marcus). From 1951 to 1964 Marcus was on the faculty at Brooklyn, Polytechnic Institute. During this period he developed important theoretical ideas on electron transfer in chemical reactions. From 1964 to 1978 he was at the University of Illinois, and since 1978 he has been at the California Institute of Technology. His recent scientific work has focused on electron transfer, unimolecular reaction theory, and mass independent isotope effects. Marcus was awarded the Nobel Prize in Chemistry in 1992. (Photo credit: Marcus with students, Chemistry Department, California Institute of Technology)

and Marcus first obtained the solution for a single ladder beginning with some particular energy and then integrated over E^{\ddagger} in the interval ΔE to obtain the total rate constant. The step size, ΔE , enters as a parameter. The frequency ω_a for activating collisions was related to that for deactivating ones using microscopic reversibility, $\omega_a = \omega_d \exp(-\Delta E/kT)$. The total collision frequency is $\omega = \omega_a + \omega_d$. The individual low pressure rate constants for formation of XYZ are then calculated for each channel (Equations 14.50 and 14.51) using the equations developed above and choosing the parameters, $\eta = 1.18$ and $\Delta E = 210 \text{ cm}^{-1}$ to fit the experimental low pressure recombination rate constant ratios, $(6 + 88)/(6 + 66)$ and $(8 + 66)/(8 + 88)$ and agreement (or not) with the other seven ratios Fig. 14.6 tests the theory. The η parameter reduces the recombination rate for symmetric isotopomers, XYX , presumably due to a lower density of states which makes collisional energy transfer less efficient for these molecules, and ω smaller. Calculated isotope enrichments for ozone isotopomers are compared with experiment in Fig. 14.6. The agreement is excellent. The nearly mass independent fractionation observed for the asymmetric isotopomers is thus principally due to two “symmetry driven” isotope effects: (1) for the asymmetric isotopomers the difference in zero point energy of the two exit channels causes the partitioning between these channels to differ from $1/2$ and this results in a large unconventional mass dependent effect on the rate constant ratios. (2) The η effect discussed immediately above which is also a consequence

of symmetry. As a net result the formation of the asymmetric species (668 or 667, for example) is favored over the symmetric ones (676 or 686) because it can proceed through a greater number of reactive quantum states. The asymmetric ozone isotopomers contain a greater density of reactive (or coupled) states as compared to the symmetric. The asymmetric species can distribute energy better and is more likely to couple to the exit channel which leads to a stable molecule. For practical application of the theory it is a requirement that these state densities be known (or calculated) for all isotopomer species of interest, and at high precision.

An important aspect of the Gao-Marcus model is that it provides a theoretical structure for the understanding of quantum state density isotope effects in general, and is not specifically confined to the formation of ozone itself. This feature is important because as discussed above we are now aware that MIF's occur widely in nature. The theory aids in prediction of where MIF's will be likely found, and once found, in rationalizing how they were chemically produced.

14.4.1 Comment

The work of Thiemens, Mauersberger, and their collaborators has now definitively established a pervasive mass independent isotope fractionation for oxygen containing molecules found in the atmosphere, upper atmosphere, and in space. These results, initially surprising because they are inconsistent with ordinary equilibrium isotope effect theory, have since been rationalized by Gao and Marcus using a chemical mechanism which invokes unimolecular rate theory and density of quantum state arguments. A merit of the chemical mechanism for the oxygen isotope anomaly is that only one oxygen reservoir is required in the solar nebula.

Further Reading

- Gao, Y. Q., Marcus, R. A. On the theory of the strange and unconventional isotopic effects in ozone formation. *J. Chem. Phys.* **116**, 137 (2002).
- Holbrook, K. A., Pilling, M. J., and Robertson, S. H. *Unimolecular Reactions*, Wiley, New York (1996).
- Marcus, R. A. Mass independent isotope effect in the earliest processed solids in the solar system. A possible chemical mechanism. *J. Chem. Phys.* **121**, 8201 (2004).
- Marcus, R. A and Rice, O. K., The kinetics of the recombination of methyl radicals and iodine atoms. *J. Phys. Chem* **55**, 894 (1951). Marcus, R. A., Unimolecular dissociations and free radical recombination reactions. *J. Chem. Phys.* **20**, 359 (1952).
- Mauersberger, K., Krankowsky, D., Janssen, C., Schinke, R. Assessment of the ozone isotope effect. *Adv. Atomic, Mol. Opt. Phys.* **50**, 1 (2005).
- Rabinovitch, B. S., Setser, D. W., Unimolecular decomposition and some isotope effects of simple alkanes and alkane radicals. *Adv. Photochem.* **3**, 1 (1964).

- Schneider, F.W. and Rabinovitch, B. S., The unimolecular isomerization of methyl-d₃ isocyanide. Statistical-weight inverse secondary intermolecular kinetic isotope effects in nonequilibrium thermal systems. *J. Am. Chem. Soc.* **85**, 2365 (1963).
- Thiemens, M. H. History and applications of mass-independent isotope effects. *Ann. Rev. Earth Planet. Sci.* **34**, 217 (2006).
- Thiemens, M. H. and Heidenreich, J. E. The mass independent fractionation of ozone. A novel isotope effect and its possible cosmochemical implications. *Science* **219**, 1073 (1983).

Author Index

A

Abbott, M.M., 426
Abrams, S.A., 310
Abrosimov, V.K., 407
Adediran, S.A., 373
Agmon, N., 194
Alej, M., 406
Allison, T.C., 200
Anderson, J.B., 183
Anderson, V.E., 369
Arrhenius, S., 117
Aston, F.W., 1, 2, 6, 14, 19–23, 27, 29–31, 34,
246, 264
Avery, D.G., 287
Avogadro, A., 3

B

Babcock, H.D., 30
Baertschi, P., 149
Bainbridge, K.T., 34
Balmer, J., 17, 18
Banerjee, B., 379, 384
Bardeen, J., 173
Bardo, R.D., 47, 50
Bartell, L., 408–409
Bates, R.C., 358, 359
Battino, R., 178
Becker, E.W., 267
Becquerel, H., 1, 4, 5
Beers, Y., 392
Bell, J.B., 372
Bell, R.P., 121, 189–192, 395
Bender, M.L., 329
Benedict, M., 251, 252, 264, 286
Berzelius, J.J., 3, 4
Bierbaum, V.M., 328, 329
Bigeleisen, J., 93–96, 101, 105, 111, 127,
130–132, 163–165, 271, 273, 359, 407
Bigelow, T.S., 258

Bird, R.B., 426
Birge, R.T., 31
Bjerrum, N., 61
Blades, A.T., 440
Blanchard, J.S., 372
Bleakney, W., 32
Bohr, N., 24
Boltzmann, L., 86
Born, M., 33, 39, 41
Boys, S.F., 52
Bragg, W., 17
Brickwedde, H.G., 31
Bridge, N.J., 392
Briggs, G.E., 347
Bronsted, J.N., 23, 190
Buckingham, A.D., 392
Buist, G.J., 329

C

Calado, G., 171
Carnot, S., 4
Chacko, T., 296
Chadwick, J., 24
Chialvo, A.A., 426
Chowdhury, S., 379, 384
Christiansen, J.A., 428
Clayton, R., 443, 444
Cleland, W.W., 349, 367, 368, 375, 377
Clough, S.A., 392
Clusius, K., 259, 261–263
Clusius, R., 4
Cohen, K., 287
Cole, D.R., 296
Coltrin, M.E., 194, 197, 198
Cook, P.F., 372, 375, 377
Cooper, L.N., 173
Coplen, J., 299
Copley, S.D., 373
Craig, H., 300

Cramer, C.J., 342
 Crespi, H.L., 311
 Criss, R.E., 297
 Cross, P.C., 68
 Curie, M., 5
 Curie, P., 5
 Curtiss, C.F., 426
 Cyvin, S.J., 412

D

Dalton, J., 1–3, 5
 Davies, E., 287
 Debye, P., 19, 147, 391, 393, 394
 Decius, J.C., 68
 de Hevesy, G., 2, 7, 9, 13, 23
 Dempster, A.J., 34
 DeNiro, M.J., 305
 Deraniyagala, S.A., 373
 Devi-Kesavan, L.S., 387
 Dewar, J., 18
 Dickel, G., 255, 259, 361, 363
 Diedrich, D.L., 183
 Diehl, P., 412
 Dieke, G.H., 30
 Doctor, D.H., 311
 Drakopoulos, P.G., 392
 Drude, P., 149
 Dutta-Choudhury, M., 155

E

Eckart, C., 192
 Ehrlich, J.J., 372
 Einstein, A., 5, 10, 19, 20, 22, 147
 Ellingson, B.A., 377
 Emiliani, C., 296
 Epstein, S., 305, 306
 Evans, M.G., 118
 Eyring, H., 33, 117, 118, 181, 196

F

Fajans, K., 1, 2, 6–10, 13, 14, 23, 24
 Fenske, M.R., 251
 Fernandez-Ramos, A., 377
 Fetzer, C., 159
 Fleck, A., 9
 Fock, V., 51–53
 Frankel, B.A., 373, 374
 Frisone, G.J., 329
 Froese, R.D., 388
 Fujii, Y., 136, 287
 Fuks, S., 164, 165

G

Galimov, E.M., 304
 Gao, J., 383
 Gao, Y.Q., 446–450
 Garrett, A.B., 7
 Garrett, B.C., 377
 Gawlita, E., 369
 Geib, E., 270
 Geiger, H., 15
 Giaque, W.F., 30, 31, 33
 Gibbs, J.W., 81
 Glasstone, S., 117
 Goldstein, E., 18
 Gold, V., 363
 Goodwin, D.H., 295
 Goorvitch, D., 397
 Grachev, A.M., 301
 Graham, T., 249
 Griffiths, H., 311
 Grigor, A.F., 407, 416
 Gruneisen, E., 157, 158, 165, 173

H

Haas, A., 25
 Haldane, J.B.S., 347, 348
 Halevi, E.A., 392, 397
 Hamilton, W.R., 37, 38, 40, 42–44
 Hammett, L.P., 43, 330
 Hansen, P.E., 405
 Harkins, W.D., 2, 20–24, 26, 27, 31
 Hartley, H., 282
 Hartree, D.R., 51–53
 Hayes, A., 23
 Heidenreich, G.E.,
 Heitler, W., 51
 Helmholtz, H., 80
 Henderson, C., 416
 Hengge, A.C., 342
 Henry, W., 85
 Hermes, J.D., 365, 368, 375
 Hertz, H., 4
 Herzberg, G., 111, 117, 396
 Hirschfelder, J.O., 416
 Hirschi, J., 326
 Hoefs, J., 311
 Hogfeldt, E., 359
 Hohenberg, P., 52
 Holbrook, K.A., 428, 432, 434, 436
 Honigschmid, O., 14
 Hopfner, A., 156
 Horita, J., 296
 Houk, K. N. 337–339
 Humphrey, J.S., 323

Hunt, R.H., 397
Hwang, C.C., 372

I

Imes, E.E., 25
Ingold, C.K., 333
Ishida, T., 105
Ivanov, E.V., 407

J

Jahren, A.H., 303
Jakli, G., 159, 166, 171
Jameson, C.J., 403
Jancso, G., 159, 161, 169, 171
Janssen, C., 450
Jenkins, F.A., 29
Jevons, W., 26, 29
Johnson, B.R., 183
Johns, T.F., 275
Johnston, H.L., 30, 31
Jones, M.E., 372

K

Kaiser, E.W., 392, 397
Kassel, L.S., 428, 448, 449
Kato, S., 328, 329
Katz, J.J., 311
Keesom, W.H., 19
Kelleher, N.L., 373
Kendall, C., 299
Kiefer, P.M., 373
King, A.S., 31
Kirkwood, J.G., 33, 97–99, 102
Kistemaker, J., 287
Kleindienst, D.B., 311
Klein, G.P., 392
Kleinman, L.I., 50
Klinman, J., 377
Kohen, A., 149
Kohn, W., 52
Kooner, Z., 236, 497, 416
Koshi, M., 217
Krankowsky, D., 450
Kratzer, A., 25
Kresge, A.J., 388
Kruger, R.G., 373
Kuhn, W., 149
Kurz, J.L., 334

L

Laughton, P.M., 359
Laurie, V.W., 392

Lawrence, E.O., 257
Lee, C.C., 244
Lennard Jones, J.E., 146, 162
Levi, H.W., 286
Levine, I., 396
Levine, I.M., 53
Lewandowicz, A.J., 386
Lewis, G.N., 31, 33
Lewis, I.C., 54
Limbach, H.H., 149, 229, 230
Li, N.C., 359
Lindemann, F.A., 2, 14, 19–20, 28, 32, 147, 148, 246, 264, 428
London, F., 51, 398
London, H., 264, 273, 275
Loomis, F., 25
Lopes, J.N.C., 163
Lorentz, H.A., 399
Lorenz, L., 399
Lowe, B.M., 359, 362
Luszczuk, M., 239
Lyman, T., 17, 18

M

MacInteer, B.B., 276
Maessen, B., 160
Marcus, R.A., 194, 197–199, 428, 446–450
Marsden, F., 15
Mason, J., 244
Mathur, R., 359
Matsson, O., 386
Mattsen, O., 336
Matuchka, M., 281
Mauersberger, K., 447, 450
Maxwell, E., 174
Maxwell, J.C., 4
Mayer, J., 112
Mayer, M.G., 93–95, 101, 111, 112, 130
Mayezawa, T., 70
McCafferty, D.G., 373
McCarthy, D.L., 373
McCoy, H.N., 6, 13
McKellar, A., 29
McQuarrie, D.A., 86, 89, 91, 92
McSween, H.J., 311
Melander, L., 342
Melnichenko, Y., 243
Mendeleev, D.I., 3, 10, 14
Menshutkin, N., 332–334
Menzel, D.H., 31
Michaelis, L., 344–346, 358
Milewska, A., 176

Miljevic, N., 155
 Miller, D.L., 307
 Millikan, R.E., 5
 Mislow, K., 324
 Moos, N.W., 282
 Morokuma, K., 385
 Morse, P.M., 56
 Moseley, H.G.J., 2, 14, 16–18
 Muenter, J.S., 392, 397
 Mulliken, R.S., 23, 26–30, 51
 Murphy, G.M., 31
 Mylonakis, S.G., 321

N

Nakamura, T., 217
 Naudé, R., 31
 Nernst, W., 19, 33
 Nier, A.O.C., 34, 287
 Northrop, D.B., 349, 388

O

O'Leary, D.J., 228
 O'Leary, M.H., 349, 368, 369, 372
 Onsager, L., 393
 Oppenheimer, J.R., 33, 39, 41

P

Paabo, M., 358, 359
 Padua, A.A.H., 163
 Paneth, F., 2, 13
 Paneth, P., 332, 335, 369, 372, 384, 386
 Phillips, J., 279
 Pigford, T.H., 286, 287
 Pilling, M.J., 428, 450
 Pisais, N., 300
 Pitzer, K.S., 414
 Planck, M., 5, 19, 26
 Plyler, E.K., 397
 Polanyi, J.C., 33
 Polanyi, M., 118, 181
 Polyakov, V.B., 426
 Pople, J., 52
 Pratt, R., 373
 Prausnitz, J.M., 426
 Prigogine, I., 171, 172
 Prout, W., 3, 22

Q

Quack, M., 392
 Quinn, D.M., 365

R

Rabinovich, I.B., 178, 179
 Rabinovitch, B.S., 437–441
 Rabinovitch, I.B., 407, 416
 Raczkowski, A.W., 50
 Rae, H.K., 268
 Raimondi, L., 337
 Ramsperger, H.C., 449
 Raoult, F.M., 85
 Ravid, B., 392, 397
 Rayleigh, L., 297
 Raynes, W.T., 406
 Rebelo, L.P.N., 146, 153, 163, 171, 177, 236, 237, 239, 243, 417, 420, 423, 425
 Redlich, O., 60, 70
 Reuben, J., 229
 Reynolds, C.A., 174
 Ribnikar, S.V., 164, 165
 Rice, O.K., 152, 428, 448, 449
 Richardson, F.M., 311
 Richards, T.W., 14
 Rife, J.E., 367
 Risley, J.M., 404
 Roberts, G.C.K., 226
 Robertson, R.E., 321, 329, 359
 Robertson, S.H., 428
 Robinson, D.E., 373
 Rock, P.A., 253
 Roentgen, W.C., 4
 Roskos, R.R., 412
 Ross, W.H., 6, 13
 Rothman, L.S., 392
 Russell, A.S., 9
 Rutherford, E., 2, 5, 6, 7, 9, 13–17, 20, 24
 Rydberg, J., 17, 28, 31

S

Saunders, M., 130
 Saunders, W.H., 326, 377
 Schaad, L., 209, 213, 325–327, 355
 Schachtschneider, J.N., 70
 Scharlin, P., 178
 Scher, C., 392, 397
 Schimerlik, M.I., 367
 Schinke, R., 450
 Schlawlow, A.L., 282
 Schneider, F.W., 437–439
 Schowen, R.L., 360, 364
 Schramm, V.L., 370
 Schrieffer, R., 173
 Schrödinger, E., 29, 33, 37, 39–44, 47–49, 51, 52
 Seltzer, S., 321

Sergeyev, M.M., 244
 Setser, D.W., 441
 Severinghaus, J.P., 301
 Shakleton, N.J., 300
 Sham, L.J., 53
 Shendarovich, G., 229
 Shiner, V.J., 321, 323
 Sicinska, D., 335
 Singleton, D.A., 232, 326
 Smiley, J.A., 372
 Smith, D.G., 362
 Snyder, R.G., 70
 Soddy, F., 1, 2, 6–11, 13–16, 18, 23, 24
 Spevack, J.S., 270
 Spindel, W.S., 253, 262, 263, 269
 Starke, K., 263
 Staveley, L.A.K., 407
 Steele, W.A., 407, 416
 Stern, M.J., 129, 320, 321, 329
 Stern, O., 19, 28
 Stirling, J., 87
 Storer, J.W., 337
 Streitwieser, A., 321
 Swain, C.G., 327
 Szydlowski, J., 176

T

Tabisz, G.C., 392
 Taft, R.W., 43
 Tang, P., 359
 Taylor, T.I., 269
 Teller, E., 60, 70
 Thiemens, M.H., 444–446, 450
 Thomas, A.A., 232
 Thomson, J.J., 5, 14, 18–23
 Thornton, E.R., 281, 329
 Tiffany, W.B., 282
 Tonakura, K., 217
 Toth, R.A., 397
 Truhlar, D.G., 182, 200, 317, 335, 377, 380,
 381, 383, 384
 Tzias, P., 166

U

Urbanczyk, A., 392, 401, 402
 Urey, H., 1, 2, 31–33, 293, 294, 306

V

van den Broek, A., 2, 14–18
 van der Merve, A., 304
 van der Waals, J.D., 149, 167, 382, 408, 409,
 413–415, 418, 421
 Van Etten, R.L., 404
 Van Hook, W.A., 146, 149, 153, 155, 161, 166,
 167–169, 171, 236, 237, 239, 240, 243,
 264, 279, 244, 392, 401, 402, 407, 416,
 417, 420, 423, 425
 Van Ness, H.C., 426
 Van't Hoff, J.H., 178
 Verkouteren, R.M., 311
 Villani, S., 267Villano, S.M., 328, 329
 Visak, Z.P., 177
 Von Liebig, J.F., 4

W

Wageman, W.E., 228
 Wagman, W.E., 406
 Waldman, L., 101Washburn, E.W., 32, 33
 Westaway, K.C., 322, 331
 Westheimer, F., 366
 Wieczorek, S., 392, 401, 402
 Wignall, G., 243
 Wigner, E.P., 33, 121, 122, 126, 147, 189
 Wilczura, H., 243
 Wilson, A.H., 5
 Wilson, E.B., 68
 Wilson, E.D., 21, 23
 Winter, N.W., 183
 Woehler, F., 4
 Wolff, H., 156
 Wolfsberg, M., 47, 50, 62, 89, 127, 134, 135,
 146, 149, 153, 160, 320, 321, 329, 392,
 417, 420, 423, 425
 Wong, W.W., 310

Y

Yang, W., 373
 Yato, Y., 164, 165

Z

Zarzycki, R., 311
 Zimm, B., 244
 Zywockinski, A., 241

Subject Index

A

AB approximation, 151–152
Abundance standards, 290–291
Acentric factor, 414
Acetic acid, 309
Acid ionization isotope effects, 359
Action integral (semi-classical), 192
Activated complex, 117, 118
Active sites, 347, 351–352
Activity, activity coefficient, 133
Adiabatic approximation, 42
Adiabatic correction, 44–51, 130
Adiabaticity in tunneling, 199
Adiabatic modes in unimolecular processes, 432
Alcohol, 309
Alpha-secondary isotope effects, 320–322
Alternative paths, S_N2 and E_2 , 327–329
Anharmonic corrections, 134, 157–160
Anharmonicity, 323
 G_0 correction, 135
Apoenzyme, 343
Aptian $\delta^{13}\text{C}$ signals, 302–303
Aqueous solvent isotope effects, 358–365
Argon isotope separation, 260
Associated model building with energy refinement (AMBER), 379
Atomic number, 15
Atomic vapor isotope laser separation (AVLIS), 285–286
Average molecular partition function, 144

B

Background contamination, mass spectroscopy, 218
Barrier penetration, 189
Basis functions, 53

Becke 3-Parameter, Lee, Yang and Parr (B3LYP), 52–53
Benzyl chloride S_N2 reaction with CN, 330–331
Beta decay, 10
Beta-secondary isotope effects, 322–323
Bigeleisen–Mayer equation, 93–96
Blue shift, 146, 147, 149, 155, 166
Boil-up, 273–274
Boltzman’s constant, 86, 87
Bond-energy-bond-order-vibration (BEBOVIB), 329
Bond order dependence of KIE, 335–336
Bond strength hypothesis, 322
Born–Oppenheimer approximation, 37, 42
 corrections, 42
Born–Oppenheimer potential, 55, 56, 59, 61
Born–Oppenheimer surface, 188
Boron nitride (BN), 45
Boron oxide (BO), 27–28
 state mixing, 44
Bottle-necking, 285
Bristlecone pines, 305–306
Bruce deuterium plant, 271, 272

C

Calcite-water equilibrium, 293
Calutron, 256, 257
Canadian-deuterium-uranium (CANDU) reactor, 268
Canonical partition function Q , 86
Canonical process, 428
Canonical variational transition state theory (CVTST), 187, 382
Carbonium ion transition states, 321
Cartesian coordinates, calculations, 62–67
Cartesian displacement coordinates, 62, 68–71
Cartesian momenta, 38

- Cascade, 247–248
 countercurrent, 249–251
 ideal, 248, 251–253
 recycle, 249
 simple, 249–251
 squared off, 248
 tapered, 248
 Cathode rays, 5
 C_3 ^{13}C cycle, 304
 C_4 ^{13}C cycle, 304
 Cell model, 150–151
 ^{13}C enrichment, paleo-organics, 301–302
 Centrifuge, 264–267
 Chemical potential, 83
 condensed phase, 141
 vapor, 140
 Chemical reflux isotope exchange, 269–270
 Chemical shift isotope effects, 228
 Chemistry at Harvard macromolecular
 mechanics (CHARMM), 379
 Chromatography, 277–282
 IE's, 177–179
 CI, 53
 Classical harmonic oscillator, 57
 Classical trajectory calculations, 185–186
 Classification of molecular energy levels,
 432–433
 Clay cores, 301–302
 $Cl + HCl$ reaction, 201
 Cloud point, 239
 Clusius Dickel thermal diffusion column, 259
 Coal, 307–308
 Column exchange (COLEX) process, 277
 Combustion trains for IRMS, 222
 Commitments, 350–351
 Competitive measurement of KIE, 208–212
 Competitive studies, single labeling, 209–210
 Complicated enzyme reactions, 351–358
 Condensation of molecules, 145–147
 Condensed phase isotope effects, 139–180
 Conjugate momenta, 69
 Continuous dilution differential refractometry,
 400–402
 Coordinate systems, 58–59
 Correction for vapor nonideality, 85–88
 Corrections to Bigeleisen-Mayer equation,
 130–132
 Correction to Henry's Law, 85
 Correction to Raoult's Law, 85
 Corresponding states calculations, 413–415
 H_2/D_2 , 422–424
 $^3He/^4He$, 422
 methane, 424, 425
 water, 424, 425
 Coulomb potential energy, 38
 Coupled motion, transition state, 375–376
 Critical density IE, 421
 Critical property isotope effects, 416, 419–422
 uncertainty, 421–422
 Cubic equations of state, 414
 Cut, 249
 Cyclopropane, isomerization, 439–440
- D**
 Dalton's law, 84
 Debye light scattering theory, 240
 Decarboxylation KIE's (enzyme), 365–366
 Decarboxylation reactions, 334–335
 Degrees of freedom, 58, 90–91
 Delta δ notation, 290
 Delta δ values, 220
 Demixing in isotopomer solutions, 172–173
 Demixing of polymer blends, 240–241
 Demixing polymer isotopomer solutions, 143
 Dendrochronology, 305–306
 Density functional theory (DFT), 52–53
 Determinant of a matrix, 75
 Deuterium
 discovery, 2, 33
 neutron moderator, 267
 production, 268
 Diagonalization, 64, 65
 Dielectric constants, 393
 Dielectric effect, 160–161
 Diels-Alder reaction, isotope effects, 336–339
 Differences between TST and VTST, 186–187
 Differential precipitation, 286–287
 Differential refractometry, 400
 Dipole moments, 389–398
 CO isotopomers, 397
 isotope effects, 392–398
 Direct method of KIE determination, 203–206
 Discovery of isotopes, 1–3
 Dispersion forces, 149
 Dispersion relations, 400
 Dissociation energy D_e , 55–56
 Distillation, 267–277
 carbon monoxide, 275–276
 column, 249–250
 hydrogen, 275
 nitrous oxide, 276
 water, 276
 Dividing surface for VTST, 182–185
 Doping, 310
 Double labeling, 208–209, 219
 Dual inlet system, IRMS, 220

E

Eckart barrier, 192
E. coli, KIE's, 372
 Eigenvalue, 40
 Eigenvalues λ , 64, 73
 Electrical properties, isotope effects, 389
 Electrolysis, 286
 Electromagnetic separation, 256–257
 Electro-migration, 286
 Electronic Schrödinger equation, 39–40
 Electronic spectra, diatomics, 29
 Electron impact (EI), 215
 Energy level density, 432
 Energy U, 78
 Enriching section, 249–250
 Enrichment factor, single stage, 248
 Enthalpy H, 78
 Entropy S, 78–79
 Environmental studies, 289–310
 Enzyme kinetics, 344–351
 Enzymes, 343–388
 Equations of state (EOS), 413–414
 Equilibrium internuclear distance, 55
 Equilibrium constants, 84, 85, 88–89
 Equilibrium isotope effects, 234–241
 Equilibrium time, 253–254
 Equivalent isotopomers, 163
 E_2 reactions, 327–329
 Error analysis of KIE measurements, 212–215
 Excess free energy
 interaction parameter c , 175
 mixing isotopes, 162, 165–166, 172–173
 solutions of isotopes, 170–173
 Excess IE's solutions of isotopes, 171
 Exchange distillation, 267–277
 boron enrichment, 276–277
 Excitation factor (EXC), 94
 Experimental measurement, KIE, 203–215

F

Fajans/Soddy rules, 10
 First law of isotopics, 42–43
 First law of thermodynamics, 77–78
 First order perturbation theory, 42
 First quantum correction, 102–106
 Flory θ point, 242
 Fluctuations in ion current, 217
 Food authentication, 308
 Force constant matrix, F, 63
 Force constants, 40, 56–58
 Forward commitment, 350
 Fractionation factors, 142–143, 170–173
 measurement, 234, 238

Free energies, 80–83
 Free energy of activation, 184
 Frequency shifts on condensation, 149, 150,
 157, 161
 Fruit juice, 308
 Fugacity, 133

G

g03, 53
 Gamma rays, 10
 Gas chromatography, 278–280
 Gaseous diffusion, 248–249
 Gas phase S_N2 and E_2 reactions, 327–329
 Gaussian computer programs, 52, 61, 62
 Gaussian type orbitals, 53
 Geib-Spevack (GS) exchange process, 252
 for deuterium separation, 271
 Geochemical studies, 289–311
 Geochemical temperature scales, 293–296
 Geometric mean, rule of, 319
 6–31G, 6–311G, 6–311**G, 53
 Gibbs free energy G, 81
 Glucose-6-phosphateogenase, 366–368
 Graham's law, 249
 Greenland ice cores, 300–301

H

Haloalkane dehalogenase, QM/MM, 385–388
 Hamiltonian, 98, 99
 function, 37, 38, 40, 65
 Hammett constants, 330
 Harmonic approximation, 56–59
 Harmonic oscillator approximation, 89–91
 Harmonic oscillator cell model (HO CM), 157,
 163, 165, 171
 Harmonic potential function, 60
 Harmonic semiclassical calculation of KIE,
 313
 Hartree-Fock approach, 51
 Hartree-Fock calculations, 381
 Heavy atom isotope effects, 319–325
 Heavy water production processes, 267–269
 $^3\text{He}/^4\text{He}$ phase diagram, 172
 Height equivalent theoretical plate (HETP),
 273
 Helmholtz free energy A, 80
 Henry's law
 coefficients, 155
 constant, 279
 Hessian matrix diagonalization, 380
 H + H_2 reaction, 197
 High concentration isotope label, SANS, 242

High pressure limit, 435
 High temperature limit, 96–103
 H₂O/D₂O solvent mixtures, 371
 Holoenzyme, 343
 Honey, 310
 Hooke's law, 56
 Hydrosphere, 296–297
 Hyperconjugation, 322
 Hyperpolarizabilities, 389–393
 Hypochlorite + ethyl chloride, 320

I

Ice cores, 298–301
 Ideal gases at equilibrium, 84–86
 Imaginary frequency, 184
 Infrared (IR) intensities, 395
 Interaction of molecules, 146, 152
 Internal coordinates, 68–70
 Intrinsic isotope effects, 351
 Intrinsic reaction coordinate (IRC), 185
 Inverse secondary KIE, 437–441
 Ion cyclotron resonance (ICR), 258
 Ion fragmentation, 218
 Irreversible processes, 79
 Isomerization methyl isocyanamide, 437–439
 Isomerization of cyclopropane, 439–440
 Isotope analysis extraterrestrial samples, 442–447
 Isotope fractionation, living organisms, 302–307
 Isotope hydrology, 296–302
 Isotope perturbation, enzyme KIE's, 207–208
 Isotope-ratio mass spectrometry (IRMS), 219–224
 use, 292
 Isotopes
 discovery, 1–3
 effects
 in mixed solvents, 362–365
 on solubility, 174–180
 on spectra, 25–30
 superconducting transition, 173–174
 as tracers, 1
 Isotope separation, 19, 245
 aerodynamic, 267
 centrifuge based, 264–267
 by chromatography, 280–282
 by distillation, 274–276
 energy demand, 261–264
 first attempt, 246
 practical, 255–267
 Isotopically pure reactants, 204
 Isotope exchange equilibrium, 45, 89

J

Jacobi coordinates, 192–194

K

Kanalstrahlen, 18
 K_{BOELE}, 46, 47
 Keltium, 17
 Kinetic isotope effects (KIEs), 313–341
 in *E. coli*, 372
 of hydrogen atom and molecules, 313–318
 as probes of TST structure, 329–339
 Kohn Hohenberg theorem, 52
 Kohn Sham orbitals, 53

L

Large curvature tunneling (LCT), 384
 Laser fluence, 283
 Laser isotope separation (LIS), 282–286
 deuterium separation, 285
 UF₆, 286
 uranium, 285–286
 Lattice anharmonicity, 157–158
 Least action tunneling (LAT), 199
 Level spacing, 91–92
 Limiting values of isotope effects, 96–97
 Linear combination atomic orbitals (LCAO), 51–52
 Liquid-liquid equilibria isotope effects, 238–241
 Liquid-liquid exchange, lithium enrichment, 277
 Liquid scintillation counting, 233
 L-malate to pyruvate (enzyme), 365–366
 Locating dividing surface, 187
 London dispersion theory, 398
 Lorenz-Lorentz formula, 399–400
 Low concentration isotope labeling, SANS, 244
 Lower critical solution temperature (LCST), 174–175
 Low pressure limit, 436
 Lutidines, 332–333

M

Machine calculations, 320
 Magnetic isotope effects, 225
 Magnitude of VCIE and VPIE, 153–154
 Maple syrup, 309
 Mass diffusion, 286

- Mass independent fractionation
 isotope fractionation, 427–450
 ozone, 446, 447
 theory, 448–450
- Mass scaled Jacobi coordinates, 193
- Mass spectrograph, 20
- Mass spectrometer, 34
- Mass weighted coordinates, 63, 71
- Mass weighted force constants, 63
- Matrix diagonalization, 72–75
- Matrix operations, 72–75
- Matrix transpose, 72
- Mean square amplitude of vibration, 396
- Mechanical model MVIE, 406, 408–409
- Membrane pervaporation, 286
- Menshutkin reactions, 332–334
- Meteoritic water line, 298
- Methane, ^{13}C NMR isotope effects, 405
- Methyl isocyanide, isomerization, 437–439
- Methyl malonyl-CoA mutase, 377–379
- Microbial enrichment, 286
- Microcanonical process, 428
- Microcanonical VTST, 187–188
- Minimum energy path (MEP), 184, 185
- Mixed solvents, 360–362
 KIE's, 362–365
- MMI x EXC x ZPE formalism, 124–125,
 319–320
- Modeling IE's on enzyme reactions, 379–388
- Modified intermediate neglect of differential
 overlap (MINDO), 381
- Molar volume corrections, 143
- Molar volume isotope effect (MVIE),
 165–166, 168–169, 401–402, 406–412
 for $\text{H}_2\text{O}/\text{D}_2\text{O}$, 410
 for hydrogen bonded liquids, 409–410
 temperature dependence, 407–408
 water, 168
- Molecular beam method, 394
- Molecular mechanics (MM), 379
- Molecular orbital approach, 51
- Molecular partition function q , 90
- Moment of inertia, 67, 70
- Morse function, 56
- Multiple isotope effects, enzyme reactions,
 355–356
- Muonium (Mu), 50–51
- N**
- Natural gas, 307–308
- Neon isotopes, vapor pressure, 19
- Neutron, discovery, 24
- Newton's second law, 65
- Nitrogen isotopes, 30–31
- Nitrogen KIE's of pyridines, 334
- Non-competitive KIE determination, 203–206
- Nonideal solutions, 143, 174
- No 'recrossing' assumption, 186
- Normal mode frequencies, 58, 60, 69
- Northrop notation, 349–350
- Nuclear field shift effect, 130–132, 282
- Nuclear magnetic resonance (NMR)
 coupling constant isotope effects, 403
 determinations of molecular structure,
 225–226
 measurement
 ^{13}C IE's, 231–233
 isotope effects, 225–233
 shielding isotope effects, 403–406
 spectra, isotopic methane, 228
 studies, fast exchange IE's, 231
- Nuclear overhauser effect (NOE), 226
- O**
- ^{18}O isotope thermometer, 296
- $\delta^{18}\text{O}$ measurements in mollusks, 293
- ONIOM, 385, 386
- $^{17}\text{O}/^{18}\text{O}$ enrichment, 442–447
 in meteoric samples, 443–444
 in ozone, 444
- Optical pumping, 283
- Optimised multidimensional tunneling (OMT),
 384
- Optimized potentials for liquid simulation
 (OPLS), 379
- Ortho and para hydrogen, 275
- Orthogonal polynomial expansions, 105–106
- Oxygen isotopes, 30–31
- P**
- Pair correlation function, 162
- Pair intermolecular energy, 146
- Paleo-thermometer, 293
- Partial Hessian vibrational analysis, 380
- Partial molar free energy (chemical potential),
 140, 170, 175, 179
- Particle in a box, 43
- Particle scattering, 15
- Partition functions, 88–89
- Partitioning factor, 350–351
- PDT x EXC x ZPE formalism, 124–125
- Peak shape, IRMS, 219
- Periodic table, 3–5
 modern, 23–24
- Petroleum, 307–308

- Phase space, 97, 98
 Phosphoenol-pyruvate carboxylase, 368–371
 Photochemical isotope separation, 282
 Photoionization, 284
 pH/pD isotope effects, 358–360
 Plasma separation process (PSP), 258–259
 Plate, ideal, 273
 Plejade, 13
 PM3-SRP/CHARMM, 387
 Polarizabilities, 389–393
 Polarizability
 frequency dependence, 398–400
 isotope effects, 398, 400, 402
 Polarization, bulk, 393
 Potential energy function, 37
 Potential energy surface, 37, 40
 Pressure dependence of critical demixing, 242
 Pressure dependence of rate constant, 435–436
 Primary isotope effect, 441–442
 Principal moments of inertia, 128
 Product factor (PF), 94
 Properties, isotopic waters, 168–169
 Protein data base (PDB) Pee Dee ^{13}C standard, 291
 Proton inventory, 205
 curves, 364–365
 Pseudo first order constants, 435, 436
 Pseudo-harmonic approximation, 157–158
 PSP superconducting ICR separator, 258
 PVT isotope effects, 418
 measurement, 237–238
- Q**
 Quantum mechanical harmonic oscillator, 57, 58
 Quantum mechanical/molecular modeling (QM/MM), 380–385
 Quantum mechanical tunneling, 314, 315
 Quantum mechanical VTST, 187–188
 Quaternizations of lutidines, 332
- R**
 Radioactive series, 6
 Radioactivity, 1
 Radio-isotope double labeling experiments, 234
 Radio-isotopes, 233–234
 Random binding, 354
 Rate corrections for pD isotope effect, 359
 Ratio of catalysis, 350
 Rayleigh fractionation, 296–302
 Reaction, methane + hydroxyl, 318–319
 Recrossing phenomenon, 187
 Rectilinear diameter, 416
 Redox ion exchange chromatography, 258, 280–282
 Red shift, 146, 148, 150, 154, 166, 167
 Reduced partition function ratio (RPFR), 96
 Reduced vapor pressures, 415, 419
 Redundant coordinates, 68
 Reference isotopomer pairs, 414–419
 Reference system, isotope effects, 418–419
 Reflection probability, 190
 Reflux, 250
 minimum, 251
 total, 251
 Refractive index isotope effects, 393, 400
 Relation of VPIE to vibrational dynamics, 144–147
 Remote labeling in IRMS, 223–224
 Remote labeling technique, 369–370
 Resolution, 278–280
 Reversible competitive inhibitors, 357–358
 Reversible enzyme reaction, active site, 351–352
 Reversible processes, 79
 Rice, Ramsberger, Kassel and Marcus (RRKM) mechanism, 428–442
 Rigid rotor approximation, 89–91
 Rigid rotor harmonic oscillator ideal gas, 96
 Rotational constant B_e , 396
 Rotation vibration interaction, 43
 Rovibrational NMR isotope effects, 226–231
 Rovibrational theory of NMR IE's, 403–406
 Rutherford scattering, 15–16
 Rydberg constant, 48
- S**
 Sample preparation IRMs, 222–223
 Schrödinger equation, 37–44, 47–48, 51, 52
 Sec-D KIEs on C-C bond rupture, 440
 Secondary isotope effects, 319–325
 Second law of thermodynamics, 78–79
 Selectivity, 283
 Semiclassical KIE, 315
 Separation factor r , 248
 Separation factor, single stage, 248
 Separation of chlorine isotopes, 23
 Separation of degrees of freedom, 43–44
 Separation of deuterated alkanes, 280
 Separation of neon isotopes, 23
 Separation of translation and rotation, 67
 Separation potentials, 255
 Separative unit, 247
 Separative work, 254–255

- Sequential enzyme reactions, 352–353
 Simple enzyme KIE notation, 344–346
 Simultaneous non-competitive measurements, 206–207
³⁴S isotope thermometer, 296
 Skew angle, 192–196
 Small angle neutron scattering (SANS), 242–244
 Small curvature tunneling (SCT), 199, 384
 S_N1 reactions, 320–321
 S_N2 reactions, 320–322
 Soddy's rule, 9
 Solubilities H₂ and D₂, 177, 178
 Solution
 Methylpyridine/water, 176, 177
 nitromethane/pentanol, 175
 Solvent extraction, 286
 Solvent IE's, 358, 373–375
 gas solubility, 156, 177, 178
 ionic compounds, 179
 Solvolysis reactions, 323
 Spectral band shapes, 160
 Spectroscopic precision, 151, 160
 Spinodal, 240
 SrtA transpeptidase, 373–374
 Stage, 247–255
 Standard mean ocean water (SMOW), 291
 Standards for IRMS, 219–220
 Standard state, 88
 Stark effect, 394
 State functions, 78
 Statistical weight isotope effect, 439, 441
 Steady state approximation, 347, 429
 Steric isotope effects, 323–324
 ST0-3G, 53
 Stirling's formula, 87
 Storm patterns and δ¹⁸O, 306–307
 Stripping section, 250
 Substituent effects, 42–43
 Substrate-enzyme binding, 350
 Sum rule, 71
 Swain-Schaad relation, 325–327, 355
 Symmetrical transition states, 314
 Symmetry numbers, 106–115
 factor, 95
- T**
- Teller Redlich product rule, 60, 70, 101
 Temperature dependence of critical demixing, 242
 Temperature dependence of (s/s')_f, 115–117
 Temperature dependent force constants, 152
 Temperature independent force constants, 152
- Thermal activation, 437–441
 Thermal diffusion, 255, 259–260
 THERMISTP computer program, 62
 Thermodynamic laws, 77–79
 Thermodynamic precision, 150–151
 Thermolysis of azo compounds, 321
 Third law of thermodynamics, 79
 Three center collinear reactions, 196–199
 Three isotope plot, 298
 terrestrial and extra-terrestrial samples, 302
 Total molecular energy, 38, 44
 Tracer isotopes, 310
 Transmission coefficient κ, 121
 Transition state, 117–121, 184
 early, 329
 late, 329
 loose, 330
 S_N2 reaction, 320
 structure, 329–339
 symmetric, 329
 tight, 330
 Transition state theory (TST), 33, 181–182, 313
 isotope effects, 117–127
 Transmission coefficient, 182
 Transmission probability, 190
 Tunneling, 189–199, 315
 in alcohol dehydrogenase, 376–377
 in enzyme reactions, 376–379
 Turbomole computer program, 61
 Turnover number, 345
- U**
- Unimolecular rate constants, isotope effects, 430, 437
 Unimolecular reactions, isotope effects, 427–428
 Upper critical solution temperature (UCST), 175–177
- V**
- Valence bond approach, 51
 Valence coordinates, 58–59, 61, 62, 68–70
 Van der Waals attraction, 149
 Van der Waals equation, 414
 modified, 415, 418
 Vapor nonideality, 143
 corrections, 145
 Vapor phase standard state, 140
 Vapor pressure isotope effect (VPIE), 19, 20
 benzene, 155, 165–166
 carbon disulfide, 161

- ethylene, 163–165
 - hydrocarbon/alkylamine solutions, 156
 - hydrocarbons, 149
 - inverse, 149, 167
 - measurement, 235
 - model calculations, 157
 - monatomics, 147–152
 - organic compounds, 154
 - polyatomics, 147–152
 - rare gases, 149, 162, 163
 - separated isotopes, 141–142
 - thermodynamics, 141
 - vibrational analysis, 147–152
 - water, 155, 166–170
 - Variational transition state theory (VTST), 181–182, 340–341
 - QM/MM
 - calculations, 380–385
 - H/D atom transfer, 380, 383, 384
 - proton/deuteron transfer, 380, 383
 - tests, 199–201
 - Vegetable juice, 308
 - Vibrational amplitude effects, 389–391, 396
 - Vibrational energy levels, 43–45
 - Vibrational kinetic energy, 61
 - Vibrations in diatomic molecules, 55–58, 67
 - Vibrations of polyatomics, 55, 57–58
 - Vibrations of water isotopomers, 59–60
 - Vienna standard mean ocean water (VSMOW), 291
 - Virial coefficient isotope effect (VCIE), 139, 146, 147, 153–154
 - Vostok core, 299–300
 - VPDB Vienna Pee Dee ^{13}C standard, 291
- W**
- Wave functions, 39, 42–44, 49, 51, 52
 - Weak collisions, 436
 - Whole molecule mass spectrometry, 215–219
 - Whole number rule, 21–23
 - Wigner tunneling correction, 122, 126, 189
 - Wine, 308–309
- Y**
- Younger-Dryas transition, 301
- Z**
- Zero-curvature tunneling (ZCT), 384
 - Zero of energy, 93
 - Zero point anharmonicity, 158–160
 - Zero point energy (ZPE), 19
 - contribution to rate, 315
 - factor, 94
 - Zimm analysis, 244